A QUANTITATIVE, COMPARATIVE STUDY OF SOUND PRODUCED *IN VITRO* BY PULSATILE FLOW IN AND AROUND PROSTHETIC, AORTIC HEART-VALVES

Thesis by

David Walter Suobank

In Partial Fulfillment of the Requirements

for the Degree of

Doctor of Philosophy

California Institute of Technology

Pasadena, California

1983

(Submitted May 12, 1983)

And even things without life giving sound,
whether pipe or harp,
except they give a distinction in the sounds,
how shall it be known what is piped or harped?
For if the trumpet give an uncertain sound,
who shall prepare himself to the battle?
I Corinthians 14.7,8

ACKNOWLEDGEMENTS

We gratefully acknowledge the funding provided for this project by the Donald E. Baxter Foundation, the Children's Heart Foundation of Southern California and the American Heart Association, Los Angeles Affiliate.

The generous contribution of valves for this project was provided by Shiley Laboratories, Sutter Biomedical and Edwards Laboratories.

The wonderful comments and suggestions by Dr. William Corcoran, Dr. Earl Harrison, Dr. Ajit Yoganathan, Dr. Thomas Brown, Dr. Vasilis Marmaralis were incisive and beneficial beyond measure to the overall project.

The inventive insight with regard to fabrication of experimental apparatus provided by George Griffith and Hollis Reamer made experimental work a pleasurable learning experience.

Visual documentation of the experiments on film and video tape was made possible by the expertise of Andrew Gero and Allen Goldstein.

A special thanks to Donna Johnson for her preparation of the neat, concise, clear and consistent portions of this manuscript.

The courteous manner in which each of these people assisted this work will always be warmly appreciated.

A general thank-you to all the other people I have interacted with during my post-graduate studies at Caltech: my colleagues within the Department of Chemical Engineering at Caltech; colleagues at the USC Medical School, City of Hope and Cedars of Sinai Hospitals and the Georgia Institute of Technology; and biomedical engineers from Australia, Japan, Germany and other countries throughout the world, many of whom visited Caltech during my graduate studies.

ABSTRACT

A quantitative, comparative study was made of sound produced *in vitro* by pulsatile flow in and around three designs of prosthetic aortic heart-valves. Designs studied were 25mm Bjork-Shiley, 24mm Smeloff and Starr-Edwards model 2400 valves. A digital method for the analysis of the sounds using the fast Fourier transform is presented and applied. Results are examined in both the time domain and a variety of formats in the frequency domain. Formats include original time vs. amplitude plots, power-density spectra, power-distribution functions, a 3-D (three-dimensional) surface of power-frequency-time, auxiliary views of these 3-D surfaces, and a 3-D, power-distribution surface showing the difference between two 3-D, power-distribution surfaces. Enhanced distinguishability of sound was clearly shown by the 3-D, power-difference surface which provided a very convenient means for the overall comparison of two sounds.

Attention was given to understanding effects of valvar and pulsatile conditions upon the frequency characteristics of the opening, systolic, and closing sounds. Failure modes were simulated and resulting changes of the sounds were examined. Simulated overgrowth was placed on the inner apical surface of the Starr-Edwards model 2400 valve and on the upstream struts of the Smeloff valve. Results showed that the sounds produced provided information pertinent to the simulated malfunction.

Effects of pulse rate, mean flow-rate, and mean aortic pressure associated with the normal valvar sounds were investigated. Results were interpreted in terms of the known physical changes of the valve and known changes of the pulsatile state. Under alternate pulsatile states, the total power of the opening and closing sounds were influenced primarily by the rate of change of the ventricular pressure prior to these events. The difference between systolic sounds was

much greater than between opening and closing sounds for cases involving changes of the stroke volume for each normal valve design. An increase in systolic flow rate produced a corresponding increase in the power of peaks in the spectra of the systolic sound for each design. The location of peaks within the power density spectra of opening, systolic and closing sounds were more similar during the studies of alternate, non-normal, pulsatile states of normal valves than they were during the studies of normal/abnormal valves under normal pulsatile states.

Visualization of the valve and particle trajectories and simultaneous recording of sound, flow rate, and upstream and downstream pressure, provided direct evidence of the cause of many of the acoustical events. Strouhal numbers were estimated from center-frequencies of resonance peaks associated with sounds that were related to periodic vortex shedding in flows past the struts, annular gaps and phonocatheter.

The overall results indicate that the method used could distinguish changes of valvar and pulsatile states for each of the valvar designs that were studied.

TABLE OF CONTENTS

PAPER 2

A Quantitative Method for the *In Vitro* Study of Sounds Produced by Prosthetic Aortic Heart Valves, Part II: An Experimental, Comparative Study of the Sounds Produced by a Normal and Simulated-Abnormal Starr-Edwards Series 2400 Aortic Prosthesis

PAPER 3

A Quantitative Method for the *In Vitro* Study of Sounds Produced by Prosthetic Aortic Heart Valves, Part III: An Experimental Comparative Study of the Sounds Produced by Normal and Simulated-abnormal Smeloff Aortic Prosthesis

PAPER 4
A Quantitative Method for the *In Vitro* Study of Sounds Produced by Prosthetic Aortic Heart Valves,
Part IV: An Experimental, Comparative Study of the Sounds Produced by a Normal Starr-Edwards 2400 Aortic Prosthesis Pulsed at Six Pulsatile States

PAPER 5
A Quantitative Method for the *In Vitro* Study of Sounds Produced by Prosthetic Aortic Heart Valves,
Part V: An Experimental, Comparative Study of the Sounds Produced by a Normal Smeloff Aortic Prosthesis Pulsed at Eight Pulsatile States

LIST OF TABLES

LIST OF FIGURES

GENERAL INTRODUCTION

MOTIVATIONS

Beyond its obvious purpose, as partial fullfillment toward the award of a doctoral degree in Chemical Engineering, this thesis presents the results of research that was begun to better understand the relation between sound and fluid-flow in and around prosthetic heart valves. The purpose for choosing this specific system for study lay in the fact that an immediate need existed for better understanding of the relationship between the valve design, valve condition, and pulsatile conditions and the sounds that the valve produced at these conditions. By working side-by-side with cardiologists, the author has been directed along a path which enabled this work to provide the information these professionals most urgently required to enhance diagnosis of valvar integrity by acoustical means.

The motivation for our work was initiated by Dr. Earl C. Harrison, M.D., a cardiologist at Los Angeles County-USC Medical Center, a leading authority of prosthetic heart valves, who brought the problem to the attention of Dr. Corcoran at Caltech. Auscultation had been used by medical doctors for decades to diagnose conditions inside the human body. Cardiologists, such as Dr. Harrison, were particulary well trained at listening to the sounds produced by the heart. Much work had been done during this century using these auscultation techniques to distinguish the sounds produced by normal and diseased heart-valves. It was also known that fluid mechanics played a fundamental role in the characteristics of these heart sounds. With the knowledge of successes and limitations of auscultation, the advent of prosthetic heart valves and their history of malfunction, and his own experience with the sounds produced by normal and abnormal valves, Dr. Harrison proposed that the differences in the sound pro-

duced by normal and abnormal heart-valve prosthesis could be characterized in a manner that was more quantitative than that provided by auscultation. Pioneering work by other people had also had shown the potential usefulness of computer analysis of these sounds. The primary motivation of the work was, therefore, to aid in the development of a methodology which was sensitive to the important states of prosthetic heart valves and which could ultimately be used for non-invasive diagnosis of these states. A clinically applicable instrument could then be developed which would be capable of generating useful, quantitative information about the condition of the heart and its valves and the nature of the flow of blood inside the heart. Such an instrument to be used by cardiologists must have a precisely defined mode of operation which includes a standard method of analysis and a standard, quickly-interpretable manner of depicting the data. This thesis provides one method which can be applied to the human heart, it provides experimental data obtained from pulse duplicator studies, and it provides detailed discussions and interpretations of these data. The experimental data, which are primarily of value as they relate to the *in vitro* experiments, provide a precise basis for estimating the accuracy and specificity of the analytical method under controlled conditions. These data will also be valuable, with appropriate considerations, when they are examined relative to data obtained from *in vivo* studies in the future.

The close working relationship between the cardiologists and engineers in our group produced many results which would not have occurred if we had worked independently. Nothing could have substituted the immediate dialectic that resulted from being together in the same room at the same table. Hopefully, this work will be an example of results produced by clear, combined knowledge that developed during the sustained relationships between professionals sharing different expertise.

ARGUMENT

To what extent can the state of a system be known from information obtainable from the sound that it produces? In particular, for systems in which fluids flow, how does the sound characterize the type of flow phenomena present in the system? With these general questions, let us begin.

Nature provides countless examples of systems which produce sounds primarily as a result of the flow of fluids in and around boundaries. In simple terms, the sound results from the transfer of kinetic energy, in the form of momentum, into potential energy, in the form of local regions of compression and rarefaction relative to ambient pressure at a particular region of flow. The Navier-Stokes equations provide the governing relationships balancing momentum in such a system. These perturbations of pressure propagate through the media as sound. Perhaps the first recorded description of such phenomena are the Aeolean tones produced by wires in the wind. The frequency of these tones is independent of the tension of the string and results from the shedding of vortices at regular intervals from the boundary layer at the surface of the string. These sounds can occur when a fluid flows around an object or through a gap. The frequency of the shedding of these vortices has been observed for flows in simple systems. The most commonly studied system has been flow around a rigid cylinder. Other important examples of flows in which sound can be of primary concern are: (1) sounds produced by flow inside pipes and valves in commercial production-facilities, (2) sounds produced in and around aircraft structures, (3) sounds produced in and around automobiles as a result of wind and within the engine, and (4) sounds produced in bio-systems involving fluid-flow such as the cardiovascular system and the respiratory system.

This thesis will focus attention on the sounds produced by the heart valves.

We also further restrict our attention to sounds produced by prosthetic heart-valves. These prostheses provide the fundamental components which characterize a sound-producing system. They possess all of the complexity which may be found in other systems, and, most importantly, the information obtained from their study provides very useful information which can be applied to improve the quality of human lives. At the present time approximately 80,000 heart-valve prostheses are implanted annually in humans. Each of the dozen or so major designs have been known to malfuction because of a variety of different causes. Before we discuss this specific system in detail, however, we will first outline the general factors which characterize the **state** of an acoustical system in which sounds are produced as a result of fluid-flow in and around its structure.

The systems we listed above each possess a particular mode of sound production within them, *i.e.* sounds produced by fluid-flow. In addition to these primary sounds, other sounds can be produced by these systems as a result of secondary effects produced by the flow. For example, a check valve may produce sounds when the occluder strikes structures of the valve as it opens or closes. Sometimes sounds will be produced during flow as the occluder of the valve bounces against its cage. For both of these secondary cases, the motion of the occluder is also a result of forces produced by fluid motion. Prosthetic heart valves produce both primary and secondary sounds.

The science of acoustics is involved with understanding the relationships between the state of the system as it is manifested by information contained in the sound that it produces, transmits, or absorbs. The phenomena of sound and vibration are closely connected. The vibration of a source is involved with the production of sound. The vibration of ambient fluid and/or boundaries are involved with the transmission of sound. The vibration of a boundary is also

involved with the absorption and directivity of sound.

What factors are involved when describing the state of an acoustical system? Generally, three factors must always be considered. These factors are flow characteristics, materials and geometry. Flow characteristics include all the important variables related to the flow, such as pulsatile frequency, mean flow rate, statistics of turbulent eddy distribution, etc. The variable "materials" primarily include the physical properties of the fluid, chambers, structures of the system, and internally located probes. Important geometrical factors include the size of the individual structures and their orientation relative to each other. A change in any one of these three general factors can generally produce direct, secondary changes in either of the other two factors. It is important, therefore, to note that the sound which is produced by a system is generally sensitive in various degrees to all of these changes which may occur. These changes usually do not occur independently.

What is the simplest and quickest way to interpret these acoustical data with the most specificity and accuracy? One can begin with a linear-systems approach. This approach generally yields useful results when the system is even moderately non-linear. This thesis discusses the results of applied linear systems-analysis. As we shall show, sounds produced by prosthetic heart valves can be very adequately analyzed by linear techniques. Like turbulence, acoustical phenomena, particularly the distribution of power over the frequency of the stimulus-response pair, can most easily be handled by Fourier analysis. Transfer functions can be generated in the frequency domain to relate the response to the stimulus. If one knows the nature of the stimulus, it is easy to estimate the response of the linear system given the transfer function. The linearity of the system can thus be tested by applying linear analysis. The question of specificity and accuracy of the linear method depends on factors which

are defined by the particular system being studied. Ideally, one can define a group of possible parameters which define the state of the system, then do experiments which maintain all but one of these parameters constant while varying the other, note any significant change of the observed results relative to a **normal** state, and do similar experiments independently varying each of the remaining parameters. Then, by comparing the results of each of these experiments, with the aid of a model, one begins to understand the degree of sensitivity, specificity and accuracy of the analysis and the model. These qualities are indicated by the variety of differences one sees relative to the **normal** state and the number of these different states that are similar to each other. The most accurate and specific method would detect and provide, for each parameter set of the model, a one-to-one relationship between the stimulus and response. A linear-model is useful and should be developed to support the results of the analysis. This model can be used to relate and explain the physical changes of the system in terms of these mathematical relationships. In addition, the model can be modified later if necessary to explain the results.

This heuristic has been used as a overall guide for the analytical method described in this thesis.

In Vivo vs. In Vitro Investigations

Results presented in the body of this thesis were obtained from a pulse duplicating system which is described in Part II. This *in vitro* approach offered control of the variables we mentioned above. The idea of *in vitro* study of heart valves is at least as old as Leonardo da Vinci whose notebooks contain a description of an apparatus for the study of fluid motion in and around the aortic valve. The use of such duplicators, however, to study the **sounds** produced by valves is unique

in the present work. As such, we can cite no references of earlier, *in vitro* work involving the sounds produced by prosthetic heart valves. References pertaining to sounds produced by prostheses *in vivo* are presented in the introduction of Part I. We have made every attempt to isolate information about the valve from the data we have obtained from the duplicator. The materials of construction of the duplicator define, in many respects, the system. This was a concern to which we have given full attention. By making internal measurements of the sound we have eliminated the variable of transmission through the plastic materials of the duplicator. By initially measuring sound at a variety of positions, and then using one of these positions as a standard, we have characterized and standardized the directivity of the aortic flow-section. This directivity, which is similar to the human aorta, was eliminated from the study by simply not considering it as a variable. Such consideration would best be made through studies *in vivo*. Finally, the walls of the aorta and the valvar-mount were altered in order to study the effect of these changes on the sounds. No such effect was observed. We were then confident that the primary modes of vibration which we were detecting at the phonocatheter were related to the valve and the fluid flowing in and around it. The information obtained from the sounds were considered to be related only to the prosthesis and pulsatile state.

A Brief Review of the General Subject of Turbulence Generated Noise

Flow through prosthetic heart valves is very complex and does not lend itself easily to idealized analysis to enhance understanding of the fundamental processes involved with the production of sound in and around these valves. Prosthetic heart valves produce a wide variety of flow phenomena. Examples are pulsatile, non-sinusoidal, non-axially symmetric flows; confined jets in circular,

annular, non-axial and even more complex geometries; stagnation regions; separation regions; recirculation; dynamic boundaries at the occluder; two-phase flow; and very complex wall-geometries. It is important, however, to present here a few of the more important references by authors who have dealt with general theoretical and experimental aspects of sound generated by fluid motions in simpler systems. These simplified models and their applications provide insight into the fundamental aspects of noise generation around prosthetic heart valves.

Two review articles of interest are those by Ffowcs-Williams (FFOWCS-WILLIAMS, 1969) and Reethof (REETHOF, 1978). The Ffowcs-Williams review describes approaches to the modeling of both pseudo-sound and the sound field proper, where pseudo-sound is classified as a local field independent of the compressibility of the fluid while the sound field radiates via compressible motion. Limitations and extensions of Lighthill's acoustic analogy are described and discussions are presented regarding acoustic source terms, sound induced by finite regions of free turbulence, radiation from compact aerodynamic surfaces, sources near noncompact surfaces, moving sources and sound generated by a turbulent liquid-bubble mixture. The more detailed review article by Reethof again covers many of the aspects presented in the Ffowcs-Williams paper, but emphasizes the special case of confined flow in pipes and through valves. This second review article includes topics such as turbulence generation in control valves and regulators, aerodynamic noise theory related to turbulence and flow in pipes, propagation of noise inside pipes with flow, theoretical aspects of acoustic transmission loss through pipe walls, and recent experimental results on the noise-generation mechanisms in valves and regulators and means of its reduction.

It is perhaps appropriate to begin citation of specific papers with the papers by Lighthill (LIGHTHILL, 1952 and 1954). Lighthill's acoustical analogy describes the acoustical radiation field produced by small regions of turbulence in an infinite continuous homogeneous fluid at rest. Using the exact mass and momentum balances and including mass sources and externally applied forces, Lighthill derived an inhomogeneous wave-equation with monopole sources related to mass-flow fluctuations, dipole sources related to compact fluctuating forces, and quadrupole sources related to the second order spacial derivatives of the turbulence-stress tensor. Ingard and Morse (INGARD and MORSE, 1968) show that the radiated acoustical power varies with the 4th, 6th and 8th powers of the velocity fluctuations for the monopole, dipole and quadrupole sources, respectively. Consequently, monopoles, if present, dominate the power of the sound being produced by monopoles, dipoles and quadrupoles.

The presence or absence of each of these three sources in various types of flows has been described by a number of theoretical and experimental papers. Sharland (SHARLAND, 1964) demonstrated that monopole and dipole sources cancel for a free shear layer far from a bounding surface. Ffowcs-Williams found that dipole sources integrate to zero for flows in infinite tubes with acoustically reflecting walls. Jenvey (JENVEY, 1975) examined sound produced by the flow of air through planar orifices placed in a pipe opened to the atmosphere. Measuring the sound downstream in the far field for different orifice diameters and pressure ratios, Jenvey showed that a quadrupole source model did not fit the data. He showed that the acoustic power varied with the 2nd power of the pressure gradient and the exponent of 2.4 of the orifice area.

The previous group of papers were concerned with overall, broadband acoustic power associated with sounds measured in the far field and dependence of this power on the characteristic velocity of the flow. Powell (POWELL, 1959) and

Lush (LUSH, 1971) both have examined the character of the frequency spectrum of circular free jets as a function of the characteristic mean velocity, geometry of the jet, and location in the far field. Both investigators predict a variation of acoustic intensity with f^8 at low frequencies and f^{-1} at high frequencies. The low-frequency region was related to low shear rates in the relatively thick mixing layer and the high-frequency region was related to high shear rate in the jet near the jet exit. Lush showed a shift of the predominant frequency to lower values and greater intensity as the observer approached the axis of the jet. A 15 db increase of the acoustical intensity was observed for a 50 % increase of the mean velocity of these low subsonic jets. Mach numbers in the range 0.30 to 0.87 were studied.

Another group of studies involves the influence of boundaries on the sounds produced by confined jets. These studies have generally been confined to either pseudo-sound in the boundary layer or radiated sound in the far field. Morfey (MORFEY, 1971) describes a general, modal method for estimating the propagational modes of sound in ducts with flow. The nature of the acoustic generation is assummed to be known. Known impedance boundary conditions are applied at the ends of the duct. Coupling between modes which occurs at real terminations was not modelled. Morfey then considers elementary sources which are compact in the axial direction and then shows how general sources are described by combinations of these simple sources and estimates the resulting acoustic field in terms of single-frequency modal response functions. Monopoles, dipoles and quadrupoles are treated. Results show the effect of various flows on the radiated power for a variety of sources. Corrections for the acoustic power with mean axial Mach number, Ma_z, were found to vary with $1 + Ma_z^2$. Solid body rotation of angular velocity ω_o in an axisymmetric duct modified the power further by a factor: $\frac{\omega_o}{\omega}$.

Ingard and Singhal (INGARD and SINGHAL, 1974) considered attenuation of plane waves of sound in ducts caused by visco-thermal effects and turbulence. The visco-thermal effect was expressed by the thickness of viscous and thermal boundary layers which were functions of the Mach number viscosity, fluid density, specific heats, and excitation frequency. The turbulence effect was expressed by the Mach number and friction factor.

The relationship of these papers to the present work is not a direct one. The theoretical papers were in simplified geometries under steady flow conditions. Sound was usually described only in the far field. We measured sound at the axis in the near-field under pulsatile conditions. We are presenting results, therefore, which include possible contributions from both pseudo-sound and radiated sound depending whether we are discussing flow related sounds or opening and closing sounds, respectively. Sound produced in our system by systolic flows could have been comprised of sound propagated to the catheter from other boundary layers and by the pressure fluctuations of the boundary layer of the catheter itself. Production and propagation of the opening and closing sounds are clearly understood because turbulent noise is absent and the sources are essentially monopoles and modes of sound propagation are nearly planar. Complexity of the structure of the turbulence in our system is such that no specific mechanism, such as those responsible for the mono-, di- or quadrupole sources, could be cited as responsible for the systolic sounds. Under certain conditions, however, we can predict the relative importance of specific phonomena based on observations in simple systems.

In simple tube flow, for example, noise production is a result of Reynold's stresses and pressure fluctuations. These quantities are not easily described nor measured. The classical statistical space-time analysis of pressure and velocity fluctuations have failed to provide insight into the causal processes that

initiate, develope, and characterize the turbulent struture in the boundary layer. Studies involving visualization of turbulence in boundary layers by Corino (CORINO and LUMLEY, 1969) show intermittent, very rapid and small-scale pressure changes at the wall under a turbulent boundary layer. Perhaps such bursts are responsible for part of the sounds measured in flows past prosthetic heart valves. It is more probable, based on the relative intensities of monopoles, dipoles and quadrupoles, that the systolic sounds are primarily caused by mass-flow fluctuations resulting from the vibrations of the walls and phonocatheter under the turbulent pressure fluctuations at these surfaces. The maximum Reynold's number of the flows through prosthetic heart valves was approximately 30,000, the maximum Mach number was 0.002. Maximum wall shear stresses were less than 2000 dynes/cm^2. Under these conditions it is probable that quadrupoles constitute little of the measured sound. This latter fact would account for the insensitivity of our spectra to fluid viscosity. This insensitivity would also indicate a relatively small contribution by dipoles such as those produced by turbulent bursting in the boundary layer.

We have observed a power-law relationship between the total power of the systolic sounds and the maximum systolic flow rate and maximum systolic pressure gradient. At sufficiently high flows the power increased dramatically with both of these variables. The relationship we observed between the acoustic power and mean velocity was much less than either the 4th, 6th, or 8th power laws predicted for the monopole, dipole and quadrupole sources. Our results were similar to those results of Jenvey in that the power scaled with the square of the maximum systolic pressure gradient.

This concludes the review of noise generation by turbulent flow. A comprehensive review was not possible, but the papers cited offer excellent examples of the types of work which have been done in this area. Any successful

scheme must be based on the understanding of the fundamental generation mechanisms in simpler configurations, therein lies the importance of this brief review. Further references are available at the ends of these papers.

Outline of Parts I through VII

The thesis is divided into seven Parts. Part I describes analytical considerations and the preferred method which was used to generate the results that are presented in Parts II through VI. Parts II and III describe experiments which were made to determine the sensitivity of the method to detection of abnormal **valvar** states of the Starr-Edwards 2400 and Smeloff prostheses, respectively. Parts IV, V and VI describe experiments which were made to determine the sensitivity of the method to detection of various **pulsatile** states using the Starr-Edwards 2400, Smeloff and Bjork-Shiley prostheses, respectively. We were particularly interested to determine if any of the pulsatile states produced sounds that could be mistaken for the abnormal valvar states that we had studied. Finally, Part VII describes the estimates we have made of the most probable location and frequency of vortex-shedding in the flow around the valvar-structures.

Appendix A provides important Figures and Tables. Appendix B contains a typical example of the software used for the analysis of the results presented in Part V. Appendix C is a copy of the United States Patent awarded to the author which describes a preferred method for the *in vivo* application of the heart-sound analysis described in Part I.

REFERENCES

[1] Corino, E.R., and Brodkey, R.S. (1969) A Visual Investigation of the Wall Region in Turbulent Flow. *J. Fluid Mech.*, **37**, 1-30.

[2] Ffowcs-Williams, J.E. (1969) Hydrodynamic Noise. *Annual Review of Fluid Mechanics*, **1**, 197-222.

[3] Ingard, K.U. and Morse, P.M. (1968) *Theoretical Acoustics*, Chapter II. New York: McGraw-Hill, 926 pp.

[4] Ingard, K.U. and Singhal, V.K. (1974) Sound Attenuation in Turbulent Pipe Flow. *J. Acous. Soc. Am.*, **55**, 535-538.

[5] Jenvey, P.L. (1975) Gas Pressure Reducing Valve Noise. *J. Acous. Soc. Am.*, **41**, 506-509.

[6] Lighthill, M.J. (1952) On Sound Generated Aerodynamically.I--General Theory. *Proc. R. Soc. London Ser. A*, **211**, 564-587.

[7] Lighthill, M.J. (1954) On Sound Generated Aerodynamically.II--Turbulence as a Source of Sound. *Proc. R. Soc. London Ser. A*, **222**, 1-32.

[8] Lush, P.A. (1971) Measurements of Subsonic Jet Noise and Comparison with Theory. *J. Fluid Mech.*, **46**, 477-500.

[9] Morfey, C.L. (1970) Sound Transmission and Generation in Ducts with Flow. *J. Sound Vib.*, **14**,37-55.

[10] Powell, A. (1959) On the Generation of Sound by Turbulent Jets. ASME Prepr. No. 59-AV-53.

[11] Reethof, G. (1978) Turbulence-generated Noise in Pipe Flow. *Ann. Rev. Fluid Mech.*, **10**, 333-367.

[12] Sharland, I.J. (1964) Sources of Noise in Axial Flow Fans. *J. Sound Vib.*, **1**, 302.

PAPER 1

A Quantitative Method for the *In Vitro* Study of Sounds Produced by Prosthetic Aortic Heart Valves Part I: Analytical Considerations

A Quantitative Method for the *In Vitro* Study of Sounds Produced by Prosthetic Aortic Heart Valves

Part I: Analytical Considerations

ABSTRACT

A method is presented for analyzing sounds produced *in vitro* by prosthetic aortic heart valves, and a one-dimensional harmonic model is described. Procedures for estimating physical parameters of the model are outlined for the case of transient and non-transient sounds, and a computational method is described for making comparisons between two general sounds. The Discrete Fast Fourier Transform provides a satisfactory means for the basic transformation to the frequency domain. Useful representations of the acoustical information that are considered are the original time and amplitude plots, power-density spectra, power-distribution functions, a 3-D (three-dimensional) surface of power-frequency-time, sections of these 3-D surfaces, and a 3-D, power-distribution surface showing the difference between two 3-D, power-distribution surfaces. Note is made that each representation is useful for indicating specific acoustical characteristics which may be important when either comparing or describing sounds. The spectra provide an accurate means for estimating the parameters of the model and provide clearer comparisons when compared to the time-amplitude plots. This fact is most clearly shown by the 3-D, power-difference surface. This surface provides a very convenient means for the overall comparison of two sounds. The analytical method described can be applied to data obtained from clinical studies.

Key Words- Fast Fourier Transform, sound, prosthetic heart valve, non-invasive diagnosis

1.1 INTRODUCTION

The malfunction of natural and prosthetic heart valves is a serious cardiological problem. A need exists for clearly detecting malfunctions as early as possible. The method used for this detection should preferably be noninvasive, accurate, sensitive, specific, quick, systematic, and relatively inexpensive. Diagnostic equipment employed should be easily portable to the patient's bedside. Presently, cardiologists use phonocardiography, echocardiography, and cineflouroscopy as noninvasive procedures for evaluating valvar integrity. The comprehensive text by Tavel (TAVEL, 1978) offers an excellent study of the clinical aspects of phonocardiography and particularly the effects of changes of the physiological state of man related to those changes observable in the heart sounds. Each of the present non-invasive methods, however, is sensitive only to malfunctions of an advanced nature, and as a result are not totally successful. Spectral-phonocardiography (**SPCG**) offers another means for evaluating valvar integrity.

Many studies using **SPCG** *in vivo* have been reported in the literature. One early publication using so-called "sound spectrography" was published by McKusic (MCKUSIC *et al.*, 1954). He used an analog device to depict acoustical information as plots of the sound energy within specific frequency bands. These energies were shown as horizontal contours comprised of dots of densities proportional to the sound energy.

A significant improvement for depicting acoustical information in the frequency-domain was reported by Winer (WINER *et al.*, 1965). This "contour spectrogram" was a plot of contours corresponding to iso-energy values of the energy-distribution of the sound. This plot differs from that used by McKusic in

that it is a contour plot representing energy distribution rather than energy density. A sound possessing relatively high-frequency components with significant energy-density was represented as a peak by this spectrogram. As with McKusic's plots the peak occurred at the time when this particular sound occurred. Winer's format allowed a clearer observation of changes in a sonic spectrum because it was generally easier to distinguish changes in peaks than it was to distinguish similar changes in point densities . This improvement of presenting the acoustical information in the frequency domain resulted in more successful clinical applications. A noteworthy example is the paper by Hylen (HYLEN *et al.*, 1969). Hylen investigated the frequency characteristics of spectrograms of the opening and closing sounds of Starr-Edwards model 1000 caged-ball prostheses having silicone-rubber occluders and compared these amplitudes with the degree of variance of the occluder. Hylen notices a decrease in the peak frequency of the opening sound in patients with variant poppets. He reports higher values of peak-frequencies, 1900 Hz, associated with normal aortic opening and closing relative to that of the normal ejection murmur and pulmonic closing sound, 1000 Hz. The abnmoral aortic opening sound had a peak frequency of 800 Hz as compared to 1900 Hz for the normal case.

The development of digital computers and algorithms such as the Fast Fourier Transform (**FFT**) allowed rapid calculation of discrete power-density spectra with well defined resolution of frequency. The frequency resolution of such digitally generated spectra is also better than that of similar spectra produced by analog devices. Further, modern computers allow retention and display of more of these data.

Work utilizing digital-spectral-phonocardiography (**DSPCG**) *in vivo* began in the early 1970's. An early example of **DSPCG** was published by Yoganathan (YOGANATHAN *et al.*, 1976a, 1976b and 1976c) He applied the **FFT** to the first and

second heart sounds of normal man. The sounds were analyzed by selecting typical first and second unfiltered heart sounds of 29 normal subjects. The center-frequencies of the peaks of the individual spectra were reported. The resulting spectra from each subject was then averaged and center frequencies of the average spectrum were reported. In the first heart sound two to five peaks occurred in the frequency range 10-120 Hz for the individual spectra and one peak near 30 Hz was observed in the average spectrum. The second heart sound of normal man possessed higher frequency content. In the second heart sound one or two peaks were observed in the bands 10-80 Hz, 80-220 Hz and 220-400 Hz for most of the individual spectra. No significant peak was observed in the average spectrum of the second heart sound when evaluated from recordings at either the aortic or pulmonary area.

Other research utilizing **DSPCG** has been applied *in vivo* to sounds produced by abnormal natural valves and prosthetic heart-valves. Johnson (JOHNSON, 1979) studied stenosis of natural aortic valves *in vivo*. This work showed a correlation between the pressure gradient across the aortic valve and the power of the systolic ejection murmur when this power was evaluated in specific, relatively broad bands of the spectrum. The pressure gradient then provided an indication of the degree of valvar stenosis. Durand (DURAND and GUARDO, 1979) presents a digital method for studying opening and closing sounds and provides examples of the technique by presenting results from bioprosthetic aortic valves. These investigators used digital filtering techniques to separate frequency bands which were determined by the location of peaks in the spectrum of the unfiltered opening and closing sounds. This work emphasizes the use of digital filters, the need for good frequency resolution and examination and presentation of as much of the acoustical information as is possible based on cost-effectiveness. Stein (STEIN *et al.*, 1980) compared normal aortic closing

sounds (A2) with closing sounds of stenotic natural valves and porcine xenografts which had been implanted from five to seven years. The abnormal sounds had dominant center-frequencies as high as 200 Hz compared to the normal value near 50 Hz. This shift was attributed to the increased stiffness of the abnormal valvar leaflets due to observed calification. The spectra presented in Stein's paper also show significant increases of power-density in the band from 100 to 300 Hz for these two abnormal valvar groups. These investigators presented their results via power-density spectra and concentrated their discussions upon the power density and center frequency of the harmonic peaks. Specific portions of the cardiac cycle were investigated depending upon the specific phenomenon which was to be studied. These spectral studies clearly showed the improvement which digital methods could provide for the analysis of specific heart sounds produced by normal and abnormal valves. The paper by Smith (SMITH *et al.*, 1981) offers a comparative study of the sounds produced by ball, disk, procine and bileaflet prostheses in normal states. The comparison emphasises clinical results based on auscultation of the sounds produced by these valvar designs implanted at the aortic and mitral positions. Qualitative differences, such as timing and amplitudes of the opening and closing sounds as well as duration and amplitude of systolic and diastolic ejection murmurs, are compared by using standard phonocardiographic methods.

Because the majority of investigations which have been reported were made *in vivo*, the precise condition of the valve and heart were not known accurately when sounds were measured. Therefore, acoustic models were normally not presented or applied qualitatively to explain results. The variability of particular acoustic characteristics *in vivo* results mainly from variabilities in the condition of each of the four heart valves, physiology of the heart and surrounding anatomy, the dynamic states of the heart, and the states of each of the four

heart valves. Isolation of individual contributions to the total variability, particularly any changes in the valve, by way of *in vivo* studies alone is a difficult task. Prosthetic valves should be studied at well defined pulsatile states while mounted in a well known geometry. Studies *in vitro* can be designed to investigate effects of the valvar condition, design, size, and orientation of implantation upon sounds made by the valve for closely controlled dynamic states. Other studies can be made of the effect of specific pulsatile conditions, such as pulse rate, pressure, and flow, upon the acoustic characteristics for a closely maintained valvar state. Information provided by these studies will improve our understanding of results obtained from *in vivo* studies. In addition to improving the understanding of results, the prediction of results for a hypothetical change of a valve would be very useful. Comparative studies of sounds produced *in vitro* together with the use of an accurate accoustic model can provide a means for testing such hypotheses. Through studies made *in vitro* the parameters of an acoustic model can be accurately estimated to test the models themselves.

Another area which could be improved is that of the display and interpretation of the overall information in heart-sounds. Digital information can be displayed in the form of a three-dimensional, power-frequency-time surface. If it is necessary to look more closely at a particular portion of this surface, it can be rotated. In addition, a procedure can be developed for comparing two sounds by a means of a power-difference surface. Finally, it would be useful to be able to interpret these surfaces in terms of the physical states or changes-in-state of the valve. To do that with the most understanding of the system, an acoustical model should be available which includes all of the important physical parameters of the valvar system.

This paper, Part I of a seven-part series, is primarily concerned with the display and analysis of the overall-sound data. It presents an acoustic model

and methods that we have used for displaying and analyzing acoustical information. Results are discussed in terms of the time-amplitude signal and the corresponding power-density spectra, power-distribution spectra, and power-distribution surfaces. The characteristics of each of these formats is discussed in terms of three parameters obtained from the acoustical model. These three parameters represent the effective mass, stiffness, and damping of the valvar system and provide, therefore, quantitative estimates of physical changes of the valve.

1.2 Transient and Non-transient Valvar Sounds

The dynamic motion and turbulent flow of fluid in and around heart valves produce periodic vibrations having characteristic frequency and amplitude. Research concerning the etiology of valvar sounds *in vitro* indicates that the numerous sounds can be grouped into two general categories according to the type of stimulus responsible for producing them. We label these two categories "transient" and "non-transient" sounds depending upon whether they are produced by transient or non-transient stimuli. When we speak of a transient or non-transient sound, we will be differentiating them relative to the temporal duration of the stimulus which we have determined for most of the sounds by observation of the timing of these sounds and the motion of the valve and fluid. Because the transient and non-transient stimuli usually have quite different mechanisms for their production, there is generally no confusion as to whether a particular sound should be labeled as either transient or non-transient when this labeling is done with respect to the stimuli.

Transient sounds (TS) are produced *in vitro* by impulses exerted when valve leaflets or mechanical structures collide or decelerate rapidly. These sounds are

short in duration and commonly have tonal qualities. The resulting vibrations begin to decay immediately and normally decay rapidly by way of viscous dissipation of energy within 30-75 ms after the impulse has occurred. Examples of **TS** produced by prosthetic valves *in vitro* are: the component of the opening sound caused by the collision of the occluder with the struts; the component of the closing sounds caused by the collision of the occluder with the seating structure; and, the component of the systolic ejection murmur caused by bouncing of the occluder against the struts or fluttering of leaflets of bioprostheses.

Non-transient sounds (**NTS**) are generally produced *in vitro* by turbulent flow resulting from sustained pressure gradients between the chambers separated by the valve. A primary characteristic of our definition of the **NTS** is that it will endure for as long as its associated periodic force which has only been observed to be produced by the flow. These fluid-mechanical forces are generally maintained for longer periods, greater than 100 ms, relative to the **TS** and the entire cardiac cycle. Sounds that are transient in duration can also be stimulated by brief turbulent forces resulting from transient flows through the small flow-areas which are present at the time of opening and closing of these valves. We will call these non-transients sounds even though they are brief relative to the cardiac cycle. This assignment may at first seem erroneous, but we must remember that the time scale required to produce sinusoidal forces that are sustained over more than one cycle and that have frequencies comparable to that of the sound can be less than 10 ms. Such briefly-sustained forces, brief relative to the cardiac cycle but sustained relative to the chacteristic time of the sound, are probably responsible for the sounds observed prior to valvar opening and after valvar closure and associated with backflow around the occluder and through the orifice. Visualization *in vitro* shows that the flow through these valves exhibits turbulent shear near walls, the annular gap and at

jet-interfaces. Examples of **NTS** produced *in vitro* are the systolic "murmurs" produced by mechanical and bioprosthetic valves due to some degree of stenosis inherent to their design, and diastolic murmurs associated with those valves which allow leakage around the occluder after the valve has closed. This leakage is normal for the Smeloff and Bjork-Shiley valves.

1.3 Acoustical Considerations

A complete analysis of the heart sounds based upon motion in three dimensions is a complex problem which has not yet been attacked. Still, we can apply a few reasonable assumptions and extract important information about the valves by use of a simple, one-dimensional model for interpretation of the valvar sounds. Throughout this section we will discuss the model in terms of its application *in vitro*. If we apply any assumption which cannot be applied *in vivo*, we will so note.

Remarks will be confined to vibrational frequencies in the range of 10 to 1000 HZ. For these frequencies, amplitudes of the physical vibrations producing the sounds are small. They can be described by the linear theory of sound discussed in the monograph by Lord Rayleigh (RAYLEIGH, 1896). This assumption will allow us to separate each harmonic and apply to it an independent linear equation of motion.

1.3.1 Propagation of Sounds

Pressure fluctuations can be measured with an acoustical system and described in terms of the physical parameters of the system. The system which was used for analysis throughout this discussion was the aortic-flow section of the Caltech pulse-duplicator together with the valve and fluid which it contained. A detailed

description of this duplicator and its operation is given in Chapter 2. Sounds propagated in the liquid phase were measured near the valve. Measurements can also be made non-invasively using surface-microphones. Determination of the modes of propagation of these fluctuations required solution of the equations of change for the fluid phase. The general equations describing the state of a fluid element are the relationships for the conservation of mass, momentum, and energy. For the general case, these equations are, respectively:

$$\frac{\partial \rho}{\partial t} + \nabla \cdot (\rho \vec{v}) = 0 \,, \tag{1-1}$$

$$\frac{\partial}{\partial t}(\rho \vec{v}) + \nabla \cdot \rho \vec{v}\vec{v} + \nabla p + \nabla \cdot \bar{\bar{\tau}} - \rho \vec{g} = 0 \,, \tag{1-2}$$

$$\frac{\partial}{\partial t}\rho(\bar{E} + \frac{v^2}{2}) + \vec{v} \cdot \nabla \rho(\bar{E} + \frac{v^2}{2}) + \nabla \cdot \vec{q} - \rho \vec{v} \cdot \vec{g} + \nabla \cdot p\vec{v} + \nabla \cdot \bar{\bar{\tau}} \cdot \vec{v} = 0 \,, \tag{1-3}$$

where, ρ is the density of the fluid, $\vec{v}$ is the velocity of the fluid, t is time, p is pressure, $\bar{\bar{\tau}}$ is the deformation tensor, $\vec{g}$ is the gravitational acceleration, $\bar{E}$ is the internal energy per unit mass, and q is the heat flux. For the system studied, the velocity of sound in the fluid media, a, was large relative to the maximum velocity of the flow. The Mach number was always less than 0.002 for this system when calculated relative to the maximum velocity at any point. Any acoustic disturbance generated in the system propagated approximately as would disturbances in the system with the fluid having a mean velocity of zero. Turbulent flow did generate sound, however, by interaction with the boundaries of the system.

If we solve the equations of change for the acoustically estimated pressure fluctuation, p', and assume that the fluctuations in pressure, density and velocity are small quantities, the solution for the pressure fluctuations satisfies the standard wave equation.

A mechanical model of wave propagation in a homogeneous medium is shown in Figure 1-1. This diagram shows fluid elements arranged in a cubic array and depicted as balls having identical mass, m, connected by springs having identical spring constants, k. If we consider the matrix of equilibrium to be that which exists under the prevailing influence of gravity, we can then neglect gravitational effects in the equations of change. If we do not allow the breakage of springs by local shifts of elements within the matrix, an assumption which seems reasonable for small Mach numbers and small acoustical amplitudes, then the vibrations are reversible because viscous effects will not be manifest in the continua due to these irreversible disturbances. Finally, if we compare the characteristic time scale of heat transfer, t_{heat}, to the characteristic time scale of the acoustic disturbance, t_{sound}, we find for our system that:

$$\frac{t_{heat}}{t_{sound}} = \frac{2\pi\omega\rho c_v}{k^2\lambda_o} = 10^{12} >> 1 , \tag{1-4}$$

where, k is the wave number of sound, ω is the frequency of sound, λ_o is the thermal conductivity of the fluid, and c_v is the heat capacity of the fluid at constant volume.

The equations of change for the special case when gravitational, viscous, and heat transfer effects are negligible are:

$$\frac{\partial\rho}{\partial t} + \nabla\cdot(\rho\vec{v}) = 0 , \tag{1-5}$$

$$\frac{\partial}{\partial t}(\rho\vec{v}) + \vec{v}\cdot\nabla\,\rho\vec{v} + \nabla p = 0 , \tag{1-6}$$

and

$$\frac{\partial}{\partial t}\rho(\bar{E}+\frac{v^2}{2}) + \vec{v}\cdot\nabla\,\rho(\bar{E}+\frac{v^2}{2}) + \nabla\cdot p\vec{v} = 0. \tag{1-7}$$

We will use the following constitutive relationship to express the density in

terms of the pressure of the fluid. We can define a bulk modulus, K_b, for the liquid such that:

$$K_b = -\frac{\Delta p}{\frac{\Delta V}{V}}, \tag{1-8}$$

where, V is the volume of the fluid element, ΔV is the change in volume of the fluid element, and Δp is the change in pressure required to produce the given volume change under conditions of constant chemical composition. If we choose as a reference state the density, ρ_o , and pressure, p_o, of the equilibrium state, then the density corresponding to a small change in pressure is given by the following constitutive relationship:

$$\rho = \rho_o\left[1 + \frac{(p-p_o)}{K_b}\right]. \tag{1-9}$$

We wish to solve Equations 1-5, 1-6, 1-7, and 1-9 for the pressure. It is well known that these equations describe isentropic vibrations. Taking the dot product of Equation 1-6 with $\vec{v}$ and subtracting the result from Equation 1-7 gives:

$$\frac{\partial}{\partial t}\rho\bar{E} + \vec{v}\cdot\nabla\,\rho\bar{E} + p\nabla\cdot\vec{v} = 0. \tag{1-10}$$

If we write the exact differential of the entropy in terms of the density and internal energy for a system of constant chemical composition, we obtain the relation:

$$dS = \frac{1}{T}d\bar{E} - \frac{p}{\rho^2 T}d\rho\,, \tag{1-11}$$

where, S is the entropy per unit mass of fluid, and T is the temperature of the fluid element. The subtantial derivative of specific entropy, $\frac{D\rho\bar{S}}{Dt}$ can then be written:

$$\frac{D}{Dt}\rho\bar{S} = \frac{1}{T}\frac{D}{Dt}\rho\bar{E} - \frac{p}{\rho T}\frac{D\rho}{Dt}. \tag{1-12}$$

A combination of Equations 1-5, 1-10, and 1-12 , gives:

$$\frac{D}{Dt}\rho\bar{S} = 0. \tag{1-13}$$

The exact differential of density can now be expressed in terms of the exact differential of pressure:

$$d\rho = \left(\frac{\partial\rho}{\partial p}\right)_{\bar{S}} dp = \frac{1}{a^2}dp, \tag{1-14}$$

where we have defined a velocity, a, as:

$$a^{-2} = \left(\frac{\partial\rho}{\partial p}\right)_{\bar{S}}. \tag{1-15}$$

This velocity is the speed of propagation of sound waves in the medium. Using Equations 1-9 and 1-15 we find:

$$a = \left(\frac{K_b}{\rho_o}\right)^{1/2}. \tag{1-16}$$

For water at atmospheric pressure and 25 C, $K_b = 2 \times 10^{10}$ dyne/cm^2, and a = 1450 m/s. Table 1-1 lists wavelengths corresponding to three frequencies of sound traveling through water. Using Equations 1-9, 1-16, 1-5 , and 1-6 we can derive the following two equations for the pressure and velocity fields:

$$\frac{Dp}{Dt} + (K_b+p-p_o)\nabla\cdot\vec{v} = 0 \tag{1-17}$$

$$\frac{D}{Dt}\left[\frac{\rho_o}{K_b}(K_b+p-p_o)\vec{v}\right] + \nabla p = 0. \tag{1-18}$$

We can linearize these two equations by expressing the pressure, velocity and density in terms of their time-mean and fluctuating components where the fluctuations are small relative to the time average value for each variable. We

Frequency (Hz)	Wavelength* (m)	Wavenumber* (m^{-1})
10	150	0.00667
100	15	0.0667
1000	1.5	0.667
10000	0.15	6.67

* Values based on speed of sound of 1500 m/s.

Table 1-1 **Frequencies and associated wave-numbers of sound in water.**

use the expressions:

$$\begin{aligned} p &= p_o + \varepsilon p' \\ \vec{v} &= \vec{v}_o + \varepsilon \vec{v}' \\ \rho &= \rho_o + \varepsilon \rho'. \end{aligned} \tag{1-19}$$

where ε is a dimensionless constant having a value much less than unity. Without loss of generality, we can equate the mean terms in Equation 1-19 with our reference states which we have defined previously relative to the equilibrium state of the system. In addition, because we are discussing the propagation of sound in the system and have shown that the Mach number is 0.001 for the flow of interest to us, we can obtain an approximate solution by allowing the mean velocity to be zero, *i.e.*, $\vec{v}_o = 0$. Then, using that relation and substituting the resultant form of Equation 1-19 into Equations 1-17 and 1-18 we obtain:

$$\varepsilon\left(\frac{\partial^2 p'}{\partial t^2} + K_b \nabla \cdot \frac{\partial \vec{v}'}{\partial t}\right) + \varepsilon^2\left(\frac{\partial}{\partial t}\vec{v}' \cdot \nabla\, p' + \frac{\partial}{\partial t} p' \nabla \cdot \vec{v}'\right) = 0. \tag{1-20}$$

$$\varepsilon\left(\rho_o \frac{\partial \vec{v}'}{\partial t} + \nabla\, p'\right) + \varepsilon^2\left(\frac{1}{a^2}\frac{\partial}{\partial t}\vec{v}' p' + \rho_o \vec{v}' \cdot \nabla\, \vec{v}'\right) + \varepsilon^3\left(\frac{1}{a^2}\vec{v}' \cdot \nabla\, p' \vec{v}'\right) = 0. \tag{1-21}$$

Retaining only the first order terms in ε , we can solve Equations 1-20 and 1-21 for the pressure or velocity to obtain the wave equation:

$$\frac{\partial^2 p'}{\partial t^2} - a^2 \nabla^2 p' = 0, \tag{1-22}$$

or, in terms of velocity fluctuations:

$$\frac{\partial^2 \vec{v}'}{\partial t^2} - a^2 \nabla^2 \vec{v}' = 0. \tag{1-23}$$

We can solve this equation for a cylindrical system in terms of cylindrical coordinates, (r, ϑ, z). The wave equation for the pressure fluctuation in terms of these transformed coordinates is:

$$\frac{\partial^2 p'}{\partial t^2} - a^2\left[\frac{1}{r}\frac{\partial}{\partial r}\left[r\frac{\partial p'}{\partial r}\right] + \frac{1}{r^2}\frac{\partial^2 p'}{\partial \vartheta^2} + \frac{\partial^2 p'}{\partial z^2}\right] = 0; \qquad (1\text{-}24)$$

and, the general solution is:

$$p'(r,\vartheta,z,;t)=\begin{Bmatrix}J_n(\alpha_{mn}r)\\ Y_n(\alpha_{mn}r)\end{Bmatrix}\begin{Bmatrix}\sin n\vartheta\\ \cos n\vartheta\end{Bmatrix}\begin{Bmatrix}\sin \kappa_{z,n}z\\ \cos \kappa_{z,n}z\end{Bmatrix}\begin{Bmatrix}\sin \omega_n t\\ \cos \omega_n t\end{Bmatrix} \quad \text{for } n=1,2,3,... \qquad (1\text{-}25)$$

where,

$$\kappa_{z,n} = \left[\left(\frac{\omega_n}{a}\right)^2 - \alpha_{mn}{}^2\right]^{1/2}. \qquad (1\text{-}26)$$

The problem is now to solve for the coefficients in Equation 1-25 by applying information derived from the boundary conditions and initial condition of the system. The boundaries must satisfy the equations of motion. Therefore at the boundary the normal components of pressure and velocity must satisfy the following relationship obtained using the linearized form of Equation 1-21:

$$\vec{n}\cdot\nabla\, p' = -\rho_o \frac{\partial \vec{v}'}{\partial t}\cdot\vec{n}. \qquad (1\text{-}27)$$

The initial condition which is most useful is simply:

$$p'(r,\vartheta,z;0) = 0. \qquad (1\text{-}28)$$

1.3.1.1 A Few Simplifying Assumptions Regarding the Boundaries

One can solve the wave equations directly by providing the boundary information using Equation 1-27. Either experimental information obtained from the system or information provided by reasonable assumptions about the nature of the system must be used. Let us look at our system in terms of the boundaries to see if we can make any reasonable assumptions regarding these boundaries which will allow us to simplify our problem.

The lateral dimensions of the aortic flow section are much less than the

wavelength of the highest-frequency sound produced in the flow regime of interest. The flow section is constructed of Lucite and is surrounded by ambient air. For such a system, sound propagating normal to the Lucite/air boundary will virtually all be reflected due to the nature of the relative acoustical impedances of the two substances. Because the wavelength of sound is much greater than the diameter of the cylinder, sounds normal to these walls will reflect and interfere destructively. This fact allows the assumption that the walls are acting as if they have infinite acoustical impedance. For such an impedance, Equation 1-27 states that the velocity at the wall is zero. We will assume for the time being that the walls of the cylinder are perfectly rigid *i.e.* have infinite acoustical impedance.

The only remaining boundaries of the system are the phonocatheter and the two ends of the cylinder. We will neglect any perturbing effect of the catheter on the propagation of sound because it is also small relative to the wavelength of sound as well as the length scales of the other boundaries. The downstream, axial boundary is the systemic capacitance chamber. This boundary is fabricated from Gooch tubing, a very pliable rubber. This tubing provides damping and capacitance for the high-amplitude, low-frequency pressure waves generated by the ventricular section of the pulse duplicator. We believe that this capacitance section provides the same effect upon the sound pressure waves. These waves traveling through this capacitance chamber are effectively damped. We will assume therefore that the sounds produced by the system are allowed to travel downstream to the capacitor and then are totally damped and are not reflected back to the phonocatheter to any significant extent. Through this assumption, echos are eliminated from our consideration.

The remaining boundary is the valve itself. Here we will assume that the materials comprising the valve are flexible enough to exhibit deformation upon

application of sufficiently large forces. This deformation produces a volume displacement of the adjacent fluid which can then propagate as a pressure wave through the system. This mode of sound production will endure only as long as the elastic deformation of the valve. This deformation will be damped by dissipation in the solid structure of the valve and to a lesser extent by the viscous drag of the fluid upon the valvar structures. This latter contribution should only occur when the flow rates are large, if it occurs at all.

We will use these various assumptions about the mechanical nature of our system as we apply the boundary conditions of the wave equation.

1.3.1.2 Application of the Boundary Conditions

We first note that the pressure must be finite at the axis of the tube. The coefficients of the Bessel function Y_n must vanish. From Equation 1-27, the condition of zero velocity at the wall of the tube, $r=R_o$, gives:

$$\frac{\partial}{\partial r}\left\{J_n(\alpha_{mn}R_o)\right\} = 0. \qquad (1\text{-}29)$$

This equation defines the values for α_{mn}. A listing of these values is given in Table 1-2. It is interesting to note how particular values of α_{mn} affect the nature of the propagation of mode m,n. If we solve for the wave number, $\kappa_{z,n}$, given by Equation 1-26, we find that it has a real value only for the mode m=n=0. All higher order modes produce a purely imaginary value for this wave number. These imaginary values predict exponential decay of the corresponding modes with respect to the axial coordinate. This decay rate is very rapid with distance, and for a distance of 54 cm from the origin, a sound having a frequency of 1000 Hz will decay to 2% of its amplitude at the source. This percentage is a maximum value for the specific location of the catheter from the valve and the fre-

m \ n	0	1	2	3	4
0	0	1.2197	2.2331	3.2383	4.2411
1	.5861	1.6970	2.7140	3.7261	4.7312
2	.9722	2.1346	3.1734	4.1923	5.2036
3	1.3373	2.9547	4.0368	4.6428	5.6624
4	2.0421	3.3486	4.4523	5.0815	6.1103

Values of $\alpha_{mn}R/\pi$ for the Roots of $\left[\frac{dJ_m(\alpha_{mn}r)}{dr}\right]_{r=R} = 0$.

Table 1-2 Eigenvalues of the radial component of the wave equation in cylindrical coordinates.

quencies of interest for our system. Therefore the only important radial modes which can propagate in our ideal system are planar modes for which m=n=0. For such planar modes the pressure fluctuations are now expressed by the expression:

$$p'(r,\vartheta,z;t) = p'(z;t) = \mathrm{Re}\left\{A_c e^{-i(\omega t+\kappa_z z)}\right\}, \qquad (1\text{-}30)$$

where A_c is a complex number, and 'i' represents the value $-1^{1/2}$. Equation 1-30 further reduces to the following expression after applying the initial condition given by Equation 1-28:

$$p'(z;t) = A \sin(\omega t+\kappa_z z), \qquad (1\text{-}31)$$

where A is now a real quantity. If we let z=0 at the valve orifice, then we are measuring the pressure fluctuations at a point corresponding to z=9 cm. Some of the sounds may originate at locations for z> 0 for those valves with struts projecting downstream from the orifice. As we shall now show, however, these small distances are not important relative to the small influence they have upon the phase of the fluctuations when measuring these fluctuations at distances downstream from the valve that are small relative to the wavelength of sound. Table 1-1 lists the wavenumbers corresponding to specific frequencies of sound propagating in water. Choosing the largest of these wave numbers and assuming that the downstream coordinate of the catheter, z_c, is 9.0 cm , we find that the maximum value for $\kappa_z z_c$ is 0.1 radian or approximately 6 degrees. This fact allows us to make the following approximation for the time-dependent fluctuations originating at the source, z=0, and measured by the phonocatheter at axial coordinate z=9.0 cm:

$$p'(z_c;t) \approx p'(0;t) = A \sin(\omega t). \tag{1-32}$$

Using Equation 1-27 with $\vec{n}$ being the axially directed normal at z=0, we find the following temporal relationship between the pressure fluctuations measured at the transducer and the one-dimensional diplacement-velocity at the monopolar source.

$$p'(z_c;t+\frac{\pi/2}{\omega}) \approx p'(0;t+\frac{\pi/2}{\omega}) = \frac{\rho_o}{\kappa_z}\frac{\partial \vec{v}'_z}{\partial t}. \tag{1-33}$$

The phase shift should be noted in Equation 1-33. When the acceleration of the source is a maximum, the pressure goes to zero, and when the acceleration of the source is zero, the pressure is a maximum. The pressure lags the acceleration by 90 degrees.

1.3.2 Generation of Sound: Description of the Source

The wave equation can now be solved if the boundary conditions are defined at the source, or valve. For our study *in vitro*, the important boundary condition was that at the valve. This boundary condition was sufficiently described by estimating the displacement of the surface of the valve. The wavelength of sound for the frequencies of interest was much greater than the dimensions the valve and the diameter of the aortic chamber. Consequently, the valve acted as a "simple" source. The vibrational modes of propagation were estimated as planar with a propagation vector directed parallel to the tube axis. We specified the displacement of the boundary at this simple source by solving for the general one-dimensional displacement of a forced oscillator with damping. The general oscillator was decomposed into distinct, monotonic, one-dimensional oscillators. Each planar mode was characterized by its corresponding effective mass, stiffness, and damping coefficient. A one-dimensional force balance around an

effective, structural element, or mode i, having mass, M_i, stiffness constant, K_i, damping coefficient, D_i, and externally applied forces, F(t), provides the following relation for the displacement, z:

$$\ddot{z} + 2\kappa_i\dot{z} + \omega_{o,i}^2 z = \frac{F(t)}{M_i}, \tag{1-34}$$

where the decay parameter, κ_i, is given by the relation:

$$\kappa_i = \frac{D_i}{2M_i} , \tag{1-35}$$

and the undamped frequency, $\omega_{o,i}$, is given by the relation:

$$\omega_{o,i} = \left[\frac{K_i}{M_i}\right]^{1/2} . \tag{1-36}$$

Equation 1-34 was solved for two cases, namely (1) F(t) is a series of impulses, and (2) F(t) is a superimposed sum of sinusoids.

1.3.3 The Transient Response

The transient force is short in duration and large in magnitude. It can most easily be expressed mathematically as an impulse, or series of impulses. Let this transient stimulus, $F_{t,j}(t)$, be expressed by the relation:

$$F_{t,j}(t) = \sum_{j=1}^{N_j} V_j \delta(t - t_j) , \tag{1-37}$$

where V_j characterizes the maximum amplitude of the force exerted over the finite time of the duration of the impulse j, the delta function, $\delta(t-t_j)$, acts to distribute the total force with respect to time relative to the time of impulse j, t_j, and the sum is over N_j impulses. By using the wave equation, appropriate boundary conditions, and Equations 1-34 and 1-37, and assuming that the observer of the sounds is near the source, *i.e.*, much closer than the wavelength of sound,

the transient-pressure response of mode i for a single impulse j, $p'_{t,ij}(t)$, can be shown to be expressed by the following general relation:

$$p'_{t,ij}(t) = \begin{cases} 0 & \text{for } t < 0 \\ \dfrac{\Gamma_{ij}}{\omega_{f,i}} e^{-\kappa_i(t)} \sin(\omega_{f,i}(t) - \varphi_{t,ij}) & \text{for } t \geq 0 \, . \end{cases} \tag{1-38}$$

The amplitude or gain parameter associated with mode i and impulse j, Γ_{ij}, is given by the relation:

$$\Gamma_{ij} = \frac{a\rho_o V_j K_i}{M_i^2 \omega_{f,i}} , \tag{1-39}$$

where a is the speed of sound in the fluid, ρ_o is the characteristic density of the fluid, and the free frequency of oscillation of mode i, $\omega_{f,i}$ is given by the relation:

$$\omega_{f,i} = (\omega_{o,i}^2 - \kappa_i^2)^{1/2} = \frac{1}{M_i}\left[K_i M_i - \frac{D_i^2}{4}\right]^{1/2} . \tag{1-40}$$

The phase associated with the transient response of mode i relative to the time of impulse j, $\varphi_{t,ij}$, is determined from initial conditions.

1.3.4 The Non-transient Response

The non-transient forces result from continuous forces applied by the fluid interaction with the structural components of the valve and flow-chamber during flow in and around the valve. Non-transient forces are long in duration and small in magnitude relative to the transient forces. The turbulent origin of these non-transient forces suggests that a statistical distribution of sinusoidal forces exists which corresponds in frequency to the turbulent-eddy distribution. These forces can most easily be expressed mathematically as a statistical sum of sinusoidal functions. Let the non-transient, forcing function of sinusoid k, $F_{nt,k}(t)$, associated with forcing frequency ν_k be expressed by the relation:

$$F_{nt,k}(t) = \begin{cases} 0 & \text{for } t < 0 \\ \sum_{k=1}^{N_k} V_k \sin(\nu_k t - \varphi_{nt,k}) & \text{for } t \geq 0, \end{cases} \tag{1-41}$$

where V_k is the amplitude of this sinusoidal force, ν_k is the frequency, and the $\varphi_{nt,k}$ is the phase of the kth, non-transient, sinusoidal force relative to an arbitrary time, t=0.

The associated pressure response of mode i to the non-transient stimulus k, $p'_{nt,ik}(t)$, can be shown to be given by the relation:

$$p'_{nt,ik}(t) = \begin{cases} 0 & \text{for } t < 0 \\ \dfrac{a\rho_o K_i A_{ik}}{M_i \omega_{f,i}} e^{-\kappa_i t} \sin(\omega_{f,i} t - \varphi_{t,ik}) + \dfrac{a\rho_o K_i B_{ik}}{M_i \omega_{f,i}} \sin(\nu_k t - \varphi_{nt,ik}) & \text{for } t \geq 0. \end{cases} \tag{1-42}$$

The coefficients A_{ik} are the amplitudes of the displacement corresponding to the transient response of mode i to the non-transient stimulus of sinusoid k, and are determined by the initial conditions for mode i and forcing frequency ν_k when no impulsive forces act upon the system. The coefficients B_{ik} correspond to the displacement corresponding to the non-transient response of mode i stimulated by frequency ν_k, when no impulsive forces act on the system, and are given by the relation:

$$B_{ik} = \frac{V_k}{M_i \left[(2\nu_k \kappa_i)^2 + \left[\nu_k^2 - \dfrac{K_i}{M_i} \right]^2 \right]^{1/2}} . \tag{1-43}$$

The phase corresponding to the decaying component of the response of mode i to the non-transient stimulus k, $\varphi_{t,ik}$, and the phase corresponding to the non-decaying component of the response of mode i to the non-transient stimulus k, $\varphi_{nt,ik}$, can be determined by specifying a reference time, t=0, and the initial conditions of the oscillator relative to this time.

Equation 1-42 indicates that the response of mode i to a sinusoidal stimulus

beginning at time t=0 and having frequency ν_k is comprised of two sinusoids. One of these sinusoids decays with characteristic time, κ_i, and possesses the same free-frequency, $\omega_{f,i}$, as the impulse response. The second sinusoid does not decay but is maintained by the sinusoidal force and possesses the same frequency as the force.

1.3.5 General Responses in the Time Domain

Equations 1-38 and 1-42 represent the basic transient and non-transient responses. The general response will be composed of linear combinations of these responses summed over the number of modes of the system, N_i, the number of impulses of the transient force, N_j, and the number of sinusoids of the non-transient force, N_k. The general pressure response, p'(t), is represented by the expression:

$$p'(t) = \begin{cases} 0 & \text{for } t < 0 \\ \sum_{i=1}^{N_i} \left[\sum_{j=1}^{N_j} p'_{t,ij}(t) + \sum_{k=1}^{N_k} p'_{nt,ik}(t) \right] & \text{for } t \geq 0 \ , \end{cases} \qquad (1\text{-}44)$$

where the summation is made using all values of indices i, j, and k.

1.3.6 The Transient Response as Represented in the Frequency Domain

If a time function is sampled at discrete time intervals, a Discrete Fourier Transformation can be applied to these data. The transformed data are represented by coefficients corresponding to the Fourier series. This transformation provides information about the gain in terms of the modulus of these coefficients and the phase angle in terms of the inverse tangent of the ratio of the imaginary to real parts. We have found the algorithm of Cooley and Tukey (COOLEY and TUKEY, 1965) satisfactory for these calculations.

Our task is to express the Fourier coefficients in terms of the parameters Γ_{ij}, κ_i, and $\omega_{r,i}$. Estimates of the phase parameters will not be considered. We will utilize the results obtained using continuous functional analysis and consider the discrete power-density spectra (**PDS**) as special cases of the continuous spectra.

A continuous representation for the transient response of N_i modes to a single impulse j was given by Equation 1-48. The corresponding continuous, power-density spectrum generated by continuous Fourier transformation, $P_t^{N_i}(\omega)$, is given by the relation:

$$P_t^{N_i}(\omega) = \sum_{i1=1}^{N_{i1}} \sum_{i2=1}^{N_{i2}} \frac{\Gamma_{i1j}\Gamma_{i2j}(\alpha_{i1}\alpha_{i2} + \beta_{i1}\beta_{i2})}{4\pi^2(\alpha_{i1}^2 + \beta_{i1}^2)(\alpha_{i2}^2 + \beta_{i2}^2)}, \tag{1-45}$$

where subscripts i1 and i2 refer to general mode-numbers, and α_{i1} and β_{i1} are functions of frequency defined for mode i1 by the relations:

$$\begin{aligned} \alpha_{i1} &\equiv \omega_{r,i1}^2 + \kappa_{i1}^2 - \omega^2 \\ \beta_{i1} &\equiv 2\kappa_{i1}\omega . \end{aligned} \tag{1-46}$$

For the case when i1=i2 and N_{i1}=1, Equation 1-46 expresses the **PDS** for the transient response for a single mode. Generally, the terms for which i1=i2 are the most significant terms in Equation 1-46. This significance is true even when $N_{i1} > 1$ provided κ_i is less than $\omega_{r,i}$ for all modes. Given these conditions one can estimate Γ_{ij}, κ_i, and $\omega_{r,i}$ for each oscillator from the **PDS** by a simple method that is independent of the other oscillators.

1.3.7 Parameter Estimation for the Transient Case in the Frequency Domain

If phase is neglected, each mode can be represented by a set of three parameters. A **frequency** parameter, $\omega_{r,i}$, provides information about the free frequency of vibration of the oscillator which is determined by the oscillator's inertial

coefficent, damping coefficient, and stiffness coefficient as given by Equation 1-40. A **decay** parameter, κ_i, provides information about the rate of decay of the oscillator and is proportional to the damping coefficient and inversely proportional to the inertial coefficient of the oscillator as given by Equation 1-35. A **gain** parameter, Γ_{ij}, provides information about the amplitude, or acoustical power, associated with the oscillator. This parameter is dependent on the speed of sound, density, the inertia, stiffness, and damping coefficents, and the magnitude of the impulsive force j, V_j, as given by Equation 1-39. Experimental evaluation of V_j, and the three acoustical parameters enables the calculation of the effective mass, damping and stiffness by using Equations 1-35, 1-36, 1-39, and 1-40.

Figure 1-1 shows the waveform of the response associated with a typical mode described by Equation 1-38. It illustrates the manner by which each parameter affects the form of the oscillations in the time domain. A lag time has been included to indicate the relationship between the initial time of the window, t=T, and the time when the impulse occurs, t_j. This time-domain representation of the sound provides neither easy nor accurate estimation of Γ_{ij}, κ_i, $\omega_{f,i}$, nor $\varphi_{t,ij}$. This fact becomes more apparent when more modes are stimulated.

By transforming this acoustical information into the frequency domain, we can generate the power-density spectrum (**PDS**), power-distribution function (**PDF**), and phase spectrum by algebraic manipulation of the Fourier coefficients.

The general form of **PDS** corresponding to the response shown in Figure 1-1 is shown in Figure 1-2 This plot shows the peak associated with a decaying monotonic oscillator. It can be shown that the free frequency associated with the vibration, $\omega_{f,i}$, occurs near the center of the peak. It can also be shown that the

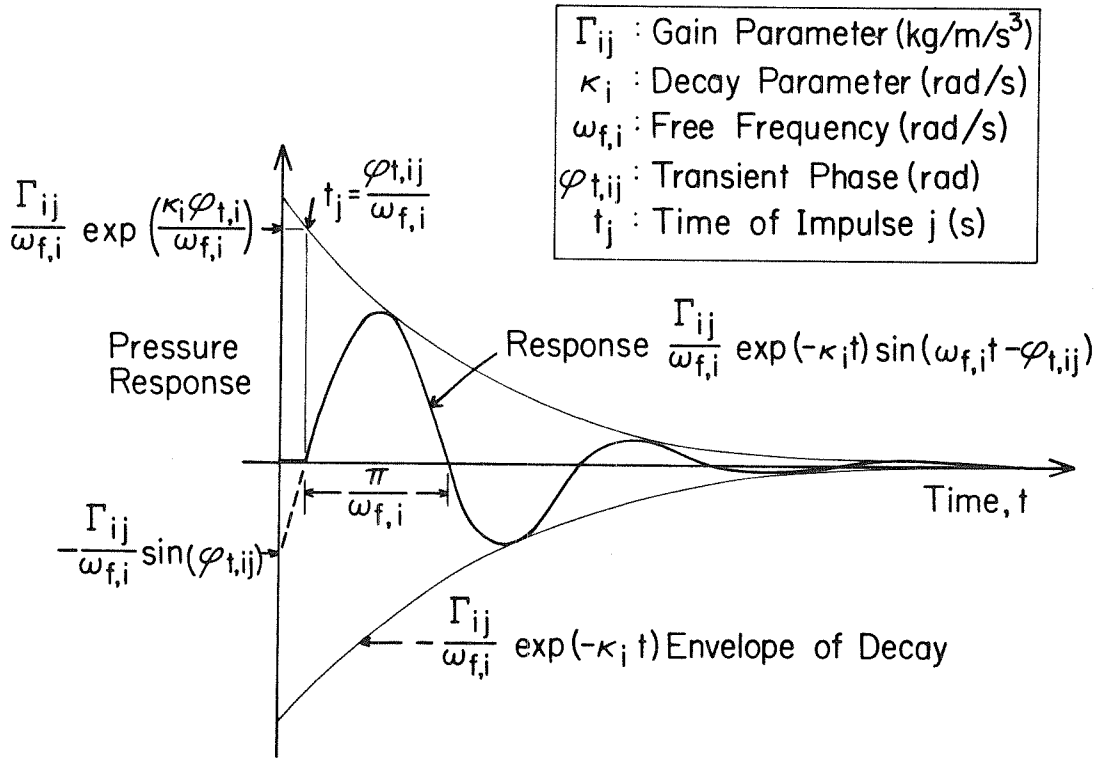

Figure 1-1. Time and amplitude response for a linear, monotonic oscillator having decay and lag.

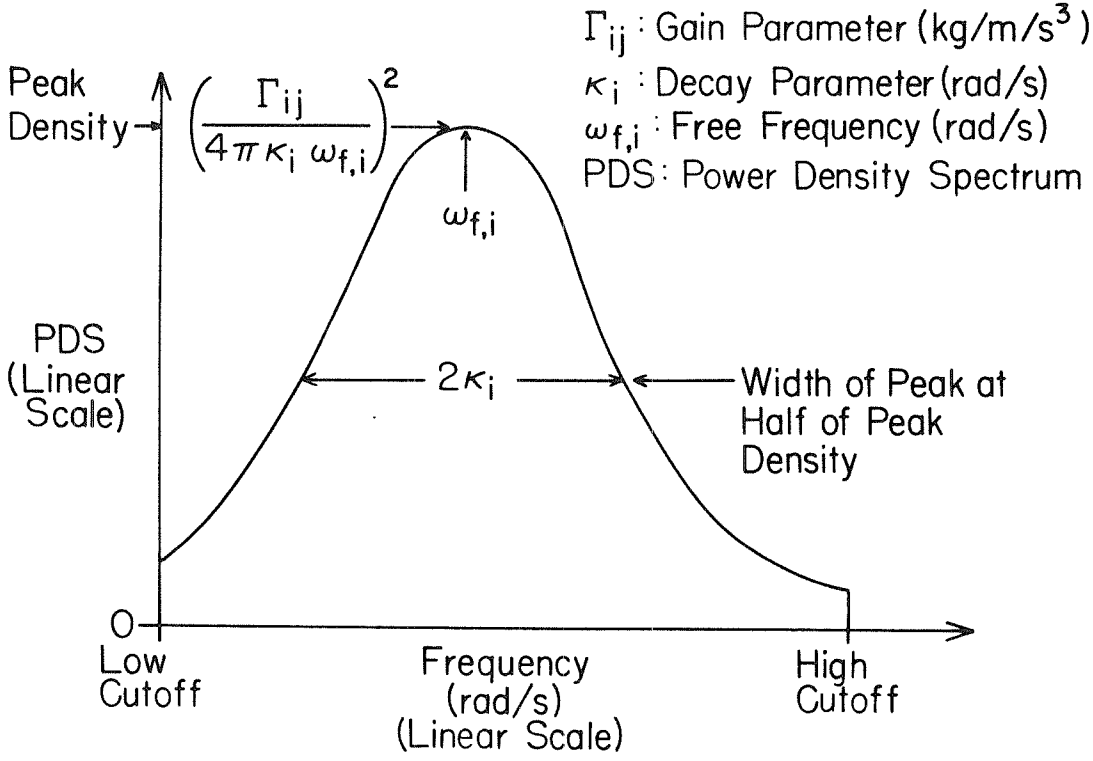

Figure 1-2. Power-density spectrum for a linear, monotonic oscillator having decay and lag.

decay parameter, κ_i, is equal to the half-width of the peak evaluated at a density that is half the value of the peak. For spectra plotted on a logarithmic ordinate, the width is evaluated 3db below the peak power density. Finally, Γ_{ij}, is related to the value of the power density evaluated at the free frequency. These three parameters determine the waveform of the time solution of the individual oscillations. We need to estimate the phase parameter if we wish to place our waveforms correctly with respect to time.

This estimation process is applicable to continuous signals of infinite duration. The effects of sampling and finite-record length upon the power-density spectrum is to produce "aliasing" and "modulation" of the spectrum, respectively. Discussions of these effects are given in the references by Brigham (BRIGHAM, 1974) and Yoganathan (YOGANATHAN *et al.*, 1976a). The gain, decay, and frequency parameters of the model can be estimated from discrete spectra using the same method provided that the data are sampled sufficiently fast and the number of data points analyzed are sufficiently great in number. The spectra for single events should be used for these parameter estimates. Some spectra will be noisy due to "modulation". A curve can be drawn through the "modulated" spectra so as to connect the peaks which exhibit a broad-band trend as shown by the examples depicted in Figure 1-3. Inflections of the corresponding **PDF** provide assistance when choosing the location of the frequency of significant peaks in the **PDS**. When the density spectra are smooth, the estimation of the parameters is an easier and accurate process. We believe that this procedure is consistent when estimating the gain, decay, and frequency parameters from both smooth and noisy spectra.

The power-distribution function, **PDF**, is the integrated form of the **PDS**. Figure 1·4 shows the **PDF** corresponding to the **PDS** shown in Figure 1-2 for the case when integration begins at the high-end frequency. The **PDF** can be normalized

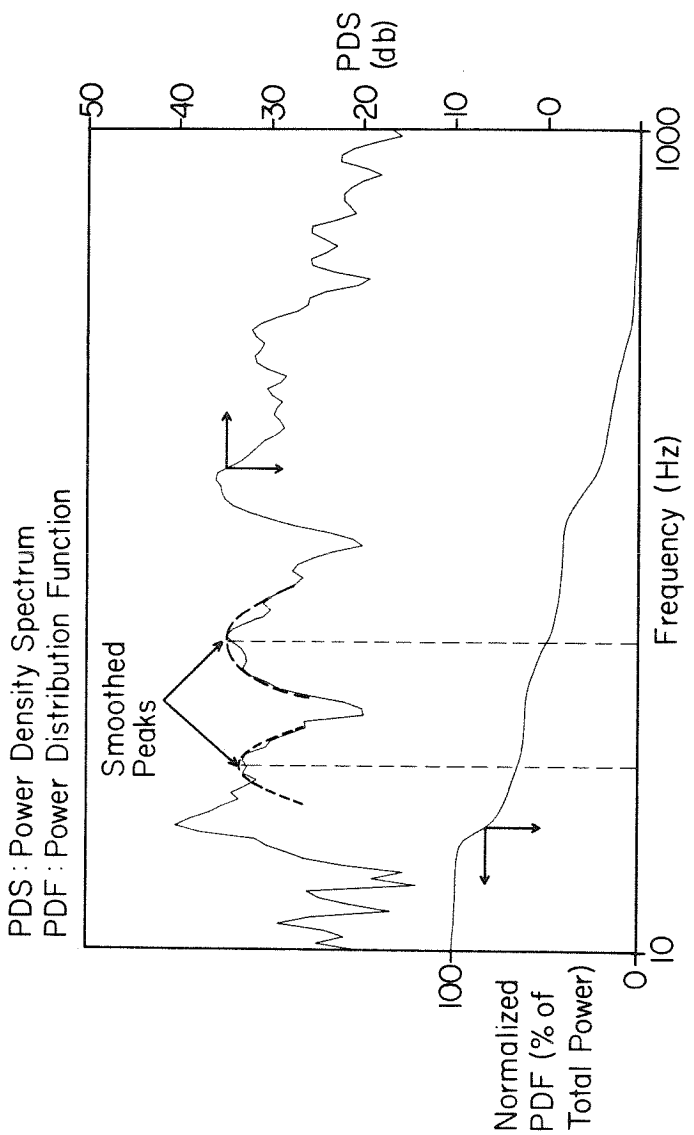

Figure 1-3. Plot depicting a typical example of the technique applied to smooth the noisier density spectra for estimating the parameters of the acoustical model.

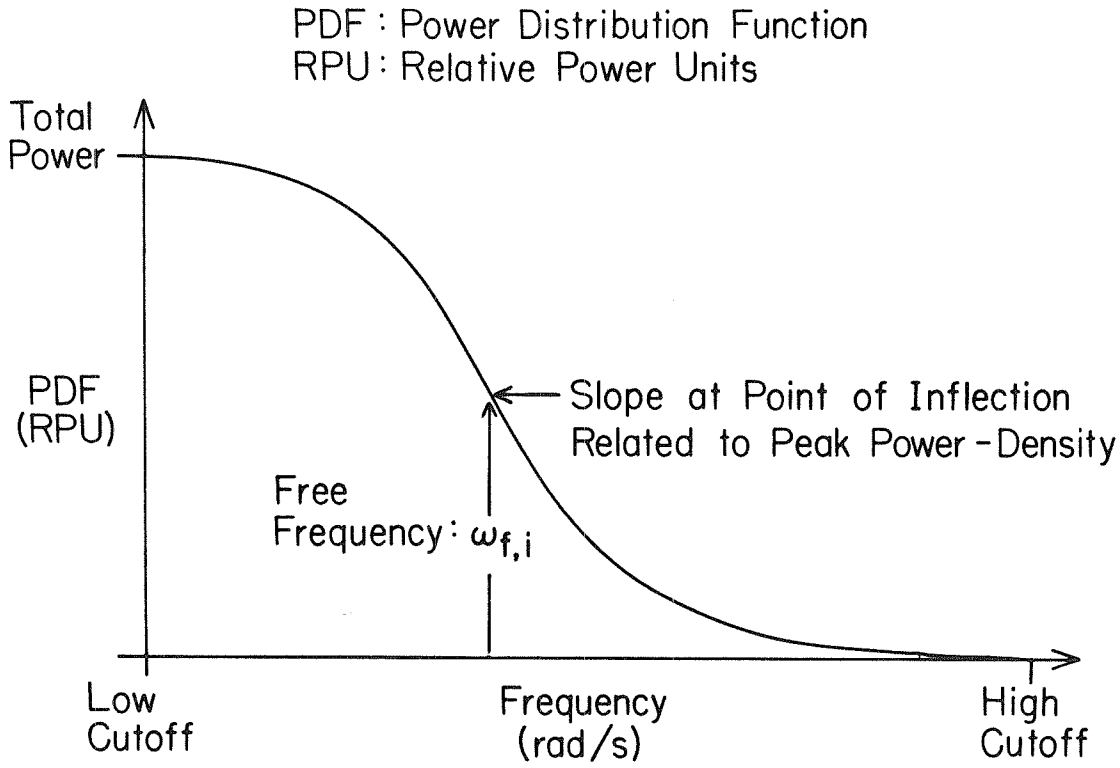

Figure 1-4. Power-distribution spectrum for a linear, monotonic oscillator having decay and lag.

with respect to the total-power over the entire bandwidth 10-1000 Hz. We have found that by integrating from the high-end frequency to the low-end frequency and **not** normalizing with respect to the total power, we can generate three-dimensional surfaces of our data that generally offer a very clear view of the acoustical information for one full cardiac cycle. The **PDF** is not, however, a convienient plot for accurately estimating Γ_{ij}, κ_i, nor $\omega_{f,i}$. It provides overall information, however, about the relative values of these parameters, and it is most useful for rapid, overall comparisons between two sounds.

If we consider the sound generated by the valve as the response to impulses the **PDS** corresponding to these impulse-responses is the "transfer function" for such a valvar system. A specific physical change of the valve should show up as a specific change in the **PDS**. By keeping non-valvar aspects constant while perturbing the valvar condition, we can interpret changes in the **PDS** of the sounds as being characteristic to changes of the valvar system. These facts are applicable to the transient response.

1.3.8 Parameter Estimation for the Non-transient Response in the Frequency Domain

Vibrations are produced by the turbulent flow of blood around the structures of the valves. In turbulent flow a wide range of length scales is present and corresponds to the wide range of eddy sizes in the turbulent motion. The structures of the valve and surrounding chamber can be stimulated by momentum transport from these eddies. The precise nature of these forces is not clear for flow in and around prosthetic heart valves. The work of Johnson (JOHNSON, 1979) shows a correlation between the degree of aortic stenosis and the acoustical power over a broad-frequency band for systolic murmurs *in vivo*. This fact suggests that a correlation may exist between the nature of the perturbed flow and

the distribution of turbulent eddies as well as between the eddy distribution and the acoustical-power distribution.

If we consider a statistical distribution of eddy sizes as the cause of the applicable forces, a linear sum of sinusoids is a reasonable first approximation for the non-transient forces. The discrete **PDS** corresponding to a sinusoid of finite duration is simply the **PDS** of the digitized window used during sampling and centered at the frequency corresponding to the sinusoid. For a cosine-smoothed window, which is common usage, the **PDS** is a relatively sharp peak with low-amplitude, side lobes. The superposition of such peaks for continuously varying frequencies will result in a spectrum having few distinct peaks. One can generally characterise the spectrum for these sounds by a single set of parameters. We can use the same method to estimate a single set of parameters for the non-transient case as we have described for the transient response. Of course, the physical meaning of the parameters is not related to the physical parameters of the materials of the valve but rather to the turbulence and geometry of the valve and chambers. The work of Kim (KIM and CORCORAN, 1974) showed that a decrease in the effective flow area for restricted flow in a tube increased the center frequency of the **PDS** as well as the total power over corresponding bandwidths. These changes should increase the values of the gain, decay, and frequency parameters as estimated by the process outlined for the transient response. The work of Gupta (GUPTA *et al.*, 1975) showed that for flow in tubes a coupling effect occurs for tube-flow between the natural resonance frequency of the tube and the turbulence spectra. Modeling of these non-transient sounds deserves further detailed consideration for the case of flow in and around prosthetic heart valves.

1.4 A Method for Digital Analysis of Acoustic Data

We have found the following method to be a most convienient means for analyzing sounds produced by prosthetic heart valves. The analog data were digitized on a PDP 11/45 computer. Sound data were digitized at 2000 samples per second. The frequency resolution using this sampling rate and a 100-ms-time window was 8.7 Hz. Pressure and flow data were digitized at 200 samples per second. Each experimental file, containing approximately 30 seconds of raw data, was plotted, and an initiation time was chosen at the beginning of each cycle to be analyzed. This initiation time was selected as the time occurring 120 ms prior to the first component of sound. The sound data were then weighted by the cosine-smoothed window shown in Figure 1-5. Zeros were added to these 200 data points to give a total of 256 values for input to the **FFT**. We also generated spectra using a window length of 120 ms by using 240 data points and 16 zeros. For this 20%-larger window, the total power increased correspondingly for each window in the cycle, but the shapes of peaks remained the same. We used the shorter window to achieve better temporal resolution because the differences were not significant relative to the analysis. The **FFT** was applied to the 100-ms extract of data. The modulus of the complex coefficients associated with each discrete frequency was calculated and stored. The window was shifted 20 ms ahead in time and the **FFT** repeated as depicted in Figure 1-6. After shifting the window 43 times, one pulsatile cycle was spanned. A new cycle was selected and the entire process repeated for a total of ten cycles. Average values for ten cycles were then stored. Information was retained only in the frequency band of 10-1000 Hz. The lower limit of 10 Hz was determined by the lower operating limit of our transducer. The 1000 Hz upper limit was determined by the Nyquist frequency. The temporal shift in window position was

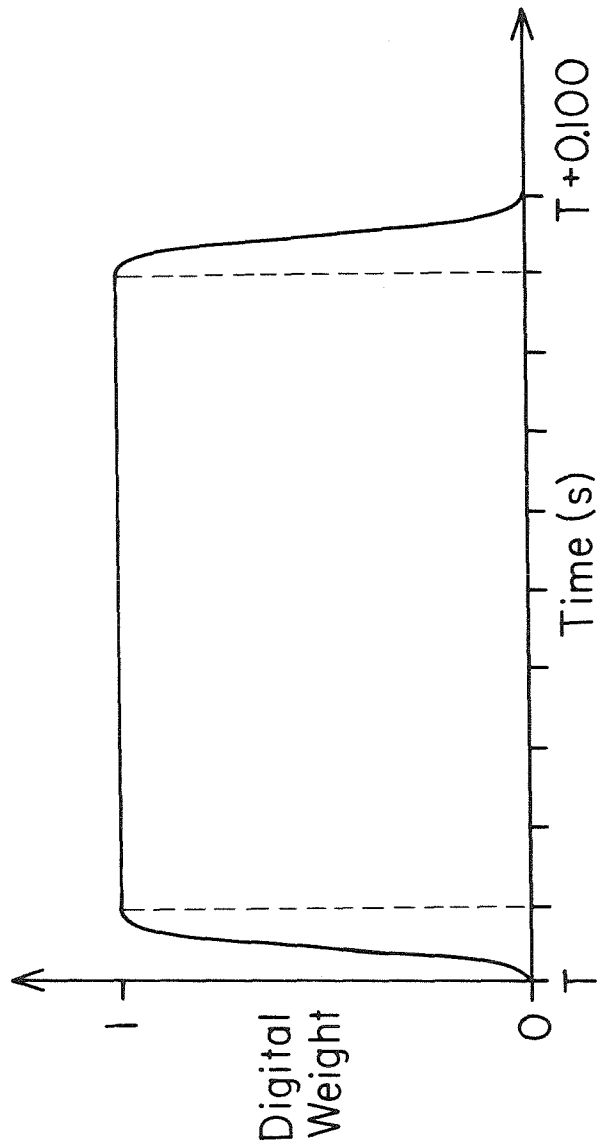

Figure 1-5. The digital window applied to the sampled data prior to the fast Fourier transformation.

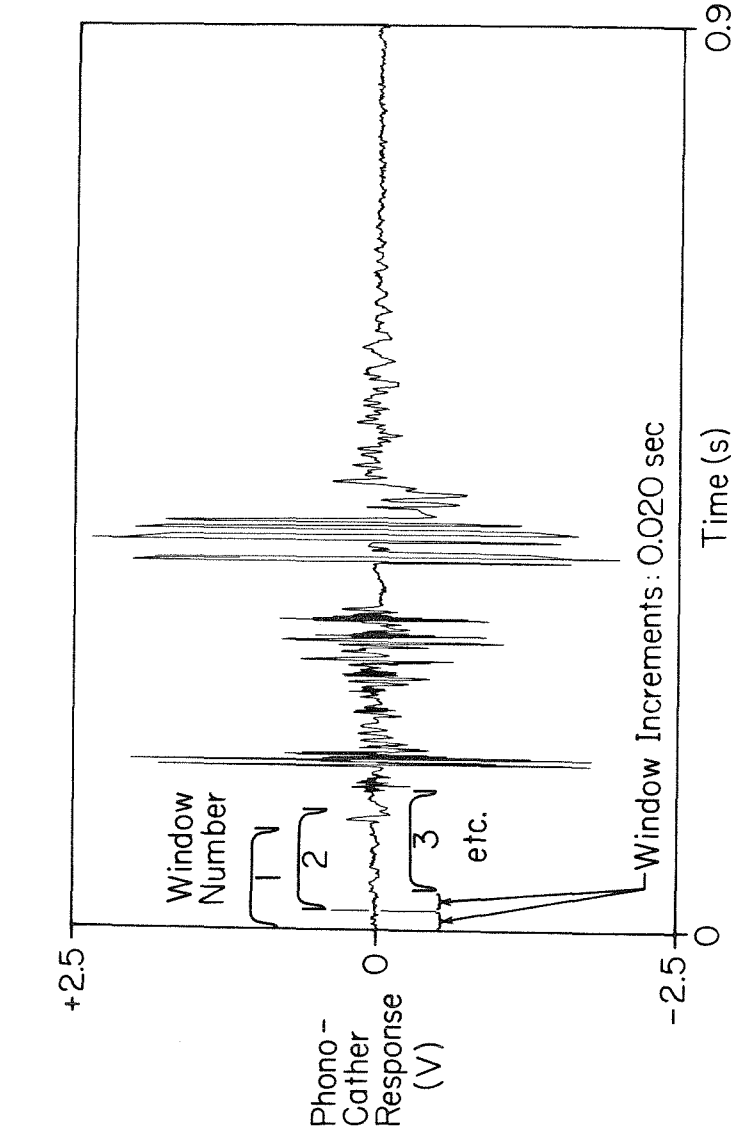

Figure 1-6. Temporal location and movement of the windows when the window length is 100 ms and the increment of the starting time of each successive window is 20 ms.

chosen by considering the timescale of events in the sound cycle and by the time and cost of computing. The cost factor becomes significant as one begins to double the number of data points for each window. The window length should be small with respect to the cycle length to allow for differentiation of events in the cycle. The window length must also balance with the sampling rate so as to provide enough points for the **FFT**, remembering that the resolution of the frequency domain is proportional to the number of data points used for the calculation of the spectra. A satisfactory window length was found to be 100 ms for a digitization rate of 2000 samples per second.

The result of these steps is a stored matrix of 128 discrete Fourier coefficients for 43 separate windows averaged over 10 cycles. Each window increment represents 20 milliseconds of real time. Successive windows possess 80% overlap with the preceding window. The average power-distribution functions were generated from the Fourier coefficients for each frequency and window and were stored for plotting purposes. A simple trapezoidal rule was used in the integration.

The power-distribution spectrum associated with each window was aligned and plotted to form a third axis representing the time associated with the beginning of each window in real time. Figure 1-7 shows a typical example of this type of plot. This particular figure shows the power distribution over frequency and time for a normal Starr-Edwards series 2400 aortic prosthesis. The value of the power-distribution for the lowest frequency, 10 Hz, is equal to the total-power for that window for the frequency band of 10-1000 Hz. A search was performed over the total power for each window, and windows for which a maximum total-power occurred were generally found to encompass the opening sound, murmur, and closing sound of the valves. If these windows did not encompass a particular event of interest, the program enabled the analyst to insert specific window

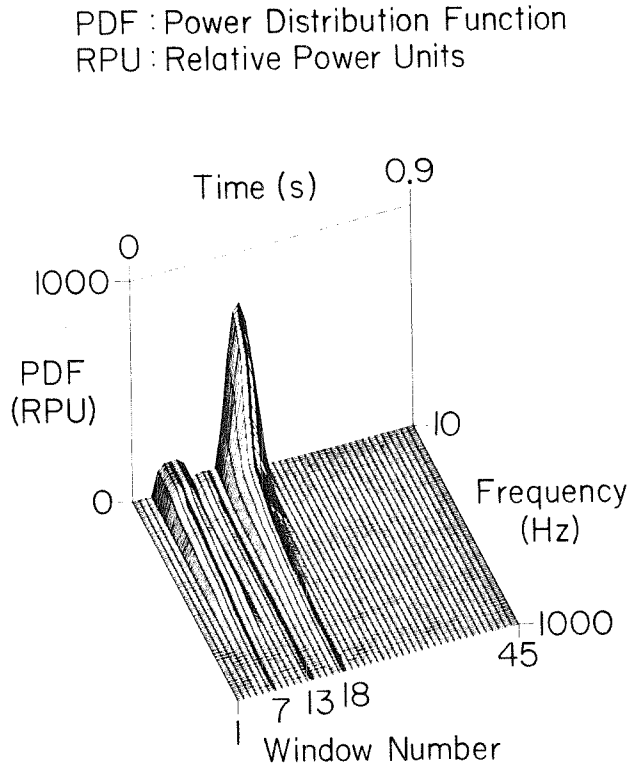

Figure 1-7. Power-frequency-time surface depicting the distribution of power in relative power units (RPU) corresponding to the sounds produced by a normal Starr-Edwards 2400 prosthesis operating *in vitro*.

numbers. For these selected windows, a plot was generated of the **PDS** and the normalized **PDF**. Figure 1-8 shows examples of these spectra for window 7 which encompasses the opening sound of the valve and which was previously depicted as a portion of the surface shown in Figure 1-7. The parameter set was manually generated from the **PDS**. We had aligned the normalized **PDF**s to form a normalized distribution surface, but these surfaces were not as informative as the non-normalized versions. A two-dimensional projection upon the power-time plane of selected contours of the power-distribution surface is shown in Figure 1-9 This type of plot offers quantitative information regarding the power in specific frequency bands. Comparisons were made between experiments by calculating the difference between corresponding matrix elements for the entire power-distribution array. Figure 1-10 shows the flat difference-surface associated with two identical sounds. Figure 1-11 depicts a typical result that we have obtained when comparing the surfaces generated from the sounds produced by a normal and abnormal Starr-Edwards series 2400 prosthesis. A detailed discussion of the information displayed in this figure is given in Part II of this series of papers. Any non-zero value of the comparison surface indicates a difference between the sounds for that window and for the frequencies in the band from the frequency of the point on the surface to the upper limit of 1000 Hz. All peaks and valleys have very precise meanings. A location on the surface having a relatively large **slope** indicates the window and frequency corresponding to larger differences in power-density. If the slope is directed parallel to the frequency axis, then this difference occurs predominantly with respect to frequency. Similarly, if the slope is directed parallel to the time axis, then this difference occurs predominantly with respect to time. Surfaces generated by aligning density spectra were not found to be as informative as the corresponding surfaces developed from distribution functions. The undulating nature of

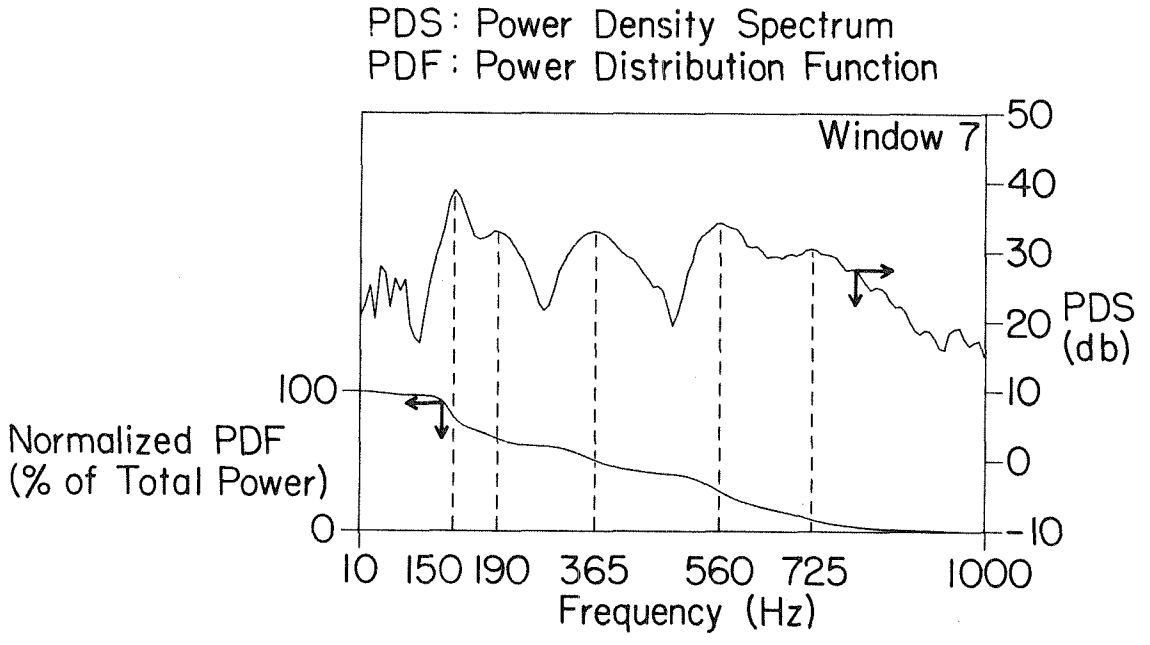

Figure 1-8. Power-density spectrum and normalized power-distribution spectrum corresponding to window 7 which encompassed the opening sound of the normal Starr-Edwards 2400 prosthesis operating *in vitro*.

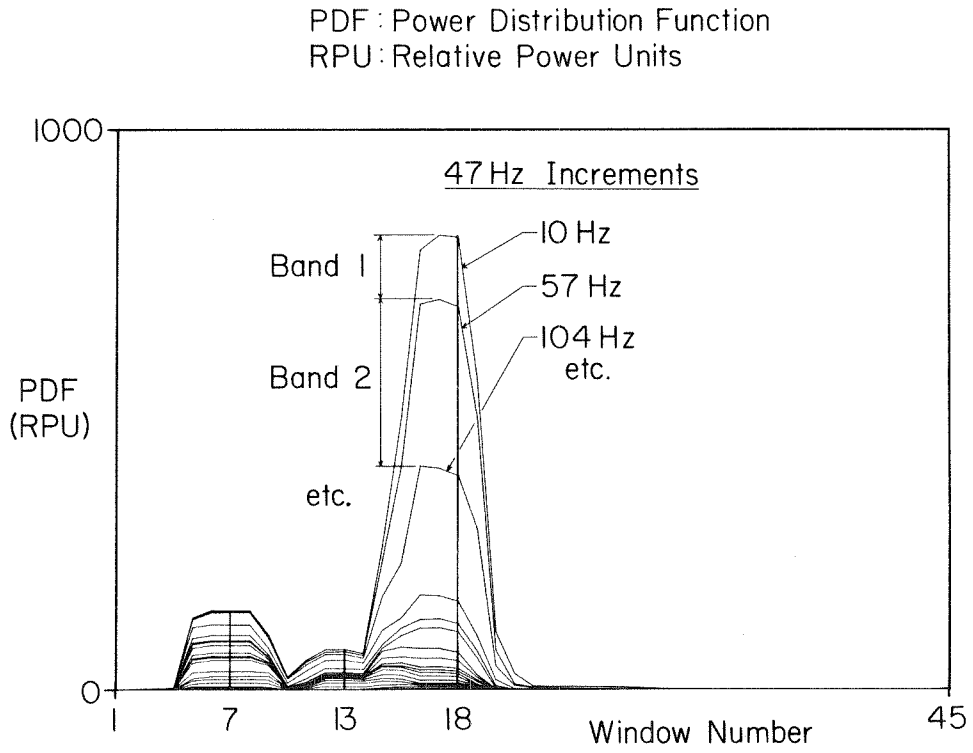

Figure 1-9. Power distribution in relative power units (RPU) as depicted by projecting every sixth frequency contour onto the power-time plane.

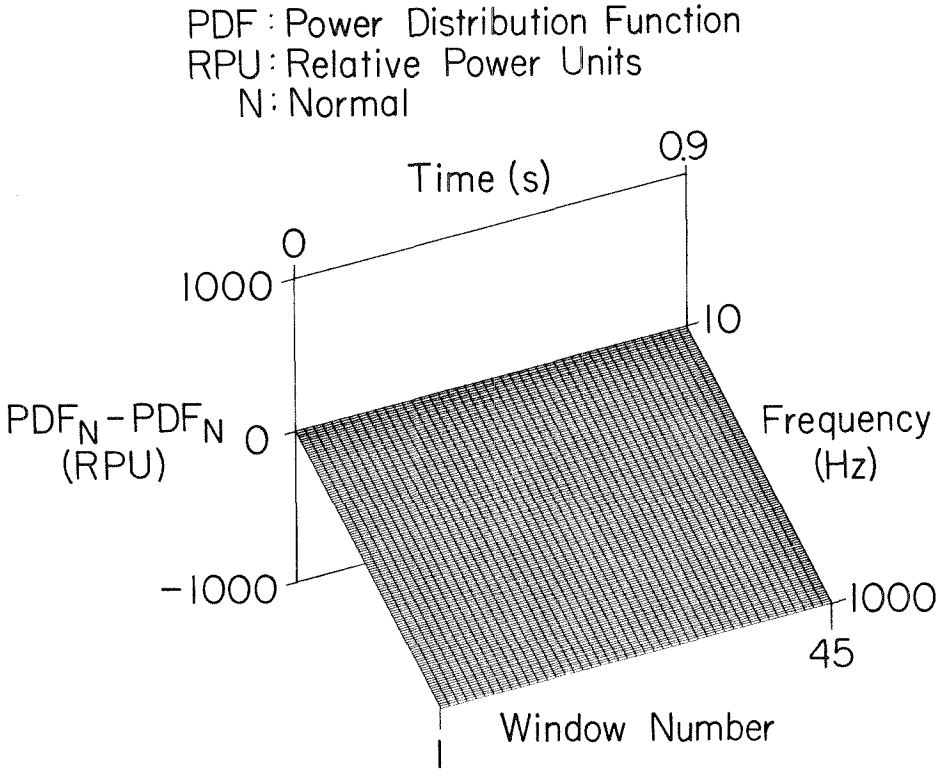

Figure 1-10. Power distribution depicting the difference between two identical power-frequency-time surfaces.

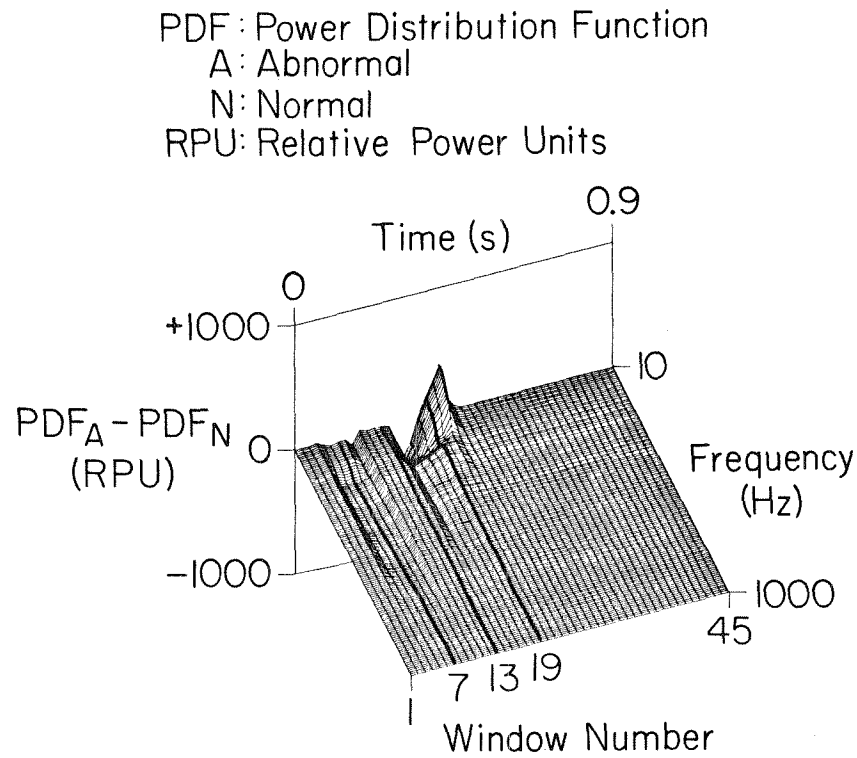

Figure 1-11. Power-distribution surface depicting the difference between the power-frequency-time surfaces corresponding to a normal Starr-Edwards 2400 prosthesis and the same valve having a simulated overgrowth on the apex of the cage as measured *in vitro*.

the power-density surfaces obscured many regions of the surface.

The phase spectra were generated but were difficult to interpret. Temporal changes, however, can be depicted by the difference-surfaces. Also, the original plots of time and amplitude precisely show the timing of most events.

1.5 CONCLUSIONS AND RECOMMENDATIONS

Studies of the sounds produced by prosthetic aortic heart valves *in vitro* offer useful information relative to the relationship between the condition and/or dynamics of the valve and the sounds which it will produce. *In vitro* tests also permit accurate testing of acoustical models.

A linear one-dimensional model can be used to describe the major physical characteristics of a prosthetic valvar source of sound. The power-density spectrum for the transient response provides the transfer function of this valvar system. The power-density spectrum for the non-transient response provides information about the degree of intensity of turbulence and of perturbance of flow of fluid through the valve. Fourier analysis of the sounds offers quantitative comparisons of two sounds. This comparison is generally more sensitive and accurate than comparisons made between representations in the time domain. Power-density spectra best depict the frequencies where the significant acoustical powers are located, the relative magnitudes of the powers at these frequencies, and, for the case of transient sounds, the relative decay rate of sounds at these frequencies. Power-distribution spectra best depict the total energy of sound within a window as well as the relative manner in which the component-frequencies contribute to this total power. The three-dimensional power-frequency-time surface depicts the overall sound in a manner which is most convienient for viewing the relative power between frequencies bands for

each window. A three-dimensional, power-frequency-time surface showing the difference between two of the previous surfaces clearly depicts the frequencies and windows where differences occur between two general sounds and whether these differences occur predominantly with respect to frequency or time. A matrix of the digital values used to generate these surfaces can be analyzed quantitatively and stored for later comparisons between matrices corresponding to other sounds. A comprehensive library of these matrices can be developed to be used for future comparisons. Recommendations regarding experimental aspects of this work are presented in Paper III of this series.

1.6 ACKNOWLEDGEMENTS

Funding for this project was provided by the Donald E. Baxter Foundation, the Children's Heart Foundation of Southern California, and the American Heart Association, Greater Los Angeles Affiliate.

1.7 NOMENCLATURE

a	Speed of sound, m/s
A	Amplitude of pressure fluctuations, $kg/m/s^2$
A_c	A complex number corresponding to the amplitude of pressure fluctuations, $kg/m/s^2$
A_{ik}	Amplitude of displacement of decaying component of mode i produced by sinusoidal non-transient force k, m
B_{ik}	Amplitude of displacement of non-decaying component of mode i produced by sinusoidal non-transient force k, m
c_v	Heat capacity at constant volume, kg/m/s/K
D_i	Damping coefficient, kg/s
$\overline{E}$	Internal energy per unit mass, m^2/s^2
$F(t)$	Force described as a function of t, $kg\ m/s^2$
$F_{t,j}(t)$	Transient force j described as a function of t, $kg\ m/s^2$
$F_{nt,k}(t)$	Non-transient force k described as a function of t, $kg\ m/s^2$
$F_{o,j}$	Amplitude of non-transient forcing function associated with forcing frequency ν_j, $kg\ m/s^2$
$\vec{g}$	Acceleration of gravity, m/s^2
k	Wave number of acoustical phase fronts, m^{-1}
K_b	Bulk modulus, $kg/m/s^2$

K_i	Stiffness coefficient of mode i, kg/s^2
M_i	Inertial coefficient of mode i, kg
$\vec{n}$	Unit normal vector, m
N_i	Total number of modes
N_j	Total number of impulse forces
N_k	Total number of sinusoidal forces
$P_t^{N_i}(\omega)$	Value of total power-density spectrum associated with frequency ω for a single transient stimulation of N_i oscillators, $kg/m/s^2$
PDF	Designates power distribution functions, RPU
PDS	Designates power-density spectra, db
p	Total pressure, $kg/m/s^2$
p_o	Pressure at equilibrium state, $kg/m/s^2$
$p'(t)$	Total pressure-response as a function of t, $kg/m/s^2$
$p'_{t,ij}(t)$	Transient pressure-response of mode i, stimulated by impulse j, described as a function of t, $kg/m/s^2$
$p'_{nt,ik}(t)$	Non-transient pressure response of mode i, stimulated by sinusoid k, described as a function of t, $kg/m/s^2$
$\vec{q}$	Heat flux, $kg/s/m^2$
r	Radial coordinate of cylindrical coordinate system, m
RPU	Designates relative power units
S	Entropy per unit mass, $m^2/s^2/K$
T	Time associated with beginning of window, s
T	Temperature, K
t	Time variable, s
t_{heat}	Characteristic time associated with heat transfer, s
t_{sound}	Characteristic time associated with acoustic disturbance, s
t_j	Time associated with impulse j, s
$\vec{v}$	Total velocity at a point, m/s
V	Volume of fluid element,m^3
V_j	Temporal density of transient forcing function, kg m/s
V_k	Amplitude of non-transient force associated with sinusoid k, $kg\ m/s^2$
z	Axial component of cylindrical coordinate system, m
z	Displacement of oscillator, m
z_c	Distance from source to catheter, m
α_{mn}	Eigenvalue of Bessel functions, m^{-1}
α_{i1}	A specific function of frequency associated with mode i1, $(rad/s)^2$
β_{i1}	A specific function of frequency associated with mode i1, $(rad/s)^2$
Γ_{ij}	Gain parameter associated with mode i and impulse j, $kg/m/s^3$
$\delta(t-t_j)$	Distribution of transient force with respect to time relative to t_j, s^{-1}
ε	A small dimensionless constant
κ_i	Decay parameter of mode i, rad/s
$\kappa_{z,n}$	Wave number of mode n in z direction, m^{-1}
λ_o	Thermal conductivity of fluid, kg/m/s/K
ν_k	Frequency of sinusoidal forcing function k, rad/s

ρ	Instantaneous density of fluid, kg/m^3
ρ_o	Density of fluid at equilibrium, kg/m^3
Σ	Summation operator
$\mathbb{T}$	Deformation dyad, $kg/m/s^2$
$\varphi_{nt,ik}$	Phase of non-decaying oscillator associated with mode i and sinusoidal force k, rad
$\varphi_{nt,k}$	Phase of non-decaying stimulation associated with sinusoidal force k, rad
$\varphi_{t,ij}$	Phase of decaying oscillator associated with mode i and impulse j, rad
$\varphi_{t,ik}$	Phase of decaying oscillator associated with mode i and sinusoidal force k, rad
ϑ	Azimuthal component of cylindrical coordinate system, dimensionless
ω	Frequency variable, rad/s
$\omega_{o,i}$	Frequency of oscillations of mode i without damping, rad/s
$\omega_{f,i}$	Free frequency of oscillation of mode i with damping, rad/s

Subscripts and superscripts

	Operator for intrinsic differentiation with respect to time
	Indicates a fluctuating component
b	Indicates a bulk quantity
c	Indicates a value associated with the phonocatheter
f	Indicates a frequency with damping present
heat	Indicates a variable associated with heat transfer
i	Indicates arbitrary mode number i
j	Indicates arbitrary impulsive force number j
k	Indicates arbitrary sinusoidal force number k
N_i	Indicates the total number of i-modes
nt	Indicates non-transient variable
o	Indicates a characteristic value
$\bar{S}$	Indicates a quantity evaluated at constant specific-entropy
t	Indicates transient variable
v	Indicates a value determined with constant volume

1.8 REFERENCES

[1] Adolph, R.J., Stephens, J.F., and Tanaka, K. (1970) The Clinical Value of Frequency Analysis of the First Sound in Myocardial Infarction. *Circulation*, **41**, 1003-1014.

[2] Brigham, E.O. (1974) *The Fast Fourier Transform* Prentice-Hall, Englewood Cliffs, NJ, 91-147, 198-223.

[3] Cooley, J.W., and Tukey, J.W. (1965) An Algorithm for Machine Calculation of Complex Fourier Series. *Math. Computation*, **19**, 297-301.

[4] Durand, L.G., and Guardo, R. (1979) Analyse Spectrale du Phonocardiogramme L'apport des Techniques Recentes. *Union Medecale du Canada*, **108**, 835-845.

[5] Gupta, R., Miller, J.W., Yoganathan, A.P., Udwadia, F.E., and Corcoran, W.H., (1975) Spectral Analysis of Arterial Sounds: A Noninvasive Method of Studying Arterial Disease. *Medical and Biological Engr.*, **13**, 700-705.

[6] Hylen, J.C., Kloster, F.E., Herr, R.H., Starr, A., and Griswald, H.E. (1969) Sound Spectrographic Diagnosis of Aortic Ball Variance. *Circulation*, **39**, 849-858.

[7] Johnson, C. (1979) Tape Recording of paper to be published as presented November 1979 at the annual meeting of the American College of Cardiology.

[8] Kim, B.M. and Corcoran, W.H. (1974) Experimental Measurements of Turbulence Spectra Distal to Stenoses. *J. of Biomechanics*, **7**, 335-342.

[9] McKusic, V.A., Talbot, S.A., and Webb, G.N. (1954) Spectralphonocardiography: Problems and Prospects in the Application of the Bell Sound Spectrograph to Phonocardiography. *Bull. John Hopkins Hosp.*, **94**, 187-198.

[10] Rayleigh, J.W.S. (1945) *The Theory of Sound*, Vols. 1 and 2, Dover Press, Vol. 1: pp. 19-42, 91-170, Vol. 2: pp. 109-114, 246-250, 312-320.

[11] Smith, N.D., Raizada, V., and Abrams, J. (1981) Auscultation of the Normally Functioning Prosthetic Valve. *Ann. Int. Medicine*, **95**, 594-598.

[12] Stein, P.D., Sabbah, H.N., Lakier, J.B. and Goldstein, S. (1980) Frequency Spectrum of the Aortic Component of the Second Heart Sound in Patients with Normal Valves, Aortic Stenosis and Aortic Porcine Xenografts. *American J. of Cardiology*, **46**,48-52.

[13] Tavel, M. E. (1978) *Clinical Phonocardiography and External Pulse Recording*, Chicago, Year Book Medical Pub., Inc., Third Edition, 391 pp.

[14] Winer, D.E., Perry, L.W., and Coure, C.A. (1965) Heart Sound Analysis: A Three-Dimensional Approach. *Amer. J. Cardiol.*, **16**, 547-551.

[15] Yoganathan, A.P., Gupta, R., Udwadia, F.E., Miller, J.W., Corcoran, W.H., Sarma, R., Johnson, J.L., and Bing, R.J. (1976a) Use of the Fast Fourier Transform for Frequency Analysis of the First Heart Sound in Normal Man. *Med. and Biol. Engr.*, **14**, 69-73.

[16] Yoganathan, A.P., Gupta, R., Udwadia, F.E., Corcoran, W.H., Sarma, R., and Bing, R.J. (1976b) Use of the Fast Fourier Transform for the Frequency Analysis of the Second Heart Sound in Normal Man. *Med. and Biol. Engr.*, **14**, 455-460.

[17] Yoganathan, A.P., Gupta, R., and Corcoran, W.H. (1976c) The Fast Fourier Transform in the Analysis of Biomedical Data. *Med. and Biol. Engr.*, 14, 239-245.

PAPER 2

A Quantitative Method for the *In Vitro* Study of Sounds Produced by Prosthetic Aortic Heart Valves
Part II: An Experimental, Comparative Study of the Sounds Produced by a Normal and Simulated-Abnormal Starr-Edwards Series 2400 Aortic Prosthesis

A Quantitative Method for the *In Vitro* Study of Sounds Produced by Prosthetic Aortic Heart Valves

Part II: An Experimental, Comparative Study of the Sounds Produced by a Normal and Simulated-Abnormal Starr-Edwards Series 2400 Aortic Prosthesis

ABSTRACT

A comparative study was made of the sounds produced by a normal, Starr-Edwards 2400, aortic valve prosthesis with those produced by the same valve but having a simulated overgrowth at the apex of the struts. Comparisons were made over the entire cardiac cycle for (1) time and amplitude, (2) power-density spectra, (3) power-distribution spectra, (4) power-distribution surfaces associated with individual valves, and (5) a 3D, power-distribution-difference surface. Power-density spectra were compared for portions of the cycle corresponding to the opening, systolic, and closing sounds of the valve. Physical parameters of an acoustical model were estimated from the power-density spectra. These parameters were then compared and discussed in terms of the physical condition of the valve.

The results showed that each comparison gave information pertinent to the simulated malfunction. Opening, systolic, and closing sounds, respectively, were different for each valve. The opening sound of the abnormal valve displayed a much lower frequency. Systolic sounds for the two valves were similar in frequency, but the abnormal valve produced more total power for this sound. The closing sound of the abnormal valve occurred later than that of the normal valve. These differences were more clearly seen when viewed in the frequency domain.

Key Words- Starr-Edwards 2400 prosthesis, sound, fast Fourier transform, *in vitro* comparison

2.1 INTRODUCTION

The majority of investigations of heart sounds have been made *in vivo*, and the precise state of the valve and heart were not known at the time the sounds were measured. Acoustic models were normally not presented or applied qualitatively to explain results. If models had been made, the sources of variability in the emanating sound would have had prime focus. Contributions to that variability would have been from the physiology of the heart and surrounding anatomy, the dyanamic state of the heart, and the performance of the four heart valves. Isolating these contributions to the total variability by *in vivo* studies alone is difficult. The valves should be studied at well defined pulsatile states. *In vitro* studies can be designed to investigate effects of the valvar condition, design, size, and orientation of implantation upon sounds made by the valve for a closely maintained dynamic state.

The purpose of the work reported here was to examine *in vitro* the sound characteristics of a specific valve prosthesis, the Starr-Edwards 2400 aortic valve, and determine by comparative analysis whether the sound data contained sufficient, useful information for diagnostic purposes. Positive results would lead to further *in vitro* studies to provide a preliminary data bank and then to equivalent or related *in vivo* studies.

2.2 EXPERIMENTAL METHOD

2.2.1 The Caltech Pulse Duplicator

The pulse duplicator used in this study was designed to simulate both normal and other pulsatile conditions for flow in and around both the mitral and the

aortic valves. It is shown schematically in Figure 2-1. Unit 1 is the left atrial reservoir. The fluid head in this unit maintains a controllable, mean atrial pressure. Unit 2 corresponds to the left ventricle. Pumping is achieved by means of pneumatic control. Two rubber bulbs inside of closed Lucite® chambers are squeezed by pressure controlled by the inlet of air. Pumping is achieved by signals to solenoid valves. The solenoids open and close at the desired cardiac rate and in turn pressurize and evacuate the closed chamber surrounding each ventricle. The systolic time interval and pulse rate can be controlled independently. This unit also has a very flexible section for providing capacitance and damping for the ventricular action. Unit 3 is the aortic flow section where the prosthetic aortic valves are mounted for study. Figure 2-2 shows this section in more detail. The valves are mounted by sewing them to Lucite® disks. The Lucite® disks are then rigidly mounted in the flow section. The downstream edge of the valve orifice is maintained at a constant distance from the positions of the transducers for sound, pressure and flow. These positions are shown in Figure 2-2. The aortic flow section was fabricated from Lucite® and was designed to have a 1:1 geometric ratio with respect to the aortic root of a normal adult. Three sinuses of Valsalva were included, but coronary arterial flows were not. Unit 4 represents a cannulating electromagnetic flow-meter. It is rigidly connected to the aortic section so that instantaneous flow through the meter is equivalent to the flow through the valve orifice. Finally, units 5 and 6 are, respectively, an effective systemic capacitance and damper and an effective systemic resistance.

A variety of flow conditions can be obtained by adjusting variables such as the ventricular compliance and/or resistance, and the systemic compliance and/or resistance. The work reported here will be concerned with aortic valves operating at one set of operating conditions which we will call *NORMAL*. Table 2-1 is a

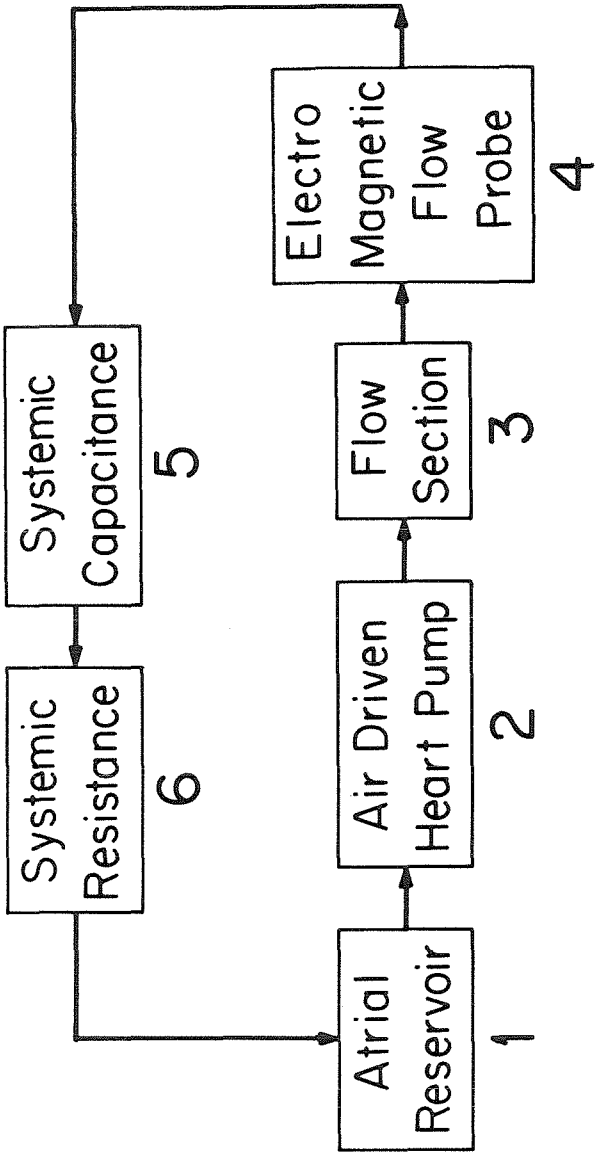

Figure 2-1. Schematic diagram of the Caltech pulse duplicator.

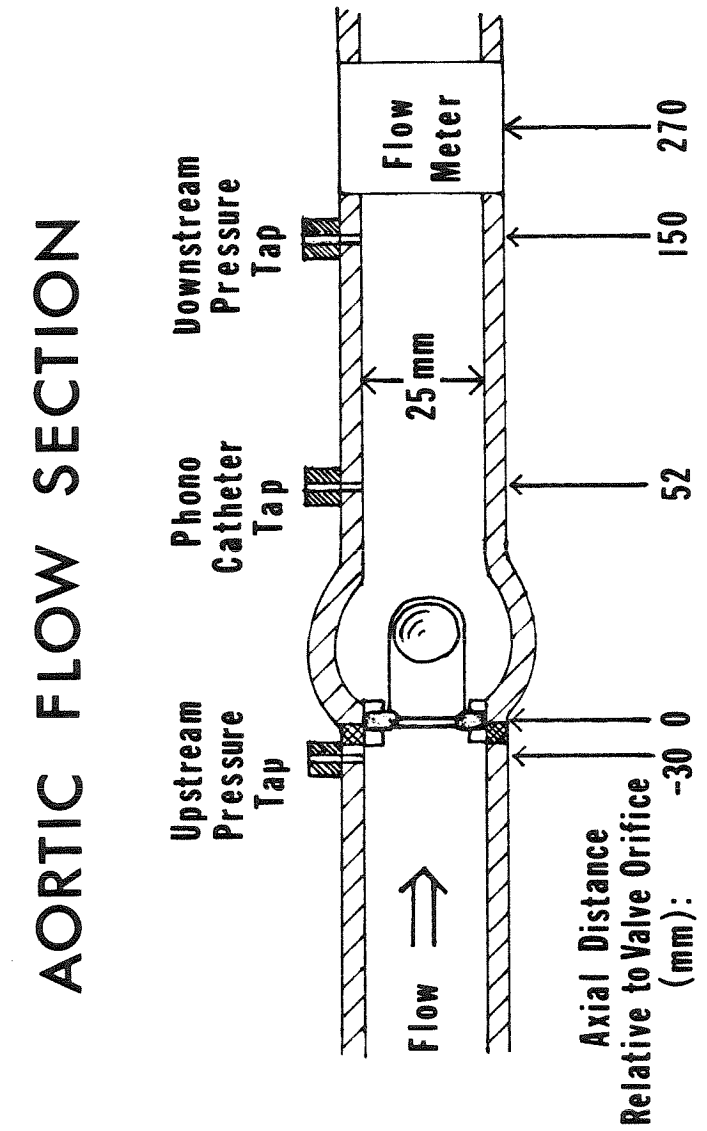

Figure 2-2. Cross section of the aortic-flow section of the Caltech pulse duplicator.

Table 2-1

Conditions for NORMAL Operation

of Pulsatile Flow System

Pulsatile Variable	Value	
Pulse Rate	70	cycles/min
Systolic Time Interval	300	ms
Diastolic Time Interval	560	ms
Stroke Volume	90	cm^3
Mean Output	5	l/min
Peak Systolic Flow	25	l/min
Minimum Aortic Pressure	80	mmHg
Minimum Ventricular Pressure	-15	mmHg

Table 2-1 Conditions for **Normal** Operation of Pulsatile Flow System.

list of values for the variables maintained for the *NORMAL* state of the pulse duplicator. All valves were studied under these pulsatile conditions. A 0.9 normal saline solution was used as a blood analog fluid. Experiments were conducted at a temperature of 23 C. Figure 2-3 shows typical flow, sound, and pressure-wave forms for the case of the Starr-Edwards 2400 prosthesis.

The pulse duplicator was designed so that the sounds at one valve are not detected in the vicinity of the other. This isolation was achieved by having the valves separated by very compliant flow sections and by use of pneumatic pumping. Ambient noises were reduced so that on a peak-to-peak basis the normal acoustical signal-to-noise ratio was approximately 60db. Consequently, the results presented represent primarily the sounds produced by the aortic valve mounted in the aortic flow section.

2.2.2 Measurement and Instrumentation

Simultaneous measurements were made of sound, ventricular pressure, aortic pressure, and volumetric flow. Sound was measured with a Millar Microtip® phonocatheter transducer (PC-480) which was placed within the aortic flow section via the first tap downstream from the valve (see Figure 2-2). The phonocatheter was positioned at the aortic axis and faced the valve. Ventricular and aortic pressures were measured using Statham P23De and P23Db transducers, respectively. Pressure measurements were made at the wall at the axial positions shown in Figure 2-2. Volumetric flow was measured with a Statham SP-7507-250, cannulating, flow probe connected to a Statham SP-2202 blood flowmeter. Each signal was amplified, filtered, and recorded on a Hewlett-Packard HP-3960, FM-tape recorder. The pressure and flow signals were low-pass filtered at a cutoff frequency of 50 Hz. The sound signal was bandpass filtered with a bandwidth of

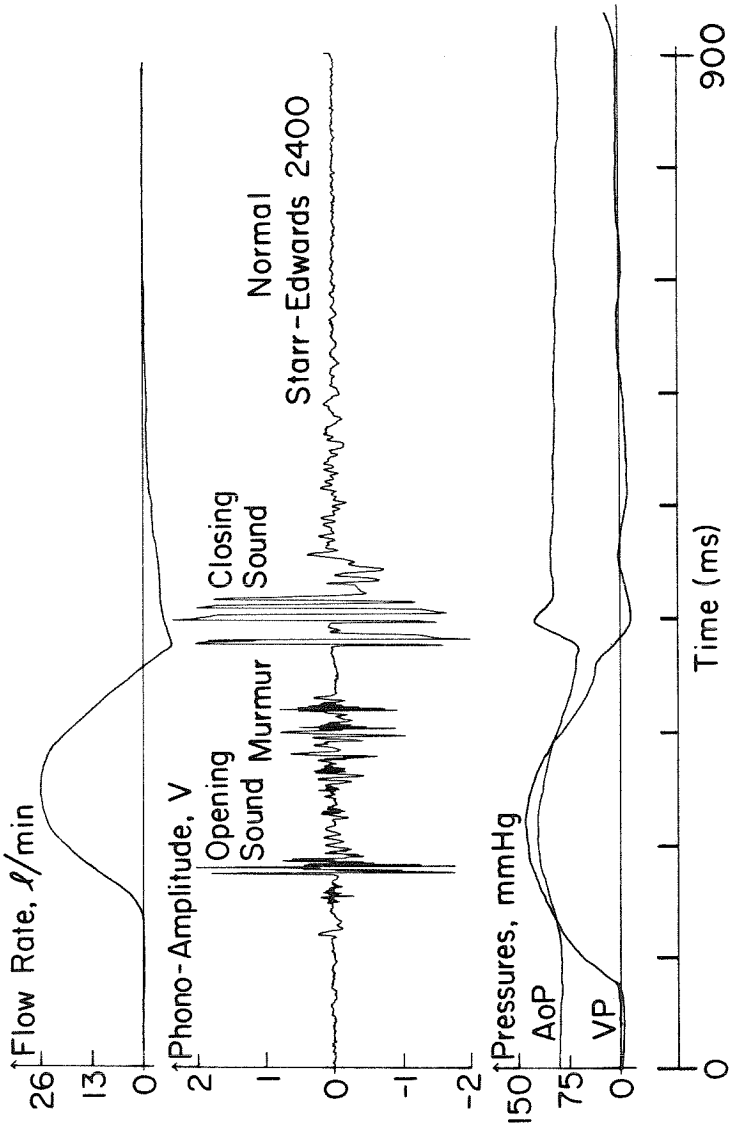

Figure 2-3. Typical data for one 860-ms cycle of the pulse duplicator showing typical flow, sound and pressure tracings corresponding to the 24-mm Starr-Edwards 2400 prosthesis.

100-5000 Hz and 12 db/octave slopes. These four signals were recorded and stored on analog tape in this format until digital analysis was performed.

The size of the valve and its orientation relative to the sinuses were noted. These variables could be important relative to the state of the system and were maintained constant in this study by using valves of identical size, 24 mm sewing diameter, and orientation. Struts of the valves were positioned so as to be opposite the the centerline of each sinus.

The same basic valve was studied for the normal and abnormal condition. Its mounting diameter was 24mm. Two valvar conditions were studied, namely, the normal valve and the same valve having a simulated overgrowth which perturbed the poppet motion. This simulated overgrowth was located at the inner apical surface as shown in Figure 2-4. The overgrowth was simulated by applying silicone rubber gel at each point and allowing it to set. This overgrowth reduced the occluder motion by 0.08 inch relative to the fully open position.

2.3 RESULTS

The results of each experiment are presented in a similar form for comparison. First, a plot of the raw, time-amplitude signal is presented. Figures 2-5a and 2-5b show 900 ms of pressure-response plotted as voltage amplitude for the two valvar conditions. These plots represent typical cycles of the ten that were used for generating the average surfaces. Each 900-ms record was analyzed, and the corresponding power distribution surfaces are plotted in Figures 2-6a and 2-6b. These figures show three-dimensional plots of power distribution as a function of frequency and window number, or time. A detailed description of the method used to develop and interpret these surfaces is presented in Part I of this series. The vertical scale is presented in terms of "relative power units" (RPU). One

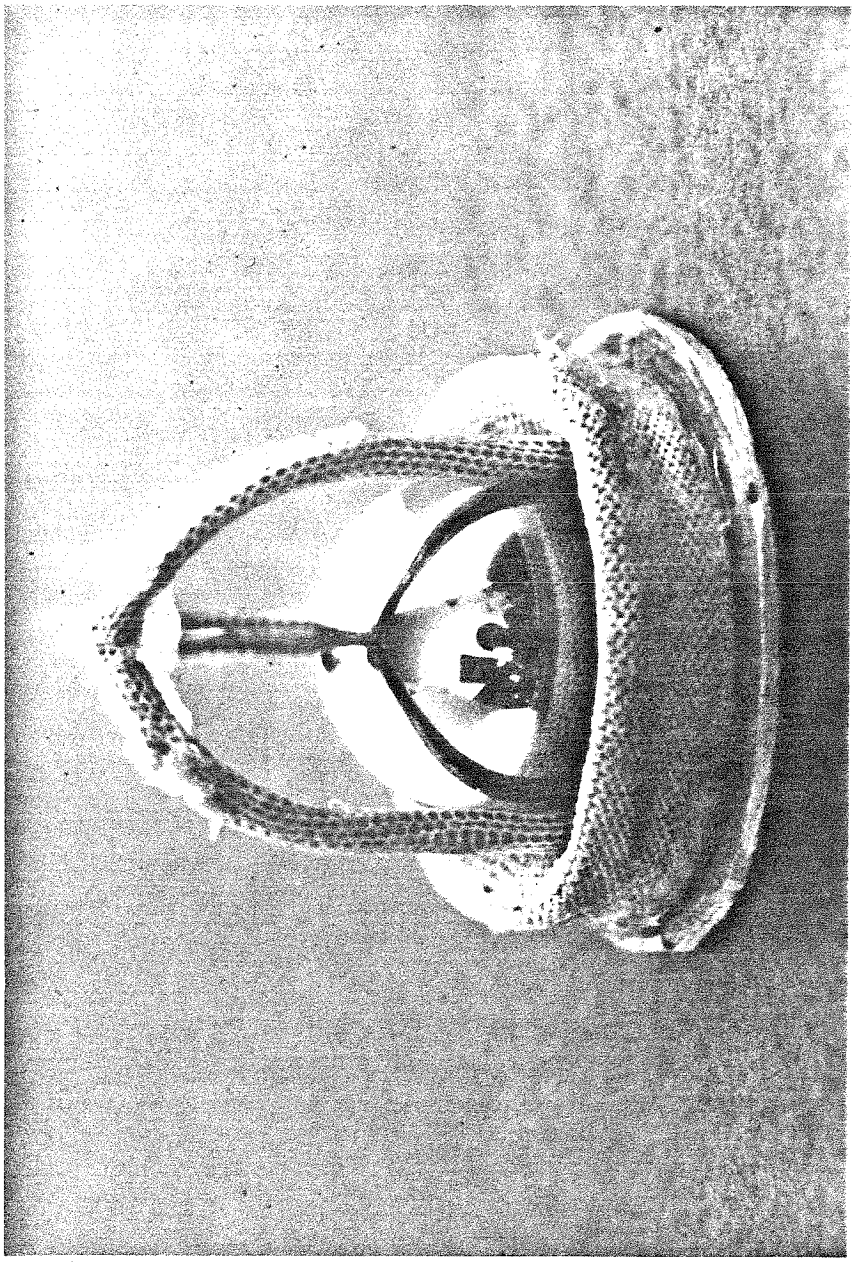

Figure 2-4. Photograph showing the Starr-Edwards 2400 prosthesis studied for the case having a simulated overgrowth on the apex of the cage.

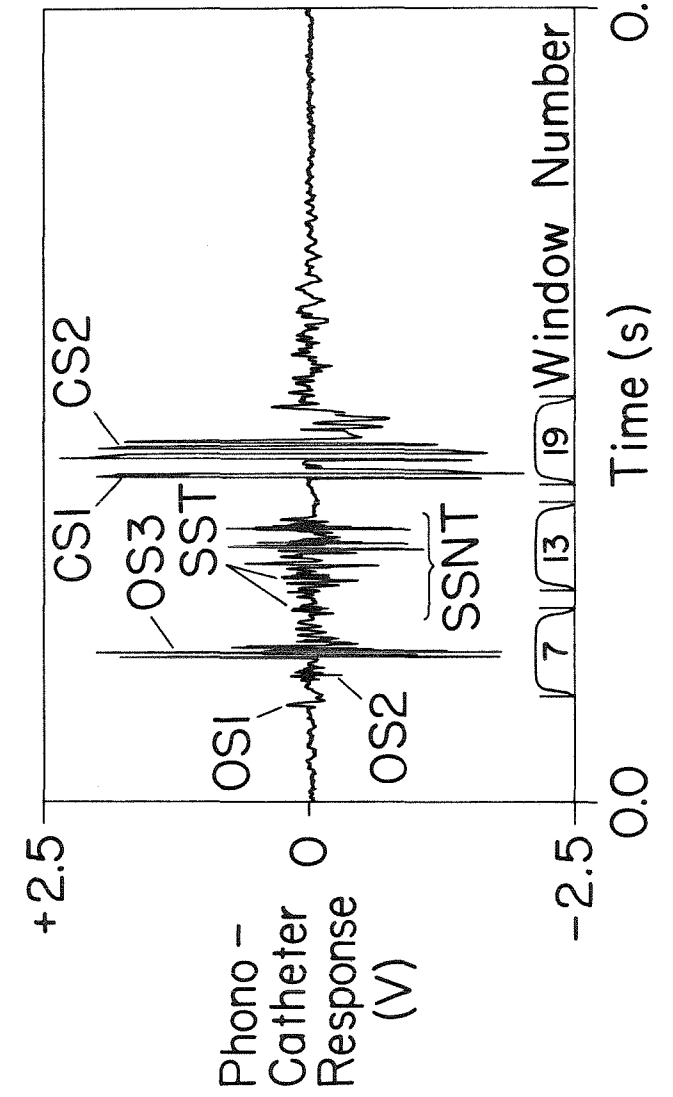

Figure 2-5a. Amplitude and time tracings of the sounds produced by the Starr-Edwards 2400 prosthesis operating at the NORMAL state *in vitro*: normal valve.

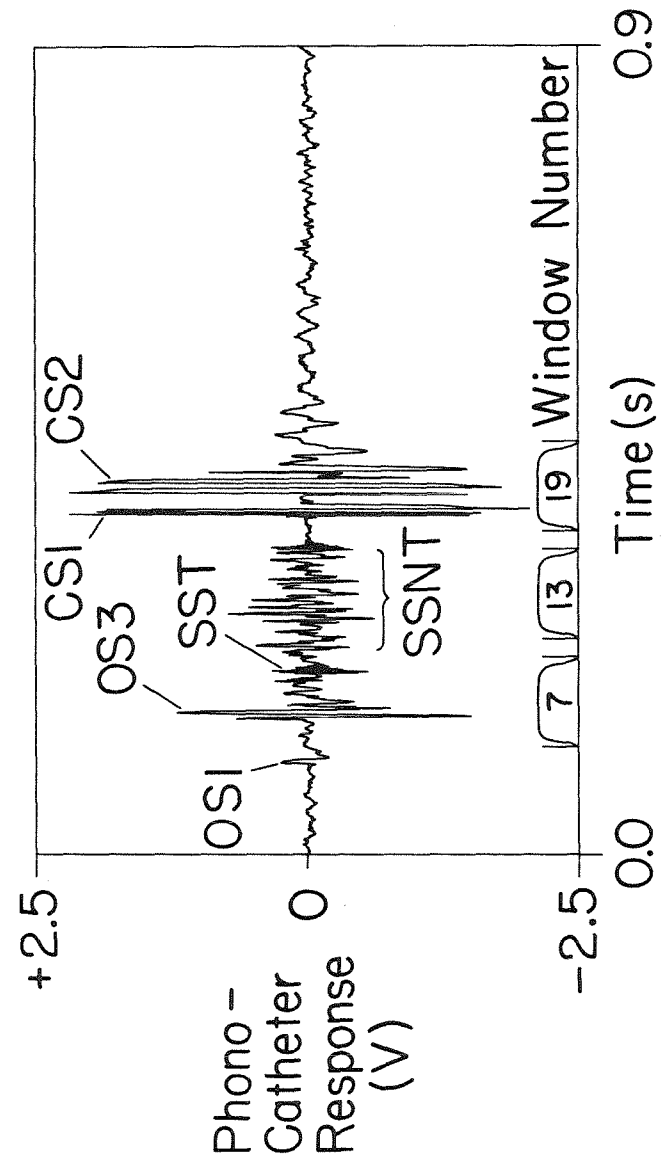

Figure 2-5b. Amplitude and time tracings of the sounds produced by the Starr-Edwards 2400 prosthesis operating at the NORMAL state *in vitro*: valve with simulated apical overgrowth.

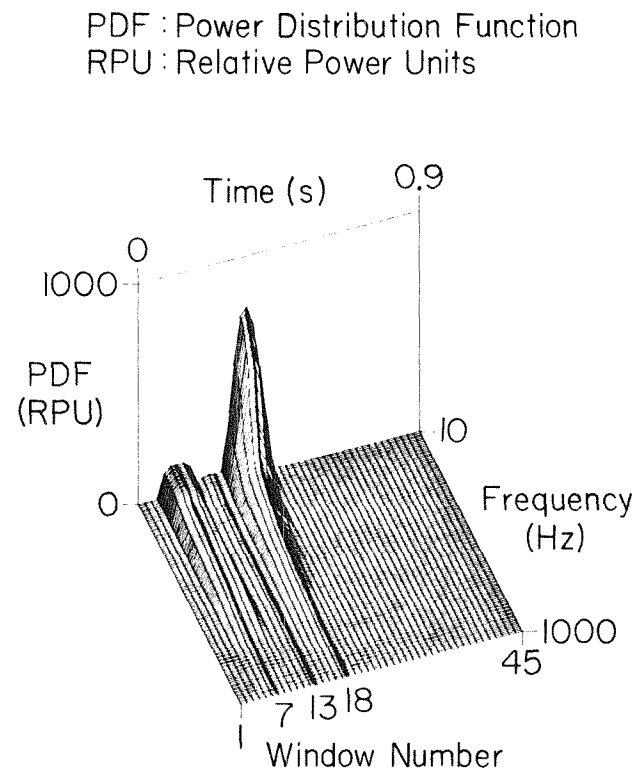

Figure 2-6a. Power-frequency-time surface depicting the power distribution in relative power units (RPU) averaged over ten typical cycles: normal valve.

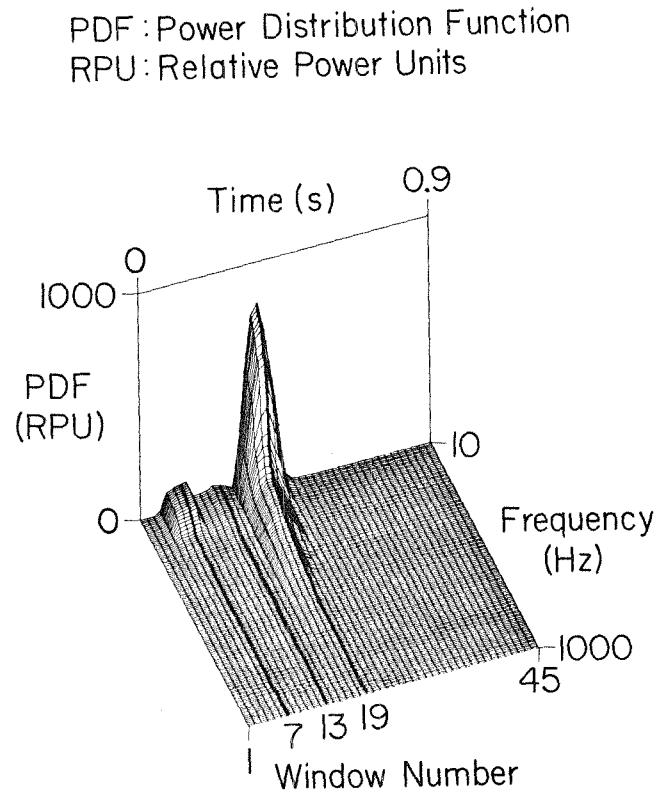

Figure 2-6b. Power-frequency-time surface depicting the power distribution in relative power units (RPU) averaged over ten typical cycles: valve with simulated apical overgrowth.

relative power unit is equivalent to the minimum power-density for the **PDS** of a typical 100-ms record of ambient background noise in the system. The conversion from relative power units to absolute power units can be determined if the gain of the heart-sound amplifier is known. By maintaining a fixed amplifier gain, however, the relative power units as presented in these results are equivalent to each other, and therefore, comparisons can be made among all experiments and figures in terms of RPU without converting to actual units. Sometimes it is convenient to have the computer generate two-dimensional plots corresponding to selected sectional views of the power-distribution surface. These sectional views can be generated parallel to either the time axis or frequency axis for any window number or frequency of interest. Figures 2-7a and 2-7b show the distribution of power plotted with respect to time for various iso-frequency contours for the two valves. The power level associated with the ordinate in these figures is that power that lies between the frequency associated with a particular contour and 1000 Hz. The contour with maximum power is that corresponding to the total power for that window, ie., the total power between frequencies 10 and 1000 Hz. The contour immediately below that is associated with the frequency band from 57 to 1000 Hz. The remaining contours are associated with bands having lower limits of integration of 104, 151, 198, etc., to 998 Hz in increments of 47 Hz. Table 2-2 lists the upper and lower frequency limits of each "band" for adjacent contours. These odd numbers are a result of the frequency resolution, 8.7 Hz, of the **FFT** for our setup and the fact that each "band" in Figure 2-7 is composed of 6 of these narrower bands.

Figures 2-8a, 2-8b, and 2-8c and 2-9a, 2-9b, and 2-9c show the power-density spectra (**PDS**) and normalized power-distribution functions (**PDF**), *i.e.* normalized with respect to the total power of each window, associated with three important windows for each condition of the valve, respectively. These three windows

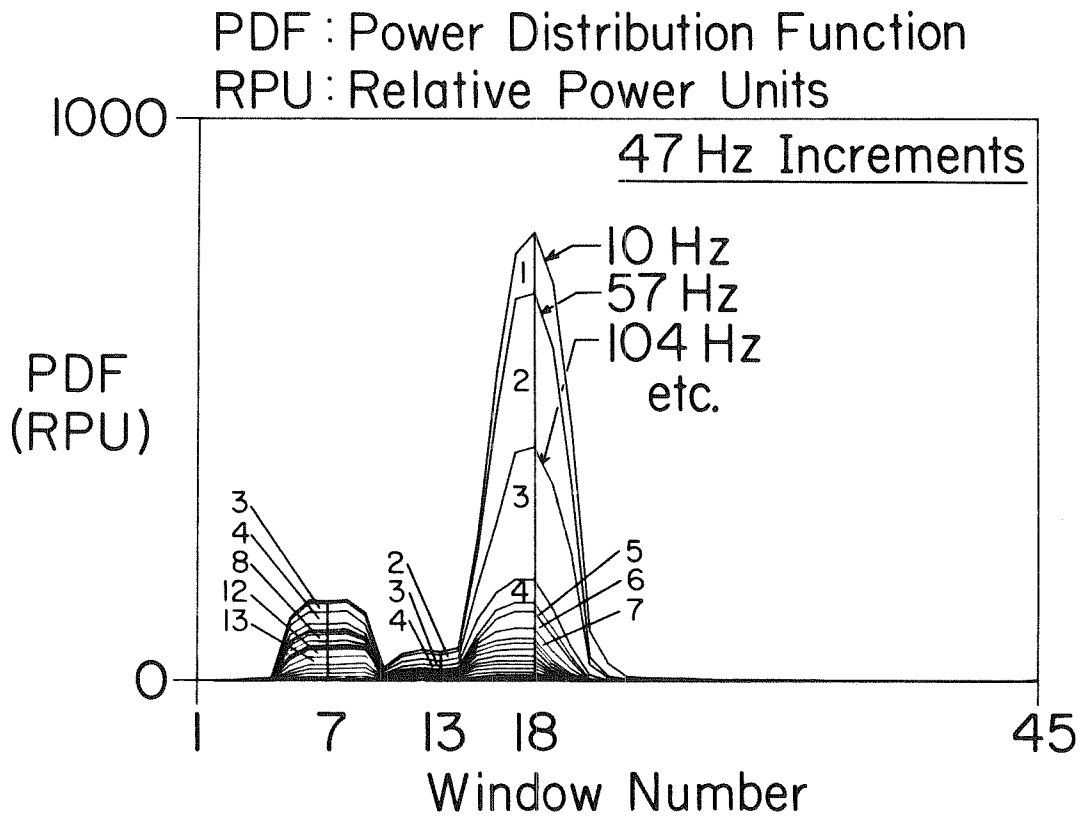

Figure 2-7a. Power distribution in relative power units (RPU) obtained by projecting every sixth frequency contour onto the power-time plane: normal valve.

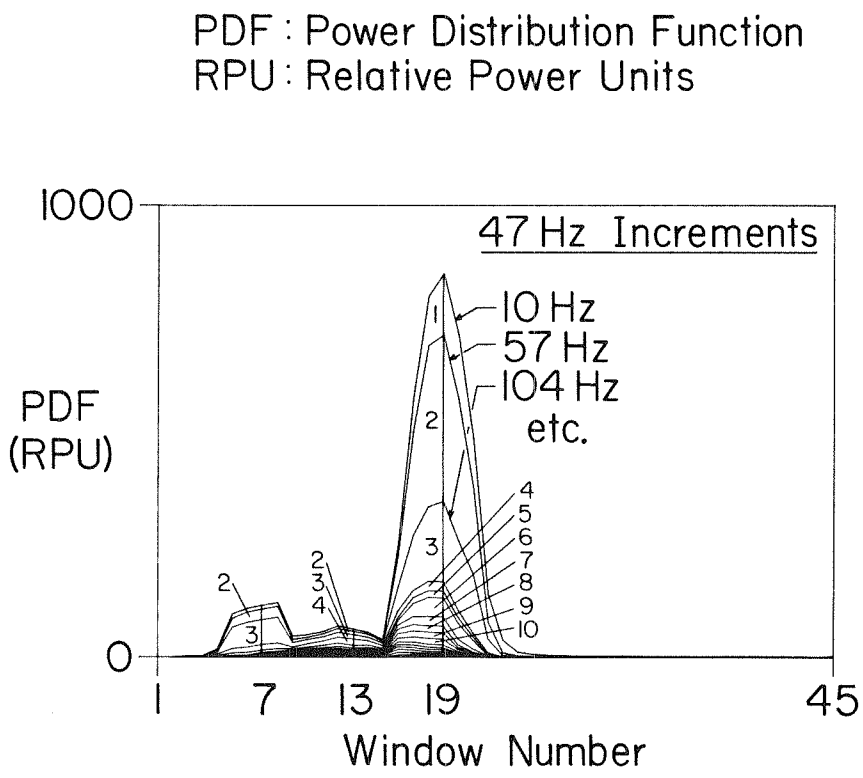

Figure 2-7b. Power distribution in relative power units (RPU) obtained by projecting every sixth frequency contour onto the power-time plane: valve with simulated apical overgrowth.

Table 2-2

Band Numbers

and Their Associated Frequencies

Band (Number)	Frequency Range (Hz)
1	10- 57
2	57-104
3	104-151
4	151-198
5	198-245
6	245-292
7	292-339
8	339-386
9	386-433
10	433-480
11	480-527
12	527-574
13	574-621
14	621-668
15	668-715
16	715-762
17	762-809
18	809-856
19	856-903
20	903-950
21	950-997

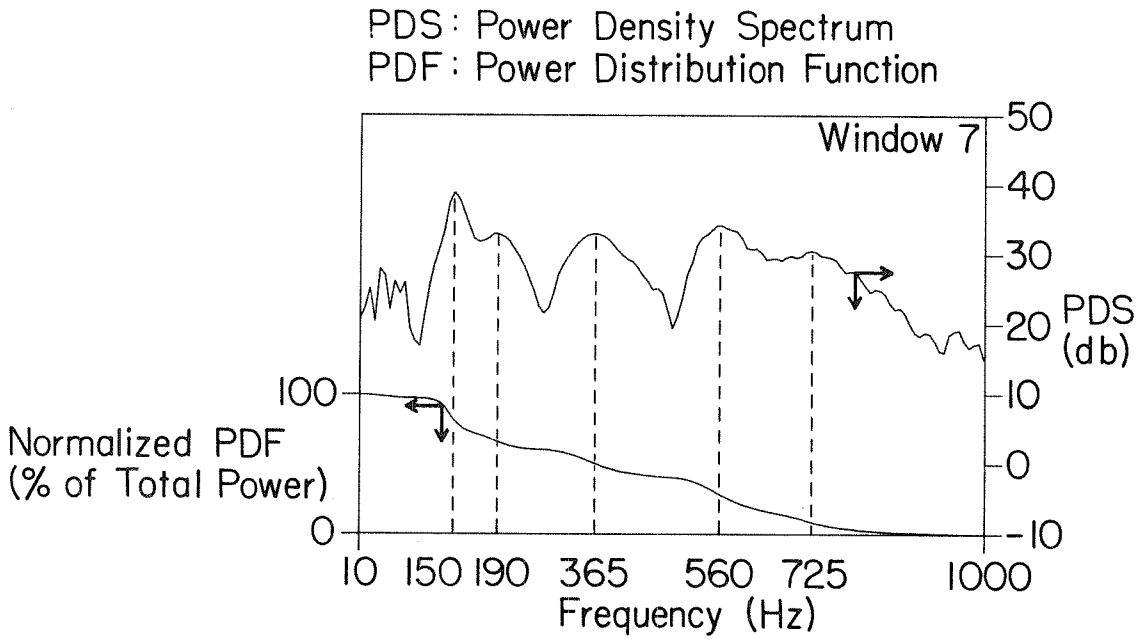

Figure 2-8a. Power-density spectra and normalized-power-distribution functions associated with the normal Starr-Edwards 2400 prosthesis: opening sound.

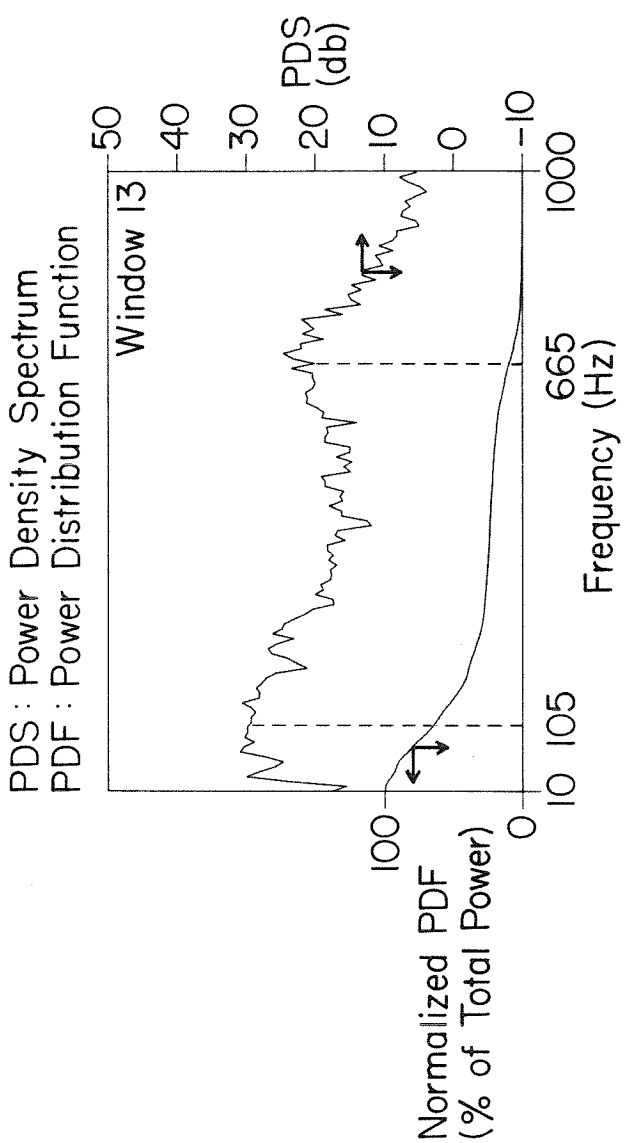

Figure 2-8b. Power-density spectra and normalized-power-distribution functions associated with the normal Starr-Edwards 2400 prosthesis: systolic sound.

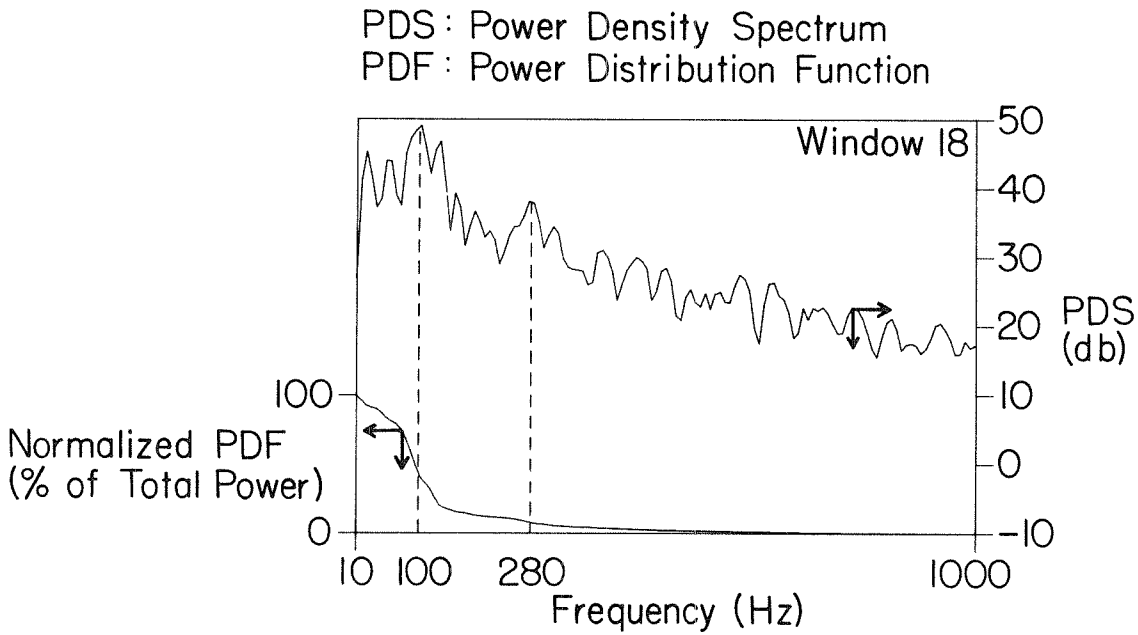

Figure 2-8c. Power-density spectra and normalized-power-distribution functions associated with the normal Starr-Edwards 2400 prosthesis: closing sound.

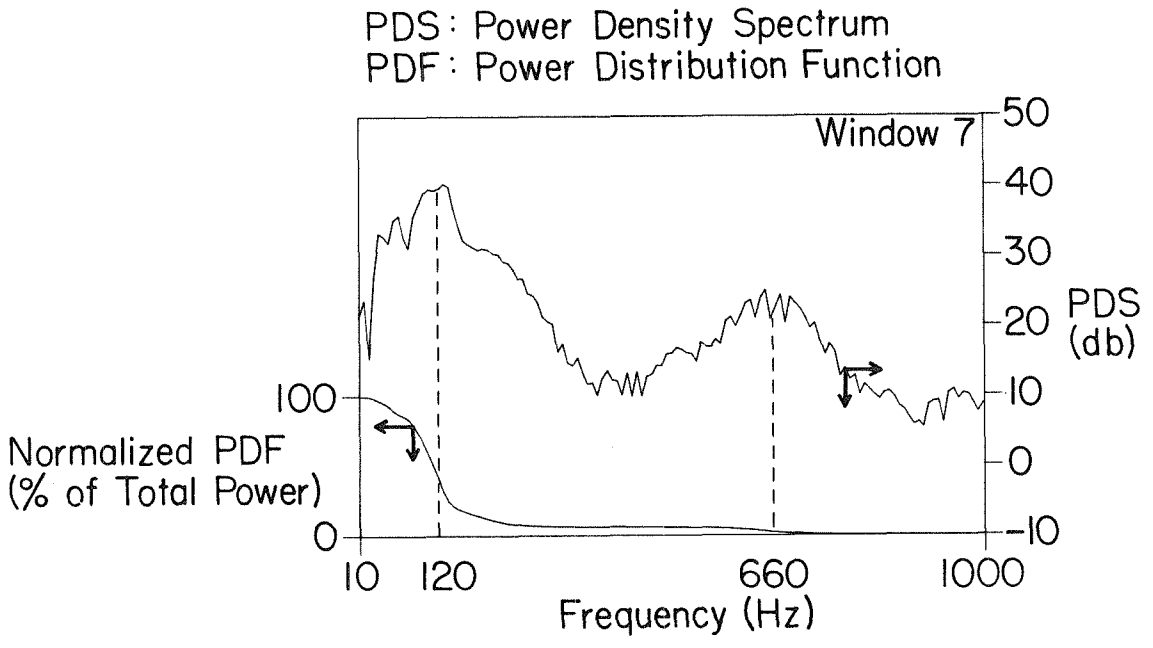

Figure 2-9a. Power-density spectra and normalized power-distribution functions associated with the Starr-Edwards 2400 prosthesis having the simulated apical growth: opening sound.

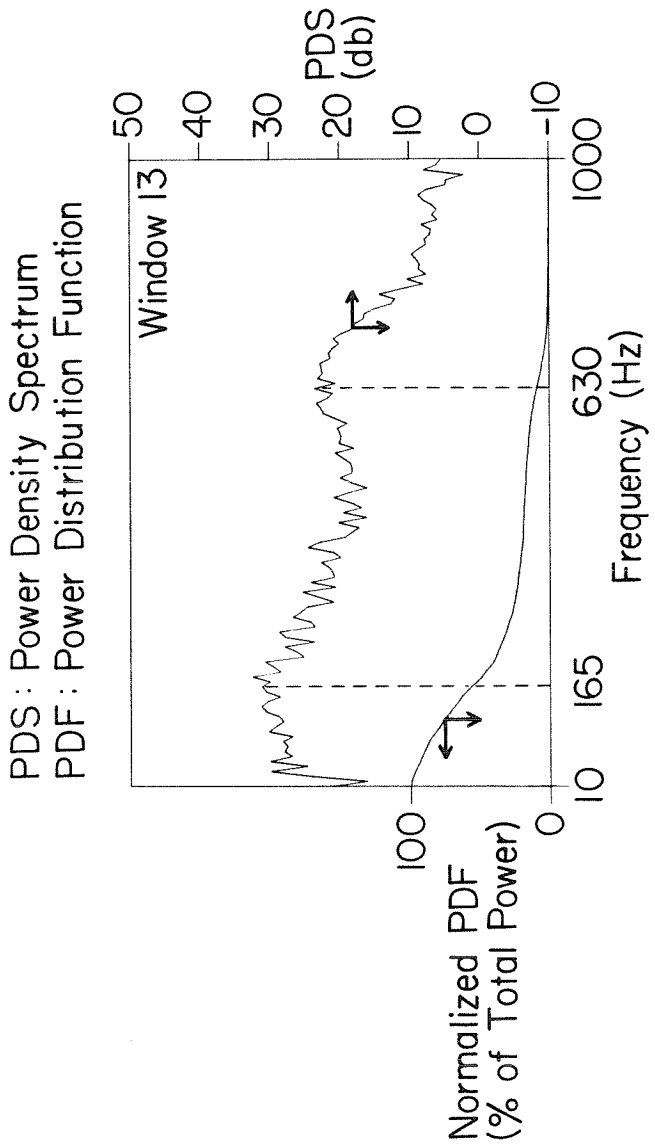

Figure 2-9b. Power-density spectra and normalized power-distribution functions associated with the Starr-Edwards 2400 prosthesis having the simulated apical growth: systolic sound.

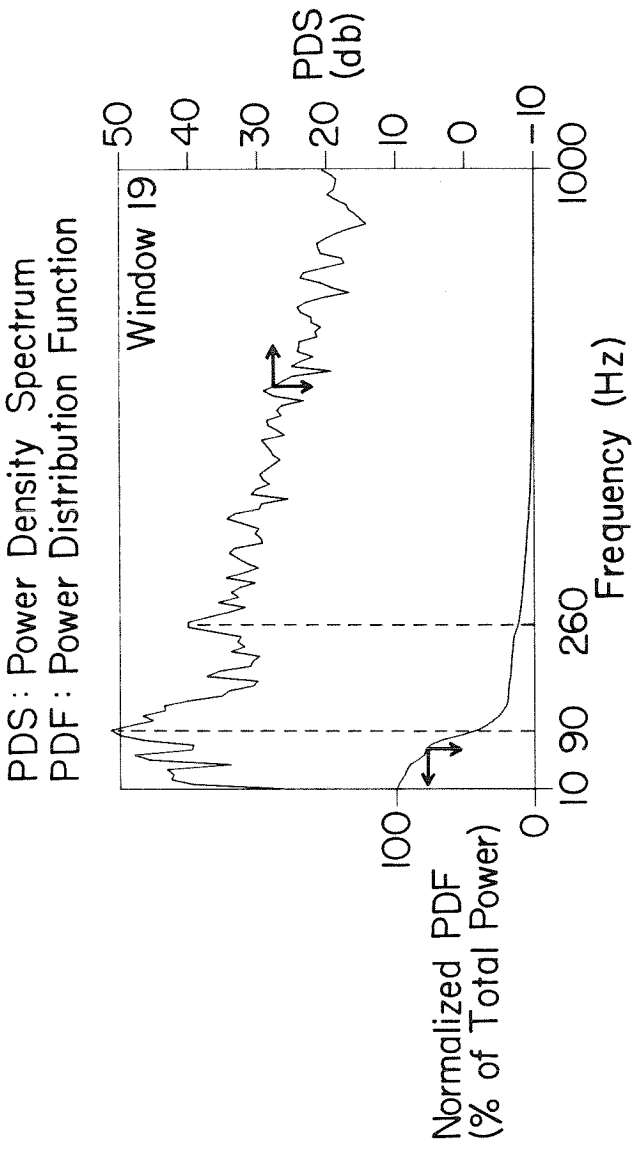

Figure 2-9c. Power-density spectra and normalized power-distribution functions associated with the Starr-Edwards 2400 prosthesis having the simulated apical growth: closing sound.

are the 100 ms windows which encompass the opening sound, systolic sound, and closing sound, respectively. The **PDS** is the top curve and is plotted in units of decibels relative to the average ambient sound level in the system. The **PDF** is plotted below the **PDS** on a basis of percent of total power for that window. Table 2-3 lists the parameters estimated for significant peaks that were found in the **PDS** shown in Figures 2-8 and 2-9. Finally, Figure 2-10 shows the comparison-surface associated with the distribution-surfaces corresponding to the normal and abnormal states of the valve.

2.4 DISCUSSION OF RESULTS

2.4.1 The Normal Starr-Edwards 2400 Prosthesis

The Starr-Edwards 2400 prosthesis is a caged-ball type of valve. The occluder, struts and orifice are made of Stellite. Three downstream struts are covered on their outer surfaces by teflon fabric. This fabric also provides the material of the sewing ring. The occluder rests in the open position against the inner surface of the apex of the cage where the three struts connect. It rests in the closed position against numerous, small Stellite supports which protrude slightly through the sewing cloth. If this fabric at these protusions becomes frayed, then backflow can occur, however, backflow is normally not present with this valvar design after the occluder has seated properly. The Starr-Edwards series 2400 (SE2400) prosthesis exhibits three major acoustical events when operating in a normal manner *in vitro*, *i.e.* **NORMAL** pulse mode and normal valve condition. These events will be called "opening" sound, "systolic" sound and "closing" sound.

Parameters Estimated for

Significant Harmonic Peaks

Event	Frequency,$f_{f,i}$; Decay, k_i; Power-density, G_i (Hz,Hz,db)	
	Starr-Edwards 2400 Normal	Starr-Edwards 2400 Abnormal
Opening Sound	150,16,38	120,27,40
	190,27,40	
	365,45,33	
	560,40,34	
	725,70,30	660,60,25
Systolic Sound	105,60,31	165,90,32
	665,80,24	630,80,24
Closing Sound	100,40,49	90,30,51
	280,30,38	260,25,40

Table 2-3 Parameters Estimated for Significant Harmonic Peaks of the Sounds of the Nomral and Abnormal Starr-Edwards 2400 Prosthesis.

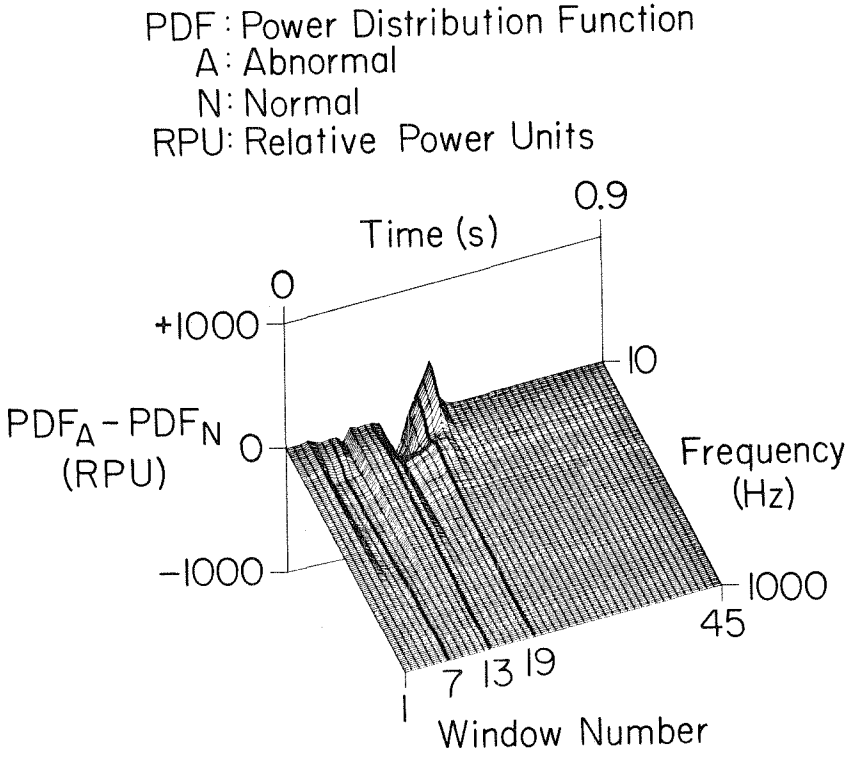

Figure 2-10. Power-frequency-time surface showing the power-difference in relative power units (RPU) generated by subtracting the surface associated with the normal prosthesis from that associated with the same valve but having the simulated apical overgrowth.

2.4.1.1 Response in the Time-Domain

In Figure 2-5a we see that the opening sound itself has three components corresponding to three different dynamic motions of the poppet. The first-component of the opening sound, OS1, is of low amplitude with a peak-to-peak voltage (vpp) of approximately 0.5 vpp. The frequency of the sound of this component is approximately 50 Hz. This sound corresponds in time with the poppet leaving the orifice. The second component of the opening sound, OS2, is another low-amplitude event with relatively high-frequency content of approximately 620 Hz. This component coincides in time with lateral collisions of the Stellite poppet with the Stellite struts as the occluder travels toward the apex of the cage. The third component of the opening sound, OS3, is a powerful opening "click". This sound is high in amplitude, 4 vpp, and has a high-frequency component of approximately 600 Hz.

The systolic sound occurs after the rapid decay of the third component of the opening sound and is coincidental with the systolic-flow period. This sound is actually a temporal overlapping of two components. One is transient and the other is non-transient. The transient component, SST, is similar in frequency to the second component of the opening sound and again is attributed to lateral and/or apical collisions between the occluder and the struts. Near 650 Hz, these "clicks" have a comparable frequency content, but they are much lower in amplitude than the third component of the opening sound. At the same time a low-frequency murmur, SSNT, is present. The amplitude of the total murmur is approximately 2 vpp.

The third major sound is the closing sound which has two components, CS1 and CS2. Both components have relatively large amplitudes of approximately 4.5 vpp. Unlike the opening sound, however, the frequency content for these

components is much lower and is approximately 130 Hz. These two events are attributed to bounces of the occluder analogous to the apical component of the opening sound, OS3, but in this case the bouncing occurs at the orifice. The etiology of the closing sound, however, differs from that of the opening sound in two ways, namely, (1) the geometry of the colliding surfaces is different and (2) the backward directed forces from pressure are larger across the valve. The latter condition produces greater decelerations of the occluder. There may be some non-linear effects occurring within the system during the production of these closing sounds.

2.4.1.2 Response in the Frequency Domain

The overall, power-distribution surface for the sounds just described is shown in Figure 2-6a. Windows 7, 13, and 18 have been enhanced for easier identification of those contours corresponding to windows encompassing the opening sound, systolic, and closing sound, respectively. In order to quantitatively estimate the power within various frequency bands we can either use scales together with Figure 2-7a or have the computer print the values of interest. For Figure 2-7a we have enhanced windows 7, 13, and 18, with vertical lines to identify those windows for which the **PDS** and **PDF** were individually plotted. The mean plus-or-minus standard deviation of total power for 10 cycles for windows 7, 13, and 18 are 141± 8, 52± 31, and 798± 39 relative power units (RPU), respectively. Table 2-4 lists these values. We will now examine the sounds within each of these three windows in detail.

Referring to the opening sound, as represented by window 7 in Figure 2-7a, five bands have power exceeding 10 RPU. These bands are numbers 3, 4, 8, 12, and 13. Here we are using the numbering sequence listed in Table 2-2. If we now

Statistics for the Total Power

Associated with Specific Windows

in Relative Power Units (RPU)

Valve	Mean Total-Power ± std. dev.		
	Opening Sound	Systolic Sound	Closing Sound
Normal Starr-Edwards 2400	141± 8	52± 31	798± 39
Abnormal Starr-Edwards 2400	115± 5	63± 32	850± 34

Table 2-4 Statistics for the Total Power Associated with Specific Windows in Relative Power Units (RPU) for the Sounds of the Normal and Abnormal Starr-Edwards 2400 Prosthesis.

examine the **PDS** for window 7 in Figure 2-8a, we see that there are resonance peaks centered at 150, 190, 365, 560, and 725 Hz. The **PDF** possesses obvious inflection points at these frequencies. The information is essentially the same, yet different views of this information are often useful in practice, and it is helpful to become acquainted with at least these two views and to be able to quickly interpret density spectra in terms of distribution functions. It will generally be best to examine both the **PDS** and **PDF**.

Referring again to the systolic sound, window 13 in Figure 2-7a, we see three bands with powers greater than 5 RPU. These bands are numbers 2, 3, and 4. When we examine the **PDS** in Figure 2-8b, we find a broad peak centered at 105 Hz corresponding with these bands. Another peak at 665 Hz corresponds to the relatively wide bands, 13 and 14, in Figure 2-7a. The **PDF** possesses two general inflection points near frequencies of 150 and 660 Hz.

Finally, the closing sound, window 18 of Figure 2-7a, has seven bands with powers greater than 10 RPU. These bands are numbers 1, 2, 3, 4, 5, 6, and 7. Bands 1, 2, 3, 4, and 6 have powers greater than 30 RPU. These more powerful bands encompass peaks at 100 Hz and 280 Hz in the **PDS** as seen in Figure 2-8c. These two peaks correspond in frequency to inflection points in the **PDF**. The inflection at higher frequency has a smaller slope than the inflection at lower frequency because the power-density is much less at that frequency. It is very important to remember that the **PDS** is being plotted on a logarithmic scale (db), and the **PDF** is generated from corresponding linear values and plotted on a linear scale. A 3-db rise in the **PDS** corresponds to a doubling of the actual value of the power-density.

2.4.2 The Starr-Edwards 2400 Prosthesis With Simulated Apical Overgrowth

A photograph of the actual valve used for this study is shown in Figure 2-4. We expected to see changes in the opening sound and possibly the murmur as compared to the normal valve. This simulation also changed the frequency content of the closing sound. Table 2-5 lists the effective area of flow for the normal and abnormal valve calculated using the standard orifice equation, the peak systolic flow rate and peak systolic pressure gradient.

2.4.2.1 The Response in the Time Domain

The opening sound depicted in Figure 2-5b has a similar first-component, OS1, as the normal Smeloff valve. The second component is absent. The third component, OS3, is significantly different in amplitude and frequency. These three observations suggest that the occluder leaves the orifice in a normal fashion, travels downstream with fewer lateral collisions, and strikes the apex producing sounds having different amplitude and frequency than those of the normal valve.

The systolic sound is greater in overall amplitude than compared to normal. This change is due to the change of flow as indicated by the reduced area of effective flow. The number of transient events, or sounds, SST, has been reduced.

The closing sound exhibits a bounce, but now the first event, CS1, is greater in frequency. If the closing sound is in part produced by the pinching off of back flow through the valve, this change could indicate that the closure was asymmetric. The closing sound occurs later than that for the normal case. This delay could be due to a reduction in viscous shear at the surface of the occluder

Effective Flow Areas for the Normal Starr-Edwards 2400 Prosthesis and the Same Valve Having Simulated Apical Overgrowth

Valve	Effective Flow Area (cm^2)
Normal Starr-Edwards 2400	2.85
Abnormal Starr-Edwards 2400	2.46

Table 2-5 Effective Flow Areas for the Normal Starr-Edwards 2400 Prosthesis and the Same Valve Having Simulated Apical Overgrowth.

due to flow perturbations created by the apical overgrowth or from sticking of the apical overgrowth with the occluder.

2.4.2.2 The Response in the Frequency Domain

A distribution-surface based on abnormal sounds is shown in Figure 2-6b. The opening sound is seen to have significantly less power in the high-frequency range than in the normal case. The systolic sound is now more powerful overall. The closing sound is similar in shape, but the window containing the maximum total-power is delayed by 20 ms. The total power associated with windows 7, 13, and 19 are 115± 5, 63± 32, and 850± 34 RPU, respectively. If we examine Table 2-4 we see that the total power of the murmur and closing sounds, respectively, is not significantly different from the normal cases. The opening sound is different by a statistically significant amount.

The opening sound, as represented by window 7 in Figure 2-7b, has two bands with power greater than 10 RPU. These band numbers are 2 and 3. Two peaks occur in the **PDS** shown in Figure 2-9a. They are centered at 120 and 660 Hz. Here is a clear case for which we can confidently assign a specific resonance peak to a specific vibration of the valve. The peak at 120 Hz is related to the occluder striking the simulated overgrowth. The peak at 660 Hz is related to the occluder striking the stellite struts. The normal peaks at 365 Hz and 560 Hz have now virtually disappeared. The **PDF** shows two significant inflection points at 120 and 660 Hz. Here we can see the effect that a 15db difference between peaks of the **PDS** will have upon the slopes at the inflection points of the corresponding **PDF**.

The systolic sound, as represented by window 13 in Figure 2-9b, is similar to that for the normal prosthesis. Band numbers 2, 3, and 4 for window 13 have

power exceeding 5 RPU and bands 13 and 14 have power of 3 RPU. These bands correspond to the two broad peaks in the PDS and two inflection points in the PDF shown in Figure 2-9b. Generally speaking the power density over most of the 100-600 Hz range is 1-2 db greater for the abnormal valvar murmur. This explains the 10 RPU increase in the averaged total-power. This difference is more clearly evident by inspecting Figures 2-8b and 2-9b, and can also be seen by inspecting the numerical values in this frequency band. Inspection of the two peaks near 660 Hz in Figures 2-8b and 2-9b shows a decrease in the center frequency for the abnormal valve. This observation suggests that the transient component of the systolic sound, caused by collisions of the occluder with the struts, has a greater effective mass. The center frequency of the peak power-density of the non-transient component has increased, which again suggests that the turbulent intensity increased as a result of a decrease in the effective area of flow.

The closing sound of the abnormal valve, as represented by window 19 in Figure 2-7b, is similar to that of the normal valve. Band numbers 1-10 for window 19 have power exceeding 10 RPU. Bands 6 and 7 possess significantly greater power as compared with the bands for the normal case. Differences of power between the two valves are evident for bands 2, 3, and 6 as seen by comparing windows 18 and 19 of Figures 2-7a and 7b, respectively. This difference can also be seen by inspecting the two PDS shown in Figures 2-8c and 2-9c at frequencies near 100 Hz and near 260 Hz where the abnormal closing sound has an additional power-density of 2 db. The values of the total power of the closing sounds for the two cases, as listed in Table 2-4, are significantly different. Finally, the abnormal closing sound is delayed by 20 ms as compared to that of the normal valve.

2.4.3 Examination of Differences Using a 3D-Difference Surface

A synopsis of the overall differences between the sounds produced by the normal and abnormal valves is conveniently conveyed by examining the 3D, difference-surface developed by subtracting the normal power-distribution surface from the abnormal. Figure 2-10 is that surface for the two valvar conditions we have been examining. This surface is a plane with a power distribution of zero when the power distributions associated with each case for a given frequency and window are identical. A negative value means that the abnormal case has less power for that window for frequencies greater than the frequency at that point and less than 1000 Hz. Similarly, a positive value means the abnormal case has more power for that window for frequencies greater than the frequency at that point and less than 1000 Hz. Because the slope of the distribution surface parallel to the frequency axis is proportional to the **PDS** at that frequency, another way of looking at this difference surface is by noting that a positive slope occurs at frequencies where the normal **PDS** is greater than the abnormal **PDS** and that a negative slope occurs at those frequencies where the normal **PDS** is less than the abnormal **PDS**. Slopes have been defined with respect to the positive direction of the frequency axis.

The major change in the opening sound was the decrease of the frequency content of its third-component, the opening click, near 660 Hz. This difference is clearly displayed in Figure 2-10 by the negative values for frequencies less than 660 Hz and by the positive slope at 660 Hz for the contour corresponding to window 7.

For the systolic sound the most noticeable change was the greater power-density for all frequencies. This difference is clearly displayed in Figure 2-10 by window 13 which has positive values and a negative slope over the entire

bandwidth from 10 to 1000 Hz.

One major change in the closing sound was a delay of this event with respect to the opening sound. This difference is clearly displayed in Figure 2-10 by the tall, valley-peak structure along the 10-Hz contour between windows 15 and 23. Redistribution of power in bands 2, 3, and 6 can also be seen by the undulation of the window-19 contour between 80 and 250 Hz.

In sum, the comparison between the power distributions for the normal and abnormal valves displays what we anticipated. Differences are immediately evident from valleys or peaks. We have also been able to extract information from the location and shape of these structures. By relating the **PDS** and **PDF** of the original surfaces to the difference-surface we have analyzed changes over the entire cardiac cycle in terms of the differences between power-distribution surfaces.

2.4.4 Comparisons Between Harmonic Model Parameters

The next point to be discussed is the estimation of the gain, Γ_i , decay, κ_i, and free frequency, $\omega_{f,i}$, for the **PDS** depicted in Figures 2-8abc and 2-9abc. These parameters have been estimated graphically from Figures 2-8abc and 2-9abc. Phase parameters will not be presented. Table 2-3 lists the results of this estimation. Entries are for peaks within each **PDS** for which estimation was relatively easy. The table entries in order correspond to the frequency, $f_{f,i}$, decay, k_i, and gain, G_i , parameters associated with peak i and having units of Hz, Hz, and db, respectively. These table entries are related to the acoustical parameters defined in Paper I by the following relations:

$$f_{f,i} = \frac{\omega_{f,i}}{2\pi}, \tag{2-1}$$

$$k_i = \frac{\kappa_i}{2\pi} \tag{2-2}$$

and,

$$G_i = 20 \log \left(\frac{\Gamma_i}{4\pi R_{RPU} \kappa_i \omega_{f,i}} \right). \tag{2-3}$$

The entry corresponding to the power-density, G_i, has been normalized with respect to R_{RPU} which is the minimum value of the power density over the band 10 to 1000 Hz associated with a typical 100-ms window encompassing ambient noise in the system. This reference value was identical for each **PDS**. We also set the value R_{RPU} = 1RPU. Thus the value of Γ_i estimated using Equation 2-3 has units of RPU/s^2.

The normal opening sound has five distinct peaks centered between 150 and 725 Hz as opposed to the two peaks for the abnormal valve centered at 120 and 660 Hz. There is an obvious loss of power at frequencies of 220, 375, and 575 Hz and a possible shift of the two remaining peaks to lower frequencies for the abnormal valve. The abnormal peaks at 120 Hz and 660 Hz possess 2 db more power and 5 db less power, respectively, than the nearest corresponding normal peaks having greater center-frequencies. A shift to lower frequencies is predicted by Equation 1-7 when the effective damping parameter, κ_i, increases while the mass-specific stiffness coefficient, $\frac{K_i}{M_i}$, remains constant. If $\frac{K_i}{M_i}$ should decrease due to either a decrease in stiffness or an increase in mass of that mode while the mass-specific viscous coefficient remains constant, the free frequency would also decrease. If we assume that the 720-Hz peak for the normal valve and the 660-Hz peak for the abnormal valve result from the same vibrational mode of the valve, say the vibration of the struts, we can estimate the

relative changes occurring in D_i and M_i for constant K_i using Equations 1-35, 1-36, and 1-40 in Part I of this series. We find that a broadening and lowering of frequency for any given peak predicts an increase in M_i and an increase in D_i. For this case our model has predicted additional mass associated with the simulated overgrowth and an increase in damping also due to the simulated overgrowth.

The systolic sound in each case has two distinct peaks, one near 100 Hz and another near 650 Hz. The peak at lower-frequency has been associated with turbulence, and the peak at higher-frequency has been associated with collisions of the occluder and struts. The change in the peak associated with turbulence is toward a higher-frequency. This result is probably due to a change in the eddy distribution in the flow. As we mentioned in the Part I, we can attribute changes in these parameters that we have estimated for the murmur to changes in the turbulent-eddy distribution and/or resonance of the aortic chamber. For this present comparison the latter effect is non-changing. The peaks located at 665 Hz for the normal valve and at 630 Hz for the abnormal valve can be discussed in terms of the transient model. Again, if we assume these peaks result from the same mode of vibration and we also assume that the stiffness coefficient remains constant, then, using Equations 1-35, 1-36 and 1-40, in Part I, we find that the acoustical parameters predict a mass increase and an increase in the effective damping for the abnormal Starr-Edwards 2400 valve. The center frequency of the low-frequency peak for the abnormal case is 165 Hz as compared to the normal value of 105 Hz. The broadening of the low-frequency portion of the spectrum is indicative of an increase in the turbulence intensity and indicates a corresponding decrease in the effective-flow area of the valve due to the apical overgrowth.

The PDS of closing sounds for the two valves are similar, and we do not predict any changes in the modes associated with these sounds. This result is consistent with the fact that nothing has changed relative to the mechanical properties of the structures involved in this acoustical event which is the collison of the occluder with the orifice.

2.5 CONCLUSIONS

The development of a systematic, digital analysis of valvar sounds has been described for an *in vitro* comparison of a normal and an abnormal condition of a Starr-Edwards 2400 aortic valve design. The comparisons were presented and discussed in terms of time-amplitude plots, power-density spectra, power-distributions, three dimensional, power-distribution surfaces, physical parameters estimated for a simple acoustic model, and finally by a three-dimensional, power-difference surface.

The Starr Edwards 2400 aortic prosthesis produced an opening sound, systolic sound, and closing sound during each cardiac cycle for each of the two valvar conditions. The valve lost significant amounts of power in the 600-Hz range of its opening sound when overgrowth was simulated at the inner apical surface. The abnormal valve produced a more powerful systolic murmur, and it possessed a 14% smaller effective-flow area calculated from peak-systolic-flow and pressure-drop data. The systolic murmur possessed greater power densities over the entire 10 to 1000 Hz range. The abnormal closing sound was delayed approximately 40 ms. It also possessed more power for frequencies between 200 to 400 Hz while having less power near 120 Hz. All of these differences were observed through the three-dimensional, power-distribution-difference surface.

We believe the method we have described offers a generally applicable method

for comparison and evaluation of valvar sounds. Both rapid qualitative comparisons and detailed quantitative comparisons can be made depending on the particular need of the analyst. The detail that can be achieved by examination of the spectra has only begun to be understood. When sufficient amounts of comparative data have been stored in a data bank, estimation of acoustical parameters may one day offer one of the most accurate non-invasive methods for characterizing heart-valve integrity *in vivo*.

2.6 RECOMMENDATIONS

Recommendations regarding the theoretical and experimental apects of this study are presented in Paper III of this series.

2.7 ACKNOWLEDGEMENTS

Funding for this project was provided by the Donald E. Baxter Foundation, the Children's Heart Foundation of Southern California, and the American Heart Association, Greater Los Angeles Affiliate.

2.8 NOMENCLATURE

Nomenclature

D_i	Damping coefficient, kg/s
$f_{f,i}$	Frequency of damped oscillations of mode i, Hz
G_i	Gain associated with power density spectrum, db
K_i	Stiffness coefficient, kg/s^2
k_i	Decay frequency, Hz
M_i	Inertial coefficient, kg
PDF	Designates power distribution functions
PDS	Designates power density spectra
R_{RPU}	Reference value for power-density spectrum, RPU
RPU	Designates dimensions of relative power units
vpp	Designates dimensions of volts peak-to-peak
Γ_i	Gain parameter associated with mode i, RPU/s^2

κ_i Decay parameter of mode i, rad/s
$\omega_{f,i}$ Frequency parameter of damped oscillations of mode i, rad/s

Subscripts

f Indicates value associated with frictional loss of energy
i Indicates value associated with mode number i
j Indicates value associated with impulse number j

PAPER 3

A Quantitative Method for the *In Vitro* Study of Sounds Produced by Prosthetic Aortic Heart Valves Part III: An Experimental Comparative Study of the Sounds Produced by Normal and Simulated-abnormal Smeloff Aortic Prostheses

A Quantitative Method for the *In Vitro* Study of Sounds Produced by Prosthetic Aortic Heart Valves

Part III: An Experimental Comparative Study of the Sounds Produced by Normal and Simulated-abnormal Smeloff Aortic Prostheses

ABSTRACT

An *in vitro* study was made of the sounds produced by a normal, Smeloff-aortic-valve prosthesis and compared for the entire cardiac cycle with the same valve having a simulated overgrowth on the upstream struts. Time and amplitude information, power-density spectra, power-distribution functions, and 3-D, power-frequency-time surfaces were compared. Power-density spectra and power-distribution functions were compared in more detail for those portions of the cycle corresponding to the opening, systolic, and closing sounds of the valve. Parameters for the acoustical model were estimated from these power-density spectra. All results were then compared and discussed in terms of the physical changes in the valve.

Each comparison gave useful information about the simulated malfunction. Opening, systolic, and closing sounds were different for each case. More power was displayed in the opening sound of the abnormal valve, and the systolic sound was early. The closing sound of the abnormal valve had a lower frequency content, and a diastolic sound was observed only for the abnormal valve. Use of the frequency domain gave additional understanding of differences in performance.

Key Words- Smeloff prosthesis, sound, fast Fourier transform *in vitro* comparison

3.1 INTRODUCTION

Papers I and II in this series of three papers described, in order, the basic principles of sound analysis in heart-valve studies and the analysis of sounds in an *in vitro* study of a Starr-Edwards 2400 aortic prosthesis. This present paper presents a similar study of a Smeloff aortic prosthesis. A description of the pulse duplicator and the experimental method used to obtain the present results was provided in Part II of this series.

3.2 RESULTS

The same basic Smeloff valve was studied for both the normal and abnormal condition. Its mounting diameter was 24 mm. Two valvar conditions were studied, namely, the normal valve and the same valve having a simulated overgrowth which perturbed the poppet motion. The simulated overgrowth for the Smeloff valve was located on each of the three upstream struts as seen in Figure 3-1. The overgrowth was simulated by applying silicone-rubber gel on each strut and allowing it to set.

Comparisons are similar to those presented in Paper II for the Starr-Edwards 2400 valve; as a result, comparisons can also be made between the results presented in the present paper and those in Paper II because the experimental method was the same for each study. Comparisons should be made between all of the analogous figures in Papers II and III. In the following discussion we will primarily focus on the results related to two conditions of the Smeloff valve.

3.3 DISCUSSION OF RESULTS

3.3.1 The Normal Smeloff Prosthesis

The normal Smeloff valve is of the caged-ball variety. The spherical occluder is made of a silicone rubber polymer. Two sets of struts, three upstream and three downstream, are made of Stellite as well as the orifice. Teflon cloth provides the material for the sewing ring. The diameter of the occluder is generally from 0.004 to 0.009 inch less than the diameter of the orifice. This design feature allows backflow during diastole through the resulting annular gap that is normal for this valvar design. When fully open the occluder is checked from further motion downstream by the downstream struts and when closed its motion is checked by the upstream struts in such a way that the equator of the occluder resides at the orifice. Neither set of struts of the Smeloff valve meet to form an "apex".

3.3.1.1 Response in the Time Domain

The Smeloff prosthesis exhibits four major acoustical events when operating in a normal manner *in vitro*. These events are an opening, systolic, closing and diastolic sound. The time-amplitude tracing shown in Figure 3-2a clearly indicates these four events.

The opening sound has two components. The first-component of the opening sound, OS1, is very similar to that we have observed for the Starr-Edwards 2400 prosthesis. It is low in amplitude, 0.4 volt peak-to-peak (vpp), and has a lower frequency content as compared to the second component. The second component of the opening sound, OS2, is greater in amplitude and frequency as compared to the first component. The origins of these two sounds correspond

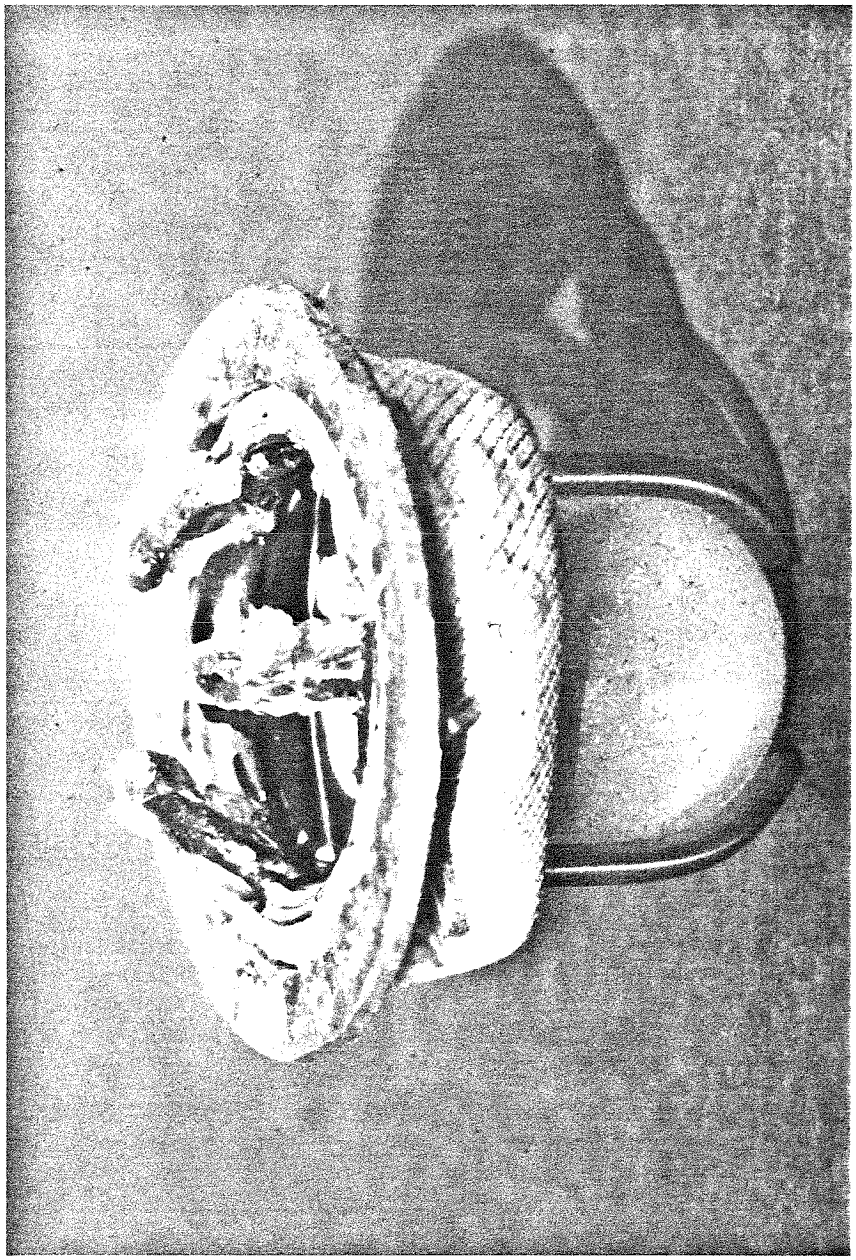

Figure 3-1. Photograph showing the Smeloff prosthesis studied for the case having a simulated overgrowth on all three upstream struts.

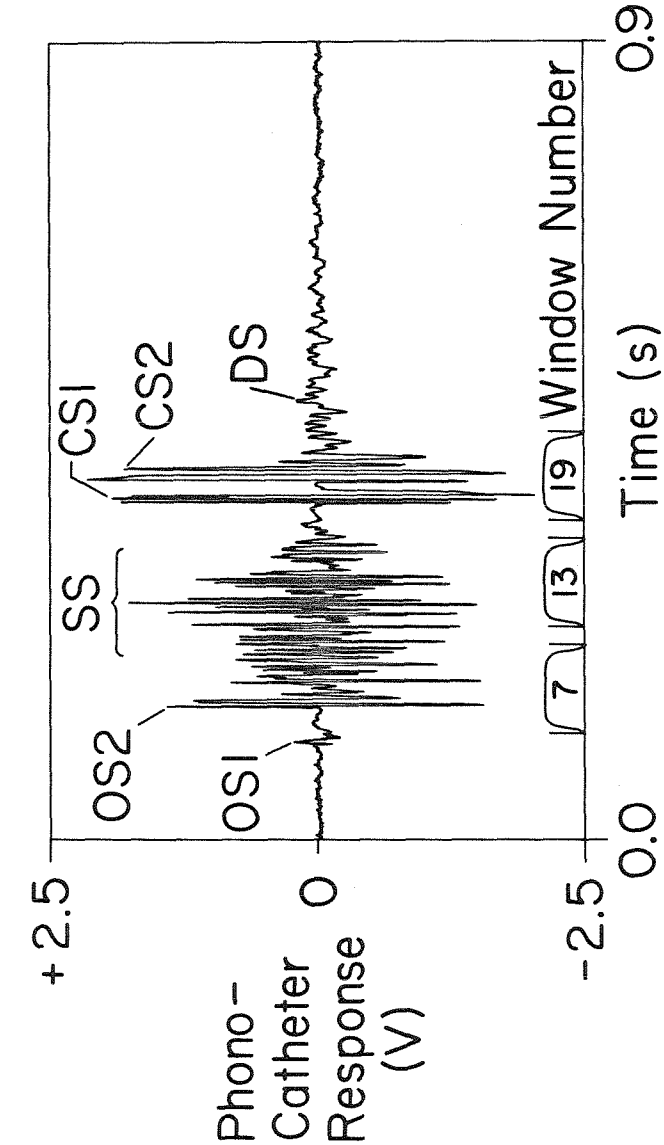

Figure 3-2a. Amplitude and time tracings of the sounds produced by the Smeloff prosthesis operating at the NORMAL state *in vitro*: normal valve.

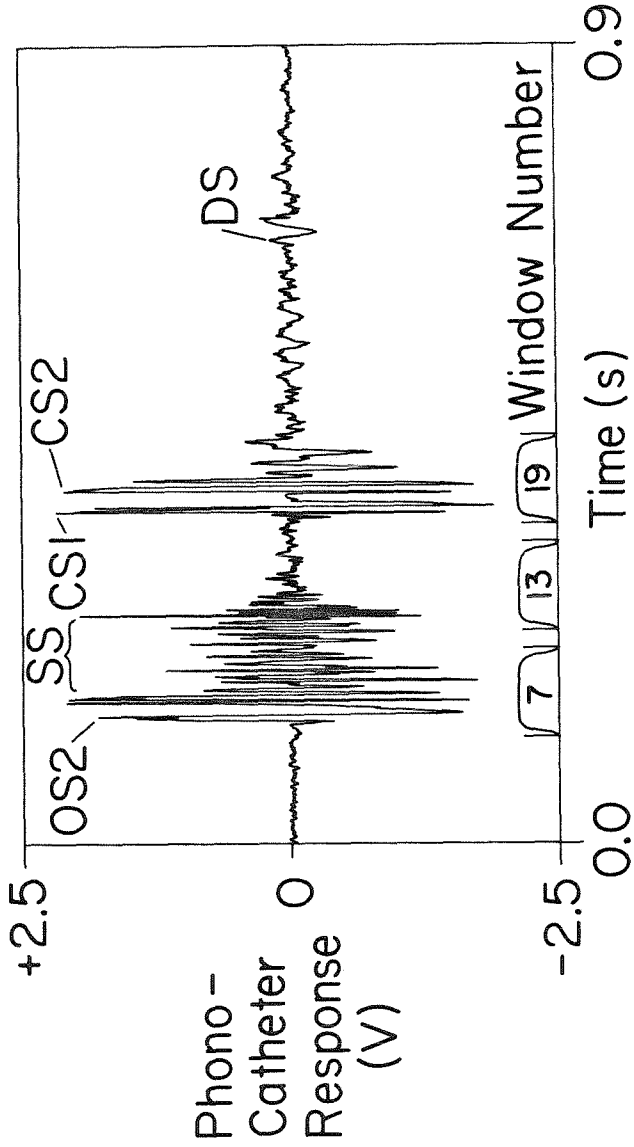

Figure 3-2b. Amplitude and time tracings of the sounds produced by the Smeloff prosthesis operating at the NORMAL state *in vitro*: valve with simulated overgrowth on all three, upstream struts.

to the times when the occluder leaves the orifice and when it strikes the cage extremities, respectively.

One can see from Figure 3-2a that the systolic sound, SS, begins before the complete decay of the second component of the opening sound. In this respect it appears to occur earlier than the systolic sound for the Starr-Edwards 2400 prosthesis as can be seen by comparing Figure 3-2a with Figure 2-5a in Paper II. The systolic sound of the normal Smeloff valve characterized by window 13 has significantly greater amplitude than that for the Starr-Edwards 2400 prosthesis. This systolic sound is also a superposition of transient sounds produced by occluder/strut collisions and a non-transient murmur produced by turbulence. The transient components of the systolic sound of the Smeloff valve are comparable in frequency to the murmur and are not distinctly seen in the time and amplitude tracings as they were for the Starr-Edwards valve.

The closing sound is high in amplitude, 4 vpp, and has two components. The first component, CS1, has a high center-frequency content and the second, CS2, a lower center-frequency. The closure mechanism is different for the Smeloff valve than for the Starr-Edwards 2400 prosthesis. We believe that it is this difference between seating mechanisms that is primarily responsible for the high-frequency sounds for the normal Smeloff valve. The first component of closure is probably produced by the "pinching off" of the reverse-annular jet just prior to valvar closure. This first component of the closing sound of the Smeloff valve is similar to that of the abnormal Starr-Edwards 2400 valve. Thus, it appears that a sound that is normal for one valvar design may be similar to that which is abnormal for another design. The second component of the closing sound is produced by rebound of the occluder in the vicinity of the orifice.

The early NT diastolic sound, DS, is produced by backflow. This sound was louder when measured upstream.

3.3.1.2 Response in the Frequency Domain

The overall, power-distribution surface for the sounds just described is shown in Figure 3-3a. Windows 7, 13, and 19 have been enhanced for easier identification of those contours corresponding to windows encompassing the opening, systolic, and closing sounds, respectively. It shows an asymmetric peak at lower frequencies for window numbers from 3 to 15 corresponding to the opening/systolic complex. The peak corresponding to closure is more symmetric and has greater power than this opening/systolic complex. This opening/systolic complex is quite different from the corresponding opening and systolic peaks generated for the Starr-Edwards 2400 valve. It results from the early systolic sound. The closing sound is more similar to that of the Starr-Edwards 2400 valve.

Examination of the projection of the power-distribution surface upon the power-time plane shown in Figure 3-4a, the opening-sound, window 7, shows a total power of 247 RPU with bands 2 to 7 each having power greater than 10 RPU. Table 3-1 lists the mean and standard deviation of the total-power associated with the special windows for this valve as well as the abnormal valve. Table 2-2 of Paper II provides the values of the frequencies associated with specific "band numbers". The standard deviation of the total power of window 7 based on ten cycles was 30 RPU. The power-density spectrum (PDS) depicted in Figure 3-5a shows broad peaks at 130, 250, and 600 Hz. The peak at 600 Hz is interesting in that it was not readily predictable from the time-amplitude plot. The power-distribution function (PDF) exhibits inflections at each of these three frequencies. The major difference between this opening sound and those of both the normal and abnormal Starr-Edwards 2400 valve is that the total-power associated with window 7 is significantly greater for the normal Smeloff valve.

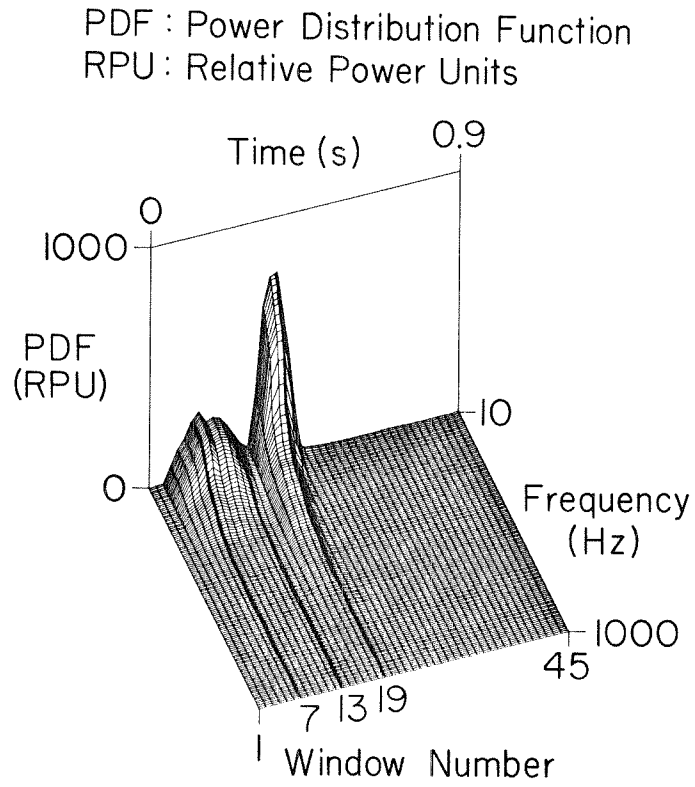

Figure 3-3a. Power-frequency-time surface depicting the power distribution in relative power units (RPU) averaged over ten typical cycles: normal valve.

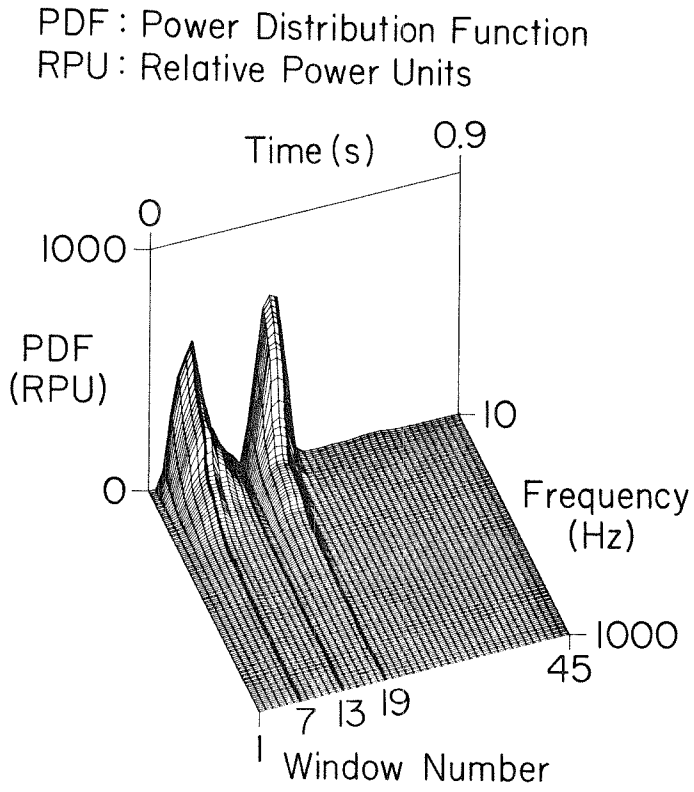

Figure 3-3b. Power-frequency-time surface depicting the power distribution in relative power units (RPU) averaged over ten typical cycles: valve with simulated overgrowth on all three upstream struts.

cies for window numbers from 3 to 15 corresponding to the opening/systolic complex. The peak corresponding to closure is more symmetric and has greater power than this opening/systolic complex. This opening/systolic complex is quite different from the corresponding opening and systolic peaks generated for the Starr-Edwards 2400 valve. It results from the early systolic sound. The closing sound is more similar to that of the Starr-Edwards 2400 valve.

Examination of the projection of the power-distribution surface upon the power-time plane shown in Figure 3-4a, the opening-sound, window 7, shows a total power of 247 RPU with bands 2 to 7 each having power greater than 10 RPU. Table 3-1 lists the mean and standard deviation of the total-power associated with the special windows for this valve as well as the abnormal valve. Table 2-2 of Paper II provides the values of the frequencies associated with specific "band numbers". The standard deviation of the total power of window 7 based on ten cycles was 30 RPU. The power-density spectrum (**PDS**) depicted in Figure 3-5a shows broad peaks at 130, 250, and 600 Hz. The peak at 600 Hz is interesting in that it was not readily predictable from the time-amplitude plot. The power-distribution function (**PDF**) exhibits inflections at each of these three frequencies. The major difference between this opening sound and those of both the normal and abnormal Starr-Edwards 2400 valve is that the total-power associated with window 7 is significantly greater for the normal Smeloff valve.

The systolic sound, represented by window 13 of Figure 3-4a, has a total-power of 143± 68 RPU with bands 2 to 5 each having power greater than 10 RPU. The **PDS** has a broad peak centered at 150 Hz as shown in Figure 3-5b. The **PDF** has an inflection point at 150 Hz. This systolic sound is more powerful over all frequencies as compared to either condition of the Starr-Edwards 2400 valve. This increase in power is partly due to a smaller, effective-flow area as compared with the Starr-Edwards 2400 prosthesis.

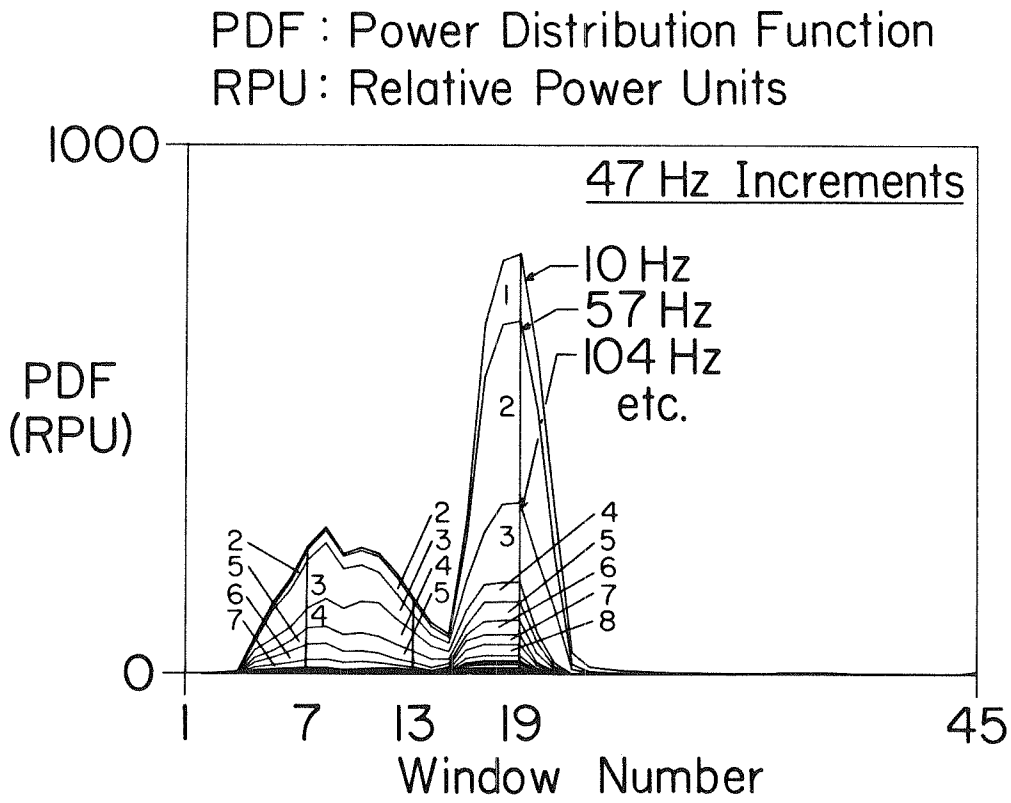

Figure 3-4a. Power distribution in relative power units (RPU) obtained by projecting every sixth frequency contour onto the power-time plane: normal valve.

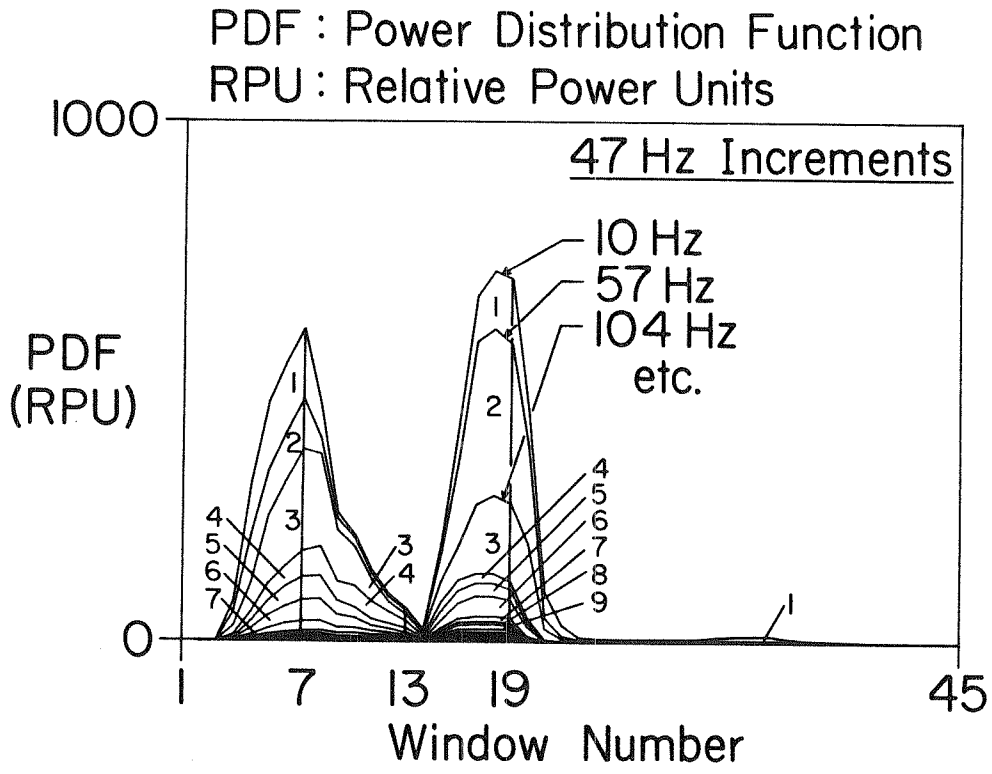

Figure 3-4b. Power distribution in relative power units (RPU) obtained by projecting every sixth frequency contour onto the power-time plane: valve with simulated overgrowth on all three upstream struts.

Statistics for the Total Power

Associated with Specific Windows

in Relative Power Units (RPU)

Valve	Mean Total Power ± std. dev.		
	Opening Sound	Systolic Sound	Closing Sound
Normal Smeloff	247± 30	143± 68	796± 36
Abnormal Smeloff	600± 83	63± 59	697± 52

Table 3-1 Statistics for the Total Power Associated with Specific Windows in Relative Power Units (RPU) of the Sounds of the Normal and Abnormal Smeloff Prosthesis.

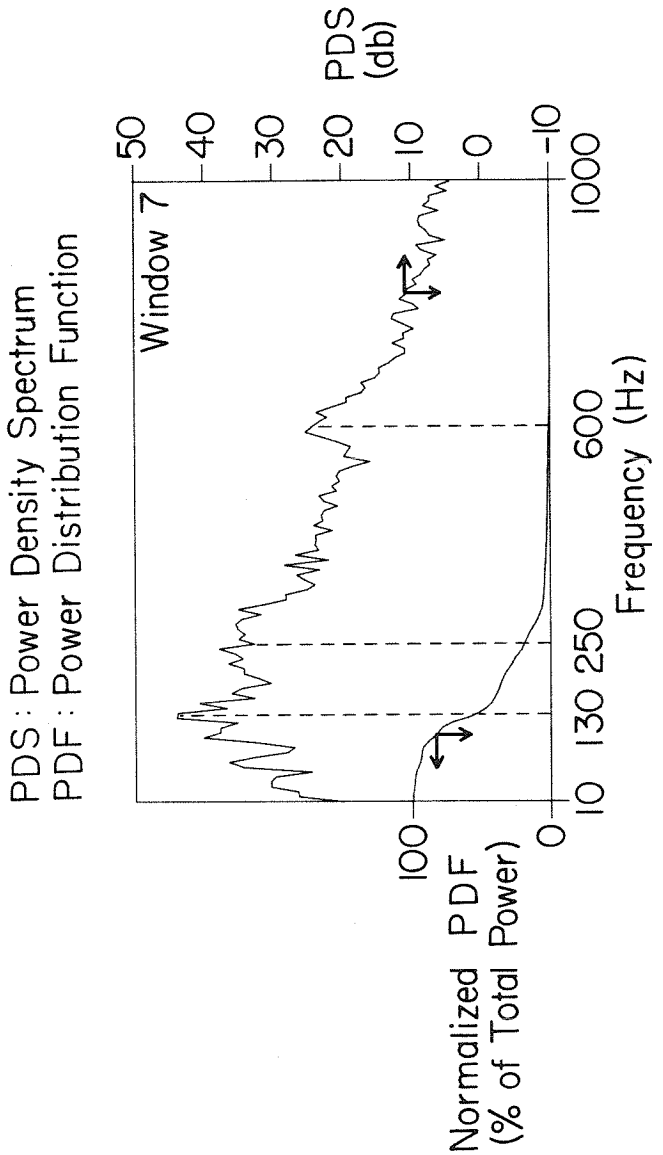

Figure 3-5a. Power-density and normalized-power-distribution functions associated with the normal Smeloff prosthesis: opening sound.

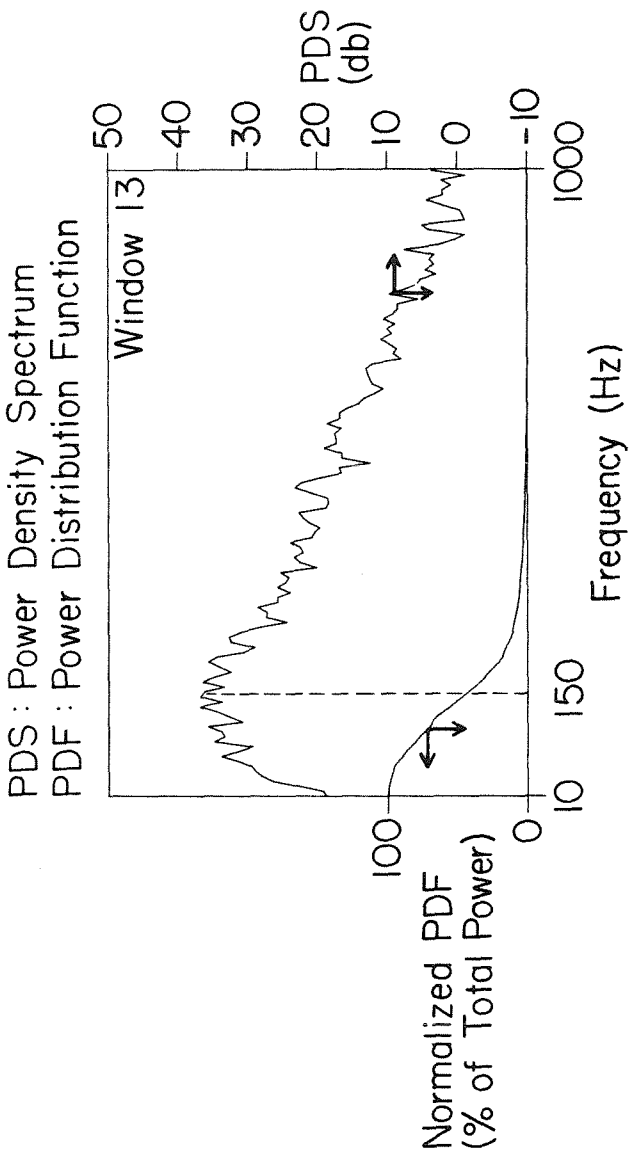

Figure 3-5b. Power-density and normalized-power-distribution functions associated with the normal Smeloff prosthesis: systolic sound.

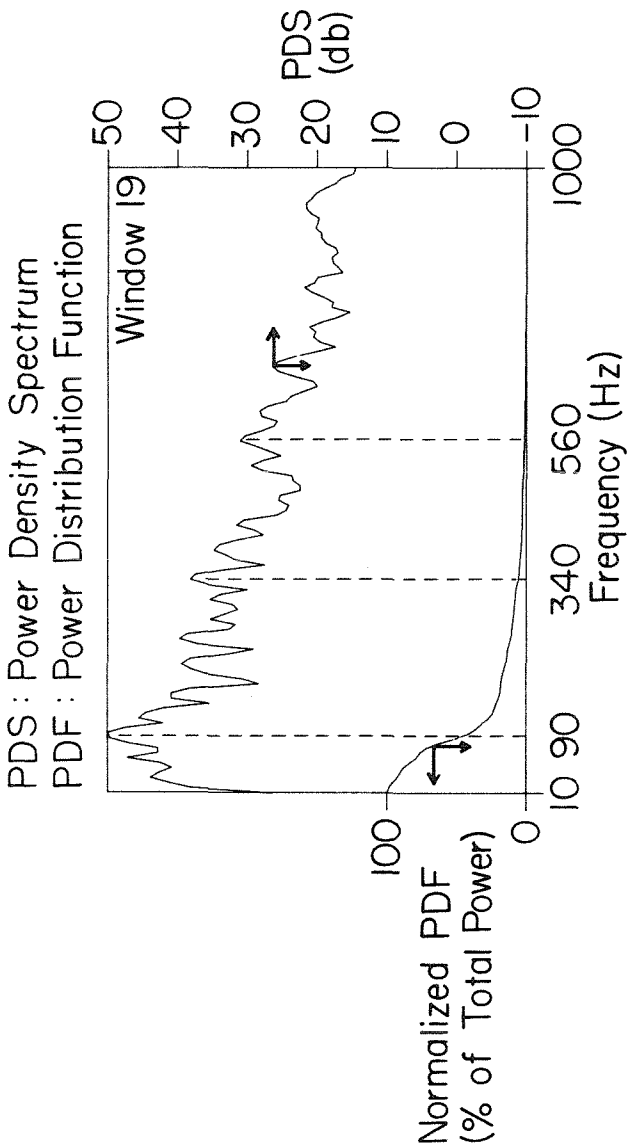

Figure 3-5c. Power-density and normalized-power-distribution functions associated with the normal Smeloff prosthesis: closing sound.

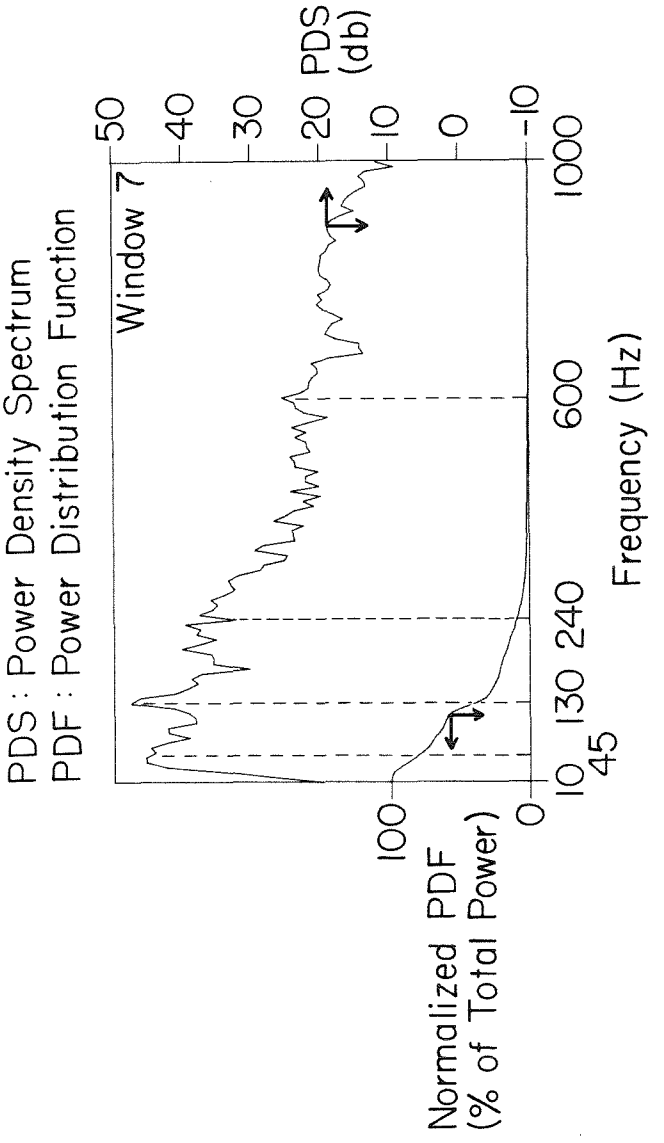

Figure 3-6a. Power-density spectra and normalized power-distribution functions associated with the Smeloff prosthesis having the simulated overgrowth on all three upstream struts: opening sound.

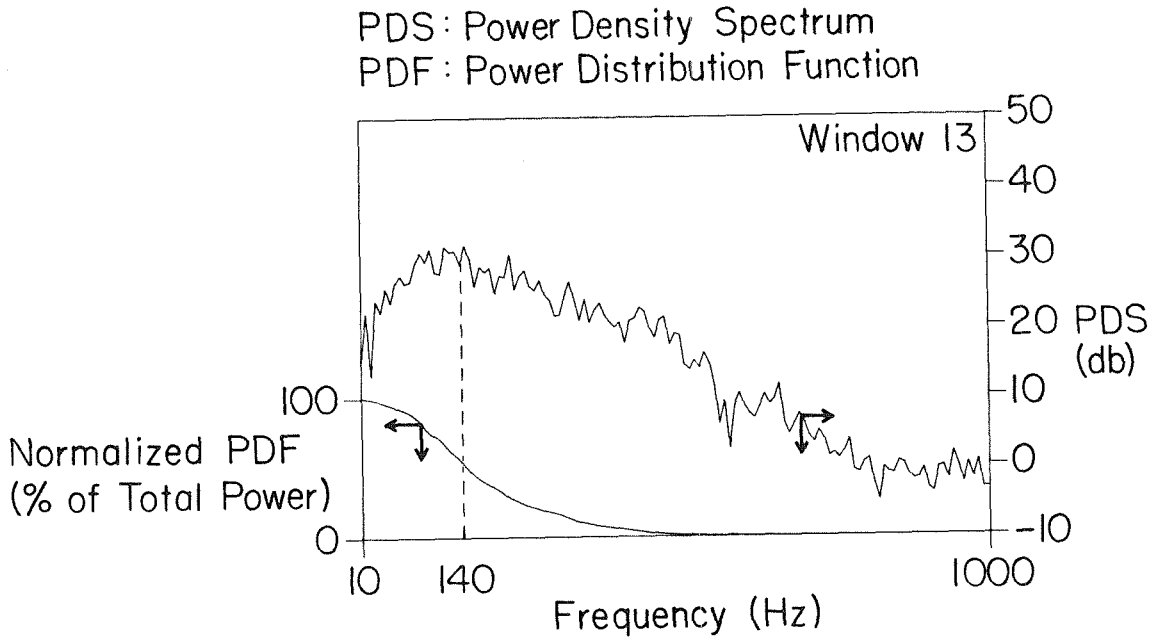

Figure 3-6b. Power-density spectra and normalized power-distribution functions associated with the Smeloff prosthesis having the simulated overgrowth on all three upstream struts: systolic sound.

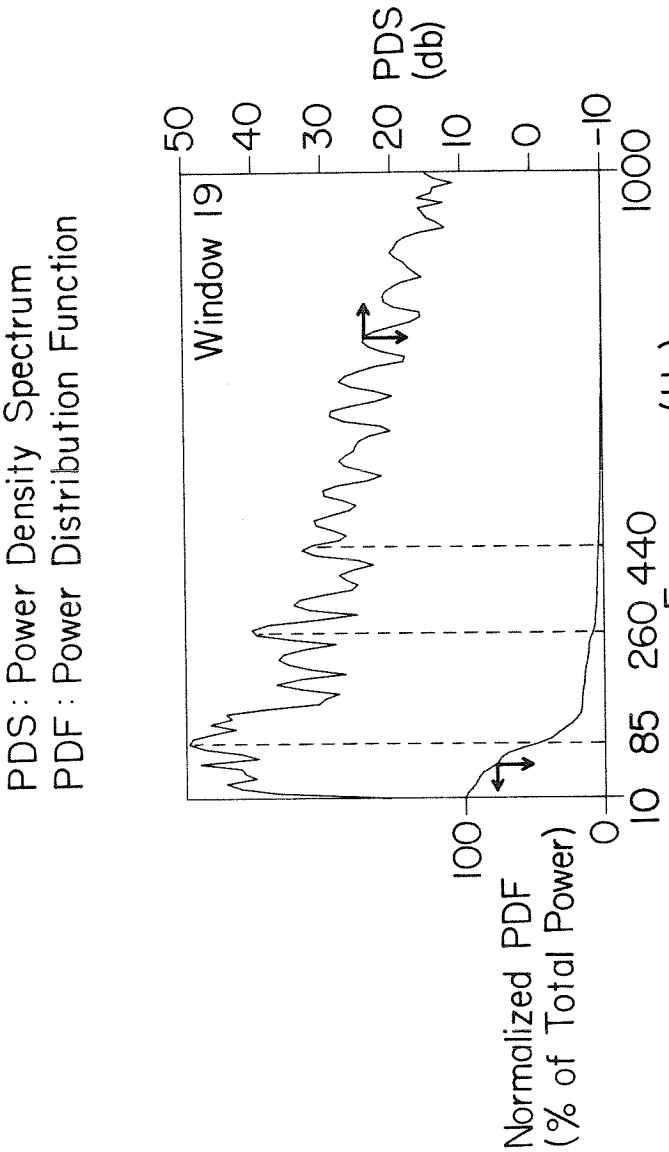

Figure 3-6c. Power-density spectra and normalized power-distribution functions associated with the Smeloff prosthesis having the simulated overgrowth on all three upstream struts: closing sound.

The systolic sound, represented by window 13 of Figure 3-4a, has a total-power of 143± 68 RPU with bands 2 to 5 each having power greater than 10 RPU. The **PDS** has a broad peak centered at 150 Hz as shown in Figure 3-5b. The **PDF** has an inflection point at 150 Hz. This systolic sound is more powerful over all frequencies as compared to either condition of the Starr-Edwards 2400 valve. This increase in power is partly due to a smaller, effective-flow area as compared with the Starr-Edwards 2400 prosthesis.

The closing sound, window 19 of Figure 3-4a, has a total-power of 796± 36 RPU with bands 1 to 8 having power greater than 10 RPU. Band 2 with 330 RPU contains a large peak at 90 Hz in its **PDS** and an inflection point in its **PDF** as shown in Figure 3-5c. Band 8 has 30 RPU and contains a peak at 340 Hz in its **PDS** and a smaller inflection point in its **PDF**. The closing sound of the normal Smeloff prosthesis is more similar to the closing sounds of both the normal and abnormal condition of the Starr-Edwards 2400 valve. The temporal position of the window having maximum total-power for the closing sound of the Smeloff valve is the same as that for the abnormal Starr-Edwards 2400 valve.

3.3.2 The Smeloff Prosthesis With Simulated Overgrowth

An overgrowth was simulated on the valve with material similar to that described in Paper II. It was placed upon the upstream struts of the prosthesis as shown in Figure 3-1. We expected to modify the closing sound of the valve by excluding the occluder from regions inside the orifice. As we will show, the opening and systolic sounds were also changed.

3.3.2.1 Response in the Time Domain

One change in the sound of the abnormal valve, as shown in time and amplitude

tracing shown in Figure 3-2b, is the absence of the first component of the opening sound which is normally produced by the occluder leaving the orifice. The simulated overgrowth has prevented the occluder from being within the orifice. Thus, the unseating sound is absent. The second component of the abnormal opening sound, OS2, is high in amplitude. It is slightly lower in frequency than the corresponding component of the normal Smeloff valve.

The systolic sound, SS, begins before the decay of the second component of the opening sound, and it is greater in amplitude relative to the normal systolic sound. This systolic sound is again comprised of a superposition of sounds caused by both turbulent noise and occluder-strut collisions. One unique quality of the abnormal systolic sound is its early decay which can be seen by comparing the power-distributions of window 14 for the normal and abnormal cases as shown in Figures 3-4a and 3-4b, respectively. This early systolic sound could be related to changes produced by the large regurgitative flow that occurred during diastole. This regurgitation causes a lower aortic pressure at the end of diastole. As a result, the time at which the valve opens is shifted to an earlier time. Also, the acceleration of the occluder is greater than normal, flow develops more rapidly, and, for a fixed systolic time interval, the flow subsides earlier. Again, the overall increase in amplitude of the systolic sound is a result of a decrease in the effective-flow area from a normal value for the case having simulated overgrowth as indicated by the values presented in Table 3-2.

The closing sound has two components and both components have relatively large amplitudes. The first component, CS1, has lost its high frequency sound which we have attributed to the "pinching off" of the annular flow prior to closure. Backflow continues at a greater rate than for the normal case, but the increase of the annular area of flow is greater relative to the increase of the backflow. As a result, the local shear should be lower at the surfaces of the

Effective Flow Areas for the Normal Smeloff Prosthesis

and the Same Valve Having Simulated Growth on the Upstream Struts

Valve	Effective Flow Area (cm^2)
Normal Smeloff	3.06
Abnormal Smeloff	2.43

Table 3-2 Effective Flow Areas for the Normal Smeloff Prosthesis and the Same Valve Having Simulated Growth on the Upstream Struts.

orifice and occluder, and in any jets in the backflow of fluid. The second component of the closing sound, CS2, is similar to that of the normal valve.

A fourth major sound is produced by the abnormal Smeloff valve. It was more instense when compared with the normal case. This diastolic sound, DS, is attributed to the regurgitative backflow through the insufficient valve. Total regurgitation was estimated from the flow data to be 20% of the stroke volume with approximately 20% of this fraction related to closure. By inserting the phonocatheter into the upstream port where we measured the ventricular pressure, we heard, qualitatively, a more intense diastolic murmur than was heard downstream. This result indicates that the intensity of the diastolic sounds produced by aortic valves would be expected to be more intense at the apex rather than the aortic position when these sounds are examined *in vivo*.

3.3.2.2 Response in the Frequency Domain

The power-distribution surface based on abnormal sounds is shown in Figure 3-3b. It has a very large, asymmetric peak at low frequencies for windows spanning the opening and systolic sounds. The asymmetry is similar to that of the normal valve, but the values are now much greater. The windows encompassing the late-systolic sounds, windows 13 and 14, possess sound having less total-power relative to the normal Smeloff valve. The closing sound is depicted by the symmetric peak with a relatively large value of total-power.

The opening sound, as represented by window 7 in Figure 3-4b, has a total-power of 600± 83 RPU with bands 1 to 7 having powers greater than 10 RPU. Band 1 has a power of 135 RPU and encompasses a peak centered at 45 Hz as shown in Figure 3-6a. Band 3 has a power of 180 RPU and encompasses a peak centered at 130 Hz in Figure 3-6a. Band 6 has a power of 40 RPU and contains

the peak centered near 240 Hz in the **PDS**. The major differences between the opening sounds of the normal and abnormal Smeloff valve is the greater power density near 45 Hz for the abnormal case. The total-power of the abnormal opening sound is nearly 140% greater than that for the normal valve. The difference between the distribution of the power over frequency can be observed by inspecting the corresponding normalized distributions in Figures 3-5a and 3-6a.

The systolic sound, as represented by window 13 shown in Figure 3-4b, has a total-power of 63± 59 RPU with bands 3 and 4 having power greater than 10 RPU. These bands encompass the broad peak centered near 140 Hz in the **PDS** as shown in Figure 3-6b. For frequencies greater than 100 Hz, this sound has a broader distribution of power as compared to the normal Smeloff valve. The power-densities are such that the total-power of window 13 is more than 100% greater than that of the normal valve.

The closing sound, as represented by window 19 shown in Figure 3-4b, has a total-power of 697± 52 RPU with bands 1 to 7 and 9 having power greater than 10 RPU. Band 2 encompasses a peak centered near 85 Hz in the **PDS**, and band 6 encompasses a peak centered near 260 Hz in the **PDS** as shown in Figure 3-6c. Corresponding inflections occur in the **PDF**. If we inspect the **PDF** in terms of the numerical values we find that the abnormal closing sound has significantly less power in bands 7, 8 and 13. For example, band 8 normally has 25 RPU while the abnormal value is 2 RPU. Thus, the major difference between the closing sounds is the loss of power near 340 Hz and 560 Hz for the abnormal valve.

3.3.3 Examination of Differences Using a 3D, Power-Difference Surface

The difference surface developed by subtracting the normal power-distribution

surface from the abnormal surface is shown in Figure 3-7. It, again, shows each of the major differences that we have discussed in terms of the spectra and individual surfaces.

The large difference between the total-power associated with the opening sounds for each valve, is illustrated by the large peak between windows 3 through 9 along the 10-Hz contour. Window 7 has an abnormal total-power which is 353 RPU greater than the value for the normal valve. This difference represents an abnormal increase of 140%. The major difference in the power-distribution of window 7 at frequencies near 45 Hz and 130 Hz is indicated by the positive values for frequencies less than 130 Hz and by the large, negative slope near 45 Hz and 130 Hz.

The early systolic murmur associated with the abnormal valve and the subsequent decrease of total-power for window 13 is shown by the valley in the region of window 13 along the 10-Hz contour. If this region does not appear as a valley, the reader should place a ruler between the points (window 1, 10 Hz) and (window 45, 10 Hz) and observe the deflections of the 10-Hz contour below the straight edge. This valley extends over the frequency domain between 10 and 250 Hz. The positive slope, parallel to the frequency axis, in this region, indicates that the normal valve possesses greater power-density between 10 Hz and 250 Hz.

One major difference between the normal and abnormal closing sounds was the early closure observed for the abnormal case. This difference is shown by the difference-surface as a peak-valley complex along the 10 Hz contour between windows 14 and 22. This peak-valley complex is similar to that for the previous comparison between Starr-Edwards 2400 valves, but it is reversed with respect to time because the time shift is now in the opposite sense. This peak-valley

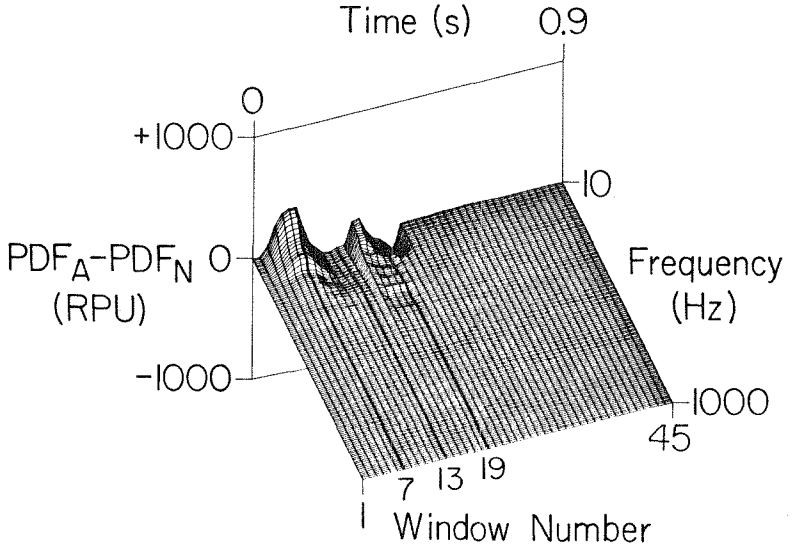

Figure 3-7. Power-frequency-time surface showing the power-difference in relative power units (RPU) generated by subtracting the surface associated with the normal prosthesis from that associated with the same valve but having the simulated overgrowth on all three upstream struts.

complex is smaller in amplitude because the time-difference, 15 ms, is smaller for these peaks as compared to 20 ms for the Starr-Edwards 2400 valves. The small valley and undulations along the window-19 contour, which extend from 10 Hz up to 450 Hz, illustrate the lower power-densities near 450 Hz for the abnormal closing sound and the redistribution of the power over this frequency band, respectively. These lower densities were attributed to the absence of the "pinching off" of the annular jet prior to valvar closure.

If the surface is viewed obliquely along the 10-Hz contour, one can see a small peak near window 33. This peak illustrates the abnormal, low-intensity diastolic sound associated with regurgitation. The negative slope between 10 and 100 Hz indicates the larger abnormal power-densities between these frequencies.

All of the differences between sounds produced by the Smeloff valves were not clearly illustrated by the difference-surfaces we have generated. Obscured differences generally occur within the higher frequency domain. The information is there. In order to bring-out the peak or valley more distinctly, a weighting of the data will probably be necessary. If one is viewing the information, however, in terms of the individual **PDS**, even these subtle differences can generally be observed. The parameters associated with the harmonic model will also illustrate these differences. Therefore, it will be necessary to refer to the **PDS** and **PDF** to obtain more details of this acoustical information.

3.3.4 Comparisons Between Harmonic Model Parameters

The gain, decay and frequency parameters can be estimated by a similar method as that described in Papers I and II. Table 3-3 lists the results of this estimation. Entries are for peaks within each **PDS** for which estimation was relatively easy. The table entries in order correspond to the frequency, $f_{f,i}$, decay, k_i, and

Parameters Estimated for

Significant Harmonic Peaks

Event	Frequency, $f_{r,i}$; Decay, k_i; Power-Density, G_i (Hz,Hz,db)	
	Smeloff Normal	Smeloff Abnormal
Opening Sound	130,10,44 250,50,38 600,30,25	45,30,45 130,16,45 240,40,41 600,25,25
Systolic Sound	150,90,37	140,100,32
Closing Sound	90,30,50 340,40,38 560,50,31	85,42,49 260,33,41 440,55,34

Table 3-3 Parameters Estimated for Significant Harmonic Peaks of the Sounds of the Normal and Abnormal Smeloff Prosthesis.

gain, G_i, associated with peak i and having units of Hz, Hz, and db, respectively. These table entries are identical to the acoustical parameters defined in Paper II.

The **PDS** corresponding to the opening sounds associated with window 7 for the two conditions of the Smeloff prosthesis differ most significantly for the frequency-bands 10-100 Hz and 700-1000 Hz. The **PDS** for window 7 for the abnormal valve possesses far greater power-densities for each of these two frequency ranges. The 45-db peak at 45 Hz is the cause of the large difference in the total-powers associated with window 7 for the normal and abnormal Smeloff prostheses. A 20-db peak at 800 Hz contributes a lesser amount to this difference in total-power. Peaks at 130 Hz and near 250 Hz are similar for each condition, with the abnormal peaks being 1 db and 3 db greater than corresponding normal peaks, respectively. It is difficult to clearly explain these differences in terms of physical transformations of specific oscillators. The abnormal peak at 45 Hz represents the stimulation of an abnormal mode of vibration. Because window 7 in each case encompasses both the opening sound and the systolic sound, these additional low and high-frequency peaks could be a result of changes in the dynamics of the occluder motion upon impact with the struts or they could result from the perturbed flow due to the overgrowth. These peaks are "additional". We attribute these peaks to new physical modes which have been stimulated.

The systolic sound, as represented by window 13, has similar power-distributions for each case. The normal **PDS** has greater power-density over all frequencies. The only frequency with significantly more power in the normal case is that near 600 Hz. The normal valve has a systolic sound which extends later into systole. Therefore window 13 still encompasses a major part of this sound which apparently includes the harmonic oscillation which produced the

peak at 600 Hz for the normal opening sound. Window 13 for the abnormal valve encompasses little of this early systolic sound.

If we compare the PDS for the closing sounds of the two valves, as represented by window 19 in Figures 3-5c and 3-6c, we find that the power-density for frequencies near 340 Hz is 10 db lower for the normal valve than for the abnormal closing sound. The power has been redistributed within the range 200 to 600 Hz. It appears that the power-density of the peaks at 340 and 560 Hz has shifted to corresponding lower frequencies for the abnormal case. The power of the normal peak at 340 Hz is, perhaps, now being incorporated as part of the power of the abnormal peak at 260 Hz, and the power of the normal peak at 560 Hs is now part of the power of the abnormal peak at 440 Hz. It is possible that the increased backflow through the valve during diastole and the damping of the closing sound caused by the overgrowth have both contributed to these changes between the closing sounds. The decrease of the frequency of a specific mode would be indicative of either an increase in the mass of the oscillator associated with that mode or a decrease in the stiffness of the oscillator associated with that mode, provided the damping remained constant. Physical changes as described by the effective mass, stiffness, or damping coefficients associated with specific oscillators are more difficult to interpret for the Smeloff valve because the frequency of the sounds produced by collisions between the struts and occluder is similar to the frequency of sounds produced by the flow. As a result, the density-spectra associated with oscillators corresponding to the two sounds are superimposed. The changes in the frequencies associated with the significant peaks of the closing sounds for the normal and abnormal valve probably result from a combination of these changes. In general the parameters do not explain the physical changes as clearly as they did for the Starr-Edwards 2400 prosthesis. The information provided by the Starr-Edwards-2400

study does provide support, however, for the conclusions we have been making about the parameters for the case of the Smeloff valve.

3.4 CONCLUSIONS

A systematic, digital analysis of valvar sounds has been applied to an *in vitro* comparison of a normal and abnormal condition of a Smeloff aortic prosthesis. Time-amplitude plots, power-density spectra, power-distributions, three dimensional, power-distribution surfaces, a three-dimensional, power-difference surface, and physical parameters estimated for a simple acoustic model were used in the comparison.

An opening/systolic sound and a closing sound were studied for each cardiac cycle of the two valvar conditions. The opening sound and systolic sound overlapped in time for each condition of the valve. The systolic sound subsided earlier for the valve with simulated overgrowth on its upstream struts, and it possessed a broader distribution of power. The closing sound of the abnormal valve was 15 ms earlier than the normal closing sound, and its power-density near 450 Hz was significantly less than the normal case. The closing sound of the normal valve had a high-frequency component at the time of initial closure. The abnormal valve did not. This difference was attributed to changes that occurred in the seating of the valve and possibly to the loss of a "pinched-off" back-jet at the time of closure of the abnormal valve. A diastolic murmur was produced by the abnormal valve. This murmur was low in frequency, 10 to 100 Hz, and low in amplitude. Each of these differences was observed through the 3D, power-distribution-difference surface.

The general conclusion is that we are able to differentiate each condition of the valves we have studied *in vitro*. We believe the method we have described

offers a generally applicable method for comparison and evaluation of valvar sounds.

3.5 RECOMMENDATIONS

Many questions remain unanswered. How do the dynamic variations of heart rate, change of blood pressure with time, hypertension, etc. affect the acoustic-power distributions? How does each individual's anatomy affect the transmission of sounds from the valve to the transducer? How does the size of valve affect particular sounds? Is the implanted orientation of the prosthetic valve a significant factor relative to the acoustic-power distributions? Each of these questions must be answered for each valve design. And ultimately, these questions will have to be answered by doing the studies *in vivo*.

Some of the questions raised above can be answered by examining the results of *in vitro* studies. Specifically, those studies which examine the effects of different pulsatile modes, valve orientation, and valve size upon the sounds are perfectly applicable for comparative studies *in vitro*. We have begun to photograph the motion of the occluder simultaneously with the tracing signals for sound, flow, and pressure in order to show the simultaneous comparison of occluder events and corresponding sounds. From these films one can estimate the deceleration of the occluder for purposes of providing information relative to the forcing function of the harmonic model for transient sounds. Studies of the correlation between sounds recorded internally and externally will be of value for future non-invasive work.

Determination of a relation between turbulent eddy distribution and the corresponding accoustic power-distribution at a point in the flow will be useful information relative to the estimation of shear components by use of non-

invasive acoustical methods. This study could be accomplished *in vitro* by investigations using laser anemometers together with a pulse duplicator. The information obtained from such a study could be of value by providing data to be used for the stimulus function of a model which could be analyzed with procedures similar to those used for the harmonic model of transient sounds.

The 3D, power-frequency-time surface should be improved. In particular, some work should be directed to obtaining better relative resolution of power distribution in the higher-frequency range.

An understanding of the non-linear characteristics of the system particularly with respect to the closing sound will be useful in future modelling.

Finally, a library must be generated for storage of acoustical information in the form of power-distribution matrices. This library would be used in all comparative studies. Of course, comparisons between libraries would be valid only if the same methods were used to generate each library.

3.6 ACKNOWLEDGEMENTS

Funding for this project was provided by the Donald E. Baxter Foundation, the Children's Heart Foundation of Southern California, and the American Heart Association, Greater Los Angeles Affiliate.

3.7 NOMENCLATURE

Nomenclature

$f_{f,i}$	Frequency of free, damped oscillations of mode i, Hz
G_i	Gain associated with power density spectrum, db
k_i	Decay frequency, Hz
PDF	Designates power distribution functions
PDS	Designates power-density spectra
RPU	Designates dimensions of relative power units

vpp Designates dimensions volts peak-to-peak

Subscripts

f Indicates value associated with frictional loss of energy
i Indicates value associated with mode number i

PAPER 4

A Quantitative Method for the *In Vitro* Study of Sounds Produced by Prosthetic Aortic Heart Valves Part IV: An Experimental, Comparative Study of the Sounds Produced by a Normal Starr-Edwards 2400 Aortic Prosthesis Operating at Six Pulsatile States

A Quantitative Method for the *In Vitro* Study of Sounds Produced by Prosthetic Aortic Heart Valves

Part IV: An Experimental Comparative Study of the Sounds Produced by a Normal Starr-Edwards 2400 Aortic Prosthesis Operating at Six Pulsatile States

ABSTRACT

An *in vitro* study was made of the sounds produced by a normal, Starr-Edwards aortic-valve prosthesis and compared for the entire cardiac cycle with the same valve operating at six different pulsatile states. Time and amplitude information, power-density spectra, power-distribution functions, and 3-D, power-frequency-time surfaces were compared. Power-density spectra and power-distribution functions were compared in more detail for those portions of the cycle corresponding to the opening, systolic, and closing sounds of the valve. Parameters for the acoustical model were estimated from these power-density spectra. All results were then compared and discussed in terms of the pulstatile changes.

Useful information about the pulsatile state was provided by this analysis. The opening sounds and closing sounds were influenced primarily by the rate of change of the ventricular pressure prior to these events. The systolic sounds were primarily influenced by the systolic flow rate. The difference between systolic sounds was much greater than between opening and closing sounds for all cases. An increase in systolic flow rate produced a corresponding increase in the power of peaks in the spectra of the systolic sound. The location of peaks within the power density spectra were very similar for these states when compared to previous studies involving abnormal valves operating at similar pulsatile states.

4.1 INTRODUCTION

In Parts II and III of this series of papers we asked the question whether a malfunctioning prosthetic heart valve could be detected by analysis of the sound which it produced. The answer to this question for the two specific examples which we had studied was affirmative. The second major question which we must answer to understand the specificity of the analysis is whether any alternate pulsatile states (APS) could produce a sound similar to that of abnormal valves when the valve is itself normal. We also want to know the changes which each of these APS produces in the sounds. To answer this question we pulsed a normal 24mm Starr-Edwards 2400 aortic valve at a variety of APS. Except where noted, we used a method of analysis that was identical to that described in Part I of this series. The APS studied were those involving changes in the pulse rate, changes of the stroke volume, and changes of mean aortic pressure.

4.2 EXPERIMENTAL METHOD

We pulsed the Starr-Edwards 2400 prosthesis at a normal and five APS. Table 4-1a lists the pulse rates, pressures, and flows which characterized each of these states. The entries involving the rate of change of ventricular pressure assigned to opening and closing were evaluated 20 ms prior to OS2 and CS1, respectively. Backflow was estimated from the digitized flow data and the portion due to closure was generally estimated by the area under the zero-flow line and above the negative flow region of the primary "notch" in early diastole. Unlike other valvar designs no ringing, or "notch", was observed in the flow curve at the time of closure for the Starr-Edwards 2400 valve. This lack made estimation of the closure fraction difficult for this design in our system.

Pressure, Flow and Sound* Data corresponding to experiments involving a normal 24mm Starr-Edwards 2400 valve operating at various pulsatile states

Experiment Number	306	307	308	309	310	311
Pulse Rate (cycles/min)	70	90	50	70	70	70
Max. Pressure Gradient (mmHg)	33	23	36	103	23	17
Mean Systolic Pressure Gradient (mmHg)	19	13	20	48	12	10
Mean Aortic Pressure (mmHg)	108	88	107	94	99	150
Pressure rate of change Opening (mmHg/ms)	1.3	1.0	1.6	1.6	1.0	1.6
Pressure rate of change Closing (mmHg/ms)	-1.6	-1.6	-1.2	-2.3	-1.3	-1.3
Mean flow rate (l/min)	5.5	4.1	5.8	9.2	4.2	2.9
Maximum flow rate (l/min)	26.6	19.3	29.8	47.1	21.6	16.6
Stroke volume (cc)	81	45	116	132	65	45
Total backflow (cc/stroke)	3	1	6	3	4	4
Total backflow (% of stroke volume)	4	2	5	2	6	9
Effective flow area (sq cm)	2.1	1.8	2.3	2.1	2.1	1.9
Opening window number	5	5	5	5	5	5
Average total power (RPU)	5.8	5.6	3.1	5.6	4.6	4.8
Std. deviation (RPU)	0.5	0.7	1.2	1.2	0.42	0.70
Systolic window number	12	11	12	12	12	11
Average total power (RPU)	1.3	0.3	2.4	27.1	0.8	0.6
Std. deviation (RPU)	0.24	0.06	0.71	6.5	0.24	0.22
Closing window number	21	20	22	21	21	19
Average total power (RPU)	63.5	67.4	67.3	77.1	65.7	71.0
Std. deviation (RPU)	2.6	6.1	2.9	6.1	1.5	2.5

*Filter bandwidth: 200-2000 Hz

Table 4-1a Pressure-Flow-Sound data for experiments involving the normal 24mm Starr-Edwards 2400 aortic valve.

The effective flow area, A_{eff}, was estimated by the relation:

$$A_{eff} = \frac{\dot{Q}}{1.0\Delta p^{1/2}}, \qquad (4\text{-}1)$$

where the maximum systolic flow rate, $\dot{Q}$, was in units of cm^3/sec and maximum systolic pressure gradient, Δp, was in units of dynes $/cm^2$.

Table 4-1b lists the times of the significant events of the sound, pressure and flow relative to the time of full valvar opening. For those experiments involving different pulse rates, the left ventricular ejection times corresponding to pulse rates of 50, 70, and 90 beats/min were 380, 300, and 220 ms, respectively. These values also apply to the appropriate experiments in Parts V and VI. In the present paper, experiment 306 will be called the **normal** pulsatile state for the Starr-Edwards 2400 valve. All experimental results of the **APS** will be compared with respect to this **normal** pulsatile state. The orientation of the valve for each experiment is depicted in Figure A-2 of Appendix A. The orientation was the same for each experiment. Window lengths for the sound analysis were 0.125 seconds and the data rate was 4000 points per second. Sound was filtered using an analog bandpass filter having a 200 Hz low-cutoff frequency/12 db per octave slope and a 2000 Hz high-cutoff frequency/12 db per octave slope. The low-frequency characteristics of this filter is depicted in Figure A-1 of Appendix A. It is important to note at this point that the analog filter used to filter the results presented in Parts II and III had a low cutoff frequency of 400 Hz and that used in Parts IV through VII had a low cutoff frequency of 200 Hz. Otherwise all other experimental methods and analysis were identical with those described in Part I of this series. Stroke volume was changed independently of the pulse rate and elevated the mean aortic pressure by relatively small values. Changes of the pulse rate and mean aortic pressure were obtained by changes of

Times of significant events of pressure, flow and sound relative to the time of full valvar opening in milliseconds for experiments involving a normal 24mm Starr-Edwards 2400 valve operating at various pulsatile states

Experiment Number	306	307	308	309	310	311
Start of Systolic Ejection	-20	-25	-35	-25	-35	-50
Second Component of Opening Sound (OS2)	0	0	0	0	0	0
Maximum Systolic Pressure Gradient	130	85	145	155	140	80
Maximum Systolic Flow Rate	140	95	155	155	145	90
Maximum Amplitude of Systolic Sound (SS)	160	80	155	155	145	95
First Component of Closing Sound (CS1)	265	180	350	260	245	185
End of Systolic Ejection	295	195	360	275	265	210
Second Component of Closing Sound (CS2)	310	210	380	300	290	225

Table 4-1b. Times of Significant Events of Sound, Pressure and Flow for Experiments involving the Starr-Edwards 2400 valve.

the ventricular ejection time and systemic resistance, respectively. The stroke volume increased or decreased according to these changes. Therefore, the experiments which include changes of pulse rate and hypertension also involved changes of the stroke volume.

4.3 RESULTS

The results of the six experiments are presented graphically in Figures 4-1 through 4-10. Figure 4-1 shows the maximum pressure gradient across the valve plotted as a function of the maximum flow rate for each experiment. Figure 4-2 shows a plot of the maximum pressure gradient across the valve as a function of the mean flow rate for each experiment. Figure 4-3 shows the average value of the total power of the systolic sound plotted as a function of the maximum pressure gradient rate for each experiment. Figure 4-4 shows a plot of the average value of the total power of the systolic sound as a function of the mean flow rate for each experiment. Figures 4-5 through 4-10 are separated into 7 or 8 subfigures indexed alphabetically with letters from **a** through **h**. Subfigures **a**, 4-5a through 4-10a, show the original time-amplitude plots of the sound, flow rate, and ventricular and aortic pressures for each experiment. Subfigure **b** shows the three-dimensional power-frequency-time plot corresponding to the sound. Subfigures **c** and **d** depict auxiliary views of this 3-D surface as viewed parallel to the frequency axis and time axis, respectively. Subfigures **e**,**f** and **g** depict the power-density spectra associated with windows which encompass the opening, systolic, and closing sounds of the valve. The contours corresponding to these three windows were enhanced in subfigures **b** and **c**. Finally Figures 4-6h through 4-10h depict the 3-D, difference-surfaces generated by subtracting the 3-D surface corresponding to the **normal** pulsatile state, shown in Figure 4-5b, from those corresponding to the **APS** shown in Figures 4-

6b through 4-10b, respectively. Parameters corresponding to the center-frequencies and amplitudes of each significant peak of the power-density spectra have been included with the plots. These parameters as well as the half-widths of each peak have also been listed separately for each experiment in Tables 4-2 through 4-7. These tables can be found on the pages immediately following the plots of the spectra of the closing sounds. Tables A-1 to A-6 in Appendix A conveniently list the center-frequencies and amplitudes of the peaks in the spectra of the opening, systolic and closing sounds for each experiment.

4.4 DISCUSSION OF RESULTS

4.4.1 Effects of Pulse Rate on the Sounds

The Starr-Edwards 2400 valve was pulsed at three different pulse rates. These rates were 70, 90, and 50 beats/min and corresponded to experiments 306, 307 and 308, respectively. The important values which defined the pulse mode for these experiments are listed in the first three columns of Table 4-1a. The ventricular ejection time was corrected by normal factors for these three pulse rates in order to simulate the natural, rate-dependent systolic and whole-cycle times. As a result the ratio of the systolic time interval to the whole-cycle time was not a constant but rather increased with the pulse rate. When the pulse rate varied between experiments, adjacent windows were shifted an amount proportional to the time of one complete cycle, consequently, windows 1 and 45 corresponded to the same relative moment within two consecutive cycles. For these three experiments, the stroke volume, maximum flow rate, and maximum pressure gradient changed with the pulse rate. These changes resulted from maintenance of the mean output near values of 5.5, 4.1 and 5.8 L/min for experiments 306, 307 and 308, respectively. Figures 4-1 and 4-2 show that the value

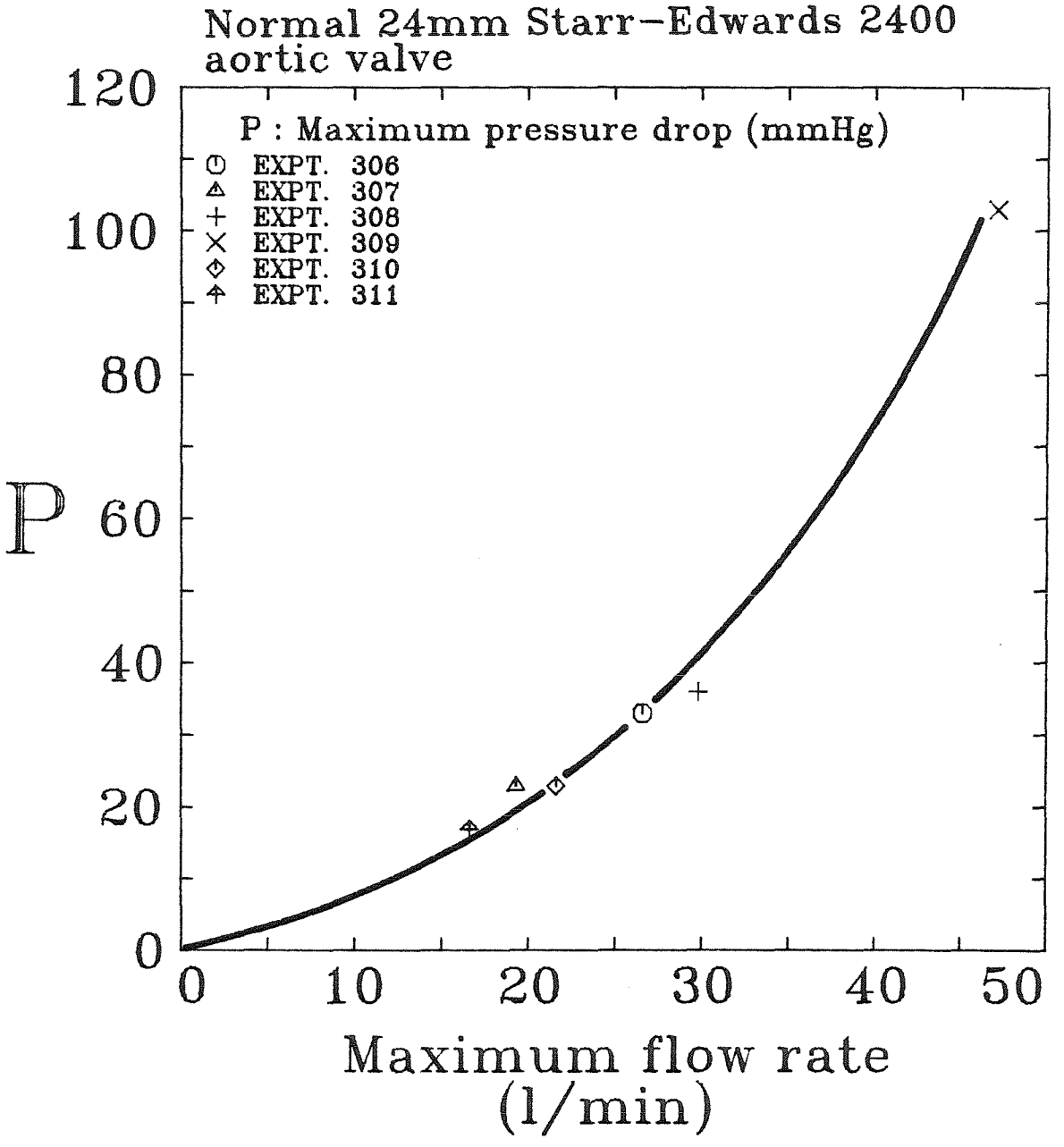

Figure 4-1 Maximum pressure gradient vs. maximum flow rate for the experiments with the normal 24mm Starr-Edwards 2400 aortic prosthesis.

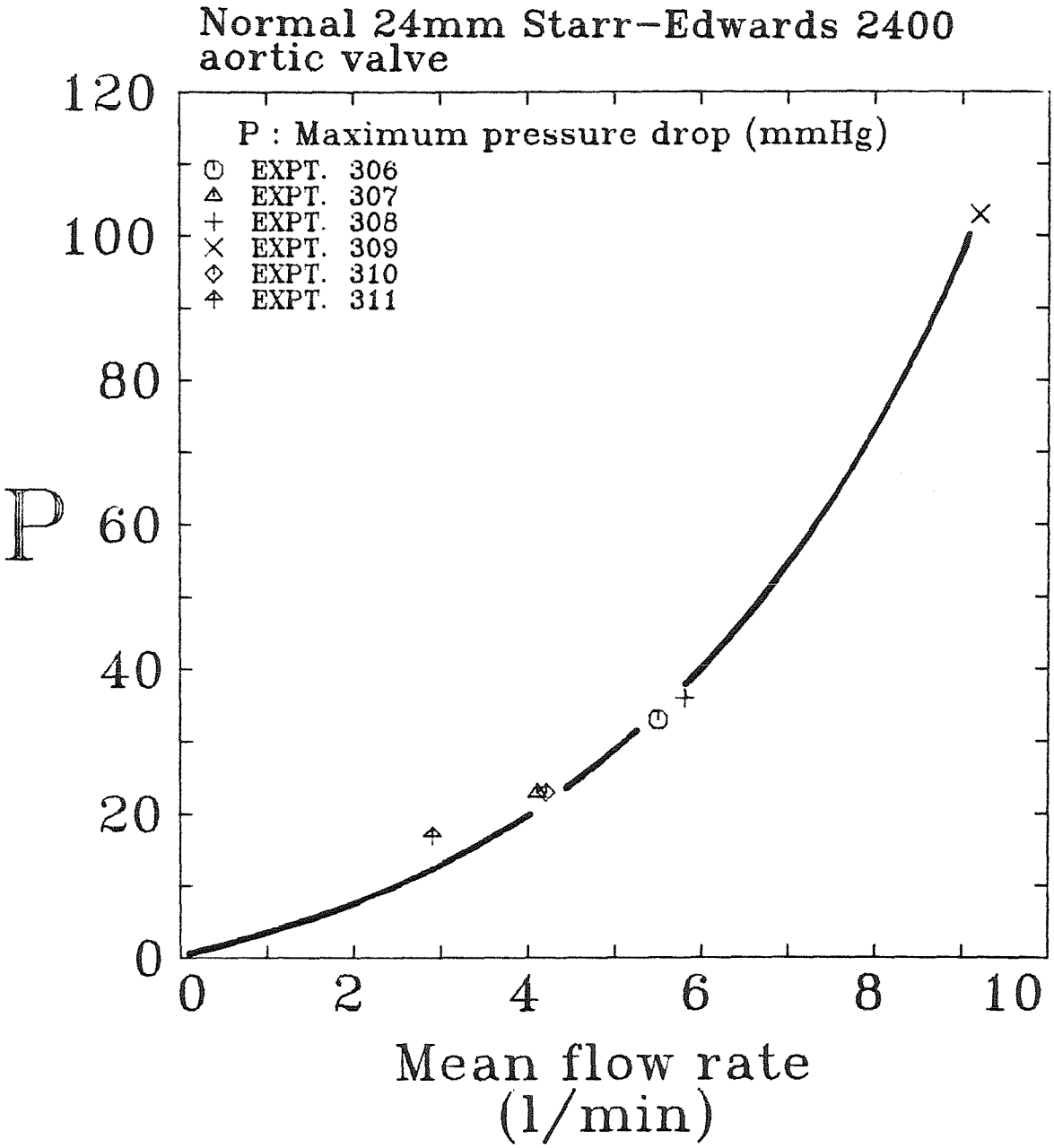

Figure 4-2 Maximum pressure gradient vs. mean flow rate for the experiments with the normal 24mm Starr-Edwards 2400 aortic prosthesis.

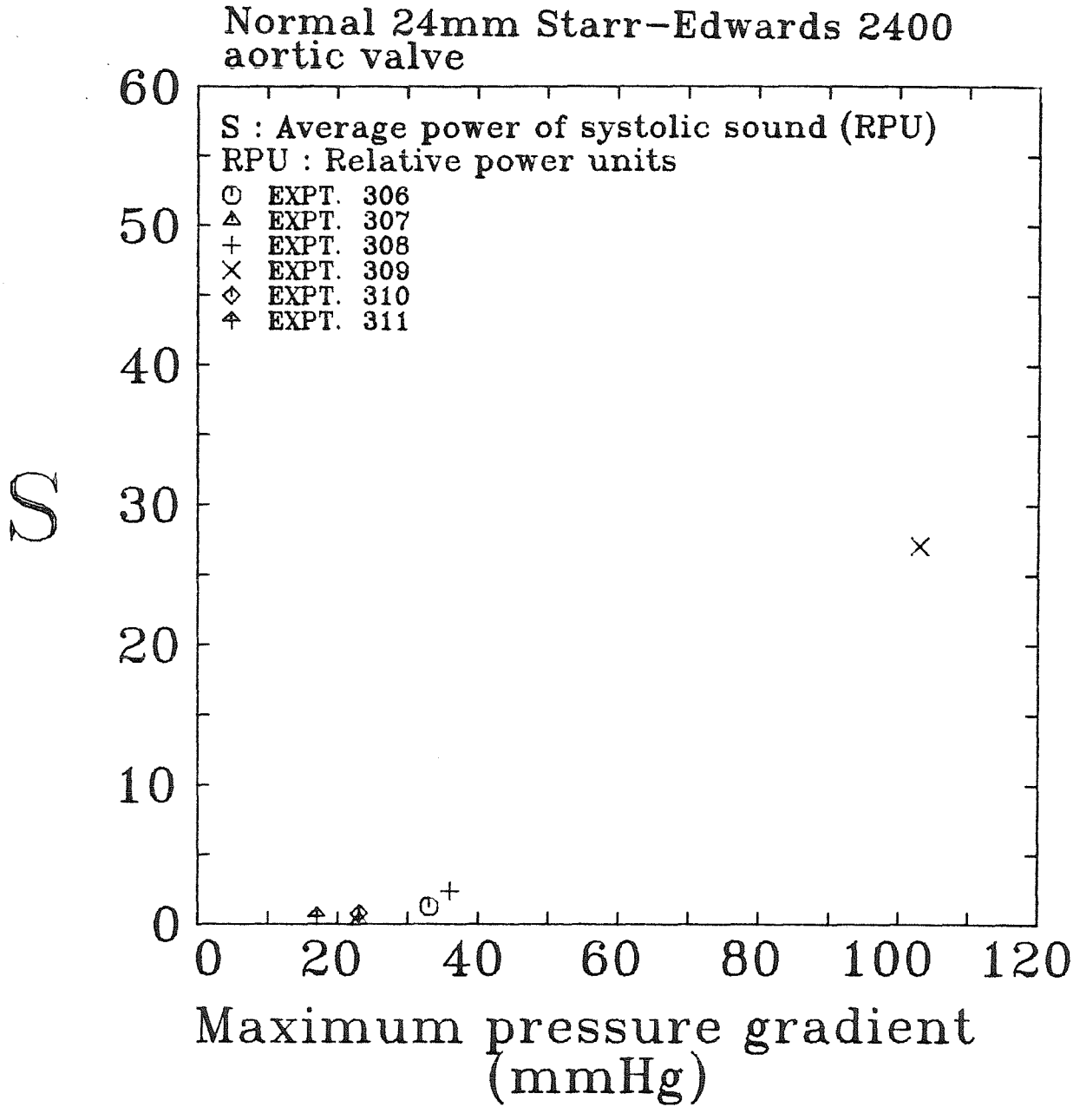

Figure 4-3 Average total-power of systolic sound vs. maximum pressure gradient for the experiments with the normal 24mm Starr-Edwards 2400 aortic prosthesis.

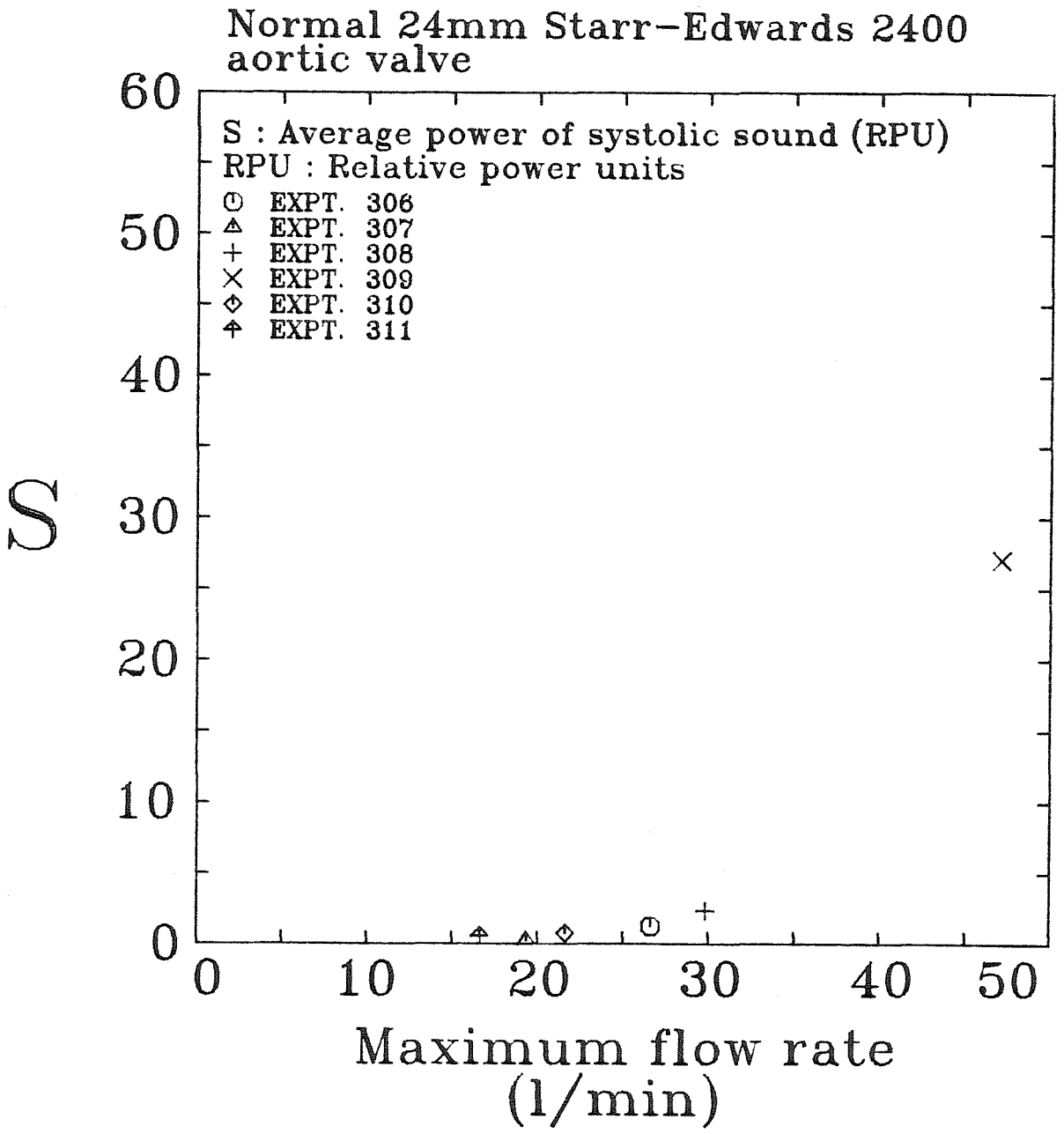

Figure 4-4 Average total-power of systolic sound vs. maximum flow rate for the experiments with the normal 24mm Starr-Edwards 2400 aortic prosthesis.

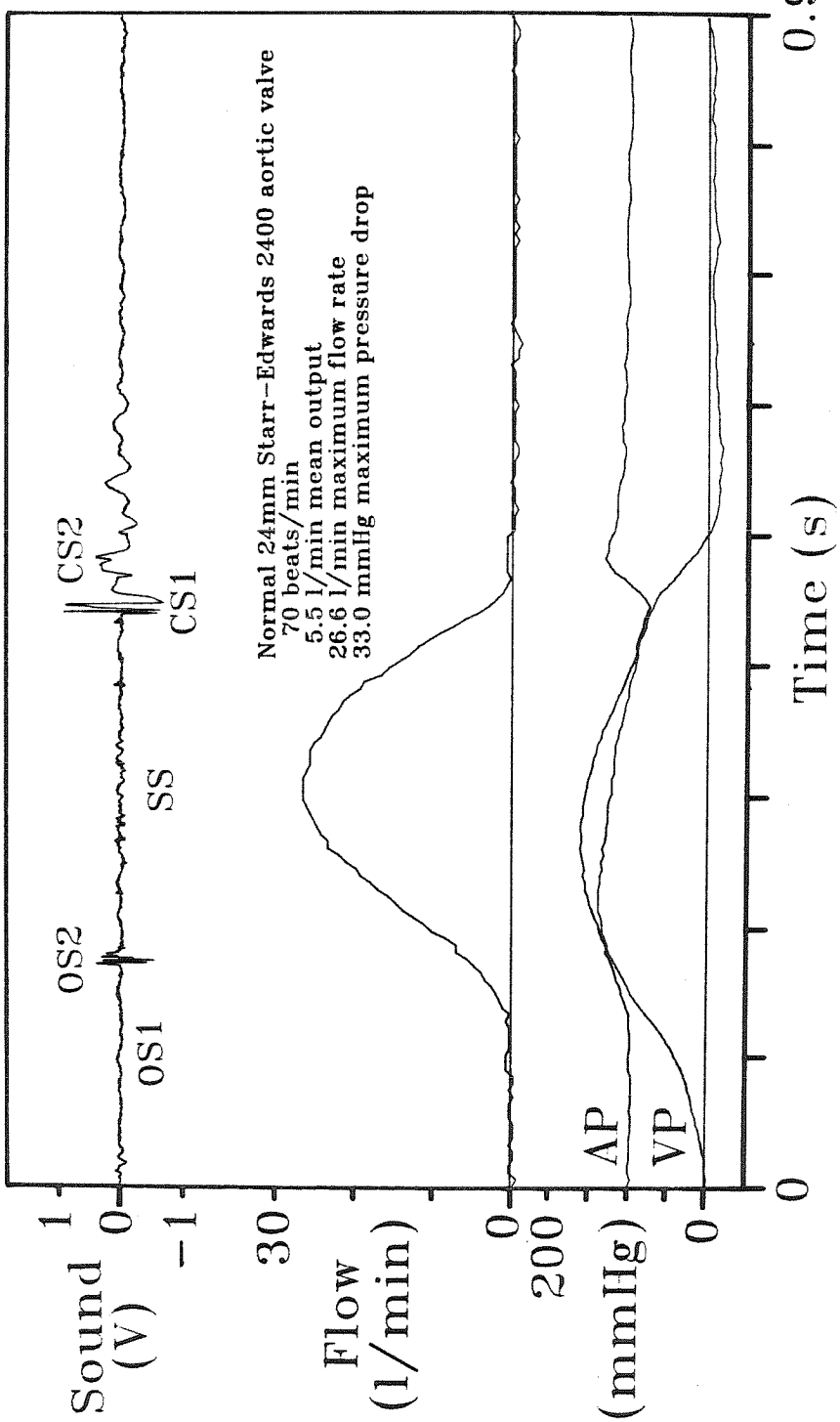

Figure 4-5a Amplitude vs. time tracings of sound, flow rate, aortic pressure and ventricular pressure associated with a typical cycle of experiment 306.

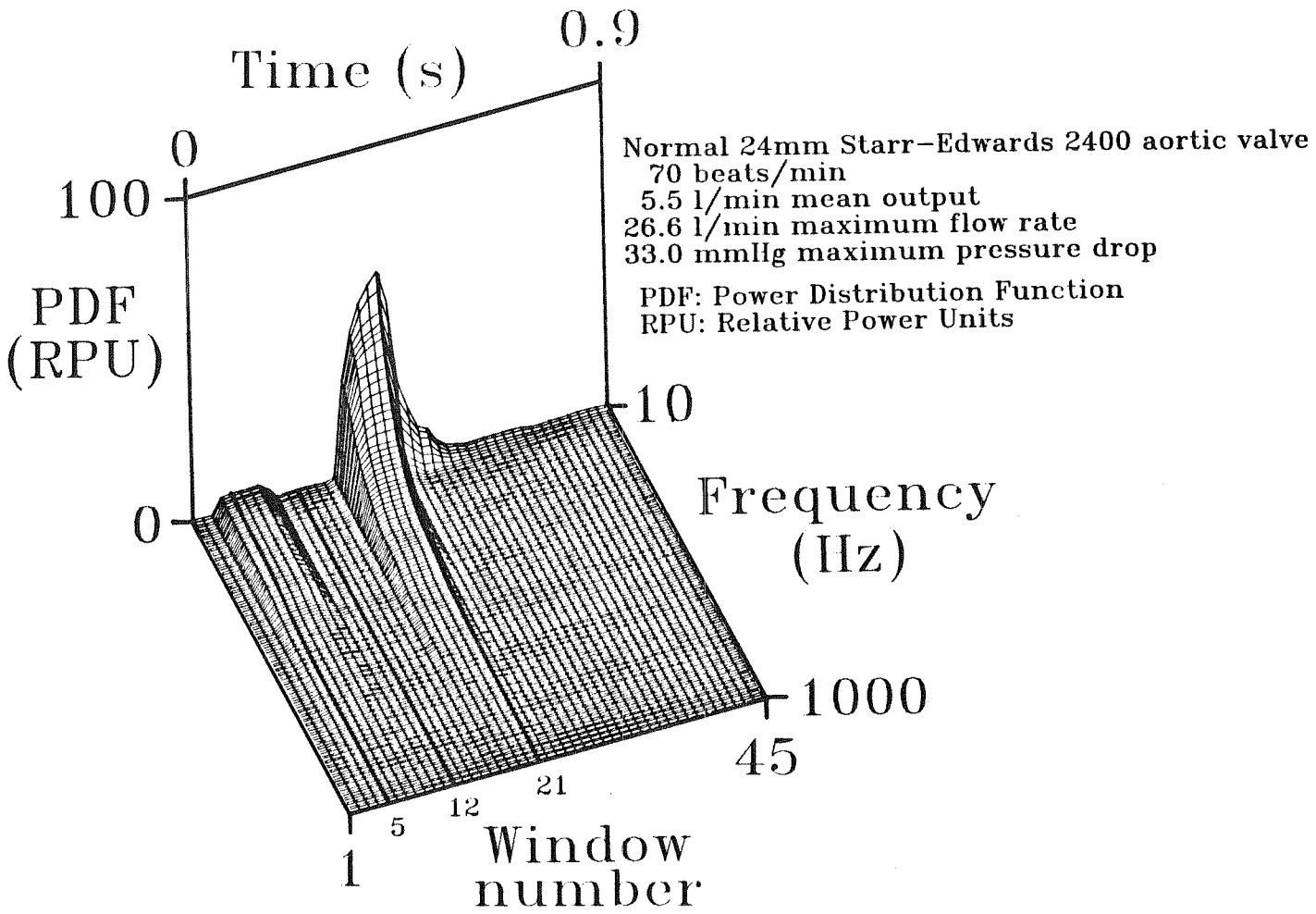

Figure 4-5b Three-dimensional power-frequency-time surface averaged over ten cycles of experiment 306.

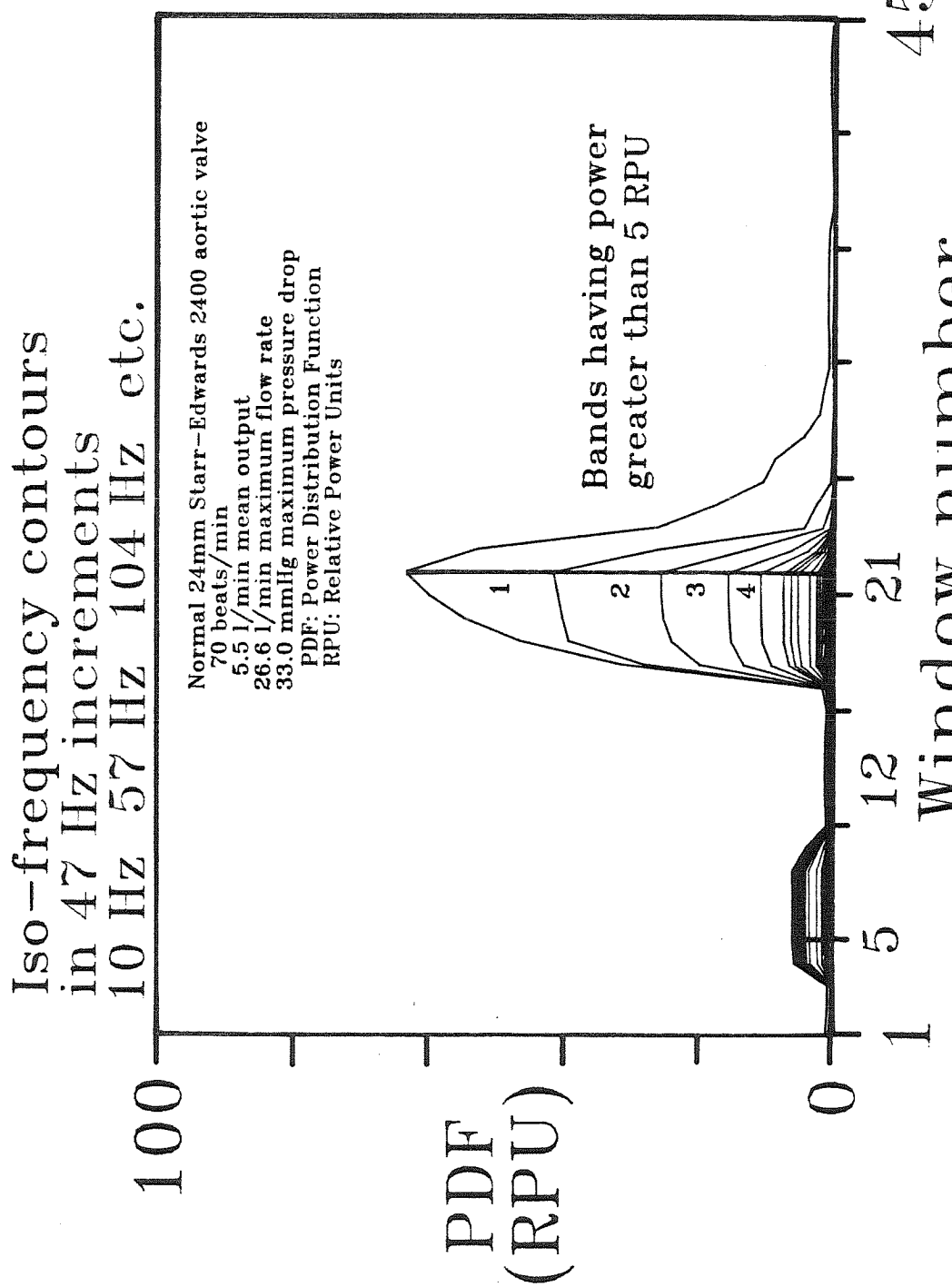

Figure 4-5c Auxiliary view perpendicular to the time axis of the 3-D power-frequency-time surface of experiment 306 showing iso-frequency contours.

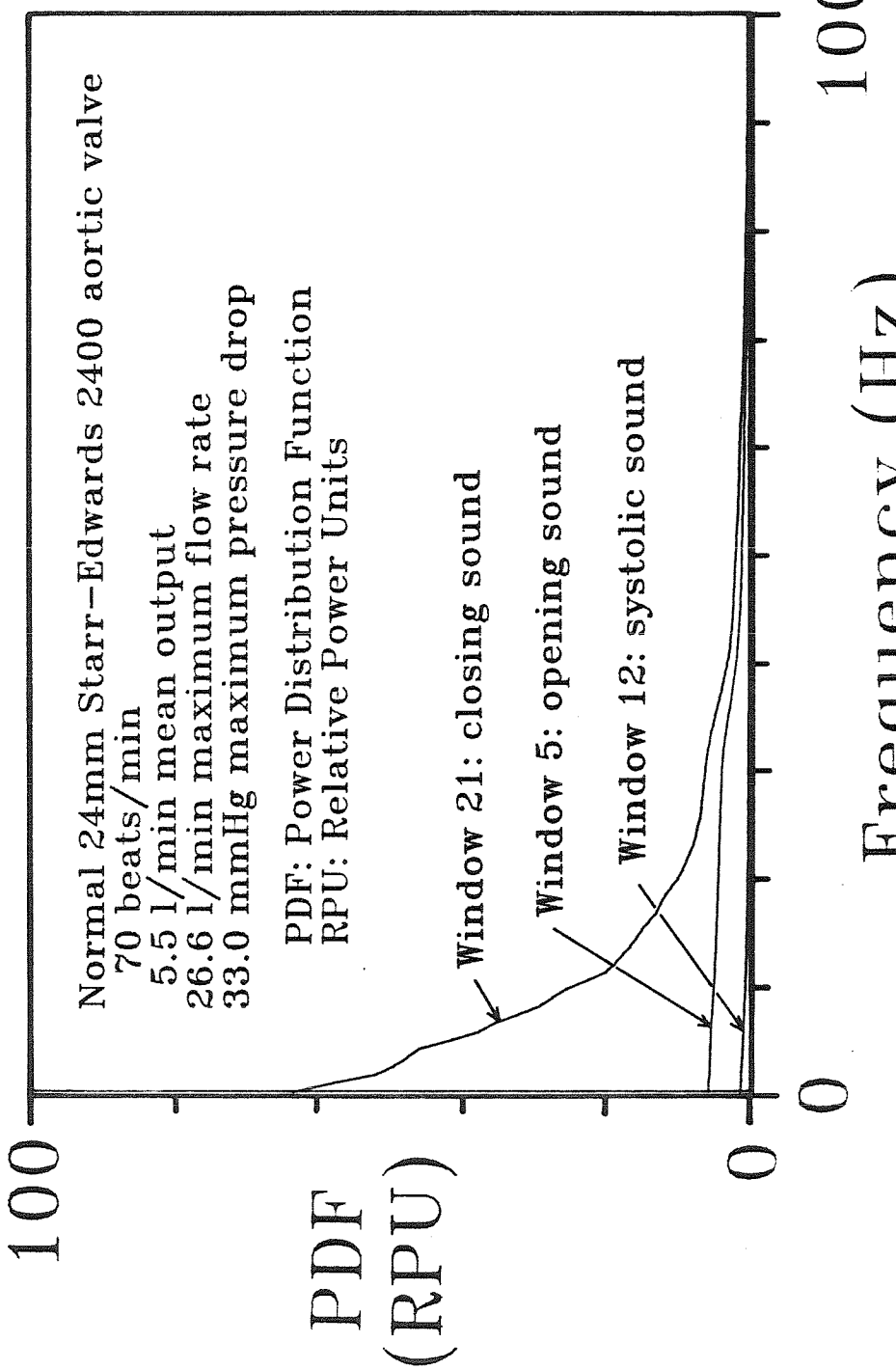

Figure 4-5d Auxiliary view perpendicular to the frequency axis of the 3-D power-frequency-time surface of experiment 306 showing power power distributions associated with windows encompassing the opening, systolic, and closing sounds.

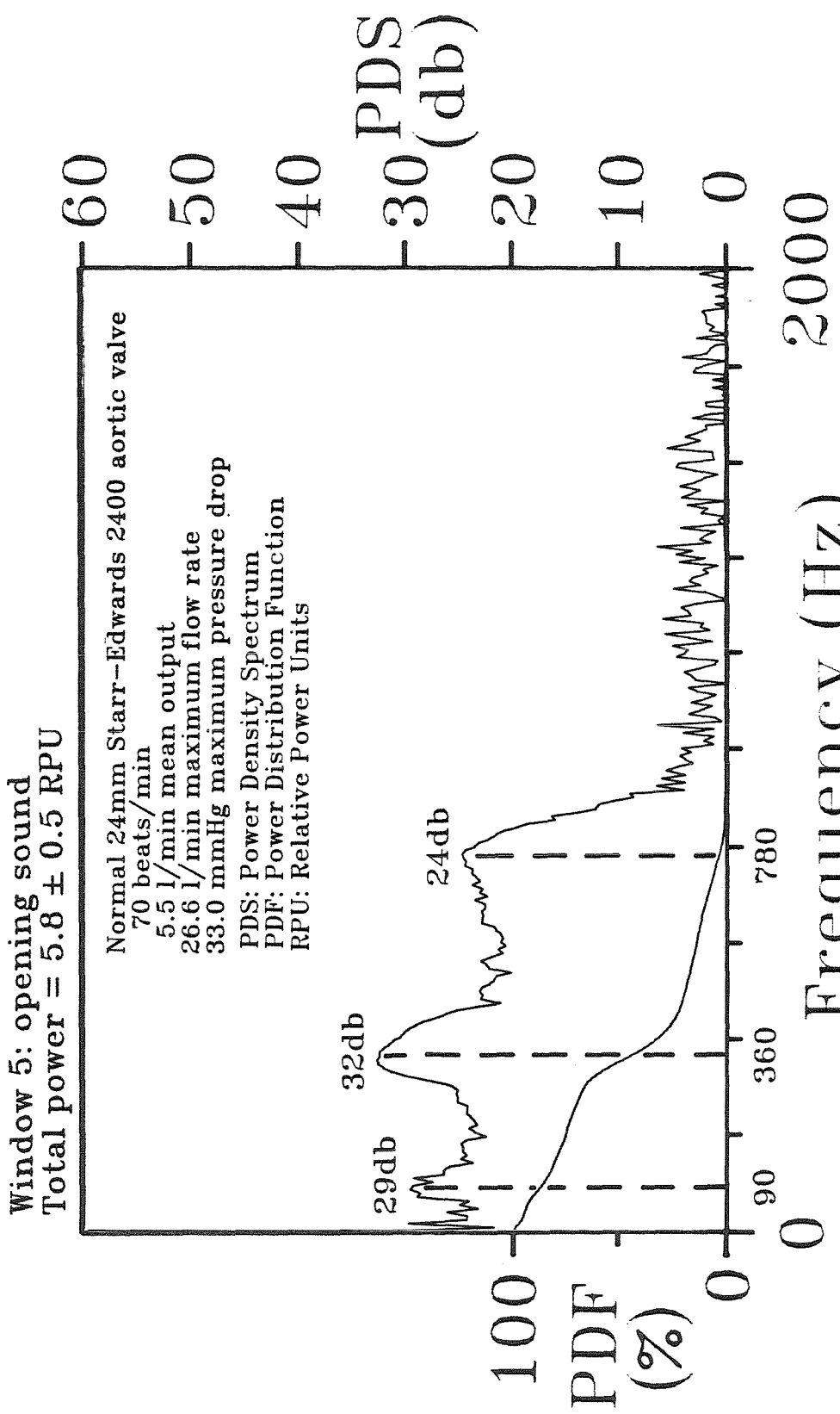

Figure 4-5e Power-density spectra and power distribution of the opening sound of experiment 306.

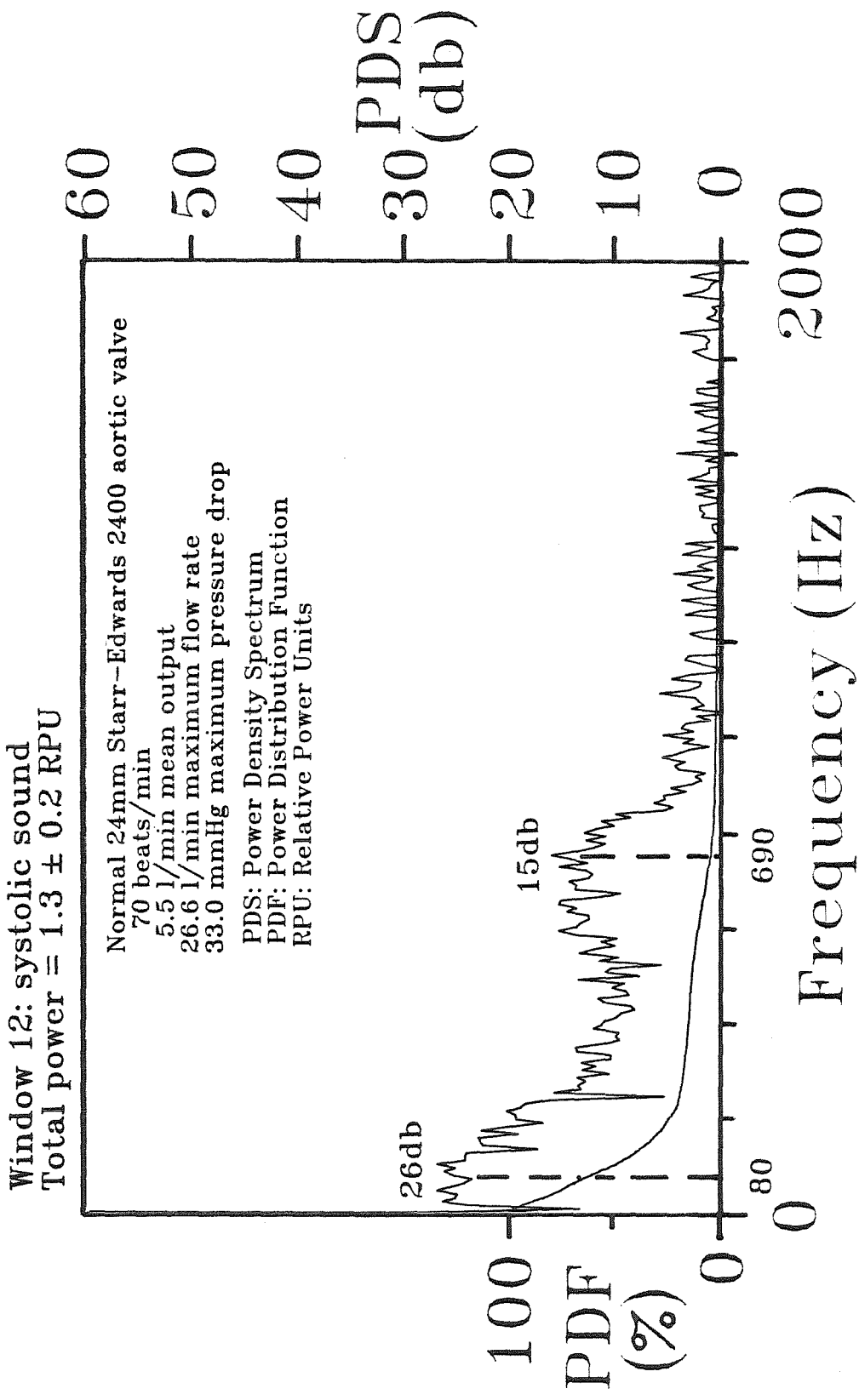

Figure 4-5f Power-density spectra and power distribution of the systolic sound of experiment 306.

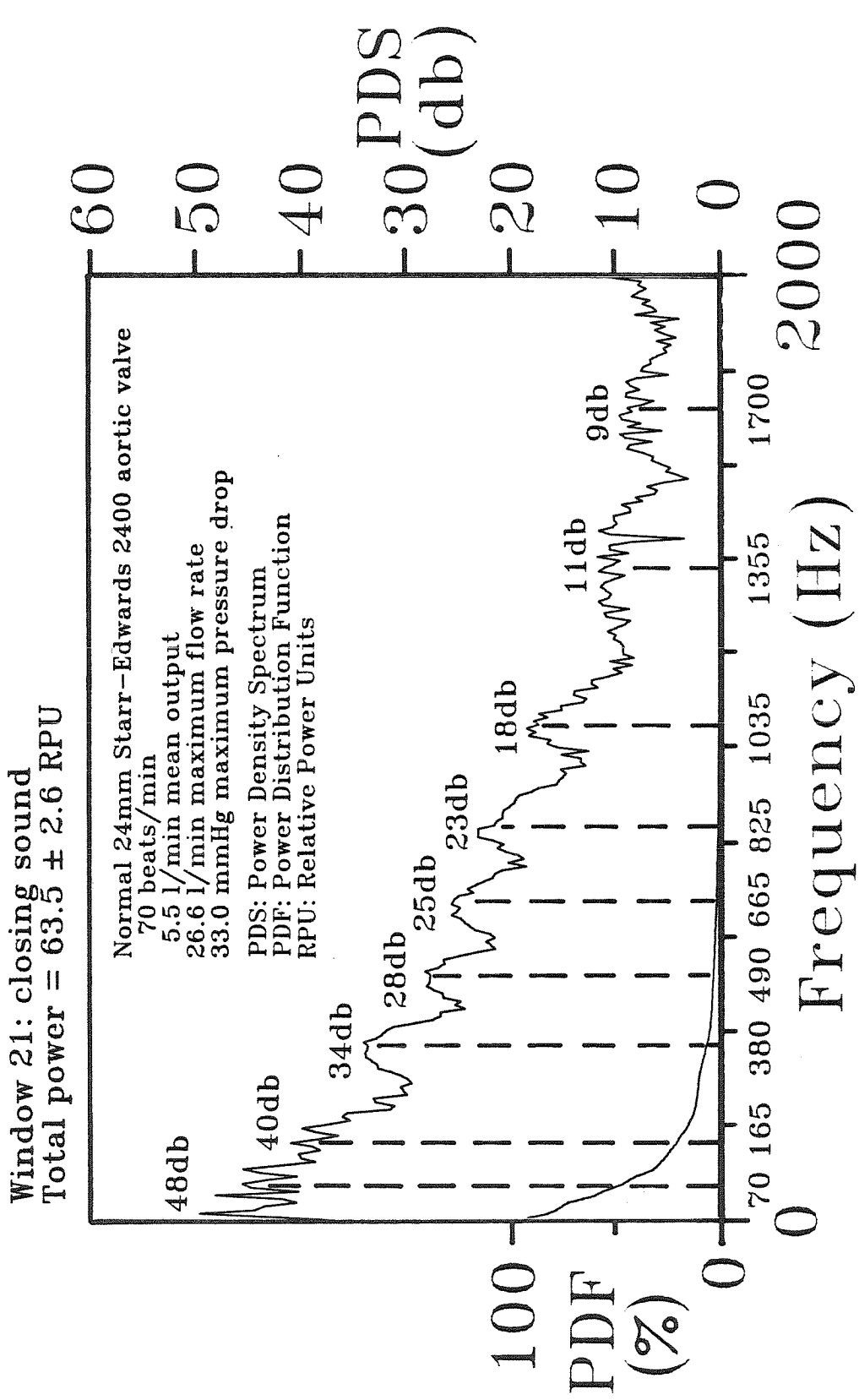

Figure 4-5g Power-density spectra and power distribution of the closing sound of experiment 306.

Parameters Estimated for

Significant Harmonic Peaks

Experiment 306

Event	Frequency, $f_{f,i}$; Decay, k_i; Power-Density, G_i (Hz,Hz,db)
Opening Sound	90,25,29
Window 5	360,45,24
	780,45,24
Systolic Sound	80, 55,26
Window 12	690,120,15
Closing Sound	70, 30,48
	165, 30,40
	380, 45,34
	490, 45,28
Window 21	665, 45,25
	825, 45,23
	1035, 45,18
	1355,150,11
	1700,110, 9

Table 4-2 Parameters estimated from significant harmonic peaks of experiment 306.

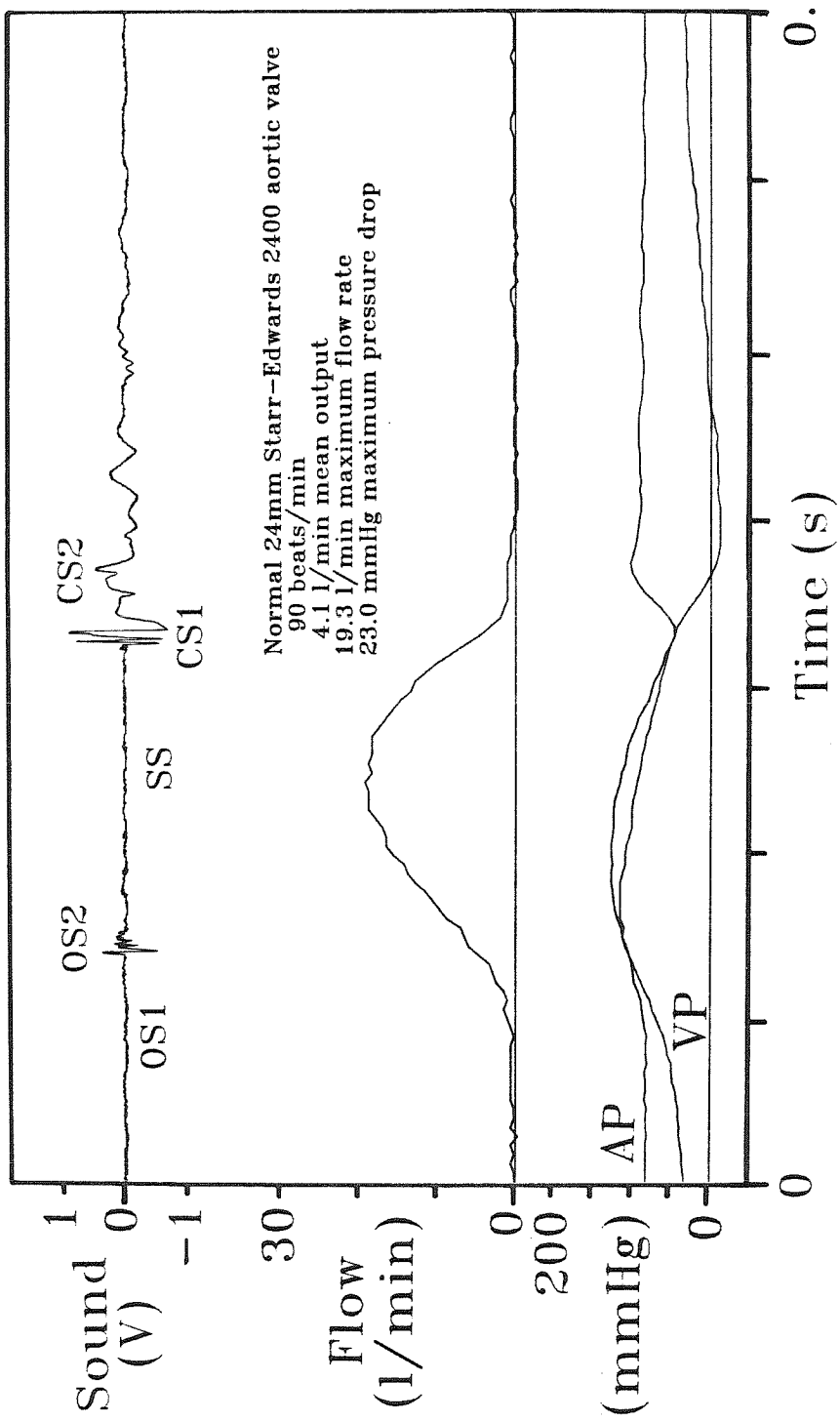

Figure 4-6a Amplitude vs. time tracings of sound, flow rate, aortic pressure and ventricular pressure associated with a typical cycle of experiment 307.

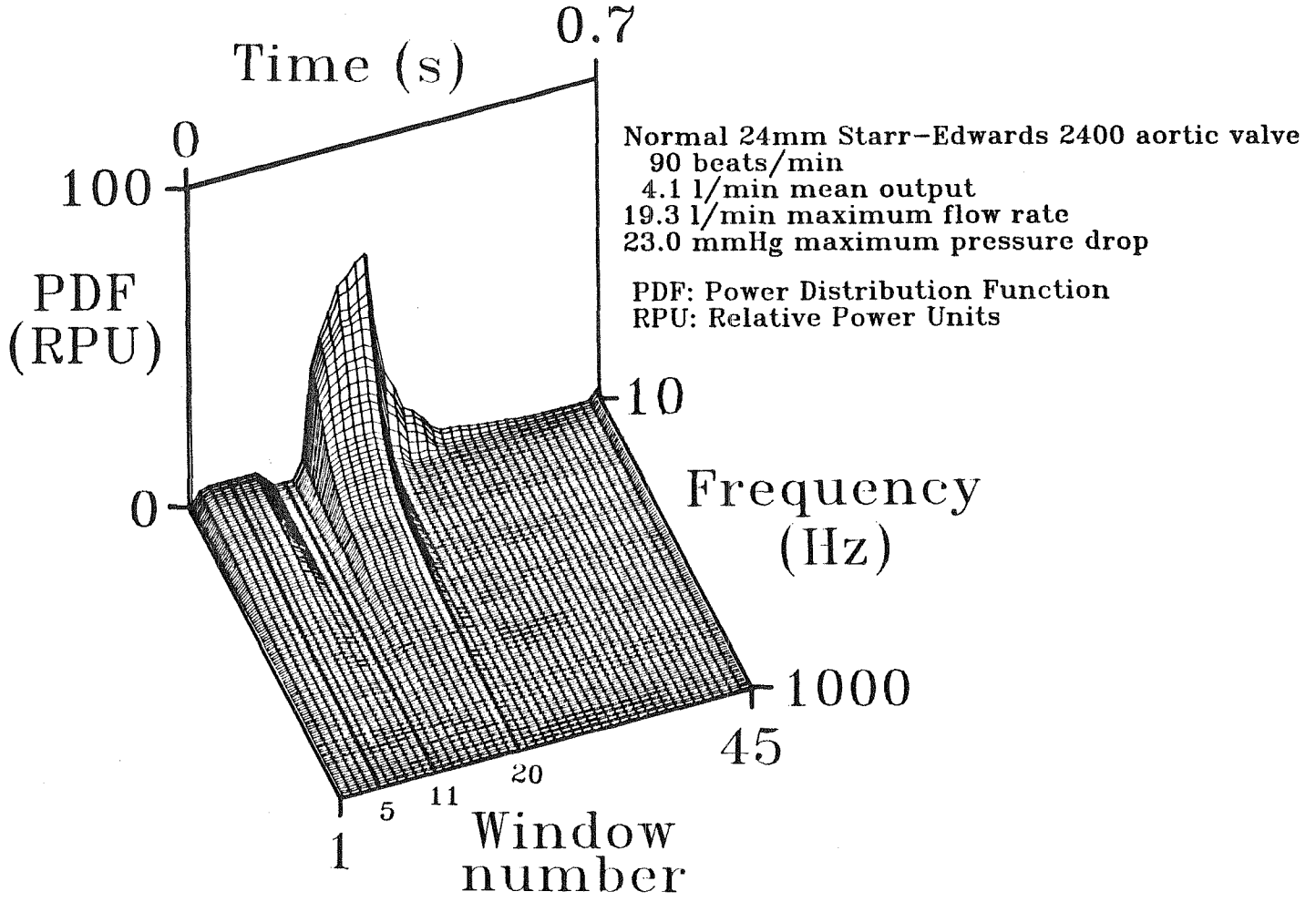

Figure 4-6b Three-dimensional power-frequency-time surface averaged over ten cycles of experiment 307.

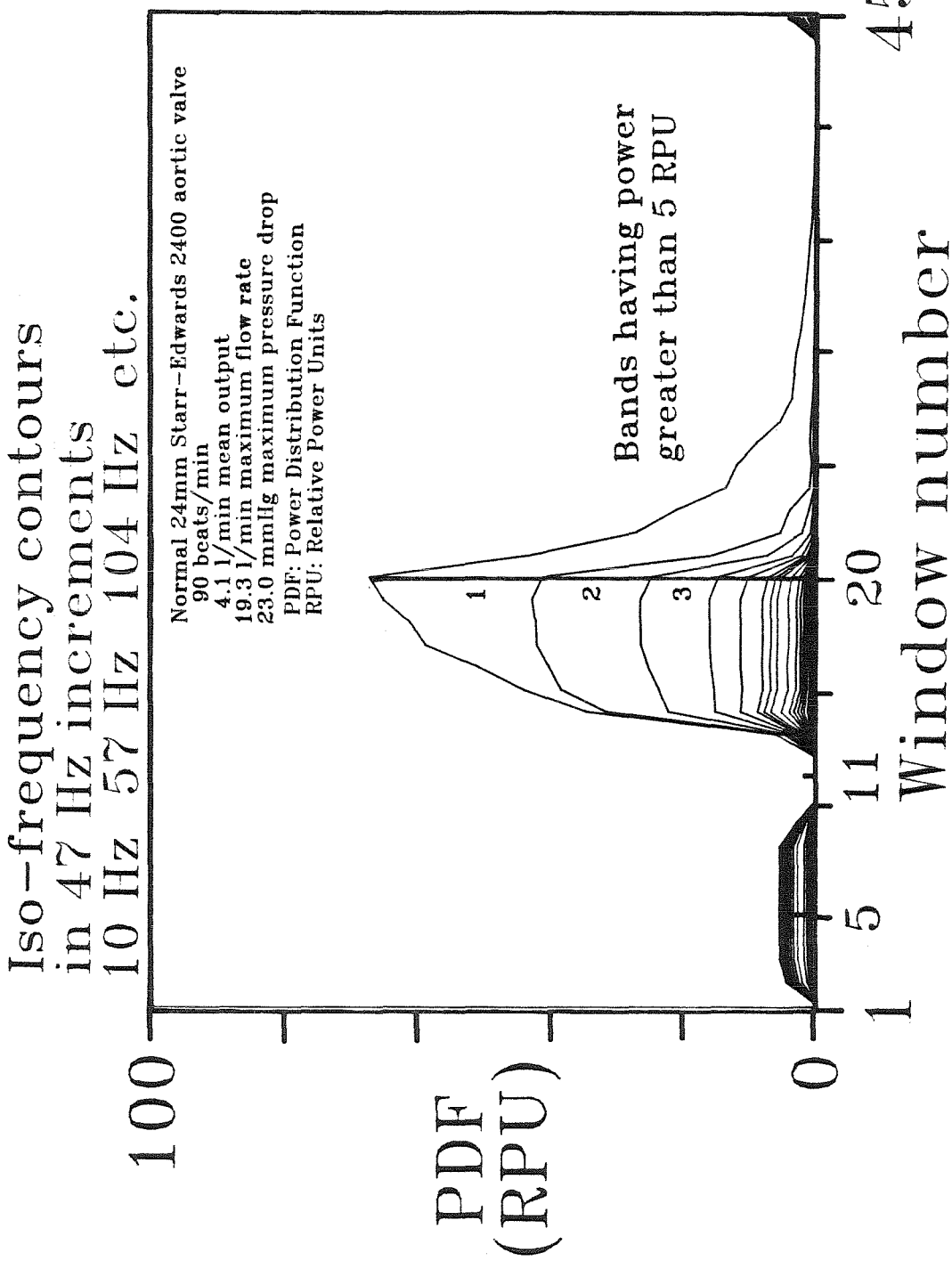

Figure 4-6c Auxiliary view perpendicular to the time axis of the 3-D power-frequency-time surface of experiment 307 showing iso-frequency contours.

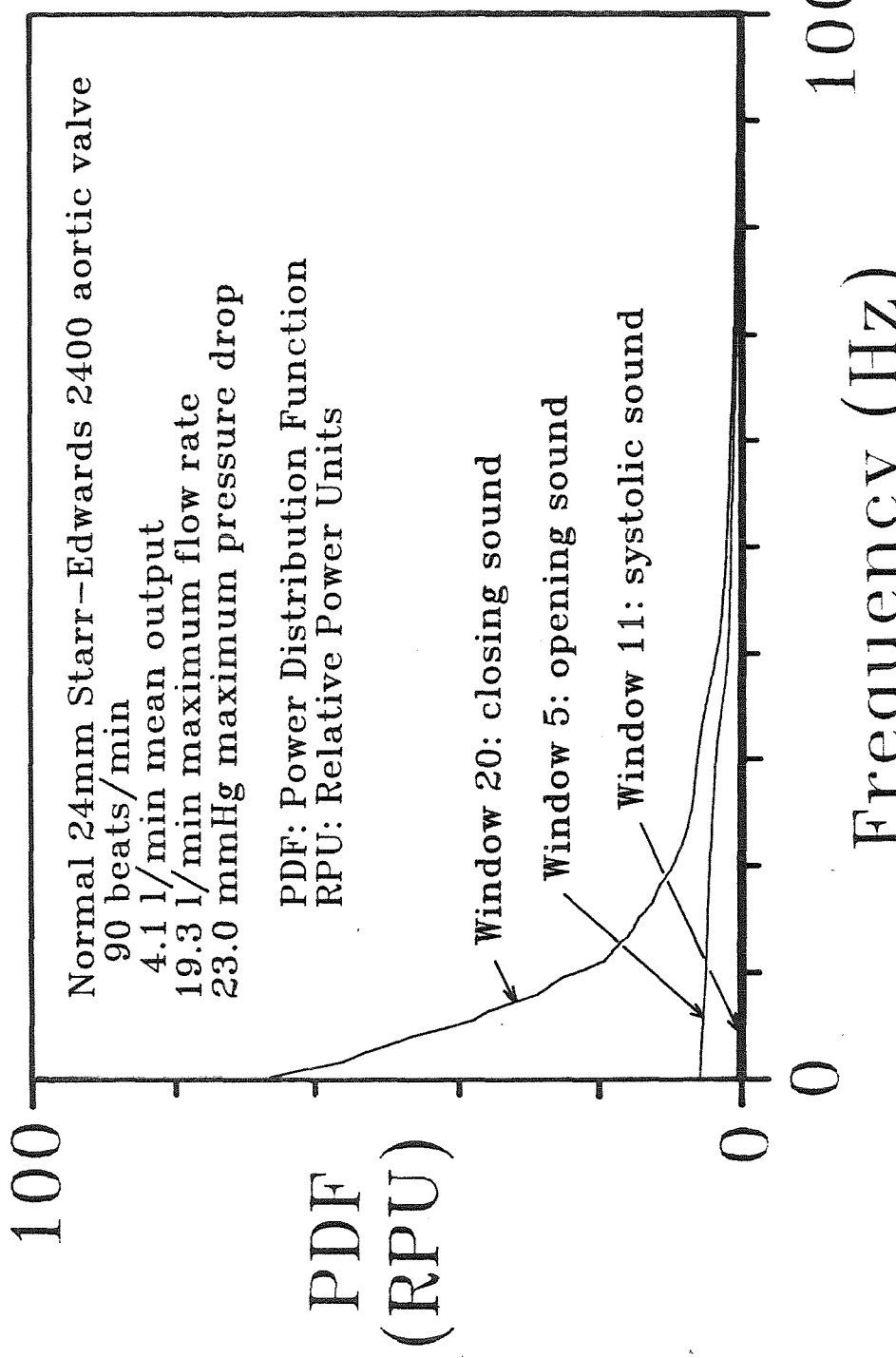

Figure 4-6d Auxiliary view perpendicular to the frequency axis of the 3-D power-frequency-time surface of experiment 307 showing power power distributions associated with windows encompassing the opening, systolic, and closing sounds.

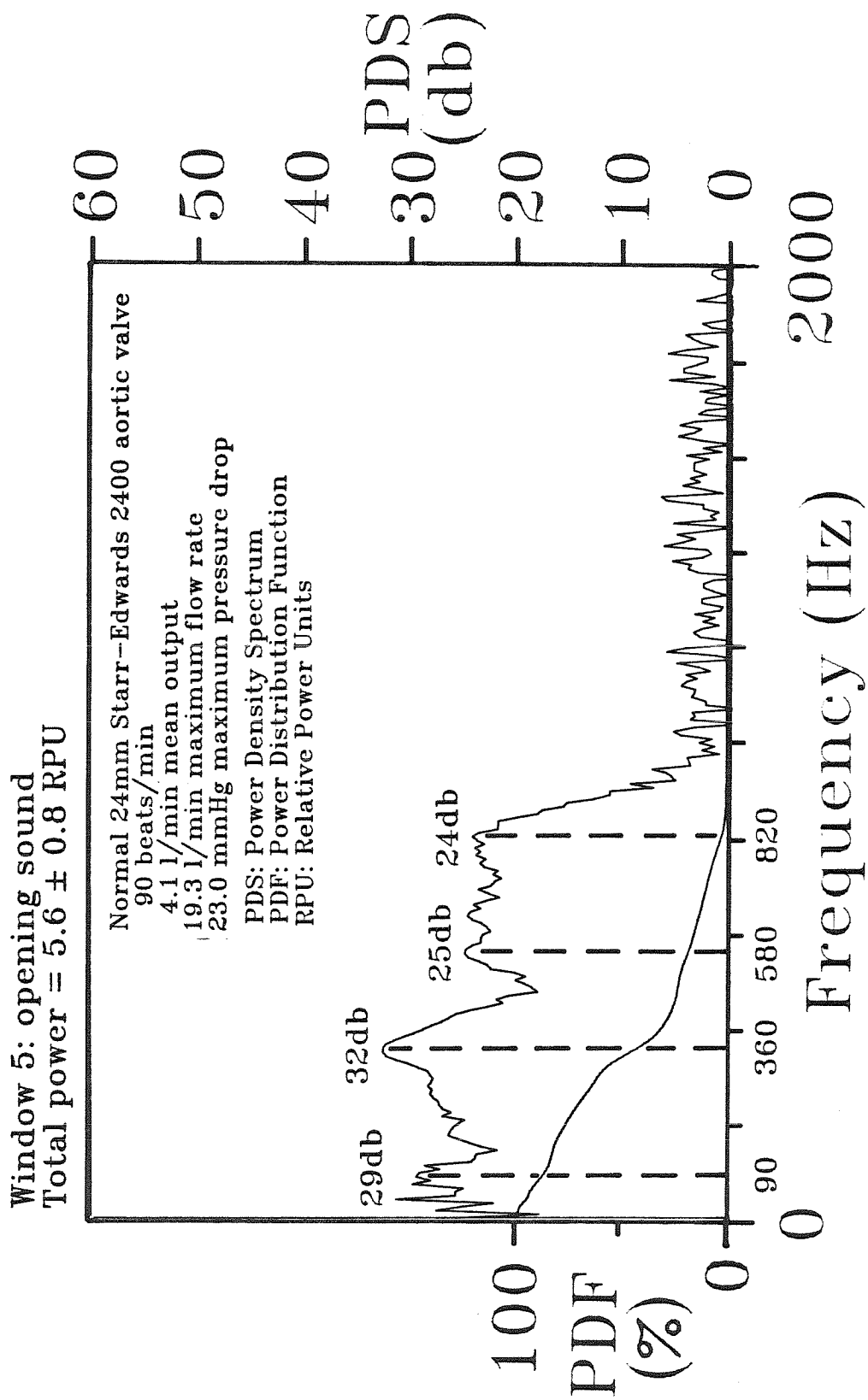

Figure 4-6e Power-density spectra and power distribution of the opening sound of experiment 307.

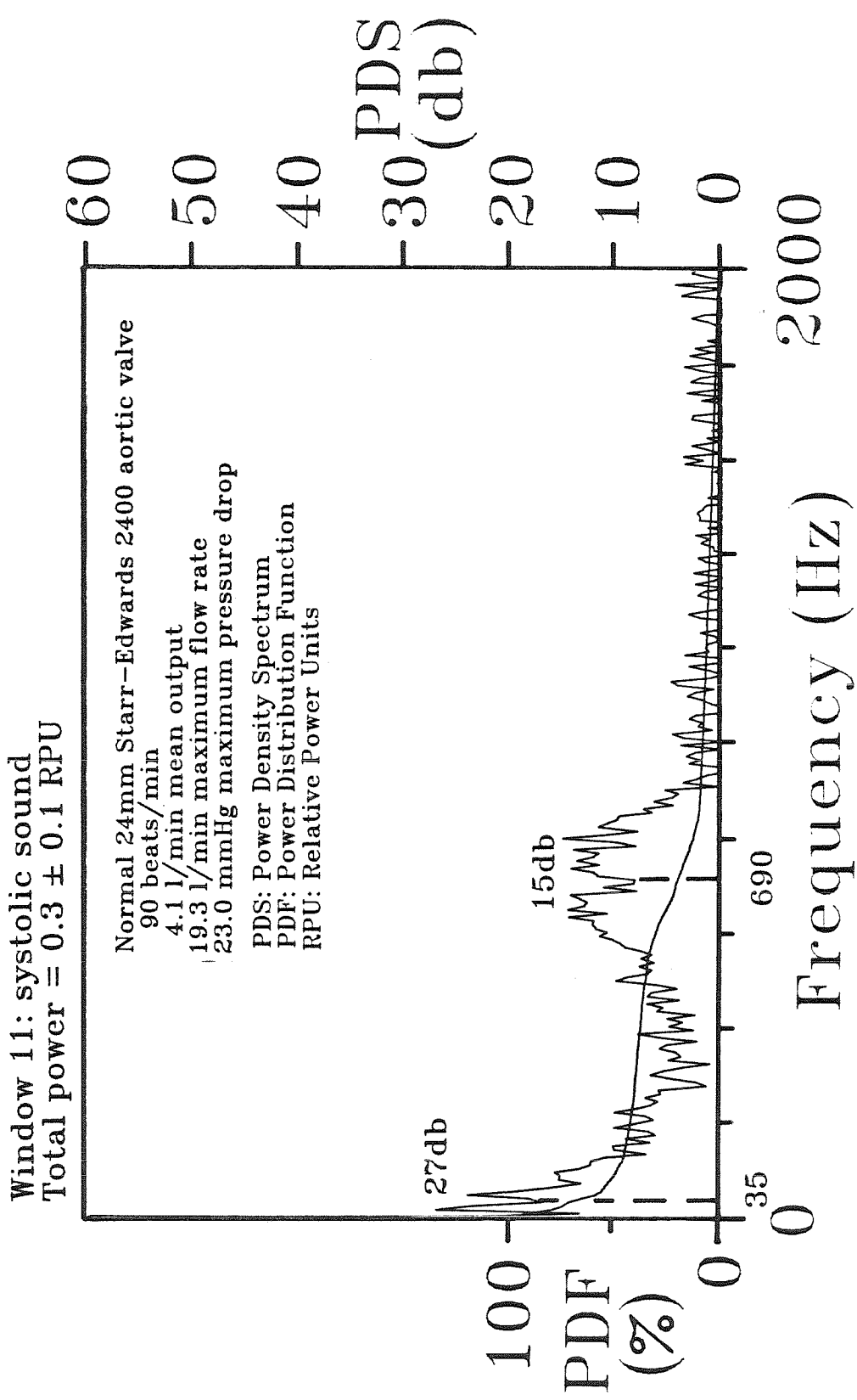

Figure 4-6f Power-density spectra and power distribution of the systolic sound of experiment 307.

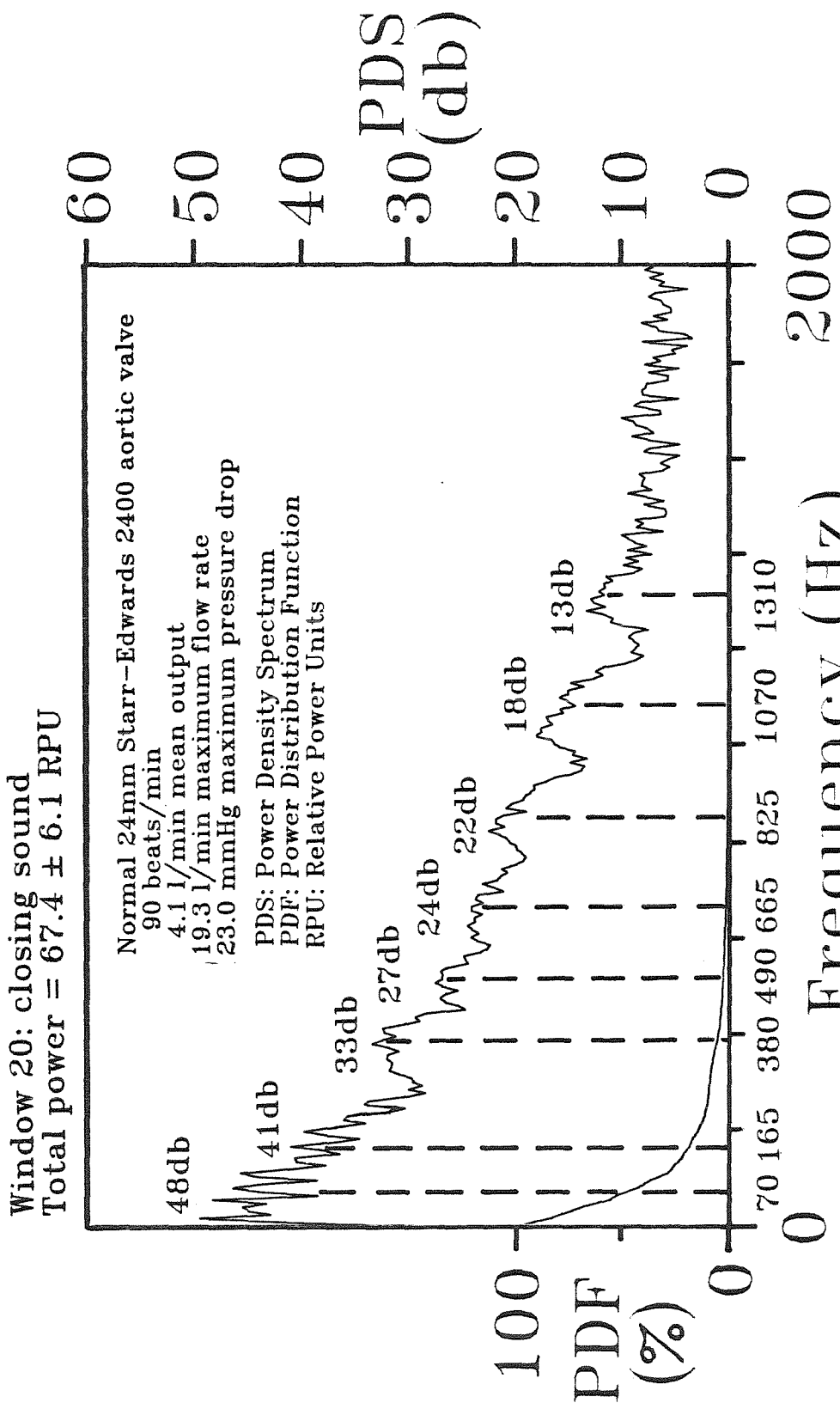

Figure 4-6g Power-density spectra and power distribution of the closing sound of experiment 307.

Parameters Estimated for

Significant Harmonic Peaks

Experiment 307

Event	Frequency, $f_{f,i}$; Decay, k_i; Power-Density, G_i (Hz,Hz,db)
Opening Sound	90,25,29
	360,35,32
Window 5	580,45,25
	820,60,24
Systolic Sound	35, 30,27
Window 11	690,120,15
Closing Sound	70,35,48
	165,45,41
	380,50,33
	490,50,27
Window 20	665,65,24
	825,65,22
	1070,50,18
	1310,50,13

Table 4-3 Parameters estimated from significant harmonic peaks of experiment 307.

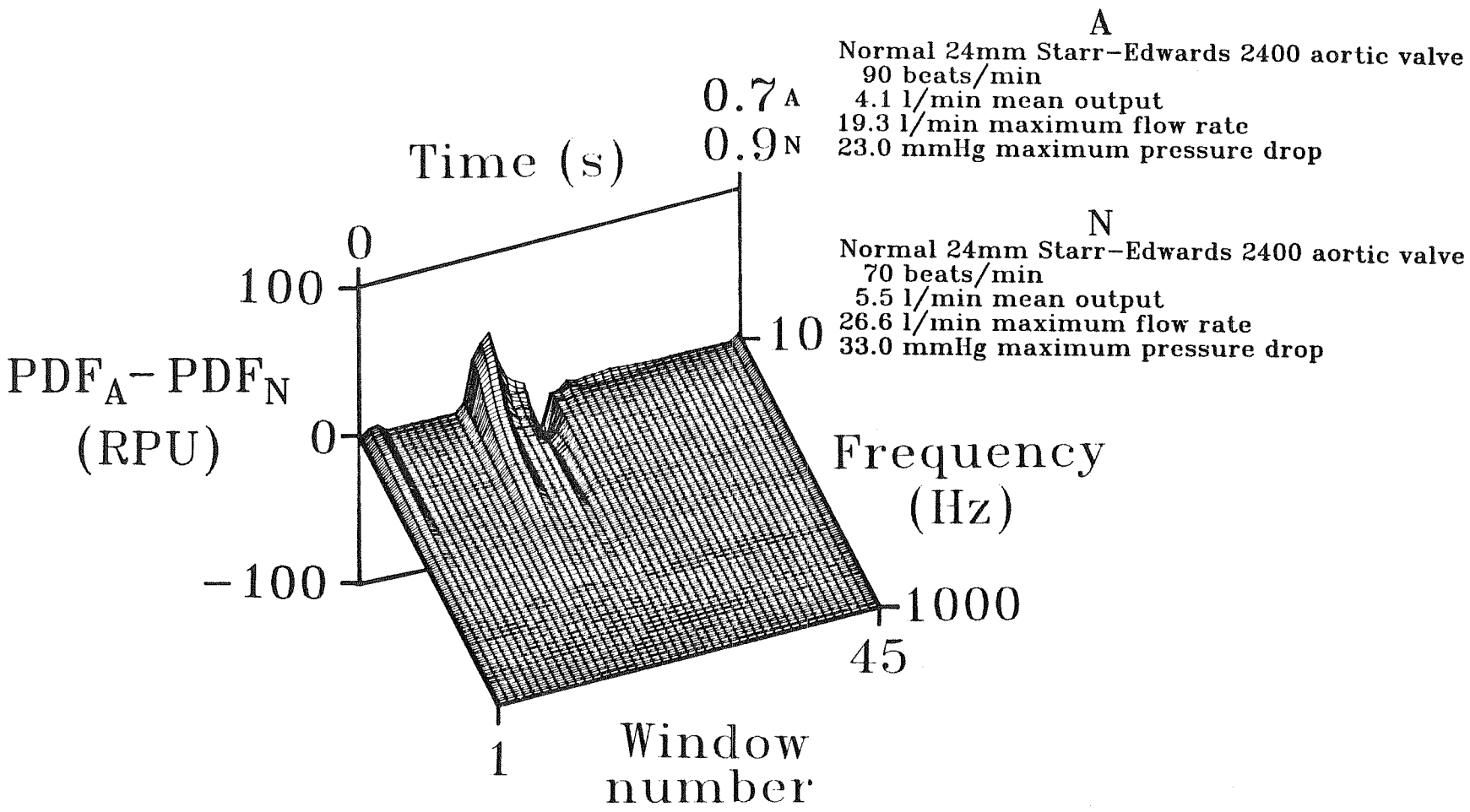

Figure 4-6h Three-dimensional surface depicting the difference between the power-frequency-time surfaces associated with experiments 307 and 306.

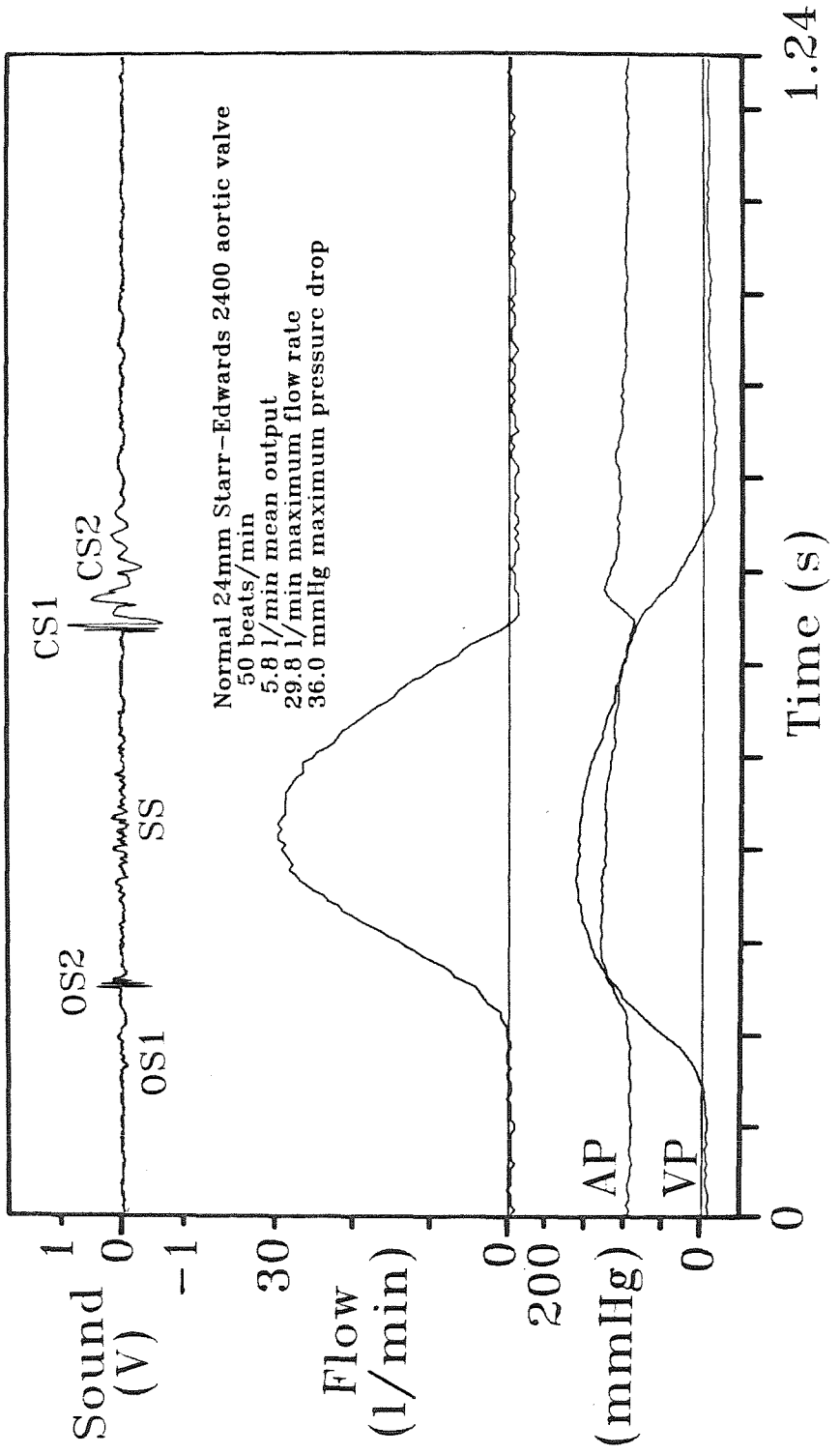

Figure 4-7a Amplitude vs. time tracings of sound, flow rate, aortic pressure and ventricular pressure associated with a typical cycle of experiment 308.

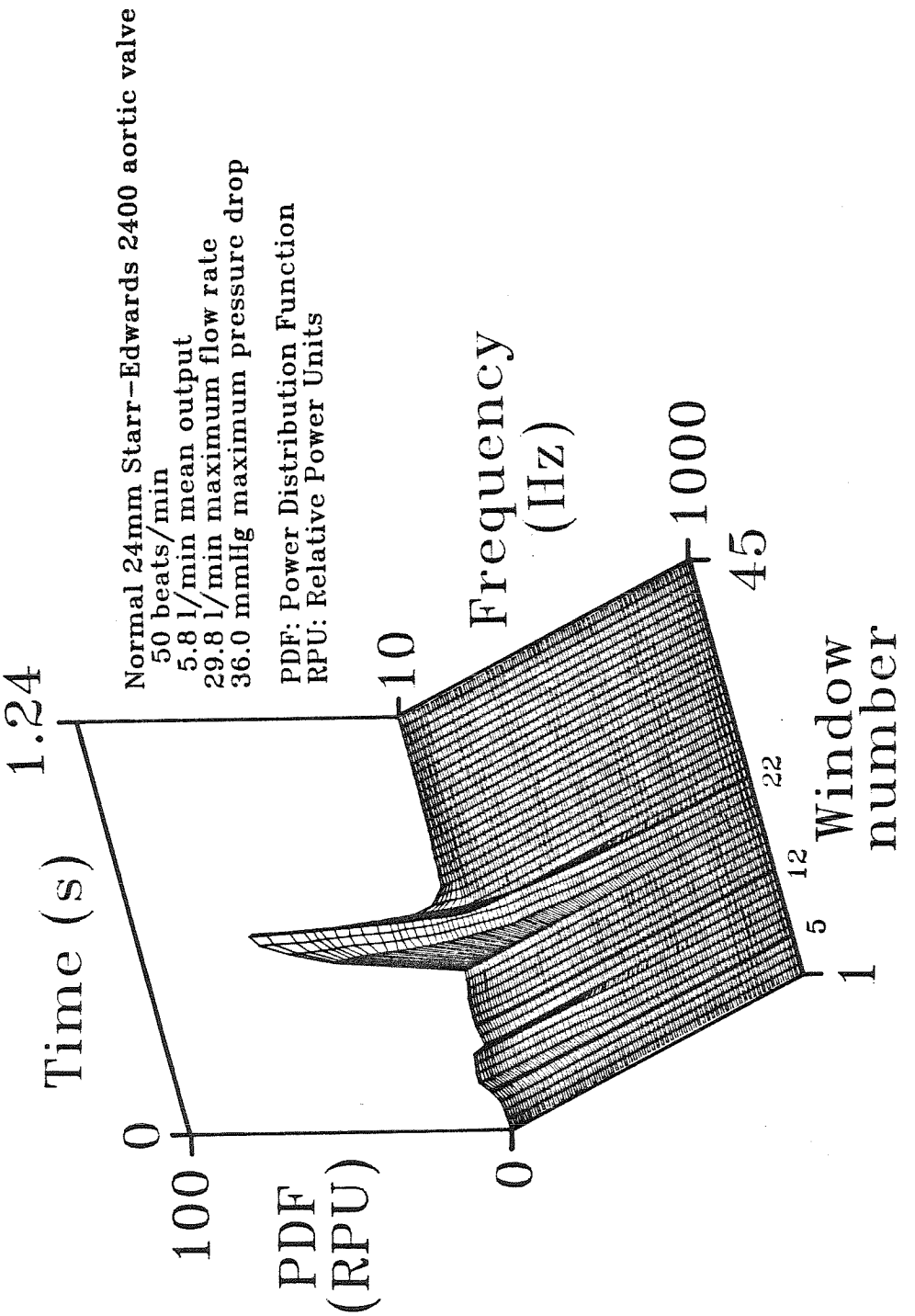

Figure 4-7b Three-dimensional power-frequency-time surface averaged over ten cycles of experiment 308.

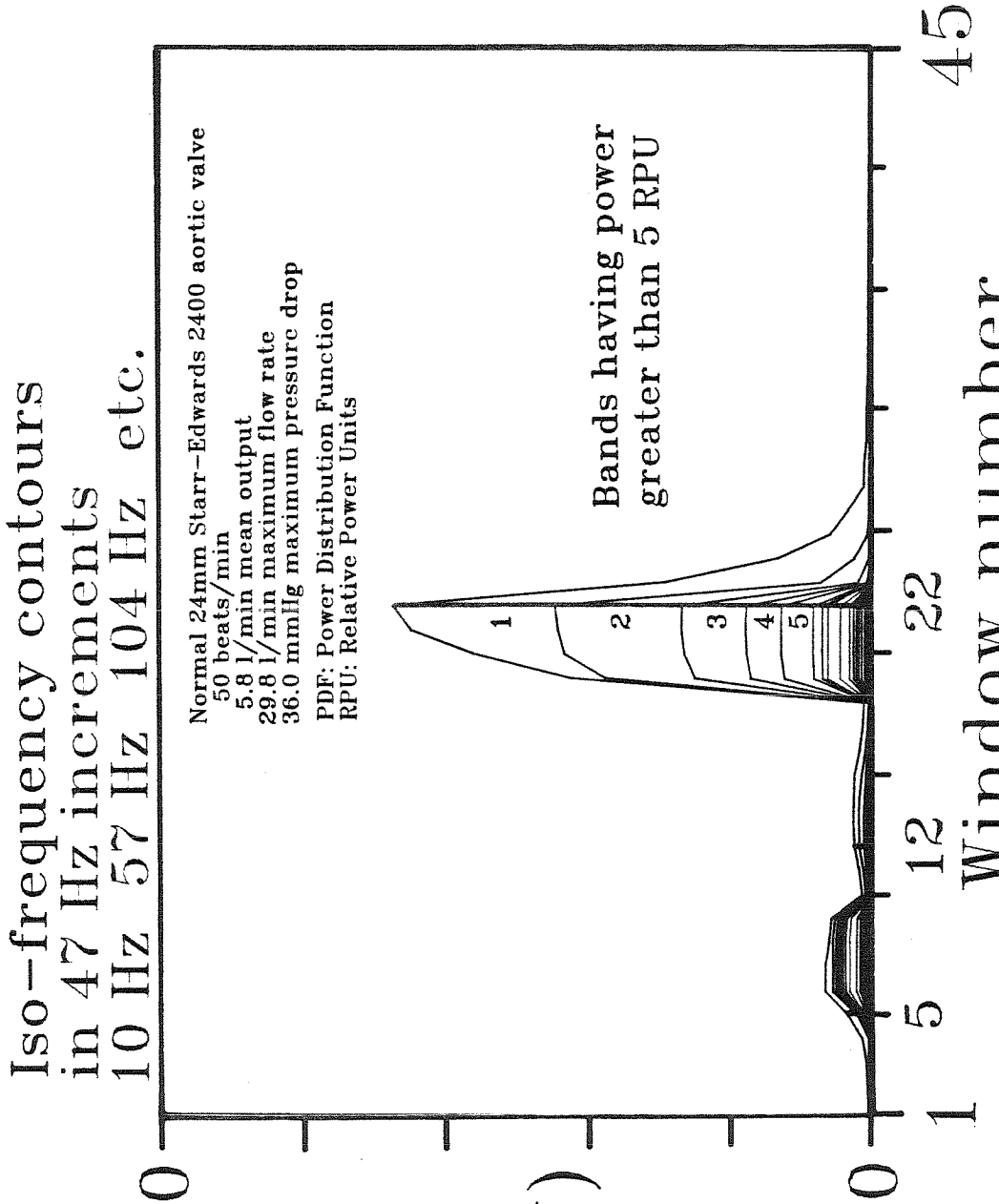

Figure 4-7c Auxiliary view perpendicular to the time axis of the 3-D power-frequency-time surface of experiment 308 showing iso-frequency contours.

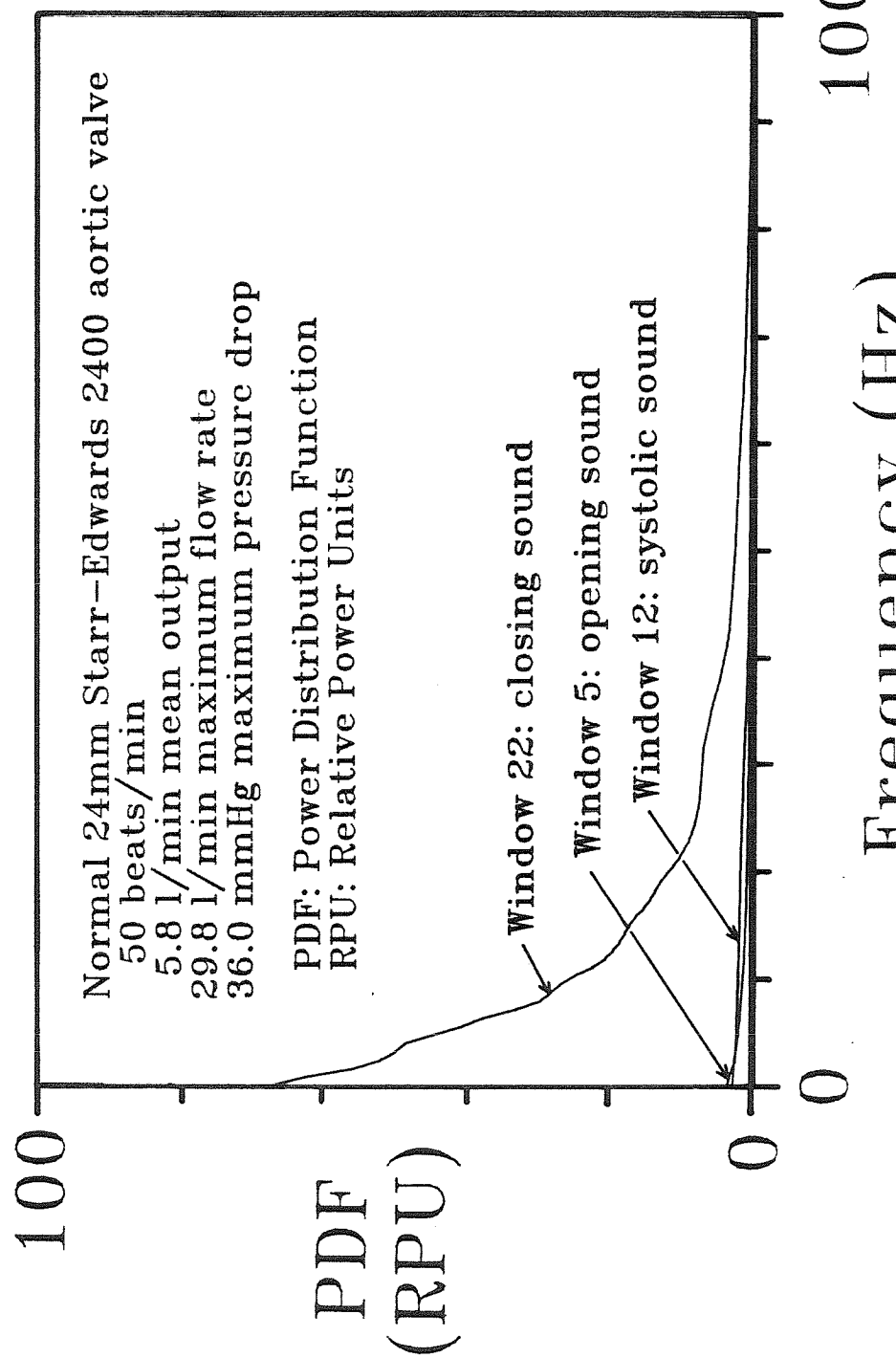

Figure 4-7d Auxiliary view perpendicular to the frequency axis of the 3-D power-frequency-time surface of experiment 308 showing power power distributions associated with windows encompassing the opening, systolic, and closing sounds.

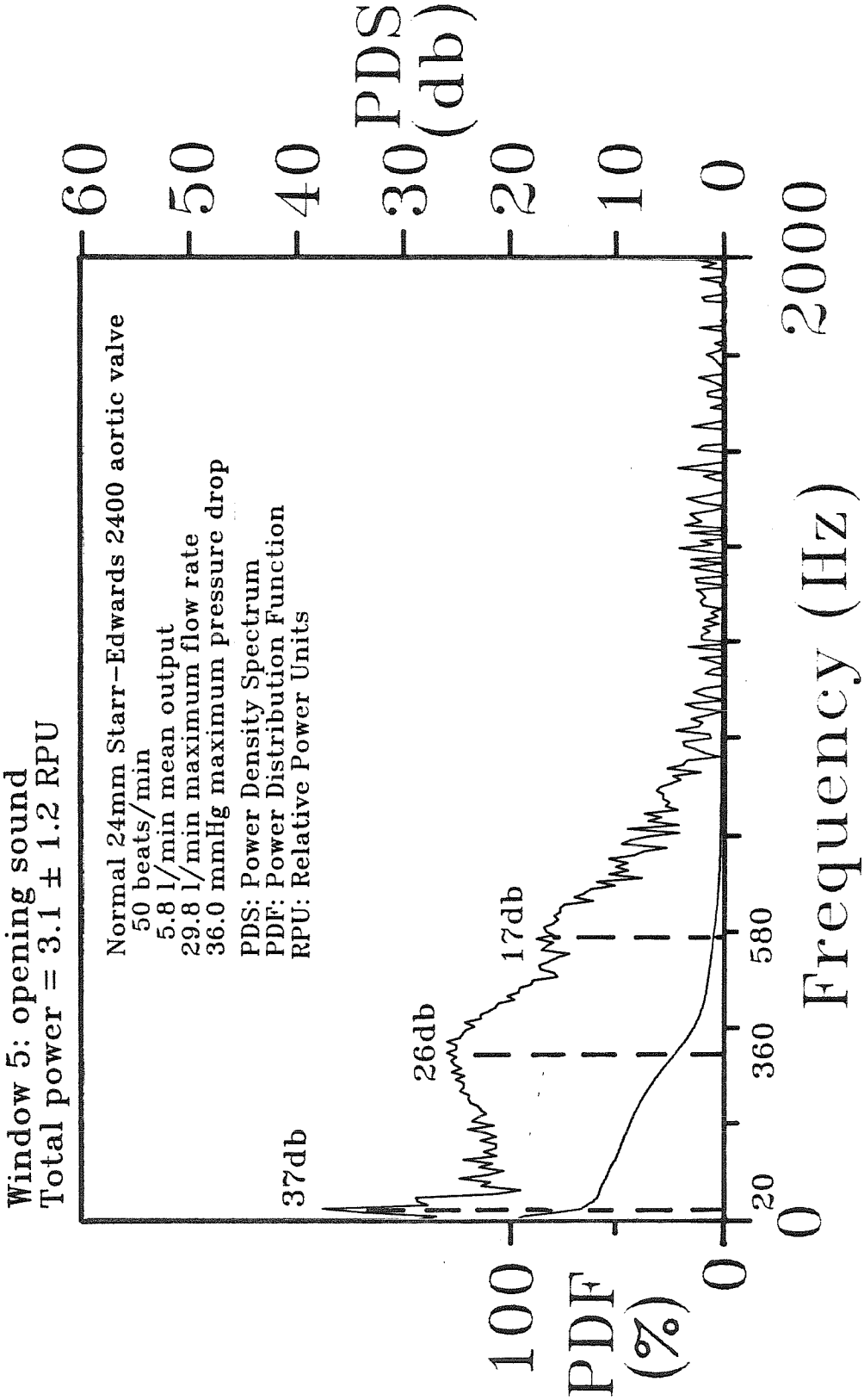

Figure 4-7e Power-density spectra and power distribution of the opening sound of experiment 308.

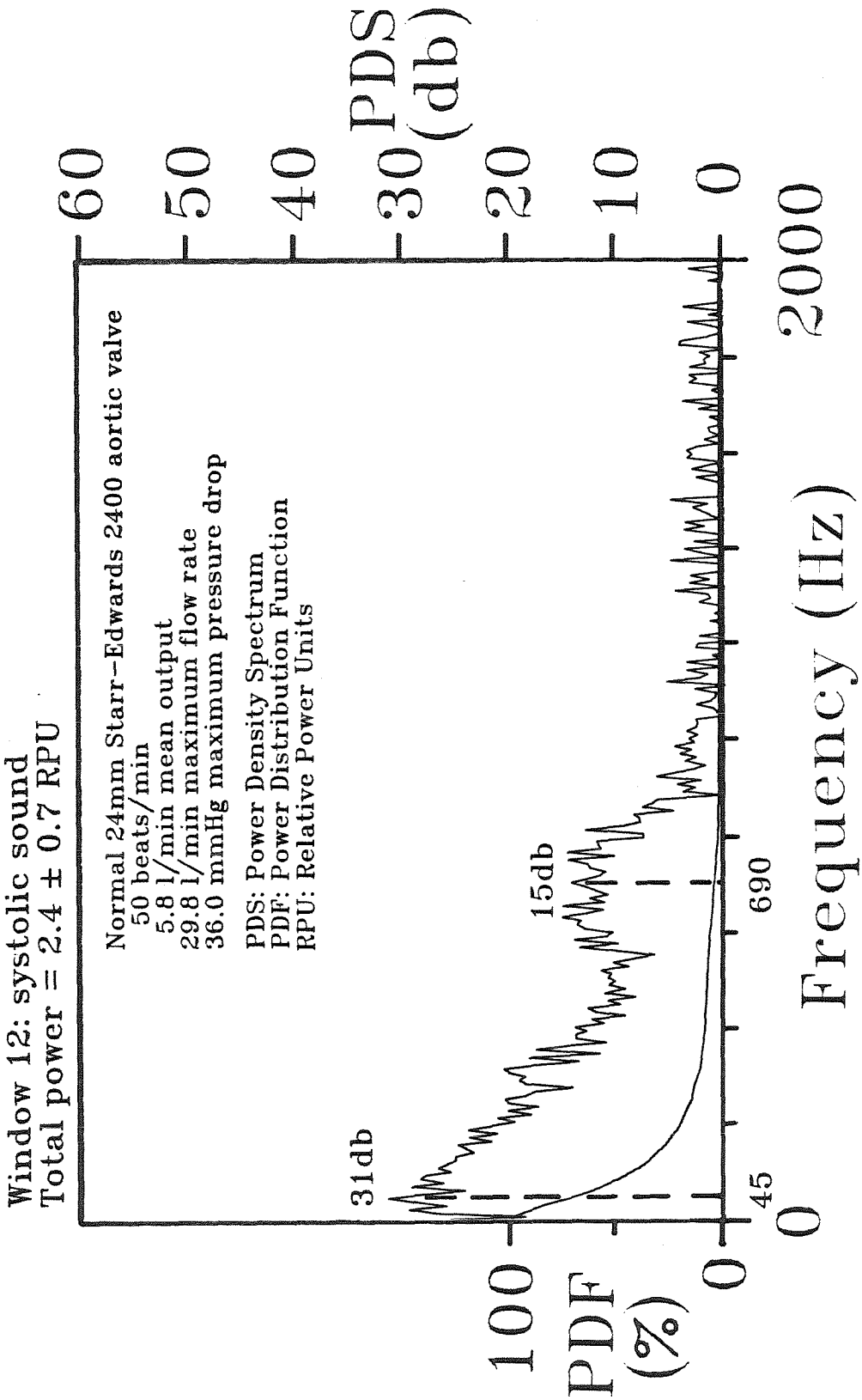

Figure 4-7f Power-density spectra and power distribution of the systolic sound of experiment 308.

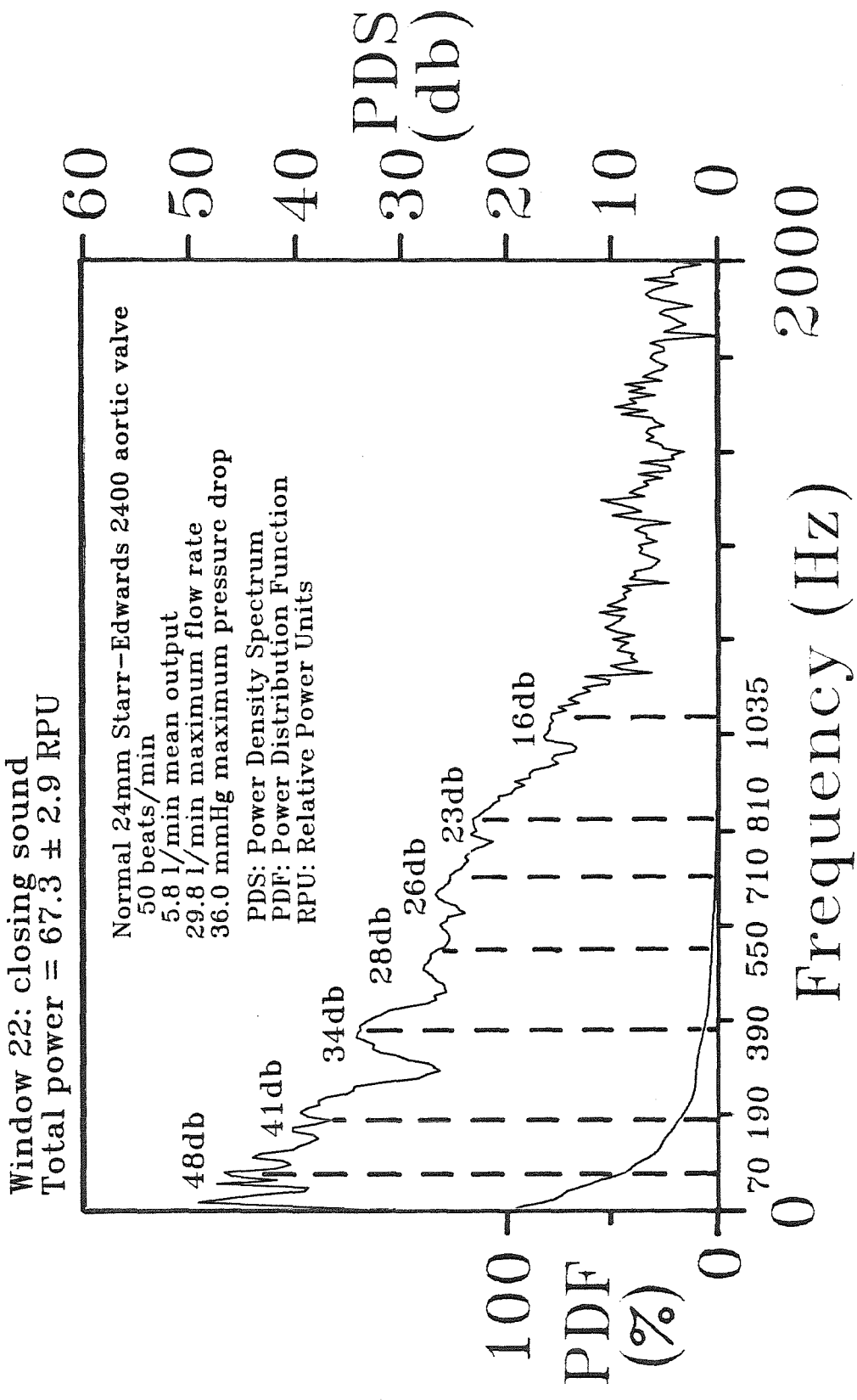

Figure 4-7g Power-density spectra and power distribution of the closing sound of experiment 308.

Parameters Estimated for

Significant Harmonic Peaks

Experiment 308

Event	Frequency, $f_{f,i}$; Decay, k_i; Power-Density, G_i (Hz,Hz,db)
Opening Sound	20, 5,37
Window 5	360,90,26
	580,80,17
Systolic Sound	45, 45,31
Window 12	690,120,15
Closing Sound	70, 35,48
Window 22	190, 45,41
	390, 50,34
	550, 50,28
	710, 50,26
	810, 45,23
	1035, 55,16

Table 4-4 Parameters estimated from significant harmonic peaks of experiment 308.

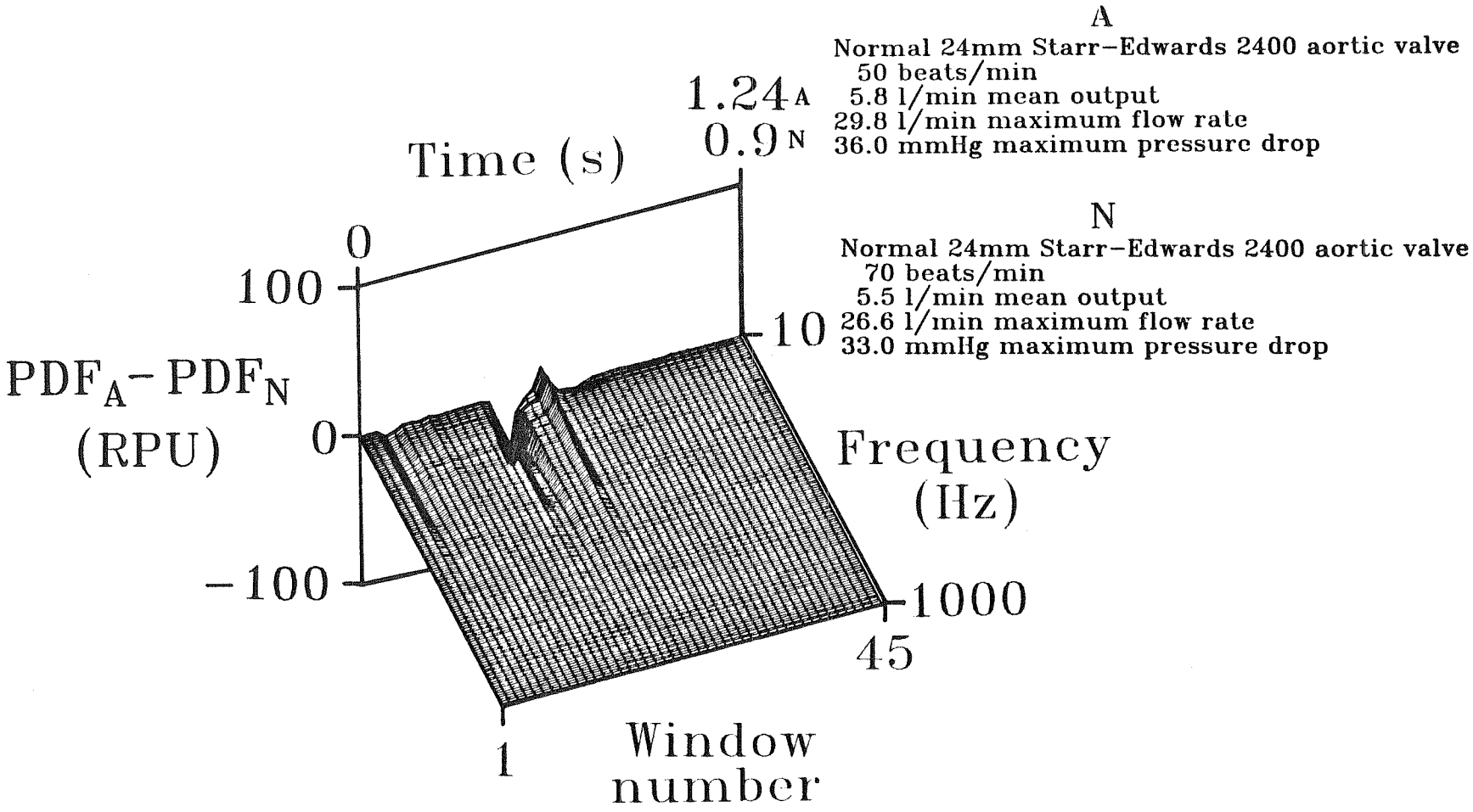

Figure 4-7h Three-dimensional surface depicting the difference between the power-frequency-time surfaces associated with experiments 308 and 306.

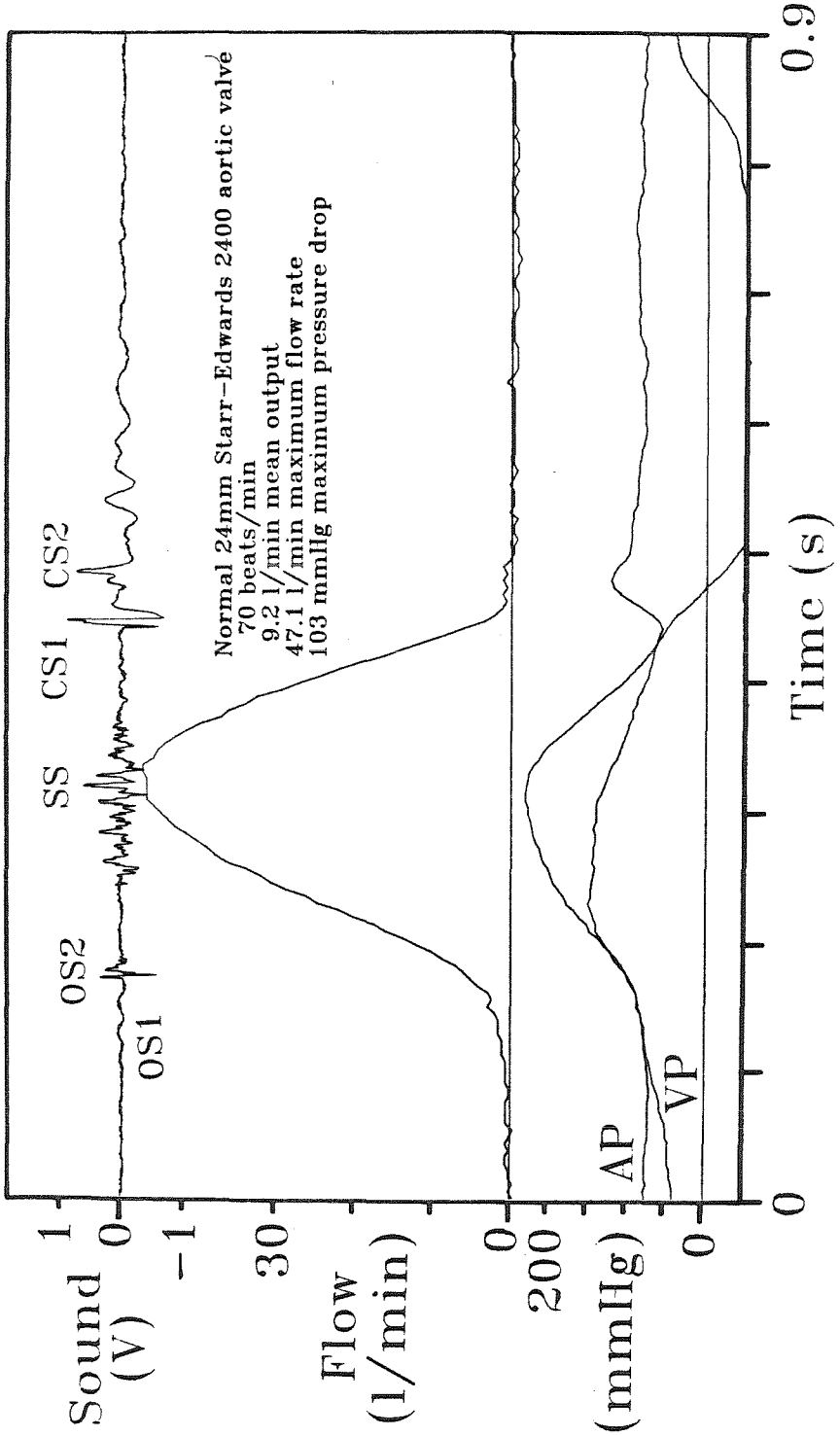

Figure 4-8a Amplitude vs. time tracings of sound, flow rate, aortic pressure and ventricular pressure associated with a typical cycle of experiment 309.

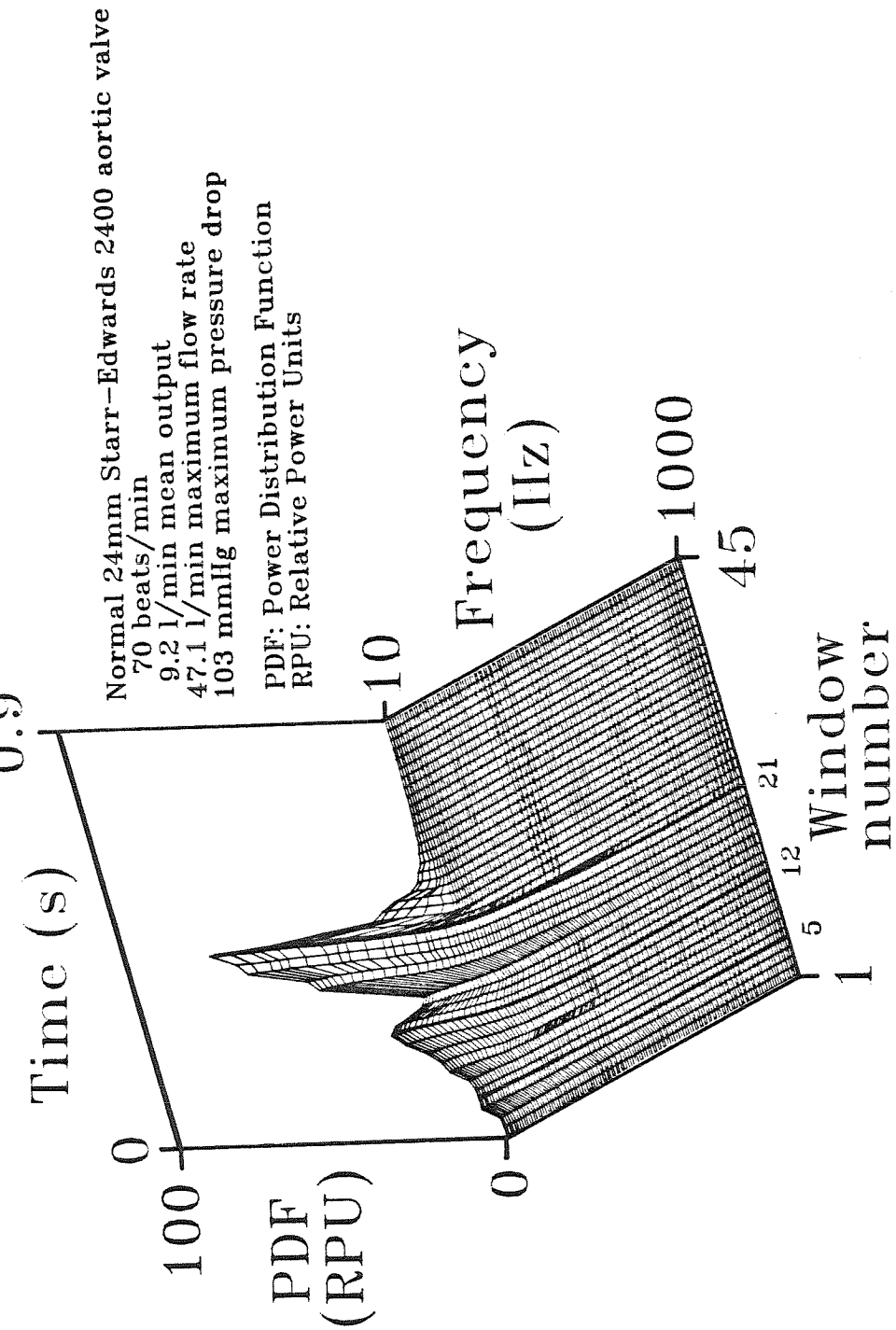

Figure 4-8b Three-dimensional power-frequency-time surface averaged over ten cycles of experiment 309.

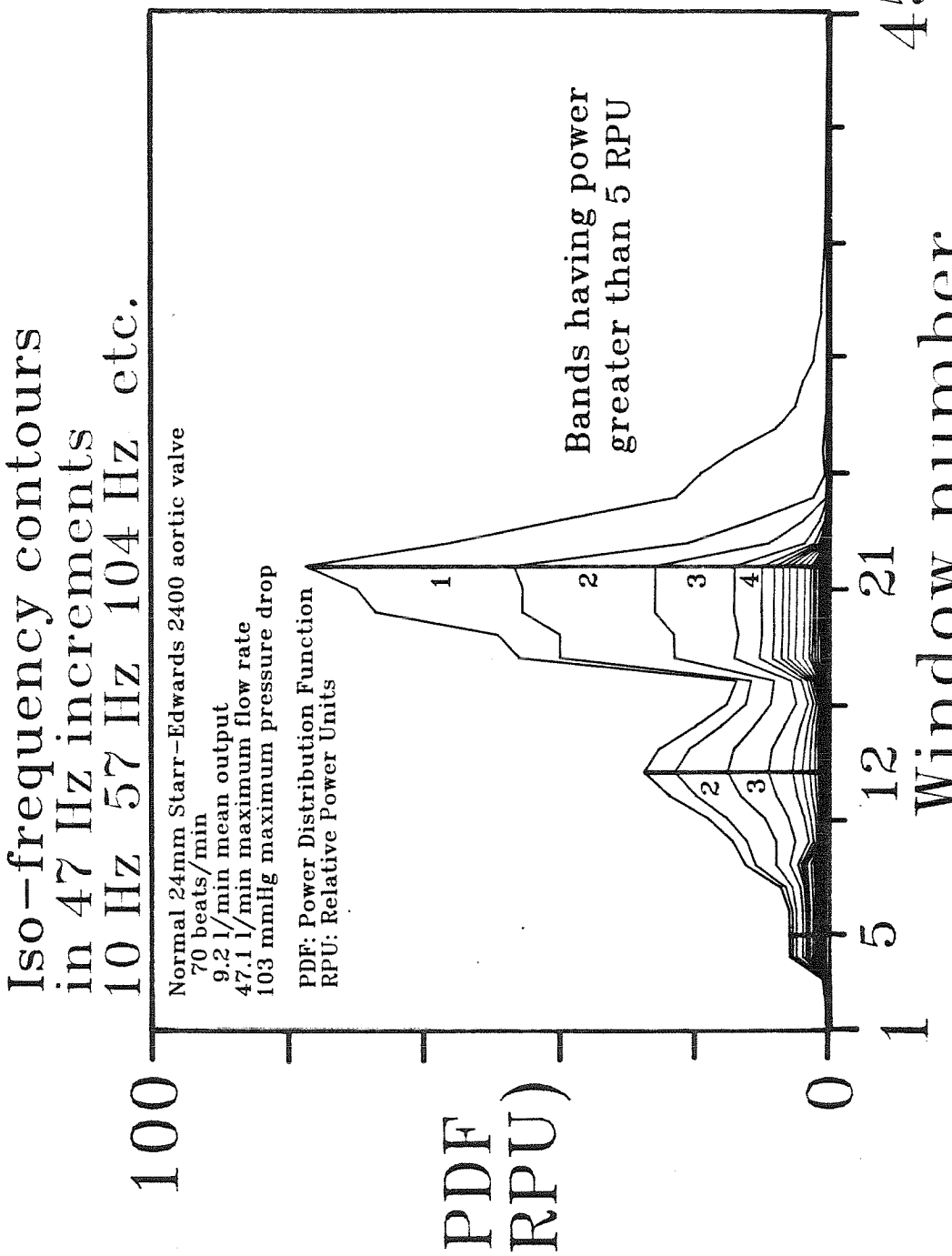

Figure 4-8c Auxiliary view perpendicular to the time axis of the 3-D power-frequency-time surface of experiment 309 showing iso-frequency contours.

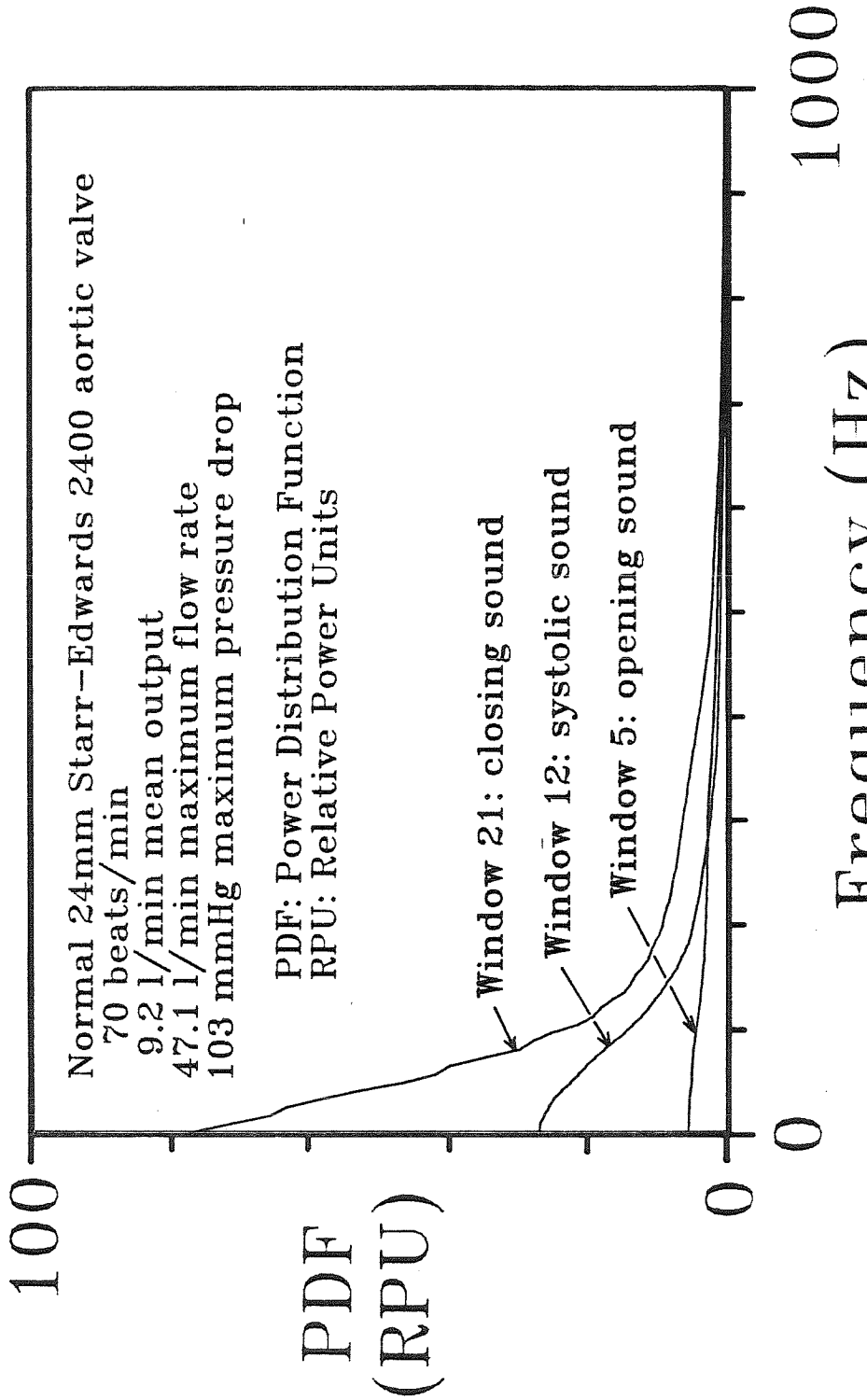

Figure 4-8d Auxiliary view perpendicular to the frequency axis of the 3-D power-frequency-time surface of experiment 309 showing power power distributions associated with windows encompassing the opening, systolic, and closing sounds.

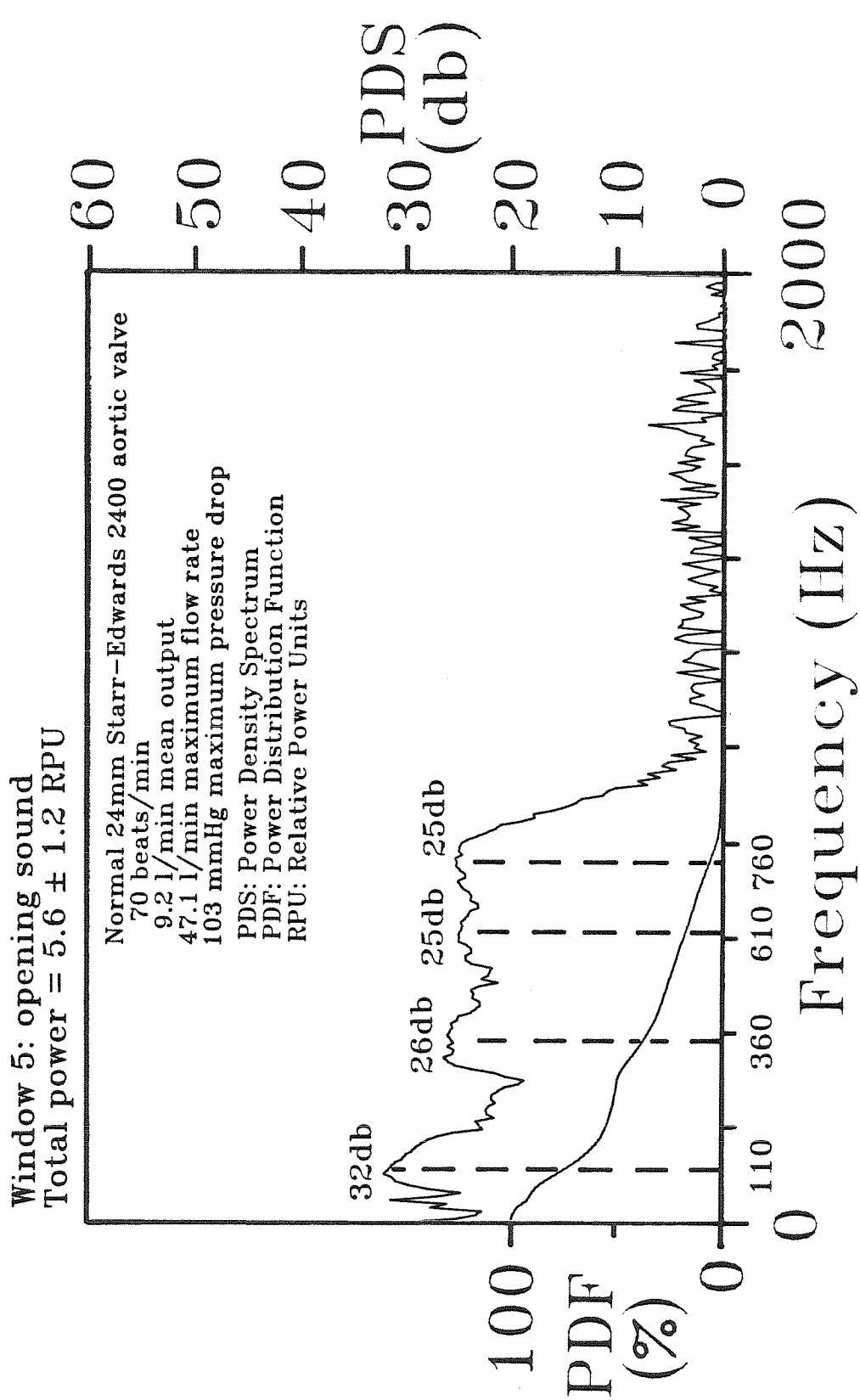

Figure 4-8e Power-density spectra and power distribution of the opening sound of experiment 309.

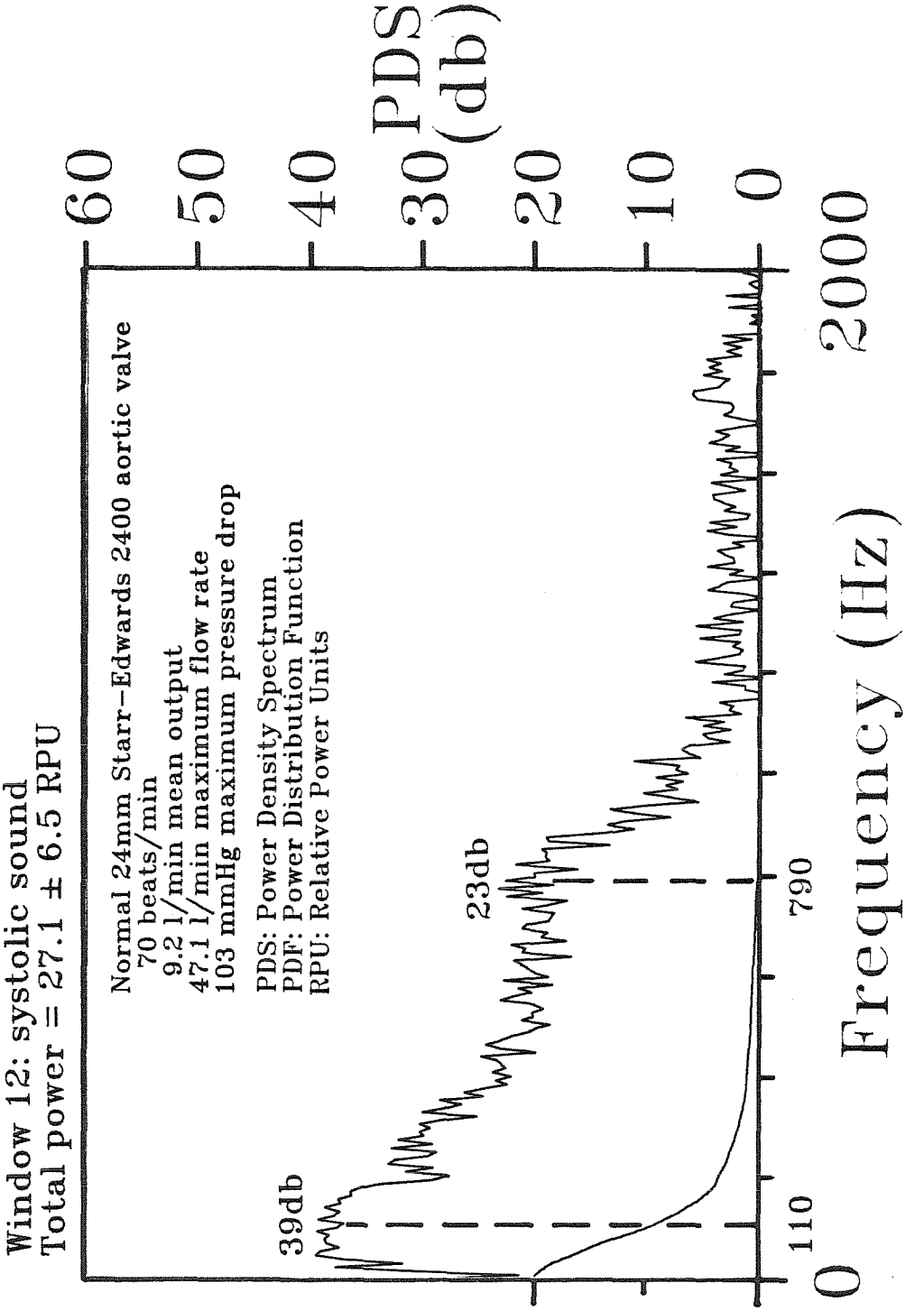

Figure 4-8f Power-density spectra and power distribution of the systolic sound of experiment 309.

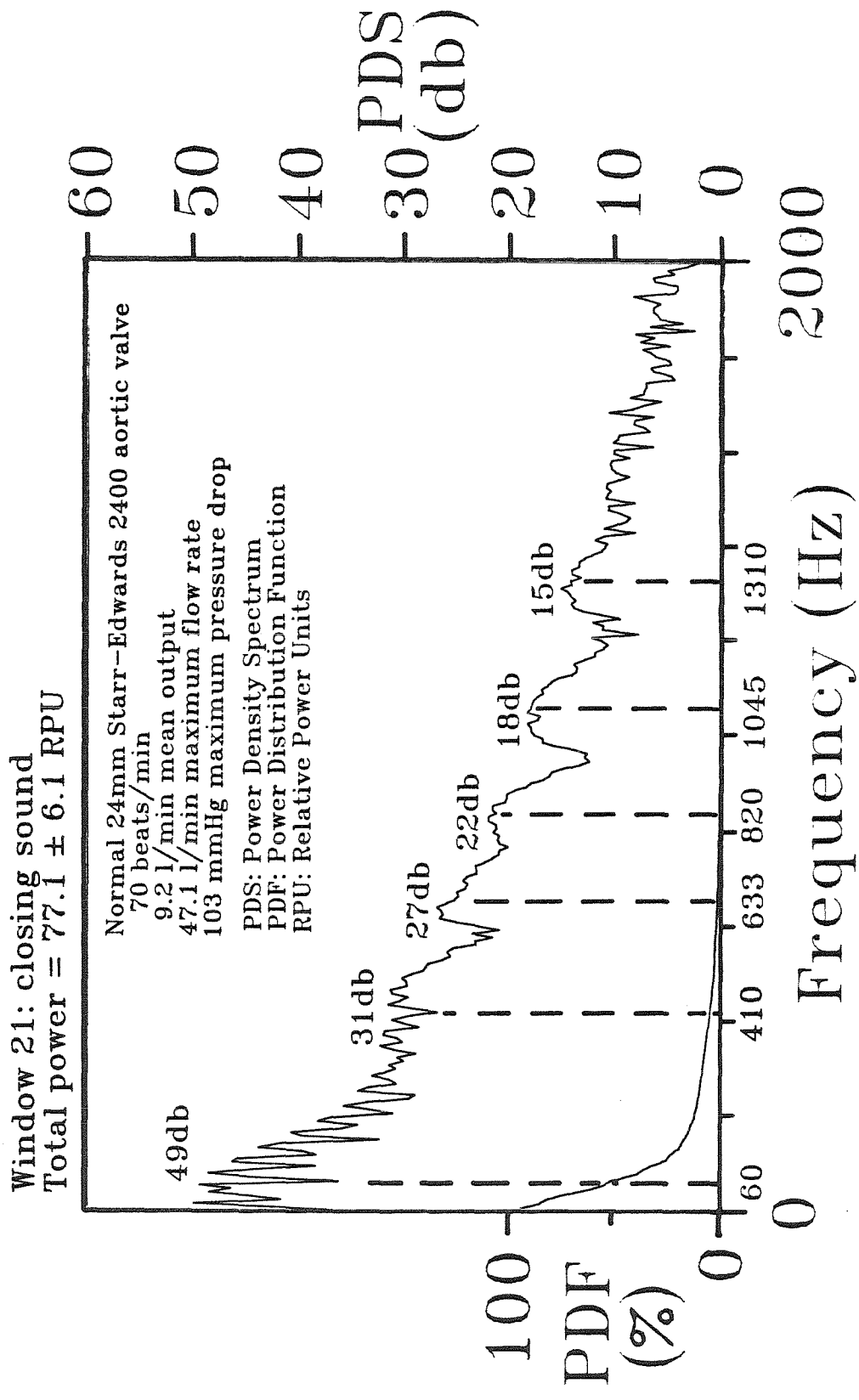

Figure 4-8g Power-density spectra and power distribution of the closing sound of experiment 309.

Parameters Estimated for

Significant Harmonic Peaks

Experiment 309

Event	Frequency, $f_{f,i}$; Decay, k_i; Power-Density, G_i (Hz,Hz,db)
Opening Sound	110,45,32
	360,65,26
Window 5	610,80,25
	760,80,25
Systolic Sound	110, 80,39
Window 12	790,120,23
Closing Sound	60,40,49
	410,70,31
	633,50,27
Window 21	820,65,22
	1045,75,18
	1310,65,15

Table 4-5 Parameters estimated from significant harmonic peaks of experiment 309.

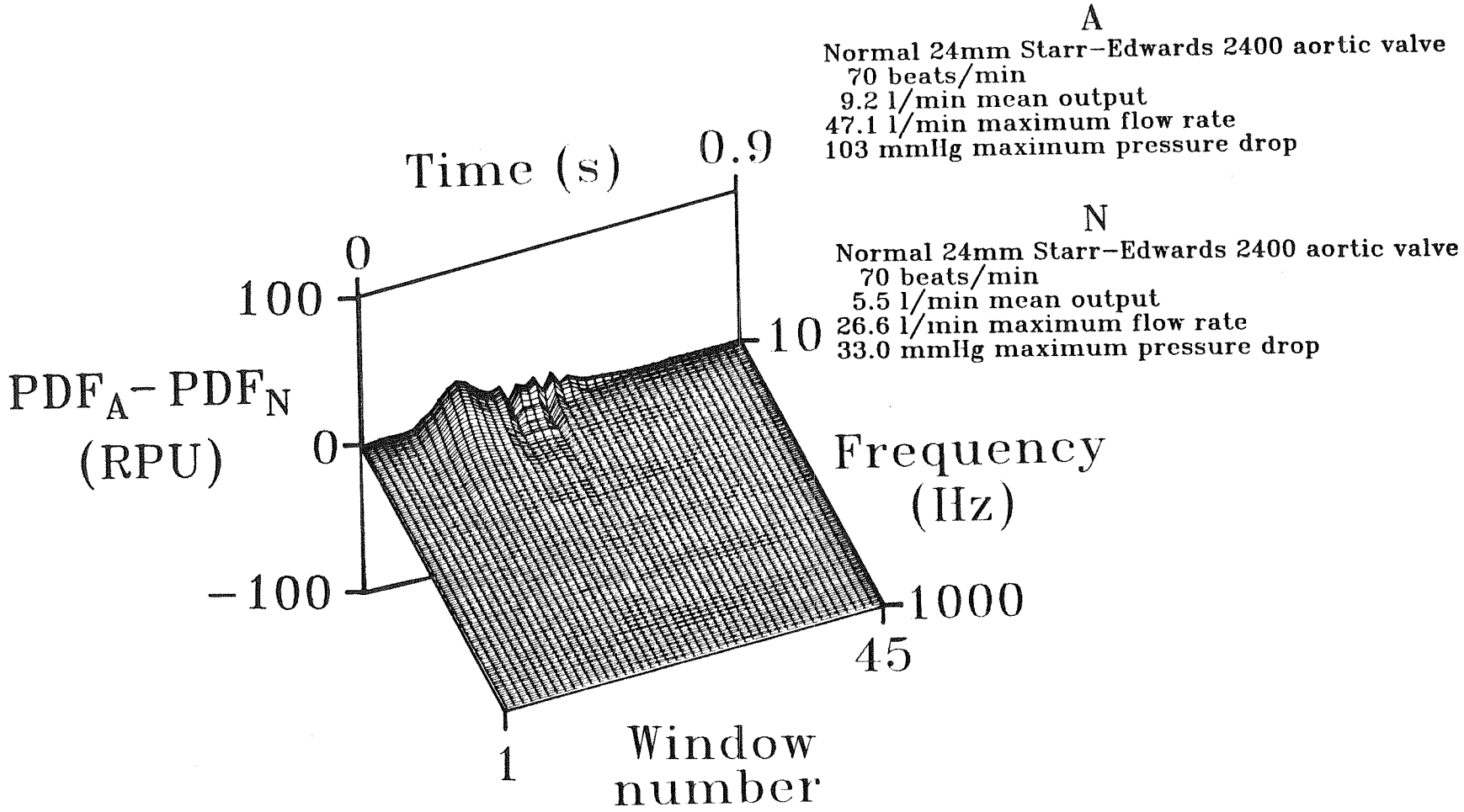

Figure 4-8h Three-dimensional surface depicting the difference between the power-frequency-time surfaces associated with experiments 309 and 306.

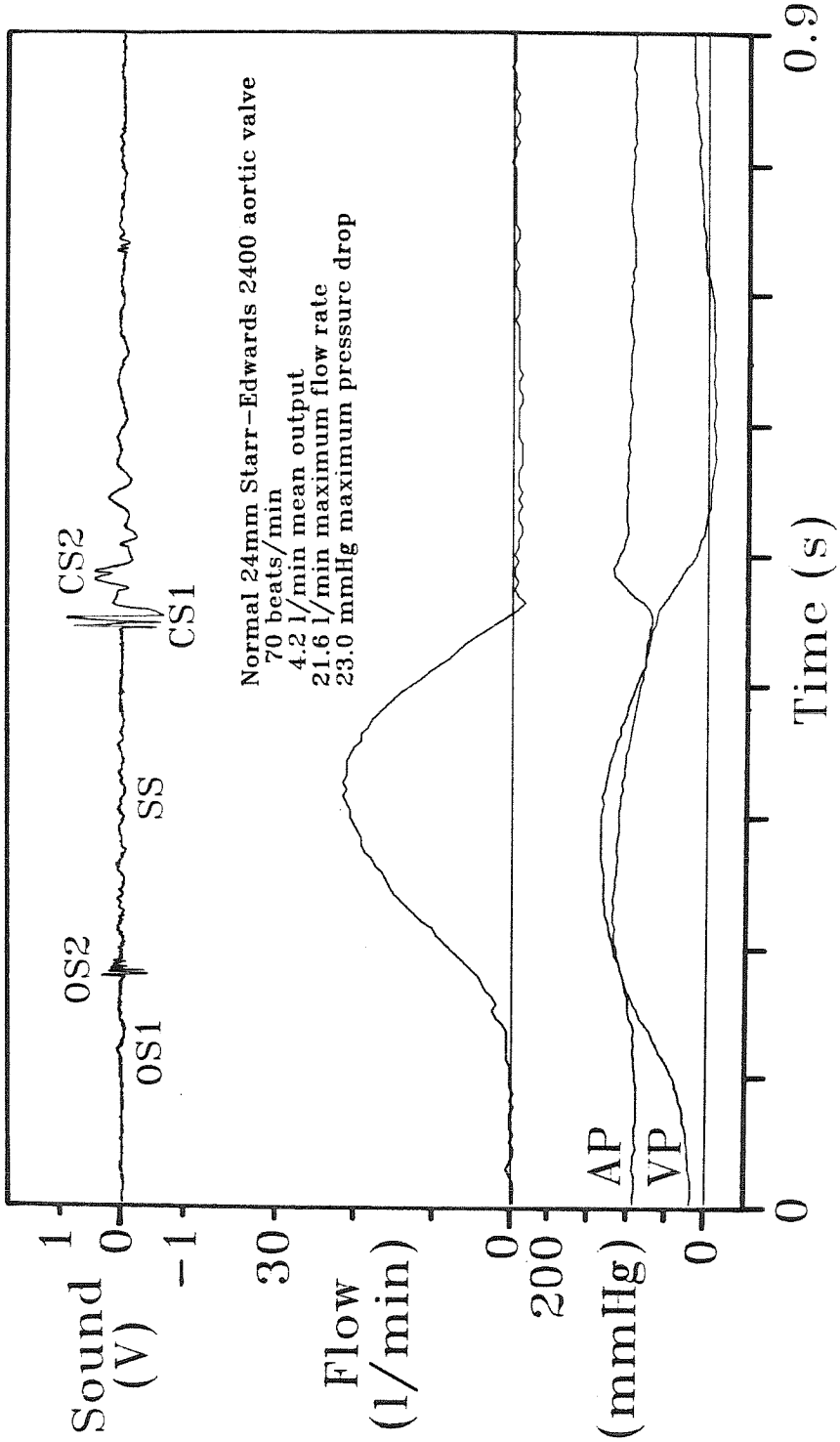

Figure 4-9a Amplitude vs. time tracings of sound, flow rate, aortic pressure and ventricular pressure associated with a typical cycle of experiment 310.

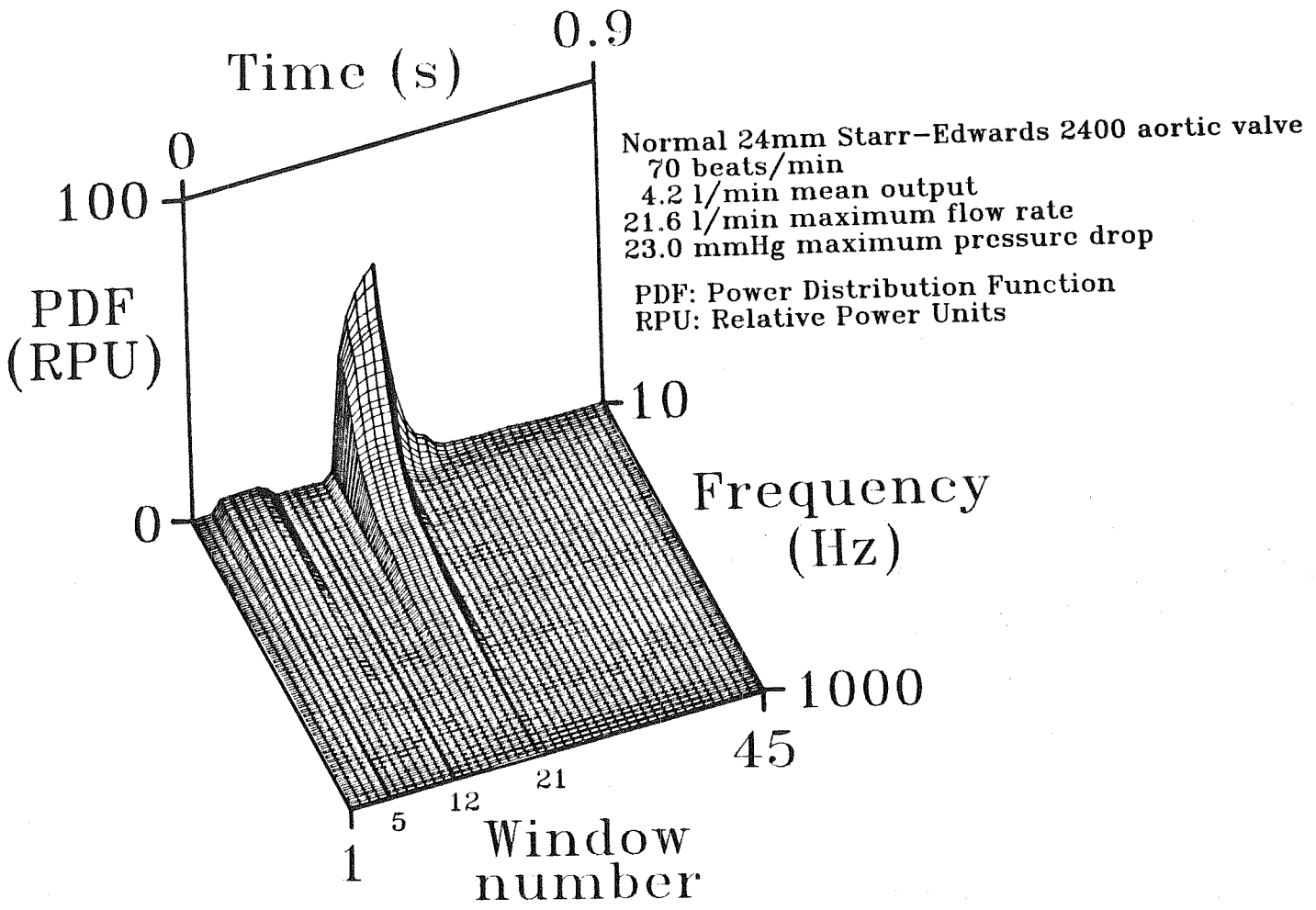

Figure 4-9b Three-dimensional power-frequency-time surface averaged over ten cycles of experiment 310.

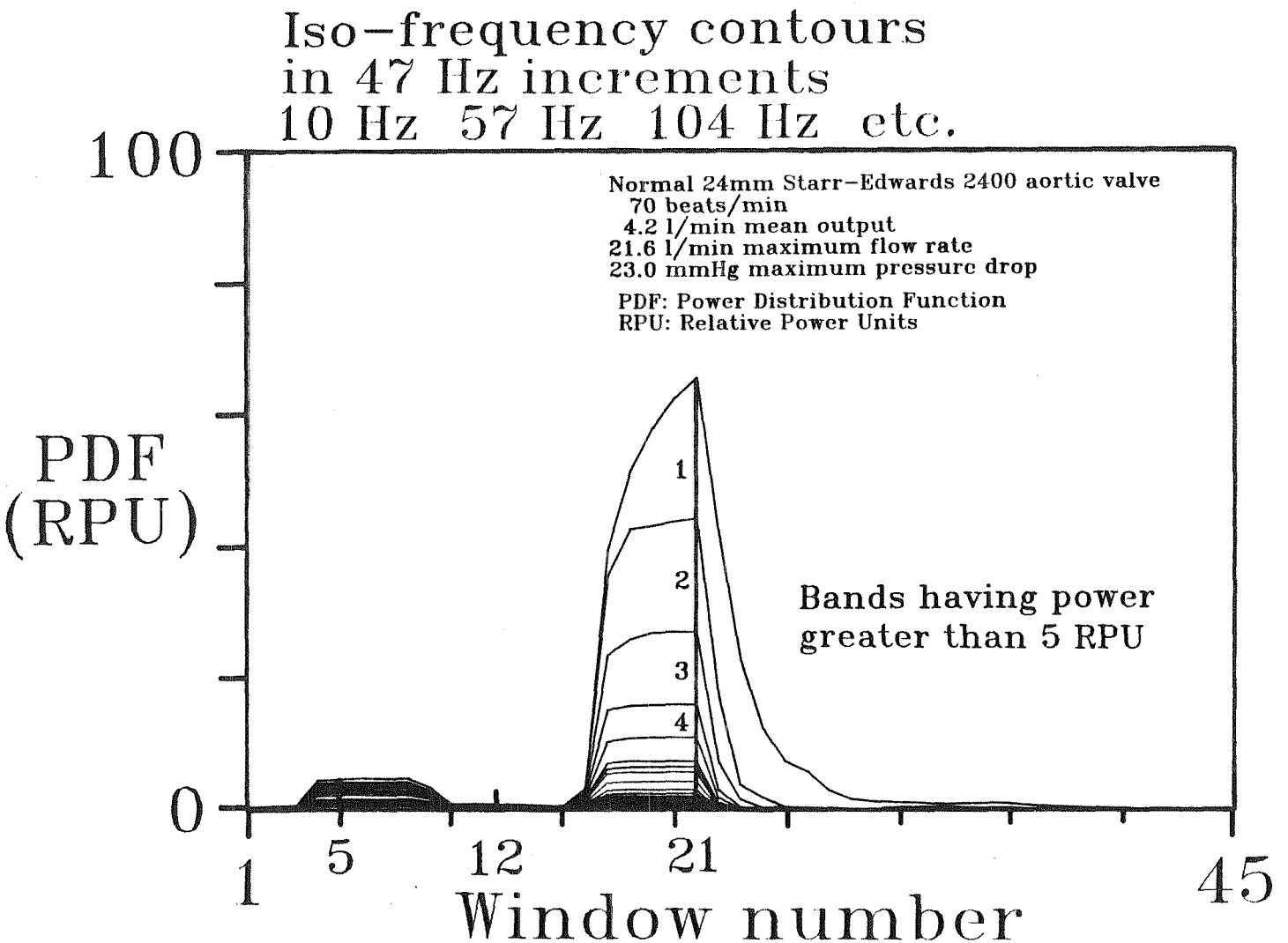

Figure 4-9c Auxiliary view perpendicular to the time axis of the 3-D power-frequency-time surface of experiment 310 showing iso-frequency contours.

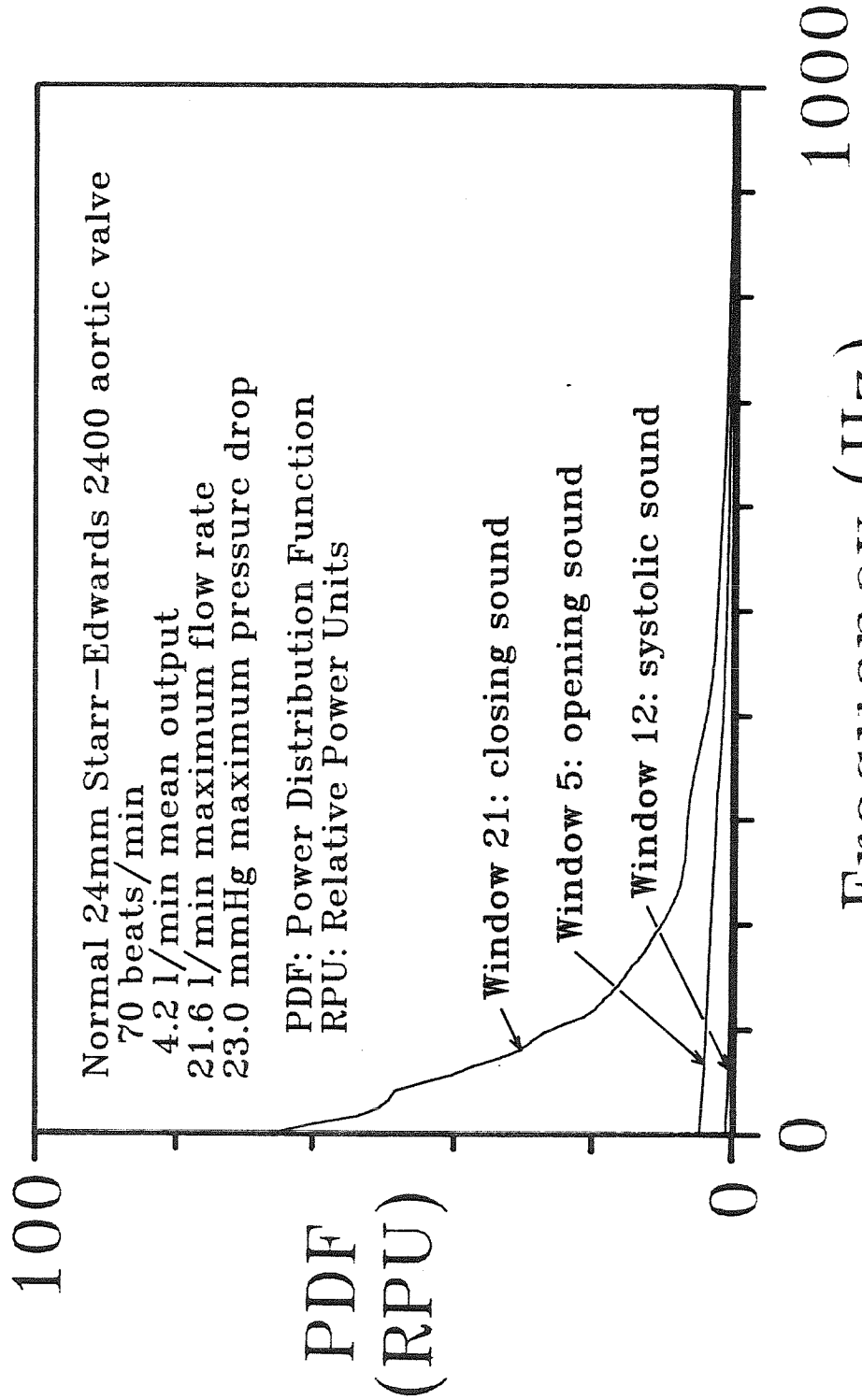

Figure 4-9d Auxiliary view perpendicular to the frequency axis of the 3-D power-frequency-time surface of experiment 310 showing power power distributions associated with windows encompassing the opening, systolic, and closing sounds.

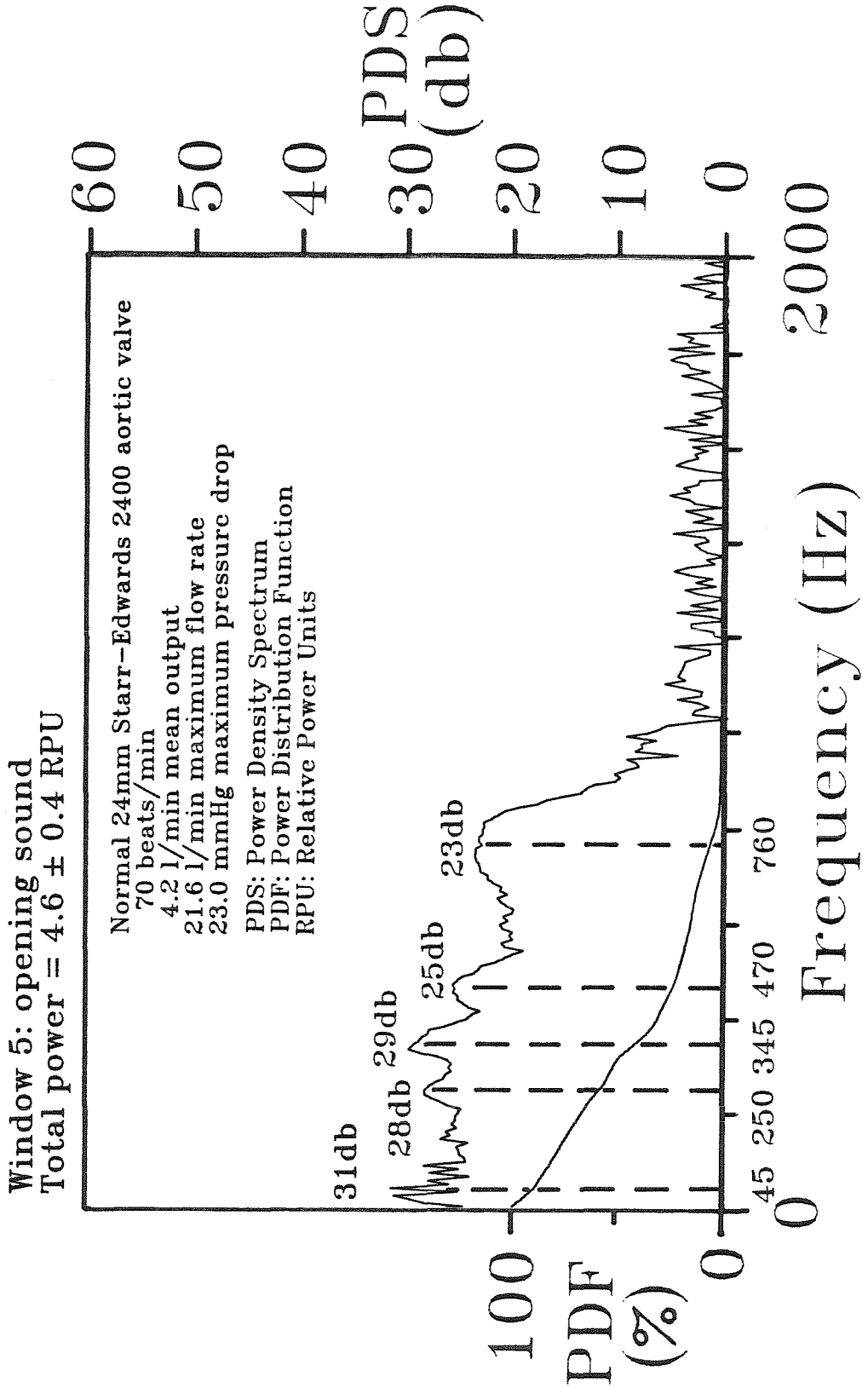

Figure 4-9e Power-density spectra and power distribution of the opening sound of experiment 310.

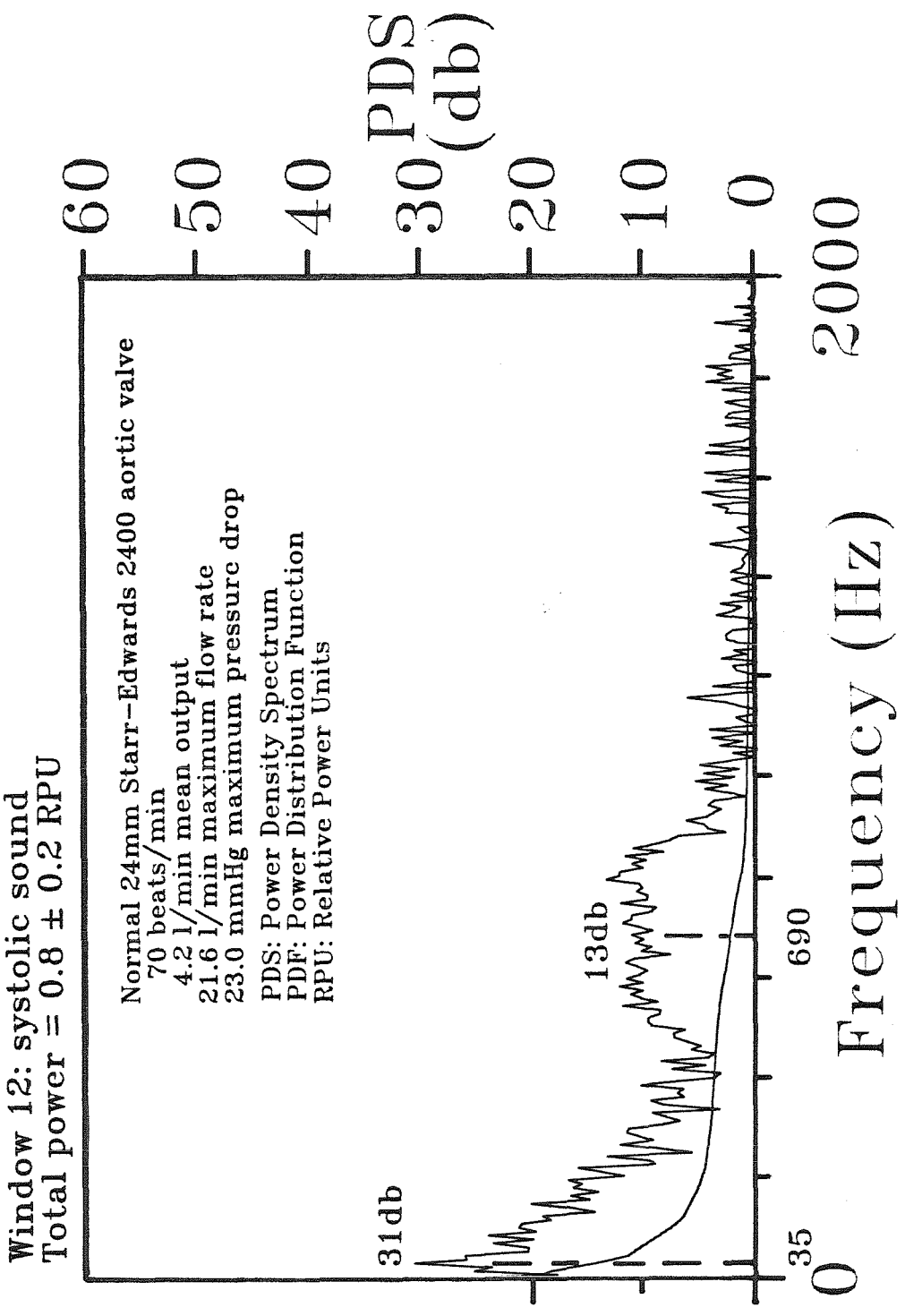

Figure 4-9f Power-density spectra and power distribution of the systolic sound of experiment 310.

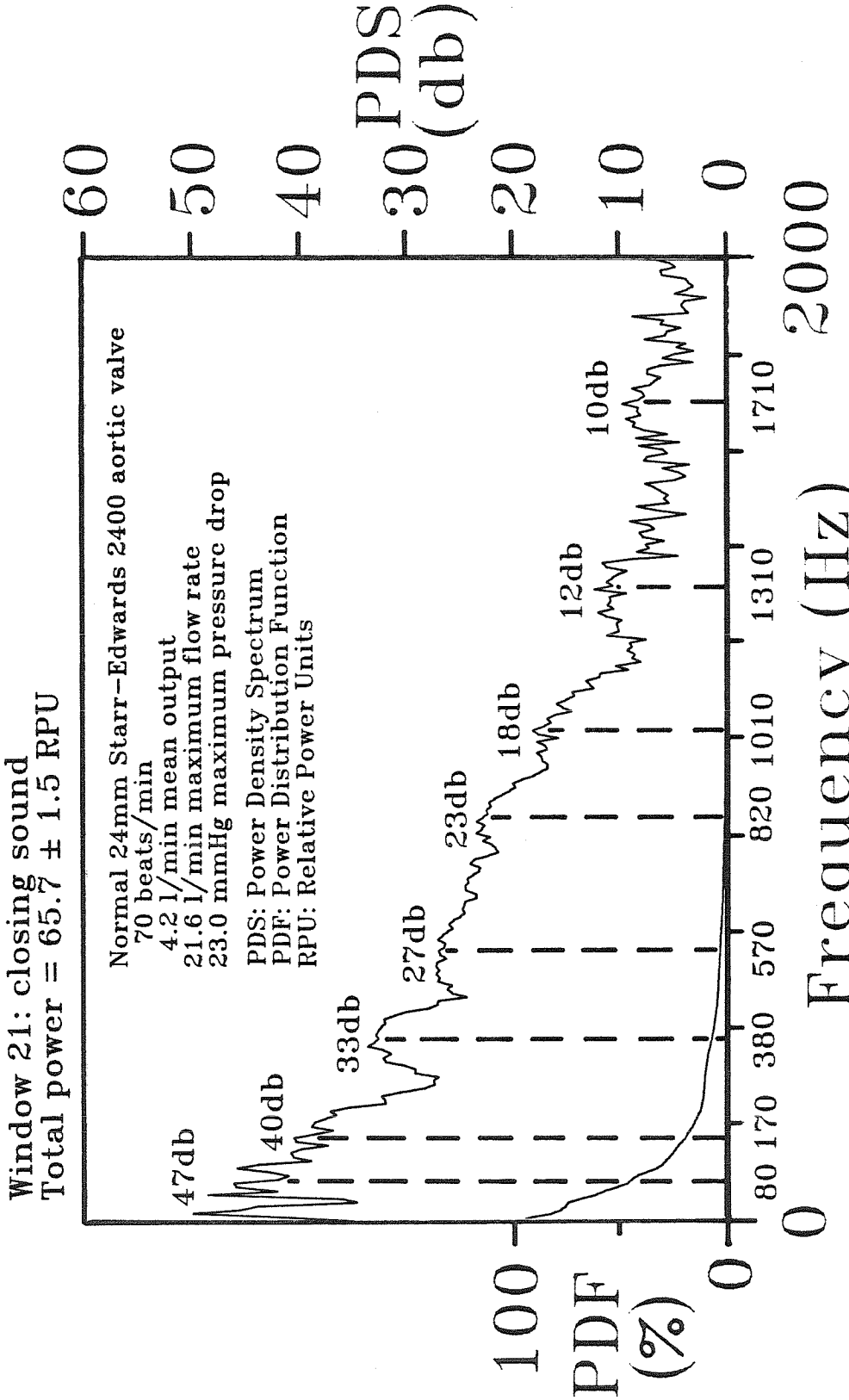

Figure 4-9g Power-density spectra and power distribution of the closing sound of experiment 310.

Parameters Estimated for

Significant Harmonic Peaks

Experiment 310

Event	Frequency, $f_{f,i}$; Decay, k_i; Power-Density, G_i (Hz,Hz,db)
Opening Sound	45,20,31
	250,35,28
Window 5	345,35,29
	470,45,25
	760,90,23
Systolic Sound	35, 15,31
Window 12	690,180,13
Closing Sound	80, 30,47
	170, 35,40
	380, 65,33
	570, 90,27
Window 21	820, 65,23
	1010, 65,23
	1310,120,12
	1710, 90,10

Table 4-6 Parameters estimated from significant harmonic peaks of experiment 310.

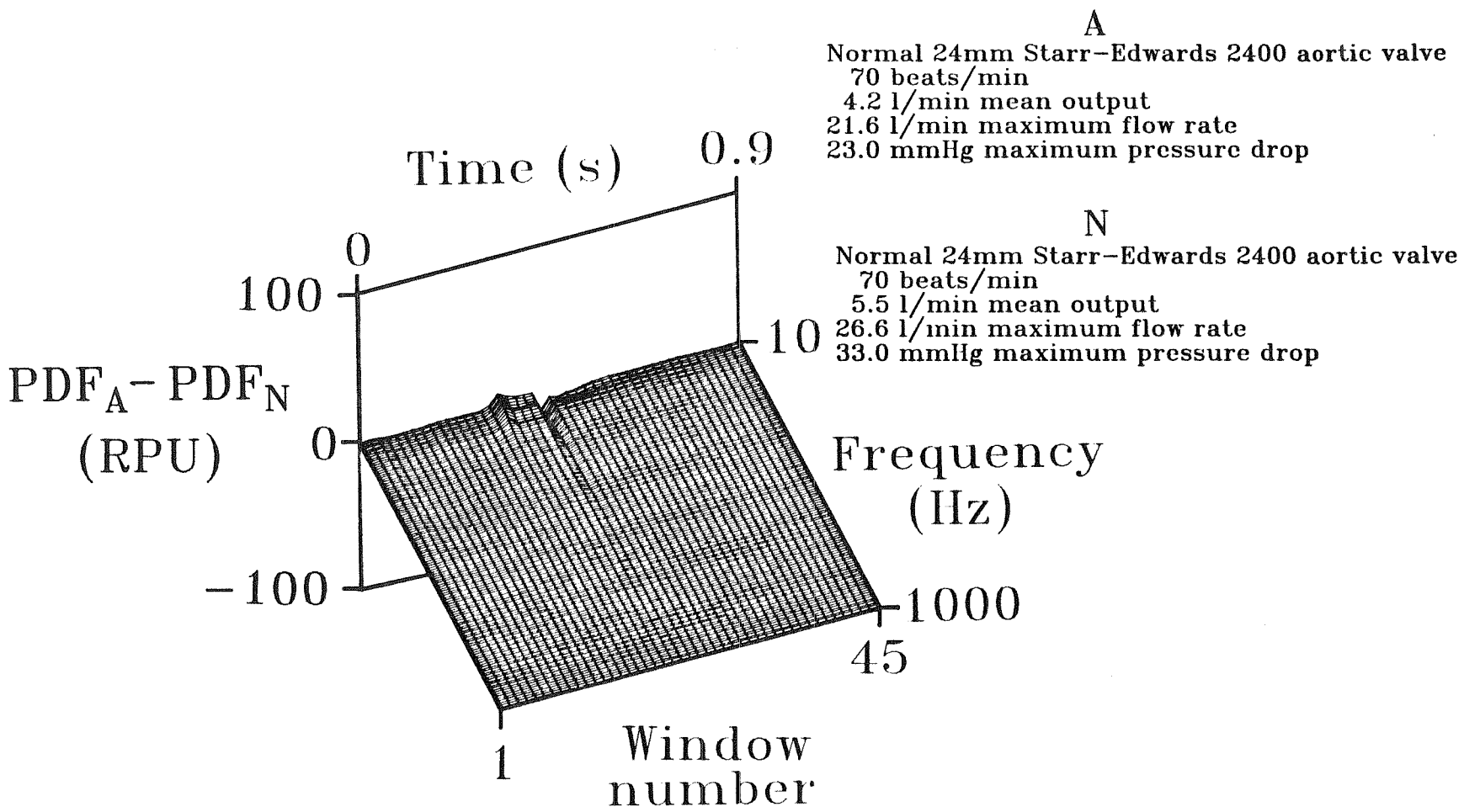

Figure 4-9h Three-dimensional surface depicting the difference between the power-frequency-time surfaces associated with experiments 310 and 306.

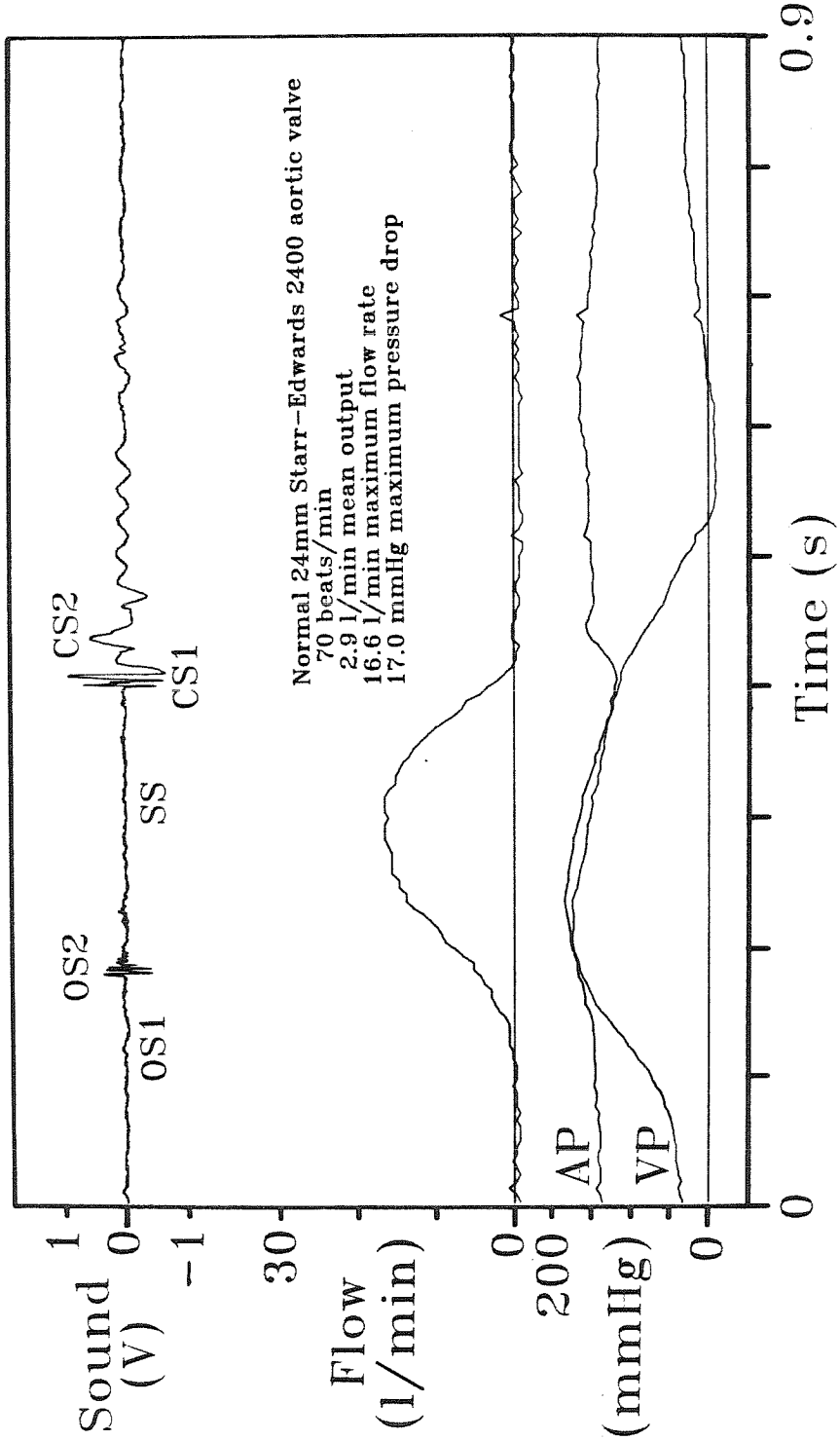

Figure 4-10a Amplitude vs. time tracings of sound, flow rate, aortic pressure and ventricular pressure associated with a typical cycle of experiment 311.

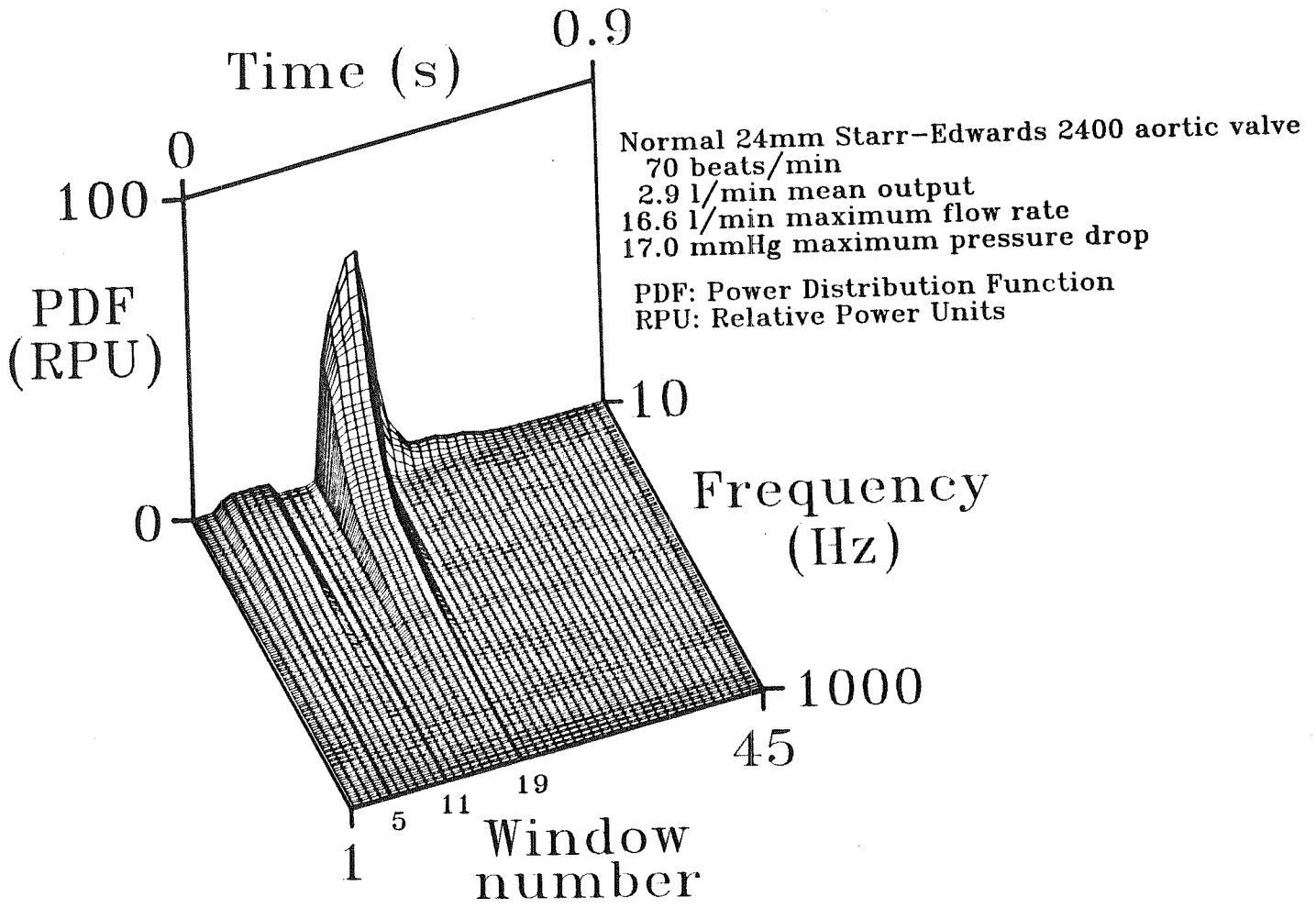

Figure 4-10b Three-dimensional power-frequency-time surface averaged over ten cycles of experiment 311.

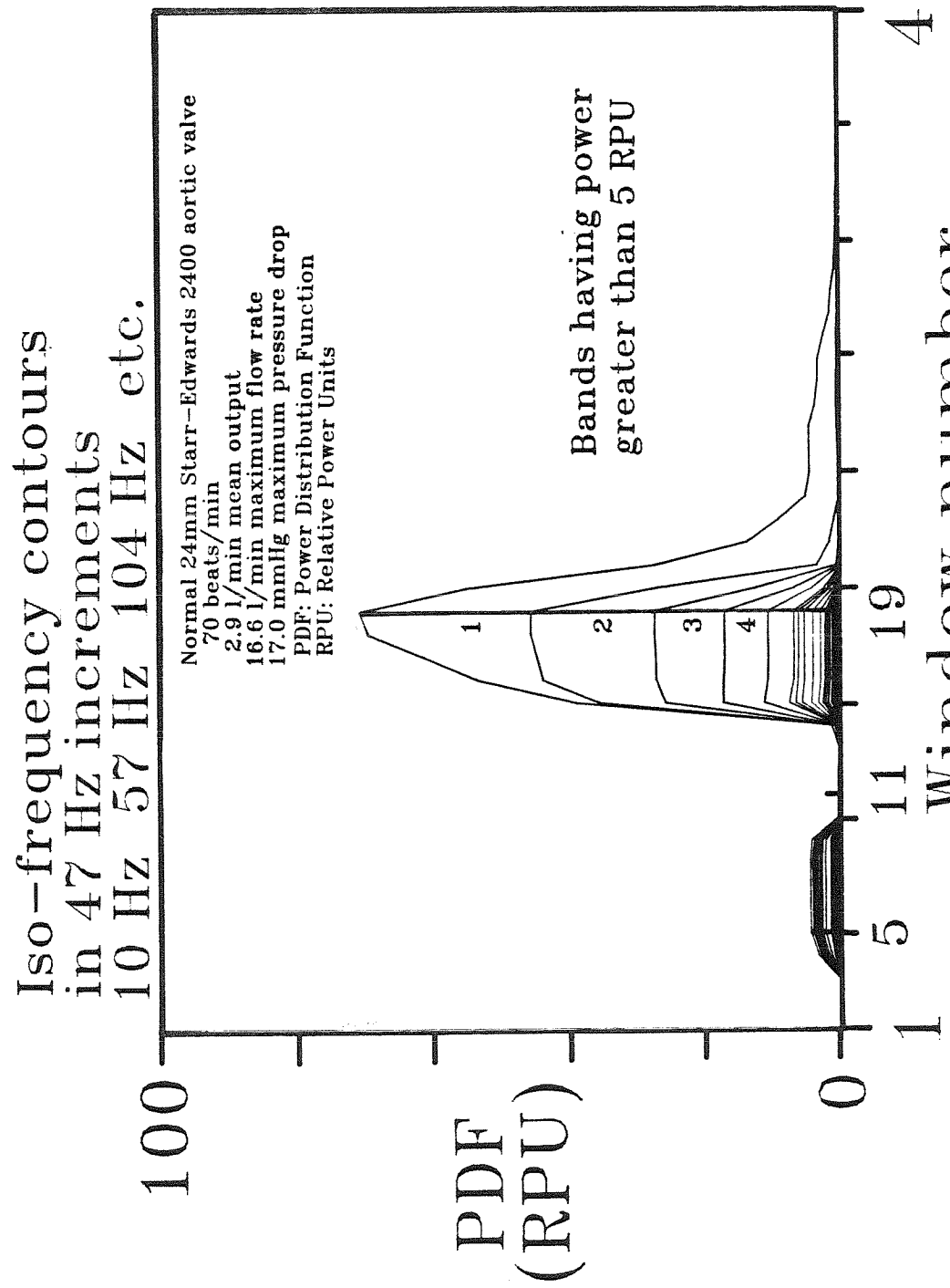

Figure 4-10c Auxiliary view perpendicular to the time axis of the 3-D power-frequency-time surface of experiment 311 showing iso-frequency contours.

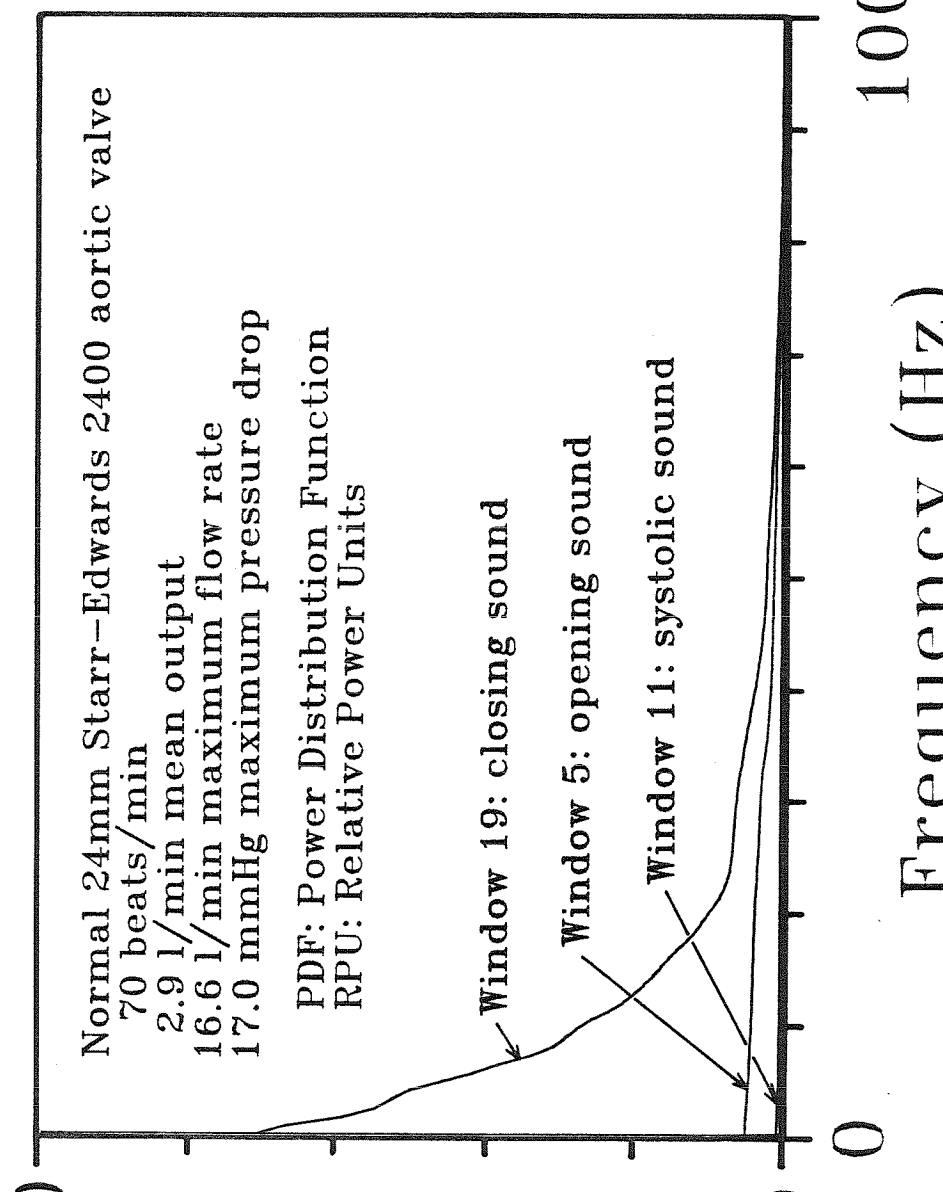

Figure 4-10d Auxiliaryview perpendicular to the frequency axis of the 3-D power-frequency-time surface of experiment 311 showing power distributions associated with windows encompassing the opening, systolic, and closing sounds.

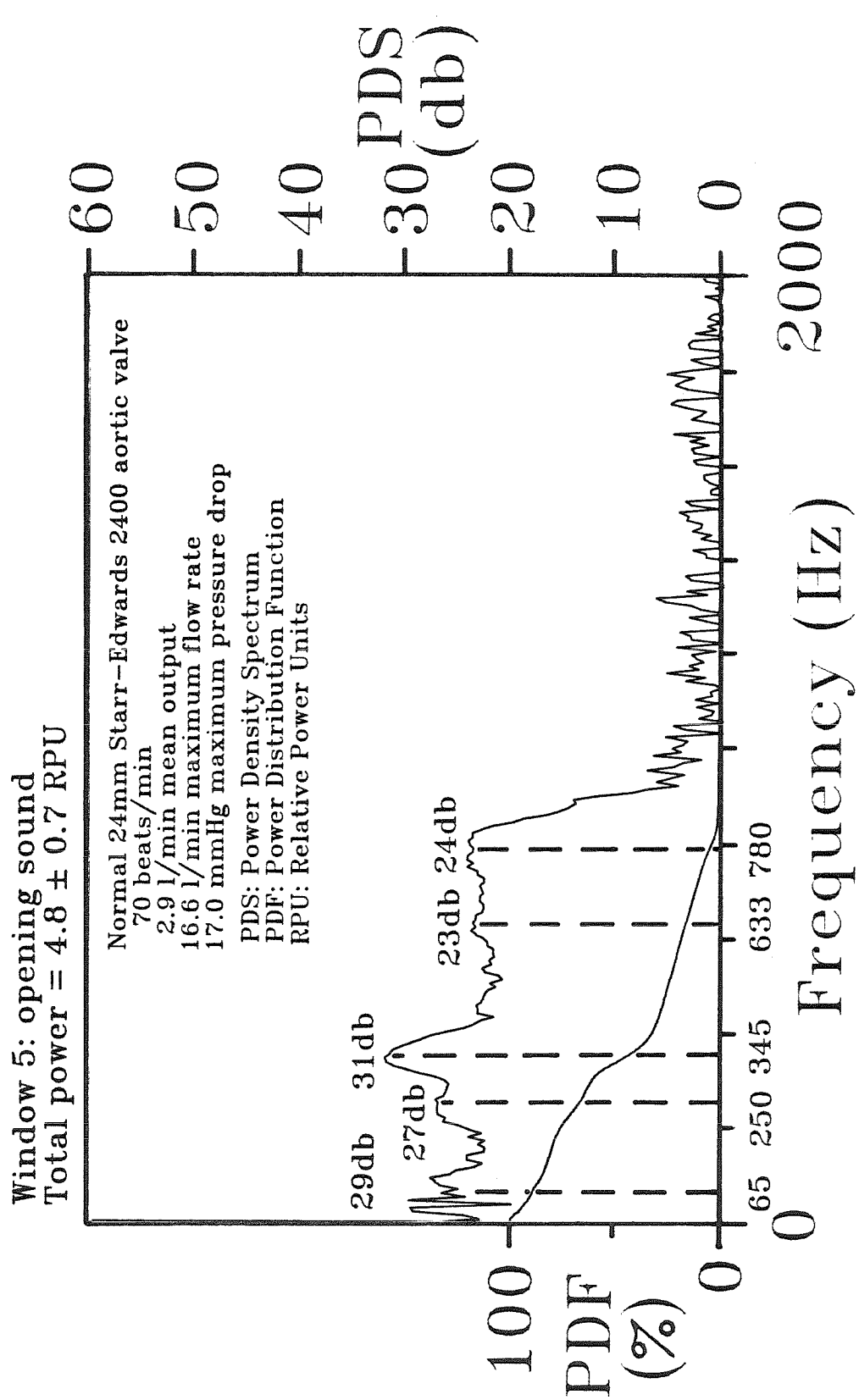

Figure 4-10e Power-density spectra and power distribution of the opening sound of experiment 311.

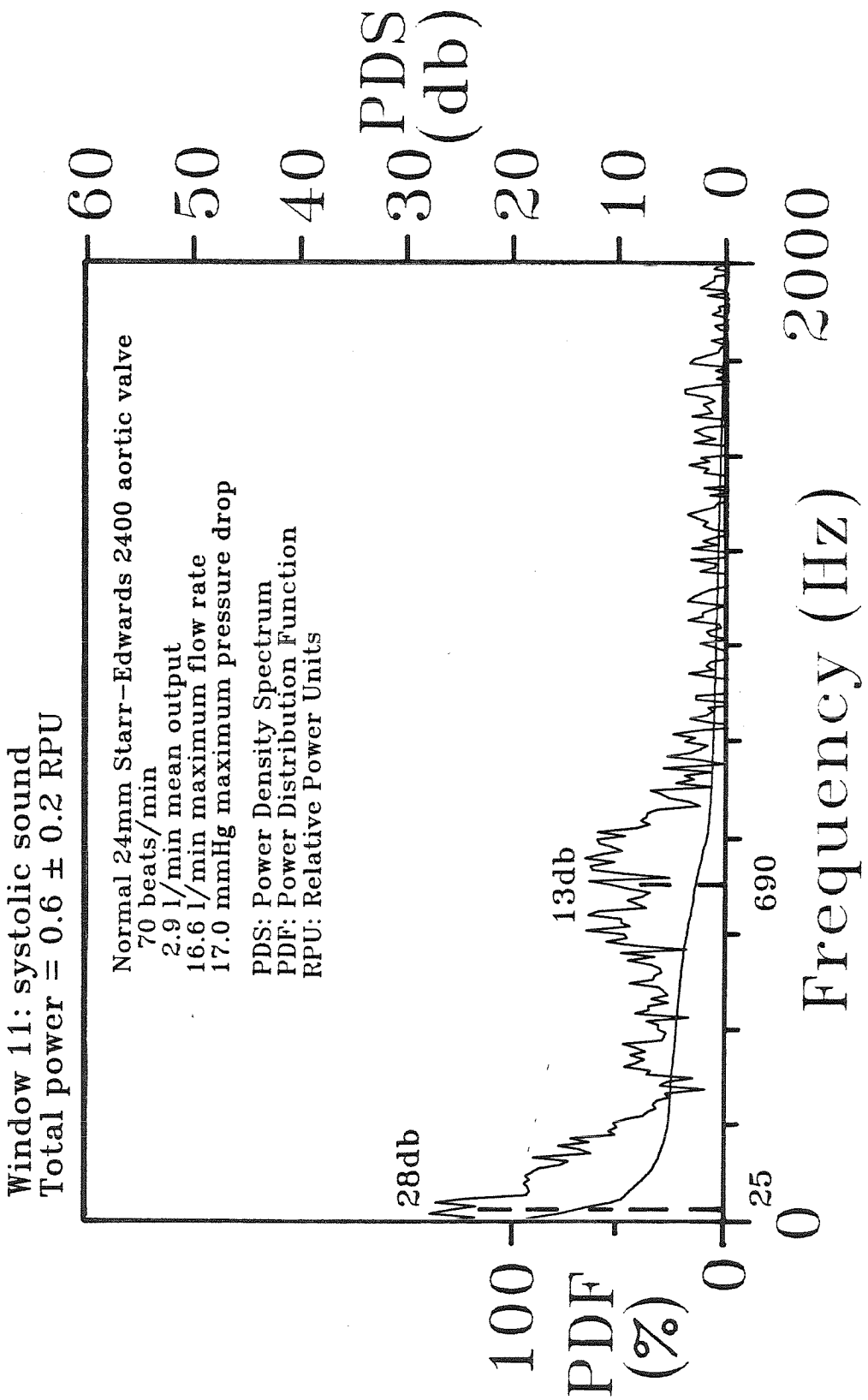

Figure 4-10f Power-density spectra and power distribution of the systolic sound of experiment 311.

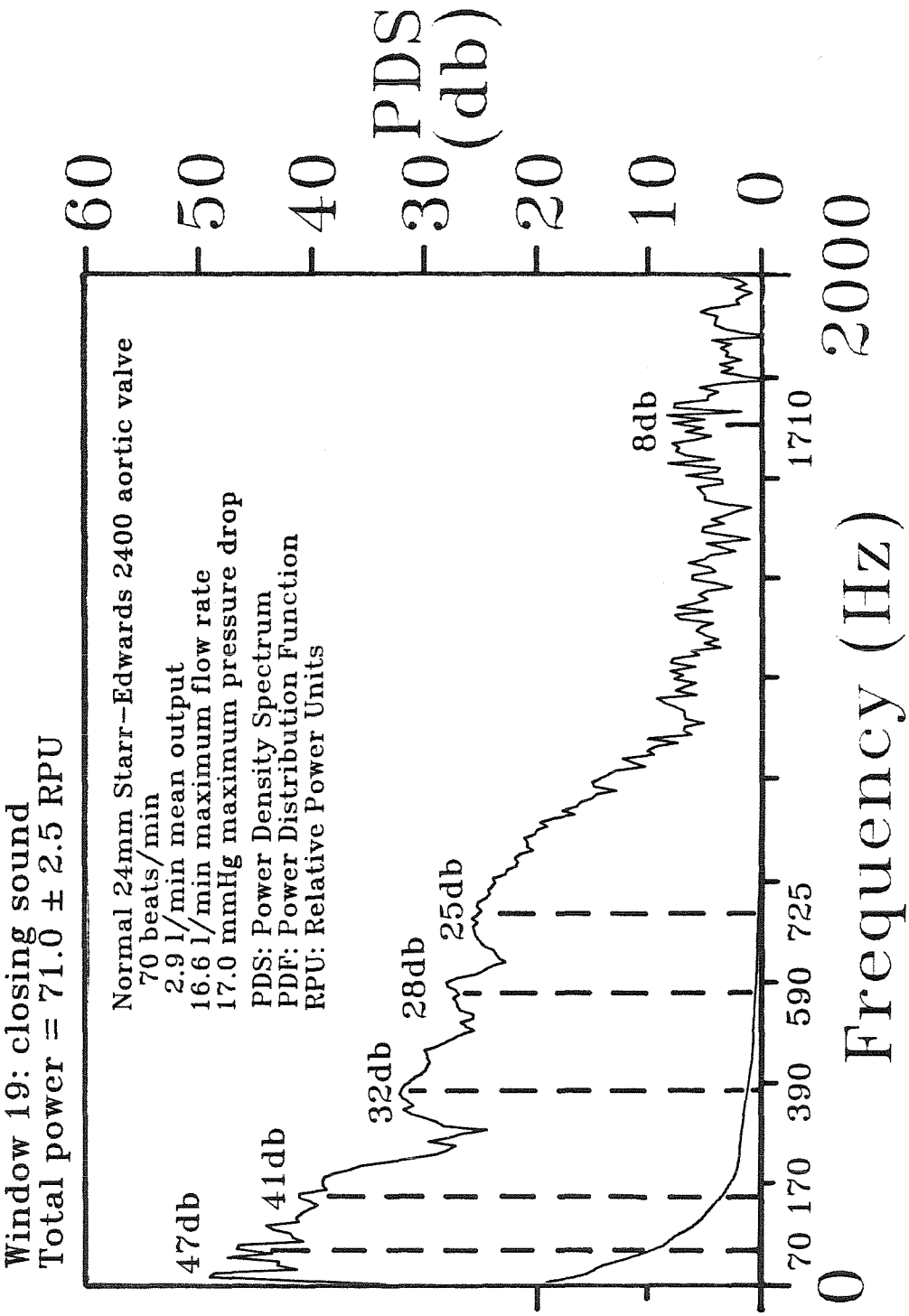

Figure 4-10g Power-density spectra and power distribution of the closing sound of experiment 311.

Parameters Estimated for

Significant Harmonic Peaks

Experiment 311

Event	Frequency, $f_{f,i}$; Decay, k_i; Power-Density, G_i (Hz,Hz,db)
Opening Sound	65,45,29
	250,45,27
Window 5	345,35,31
	633,55,23
	780,50,24
Systolic Sound	25, 25,28
Window 11	690,180,13
Closing Sound	70, 35,47
	170, 45,41
	390, 65,32
Window 19	590, 45,28
	725,110,25
	1710,100, 8

Table 4-7 Parameters estimated from significant harmonic peaks of experiment 311.

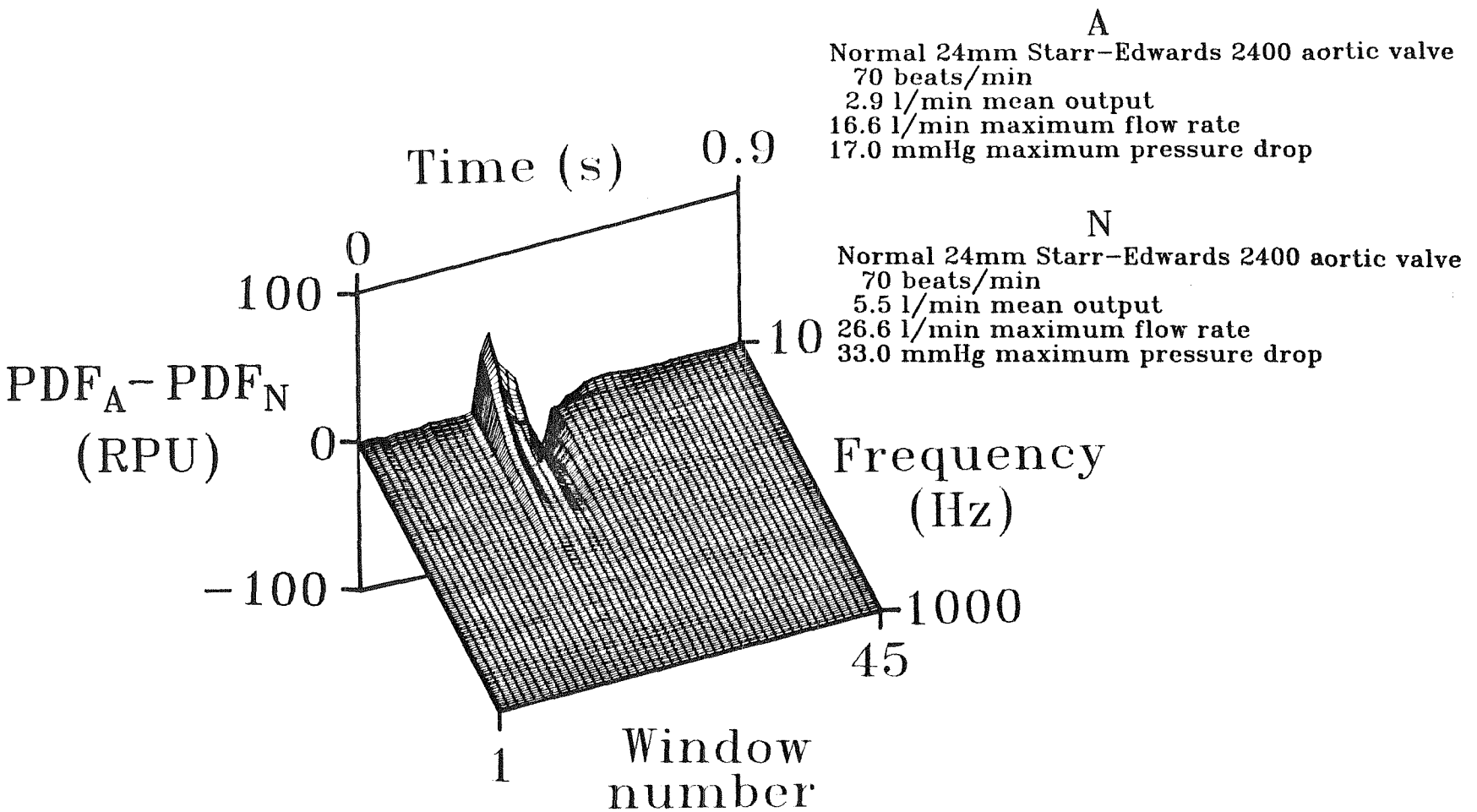

Figure 4-10h Three-dimensional surface depicting the difference between the power-frequency-time surfaces associated with experiments 311 and 306.

of the maximum pressure-gradient correlated well with the maximum, systolic flow-rate and the mean flow rate, respectively, for these three experiments. These figures also show the same correlation for the other experiments involving this valve.

4.4.1.1 The Opening Sounds

The opening sounds, OS, produced by the Starr-Edwards 2400 valve occurred as two distinct events for these three experiments. We have labeled these events OS1 and OS2 nearest their occurrence along the upper tracings of Figures 4-5a, 4-6a and 4-7a. Although OS1 may at first seem difficult to justify as a sound at all, it does correspond in time to a similar sound that we have observed produced by the Smeloff and Bjork-Shiley prostheses which are discussed in Parts V and VI of this series, respectively. From flow visualization experiments we have observed that OS1 was produced when the occluder was near its closed position while OS2 was produced when the occluder was at its totally open position. These observations suggest that OS1 was produced by vortex shedding from a confined, annular jet produced at the time of opening. The second component, OS2, was produced by the collision of the occluder with the apex of the cage. From the four tracings in Figures 4-5a, 4-6a and 4-7a it is clear that OS1 occurred at the time that the forward flow began and at the time when the ventricular pressure began its rapid increase. It is also clear that OS2 occurred 70 ms after OS1 for each of these three experiments. The time axis of these figures were each normalized with respect to the time of one pulstile cycle. The time between OS1 and OS2 is approximately constant, consequently the occluder traveled from the orifice to the apex of the cage with the same average speed. We would therefore expect to see similarities in the opening sounds for these experiments. We have chosen the initial time of each cycle such that window 5

encompassed the opening sounds of each experiment. Changes were observed between the values of the rate of change of the ventricular pressure immediately prior to the opening sound for these three experiments.

These changes produced little effect upon the power-density spectra of these opening sounds. This can be seen if one examines the peaks shown in Figures 4-5e and 4-6e and the corresponding parameters listed in Tables 4-2 and 4-3. Here one can see that the spectra have essentially the same peaks, that is to say each peak had parameters that are the same within the error of estimation and analysis.

These similarities are also shown by the window-5 contours depicted in Figures 4-2, 4-3 and 4-4, subfigures **b,c,d** and **h**. We cannot, however, compare Figure 4-7e of experiment 308 with the corresponding spectra of the opening sounds for the other two experiments because window 5 occurred prior to the time of the maximum total-power of the opening sound for this experiment as can be seen by inspecting Figure 4-7b and 4-7c. If one, however, compares window 6 between experiments 306 and 308, it is clear that the opening sounds are indeed very similar for all three of the pulse rates. Each of these opening sounds possessed clear harmonic peaks in its spectrum. These peaks were centered near frequencies of 100, 350 and 800 Hz. No significant power was observed above 1000 Hz in these opening sounds. A direct comparison of the power distributions associated with window 6 for these experiments is provided by Figures 4-6h and 4-7h. Both of these figures show similar power-distributions for these opening sounds by the flat contour corresponding to window 6 over the bandwidth of 10 to 1000 Hz. Comparisons of the opening sounds can also be made by inspecting the iso-frequency contours in Figures 4-6c and 4-7c and by comparing the power-distributions in Figures 4-6d and 4-7d.

It should be noted that these spectra differ dramatically from the corresponding spectra of the Smeloff valvar design which are discussed in Part V of this series. The opening sounds of the Bjork-Shiley design, discussed in Part VI of this series, are more similar, but are still significantly different. This unique, over-all difference in the spectra of the opening sounds for a given valvar design has been observed for each design we have studied. The reader is encouraged to make similar additional comparisons between valvar designs at comparable pulsatile states by comparing corresponding figures in Parts IV and VI and inspecting Tables A-1 through A-6 of Appendix A. The analog filter used for the analysis of the sounds produced by the Starr-Edwards 2400 and Bjork-Shiley valves had a low-cutoff frequency of 100 Hz. The analog filter used for the analysis of the sounds produced by the Smeloff valve had a low-cutoff frequency of 200 Hz. Comparisons between the results for the Smeloff valve presented in Part V and the results presented in this part and Part VI can not be made directly. Figure A-1 shows the low-cutoff characteristics of the analog filters used during the analyses of results presented in this thesis.

4.4.1.2 The Systolic Sounds

Unlike the opening sounds, the systolic sounds are quite different for experiments 306, 307 and 308. This difference is primarily a result of differences in the value of the maximum, systolic flow-rate which was 26.6, 19.3 and 29.8 L/min for experiments 306, 307 and 308, respectively. The systolic sound, SS, was labeled nearest its occurrence along the upper tracings of Figures 4-5a, 4-6a and 4-7a. By examining all four tracings in each of these three figures, one can see that the maximum intensity of the systolic sound occurred simultaneously with the maximum flow-rate and the maximum pressure-gradient. It is clear from these figures that the systolic sound-intensity increased with the

maximum flow-rate and the maximum pressure-gradient. A very good correlation existed between the power of the sound produced during systole and the value of the maximum flow rate. This correlation is shown in Figure 4-4 for these three experiments. This correlation extends to the other experiments involving the Starr-Edwards 2400 valve. The ordinate of this figure represents the total power associated with the window having the maximum total power of the systolic sound. The number of this window varied with the stroke volume. Another correlation existed between the power of the sound produced during systole and the value of the maximum, systolic pressure-gradient across the valve. This correlation is shown in Figure 4-3 for all six experiments involving the Starr-Edwards 2400 prosthesis.

The corresponding power-density spectra depicted in Figures 4-5f, 4-6f and 4-7f each show two significant peaks centered near 50 Hz and 700 Hz. The low-frequency peaks tended to increase in amplitude with the maximum systolic flow rate while maintaining the same center-frequency. The peaks near 700 Hz, however, are identical for these three spectra. The corresponding power-distributions show that the low-frequency peaks became increasingly-powerful relative to the high-frequency peak as the stroke volume increased. For experiment 307 this high-frequency peak was 30% of the total power and for experiment 308 it was 10%. If we assume that the low-frequency peak was produced by the non-transient sounds associated with flow and the high-frequency peak was produced by the transient sound associated with bouncing of the occluder, then, these facts suggest that the power of the non-transient component increased with the maximum systolic flow rate and the amount of bouncing of the occluder was not affected by these changes of pulsatile state. The assumptions about the physical cause of each peak is supported by the calculations described in Part VII of this series. In that section we estimated Strouhal

numbers of 0.07 and 0.18 for associated vortex-shedding caused by flow around the struts and the phonocatheter, respectively. The only reasonable values we obtained were those associated with flow past the phonocatheter and these had a shedding frequency of 80 Hz. Based on our calculations, the high-frequency peak could not be related to vortex shedding.

Figures 4-5, 4-6 and 4-7, subfigures b,c,d, and h, show the power distributions of these sounds. They also allow comparisons to be made between the systolic sounds and the opening and closing sounds of the valve. Because of the low values of power associated with these systolic sounds relative to the opening and closing sounds, it is not easy to compare them by inspecting these figures. A more detailed comparison could be made between these sounds if the scale of the ordinate were expanded. Such a comparison can be made using the normalized distributions plotted immediately below each density-spectrum. A direct comparison of the systolic sounds is provided graphically by the 3-D difference surfaces shown in Figure 4-6h and Figure 4-7h. Unfortunately, the vertical scale is again too large to depict the small differences of these systolic distributions.

4.4.1.3 The Closing Sounds

The closing sounds, CS, of experiments 306, 307 and 308 are very similar to each other. These sounds were comprised of two events which we have labeled CS1 and CS2 nearest their occurrence along the upper tracings of Figures 4-5a, 4-6a and 4-7a. By inspecting the flow and pressure tracings included in the same figures, we see that the closing sound, CS1, occurred at the same time as the maximum backflow, the dichrotic notch of the aortic pressure curve, and the beginning of the rapid decrease of the ventricular pressure curve. The second closing sound CS2 occurred at the same time as the peak in the diastolic aortic

pressure. The spectra of the closing sounds were similar to each other but much unlike either of the spectra associated with the opening and systolic sounds.

The similarity between closing sounds included the number, location, shape and amplitude of corresponding peaks. Each spectrum shown in Figures 4-5g, 4-6g and 4-7g had essentially the same distribution of peaks. The differences between the spectra of the closing sounds and the spectra of either opening or systolic sounds were dramatic. These "extra-sonic" differences included the number of peaks and their corresponding amplitudes. The spectra of the closing sounds have seven or eight significant peaks instead of two or three as we have seen in the case of the opening and systolic sounds. Clearly more vibrational modes were stimulated. These modes are those of the valve and/or those of the aortic flow section. It was not possible to separate the modes into either of these two catagories. It is also possible that these modes were exclusively associated by CS1 and CS2. Some of these peaks could also be associated with vortex shedding resulting from "pinched-off" backflows at the time of closure. Closing sounds of other valvar designs also exhibited many peaks compared to their opening and systolic sounds. To further complicate matters, the large power levels produced by these sounds may indicate that vibrational modes of the aortic flow-section may be included as part of these additional peaks. That is to say, some peaks may be associated with vibrational modes of this flow-section. This latter hypothesis could not, however, explain, by itself, the changes we have observed in these spectra. There were clear differences between the groupings of the peaks for each valvar design which would suggest that the design had an influence on the location and shape of the peaks. At this time we cannot relate specific peaks with more certainty to specific physical vibrations of the system. A quick comparison of the center-frequencies of the closing

sounds of each experiment involving the three valvar designs is provided by the list in Table A-5 of Appendix A.

The power distributions of the closing sounds represented by windows 21, 20 and 22 in Figures 4-5, 4-6 and 4-7, subfigures b,c,d and h, respectively, were similar in form. We observed significant differences between the timing of the closing sound with respect to the opening sound for these three experiments. These differences are shown directly by the difference-surfaces. The difference between the power distributions of experiments 306 and 307 are shown as a peak/valley combination located between 10 and 800 Hz and windows 12 and 24 in Figure 4-6h and as a valley/peak combination located between 10 and 800 Hz, and windows 16 and 25 in Figure 4-7h. The former surface indicates an early closing sound and the latter surface indicates a late closing sound relative to **normal**. The symmetry of these valleys and peaks about their flat, mid-window contour indicates the similarity of the power distributions of these sounds.

4.4.1.4 Summary of Comparisons of Pulse-Rate Experiments

The effect of pulse rates of 50, 70 and 90 beats/min upon the opening sounds of the normal Starr-Edwards 2400 valve was minor relative to changes observed in the systolic and closing sounds. A reduction of total power of the opening sound of 40% below **normal** was observed for the case having a pulse rate of 50 beats/min.

The effect of pulse rate upon the systolic sound was primarily to shift this sound earlier in systole if the corresponding stroke volume decreased. Because the stroke volume increased as the pulse rate decreased, a reduction of the pulse rate increased the power of the non-transient component of the systolic sound, centered near 50 Hz. This latter change would result from changes of

the pulse rate while maintaining a constant mean cardiac output. The transient component of the systolic sound was not affected by these changes in the pulse rate. This transient sound was attributed to the bouncing of the occluder. The lack of change of the peak associated with its sounds suggested that the bouncing associated with this peak was not affected by these changes of the pulse rate and their associated stroke volumes.

The effect of pulse rate upon the closing sound was minor with respect to frequency-content but significant relative to timing within the cardiac cycle even when this timing had been normalized with respect to the time of one cycle. The closing sound of the low-pulse rate experiment was disproportionately late and that of the high-pulse rate experiment disproportionately early. The total power of these sounds was not significantly different.

4.4.2 Effects of Stroke Volume on the Sounds

The Starr-Edwards 2400 valve was pulsed at three different stroke volumes while maintaining a pulse rate of 70 beats/min and comparable mean, aortic pressure. The experiments which will be compared are numbers 306, 309, and 310. The important values which define the pulsatile state for these experiments are listed in the appropriate columns of Table 4-1a. The stroke volumes were 81, 132 and 65 cm^3 and corresponded to mean flow rates of 5.5, 9.2, and 4.2 L/min, respectively. The maximum flow-rate and maximum pressure-gradient increased as the stroke volume increased for these three experiments. The relationship between maximum pressure gradient and flow are provided by the plots shown in Figures 4-1a and 4-2.

4.4.2.1 The Opening Sounds

The opening sounds, OS, produced by the Starr-Edwards 2400 valve during these three experiments occurred as two distinct events which we have labeled OS1 and OS2 nearest their occurrence along the upper tracings of Figures 4-5a, 4-8a and 4-9a. The occluder again began its motion downstream at about the time OS1 occurred and struck the apex of the downstream cage at the time OS2 occurred. The time interval between OS1 and OS2 was approximately 60 ms for each of these experiments. The opening sounds correspond to window 5 of our analysis. Changes were observed in the values of the rate of change of the ventricular pressure for times immediately prior to the opening sound. These changes had a significant effect upon the power-density spectra of the opening sounds for these three experiments. This can be seen if one examines the power-density spectra plotted in Figures 4-5e, 4-8e and 4-9e and the corresponding parameters that have been listed in Tables 4-2, 4-5 and 4-6. In the figures one can see that the spectra had from three to five peaks distributed over the frequency range from 10 to 1000 Hz. All three spectra had a peak centered near 780 Hz. This peak was associated with sounds produced by collisions of the occluder with the struts. The amplitudes of these peaks differed, at most, by 2 db between experiments. Besides these similar-peaks each spectrum had minor peaks which are not clearly seen in the other spectra. For example experiment 310 had a peak centered near 250 Hz. The general trends that we observed in the spectra of the opening sounds for the experiment having low stroke-volume were a 5-db increase of power between 10 and 150 Hz, a 10-db decrease of power between 200 and 300 Hz, and a relatively constant power level of 24 db near 780 Hz.

These opening sounds can be compared further by examining contours of

window 5 for the other subfigures corresponding to these three experiments. For example, Figures 4-5c, 4-8c and 4-9c indicate that the distribution of power was indeed different, but the total power was relatively constant for the opening sounds of these experiments. These figures also allow comparisons of the power distributions between opening, systolic and closing sounds. The flat contour corresponding to window 5 in Figure 4-8h indicates that the opening sound for experiment 309 has nearly the same total-power as that of experiment 306. A similar shape occurs along the contour for window 5 in Figure 4-9h. Compared to the changes of the opening sound we have observed for the abnormal valve having simulated tissue overgrowth, these changes are insignificant.

4.4.2.2 The Systolic Sounds

The systolic sounds were quite different for experiments 306, 307 and 308. This difference was primarily a result of differences in the value of the maximum systolic flow rate which was 26.6, 47.1 and 21.6 L/min during experiments 306, 307 and 308, respectively. The systolic sound, SS, is depicted nearest its occurrence along the upper tracings of Figures 4-5a, 4-8a and 4-9a. Again, by examining all four tracings, one can see that the maximum intensity of the systolic sound occurred at the same time as the maximum flow-rate and the maximum pressure-gradient. It is also clear that the systolic sound-intensity increased with the maximum flow-rate and the maximum pressure-gradient. The correlation between systolic sound and maximum flow-rate/pressure-gradient is shown in Figures 4-4 and 4-3, respectively.

The power-density spectra depicted in Figures 4-5f, 4-8f and 4-9f show these acoustical differences in the frequency domain. Each spectrum has one low-frequency peak centered below 100 Hz and one high-frequency peak centered

near 700 Hz. The **normal** spectrum, for example, had a peak centered at 80 Hz and another at 690 Hz. The spectra of the opening sound of the experiment having less stroke volume is very similar to **normal** except that the high-frequency peak was 2-db lower in amplitude and the low-frequency peak was shifted to a lower center-frequency of 35 Hz from a **normal** value of 80 Hz. These facts suggest a reduction in the bouncing of the occluder and a change in the turbulent eddy-distribution, respectively. The spectrum of the systolic sound of the experiment having more stroke volume also had two peaks. The low-frequency peak was shifted to a higher center-frequency of 110 Hz and had an amplitude 13-db greater than **normal**. The high-frequency peak was shifted to a higher center-frequency of 790 Hz. This peak also had an amplitude 8-db greater than **normal**. Thus, we would initially conclude that both the turbulence and occluder-collisions increased their acoustical productivity as the stroke volume increased. Since the total spectrum would be a superposition of the power contributed by both components of the systolic sound, the transient contribution at 700 Hz does not seem significantly different for these spectra if the broad, non-transient peak is subtracted from the total power-density. Therefore, the amount of bouncing had not changed significantly. These spectra also suggest that the power associated with the non-transient sound approached zero in the limit of zero stroke-volume at a rate faster than that associated with the transient sound produced by the bouncing of the occluder. For estimates of frequencies produced by vortex-shedding near the struts and phonocatheter for these experiments, only the low-frequency peak could be associated with shedding. Based on our estimates, if such a phenomenon existed, it would probably occur at the phonocatheter. These estimates are discussed in detail in Part VII of this series of papers. The results of our calculations are listed in Table 7-2.

Subfigures 4-5 and 4-9 b,c,d, and h, clearly show the large differences between the power distributions of these systolic sounds, particularly that associated with experiment 309. The differences between power distributions of the systolic sounds corresponding to experiment 309 and the **normal** experiment are directly shown by the peak between 10 and 700 Hz along the contour corresponding to window 12 depicted in Figure 4-8h. The reverse effect is not clearly indicated along the window-12 contour of Figure 4-9h.

4.4.2.3 The Closing Sounds

The closing sounds, CS, of experiments 306, 309 and 310 are again very similar to each other. These sounds were comprised of two events which we have labeled CS1 and CS2 nearest their occurrence along the upper tracings of Figures 4-5a, 4-8a and 4-9a. One can see from the other tracings included in these figures that the closing sound CS1 occurred at the same time as the maximum backflow, the dichrotic notch of the aortic pressure-curve, and the beginning of the rapid decrease of the ventricular pressure-curve. The second closing-sound, CS2, occurred at the same time as the peak value of the diastolic, aortic pressure. The timing of these events are **normal** for each of these experiments. The spectra of the closing sounds are, again, similar to each other but quite different from either of the corresponding spectra associated with the opening or systolic sounds.

Each of the spectra of the closing sounds that are shown in Figures 4-5g, 4-8g and 4-9g have six to eight peaks. Some of these peaks are more distinct than others. The distribution of power is also similar for these experiments. Considering the fact that these spectra are averages of ten spectra, it is perhaps reasonable to say that these particular spectra are not significantly different with

respect to the distribution of power. There is a significant difference, however, between the total power of the closing sound of experiment 309 and the closing sounds of either experiment 306 or 310. This difference also corresponds to a 60% increase in the rate of change of ventricular pressure prior to closure. Drag forces involved with the closing process could have been significantly greater during this experiment. This rapid decrease in ventricular pressure could correspond to increases in fluid velocity and drag forces on the occluder, producing a greater acceleration of the occluder toward the orifice. If this change of acceleration produced greater impulsive forces at closure, an increase of the power of the resulting closing sound would then be a reasonable consequence of these changes.

The power distributions of the closing sounds for these three experiments were represented by windows 21, 21 and 21 and depicted in Figures 4-5, 4-8 and 4-9, subfigures b,c,d and h, respectively. The center-frequencies of these three sounds do have a number of significant differences. For example the spectrum of experiment 309 lacks two peaks which are common to every other experiment with this valve, those centered near 165 and 490 Hz. The remaining peaks were similar in form but differ slightly in their amplitudes at corresponding frequencies. The total power of the closing sound of the experiment having a large stroke-volume was 13.6 RPU greater than the **normal** value of 63.5 RPU. These differences are depicted by difference-surfaces shown in Figures 4-8h or 4-9h. The overall increase of power of the closing sound of the (**APS**), experiment 309, is depicted by the peak between 10 and 500 Hz and between windows 18 and 23 in Figure 4-8h. The peak/valley combination between 10 and 500 Hz and between windows 16 and 23 in Figure 4-9h depicts the 10 ms early closing sound associated with the lower stroke volume of experiment 310. The overall similarity of the power distribution of the closing sounds between the **normal** case and

experiment 310 is depicted by the symmetry of this peak/valley combination about the flat, center-contour of window 20.

4.4.2.4 Summary of Comparisons of Stroke-Volume Experiments

The effect of stroke volumes of 65, 81, and 132 cm^3 upon the opening sounds of the Starr-Edwards 2400 valve was not significant compared to the changes we have observed with simulated tissue overgrowth discussed in Part II of this series of papers. Relative to other comparisons made in this paper they are also insignificant.

The effect of changes of the stroke volume was very significant relative to the changes produced by tissue overgrowth. The primary effect of an increase in the stroke volume was to increase the power of the low-frequency, non-transient peak of the systolic sound centered near 80 Hz, and at the same time, shift the center-frequency of this peak toward higher frequencies. The transient peak normally centered at 700 Hz did not have a significant change of power as the stroke volume changed provided the non-transient component of the spectra was subtracted from the total amplitude of these peaks.

The effect of stroke volume upon the closing sound was minor compared to the systolic sounds. The most significant effect observed was an increase of 10 RPU in the total power of the closing sound for the case having above-**normal** stroke-volume. This pulse state had a 60 % greater rate-of-change of ventricular pressure prior to valve-closure. An early closing sound was observed for the case having below-**normal** stroke volume.

4.4.3 Effects of Hypertension on the Sounds

The Starr-Edwards 2400 valve was pulsed at two different states of mean aortic

pressure at a pulse rate of 70 beats/min. The experiments which will be compared are 306 and 311. Values of the important pulsatile variables for these experiments are listed in the appropriate columns of Table 4-1a. The stroke volumes were 81 and 45 cm^3 and corresponded to mean flow rates of 5.5 and 2.9 L/min, respectively. For these three experiments, as with all other experiments involving changes in the value of the stroke volume, the maximum flow-rate and maximum pressure-gradient increased as the stroke volume increased. Since the effect of stroke-volume alone on the opening and closing sounds were minor, we expect any changes in the spectra of these sounds for the experiments involving increased mean aortic pressures to be related to hypertension. Of course, this isolation of hypertensive effects does not apply to the timing of events. When cardiac output is held constant, hypertension tends to delay the closing sound of the natural aortic valve. The early closing sounds we have observed under elevated mean aortic pressure were therefore related to the change of stroke volume.

4.4.3.1 The Opening Sounds

In a manner similar to the previous comparisons involving changes of pulse rate and stroke volume, the opening sounds, OS, produced by the Starr-Edwards 2400 valve for these three experiments occurred as two distinct events which we have labeled OS1 and OS2 nearest their occurrence along the upper tracings of Figures 4-5a and 4-10a. The **normal** time interval between OS1 and OS2, 50 ms, was the same for both experiments. We would therefore expect to see similarities in the opening sounds for these two experiments.

If one examines the power-density spectra plotted in Figures 4-5e and 4-10e and the corresponding parameters that have been listed in Tables 4-2 and 4-7

one can see that the spectra have three similar peaks with approximately the same center-frequencies of 90, 360 and 780 Hz. These peaks of the spectrum of the **APS** had 1 to 2 db less power than those of the **normal** spectrum. The spectrum of the **APS** had two additional peaks centered at 250 and 630 Hz. These additional peaks were similar to those that were observed in the spectra of the opening sound of experiment 310. The significance of these peaks is not clear but could be related to the hypertensive state. The total power of the opening sound was less for the case having increased-hypertension but the distribution of this power over the frequencies we have studied did not significantly change. This decrease of power may be a result of the occluder opening under less drag forces resulting from late valvar opening relative to the initial rise of the ventricular pressure. The drag forces on the occluder may decrease at such pulsatile states.

These power distributions of the opening sounds of these two experiments can be compared further by inspecting the contours corresponding to window 5 depicted in Figure 4-5 and Figure 4-10, subfigures b,c,d, and h. The opening sound is again more powerful than the systolic sound and less powerful than the closing sound. A direct comparison between all of these sounds is provided by Figure 4-10h. The shallow valley between 10 and 600 Hz along the contour corresponding to window 5 in Figure 4-10h indicates that the opening sound for experiment 311 had less total-power and power-density near 600 Hz than that of the **normal** experiment 306.

4.4.3.2 The Systolic Sounds

The systolic sounds were quite different for experiments 306 and 311. This difference was primarily a result of differences in the value of the maximum,

systolic flow rates of 26.6 and 16.6 L/min corresponding to experiments 306 and 311, respectively. The systolic sound, SS, was depicted nearest its occurrence along the upper tracings of Figures 4-5a and 4-10a. The systolic sound was approximately 20-ms early in the hypertensive case. The time when the maximum systolic sound occurred correlated well with the stroke volume, maximum flow rate, or alternatively the mean flow rate. This early systolic sound of the **APS** occurred during the forward acceleration of flow prior to the time of peak flow. The amplitude of the systolic sound in the time-domain for experiment 311 was much less than **normal** as we would have predicted from the results of the previous experiments involving the effect of stroke volume on this amplitude. The systolic sound-intensity again increased with the maximum flow-rate and the maximum pressure-gradient. Plots of the total power versus maximum flow-rate and pressure-gradient are shown in Figures 4-4 and 4-3, respectively.

The power-density spectra depicted in Figures 4-5f and 4-10f showed differences between these sounds in the frequency domain. Here we see that the systolic sound of experiment 311 was noticeably different from **normal**. The spectrum of the **APS** had two peaks centered near 25 Hz and 690 Hz. The peaks centered near 190 Hz are significantly less powerful within the frequency band 10-50 Hz. This fact is depicted graphically by the density-spectra as well as the distribution functions that are plotted immediately below them. The hypertensive power-distribution shown in Figure 4-10f has a steep slope spanning this low-frequency range relative to the more gradual slope of the distribution of the **normal** sound shown in Figure 4-5f. The major differences between these spectra were similar to those discussed for the experiments involving changes of the stroke volume. For example, the low-frequency, non-transient peak was shifted toward a lower center-frequency because the maximum systolic flow rate had decreased, thus, indicating a decline in the production of sound caused by the

turbulence eddy-distribution. The high-frequency, transient peak declined in total amplitude but remained constant when the decreasing, non-transient contribution to the power-density at these frequencies was subtracted from the total power-density. We have observed once again that the spectra of systolic sounds of the **APS** decrease in power as the stroke-volume decreases and occur earlier in systole as the stroke-volume decreases. The nature of these changes also suggested that the power associated with the non-transient sound approached zero in the limit as the stroke volume approached zero, at a rate faster than the power associated with the transient sound produced by the bouncing of the occluder.

Subfigures 4-5 and 4-10 b,c, and d do not show the power distributions for the systolic sounds but only indicate their relative values with respect to the opening and closing sounds. This difficulty is true also for Figure 4-10h.

4.4.3.3 The Closing Sounds

Closing sounds, CS, of experiments 306 and 311 are different from each other. They are comprised of two events, CS1 and CS2, and are labeled nearest their occurrence along the upper tracings of Figures 4-5a and 4-10a. The closing sound CS1 occurs at the same time as the maximum backflow, the dichrotic notch of the aortic pressure curve, and the beginning of the rapid decrease of the ventricular pressure curve. The second closing sound CS2 occurs at the same time as the highest value of the diastolic aortic pressure.

The spectra of the closing sounds are shown in Figures 4-5g and 4-10g. Comparing these figures, we can see that there is a difference between the two spectra at frequencies above 800 Hz. A small peak still exists at 1710 Hz but those normally near 825, 1035 and 1355 Hz have vanished in the spectrum of the

APS . The peaks of the **APS** in the range 10-800 Hz are also different in number and location. Either different modes have been stimulated or the same modes have changed their characteristic frequencies. Which of these two phenomena are occurring is not clear at this time. The total power of the closing sound of the **APS** increased by 7.5 RPU above the **normal** value of 63.5 RPU.

The power distributions of the closing sounds, represented by windows 21 and 19, are depicted in Figures 4-5 and 4-10, subfigures b,c,d and h, respectively. As we have mentioned, the shapes of these contours are similar for these two experiments. Differences do appear however in the 3-D difference-surfaces depicted in Figure 4-10h. These differences are with respect to the timing of the closing sound relative to **normal**. We would expect this difference given the shift of the window having the maximum total-power from a **normal** window-number of 21 to the value of 19 of the **APS** . This difference appears as a peak/valley combination along the 10 Hz contour between windows 14 and 24 in Figure 4-10h. Since the closing sounds are similar relative to their power distributions, the symmetry of this peak/valley combination about its mid-window contour indicates differences that are primarily temporal in character. A difference of the total powers of the two sounds is apparent by the fact that window 19, which bisects this peak/valley combination, is not flat. This fact indicates that this **APS** possesses more total-power in its closing sound particularly at the lower frequency range of 10 to 200 Hz where this contour has its greatest slope parallel to the frequency axis.

4.4.3.4 Summary of Comparisons of Hypertensive Experiments

The effect of mean aortic pressures of 108 and 150 mmHg upon the opening sounds of the Starr-Edwards 2400 aortic valve at a pulse rate of 70 beats/min

was minor compared to the changes which we have observed for the malfunctioning valve with tissue overgrowth at the apex. The location of peaks in the density-spectrum changed significantly, however, the power-distribution and total-power of these sounds were very similar for the **normal** and hypertensive cases.

The primary effect of hypertension upon the systolic sound was to shift this sound earlier in systole as the hypertension increased and to decrease the power of the non-transient component, centered near 50 Hz, as the hypertension increased. The transient peak normally centered at 700 Hz did not have a significant loss of power as the stroke volume changed provided the amplitude of this peak was estimated after the the amplitude of the broad, low-frequency, non-transient peak was subtracted at the center frequency of the high-frequency peak. The change of the systolic sound produced by hypertension was also minor relative to that produced by simulated overgrowth.

The effect of hypertension upon the closing sound of the Starr-Edwards 2400 valve was to shorten systole by reducing the stroke volume. This caused the closing sound to occur early with respect to **normal** timing. A significant loss of power occurred in the band 1000 to 2000 Hz for the hypertensive closing sound. Normal peaks centered at 825, 1035 and 1355 Hz were absent. An increase of power in the band 10 to 100 Hz was also observed and accounted for the increase of total-power of 7.5 RPU above **normal** associated with the closing sound of the hypertensive case. The temporal changes were comparable to those observed with simulated overgrowth, however, the accompanying frequency changes were quite different for the two cases. Therefore the two effects were distinguishable.

4.5 CONCLUSIONS AND RECOMMENDATIONS

It is apparent from the results presented in this paper that the effects of pulse rate, stroke volume and hypertension were significant upon the three major sounds of the Starr-Edwards 2400 valve.

The opening sounds under all of the pulsatile conditions did not change significantly relative to corresponding changes of the systolic and closing sounds. We did observe a decrease of the total power of the opening sound with a decrease of the stroke volume and rate of change of ventricular pressure evaluated 20 ms prior to OS2.

Of the three major sounds, the most significant changes occurred with respect to the systolic sounds. Unlike the Smeloff and Bjork-Shiley valves this sound occurred at the same relative time in the cycle independent of the stroke volumes we studied. We observed, however, that the total-power of the systolic sound changed dramatically and correlated very well with the stroke volume, maximum systolic flow rate, mean flow rate, and maximum systolic pressure gradient. A low-frequency peak, associated with the flow, was always present in the spectrum. The center-frequency of this peak shifted to greater values as the stroke volume increased. This peak was associated with turbulence and with vortex-shedding at the phonocatheter and struts. A high-frequency peak associated with the collisions between the occluder and cage, appeared in the spectrum of the systolic sound of each experiment. This peak had a center-frequency at 690 Hz for all experiments except that having a large stroke volume for which it shifted to 790 Hz.

The closing sounds of the valve were very powerful relative to both the opening and systolic sounds. The time of closure was later with increasing stroke volume. The total power of the closing sound increased with stroke volume and

the rate of change of ventricular pressure 20 ms prior to CS1. The spectra of these sounds were very similar for each experiment except for the case having a large mean aortic pressure. Three of the peaks of the spectrum of the closing sound for this experiment were absent. The remaining peaks were normal. For this case, the total power of the closing sound was 7.5 RPU greater than the normal value of 63.5 RPU. This particular experiment also involved a small stroke-volume. These combined effects produced this reduction of acoustical power at the time of closing. It should be noted that the opposite effect was observed for the total power of the closing sound for the hypertensive state of the Bjork-Shiley valve discussed in Part VI.

The differences we have observed for these changes of the pulsatile state are distinct from those we discussed in Part II. For example the large valley between 10 and 600 Hz along the contour of the opening sound of the difference-surface presented for the valve having tissue overgrowth in Part II was not observed for any of the opening sounds of the normal valve at the six pulsatile states we have studied. It is unlikely that this could occur with a normal valve at any reasonable pulsatile state because this high-frequency peak was associated with collisions of the occluder with a normal apical surface at the time of OS2. Such an event would always occur with a normal valve. We conclude therefore that our method is specific for identifying opening sounds corresponding to a case with tissue overgrowth at the apex of the Starr-Edwards 2400 valve amongst those sounds produced by a normal valve pulsed at the APS we have studied.

We observed some general similarities and differences between valvar designs. These topics are presented in the Conclusion section of Part VI. At that point in the text we will have had a chance to discuss the results of the experiments involving all three valvar designs under comparable pulsatile states.

Furthermore, all recommendations associated with Parts IV, V and VI are given at the end of Part VI.

4.6 ACKNOWLEDGEMENTS

Funding for this project was provided by the Donald E. Baxter Foundation, the Children's Heart Foundation of Southern California, and the American Heart Association, Greater Los Angeles and Georgia Affiliates.

PAPER 5

A Quantitative Method for the *In Vitro* Study of Sounds Produced by Prosthetic Aortic Heart Valves Part V: An Experimental, Comparative Study of the Sounds Produced by a Normal Smeloff Aortic Prosthesis Operating at Eight Pulsatile States

A Quantitative Method for the *In Vitro* Study of Sounds Produced by Prosthetic Aortic Heart Valves

Part V: An Experimental Comparative Study of the Sounds Produced by a Normal Smeloff Aortic Prosthesis Operating at Eight Pulsatile States

ABSTRACT

An *in vitro* study was made of the sounds produced by a normal, Smeloff aortic, heart-valve prosthesis and comparisons were made with sounds of the same valve operating at eight different pulsatile states. All results were then compared and discussed in terms of the pulstatile changes.

Useful information about the pulsatile state was provided by this analysis. The opening sounds and closing sounds were influenced primarily by the rate of change of the ventricular pressure prior to these events. The systolic sounds were primarily influenced by the systolic flow rate. The difference between systolic sounds was much greater than between opening and closing sounds for all cases. An increase in systolic flow rate produced a corresponding increase in the power associated with the systolic sound. These values correlated quite well. The location of peaks within the power density spectra were very similar for these eight pulsatile states when compared to the previous study involving an abnormal valvar state.

Key Words-Smeloff prosthesis, sound, fast Fourier transform

in vitro **comparison**

5.1 INTRODUCTION

This paper, Part V of a Series of VI, is concerned with the effects of eight pulsatile states upon the sounds produced by a normal 24-mm Smeloff aortic prosthesis. Part III of this series of papers was concerned with answering the question whether a malfunctioning Smeloff valve, with tissue overgrowth on its upstream struts, produced sounds that could be distinguished from the corresponding sounds of a normal valve of the same design pulsed at the same pulsatile state. The answer was affirmative for the case we studied. A linear analysis proved useful for this purpose. An equally important question was whether the sounds produced by a normal valve when it is pulsed at alternate pulsatile states **APS** were similar to the sounds produced by the abnormal valve with simulated tissue overgrowth. To answer this question we pulsed a normal Smeloff valve at a normal and seven **APS** . The states we have chosen include states which could occur between day-to-day examinations of a patient. The **APS** of interest were those involving changes in the pulse rate, changes of the stroke volume, and changes of mean aortic pressure. In addition to these pulsatile states we have also pulsed the valve at three orientations with respect to gravity.

5.2 EXPERIMENTAL METHOD

We pulsed the Smeloff prosthesis at eight pulsatile states. Table 5-1a lists the pulse rates, pressures and flows associated with these eight experiments. The entries involving the rate of change of ventricular pressure assigned to opening and closing were evaluated 20 ms prior to OS2 and CS1, respectively. Backflow was estimated from the digitized flow data and the portion due to closure was

Pressure, Flow and Sound* Data
corresponding to experiments involving
a normal 24mm Smeloff valve
operating at various pulsatile states

Experiment Number	292	293	294	295	296	297	298	300
Pulse Rate (cycles/min)	70	91	51	70	70	70	70	70
Max. Pressure Gradient (mmHg)	48	28	53	104	26	20	25	50
Mean Systolic Pressure Gradient (mmHg)	27	18	28	42	14	12	15	28
Mean Aortic Pressure (mmHg)	86	78	88	86	82	145	135	89
Opening rate of change of V. Pressure (mmHg/ms)	1.3	1.0	1.5	0.3	0.9	0.7	1.0	1.3
Closing rate of change of V. Pressure (mmHg/ms)	-1.0	-1.0	-0.7	-2.3	-0.7	-0.7	-0.7	-1.0
Mean flow rate (l/min)	4.7	2.7	4.1	8.4	2.7	1.1	1.9	4.7
Maximum flow rate (l/min)	30.7	20.2	32.8	47.5	21.1	17.5	20.7	30.5
Stroke volume (cc)	91	43	125	135	63	44	54	91
Total backflow (cc/stroke)	24	14	46	42	24	27	28	25
Backflow due to closure (cc/cycle)	2	2	2	2	2	2	2	2
Total backflow (% of stroke volume)	26	33	37	31	38	61	52	27
Effective flow area (sq cm)	2.0	1.8	2.1	2.1	1.9	1.8	1.9	2.0
Opening window number	5	5	5	5	5	5	5	5
Average total power (RPU)	34.6	29.7	32.5	15.8	30.8	25.4	27.5	32.1
Std. deviation (RPU)	5.3	2.6	6.5	3.3	3.2	4.3	5.5	4.7
Systolic window number	13	10	12	14	8	8	8	12
Average total power (RPU)	73.5	50.4	112.6	268.4	45.6	40.3	47.8	64.2
Std. deviation (RPU)	17.6	9.1	30.0	41.4	6.2	4.6	4.1	16.0
Closing window number	23	23	22	23	23	20	21	23
Average total power (RPU)	79.8	84.3	77.7	88.4	78.3	78.1	78.3	80.2
Std. deviation (RPU)	2.2	7.0	3.0	3.5	2.6	2.0	3.0	7.2

*Filter bandwidth: 200-2000 Hz

Table 5-1a Pressure-Flow-Sound data for experiments involving the normal 24mm Smeloff aortic valve.

generally estimated by the area under the zero-flow line and above the negative flow region of the primary "notch" in early diastole. The effective flow area, A_{eff} was estimated by Equation 4-1. Table 5-1b lists the times of the significant events of the sound pressure and flow relative to the time of full valvar opening. We shall call experiment 292 the **normal** pulsatile state for the Smeloff design. Most comparisons between experiments will be with respect to this **normal** state. The orientation of the valve for each experiment is depicted in Figure A-2 of Appendix A. Experimental method and analysis used for the results presented in this paper were identical with those described in Papers IV, VI and VII. Stroke volume was changed independently of the pulse rate and elevated the mean aortic pressure by relatively small values. Changes of the pulse rate and mean aortic pressure were obtained by changes of the ventricular ejection time and systemic resistance, respectively. The stroke volume increased or decreased according to these changes. Therefore, the experiments which include changes of pulse rate and hypertension also involved changes of the stroke volume.

5.3 RESULTS

The results of the eight experiments are presented graphically in Figures 5-1 through 5-12. Figure 5-1 shows a plot of the maximum pressure gradient across the valve as a function of the maximum flow-rate for each experiment. Figure 5-2 shows the maximum pressure-gradient across the valve plotted as a function of the mean flow rate for each experiment. Figure 5-3 shows a plot of the average value of the total power of the systolic sound as a function of the maximum pressure-gradient rate for each experiment. Figure 5-4 shows the average value of the total power of the systolic sound plotted as a function of the mean flow-rate for each experiment. Figures 5-5 through 5-12 are separated into eight subfigures indexed alphabetically with letters from **a** through **h**. Subfigures **a**, 5-

Times of significant events of pressure, flow and sound relative to the time of full valvar opening in milliseconds for experiments involving a normal 24mm Smeloff valve operating at various pulsatile states

Experiment Number	292	293	294	295	296	297	298	300
First Component of Opening Sound (OS1)	-45	-55	-40	-70	-40	-50	-45	-45
Start of Systolic Ejection	-20	-15	-20	-10	-10	-15	-10	-10
Second Component of Opening Sound (OS2)	0	0	0	0	0	0	0	0
Maximum Systolic Pressure Gradient	135	100	155	230	130	115	105	140
Maximum Systolic Flow Rate	140	105	185	220	140	125	125	155
Maximum Amplitude of Systolic Sound (SS)	105	50	170	185	115	95	70	135
First Component of Closing Sound (CS1)	280	190	395	325	280	235	245	290
End of Systolic Ejection	275	195	395	335	295	235	250	290
Second Component of Closing Sound (CS2)	315	235	435	365	340	280	290	330

Table 5-1b Times of Significant Events of Sound, Pressure and Flow for Experiments involving the Smeloff valve.

5a through 5-12a, show the original time-amplitude data of the sound, flow rate, and ventricular and aortic pressures corresponding to each experiment. The corresponding subfigure **b** shows the three-dimensional power-frequency-time surfaces. Subfigures **c** and **d** depict the auxiliary views of this 3-D surface as viewed parallel to the frequency axis and time axis, respectively. Subfigures **e,f** and **g** depict the power-density spectra associated with windows which encompass the opening, systolic, and closing sounds. These three windows were also enhanced in subfigures **b** and **c**. The final figures corresponding to each experiment, Figures 5-6h through 5-12h, depict the 3-D difference-surfaces generated by subtracting the 3-D surface corresponding to the **normal** case, shown in Figure 5-5b, from those corresponding to the **APS** , shown in Figures 5-6b through 5-12b, respectively. Center-frequencies and amplitudes estimated for each peak in the power-density spectra have been included with the plots. These two parameters and the decay parameter have been listed separately for each experiment in Tables 5-2 through 5-9. These tables can be found on the pages immediately following the plots of the spectra of the closing sounds. Tables A-1 to A-6 in Appendix A list the center-frequencies and amplitudes of the peaks of the spectra of the opening, systolic and closing sounds for all experiments in Parts IV, V and VI.

5.4 DISCUSSION OF RESULTS

5.4.1 Effects of Pulse Rate on the Sounds

The Smeloff valve was pulsed at three different pulse rates. These rates were 70, 91, and 51 beats/min and corresponded to experiments 292, 293 and 294, respectively. The important values which defined the pulse mode for these experiments are listed in the first three columns of Table 5-1a. The ventricular

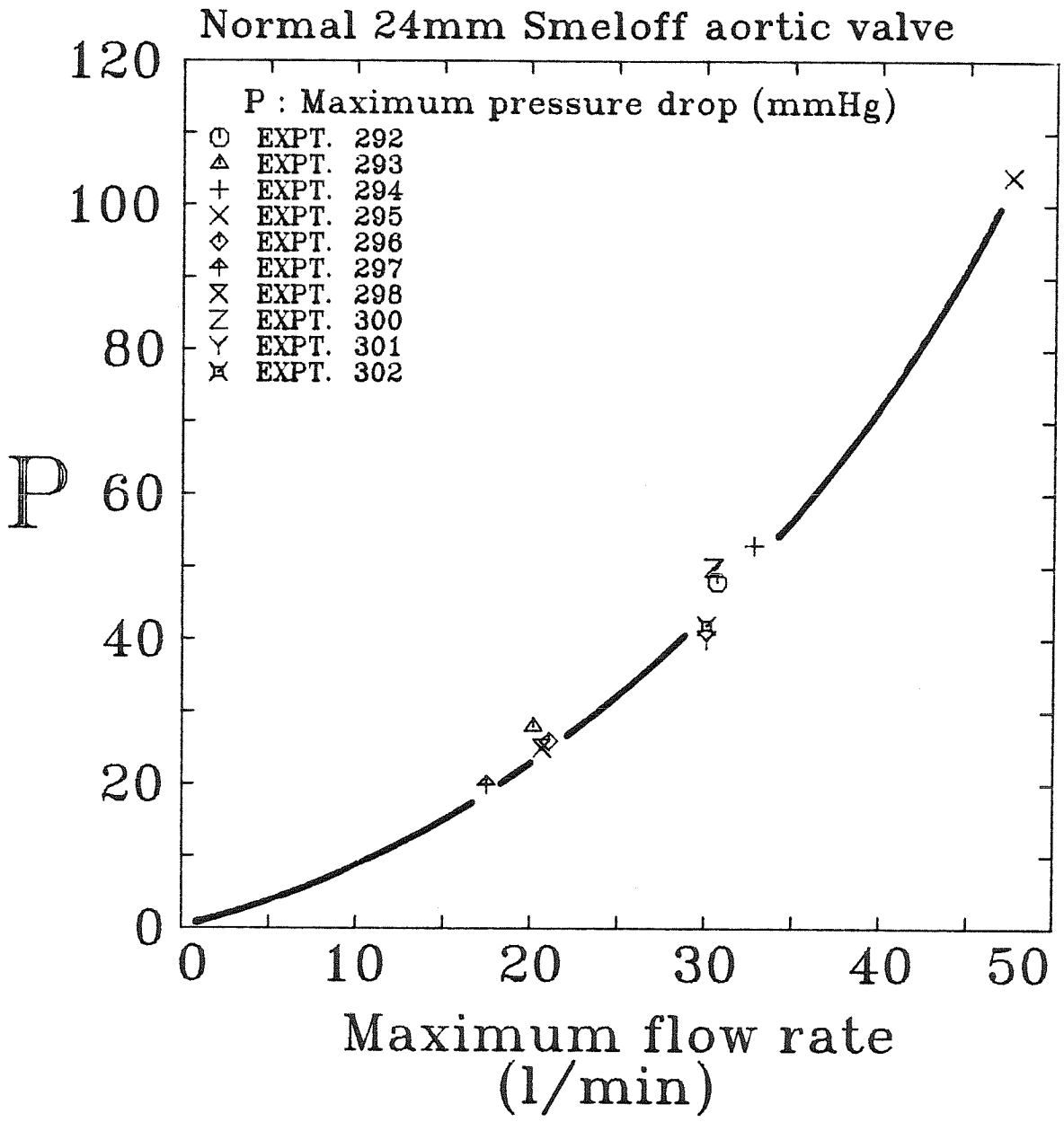

Figure 5-1 Maximum pressure gradient vs. maximum flow rate for the experiments with the normal 24mm Smeloff aortic prosthesis.

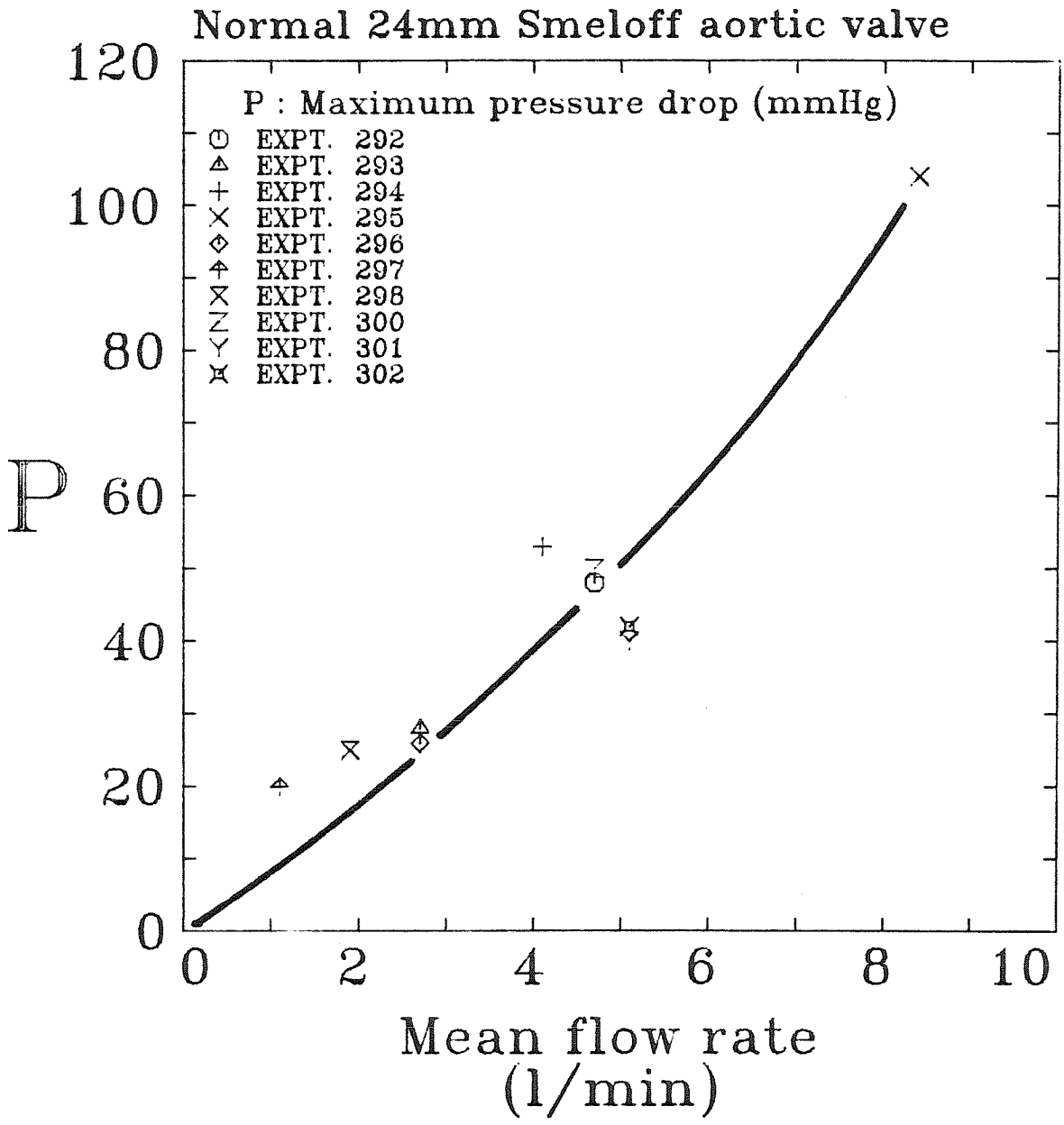

Figure 5-2 Maximum pressure gradient vs. mean flow rate for the experiments with the normal 24mm Smeloff aortic prosthesis.

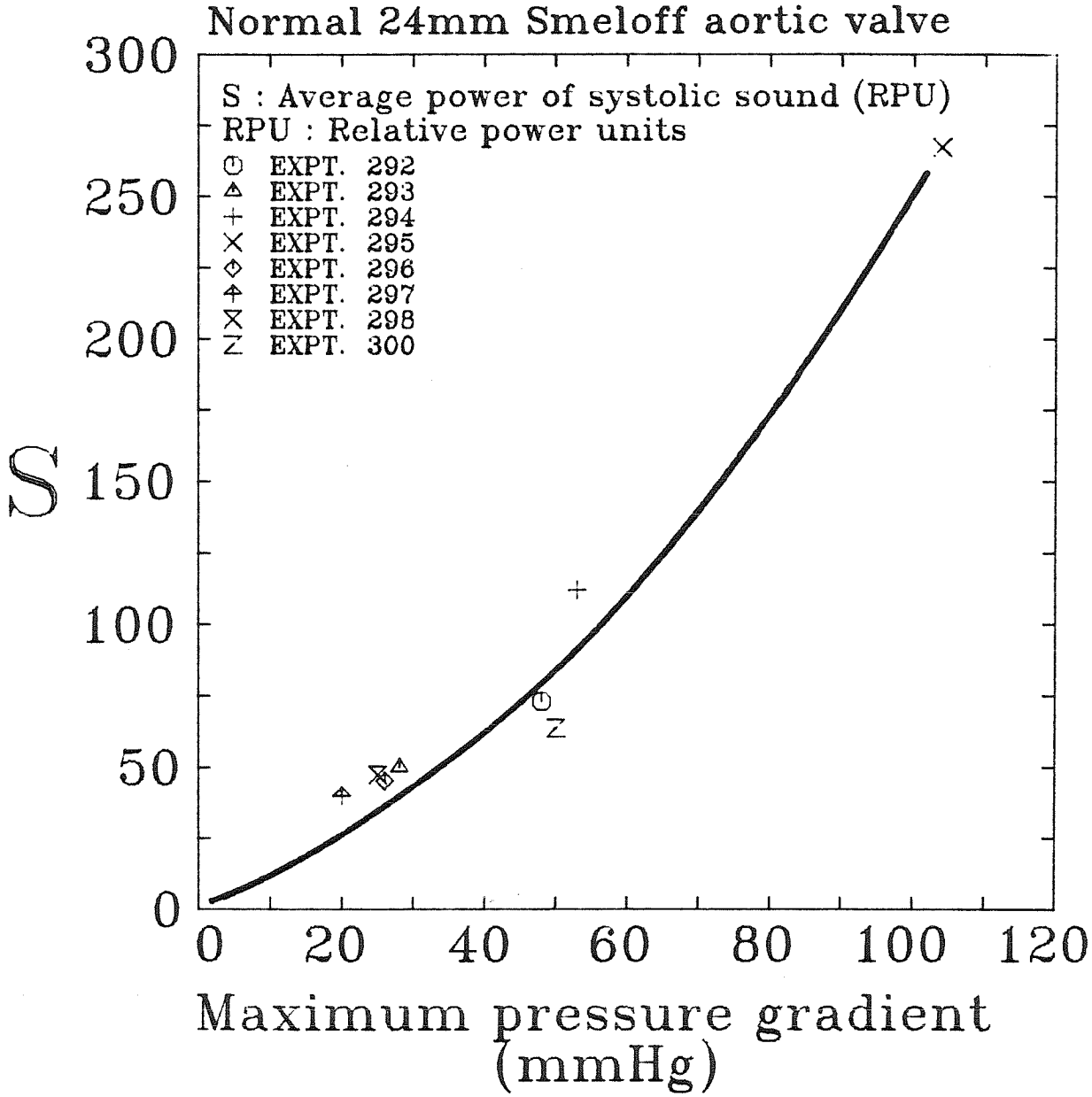

Figure 5-3 Average total-power of systolic sound vs. maximum pressure gradient for the experiments with the normal 24mm Smeloff aortic prosthesis.

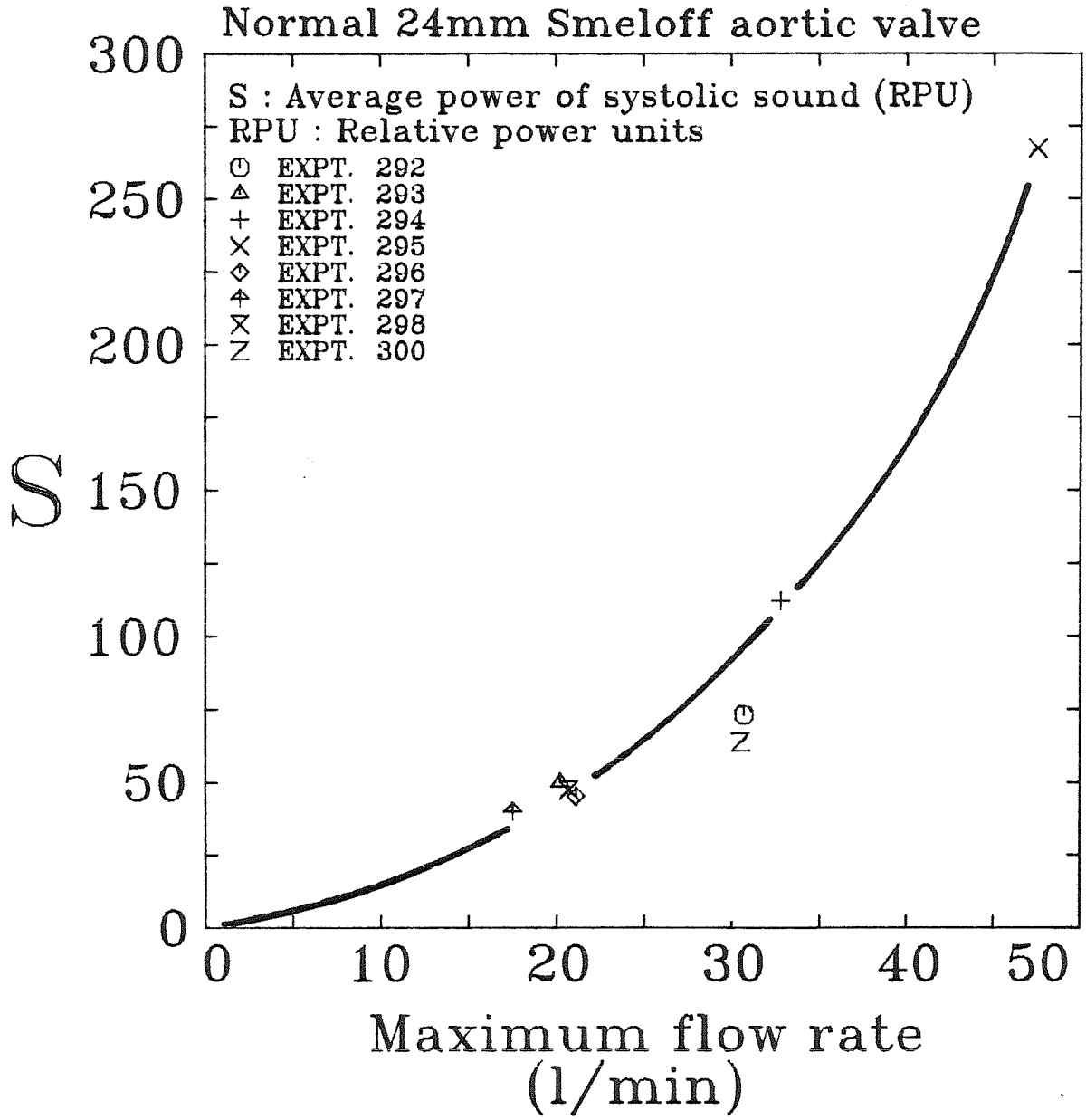

Figure 5-4 Average total-power of systolic sound vs. maximum flow rate for the experiments with the normal 24mm Smeloff aortic prosthesis.

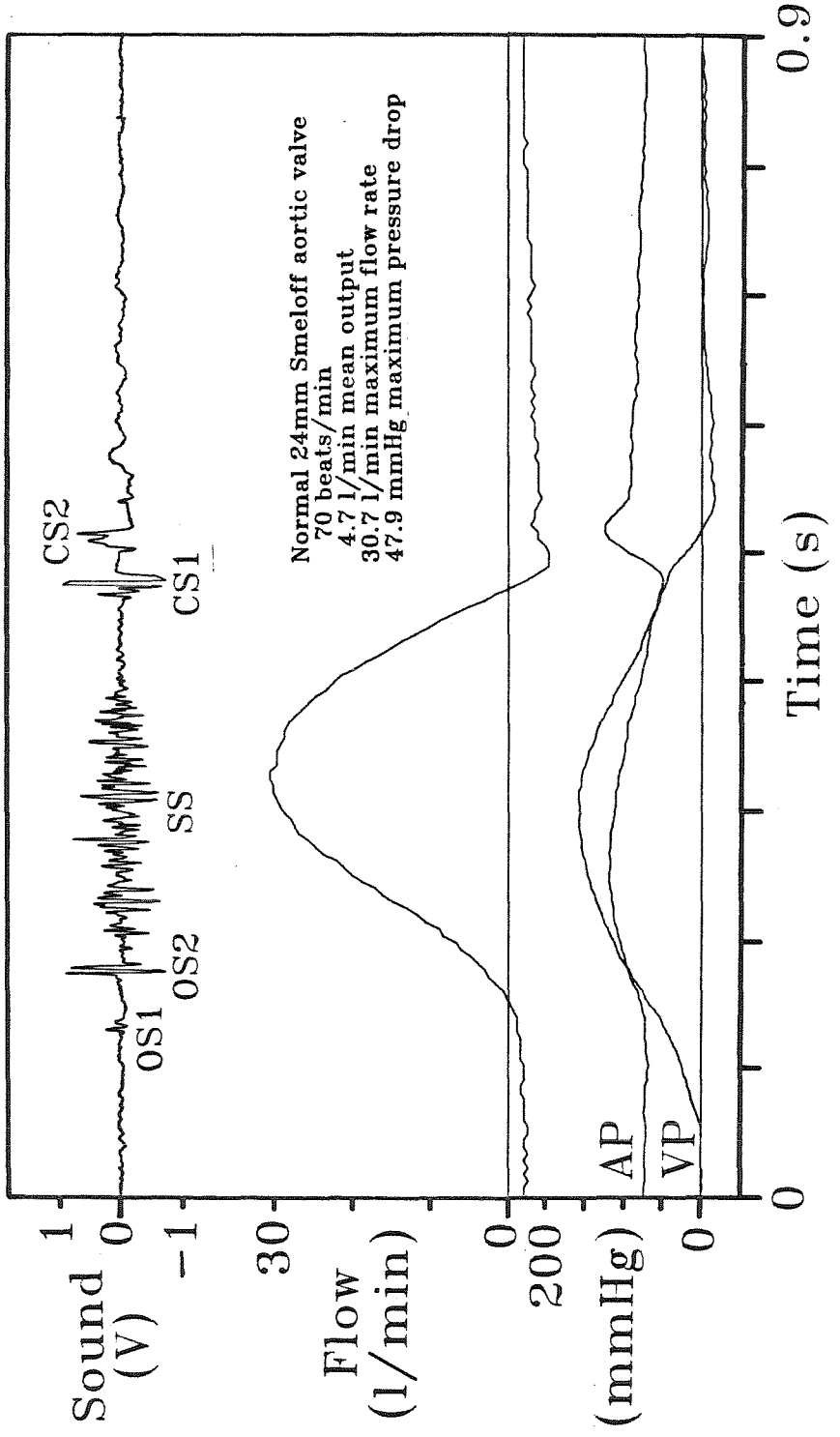

Figure 5-5a Amplitude vs. time tracings of sound, flow rate, aortic pressure and ventricular pressure associated with a typical cycle of experiment 292.

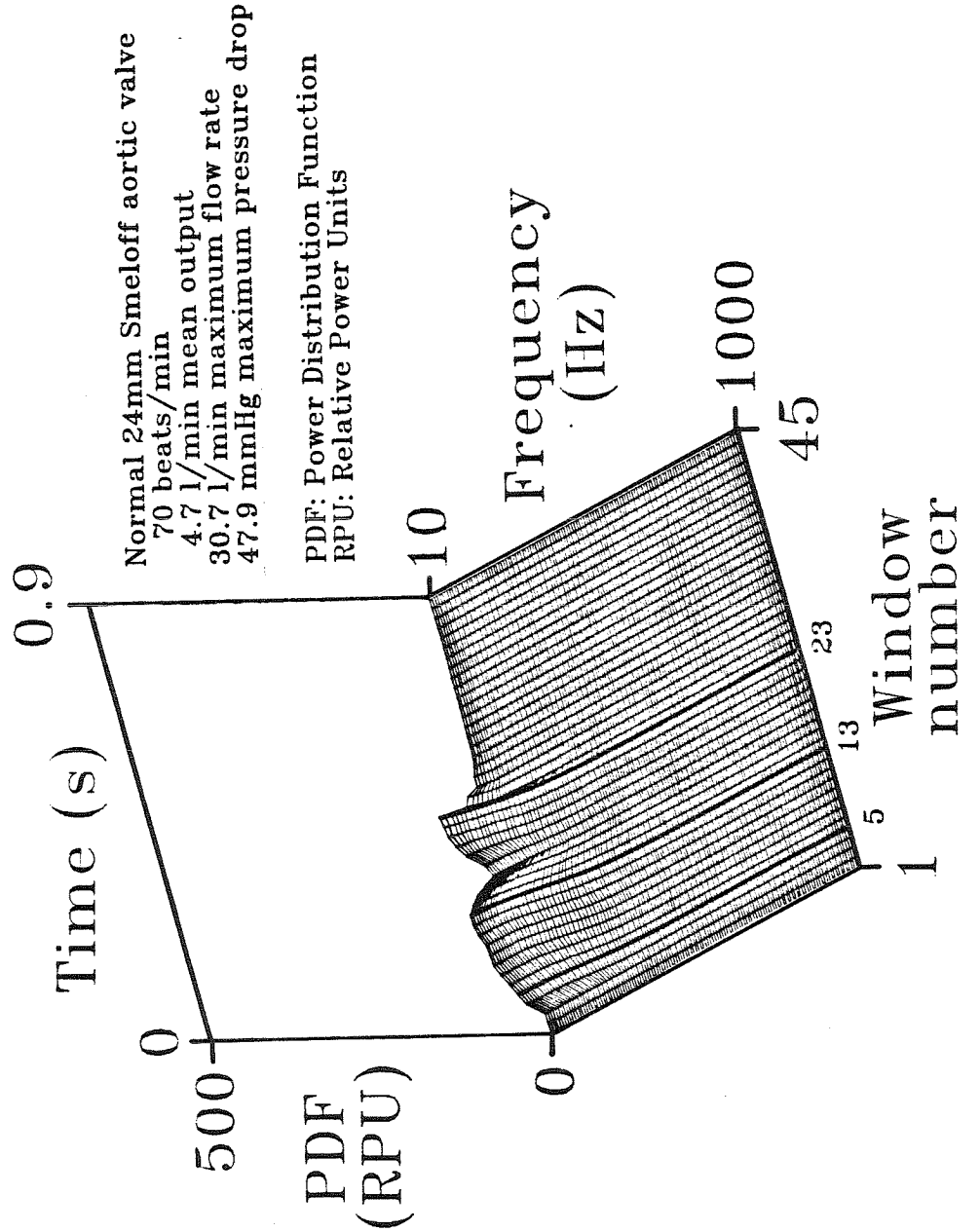

Figure 5-5b Three-dimensional power-frequency-time surface averaged over ten cycles of experiment 292.

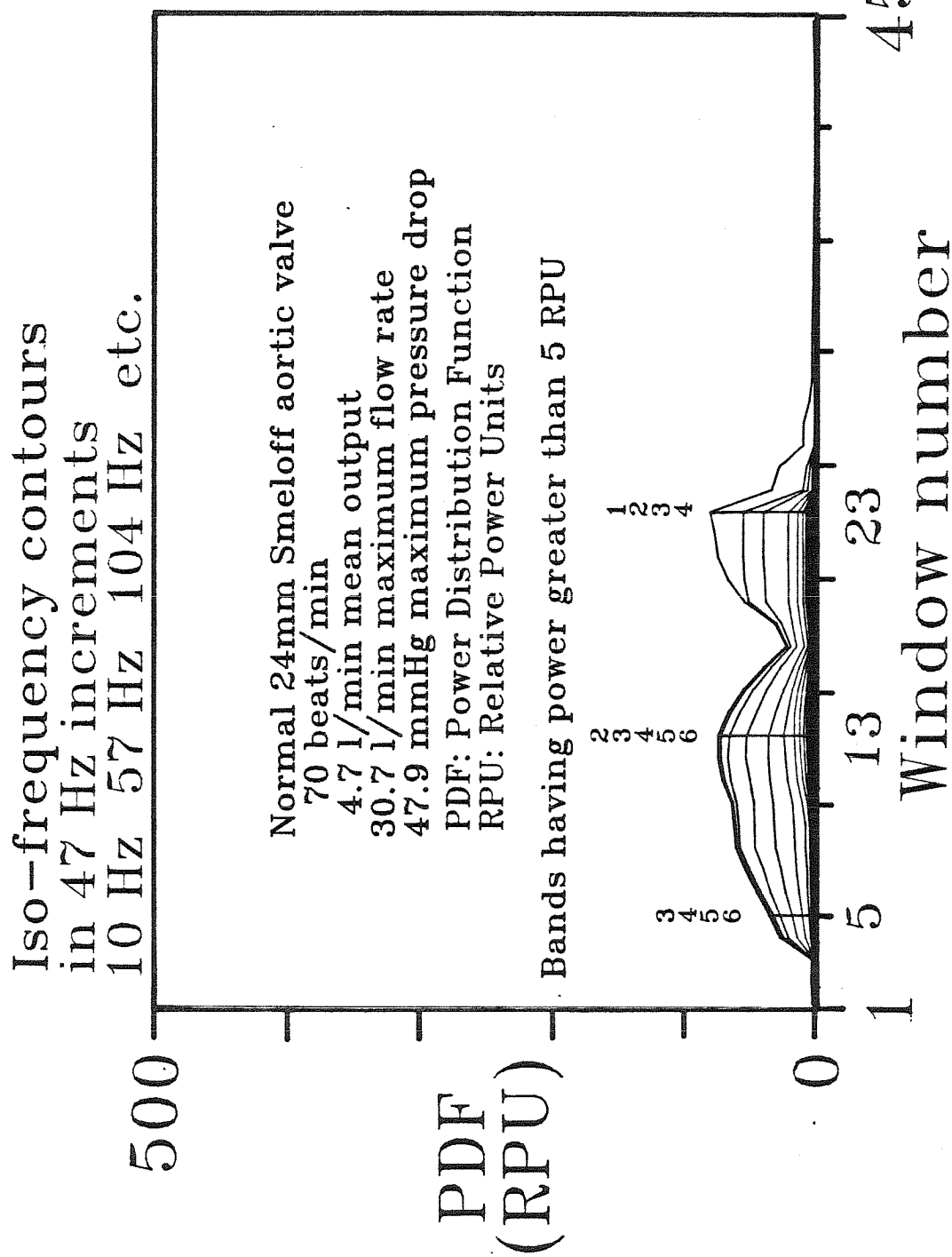

Figure 5-5c Auxiliary view perpendicular to the time axis of the 3-D power-frequency-time surface of experiment 292 showing iso-frequency contours.

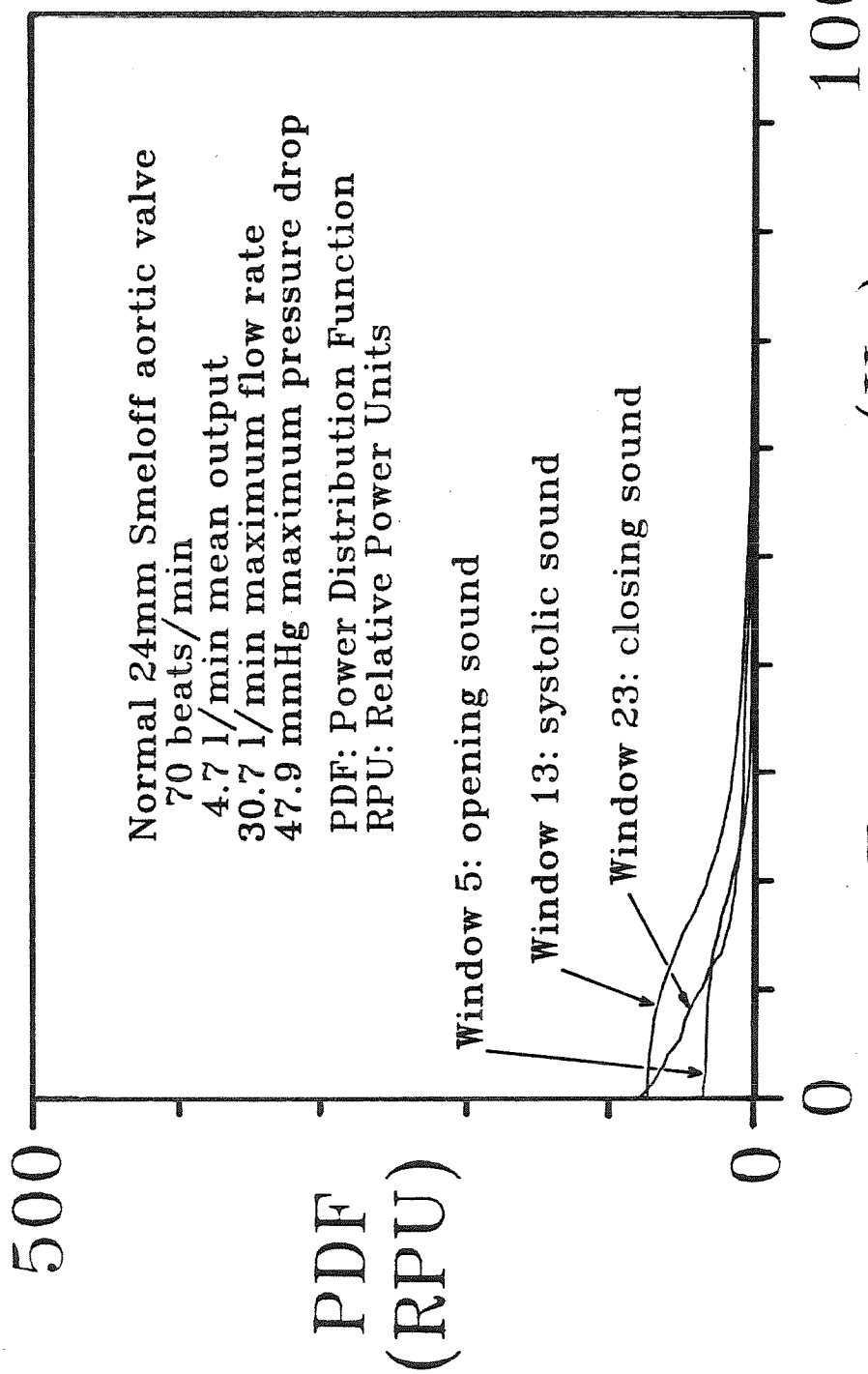

Figure 5-5d Auxiliary view perpendicular to the frequency axis of the 3-D power-frequency-time surface of experiment 292 showing power power distributions associated with windows encompassing the opening, systolic, and closing sounds.

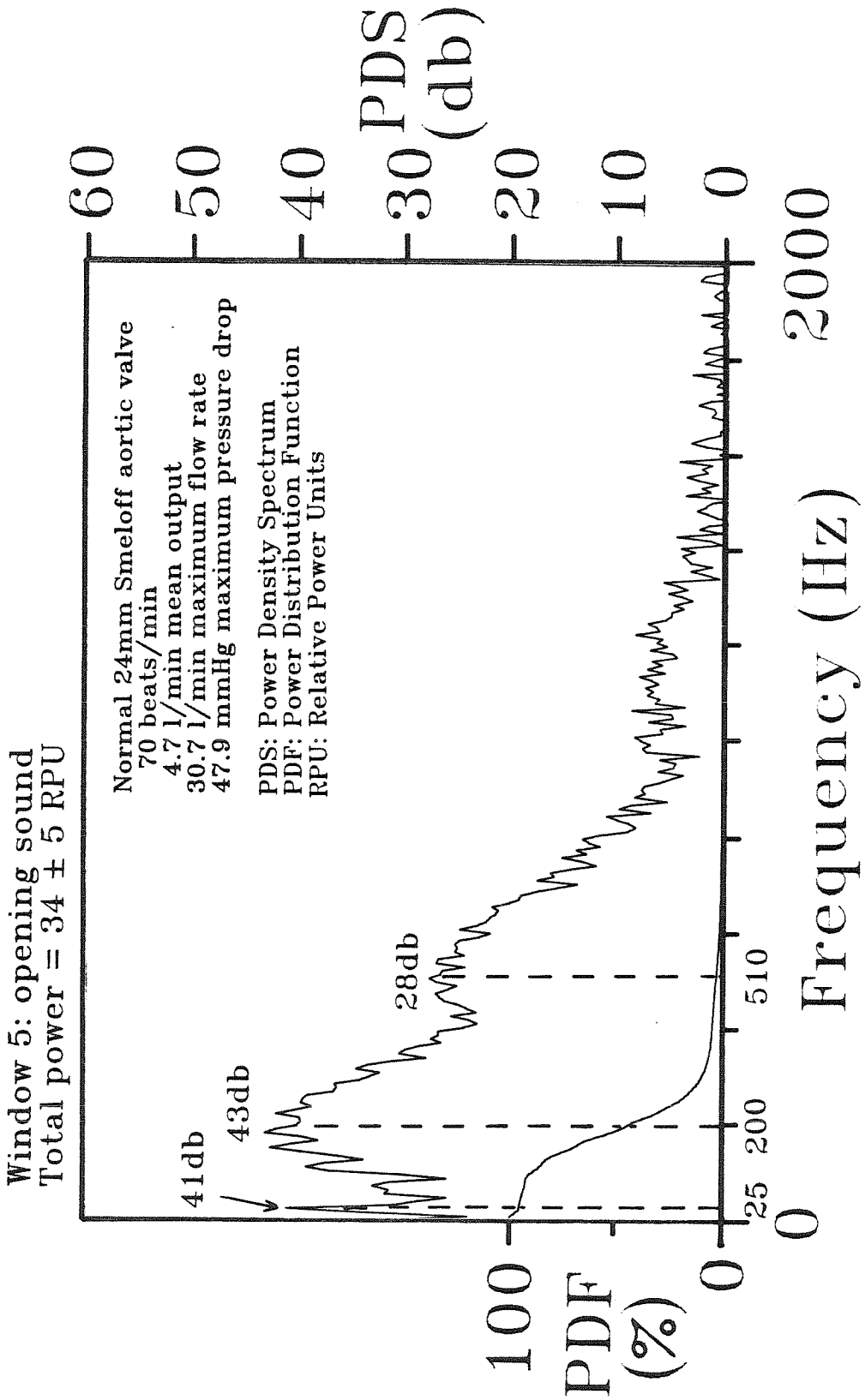

Figure 5-5e Power-density spectra and power distribution of the opening sound of experiment 292.

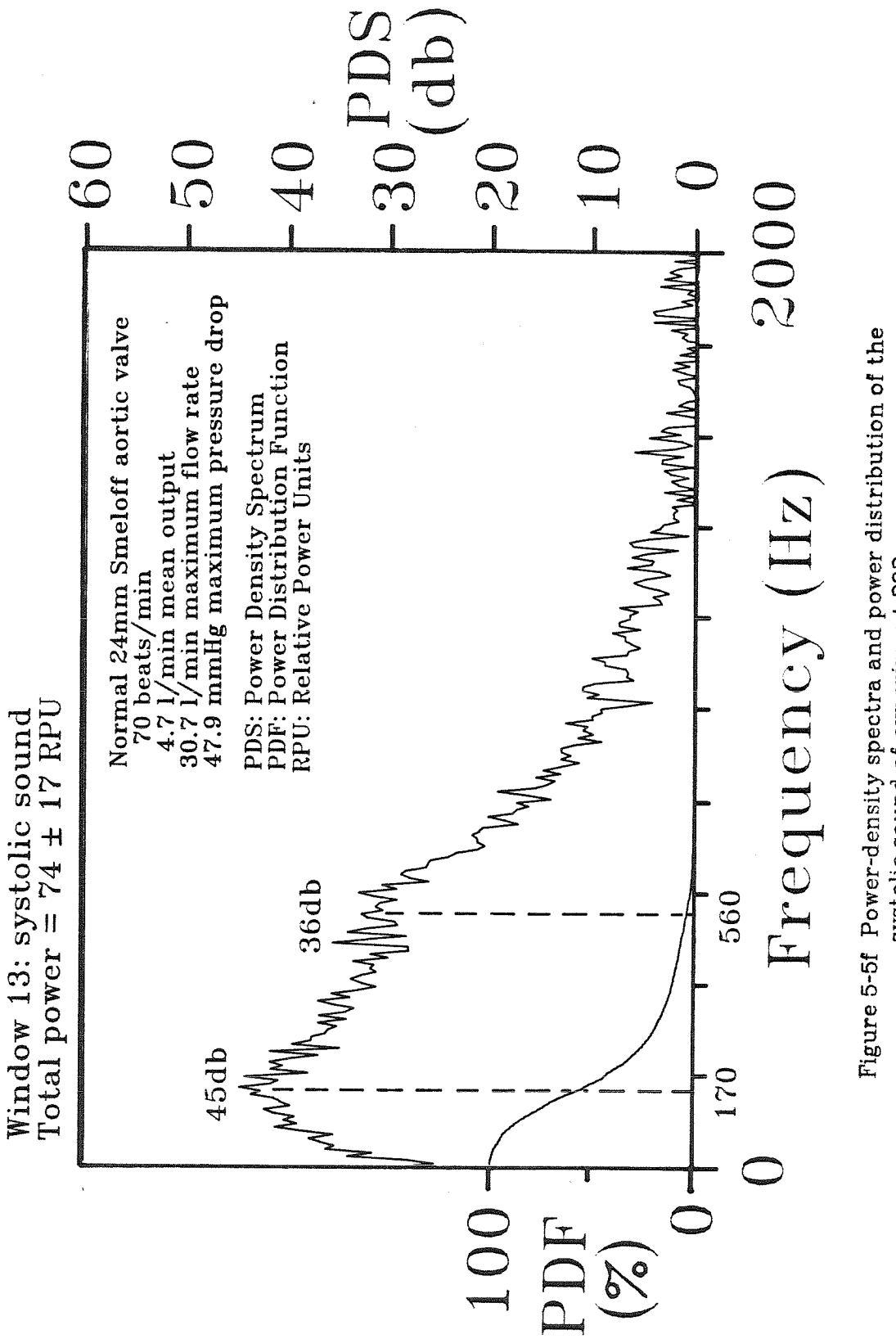

Figure 5-5f Power-density spectra and power distribution of the systolic sound of experiment 292.

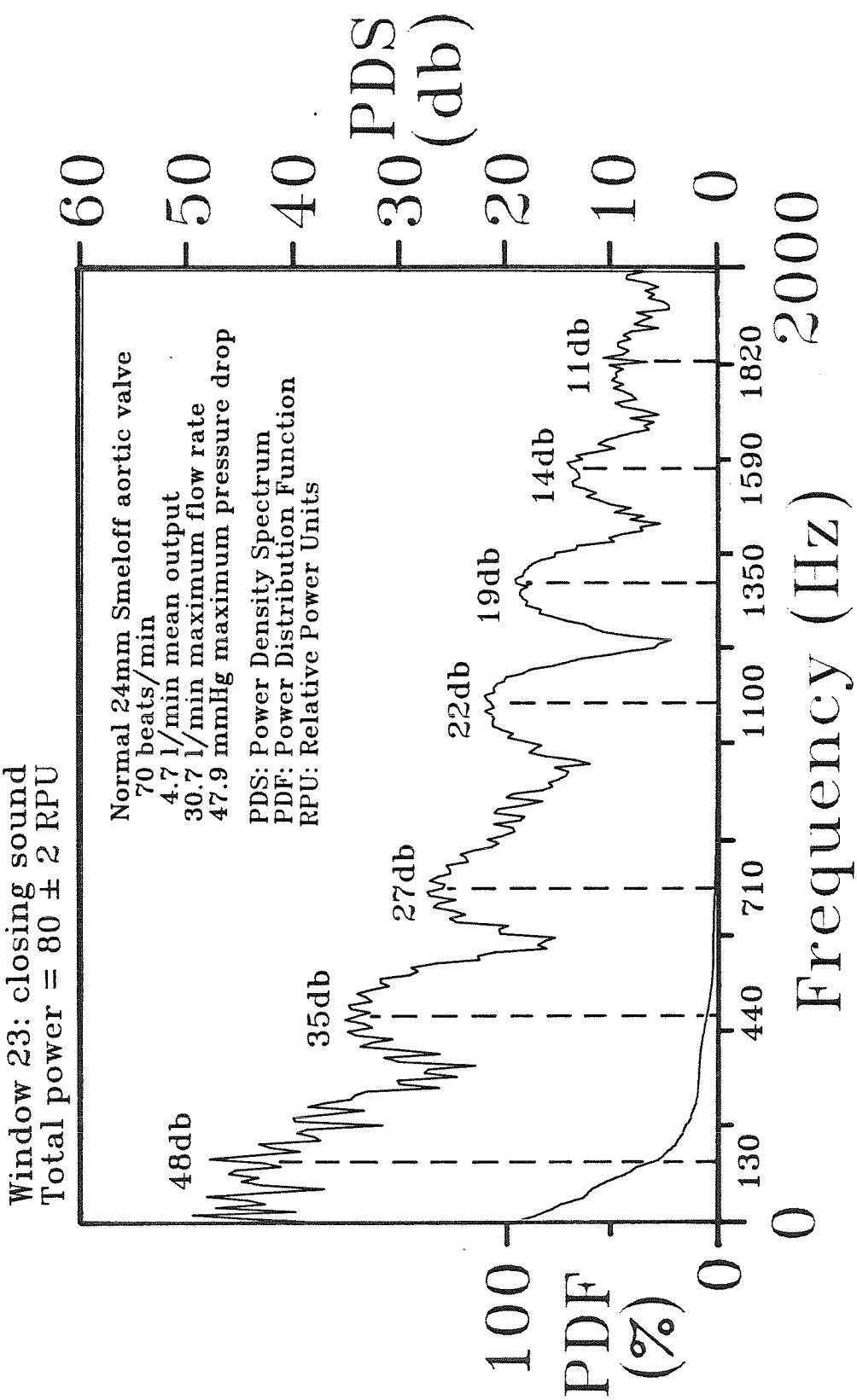

Figure 5-5g Power-density spectra and power distribution of the closing sound of experiment 292.

Parameters Estimated for

Significant Harmonic Peaks

Experiment 292

Event	Frequency, $f_{r,i}$; Decay, k_i; Power-Density, G_i (Hz,Hz,db)
Opening Sound	25, 5,41
Window 5	200,70,43
	510,80,28
Systolic Sound	170,80,45
Window 13	560,90,36
Closing Sound	130, 40,48
	440, 70,35
	710, 70,27
	1100, 70,22
Window 23	1350, 70,19
	1590, 60,14
	1820,110,11

Table 5-2 Parameters estimated from significant harmonic peaks of experiment 292.

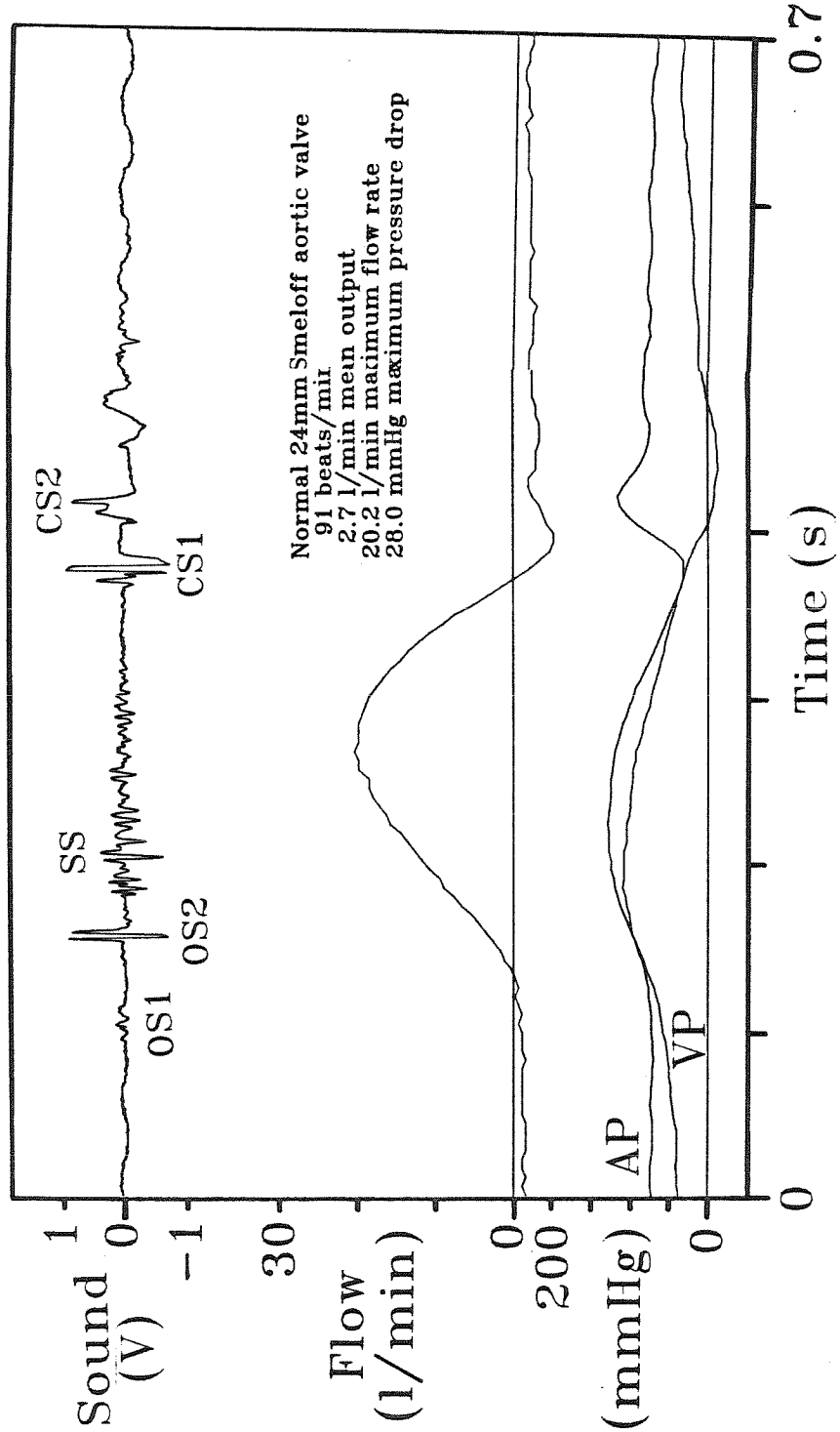

Figure 5-6a Amplitude vs. time tracings of sound, flow rate, aortic pressure and ventricular pressure associated with a typical cycle of experiment 293.

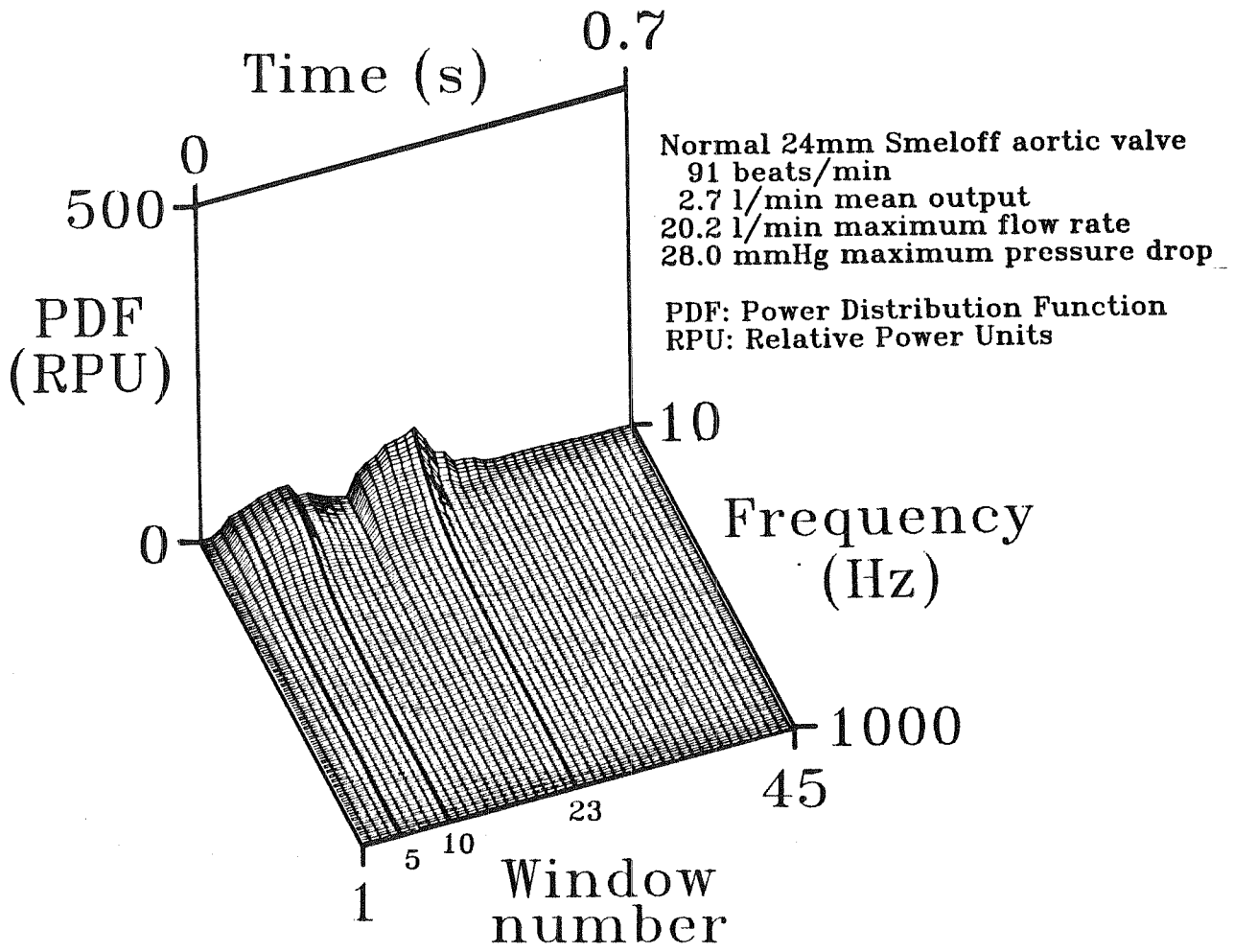

Figure 5-6b Three-dimensional power-frequency-time surface averaged over ten cycles of experiment 293.

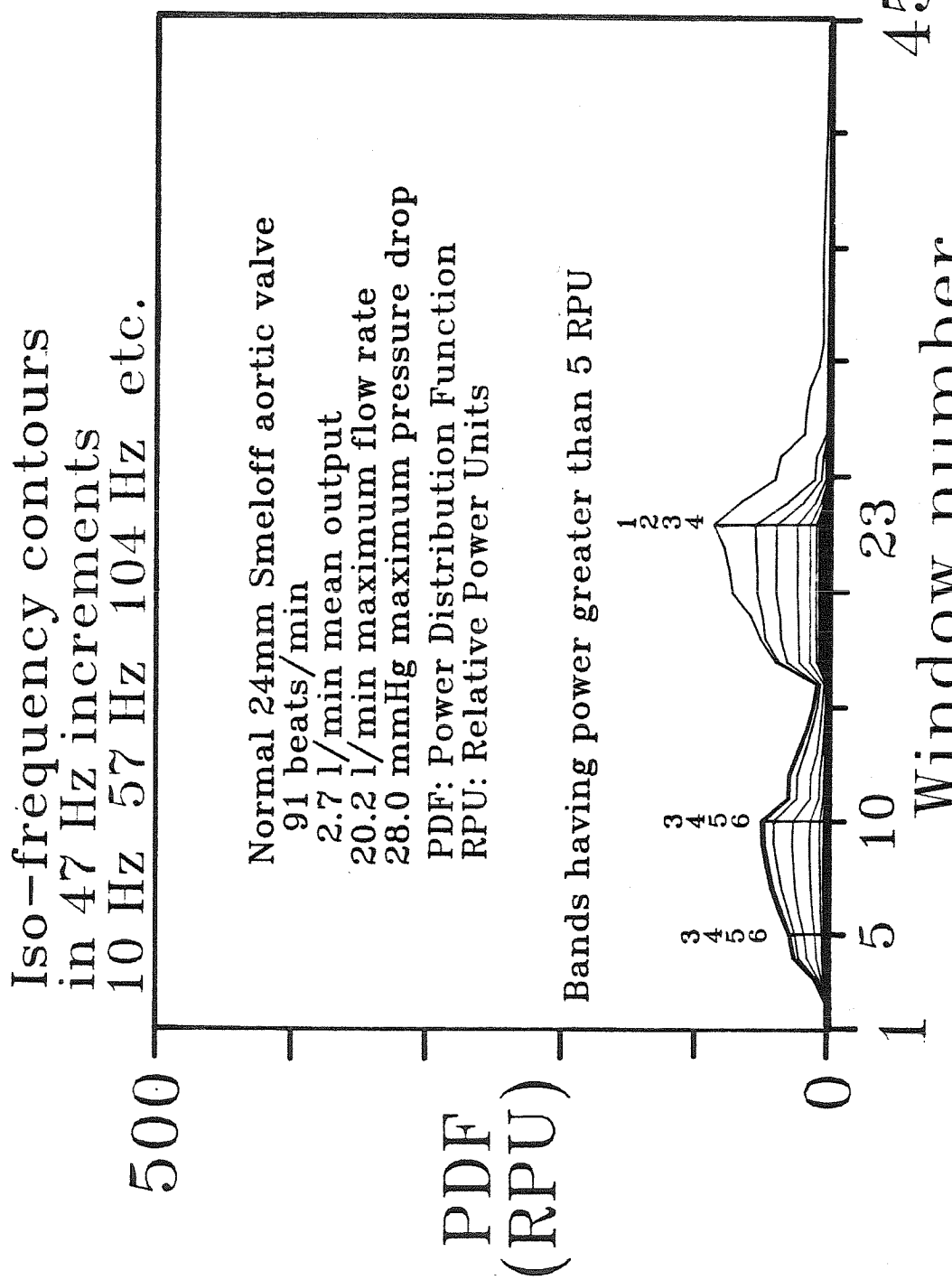

Figure 5-6c Auxiliary view perpendicular to the time axis of the 3-D power-frequency-time surface of experiment 293 showing iso-frequency contours.

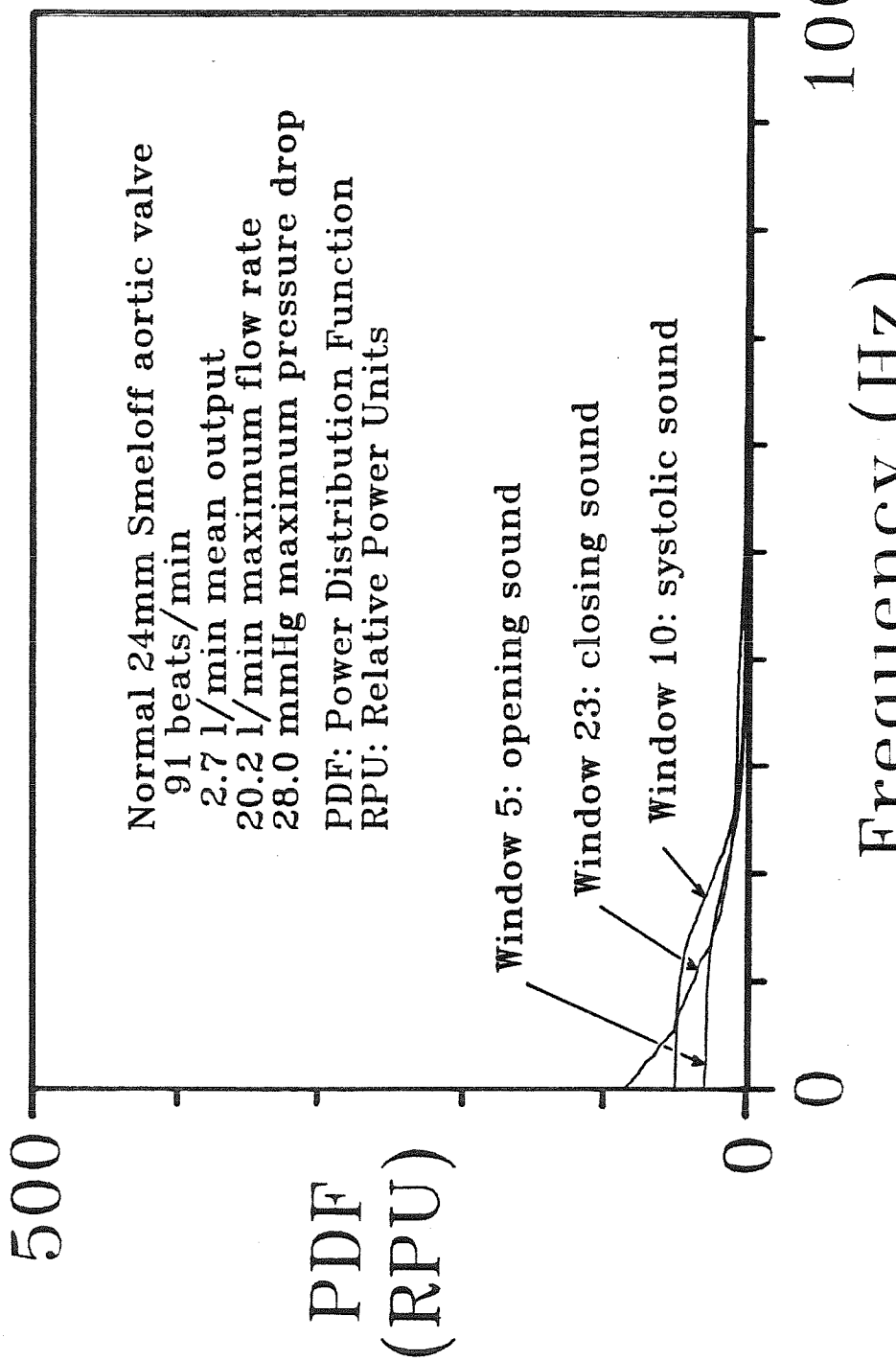

Figure 5-6d Auxiliary view perpendicular to the frequency axis of the 3-D power-frequency-time surface of experiment 293 showing power power distributions associated with windows encompassing the opening, systolic, and closing sounds.

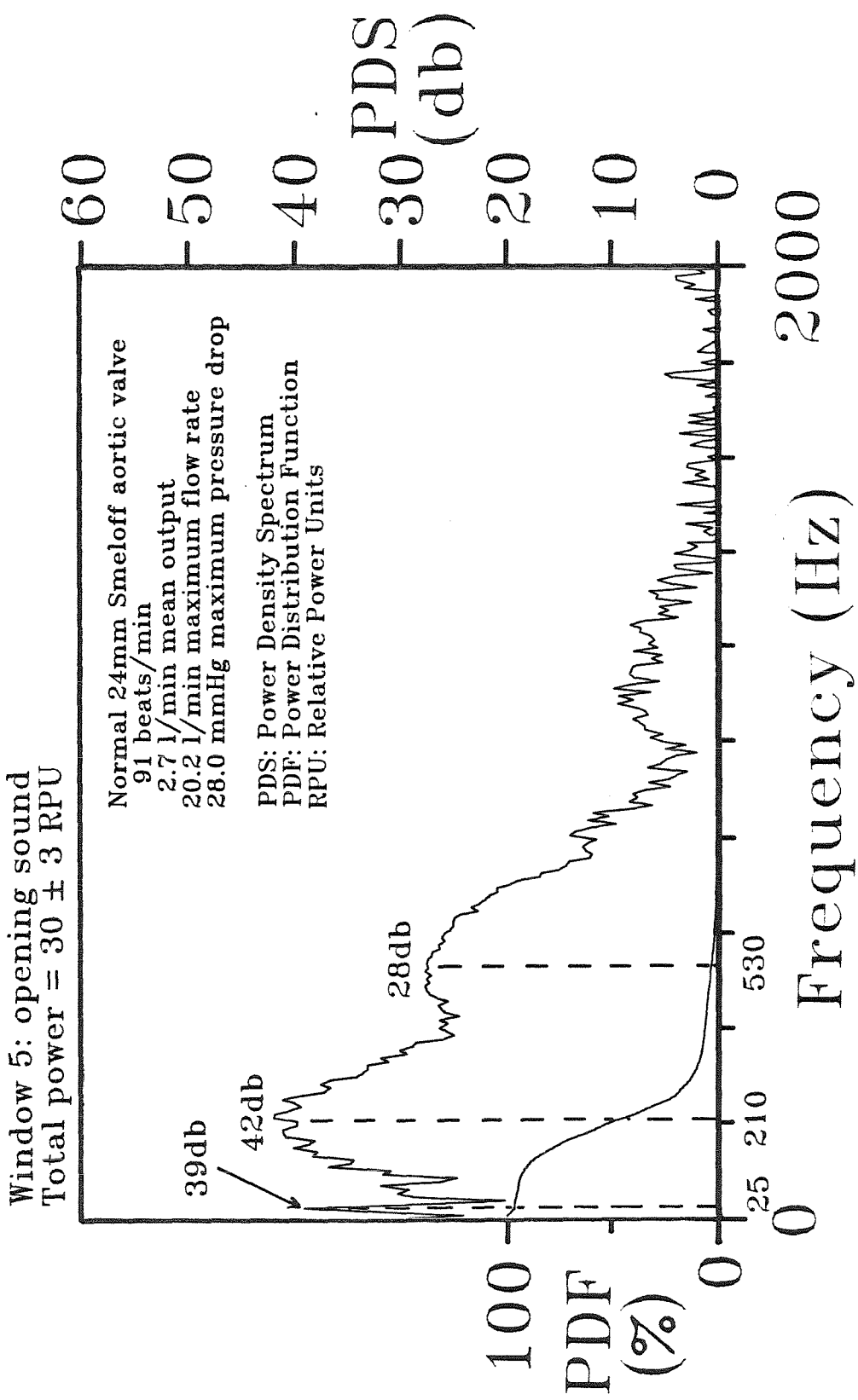

Figure 5-6e Power-density spectra and power distribution of the opening sound of experiment 393.

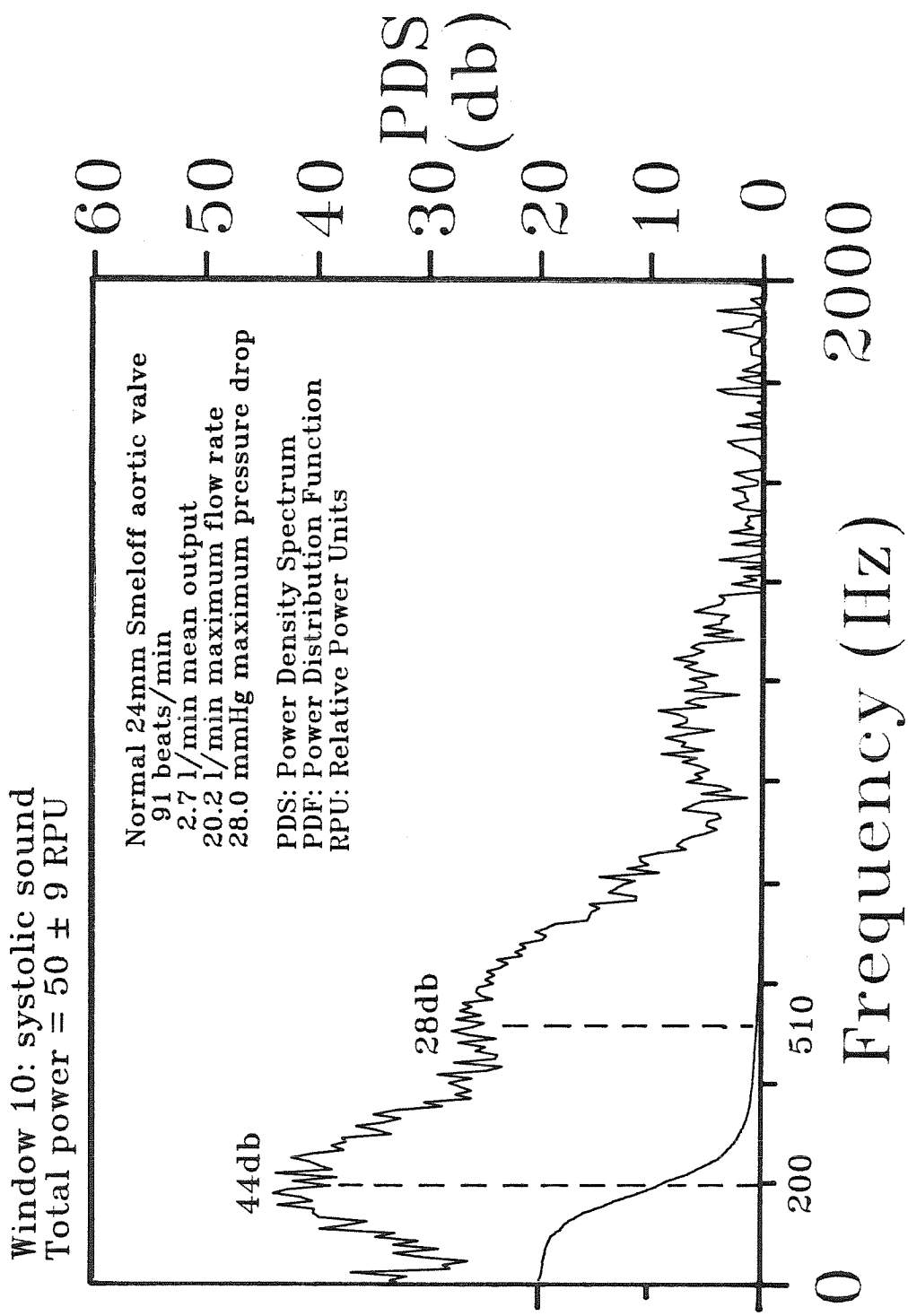

Figure 5-6f Power-density spectra and power distribution of the systolic sound of experiment 293.

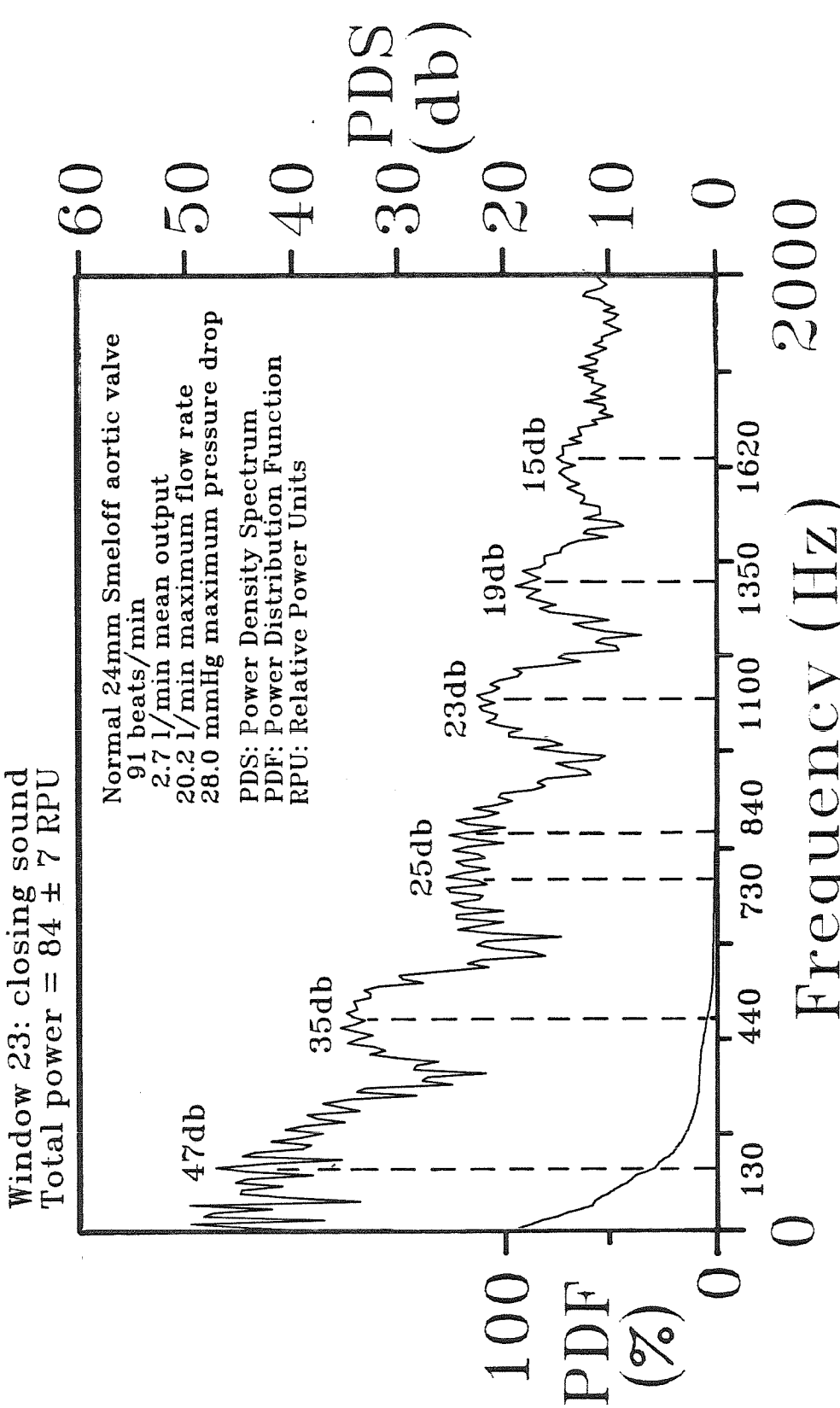

Figure 5-6g Power-density spectra and power distribution of the closing sound of experiment 293.

Parameters Estimated for

Significant Harmonic Peaks

Experiment 293

Event	Frequency, $f_{f,i}$; Decay, k_i; Power-Density, G_i (Hz,Hz,db)
Opening Sound	25, 5,39
Window 5	210, 70,42
	530,100,28
Systolic Sound	200, 70,44
Window 10	510,100,28
Closing Sound	130,40,47
	440,80,35
	730,70,25
Window 23	840,70,25
	1100,70,23
	1350,70,19
	1620,90,15

Table 5-3 Parameters estimated from significant harmonic peaks of experiment 293.

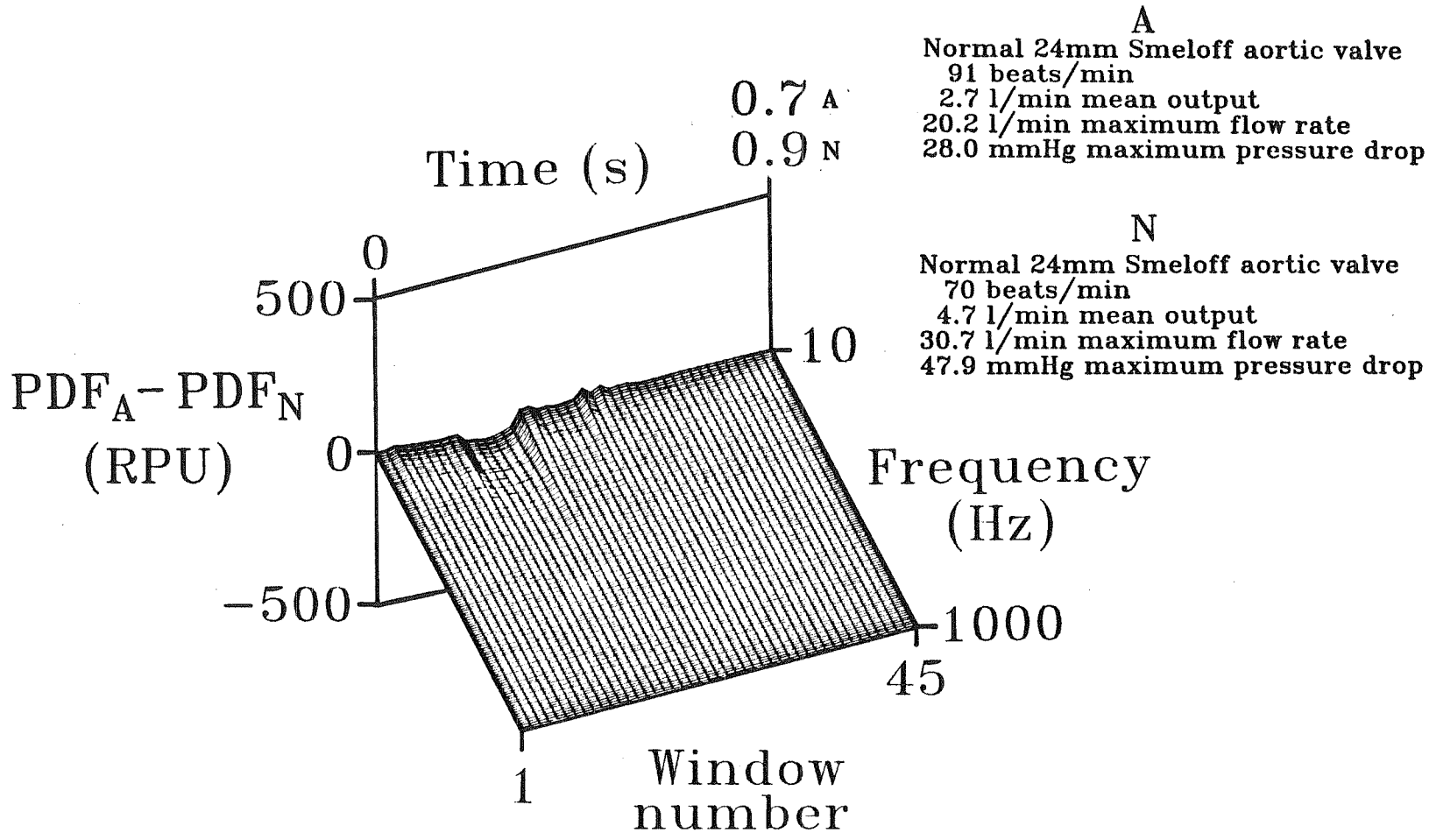

Figure 5-6h Three-dimensional surface depicting the difference between the power-frequency-time surfaces associated with experiments 293 and 292.

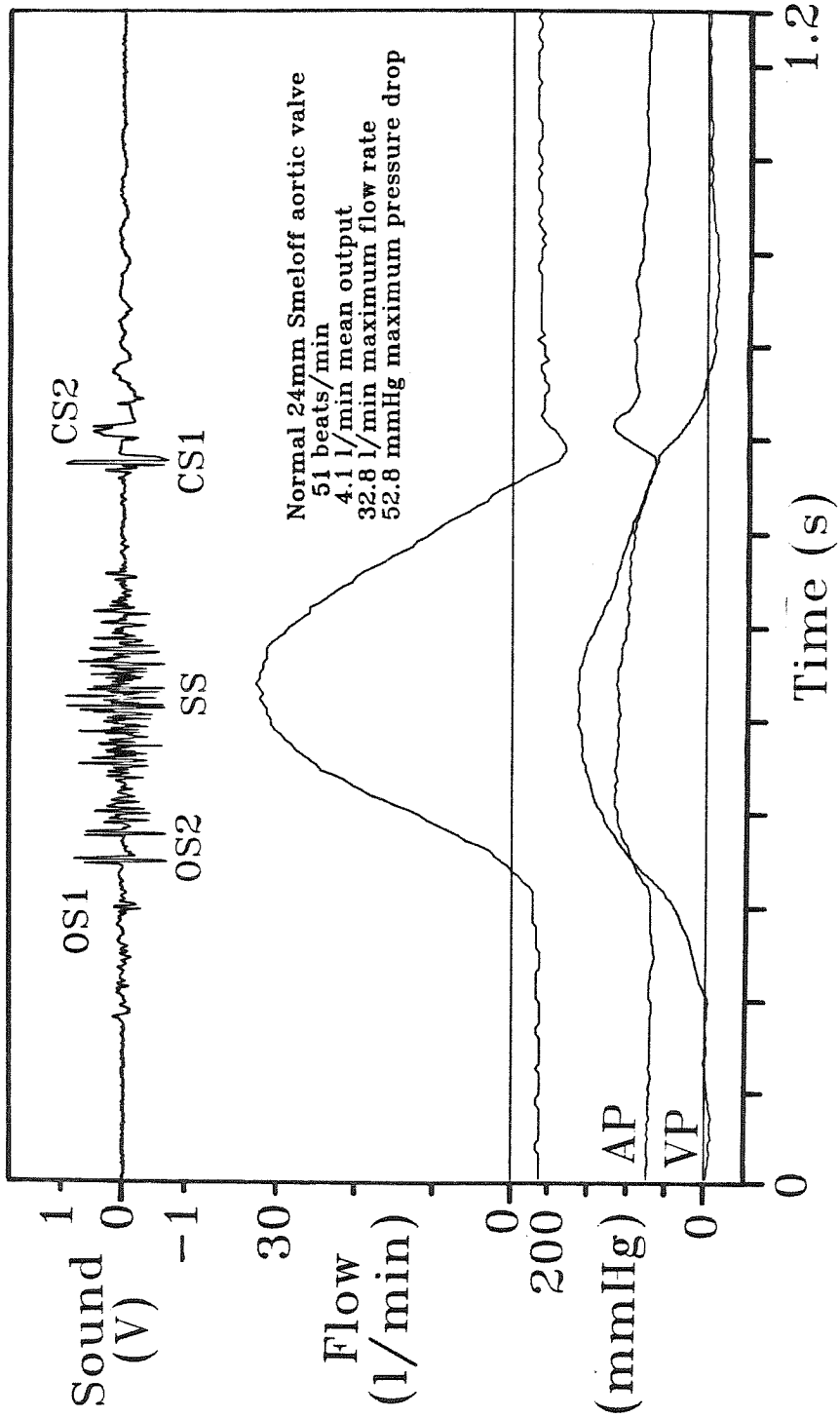

Figure 5-7a Amplitude vs. time tracings of sound, flow rate, aortic pressure and ventricular pressure associated with a typical cycle of experiment 294.

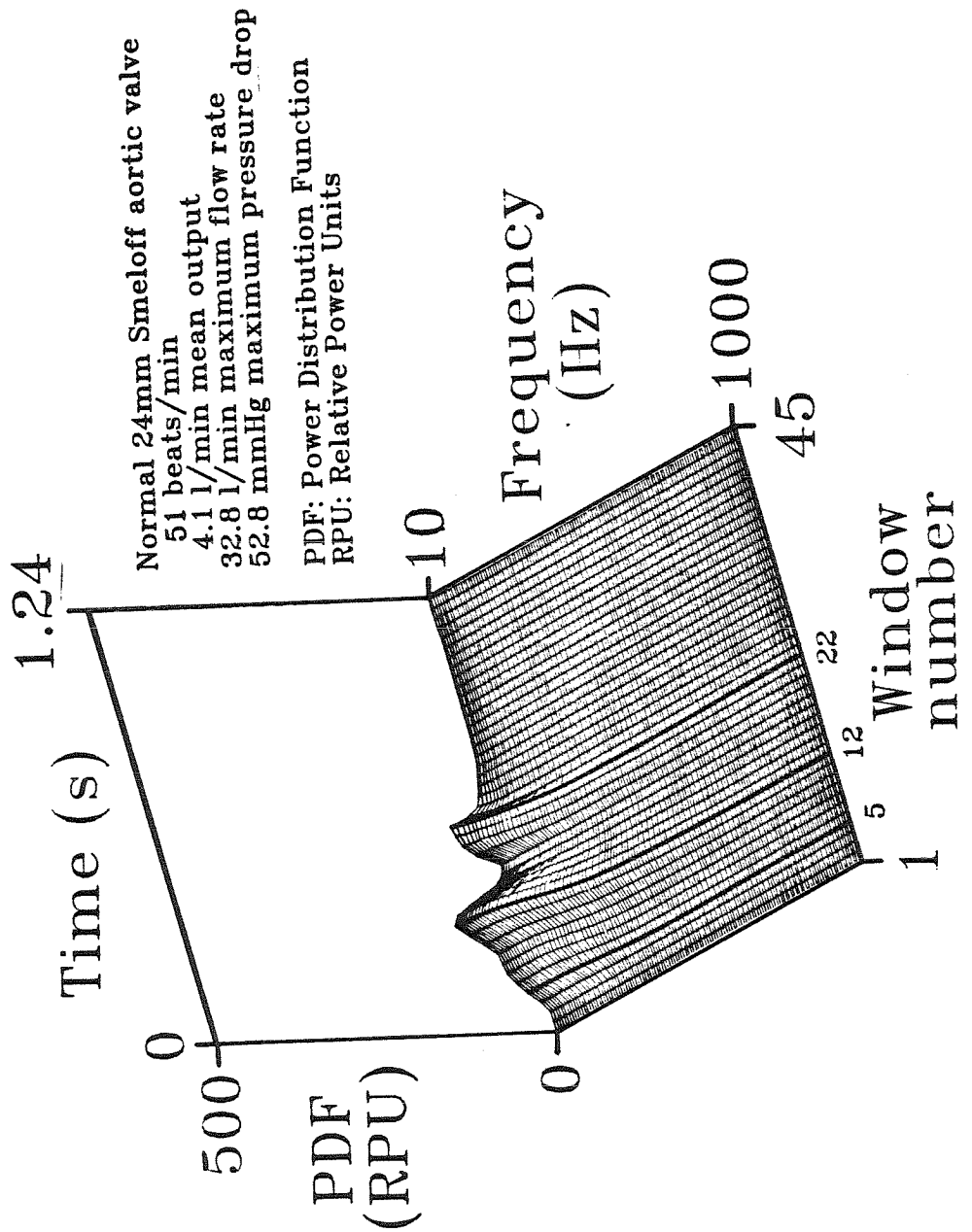

Figure 5-7b Three-dimensional power-frequency-time surface averaged over ten cycles of experiment 294.

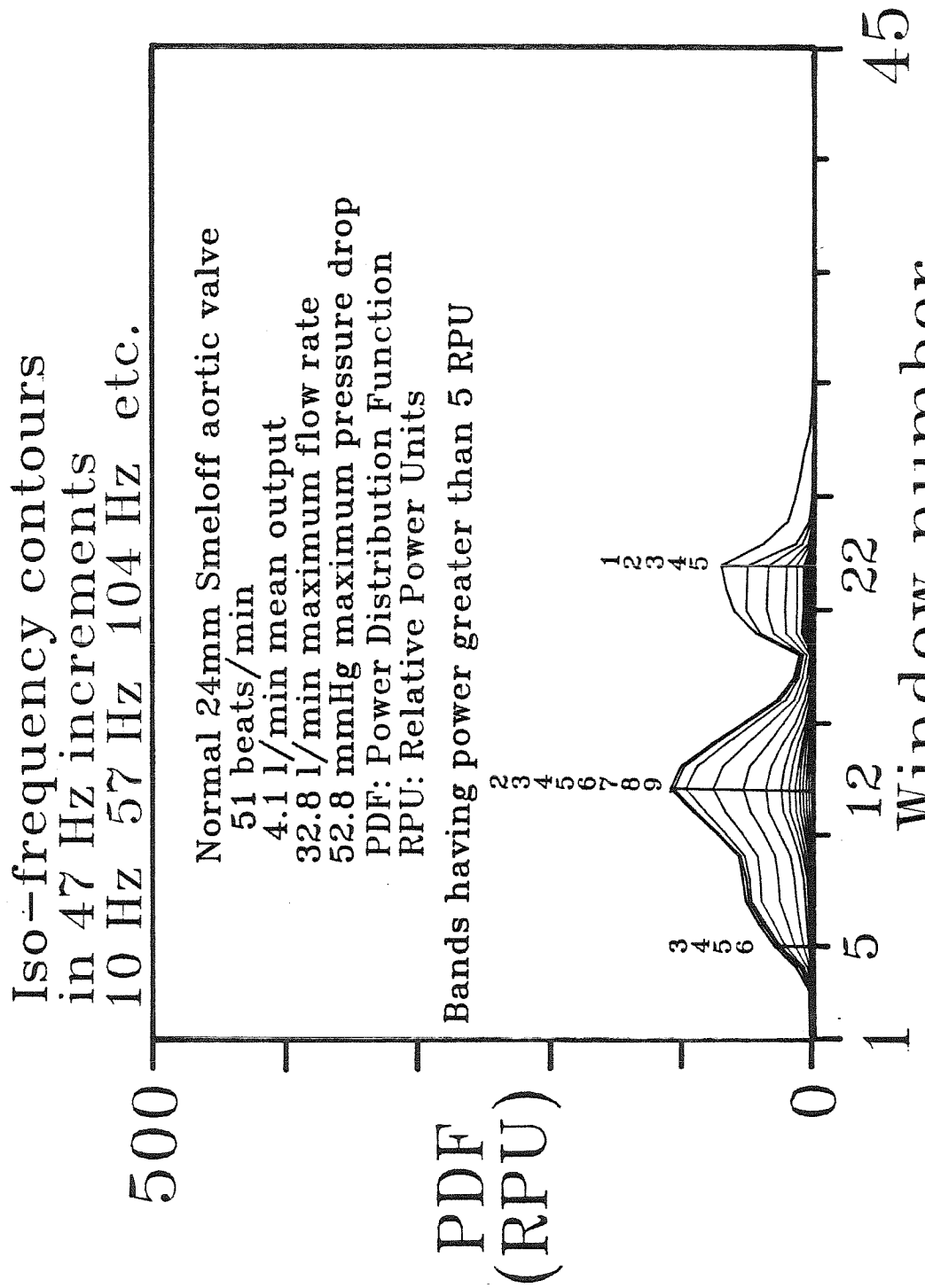

Figure 5-7c Auxiliary view perpendicular to the time axis of the 3-D power-frequency-time surface of experiment 294 showing iso-frequency contours.

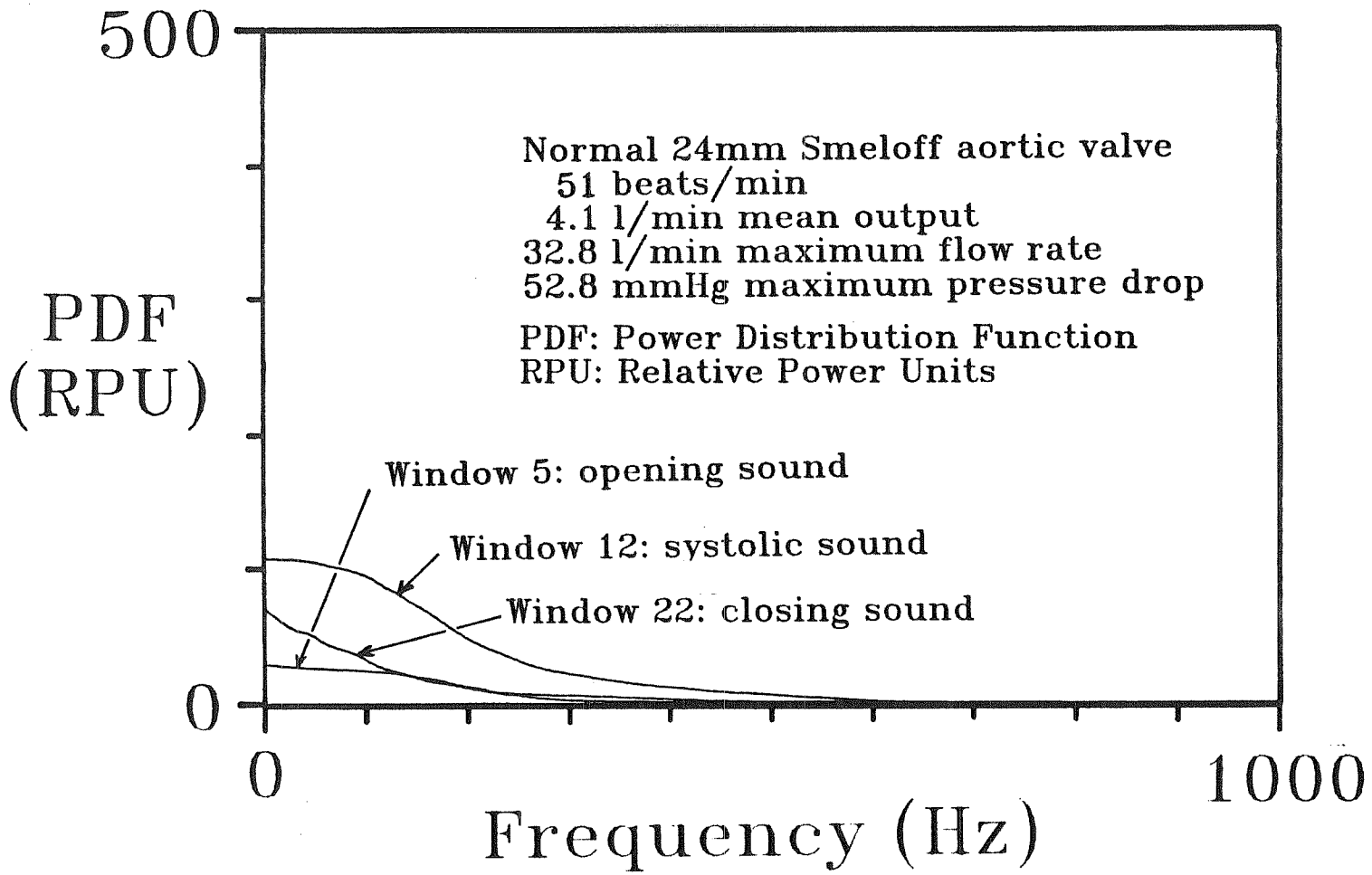

Figure 5-7d Auxiliary view perpendicular to the frequency axis of the 3-D power-frequency-time surface of experiment 294 showing power power distributions associated with windows encompassing the opening, systolic, and closing sounds.

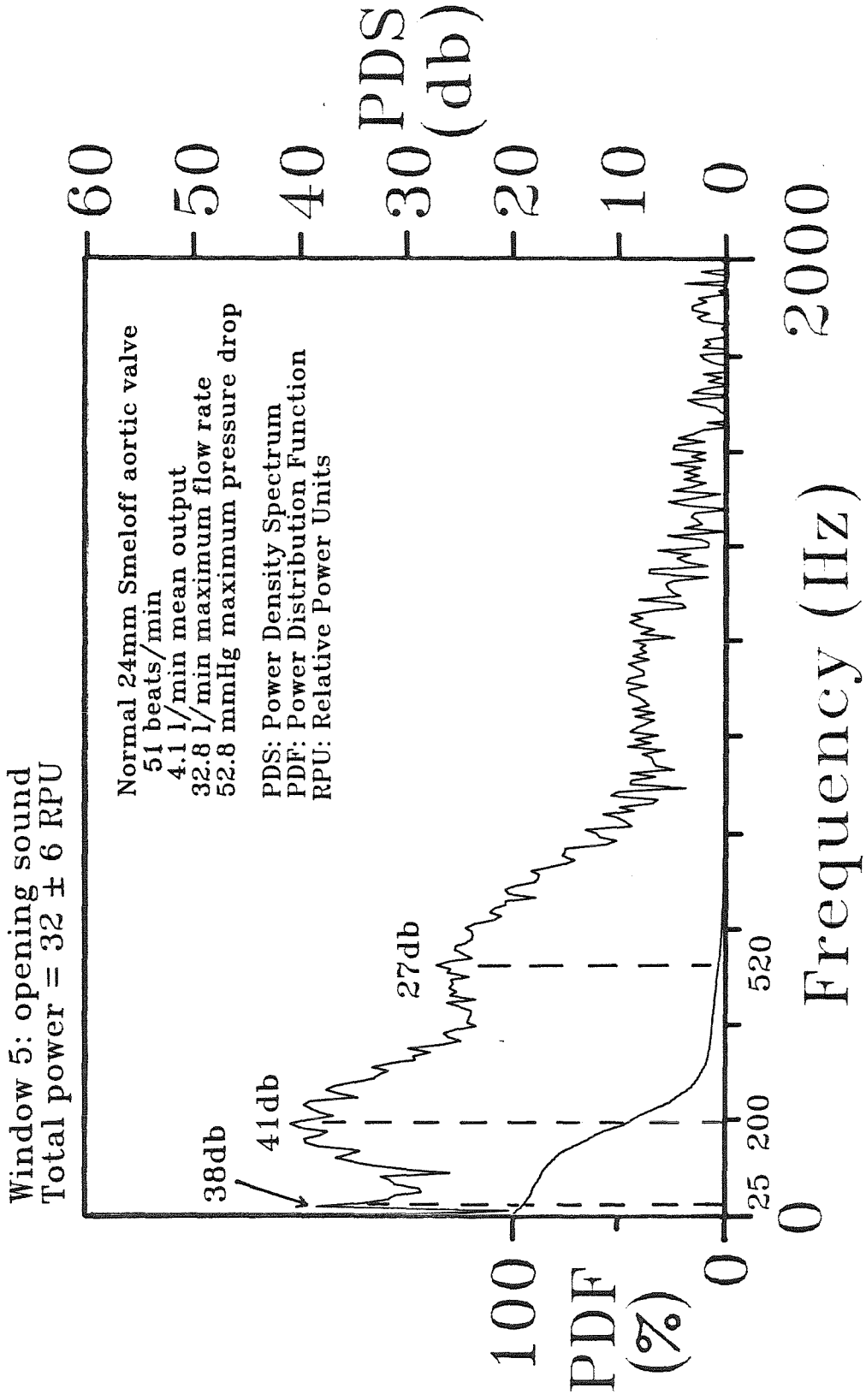

Figure 5-7e Power-density spectra and power distribution of the opening sound of experiment 294.

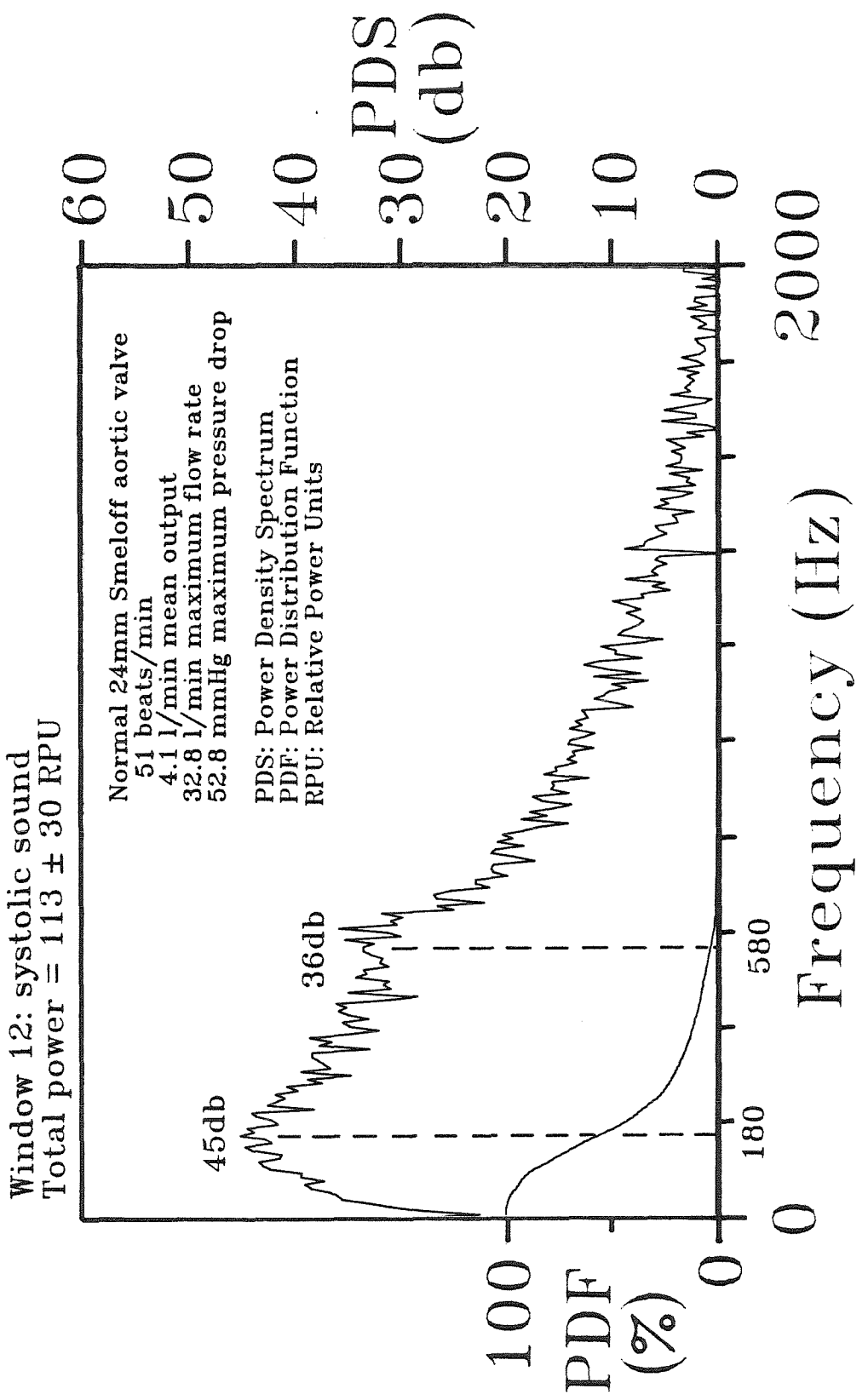

Figure 5-7f Power-density spectra and power distribution of the systolic sound of experiment 294.

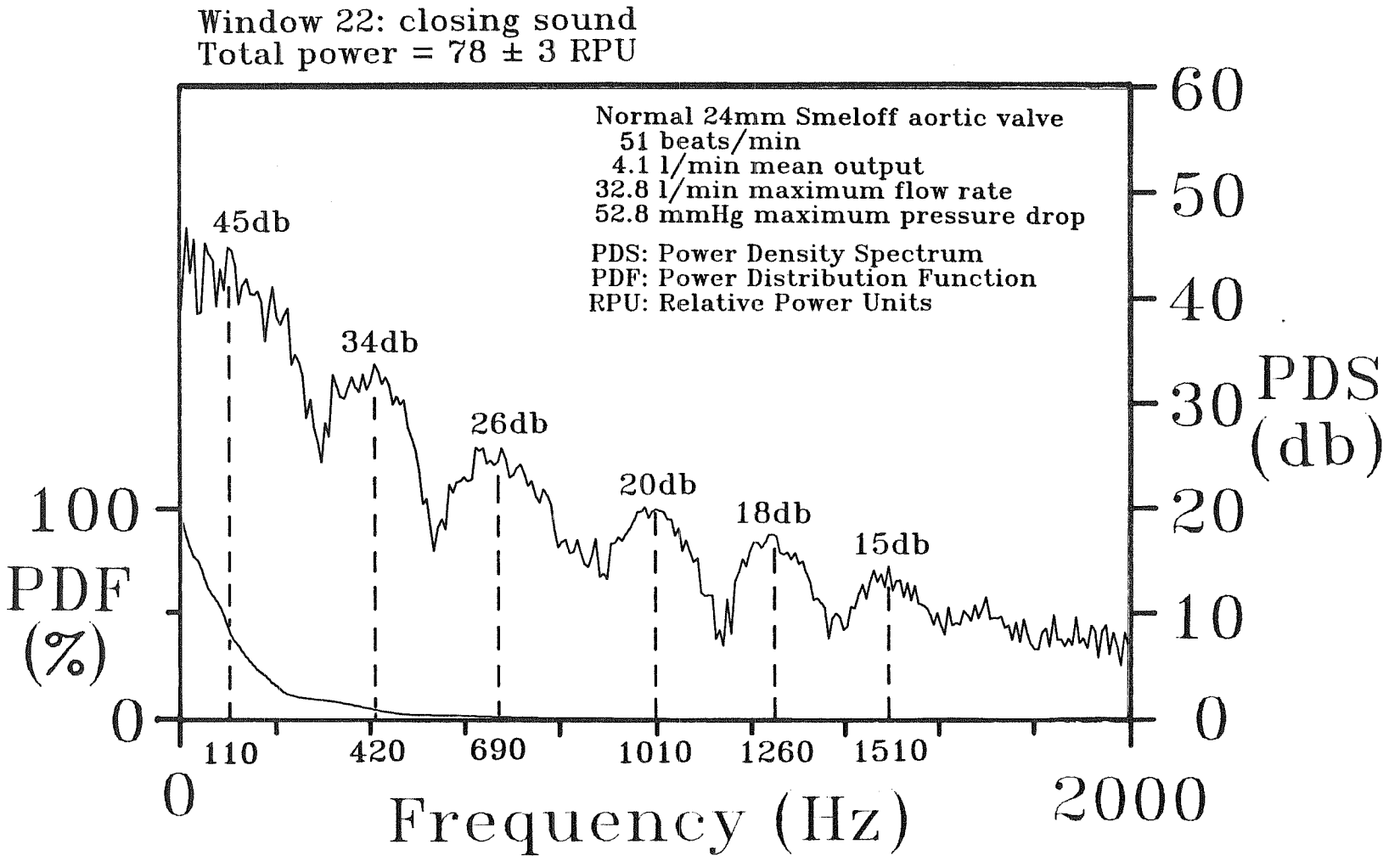

Figure 5-7g Power-density spectra and power distribution of the closing sound of experiment 294.

Parameters Estimated for

Significant Harmonic Peaks

Experiment 294

Event	Frequency, $f_{r,i}$; Decay, k_i; Power-Density, G_i (Hz,Hz,db)
Opening Sound	25, 5,38
Window 5	200,70,41
	520,80,27
Systolic Sound	180,80,45
Window 12	580,80,36
Closing Sound	110,40,45
	420,80,34
	690,90,26
Window 22	1010,80,20
	1260,80,18
	1510,80,15

Table 5-4 Parameters estimated from significant harmonic peaks of experiment 294.

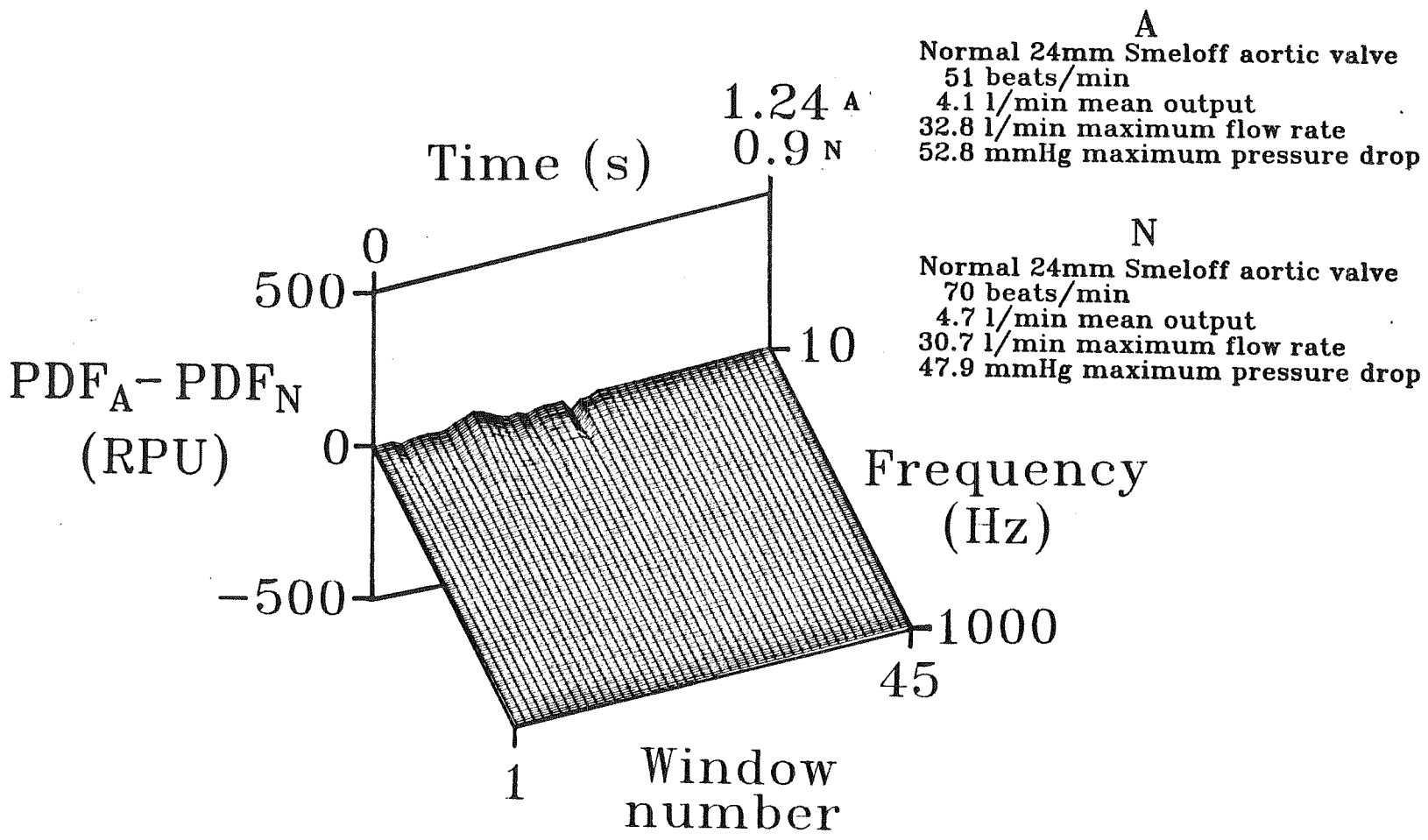

Figure 5-7h Three-dimensional surface depicting the difference between the power-frequency-time surfaces associated with experiments 294 and 292.

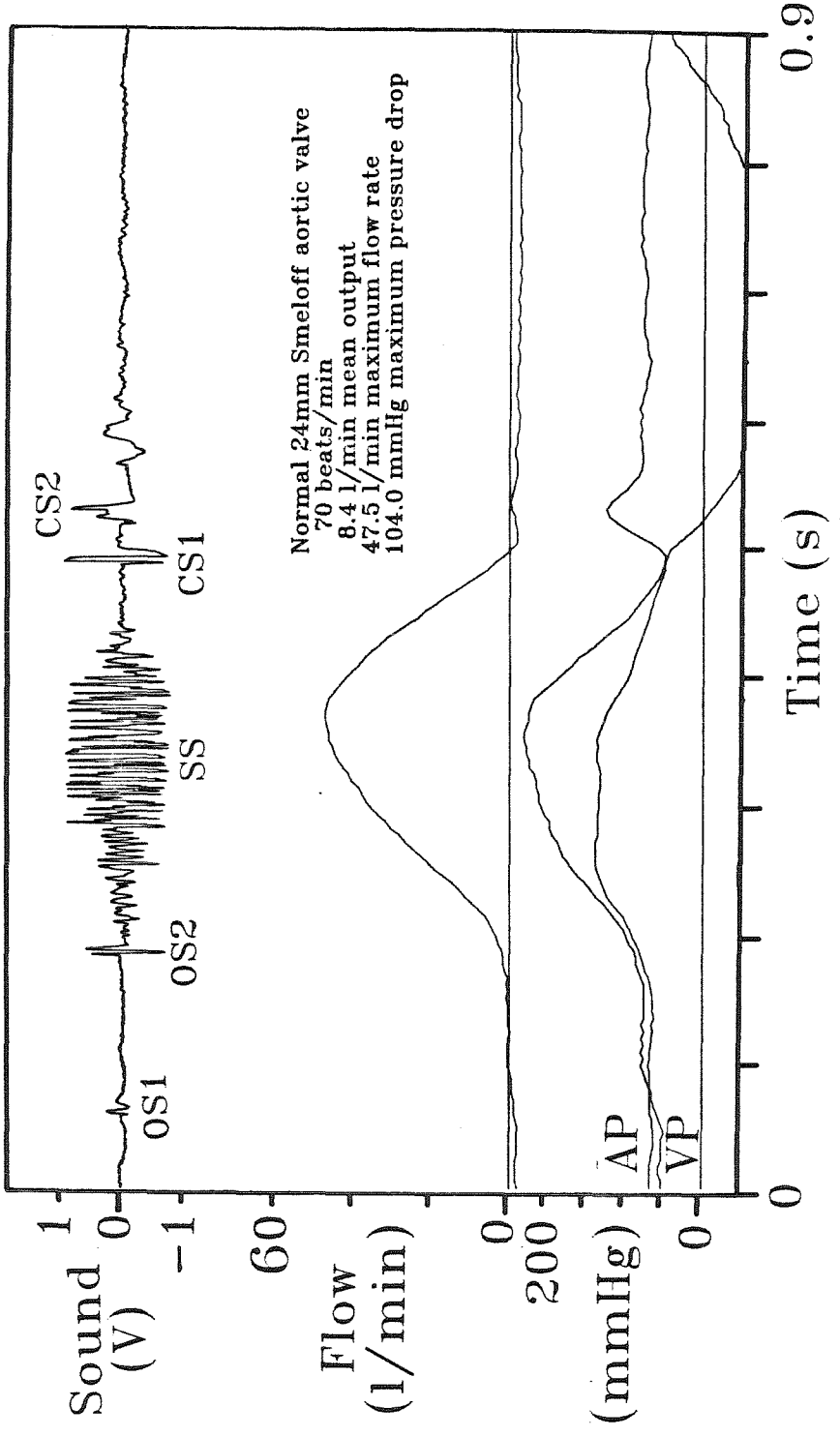

Figure 5-8a Amplitude vs. time tracings of sound, flow rate, aortic pressure and ventricular pressure associated with a typical cycle of experiment 295.

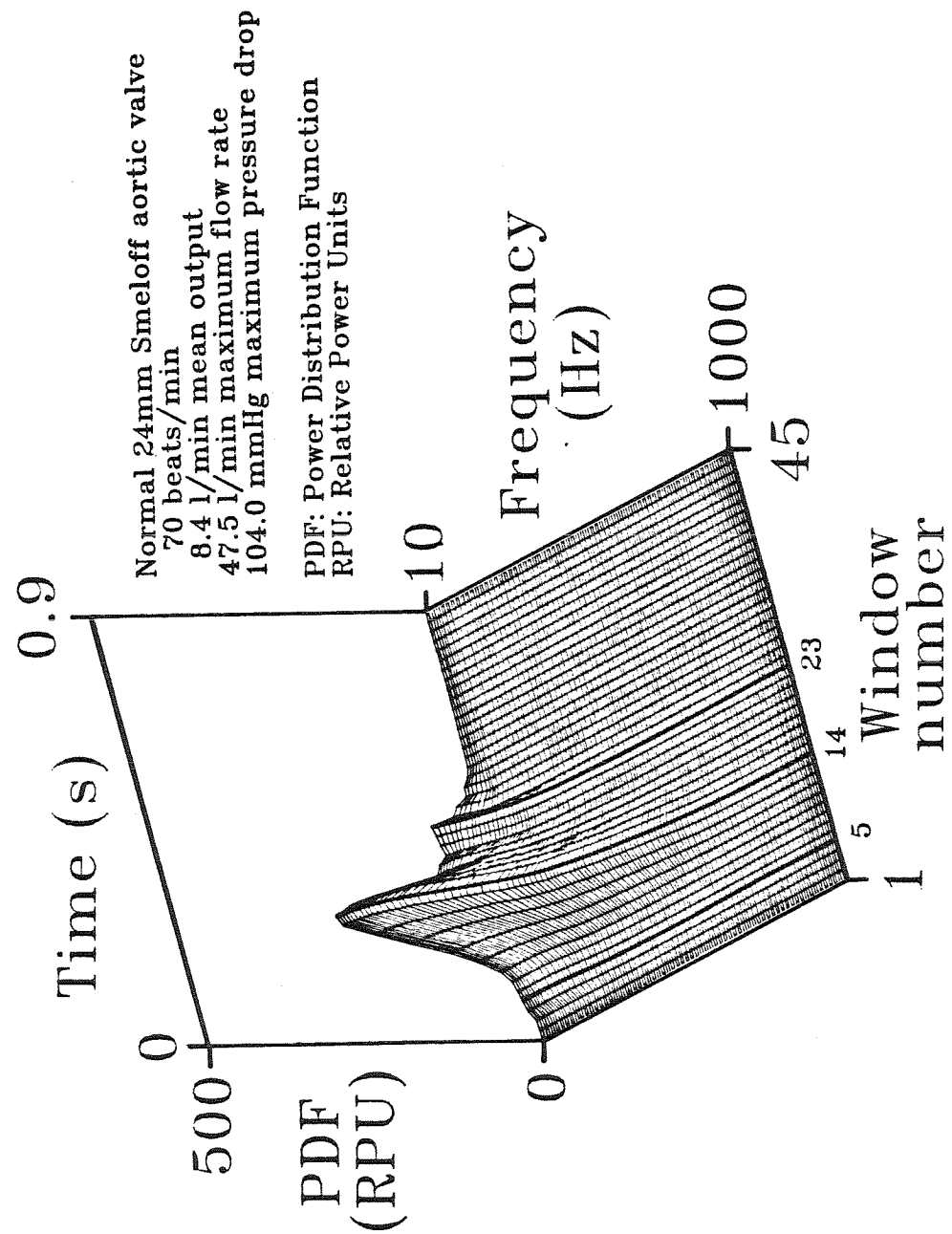

Figure 5-8b Three-dimensional power-frequency-time surface averaged over ten cycles of experiment 295.

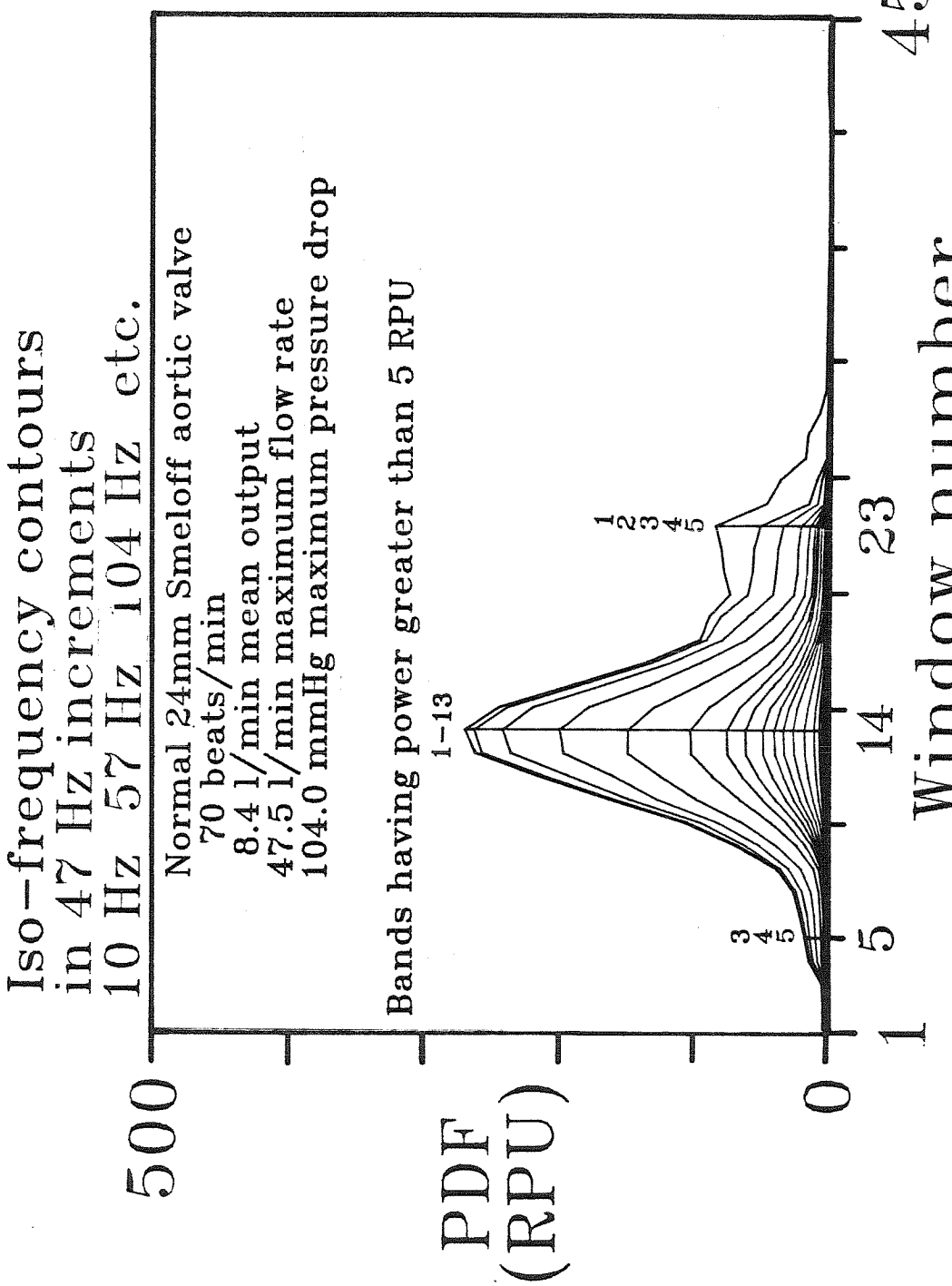

Figure 5-8c Auxiliary view perpendicular to the time axis of the 3-D power-frequency-time surface of experiment 295 showing iso-frequency contours.

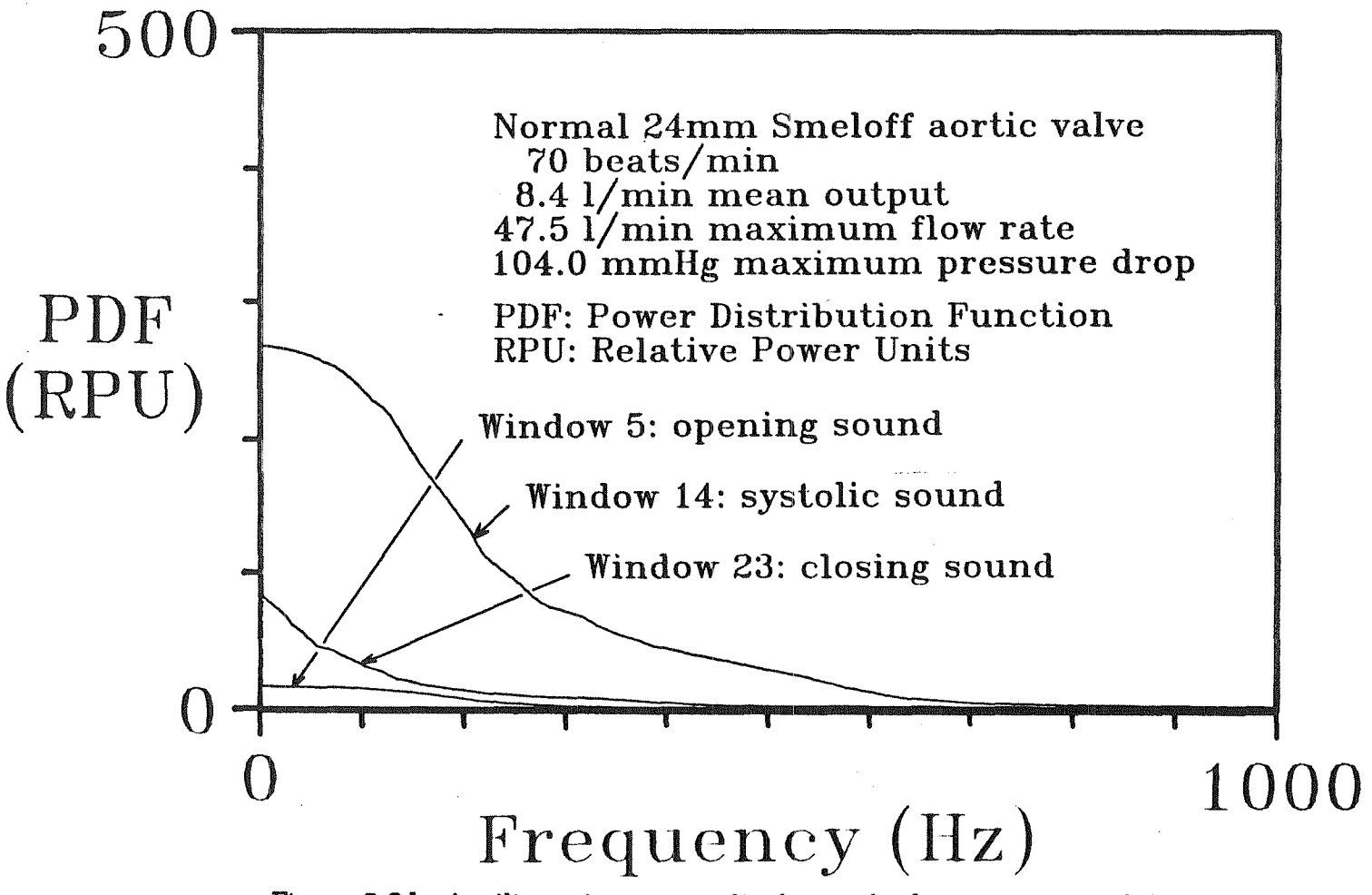

Figure 5-8d Auxiliary view perpendicular to the frequency axis of the 3-D power-frequency-time surface of experiment 295 showing power power distributions associated with windows encompassing the opening, systolic, and closing sounds.

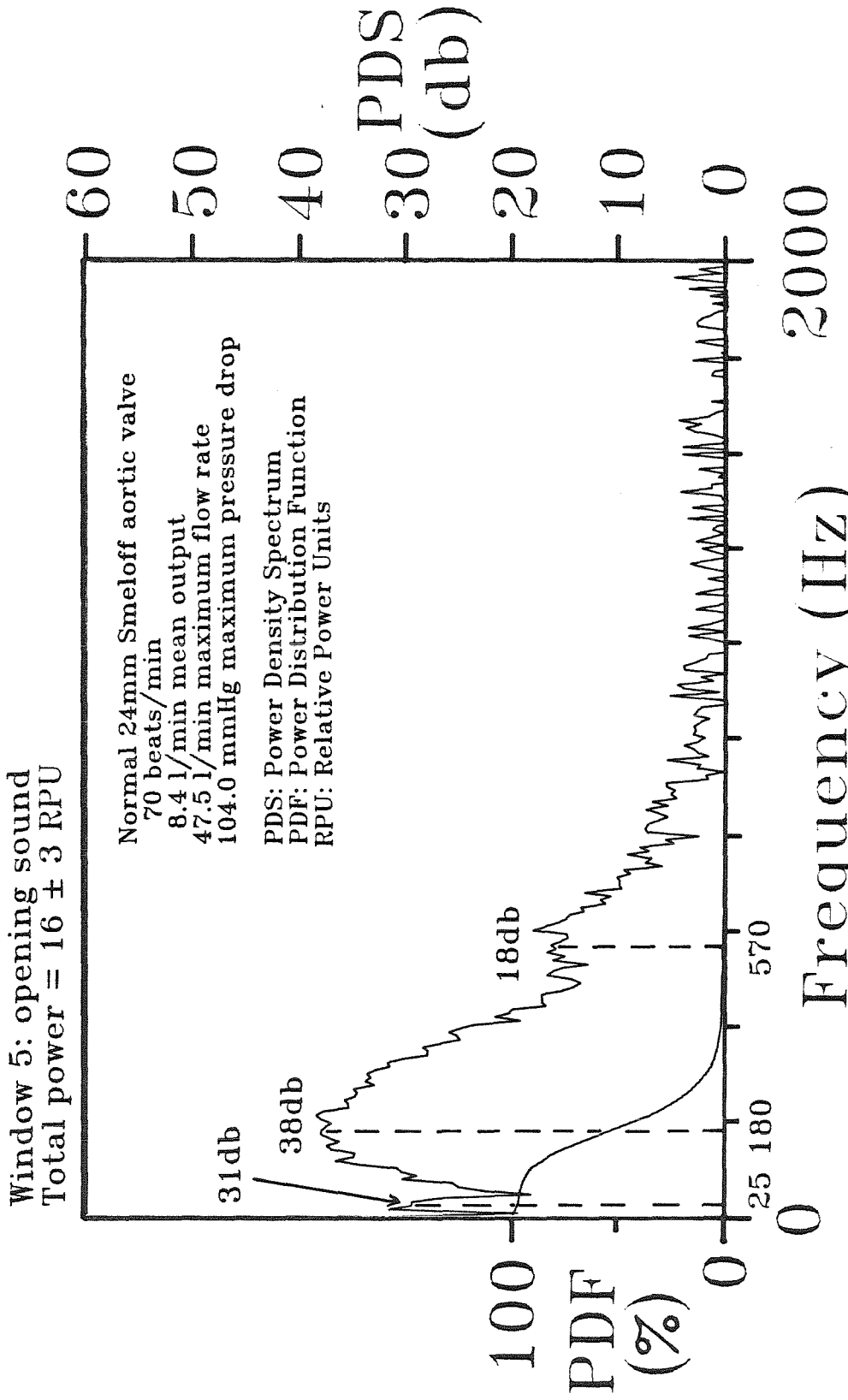

Figure 5-8e Power-density spectra and power distribution of the opening sound of experiment 295.

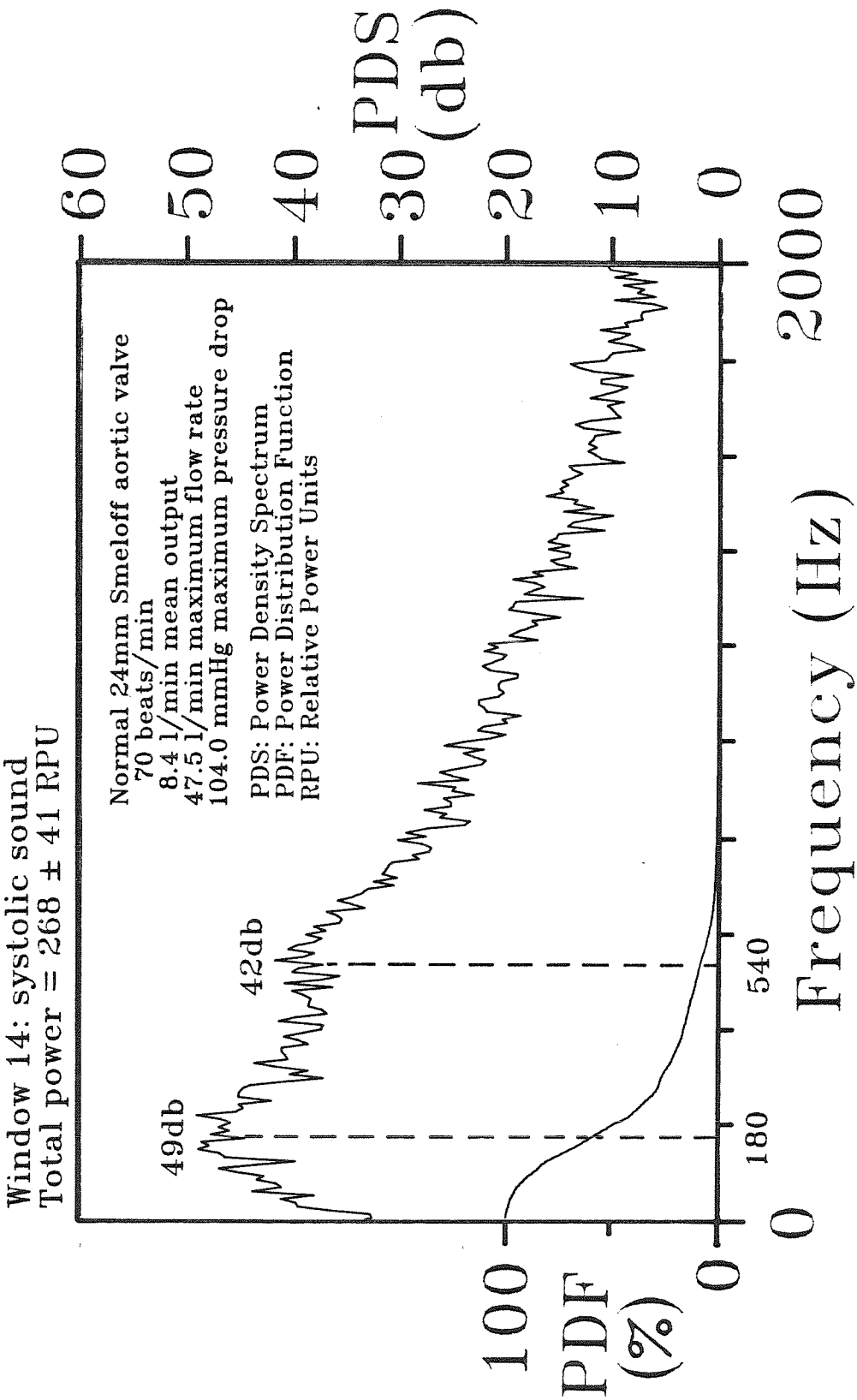

Figure 5-8f Power-density spectra and power distribution of the systolic sound of experiment 295.

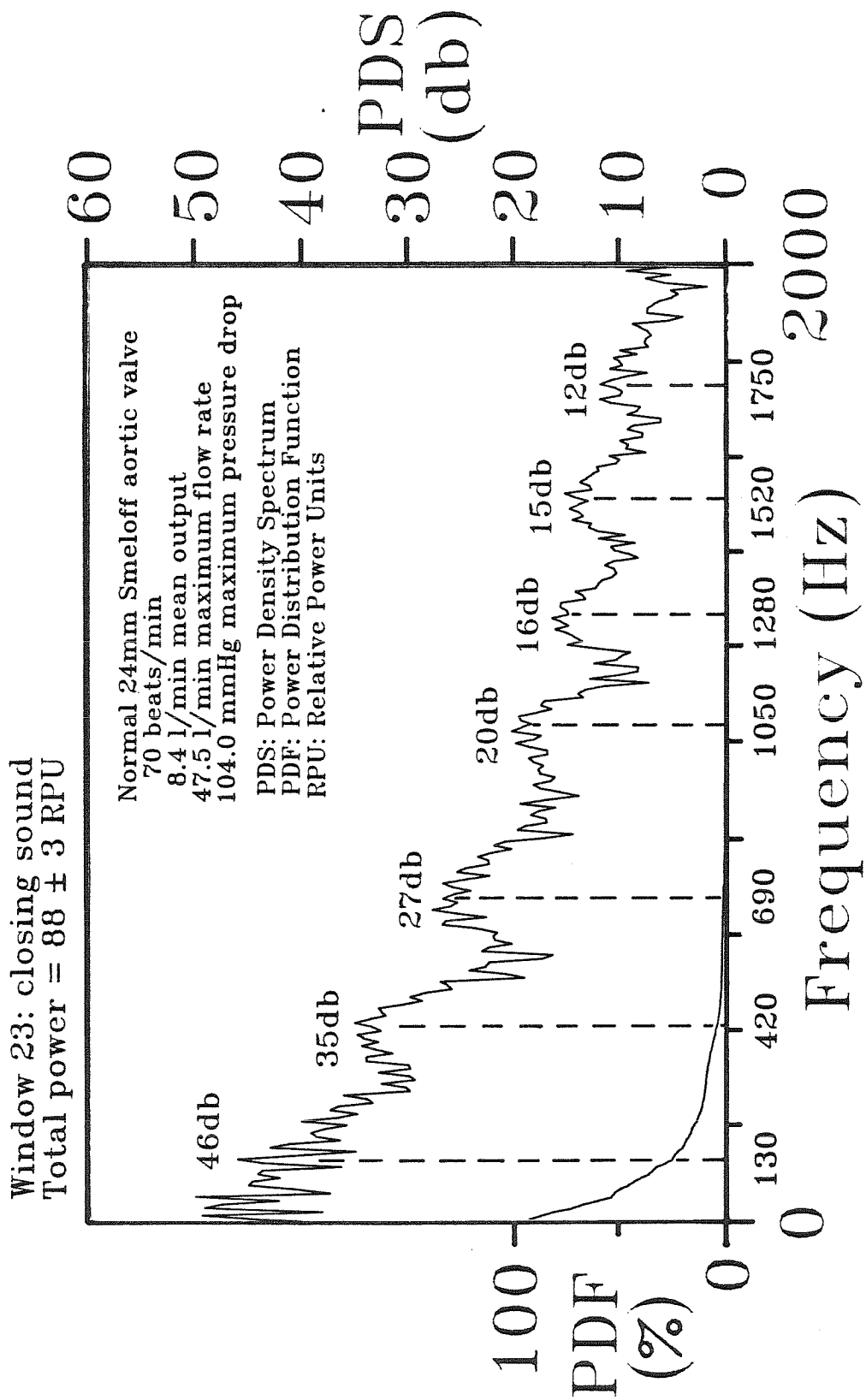

Figure 5-8g Power-density spectra and power distribution of the closing sound of experiment 295.

Parameters Estimated for

Significant Harmonic Peaks

Experiment 295

Event	Frequency, $f_{f,i}$; Decay, k_i; Power-Density, G_i (Hz,Hz,db)
Opening Sound	25,10,31
Window 5	180,70,38
	570,70,18
Systolic Sound	180,80,49
Window 14	540,90,42
Closing Sound	130,40,46
	420,70,35
	690,90,27
Window 23	1050,80,20
	1280,70,16
	1520,80,15
	1750,90,12

Table 5-5 Parameters estimated from significant harmonic peaks of experiment 294.

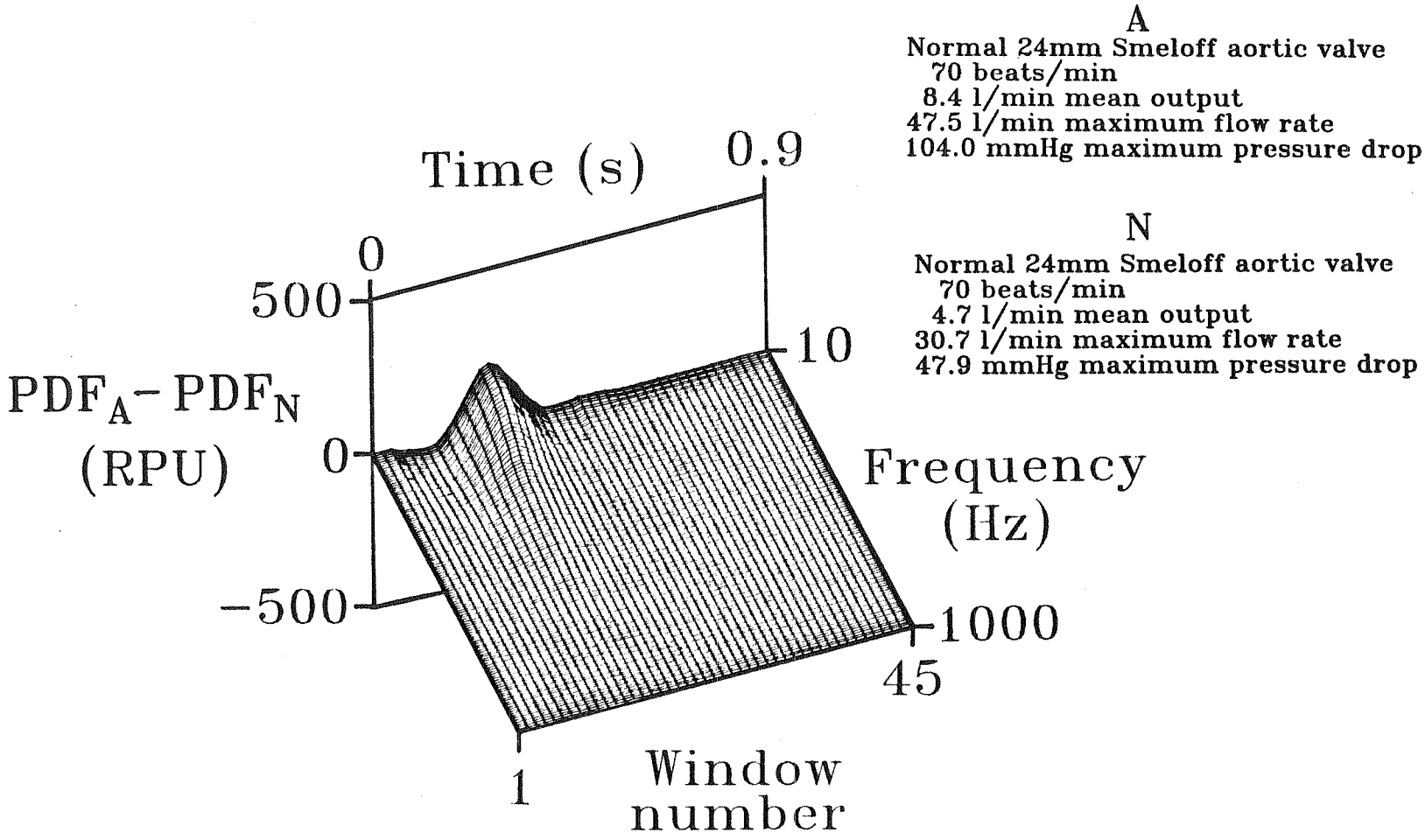

Figure 5-8h Three-dimensional surface depicting the difference between the power-frequency-time surfaces associated with experiments 295 and 292.

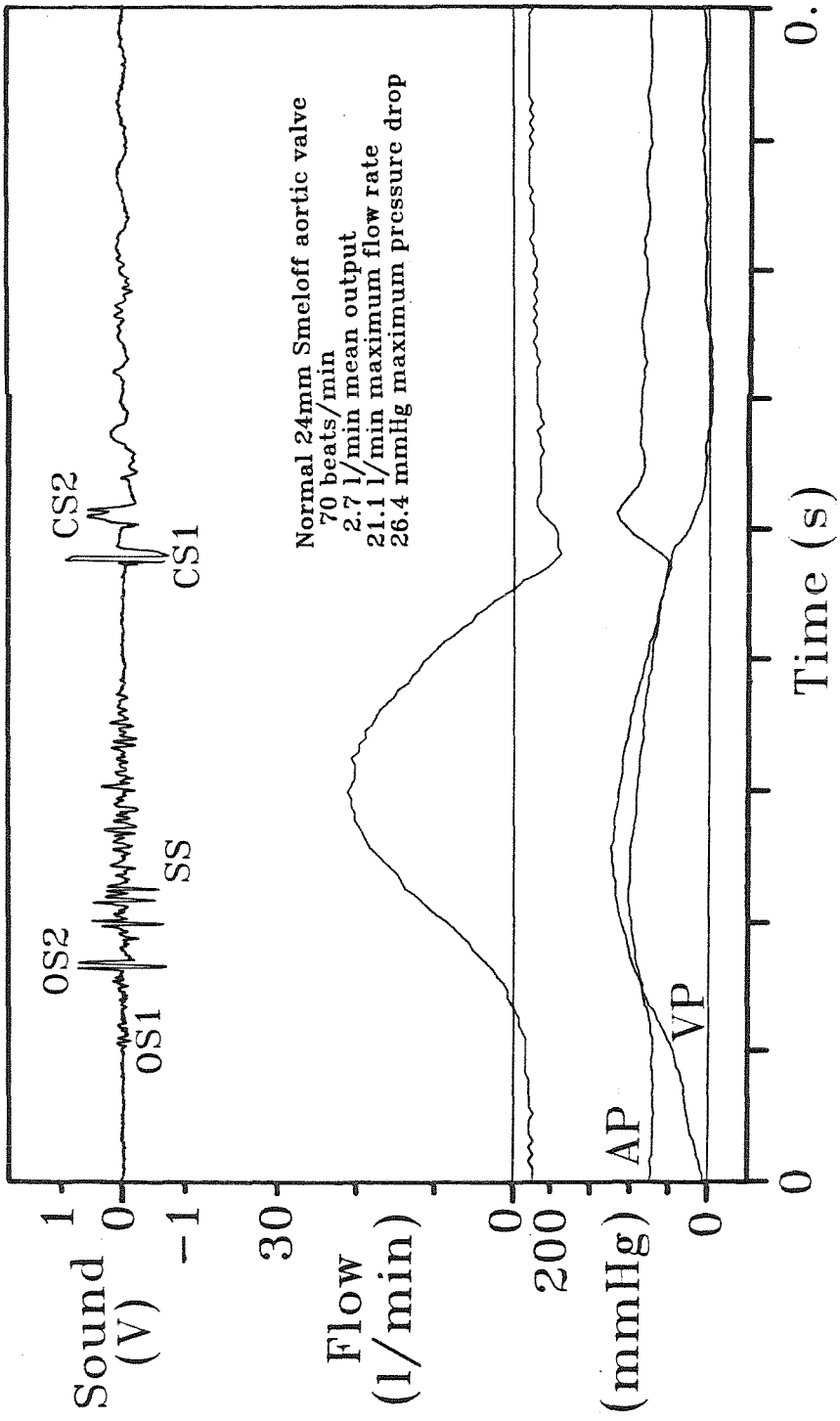

Figure 5-9a Amplitude vs. time tracings of sound, flow rate, aortic pressure and ventricular pressure associated with a typical cycle of experiment 296.

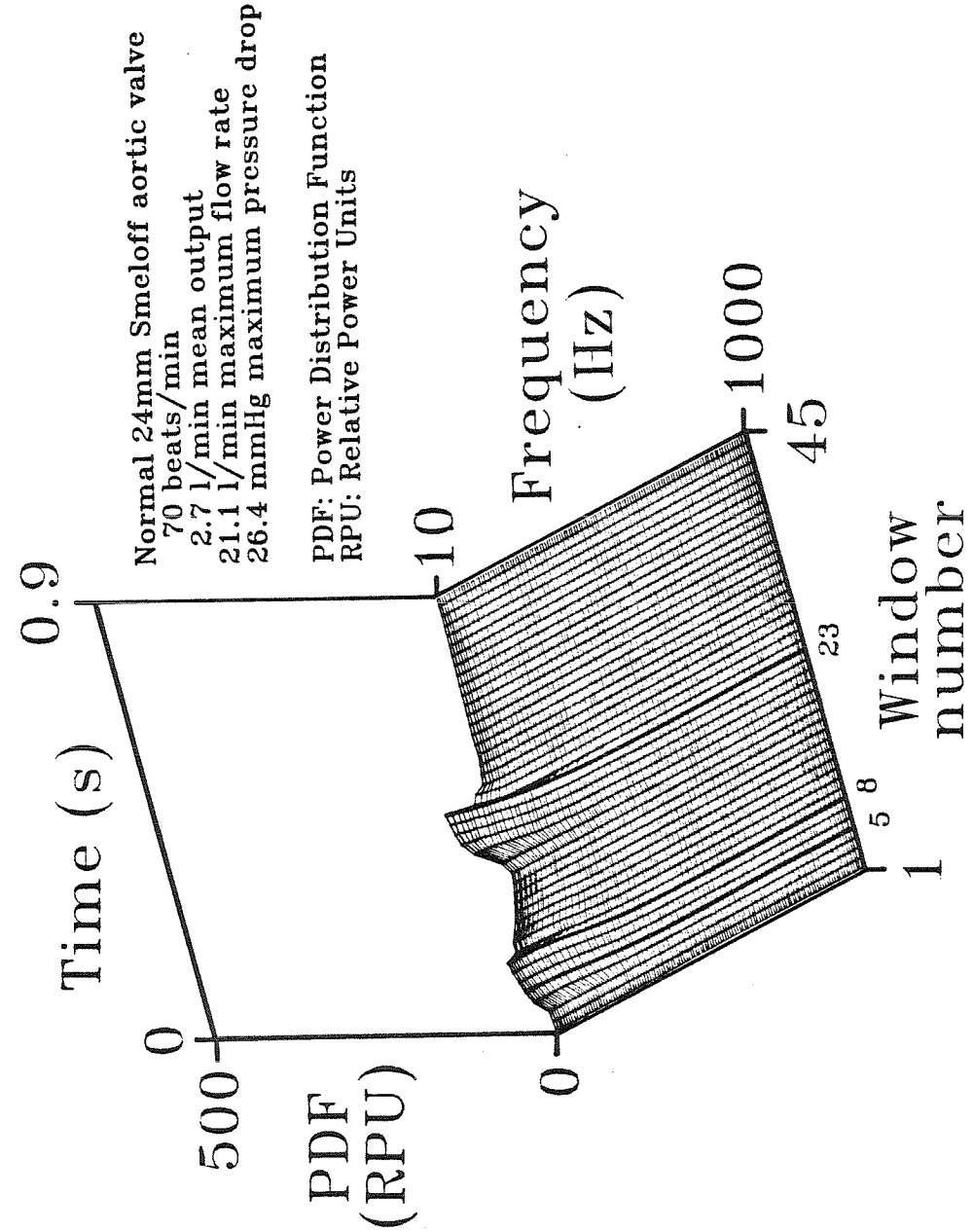

Figure 5-9b Three-dimensional power-frequency-time surface averaged over ten cycles of experiment 296.

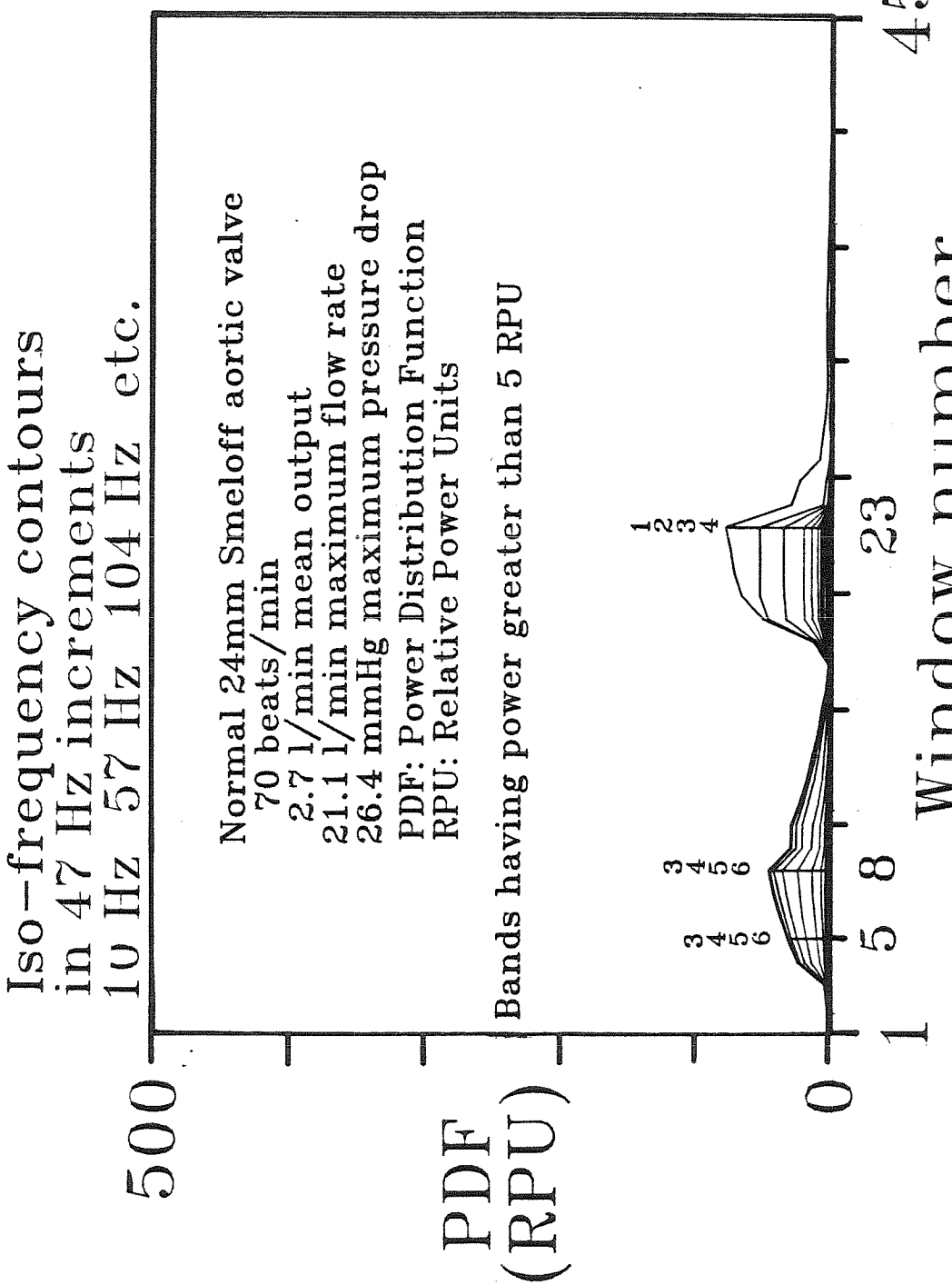

Figure 5-9c Auxiliary view perpendicular to the time axis of the 3-D power-frequency-time surface of experiment 296 showing iso-frequency contours.

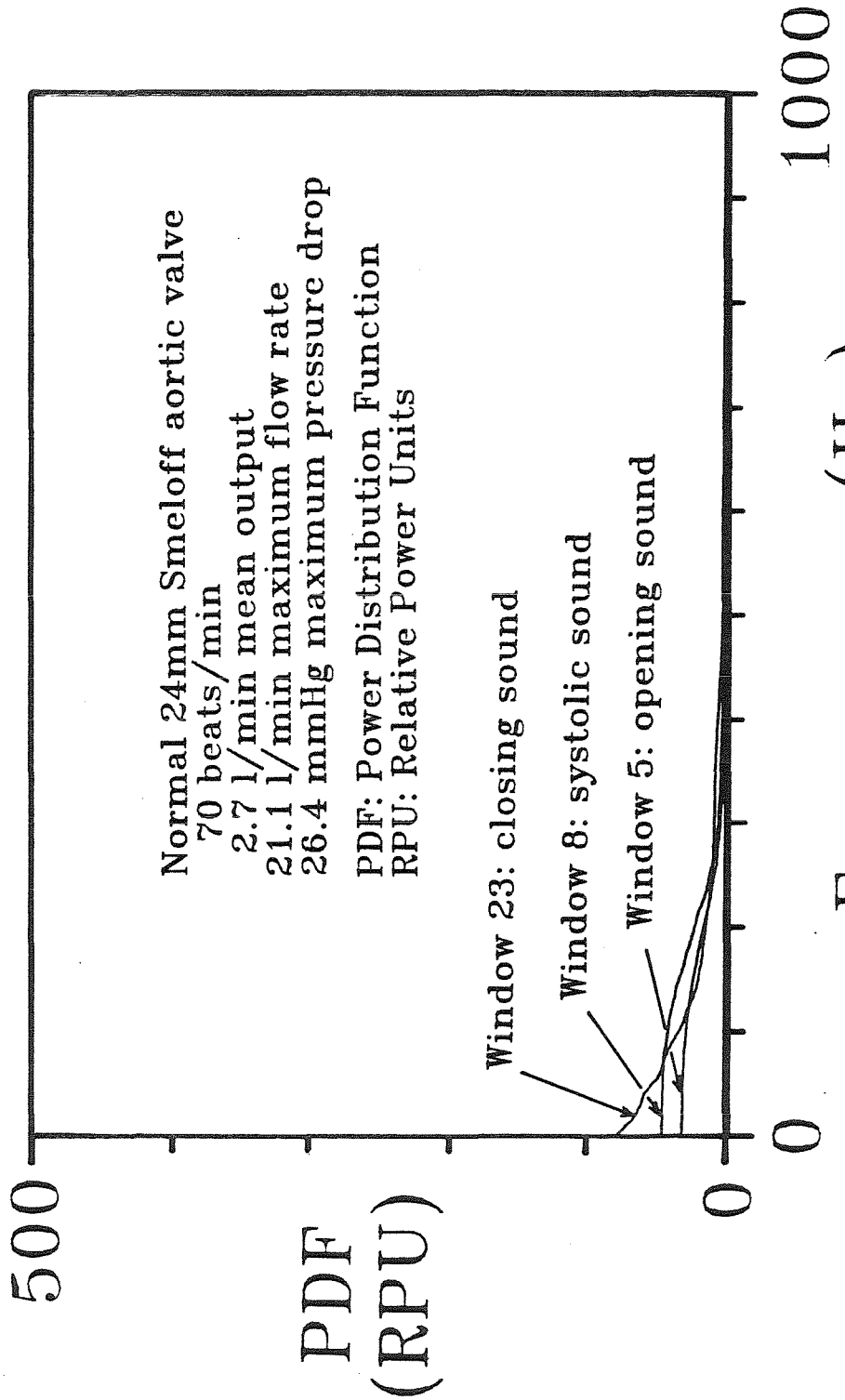

Figure 5-9d Auxiliary view perpendicular to the frequency axis of the 3-D power-frequency-time surface of experiment 296 showing power power distributions associated with windows encompassing the opening, systolic, and closing sounds.

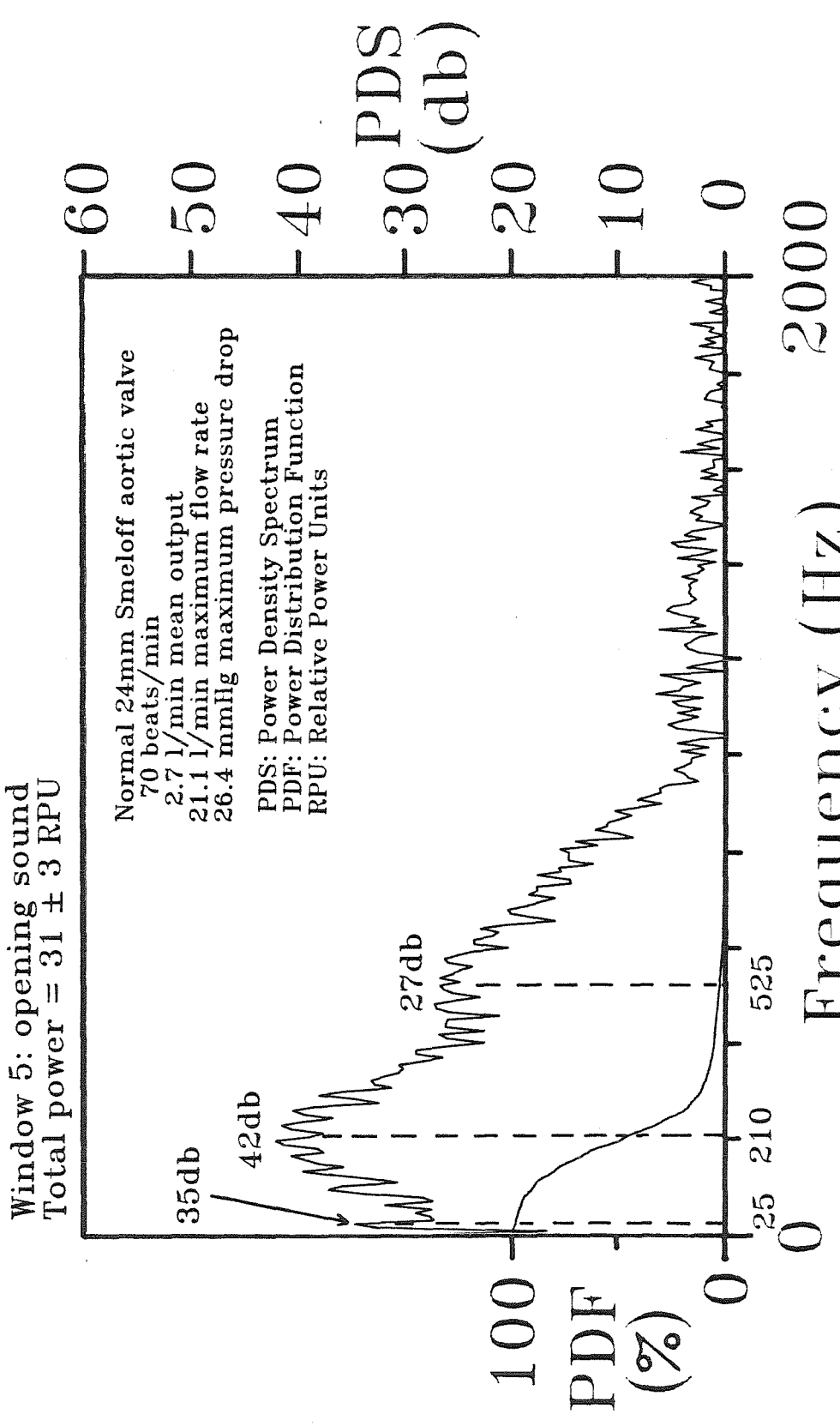

Figure 5-9e Power-density spectra and power distribution of the opening sound of experiment 296.

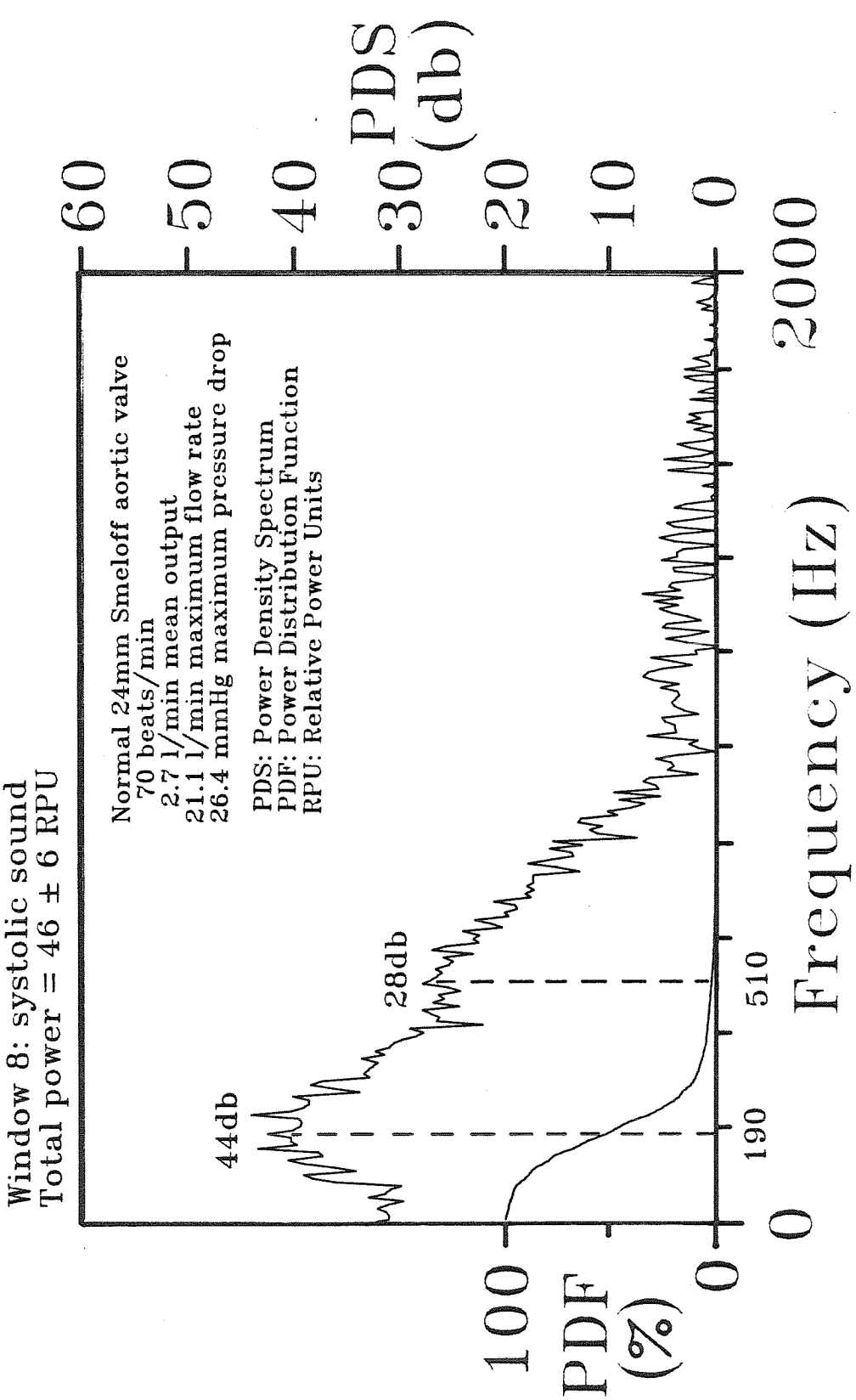

Figure 5-9f Power-density spectra and power distribution of the systolic sound of experiment 296.

Parameters Estimated for

Significant Harmonic Peaks

Experiment 296

Event	Frequency, $f_{r,i}$; Decay, k_i; Power-Density, G_i (Hz,Hz,db)
Opening Sound	25, 5,35
Window 5	210,80,42
	525,90,27
Systolic Sound	190,70,44
Window 8	510,90,28
Closing Sound	100, 40,46
	420, 70,36
	720, 70,27
Window 23	1090, 80,22
	1330, 80,19
	1590, 90,16
	1840,100,13

Table 5-6 Parameters estimated from significant harmonic peaks of experiment 296.

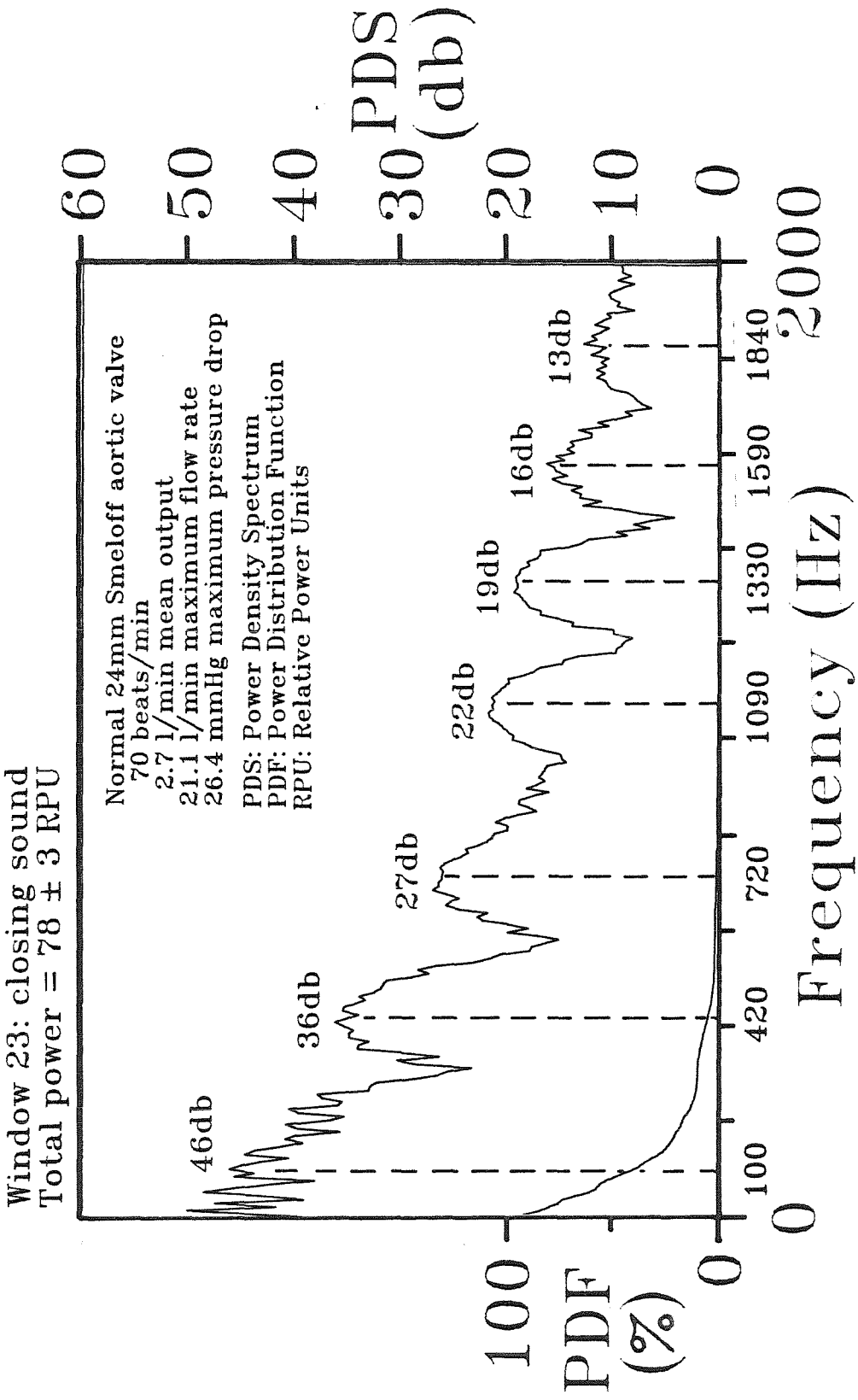

Figure 5-9g Power-density spectra and power distribution of the closing sound of experiment 296.

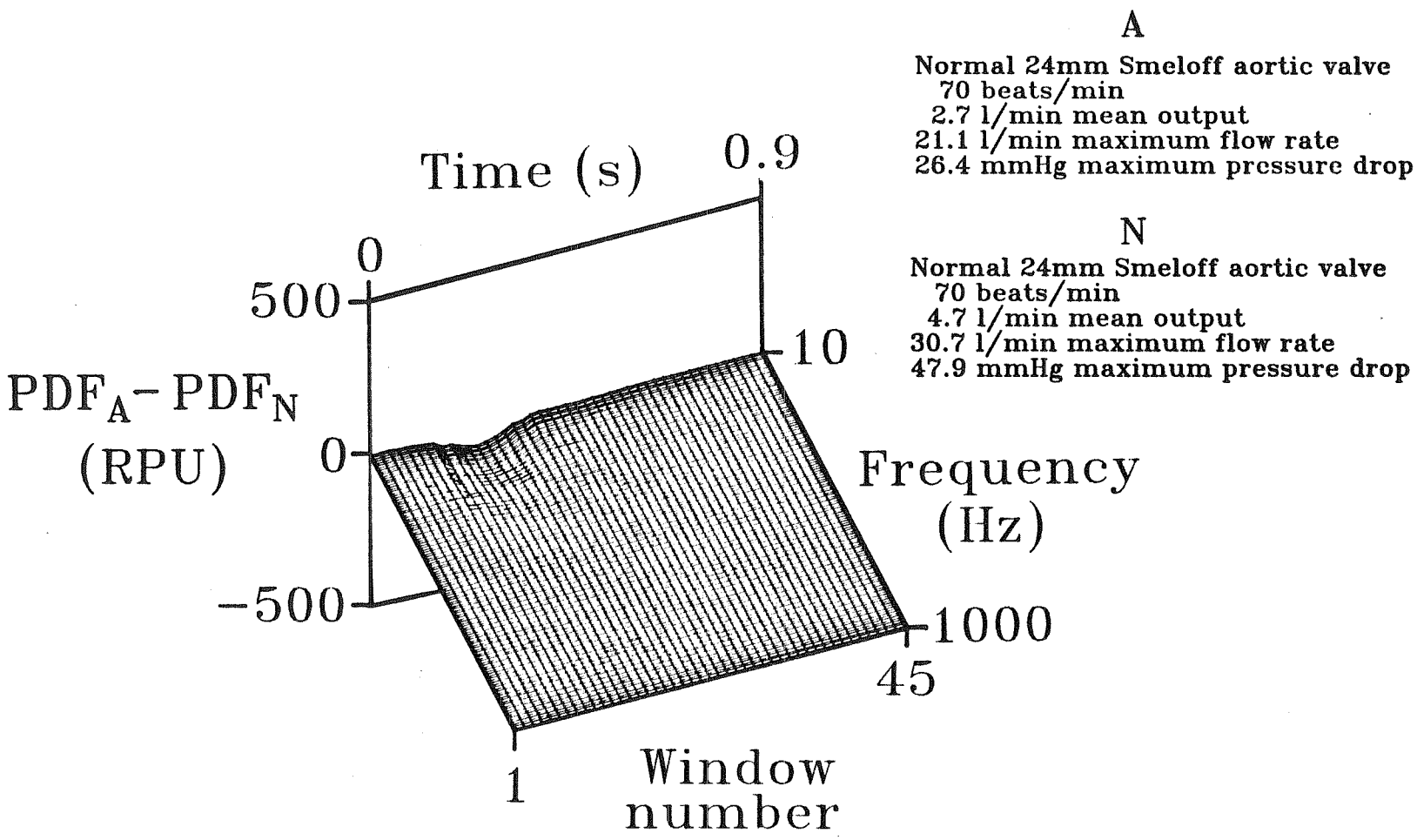

Figure 5-9h Three-dimensional surface depicting the difference between the power-frequency-time surfaces associated with experiments 296 and 292.

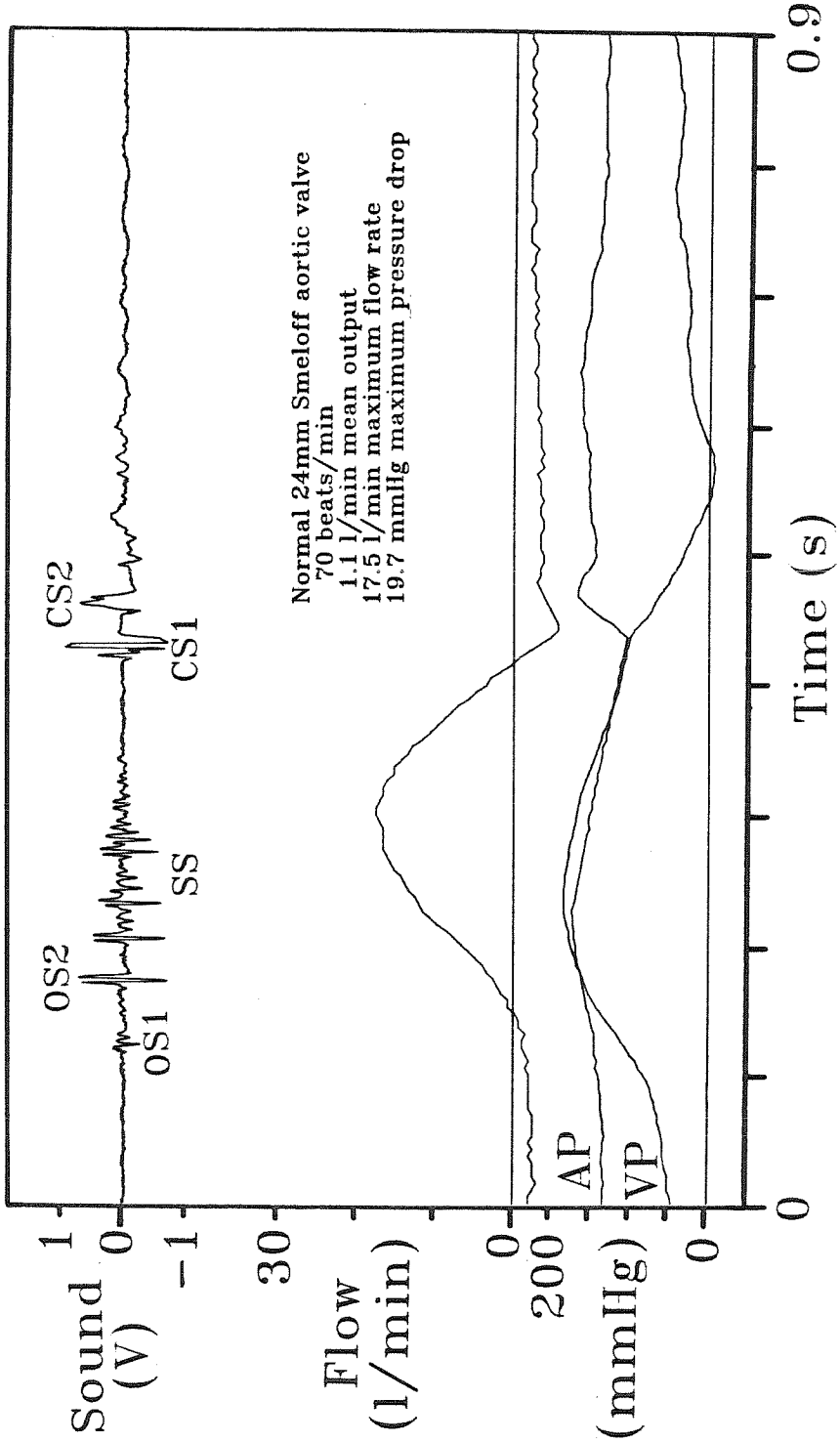

Figure 5-10a Amplitude vs. time tracings of sound, flow rate, aortic pressure and ventricular pressure associated with a typical cycle of experiment 297.

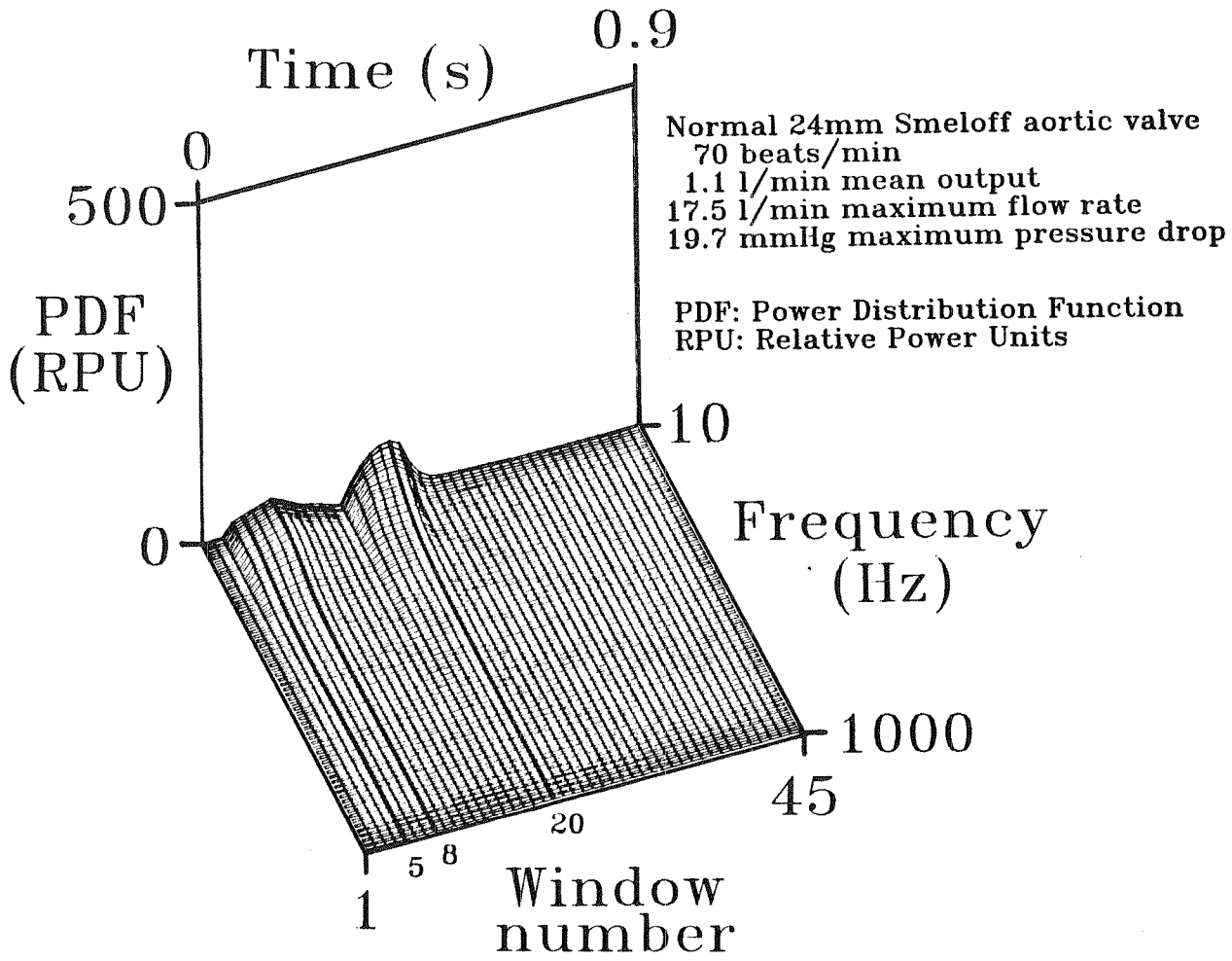

Figure 5-10b Three-dimensional power-frequency-time surface averaged over ten cycles of experiment 297.

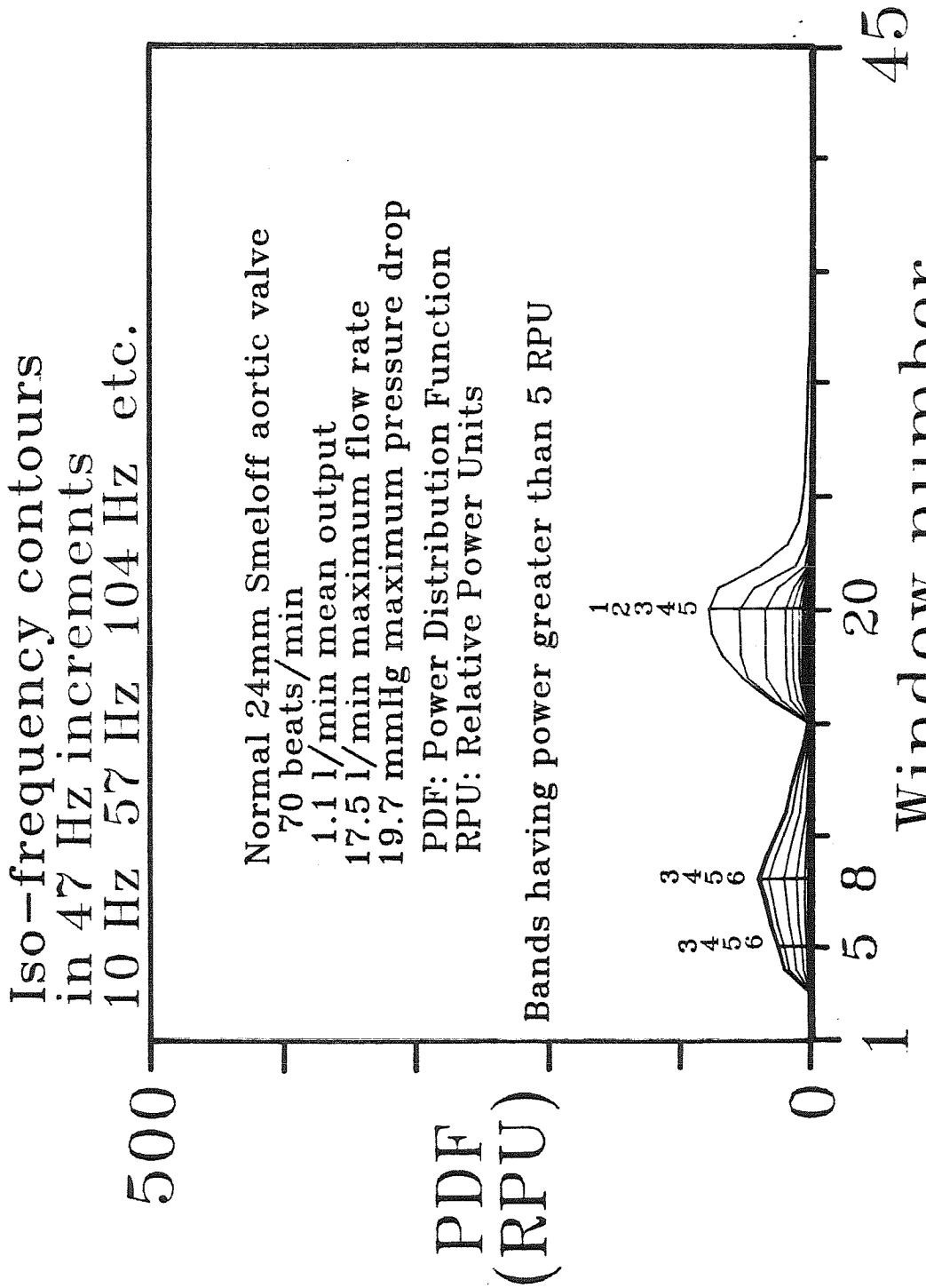

Figure 5-10c Auxiliary view perpendicular to the time axis of the 3-D power-frequency-time surface of experiment 297 showing iso-frequency contours.

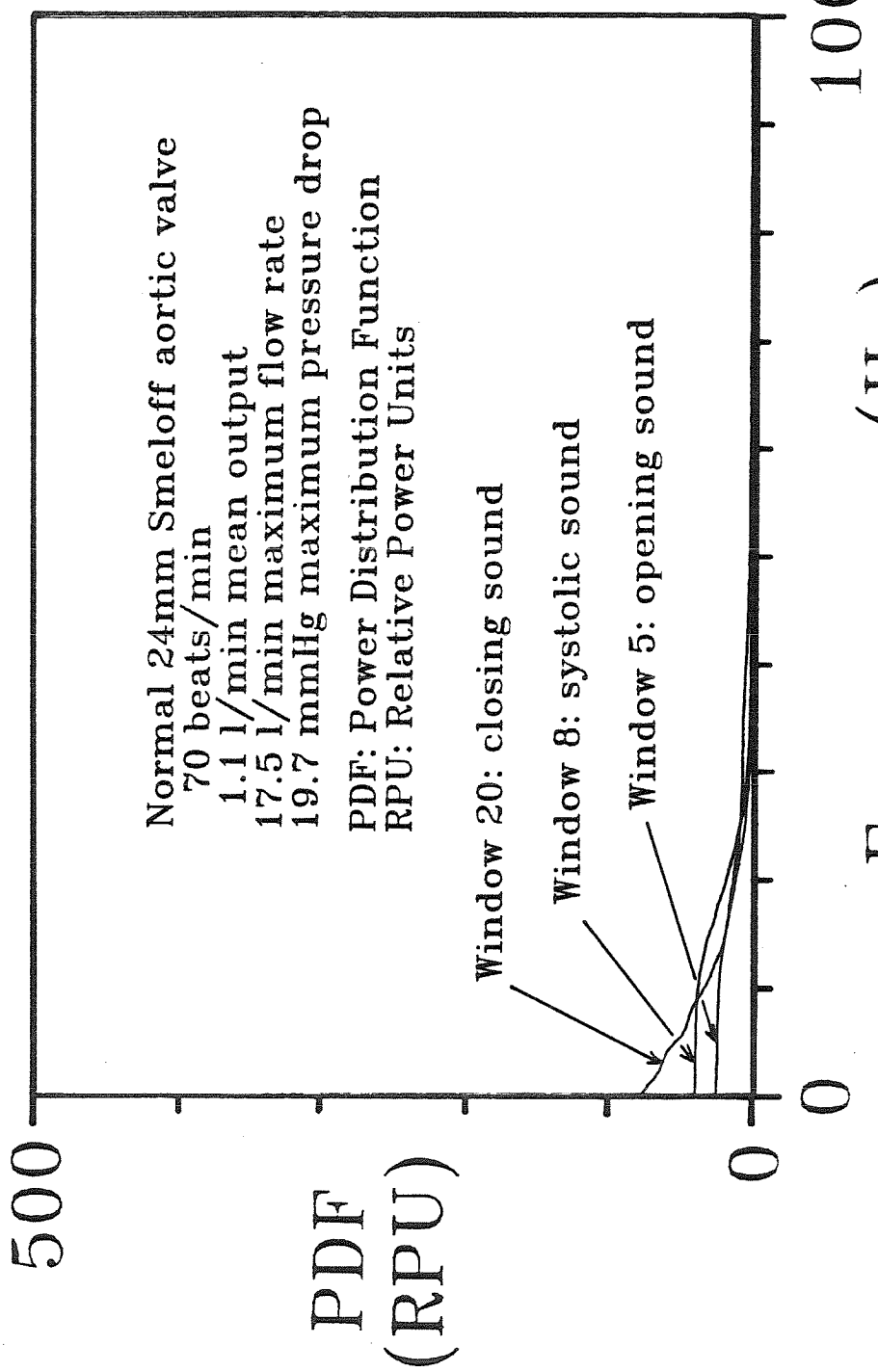

Figure 5-10d Auxiliary view perpendicular to the frequency axis of the 3-D power-frequency-time surface of experiment 297 showing power power distributions associated with windows encompassing the opening, systolic, and closing sounds.

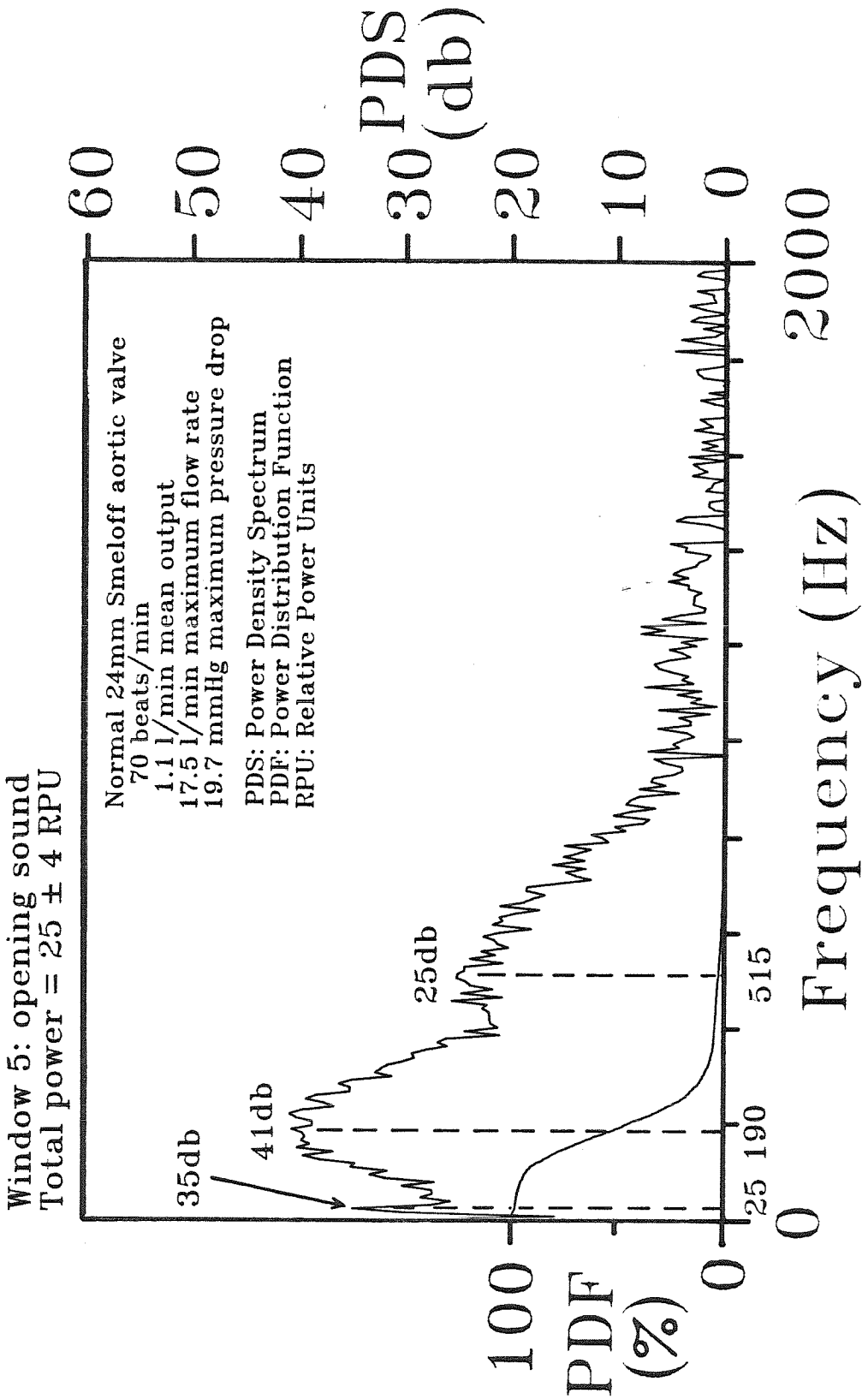

Figure 5-10e Power-density spectra and power distribution of the opening sound of experiment 297.

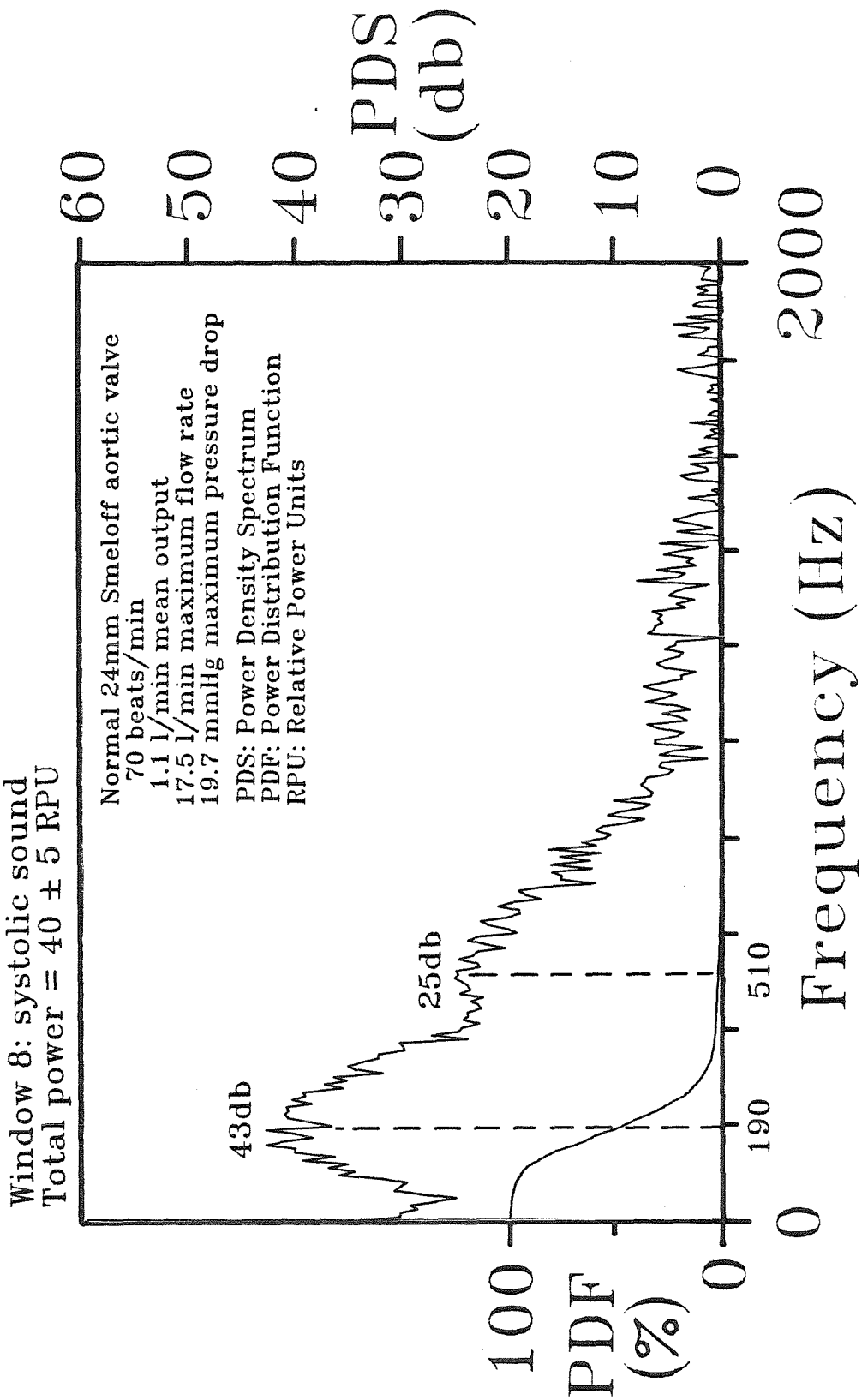

Figure 5-10f Power-density spectra and power distribution of the systolic sound of experiment 297.

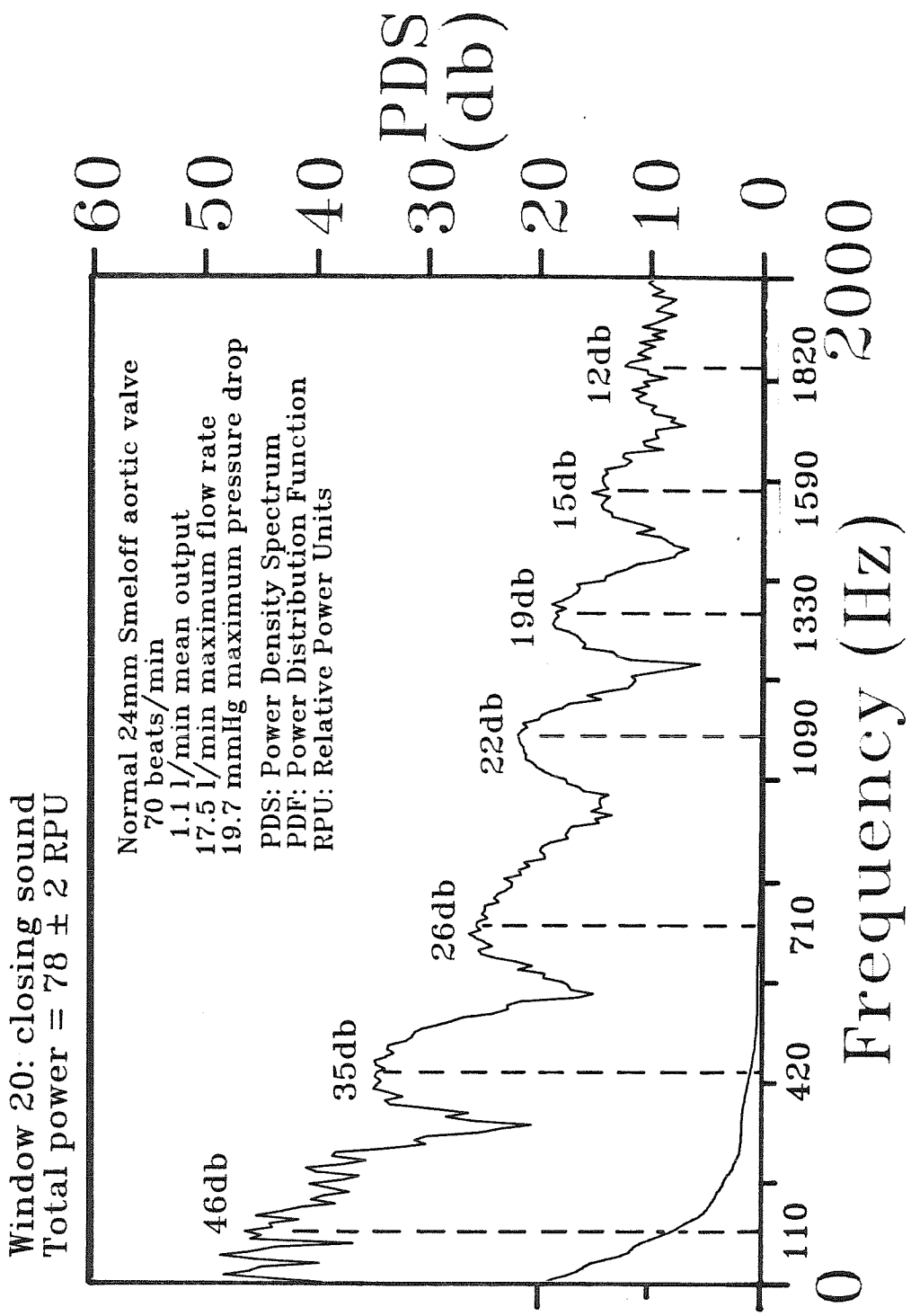

Figure 5-10g Power-density spectra and power distribution of the closing sound of experiment 297.

Parameters Estimated for

Significant Harmonic Peaks

Experiment 297

Event	Frequency, $f_{f,i}$; Decay, k_i; Power-Density, G_i (Hz,Hz,db)
Opening Sound	25, 5,35
Window 5	190,70,41
	515,90,25
Systolic Sound	190, 70,43
Window 8	510,100,25
Closing Sound	110, 40,46
	420, 70,35
	710, 80,26
Window 20	1090, 70,22
	1330, 70,19
	1590, 70,15
	1820,100,12

Table 5-7 Parameters estimated from significant harmonic peaks of experiment 297.

A
Normal 24mm Smeloff aortic valve
70 beats/min
1.1 l/min mean output
17.5 l/min maximum flow rate
19.7 mmHg maximum pressure drop

N
Normal 24mm Smeloff aortic valve
70 beats/min
4.7 l/min mean output
30.7 l/min maximum flow rate
47.9 mmHg maximum pressure drop

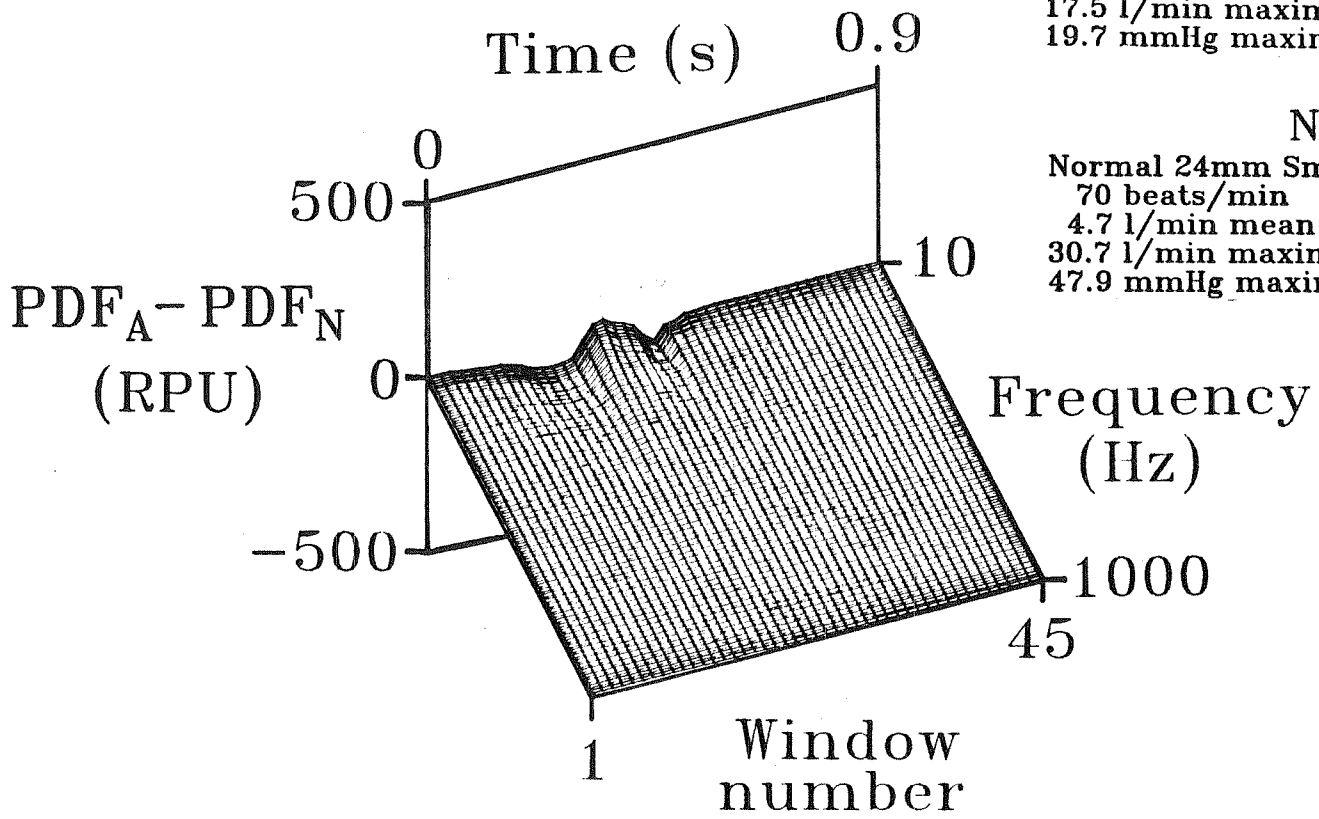

Figure 5-10h Three-dimensional surface depicting the difference between the power-frequency-time surfaces associated with experiments 297 and 292.

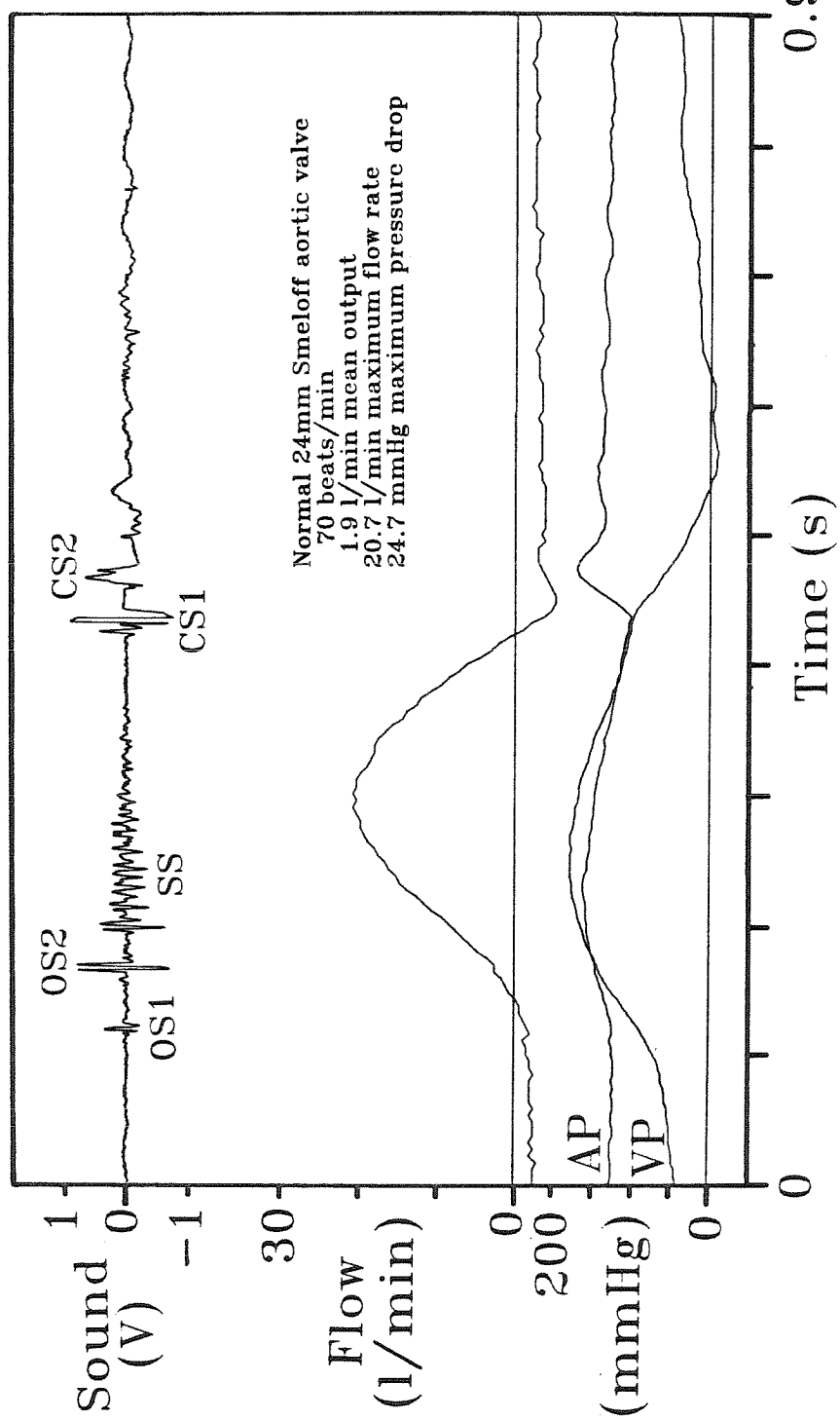

Figure 5-11a Amplitude vs. time tracings of sound, flow rate, aortic pressure and ventricular pressure associated with a typical cycle of experiment 298.

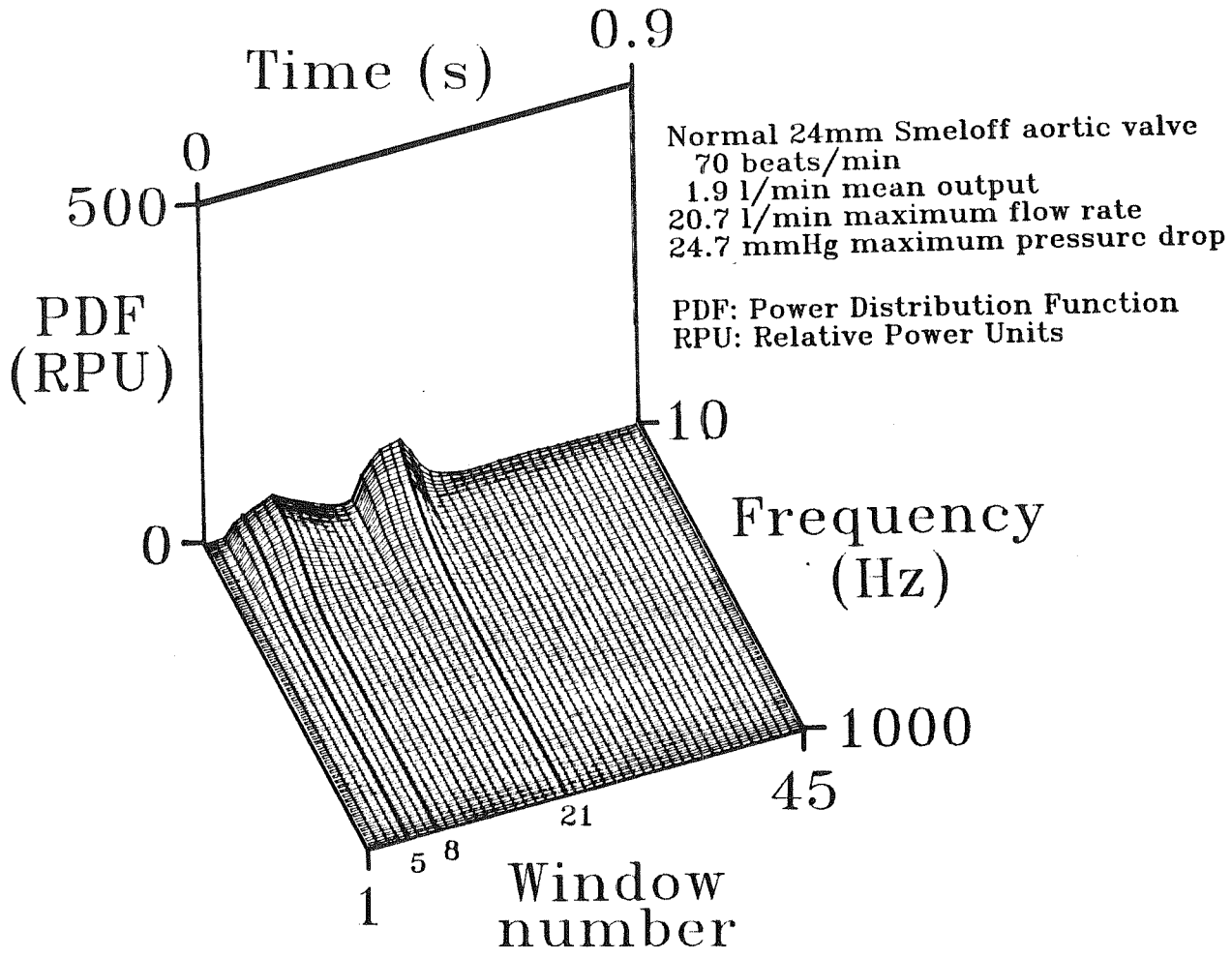

Figure 5-11b Three-dimensional power-frequency-time surface averaged over ten cycles of experiment 298.

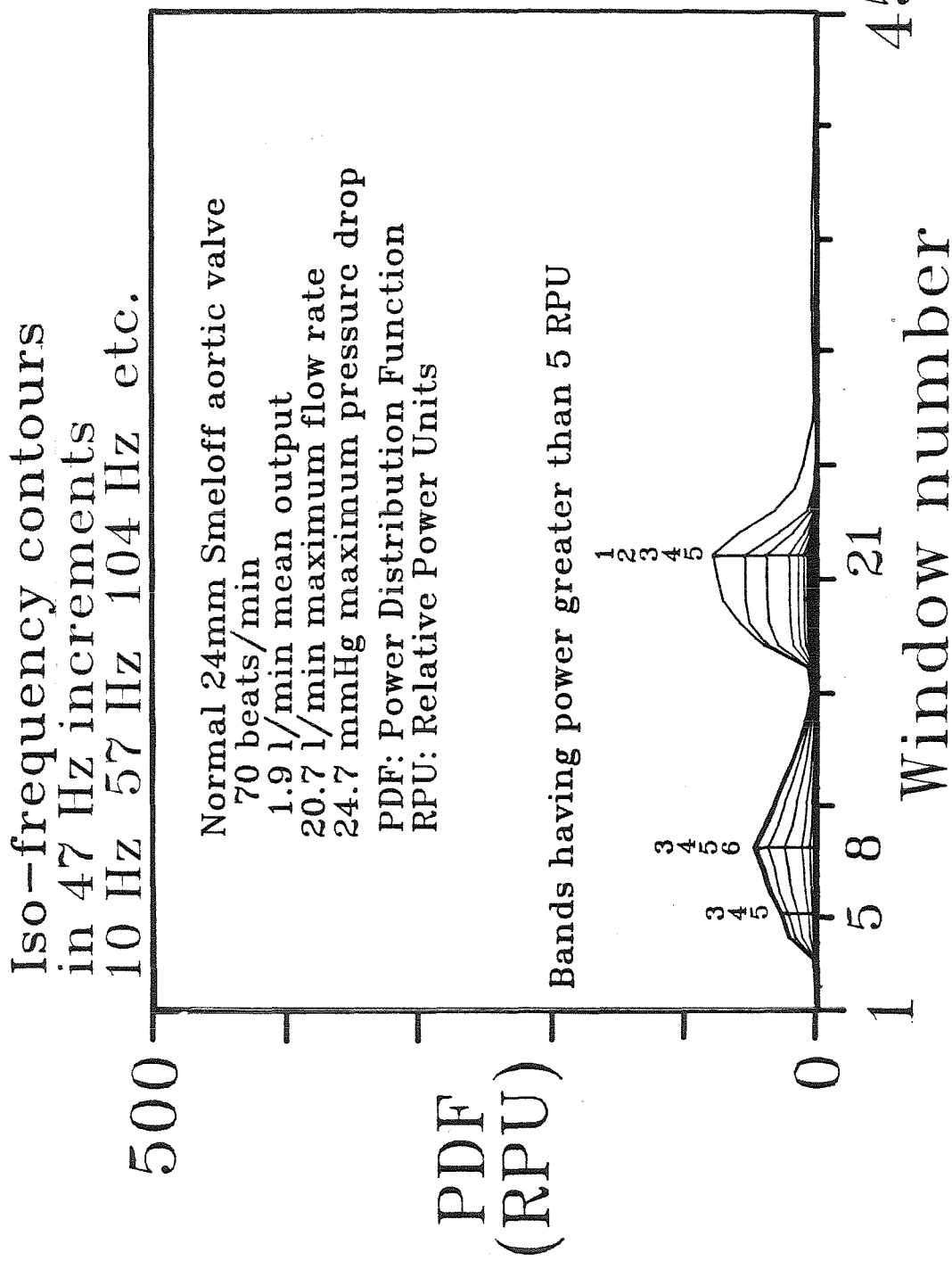

Figure 5-11c Auxiliary view perpendicular to the time axis of the 3-D power-frequency-time surface of experiment 298 showing iso-frequency contours.

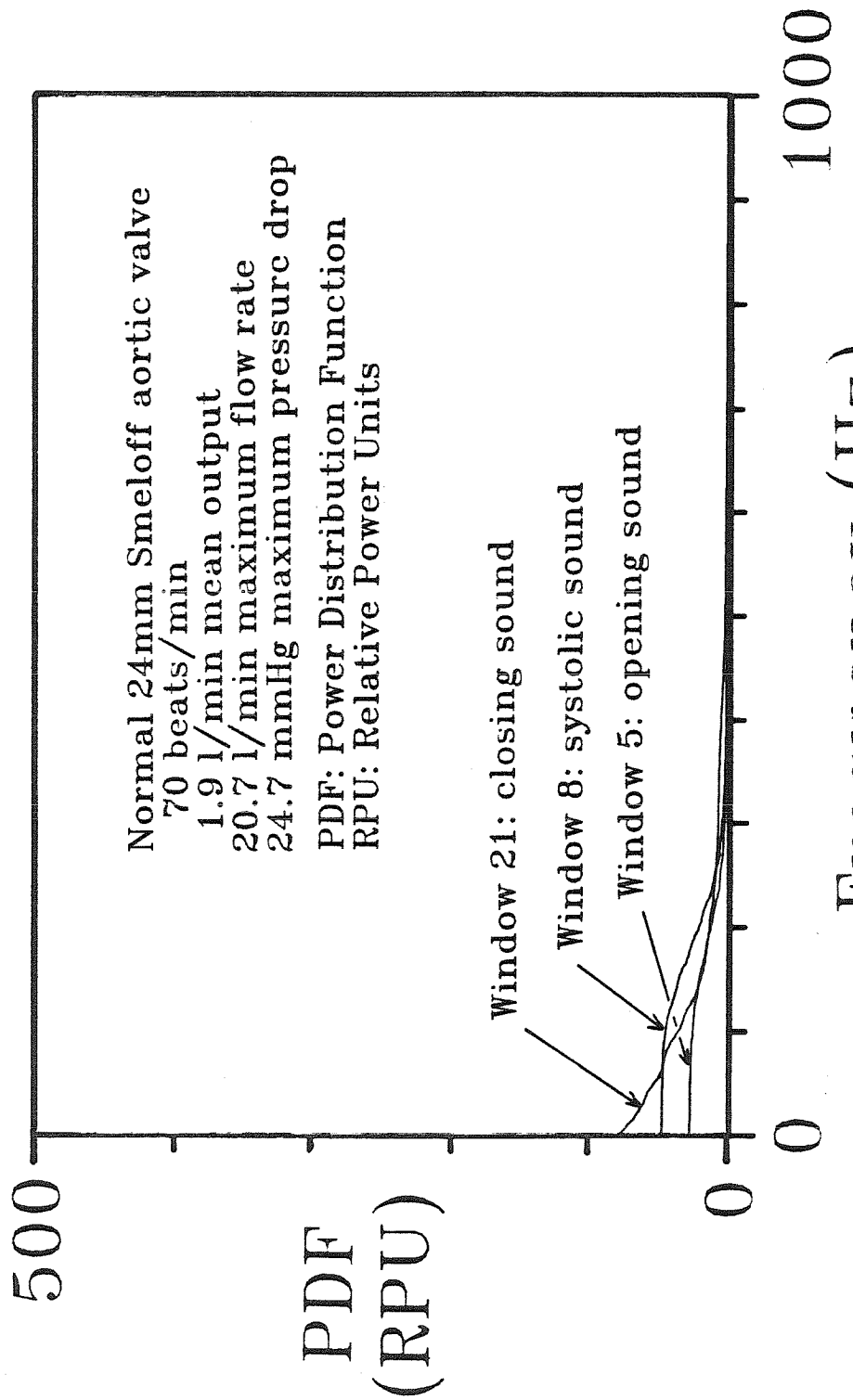

Figure 5-11d Auxiliary view perpendicular to the frequency axis of the 3-D power-frequency-time surface of experiment 298 showing power power distributions associated with windows encompassing the opening, systolic, and closing sounds.

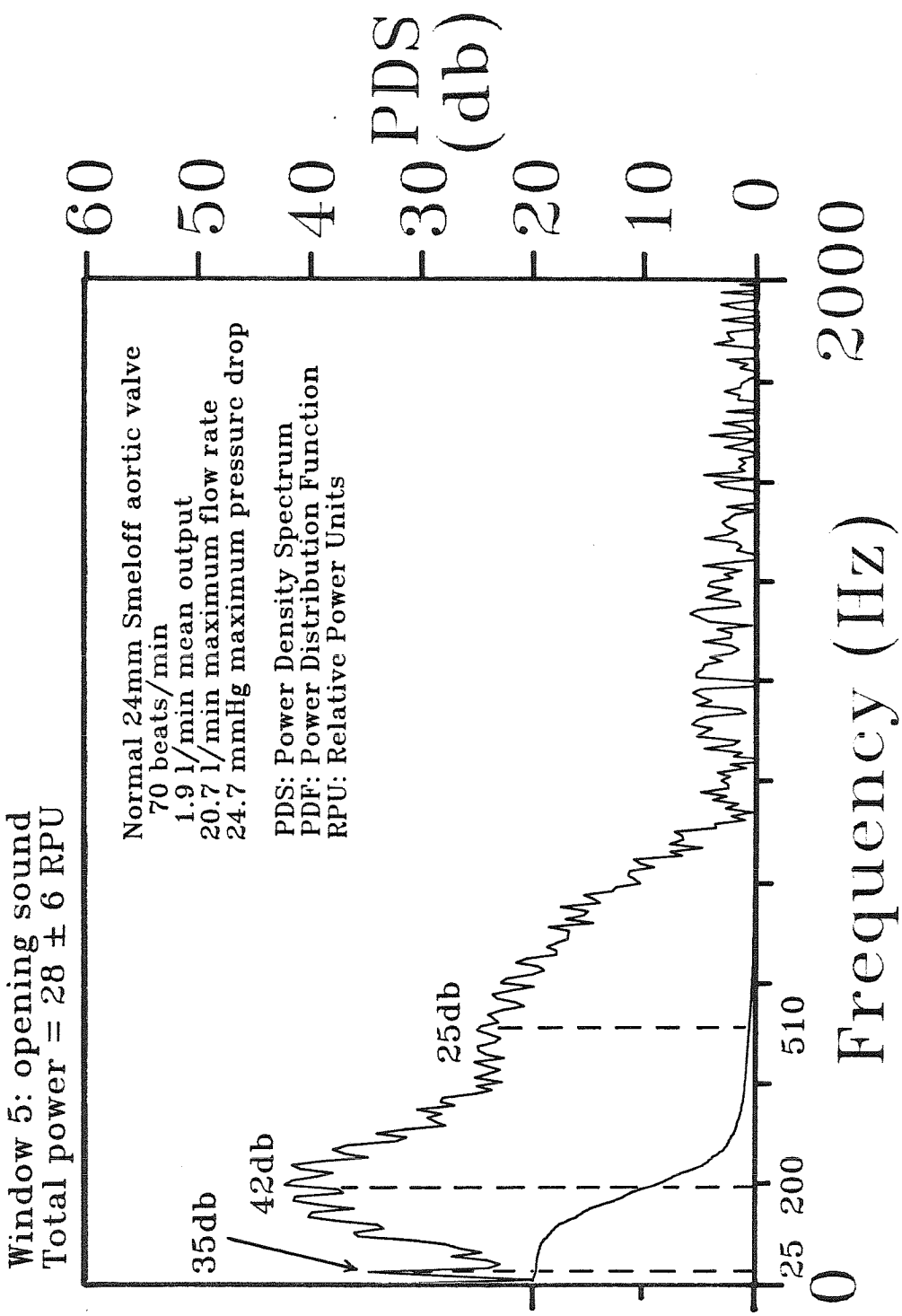

Figure 5-11e Power-density spectra and power distribution of the opening sound of experiment 298.

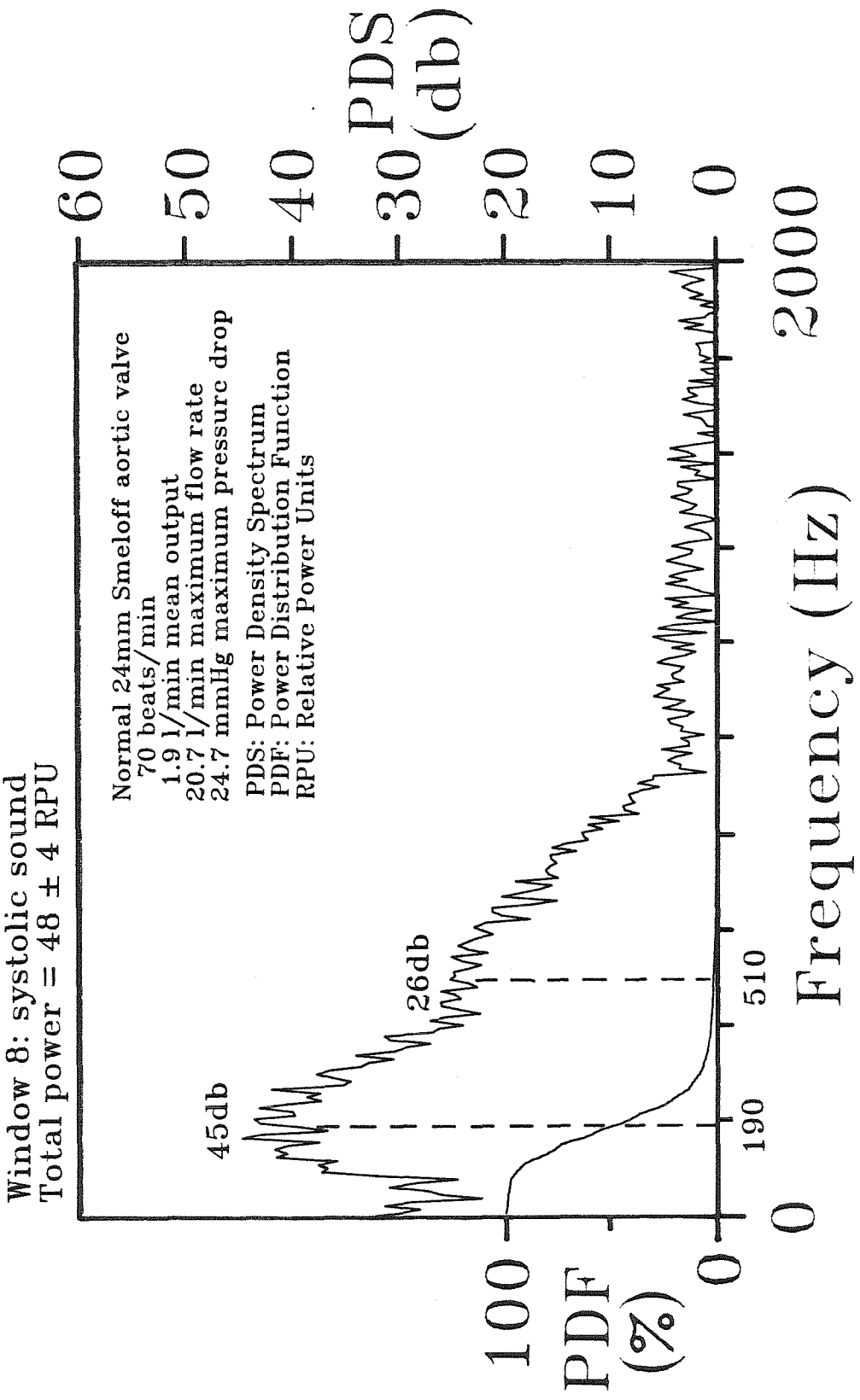

Figure 5-11f Power-density spectra and power distribution of the systolic sound of experiment 298.

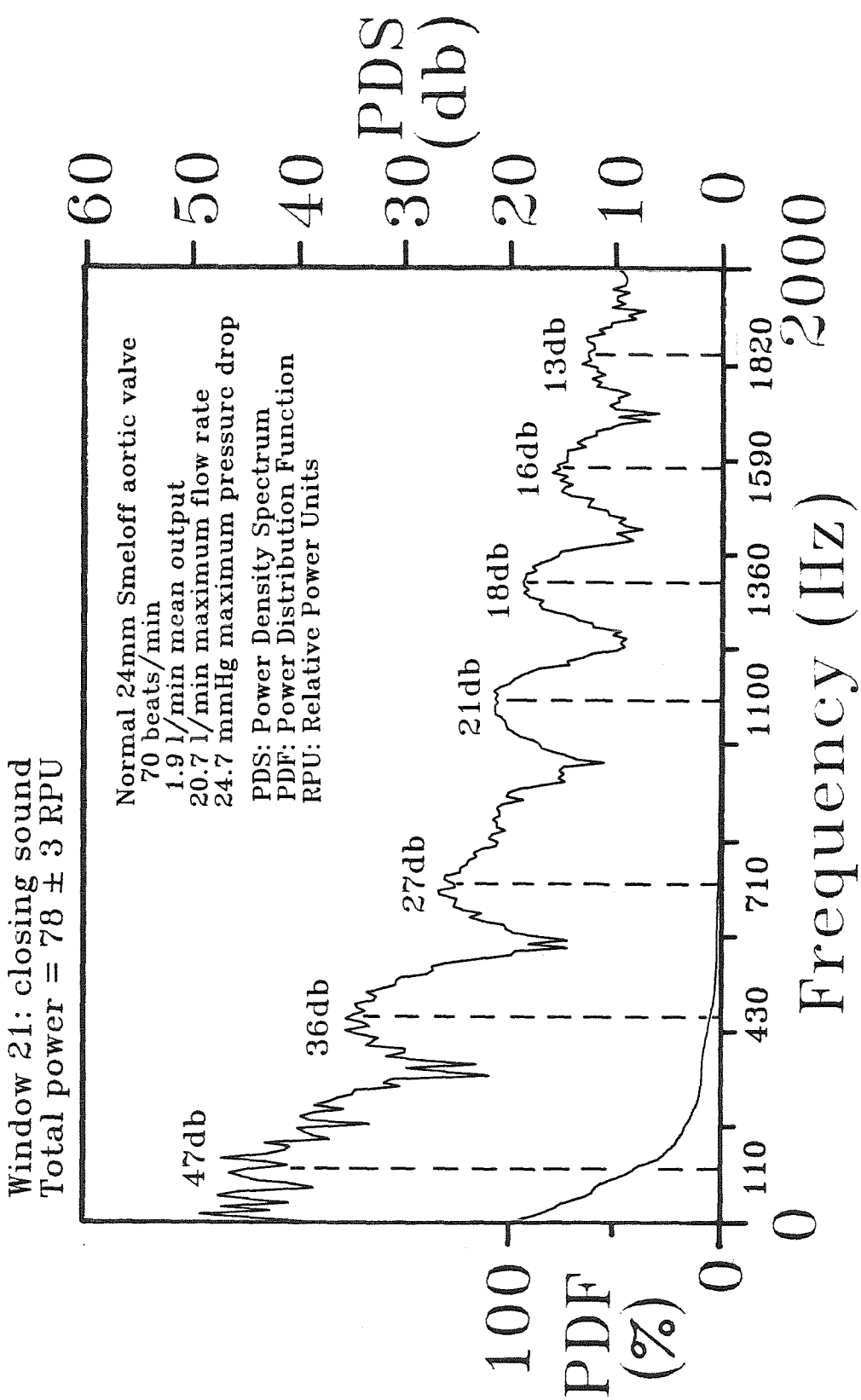

Figure 5-11g Power-density spectra and power distribution of the closing sound of experiment 298.

Parameters Estimated for

Significant Harmonic Peaks

Experiment 298

Event	Frequency, $f_{f,i}$; Decay, k_i; Power-Density, G_i (Hz,Hz,db)
Opening Sound	25, 5,35
Window 5	200, 70,42
	510,100,25
Systolic Sound	190, 80,45
Window 8	510,100,26
Closing Sound	110,40,47
	430,70,36
	710,80,27
Window 21	1100,70,21
	1360,70,18
	1590,80,16
	1820,80,13

Table 5-8 Parameters estimated from significant harmonic peaks of experiment 298.

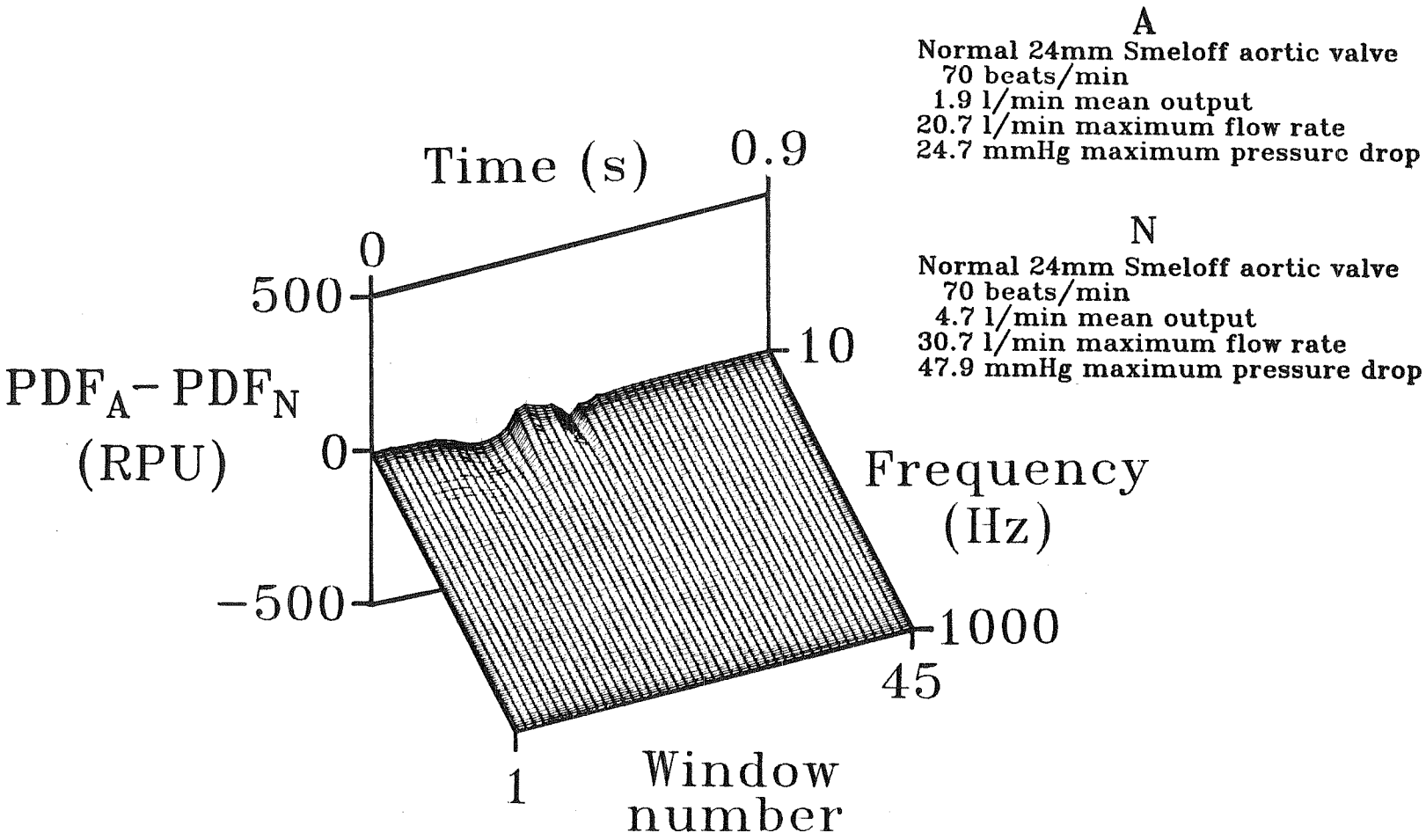

Figure 5-11h Three-dimensional surface depicting the difference between the power-frequency-time surfaces associated with experiments 298 and 292.

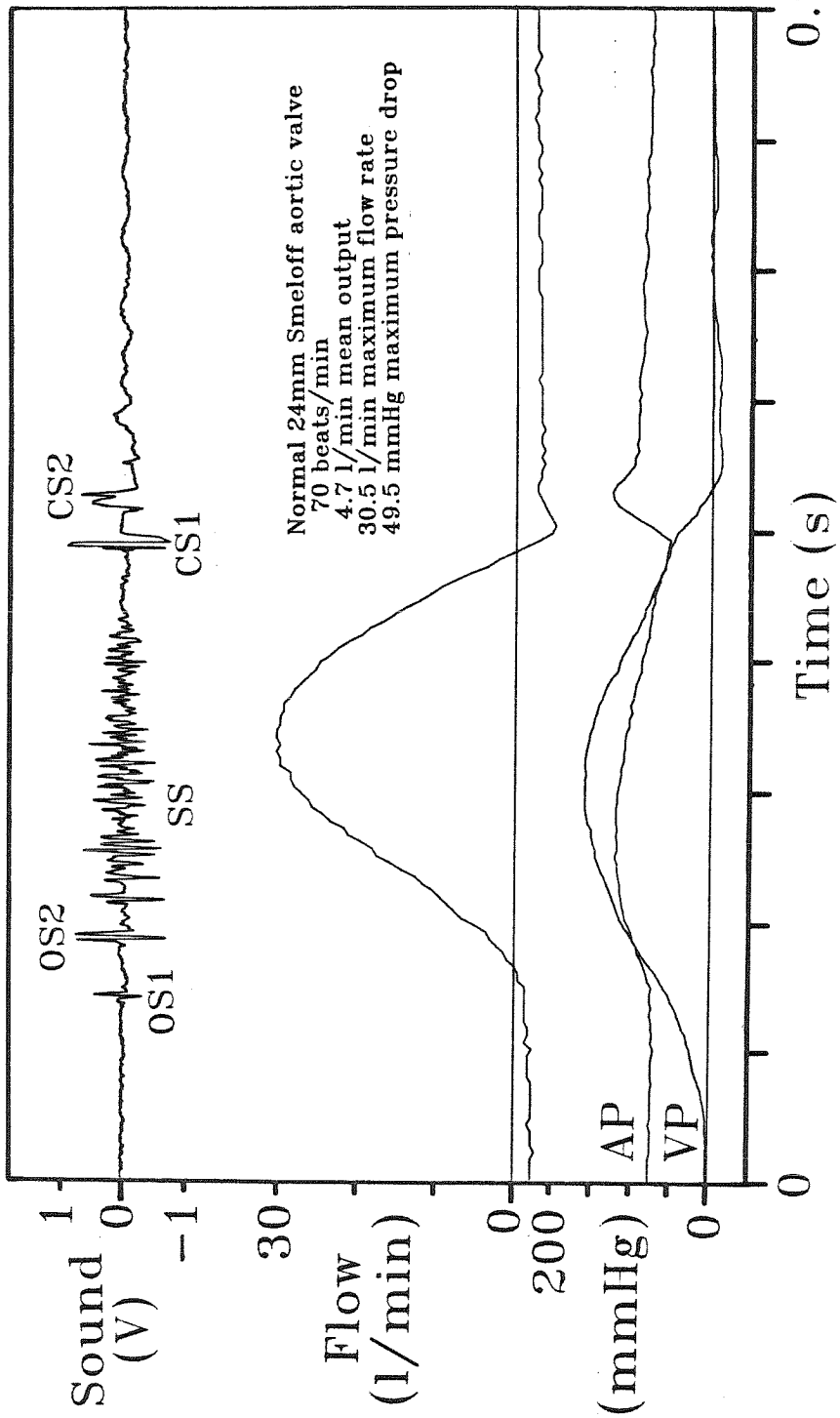

Figure 5-12a Amplitude vs. time tracings of sound, flow rate, aortic pressure and ventricular pressure associated with a typical cycle of experiment 300.

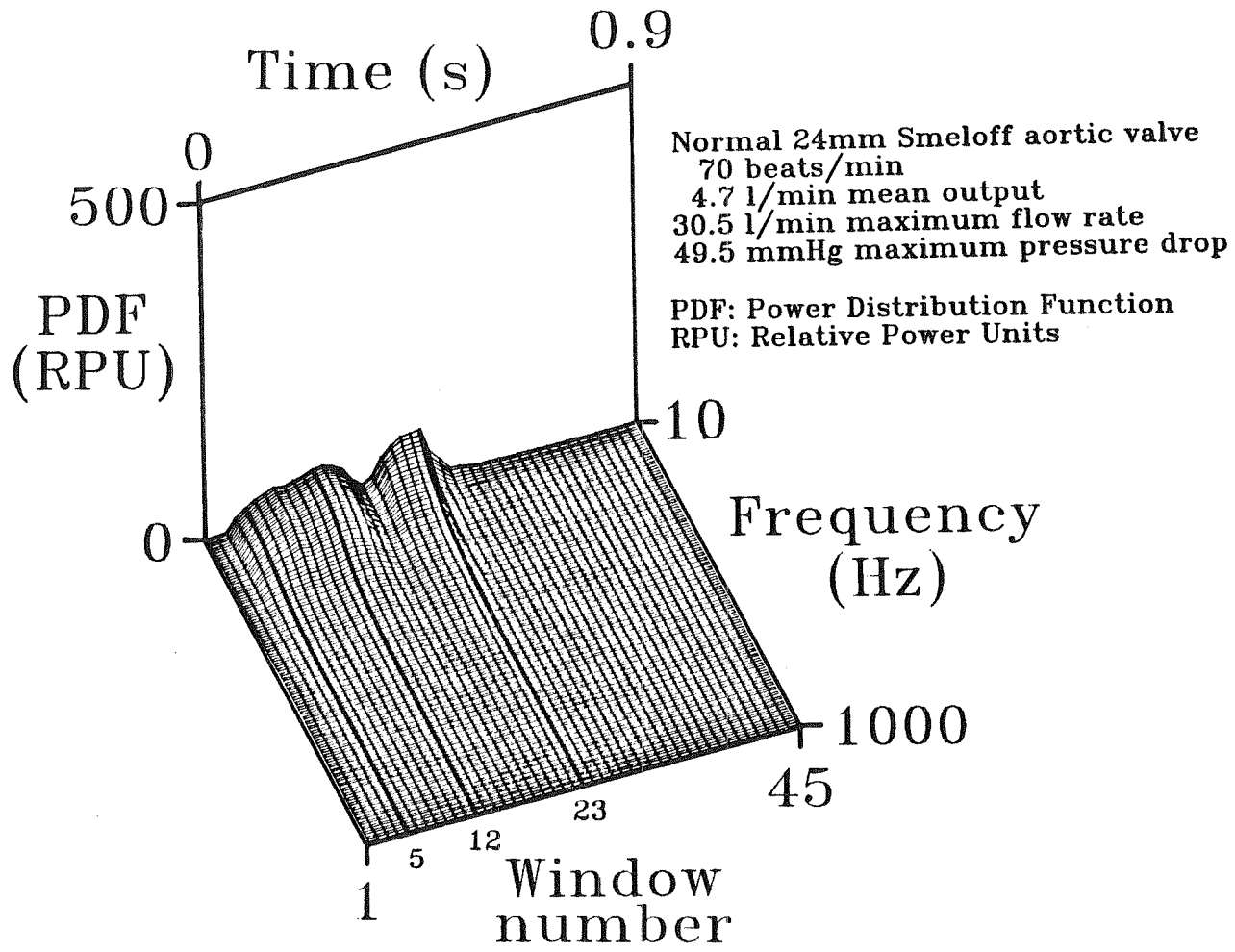

Figure 5-12b Three-dimensional power-frequency-time surface averaged over ten cycles of experiment 300.

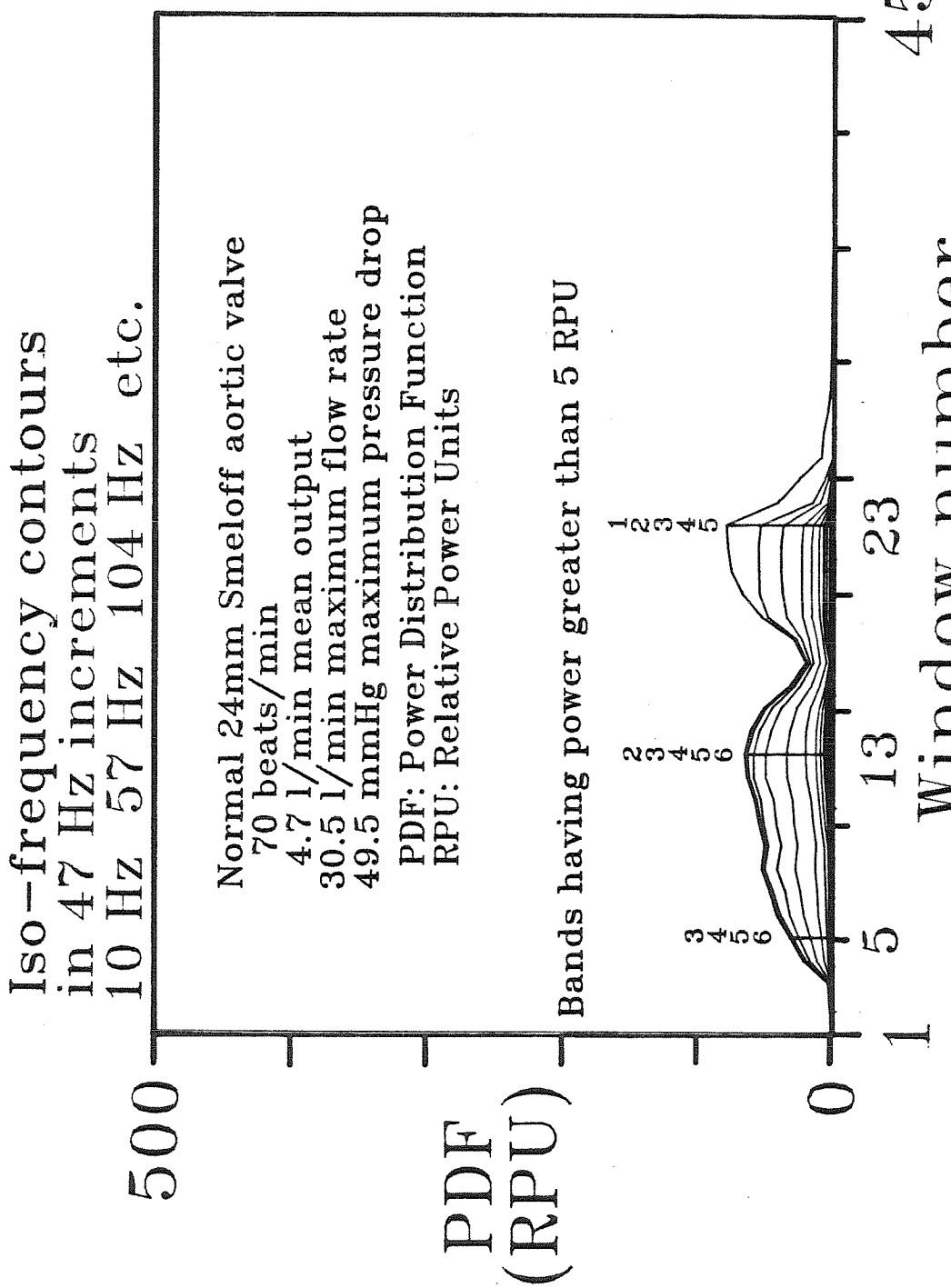

Figure 5-12c Auxiliary view perpendicular to the time axis of the 3-D power-frequency-time surface of experiment 300 showing iso-frequency contours.

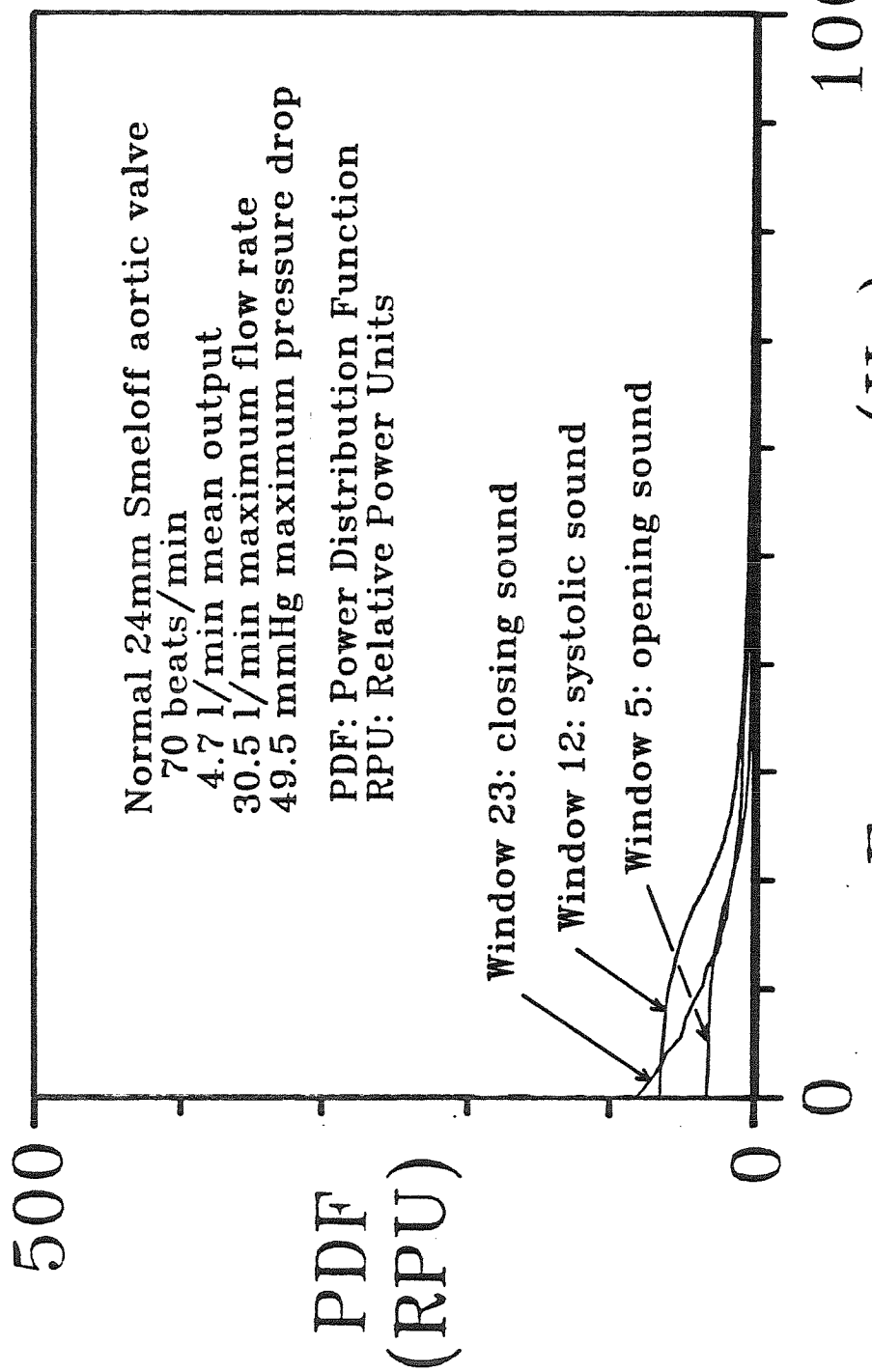

Figure 5-12d Auxiliary view perpendicular to the frequency axis of the 3-D power-frequency-time surface of experiment 300 showing power power distributions associated with windows encompassing the opening, systolic, and closing sounds.

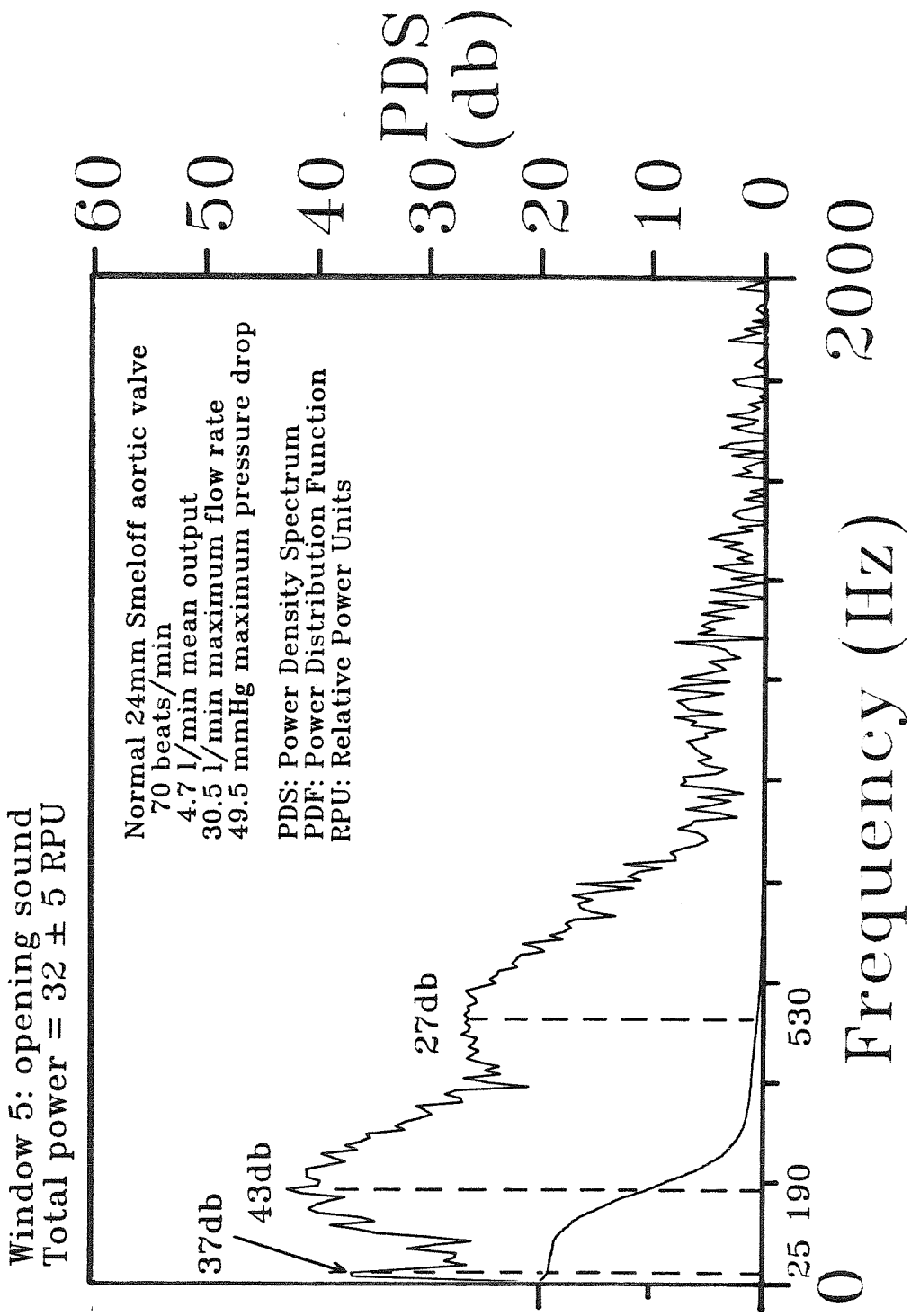

Figure 5-12e Power-density spectra and power distribution of the opening sound of experiment 300.

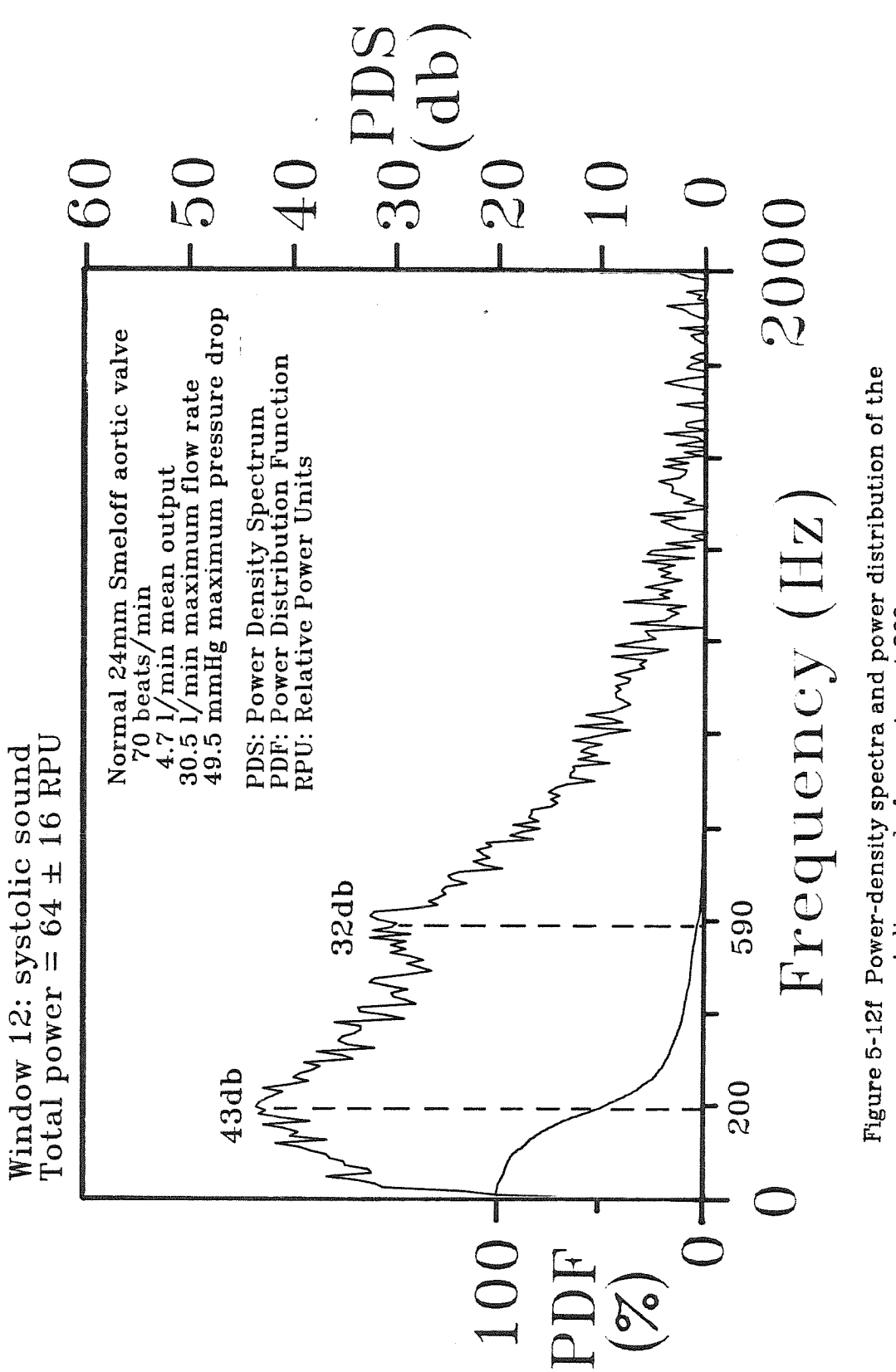

Figure 5-12f Power-density spectra and power distribution of the systolic sound of experiment 300.

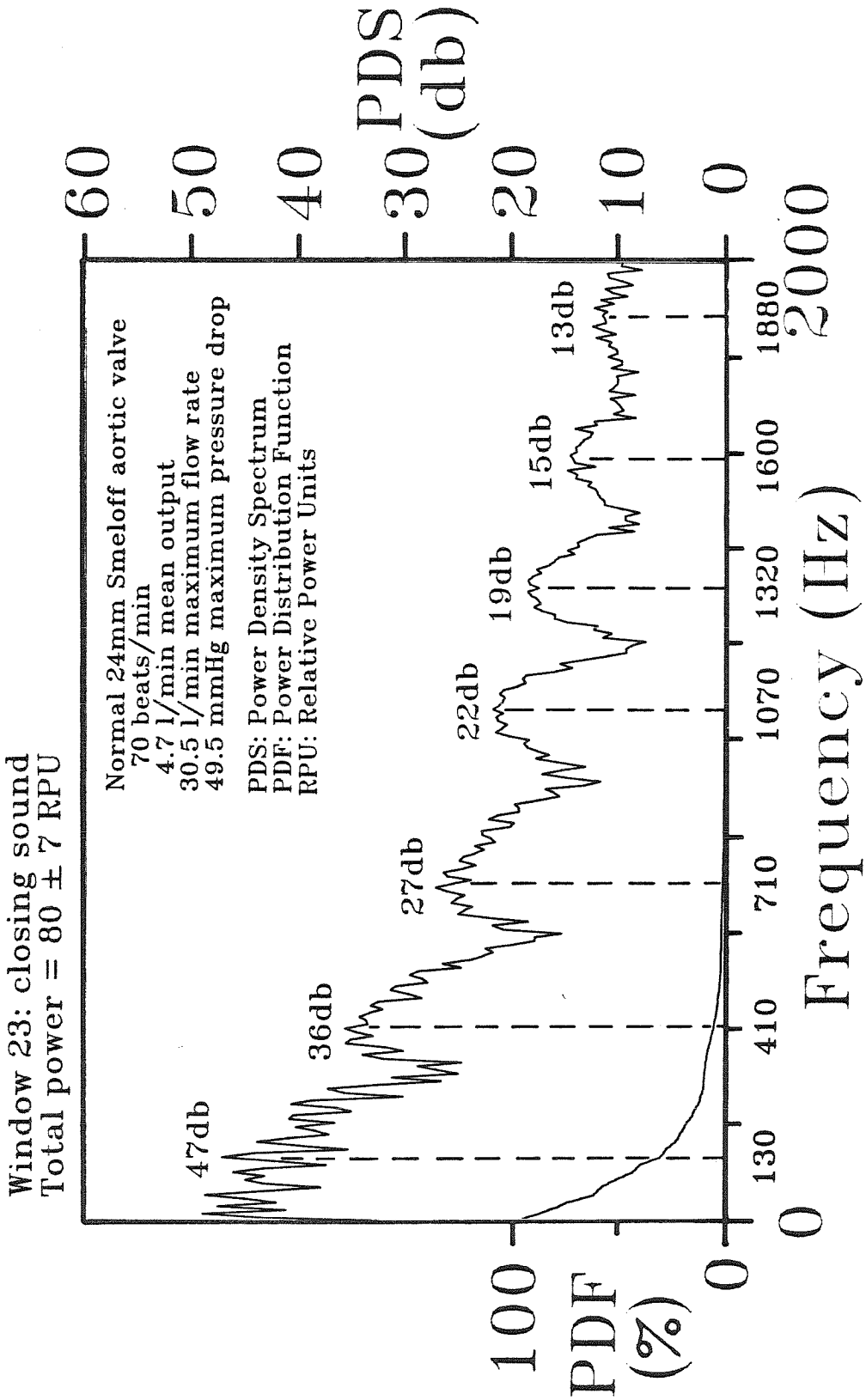

Figure 5-12g Power-density spectra and power distribution of the closing sound of experiment 300.

Parameters Estimated for

Significant Harmonic Peaks

Experiment 300

Event	Frequency, $f_{f,i}$; Decay, k_i; Power-Density, G_i (Hz,Hz,db)
Opening Sound	25, 5,37
Window 5	190, 70,43
	530,100,27
Systolic Sound	200,70,43
Window 12	590,60,32
Closing Sound	130, 40,47
	410, 70,36
	710, 80,27
	1070, 70,22
Window 23	1320, 70,19
	1600, 80,15
	1880,100,13

Table 5-9 Parameters estimated from significant harmonic peaks of experiment 300.

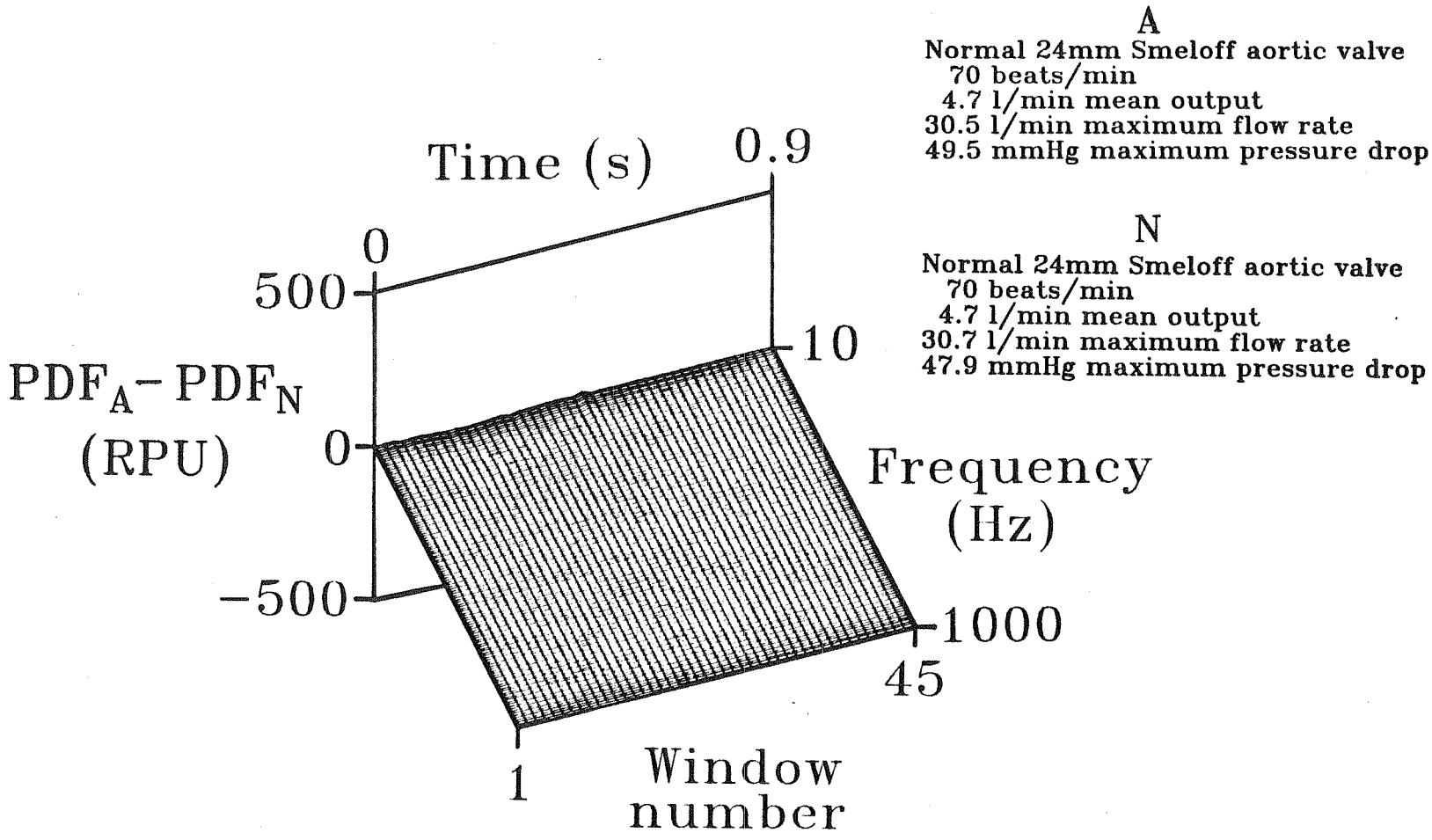

Figure 5-12h Three-dimensional surface depicting the difference between the power-frequency-time surfaces associated with experiments 300 and 292.

ejection time was corrected by normal factors for these three pulse rates in order to simulate the natural, rate-dependent systolic and whole-cycle times. As a result the ratio of the systolic time interval to the whole-cycle time was not a constant but rather increased with the pulse rate. When the pulse rate varied between experiments, adjacent windows were shifted an amount proportional to the time of one complete cycle so that windows 1 and 45 corresponded to the same relative moment within two consecutive cycles. For these three experiments, the stroke volume, maximum flow rate, and maximum pressure gradient decreased as the pulse rate increased. These changes resulted from maintenance of the mean output near values of 4.7, 2.7 and 4.1 L/min during experiments 292, 293 and 294, respectively.

5.4.1.1 The Opening Sounds

The opening sounds, OS, produced by the Smeloff valve for experiments 292, 293 and 294 occurred as two transient events which we have labeled OS1 and OS2 nearest their occurrence along the upper tracings of Figures 5-5a, 5-6a and 5-7a. Flow visualization experiments indicated that OS1 was produced when the occluder was still in its closed position while OS2 was produced as the occluder arrived at its totally open position. The four tracings in Figures 5-5a, 5-6a and 5-7a show that OS1 occurred at the same time as the forward flow began and at the time when ventricular pressure exceeded the aortic pressure. It is also clear that OS2 occurred 50 ms after OS1 during each of these three experiments. Because the time between OS1 and OS2 was approximately constant, the occluder traveled from the orifice to the apex of the cage in a time that was not affected by the pulse rates and stroke volumes simulated during these experiments. We would expect to see similarities in the spectra of the opening sounds for these three experiments.

The opening sounds correspond to window 5 of our analysis. The spectra corresponding to experiments 292, 293 and 294 are shown in Figures 5-5e, 5-6e and 5-7e and the corresponding parameters are listed in Tables 5-2, 5-3 and 5-4. Here one can see that the spectra have essentially the same peaks, that is to say each peak has center-frequencies and amplitudes that are the same within the error of their estimation. This similarity between opening sounds can be observed by comparing window-5 contours in Figures 5-5, 5-6 and 5-7, subfigures b,c,d, and h.

5.4.1.2 The Systolic Sounds

Unlike the opening sounds, the systolic sounds are quite different for experiments 292, 293 and 294. This difference is primarily a result of differences in the value of the maximum systolic flow rate which was 30.7, 20.2 and 32.8 L/min for experiments 292, 293 and 294, respectively. These systolic sounds were labeled SS nearest its occurrence along the upper tracings of Figures 5-5a, 5-6a and 5-7a. By examining all four tracings in each of these three figures, one can see that the maximum intensity of the systolic sound occurred at the same time as the maximum flow-rate and the maximum pressure-gradient. It is clear from these figures that the systolic sound-intensity increases with the maximum flow-rate and the maximum pressure-gradient. A very good correlation exists between the power of the sound produced during systole and the value of the maximum flow rate. This correlation is shown in Figure 5-4 for these three experiments. In addition, the maximum total-power of the sound produced during systole and the value of the maximum systolic pressure-gradient across the valve correlated as shown in Figure 5-3. The time-amplitude tracings in subfigures a also show that the systolic sound occurred earlier, within window 10, during experiment 293 than during either experiment 292, window 13, or

experiment 294, window 12. This difference primarily resulted from the fact that experiment 293 also had a smaller stroke volume of 43 cm^3 as compared with either experiment 292 or 294 which had stroke volumes of 91 and 125 cm^3, respectively.

The power-density spectra of the systolic sounds of experiments 292, 293 and 294, depicted in Figures 5-5f, 5-6f and 5-7f respectively, show these differences in the frequency domain. Here again, experiment 293 was noticeably different from the other two experiments. The spectra of the **normal** sound, shown in Figure 5-5f, depicts a broad, powerful peak centered at 170 Hz and a narrower, less-powerful peak at 560 Hz. The low-frequency peak corresponded to the transient sounds resulting from bouncing of the occluder during systole and the non-transient sound produced by the overall pressure-fluctuations in the turbulent flow. The transient sounds of the Smeloff valve have frequencies which are comparable to the non-transient sounds during systole. The high-frequency peak is probably related to the flow past the phonocatheter and/or the struts. Estimates of the Strouhal number for such flows are given in Table 7-1 and discussed in Part VII. These estimates suggest that the low-frequency peak could also be related to vortex-shedding at the phonocatheter, and the high-frequency peak could be related to vortex-shedding at the struts. The spectrum of the systolic-sound of experiment 294 is similar in shape to the spectrum of the **normal** systolic-sound but it possesses power-densities which are greater than **normal** over all frequencies between 10 and 1000 Hz. The spectrum of the systolic-sound of experiment 293 is different in shape and amplitude from either of those of experiments 292 or 294. The shape of this spectrum is similar to that of the spectrum of the opening sound. It is probable that for this case the power associated with the sound produced by flow was overpowered by the sound produced by the bouncing of the occluder. These results indicate that

the occluder bounced more as the maximum systolic flow-rate increased.

Subfigures 5-5 to 5-7 b,c,d, and h again show these differences in their own characteristic manner. The early systolic sound of experiment 293 is indicated by the lower window-number, window 10, associated with systole for this experiment. We can also see in these figures that the total-power of the systolic sound increases with increasing values of the maximum systolic flow-rate. We can also see that the systolic sound of experiment 294 has 35-RPU **more** total power than the closing sound. Differences between these power-distributions are plotted directly in Figures 5-6h and 5-7h. The loss of power of the systolic sound of experiment 293 is shown by the valley between 10 and 600 Hz along the contour corresponding to window 12 in Figure 5-6h. The increase of power of the systolic sound of experiment 294 is shown by the peak between 10 and 600 Hz along the contour for window 13 in Figure 5-7h.

5.4.1.3 The Closing Sounds

The closing sounds, CS, of experiments 292, 293 and 294 are very similar to each other. These sounds were comprised of two events which we have labeled CS1 and CS2 nearest their occurrence along the upper tracings of Figures 5-5a, 5-6a and 5-7a. One can see from the other tracings included in these figures that the closing sound CS1 occurred at the same time as the maximum backflow, the dichrotic notch of the aortic pressure curve, and the beginning of the rapid decrease of the ventricular pressure curve. The second closing sound CS2 occurred at the same time as the highest diastolic peak of the aortic pressure. The spectra of the closing sounds are similar to each other. They differ considerably from the spectra of their corresponding opening or systolic sounds.

The "intra-sonic" similarity is in the location, shape and amplitude of

corresponding peaks. Each spectrum shown in Figures 5-5g, 5-6g and 5-7g has essentially seven peaks. An increase in power-density for the low-frequency peaks centered near 130 Hz primarily contributes toward increased values of the average total-power of the sounds.

As we have observed with the other two valvar designs, the "extra-sonic" difference is in the number, location and amplitudes of the peaks. The spectra of the closing sounds have seven or eight significant peaks instead of two or three as we have seen in the case of the opening and systolic sounds. These extra-sonic differences can most immediately be examined by inspecting the values listed in Tables A-1 through A-6. Clearly more vibrational modes have been stimulated for the case of the closing event. Are these transformed and/or additional modes of the valve, or are they new modes of the aortic flow section? The answer is probably yes to all three hypotheses. The center-frequencies of the closing sounds produced by all three valvar designs are listed in Table A-5 for all of the experiments. We can see that some of the columns have entries that are similar between designs, while some entries are valvar-unique. The columns which are similar between valvar designs do have slightly different values. For example, notice the values near 980 Hz for the closing sound of the Bjork-Shiley valve and near 1100 Hz for the Smeloff valve. This fact may suggest that the aortic flow section is involved with these additional peaks because the general effect is not valvar dependent. On the other hand, there are clear differences between the fine-scale groupings of the peaks for each valvar design which would suggest that the design does have some additional influence on the location and shape of the peaks. At this time we can not relate these peaks with more certainty to specific physical vibrations of the system.

The power distributions of the closing sounds that are indicated by windows 23, 23 and 22 in Figures 5-5, 5-6 and 5-7, respectively are similar in form. These

similarities are shown by the flat contours of windows 23 on the difference-surface shown in Figure 5-6h and Figure 5-7h.

5.4.1.4 Summary of Comparisons of Pulse-Rate Experiments

The effect of pulse rates of 51, 70 and 91 beats/min upon the opening sounds was minor. The only significant change we observed was a reduction of the total-power of the opening sound for the experiment having a high pulse rate. This change was probably a result of an effects accompanying the decrease of the stroke-volume during this experiment, *i.e.*, lesser value of acceleration of the fluid and a decrease in the rate of change of ventricular pressure. These changes of the sound were minor with respect to those we observed in the corresponding systolic sounds.

The effect of pulse rate upon the systolic sound was primarily to shift this sound earlier in systole, decrease the power of the non-transient component, centered near 560 Hz, and shift this peak 50 Hz lower to a center-frequency of 510 Hz, all as the stroke volume decreased. The earlier systolic sound was observed for the experiment having a higher pulse rate and reduced stroke-volume even when the time-scale had been normalized with respect to the different cycle times. Vortex-shedding at the phonocatheter has been assigned a possible source of the low-frequency peak and similar shedding at the struts could account for the high-frequency peak.

The differences between closing sounds were minor with respect to changes observed for the cases involving comparisons of the opening and systolic sounds. The frequency characteristics of these sounds were not significantly different. There was also no significant change in the timing between opening and closing sounds after these had been normalized with respect to pulse rate.

5.4.2 Effects of Stroke Volume on the Sounds

The Smeloff valve was pulsed at three different stroke volumes while maintaining a pulse rate of 70 beats/min. The experiments which will be compared are 292, 295, and 296. The important values which define the pulsatile state for these experiments are listed in the appropriate columns of Table 5-1a. The stroke volumes were 91, 135, and 63 cm^3 and corresponded to mean flow rates of 4.7, 8.4, and 2.7 L/min, respectively. For these three experiments, the maximum flow-rate, and maximum pressure-gradient increased as the stroke volume increased as indicated by their values which are listed in Table 5-1a.

5.4.2.1 The Opening Sounds

In a manner similar to the previous comparisons involving changes of pulse rate, the opening sounds, OS, produced by the Smeloff valve for these three experiments occurred as two distinct events which we have labeled OS1 and OS2 nearest their occurrence along the upper tracings of Figures 5-5a, 5-8a and 5-9a. The occluder again begins its motion downstream at about the time OS1 occurs and arrives at the apex of the downstream cage at the time OS2 occurs. The time interval between OS1 and OS2, however, is approximately 120 ms for experiment 295, an increase of 140% relative to the **normal** time interval of 50 ms during experiment 292. Pressure and flows for experiment 295 were also quite different from **normal** as shown in Figure 5-8a . This figure shows that this 120-ms time-interval occurs at the same time that there is a small amount of forward flow and a small, constant difference between ventricular and aortic pressures. These differences result from the nature of the design of the pulse duplicator and its ability to pulse at this extreme flow-state of 8.4 L/min mean output. In particular the pressure waveforms had very large fluctuations

throughout diastole which may have affected the dynamics of the valve in pre- and early systole. We would therefore expect to see dissimilarities in the opening sounds for these three experiments, especially experiment 295.

The opening sounds correspond to window 5 of our analysis. Significant differences were observed between the power-density spectra of the opening sounds for these three experiments, particularly between the spectrum of experiment 295 which had the large OS1-OS2 interval and the **normal** spectrum. This can be seen if one examines the power-density spectra plotted in Figures 5-5e, 5-8e and 5-9e and the corresponding parameters that have been listed in Tables 5-2, 5-5, 5-6 and A-1 through A-6. Here one can see that each spectrum has essentially three peaks with similar center-frequencies, but the peaks for experiment 295 as shown in Figure 5-8e are much lower in amplitude. It is important to note that window 5 does not encompass OS1 for experiment 295. This fact together with the 10-db loss of power-density of the high-frequency peak at 570 Hz indicates that this peak in the **normal** spectrum was attributed to the sound OS1. Estimates of the mean-velocity required to produce vortex shedding downstream of the annular gap associated with this valve when it is closed, gave values of 25.5 cm/s and corresponding flow rates of 0.07 L/min for shedding frequencies of 570 Hz. These values are physically realistic for early systolic flows.

Figures 5-5, 5-8 and 5-9, subfigures b,c,d, and h, again show power-distributions of these opening sounds. By comparing contours of window number 5 in all of the other figures, one can again see that the opening sound of experiment 295 has less power than those corresponding to experiments 292 or 296. The valley between 10 and 200 Hz along the contour corresponding to window 5 in Figure 5-8h indicates that the opening sound for experiment 295 has significantly less power near 200 Hz than that of experiment 292. The relatively

flat contour for window 5 in Figure 5-9h indicates the similarity between the opening sounds of experiments 296 and 292.

5.4.2.2 The Systolic Sounds

The systolic sounds were significantly different for experiments 292, 295 and 296. This difference was primarily a result of differences between the values of the maximum, systolic flow-rates of 30.7, 47.5 and 21.1 L/min for experiments 292, 295 and 296, respectively. The systolic sound, SS, was depicted nearest its occurrence along the upper tracings of Figures 5-5a, 5-8a and 5-9a. Again by exam- ining all four tracings in these figures, one can see that the maximum intensity of the systolic sound occurred at the same time as the maximum flow-rate and the maximum pressure-gradient. And it is also clear that the systolic sound-intensity again increased with the maximum flow-rate and the maximum pressure-gradient. The correlation between systolic sound and maximum flow-rate and maximum pressure-gradient is shown in Figures 5-4 and 5-3, respectively. The time-amplitude tracings in subfigures **a** also show that the maximum amplitude of the systolic sound occurred earlier during experiment 296, window 8, and later during experiment 295, window 14, as compared with the **normal** window 13. The time of maximum systolic sound correlated quite well with the stroke volume, maximum flow rate and mean flow rate.

The power-density spectra depicted in Figures 5-5f, 5-8f and 5-9f show these differences in the frequency domain. Here experiment 295 was, again, noticeably different from the other two experiments. Each spectrum had two peaks centered near 180 Hz and 560 Hz. The major difference between these spectra was the amplitude of the peaks which increased as the stroke volume increased. The spectra of the **normal** systolic sound of experiment 292, as shown in Figure

5-5f, depicted a broad, powerful peak centered at 170 Hz and a narrower, less-powerful peak at 560 Hz. Both of these peaks are centered near the same frequencies as the peaks that we observed in the spectra of the opening sounds. The transient component of the systolic sound would be similar to that of OS2 if they are produced by collisions of the occluder with the struts. Considering experiment 296, we observed an 8-db loss of power for the peak at 510 Hz and an insignificant loss of power for the peak at 190 Hz. This result suggests that the peak at 190 Hz is produced by the transient part of the systolic sound which would probably remain constant for these experiments. It also suggests that the peak at 510 Hz is produced by the non-transient part of the systolic sound because this sound is primarily related to the flow rate, particularly near the phonocatheter. A correlation was observed between the maximum systolic flow rate and pressure gradient for these experiments which was similar to that involving different pulse rates. The spectra of these systolic sounds increased in power with the stroke volume and were delayed later in systole as the stroke volume increased. As the stroke volume approached zero-values the shape of the spectrum of the systolic sound became similar to that of the spectrum of the opening sound. It appears that the power associated with the sound produced by flow approaches zero in this limit faster than the power associated with the sound produced by the bouncing of the occluder.

Figures 5-8 to 5-9, subfigures b,c,d, and h, again show the differences between power-distribution functions in their own characteristic manner. Here one can see the large differences between the total-powers of the systolic sounds and their relative values with respect to the total-power of the corresponding opening and systolic sounds. Figures 5-8h and 5-9h show these differences directly by the peak between 10 and 800 Hz along the contour corresponding to window 14 in Figure 5-8h and by the valley between 10 and 600 Hz along the contour for

window 13 in Figure 5-9h. The former peak indicates that large flow rate of the APS has produced more systolic, acoustical power, while the latter valley indicates that the low flow rate of the other APS has produced less systolic, acoustical power.

5.4.2.3 The Closing Sounds

The closing sounds, CS, of experiments 292, 295 and 296 are very similar to each other. These sounds were comprised of two events which we have labeled CS1 and CS2 nearest their occurrence along the upper tracings of Figures 5-5a, 5-8a and 5-9a. One can see from the other tracings included in these figures that the closing sound CS1 occurred at the same time as the maximum backflow, the dichrotic notch of the aortic pressure curve, and the beginning of the rapid decrease of the ventricular pressure curve. The second closing sound CS2 occured at the same time as the highest value of the diastolic, aortic pressure. The only significant differences that we saw in the time domain between these experiments was the rate of change of the ventricular pressure at the time of closing. This slope was greater with increasing stroke volume because we had maintained a constant pulse rate, the flows decelerated over approximately the same amount of time for each case, a more rapid deceleration of flow occurred, and subsequently the rate of change of the ventricular pressure increased. We would, therefore, expect to see changes in the frequency characteristics of the closing sounds for these three experiments.

Each of the corresponding spectra shown in Figures 5-5g, 5-8g and 5-9g have seven peaks. These spectra were not significantly different. Again, the spectra of the closing sounds had more peaks than the corresponding spectra associated with the opening or systolic sounds.

The power distributions of the closing sounds of experiments 292, 295 and 296 can be compared by inspecting contours 23 in Figures 5-5, 5-8 and 5-9, subfigures 'b,c,d and h', respectively. These contours are similar in form but differ slightly in their amplitudes at corresponding frequencies. The total power of the closing sound of the experiment having a high stroke-volume was 8.6 RPU above that of the normal pulsatile state. An high rate of change of ventricular pressure was also observed during this experiment relative to a normal pulsatile state. The difference between power distributions of experiment 295 and normal appears as a peak at window 23 along the 10-Hz contour on the difference surface shown in Figures 5-8h. On the other hand, the flat contour for window 23 in Figure 5-9h indicates the relative similarity between power-distributions for the closing of experiments 292 and 296.

5.4.2.4 Summary of Comparisons of Stroke-Volume Experiments

The effect of stroke volumes of 63, 91, and 135 cm^3 upon the opening sounds of the Smeloff valve was significant for the case having the largest stroke volume. At the pulsatile conditions of this experiment, 295, a very small rate of change of ventricular pressure occurred prior to opening of the valve. This reduction, which resulted from the pulsatile mode of the duplicator, produced a less powerful opening sound at all frequencies. The peak normally centered at 200 Hz was 5 db less in the opening sound of the APS and the peak normally centered at 510 Hz was 10 db less during the APS. We observed an increase of the total power of the opening sound with increases of the rate of change of ventricular pressure evaluated 20 ms prior to OS2.

The effect of the stroke volume upon the systolic sound was primarily to shift this sound earlier in systole as the stroke volume decreased and to increase the

power of the non-transient component, centered near 500 Hz, as the stroke volume increased. The transient peak normally centered at 200 Hz had a significant gain of power as the stroke volume increased. The total-power of the closing sound increased by 300% relative to **normal** when the stroke volume was increased from 91 to 135 cm^3.

The effect of stroke volume upon the closing sound was minor compared to the opening and systolic sounds. The only significant effect that was observed involved an increase of 8.6 RPU in the total power of the closing sound for the case having high stroke-volume and a 100 % greater rate-of-change of ventricular pressure prior to valve-closure. We observed an increase of the total power of the closing sound with increasing magnitude of the rate of change of ventricular pressure evaluated 20 ms prior to CS2.

5.4.3 Effects of Hypertension on the Sounds

The Smeloff valve was pulsed at three different states of mean aortic pressure at a pulse rate of 70 beats/min. The experiments which will be compared are 292, 297, and 298. Values of the important pulsatile variables for these experiments are listed in the appropriate columns of Table 5-1a. The stroke volumes were 91, 44, and 54 cm^3 and corresponded to mean flow rates of 4.7, 1.1, and 1.9 L/min, respectively. For these three experiments, which had very low stroke-volumes, the maximum flow-rate, and maximum pressure-gradient decreased as the stroke volume decreased below **normal** values. As with all other experiments involving changes in the value of the stroke volume, the maximum flow-rate and maximum pressure-gradient increased as the stroke volume increased. Since the effect of stroke-volume alone on the opening and closing sounds were minor, we consider any changes in the spectra of these sounds for the experiments

involving increased mean aortic pressures to be related to hypertension. Of course, this isolation of hypertensive effects does not apply to the timing of events. When cardiac output is held constant, hypertension tends to delay the closing sound of the natural aortic valve. The early closing sounds we have observed under elevated mean aortic pressure were therefore considered to be related to the change of stroke volume during the hypertensive experiments.

5.4.3.1 The Opening Sounds

In a manner similar to the previous comparisons involving changes of pulse rate and stroke volume, the opening sounds, OS, produced by the Smeloff valve for these three experiments occurred as two distinct events which we have labeled OS1 and OS2 nearest their occurrence along the upper tracings of Figures 5-5a, 5-10a and 5-11a. The occluder again began its motion downstream at about the time OS1 occurred and arrived at the apex of the downstream cage at the time OS2 occurred. The time interval between OS1 and OS2, 50 ms, was **normal** all three experiments. The values of the rate of change of the ventricular pressure prior to the opening sound were **normal** for these three experiments. We would therefore expect to see similarities between their opening sounds. The opening sounds correspond to window 5 of our analysis. If one examines the power-density spectra plotted in Figures 5-5e, 5-10e and 5-11e and the corresponding parameters that have been listed in Tables 5-2, 5-7 and 5-8, one can see that the spectra have essentially three peaks with approximately the same center-frequencies near 25, 200 and 510 Hz. Each peak in the spectra of the **APS** had 1 to 3 db less power the corresponding peak of the **normal** spectrum. It is important to emphasize that we did not observe any change in the opening sounds that could be related to hypertension alone. Losses of power are consistent with the decreased stroke volumes of both hypertensive experiments. If

one compares the results of experiment 296, it is clear that the hypertensive state did not directly affect the changes we have observed in the spectra of the opening sounds because we would have seen similar effects by changing the stroke-volume alone.

The power distributions of these opening sounds can be compared further by inspecting the window-5 contours in Figure 5-5 , Figure 5-10 and Figure 5-11, subfigures b,c,d, and h. A direct comparison is provided by Figures 5-10h and 5-11h. The shallow valley between 10 and 200 Hz along the contour corresponding to window 5 in Figure 5-10h indicates that the opening sound for experiment 297 had slightly less power near 200 Hz than that of experiment 292. The same statement is true for the contour of window 5 in Figure 5-11h which compares the 3-D power-frequency-time surfaces of experiments 298 and 292.

5.4.3.2 The Systolic Sounds

The systolic sounds were again quite different for experiments 292, 297 and 298. This difference resulted from differences in the value of the maximum systolic flow rate which was 30.7, 17.5 and 20.7 L/min for experiments 292, 297 and 298, respectively. A systolic sound, SS, is depicted nearest its occurrence along the upper tracings of Figures 5-5a, 5-10a and 5-11a. In a manner similar to that of experiment 296 having a stroke-volume less than **normal**, the systolic sound for the hypertensive state occurs 50 to 100 ms earlier in systole relative to the **normal** timing of this sound. The time-amplitude tracings in Figures 5-10a and 5-11a depict the maximum amplitude of the systolic sound occurring within window 8 for experiments 297 and 298 as compared to window 13 for experiment 292. The time of this early systolic sound correlated quite well with the stroke volume, maximum flow rate, or alternatively the mean flow rate. This sound

occured during the forward acceleration of flow prior to the time of peak flow. The amplitude of the systolic sound in the time-domain in both experiments 297 and 298 was much less than **normal** as we would have predicted from the results of the previous experiments investigating the effect of stroke volume and the knowledge that we now have about the effects of stroke volume from the present set of experiments. Consequently, the amplitude of the systolic sound again increased with the maximum flow-rate and the maximum pressure-gradient. The correlation between systolic sound and maximum flow-rate and pressure-gradient is shown in Figures 5-4 and 5-3, respectively.

The corresponding power-density spectra depicted in Figures 5-5f, 5-10f and 5-11f show differences between these sounds in the frequency domain. Here the systolic sounds of experiment 297 and 298 were also noticeably different from those of the **normal** experiment. Each spectrum of the **APS** had two peaks centered near 190 Hz and 510 Hz. The major difference between these spectra and the **normal** spectrum was a loss of power as the stroke volume decreased. This difference was 10 db for the peaks at 510 Hz but only 2 db for the peaks at 190 Hz. Again the low-frequency peak was associated with collisions of the occluder and the high-frequency peak was associated with vortex-shedding at the phonocatheter and possibly at the struts. We have seen once again that remarks made earlier with regard to the systolic sounds of experiments involving different pulse rates and stroke volumes also apply to the present group of experiments: transient sounds and non-transient sounds occur; the spectra of systolic sounds of the **APS** decrease in power with the stroke volume, occur earlier in systole as the stroke volume decreases; and, as the stroke volume approaches zero the shape of the spectrum of the systolic sound becomes similar to that of the spectrum of the opening sound.

One new point should be emphasized relative to the power-density spectra for the systolic sounds of the hypertensive experiments. The peaks centered near 190 Hz are significantly less powerful in the lower band having frequencies form 10 to 100 Hz. This fact is depicted graphically in the spectra as well as the distribution functions that were plotted immediately below them. The distribution of power for the **APS** were flat over this low-frequency range relative to the more curved shape of the power-distribution of the **normal** systolic sound.

Subfigures 5-8 to 5-9 b,c,d, and h again show these differences in their own characteristic manner. Here we see the significant decrease of the total power of the hypertensive, systolic sounds and their early occurrance. These differences are directly shown by the valley between 10 and 600 Hz along the contour corresponding to window 13 in Figure 5-10h and by the similar valley between 10 and 600 Hz along the contour for window 13 in Figure 5-11h.

5.4.3.3 The Closing Sounds

Like all previous experiments involving the Smeloff prosthesis, the closing sounds, CS, of experiments 292, 297 and 298 were very similar to each other. They were comprised of two events, CS1 and CS2, and are labeled nearest their occurrence along the upper tracings of Figures 5-5a, 5-10a and 5-11a. Again, the closing sound CS1 occurred at the same time as the maximum backflow, the dichrotic notch of the aortic pressure curve, and the beginning of the rapid decrease of the ventricular pressure curve. The second closing sound CS2 occurred at the same time as the highest value of the diastolic aortic pressure. The spectra of the hypertensive closing-sounds were essentially identical with that of the **normal** case. These three spectra are shown in Figures 5-5g, 5-10g and 5-11g.

The power distributions of the closing sounds that are represented by windows 23, 20 and 21 and depicted in Figures 5-5, 5-10 and 5-11, subfigures b,c,d and h, respectively, are identical in form. They have comparable total-powers. Differences do appear, however, in the 3-D difference-surfaces depicted in Figures 5-10h and 5-11h. As we would expect from the previous statements, these differences are with respect to the timing of the closing sound. Such differences appear as a peak/valley combination along the 10 Hz contour between windows 17 and 24 in Figures 5-10h and 5-11h. Since the closing sounds are so similar relative to their power distributions, this peak/valley combination indicates differences that are of a purely temporal nature because they are symmetric about the mid-window contour parallel to the frequency axis.

5.4.3.4 Summary of Comparisons of Hypertensive Experiments

The effect of mean aortic pressures of 86, 145, and 135 mmHg upon the opening sounds of the Smeloff valve at a pulse rate of 70 beats/min was minor. The only significant change, a slight decrease of the total power, was explained by the secondary changes caused by reduction of the stroke volume.

The primary effect of hypertension upon the systolic sound was to shift this sound earlier in systole as the stroke volume decreased and to decrease the power of the non-transient component, centered near 500 Hz, as the stroke volume decreased. The transient component of the systolic spectrum was not significantly changed. These changes produced a corresponding decrease of the total power of the systolic sound with decreasing stroke volume. Again, these changes were explainable by changes of the stroke volume and not directly by the hypertensive condition.

The effect of hypertension upon the closing sound of the Smeloff valve was

insignificant in the frequency domain. A significantly early closing sound was observed for both hypertensive experiments. These changes were also attributed to reduction of the stroke volume.

5.4.4 Effects of Orientation on the Sounds

The Smeloff valve was pulsed at two different orientations with respect to gravity. The experiments illustrating these conditions were 292 and 300. Corresponding orientations are shown in Figure A-2 of Appendix A. The orientation of the valvar struts relative to the sinuses of Valsalva did not change but a rotation of the struts by 60 degrees was made with respect to gravity. During experiment 292, the force of gravity was directed from the center of mass of the occluder directly toward a single, lower strut, whereas during experiment 300, this force was directed between two struts. By inspecting the entries involving pressure and flow in appropriate columns of Table 5-1a, it is clear that there was essentially no other difference between the pulsatile states during these two experiments. Any significant differences would therefore be a result of the change of orientation.

5.4.4.1 The Opening Sounds

In a manner similar to the previous comparisons involving changes of pulse rate, stroke volume and mean, aortic pressure, the opening sounds, OS, produced by the Smeloff valve for these three experiments have been labeled OS1 and OS2 nearest their occurrence along the upper tracings of Figures 5-5a and 5-12a. The occluder began its motion downstream at about the time OS1 occurred and arrives at the apex of the downstream cage at the time OS2 occurred. The normal time interval between OS1 and OS2, 50 ms, is the identi-

cal for both experiments. The values of the rate of change of the ventricular pressure prior to opening were also identical. We would therefore expect to see similarities in the opening sounds for these experiments. The sounds appear identical in the time domain.

If one examines the power-density spectra of the opening sounds plotted in Figures 5-5e and 5-12e and the corresponding parameters that have been listed in Tables 5-2 and 5-9, one can see that these spectra have essentially two peaks with approximately the same center-frequencies and amplitudes.

These opening sounds can be compared further by inspecting the window-5 contours in Figure 5-5 and Figure 5-12, subfigures b,c,d, and h, which correspond to these two experiments. A direct comparison is provided by Figure 5-12h. This figure indicates no difference between the opening sounds because the contour of window 5 is flat over the band 10-1000 Hz.

5.4.4.2 The Systolic Sounds

The systolic sounds were also similar for experiments 292 and 300. The systolic sound, SS, is depicted nearest its occurrence along the upper tracings of Figures 5-5a and 5-12a. The timing of the maximum amplitude is similar for both experiments. The amplitudes of the peaks of the power-density spectra depicted in Figures 5-5f and 5-12f should not be compared because Figure 5-12f corresponds to window 12 which occurs one window prior to the window having the maximum value of total systolic power. The center-frequencies, however, can be compared are are similar in both spectra. One can compare the power-distributions of window 13 by inspecting the subfigures b,c and h of Figures 5-5 and 5-12. The similarity between these two systolic sounds is directly shown by the flat contour corresponding to window 13 in Figure 5-12h.

5.4.4.3 The Closing Sounds

Like all of the previous experiments involving the Smeloff prosthesis, the closing sounds, CS, of experiments 292 and 300 were very similar to each other. They were comprised of two events, CS1 and CS2, and are labeled nearest their occurrence along the upper tracings of Figures 5-5a and 5-12a. Timing of the closing sounds was **normal** during both experiments. The spectra of the closing sounds, shown in Figures 5-5g and 5-12g, are identical within experimental error. The power distributions of the closing sounds that are depicted in Figures 5-5 and 5-12, subfigures b,c,d and h, respectively, are identical in form. These similarities are depicted in Figure 5-12h by the flat contour corresponding to window 23.

5.4.4.4 Summary of Comparisons of Orientation Experiments

When all other factors were constant, the effect of rotating the Smeloff valve 180 degrees relative to gravity and zero degrees relative to the sinuses produced no significant changes in the sounds. The opening, systolic and closing sounds were the same within experimental error. Note especially the overall flatness of Figure 5-12h.

5.5 CONCLUSIONS AND RECOMMENDATIONS

It is apparant from the results presented in this paper that the effects of pulse rate, stroke volume and hypertension upon the three major sounds were significant for the Smeloff valve.

The opening sounds under all of the pulsatile conditions did not change significantly relative to corresponding changes of the systolic and closing

sounds. We did observe an increase of the total power of the opening sound with an increase in the rate of change of the ventricular pressure and stroke volume.

Of the three major sounds, the most significant changes occurred with respect to the systolic sounds. This sound occurred early or late depending whether the stroke volume was greater or less than **normal**. We observed that the total-power of the systolic sound changed dramatically and correlated very well with the stroke volume, maximum systolic flow rate, mean flow rate, and maximum systolic pressure gradient. A low-frequency peak, associated with the collisions of the occluder with the downstream cage, was present in each systolic spectrum, and a high-frequency peak associated with vortex shedding at the phonocatheter and possibly the struts also appeared in each systolic spectrum.

The closing sounds of the Smeloff valve were very similar relative to both the opening and systolic sounds. The time of closure was later with increasing stroke volume. The total power of the closing sound did not change significantly with increased stroke-volume. The total power of the closing sound did increase, however, with increasing magnitude of the rate of change of ventricular pressur evaluated 20 ms prior to CS1. The spectra of these sounds were very similar for each experiment except for the case having a large stroke volume. For this case, the total power of the closing sound was 8.6 RPU more than the **normal** value of 79.8 RPU. This particular experiment also involved a large rate of change of ventricular pressure at the time of closing and other extraordinary dynamics of the ventricular pressure-curve. These combined effects produced this increase of acoustical power in the closing sound.

We observed some general similarities and differences between valve designs. We shall reserve these comments for the Conclusions section of Part VI. At that time we will have discussed all three valvar designs and comments concerning

all three valves will be more appropriate. Recommendations associated with Parts IV, V and VI are given at the end of Part VI.

5.6 ACKNOWLEDGEMENTS

Funding for this project was provided by the Donald E. Baxter Foundation, the Children's Heart Foundation of Southern California, and the American Heart Association, Greater Los Angeles and Georgia Affiliates.

PAPER 6

A Quantitative Method for the *In Vitro* Study of Sounds Produced by Prosthetic Aortic Heart Valves Part VI: An Experimental, Comparative Study of the Sounds Produced by a Normal Bjork-Shiley Aortic Prosthesis Operating at Five Pulsatile States

A Quantitative Method for the *In Vitro* Study of Sounds Produced by Prosthetic Aortic Heart Valves

Part VI: An Experimental Comparative Study of the Sounds Produced by a Normal Bjork-Shiley Spherical-Aortic Prosthesis Operating at Five Pulsatile States

ABSTRACT

An *in vitro* study was made of the sounds produced by a normal, Bjork-Shiley spherical aortic-valve prosthesis and comparisons were made of the sounds produced by the same valve operating at five different pulsatile states. All results were then compared and discussed in terms of the pulstatile changes which included pulse rate, stroke volume and hypertension.

Useful information about the pulsatile state was provided by this analysis. The opening sounds and closing sounds were influenced primarily by the rate of change of the ventricular pressure prior to these events. The systolic sounds were primarily influenced by the systolic flow rate. Changes of systolic sounds were much greater than associated changes between opening and closing sounds for all cases. An increase in systolic flow rate produced a corresponding increase in the power associated with the systolic sound. These values correlated quite well. The location of peaks within the power density spectra were very similar for these states when compared to previous studies involving abnormal valvar states operating at similar pulsatile states.

Key Words-Bjork-Shiley spherical prosthesis, sound, fast Fourier transform *in vitro* comparison

6.1 INTRODUCTION

This paper investigates the effects of five pulsatile states on the sounds produced by a normal 25mm Bjork-Shiley spherical aortic heart-valve prosthesis. This prosthesis is of the tilting-disk variety. The misleading term "spherical" occluder refers to the fact that the surface of one side of the disk has a spherical shape, but the radius of curvature is very large. Thus, the term refers to only a small portion of a spherical surface. This term is used to differentiate this valve from the Bjork-Shiley convexo-concave design. The occluder is fabricated of pyrolytic carbon. It is held in place by two Stellite struts each of which originate and end at the orifice. The orifice is Stellite and the sewing fabric is Teflon. The diameter of the disk is less than the inner diameter of the orifice. Therefore, this Bjork-Shiley valve, like the Smeloff valve, has a normal amount of backflow associated with it during the diastolic period. The disk opens to approximately 60 degrees relative to its closed position. This angle causes a significant degree of asymmetry relative to the axis of the aorta. A major and minor flow region exists because the line-of-pivot is not located along the center of the disk. We have pulsed a normal Bjork-Shiley valve of the sperical occluder design at a normal and four alternate pulsatile states **APS** and compared the results in a manner similar to previous results involving the Starr-Edwards 2400 and Smeloff valves described in Papers IV and V, respectively. All experimental methods and analysis were identical with those described in Papers IV, V and VII. The **APS** of interest were those involving changes in the pulse rate, changes of the stroke volume, and changes of mean aortic pressure. Stroke volume was changed independently of the pulse rate and elevated the mean aortic pressure by relatively small values. Changes of the pulse rate and mean aortic pressure

were obtained by changes of the ventricular ejection time and systemic resistance, respectively. The stroke volume increased or decreased according to these changes. Therefore, the experiments which include changes of pulse rate and hypertension also involved changes of the stroke volume

6.2 EXPERIMENTAL METHOD

The pulse rates, pressures, flow, and acoustical powers for the opening, systolic, and closing sounds are listed in Table 6-1a for each of the five pulsatile states. The entries involving the rate of change of ventricular pressure assigned to opening and closing were evaluated 20 ms prior to OS2 and CS1, respectively. Backflow was estimated from the digitized flow data and the portion due to closure was estimated by the area under the zero-flow line and above the negative flow region of the primary "notch" in early diastole. The effective flow area, A_{eff} was estimated by Equation 4-1. Table 6-1b lists the times of the significant events of the sound pressure and flow relative to the time of full valvar opening. We shall call experiment 266 the **normal** pulsatile state for the Bjork-Shiley design. Comparisons between experiments will be with respect to this **normal** state. The orientation of the valve was the same for each experiment and it is depicted in Figure A-2 of Appendix A.

6.3 PRESENTATION OF RESULTS

The results of the five experiments are presented graphically in Figures 6-1 through 6-9. Figure 6-1 shows a plot of the maximum pressure gradient across the valve as a function of the maximum flow rate for each experiment. Figure 6-2 shows the maximum pressure gradient across the valve plotted as a function of the mean flow rate for each experiment. Figure 6-3 shows a plot of the aver-

Pressure, Flow and Sound* Data corresponding to experiments involving a normal 25mm spherical Bjork-Shiley Valve

Experiment Number	265	266	267	271	272
Pulse Rate (cycles/min)	70	70	70	52	75
Max. Pressure Gradient (mmHg)	46	10	5	21	12
Mean Systolic Pressure Gradient (mmHg)	30	5	3	12	10
Mean Aortic Pressure (mmHg)	126	92	164	116	73
Opening rate of change of V. Pressure (mmHg/ms)	2.6	1.6	1.0	1.6	1.0
Closing rate of change of V. Pressure (mmHg/ms)	-1.0	-1.0	-0.3	-0.6	-1.0
Mean flow rate (l/min)	6.8	3.6	1.2	5.6	3.0
Maximum flow rate (l/min)	40.0	20.5	14.1	29.6	22.8
Stroke volume (cc)	105	58	32	116	47
Total backflow (cc/cycle)	7	7	15	10	8
Backflow due to closure (cc/cycle)	1	1	1	1	1
Total backflow (% of stroke volume)	7	12	47	9	17
Effective flow area (sq cm)	2.7	3.0	3.0	3.0	3.0
Opening window number	5	5	5	5	5
Average total power (RPU)	2.6	1.7	0.6	1.7	0.6
Std. deviation (RPU)	0.3	0.3	0.1	0.3	0.1
Systolic window number	13	12	11	13	11
Average total power (RPU)	31.0	5.7	0.9	4.6	2.5
Std. deviation (RPU)	12.0	2.3	0.3	2.1	1.4
Closing window number	21	21	19	22	19
Average total power (RPU)	97.2	92.7	64.2	79.5	80.2
Std. deviation (RPU)	1.0	2.5	5.3	0.8	1.3

*Filter bandwidth: 200-2000 Hz

Table 6-1a Pressure-Flow-Sound data for experiments involving the normal 25mm Bjork-Shiley spherical aortic valve.

Times of significant events of pressure, flow and sound relative to the time of full valvar opening in milliseconds for experiments involving a normal 25mm spherical Bjork-Shiley valve operating at various pulsatile states

Experiment Number	265	266	267	271	272
First Component of Opening Sound (OS1)	-30	-45	-45	-50	-45
Start of Systolic Ejection	-15	-20	-10	-15	-20
Second Component of Opening Sound (OS2)	0	0	0	0	0
Maximum Systolic Pressure Gradient	155	95	85	160	110
Maximum Systolic Flow Rate	135	125	105	175	110
Maximum Amplitude of Systolic Sound (SS)	160	140	110	175	95
First Component of Closing Sound (CS1)	245	260	205	345	195
End of Systolic Ejection	255	260	205	360	200
Second Component of Closing Sound (CS2)	285	295	240	395	235

Table 6-1b Times of Significant Events of Sound, Pressure and Flow for Experiments involving the Bjork-Shiley valve.

age value of the total power of the systolic sound as a function of the maximum pressure gradient rate for each experiment. Figure 6-4 shows the average value of the total power of the systolic sound plotted as a function of the mean flow rate for each experiment. Figures 6-5 through 6-9 are separated into eight subfigures indexed alphabetically with letters from **a** to **h**. Subfigure **a** of each Figure between 6-5 and 6-9 shows the original time-amplitude tracings of the sound, flow rate, and ventricular and aortic pressures corresponding to one cycle of the associated experiment. Subfigure **b** shows the three-dimensional power-frequency-time surface corresponding to the sound. Subfigures **c** and **d** depict auxiliary views of each 3-D surface as it would be seen parallel to the frequency axis and time axis, respectively. Subfigures **e**,**f** and **g** depict the power-density spectra associated with windows which encompassed the opening, systolic, and closing sounds, respectively. These three windows were also enhanced in subfigures **b** and **c**. Finally Subfigure **h** depicts the 3-D difference-surface generated by subtracting the 3-D surface corresponding to the **normal** case, shown in Figure 6-6b, from those corresponding to Figures 6-5b, 6-7b through 6-9b, respectively. Parameters for each peak in the power-density spectra have been included with the plots. These parameters have also been listed separately for each experiment in Tables 6-2 through 6-6 which can be found on the pages which immediately follow the plots of the spectra of the closing sounds. Another list of the parameters is provided in Tables A-1 through A-6 of Appendix A. These latter tables provide quick, overall comparisons of the results of the parameter estimation. They are especially useful for comparing parameters estimated from spectra associated with different valvar designs.

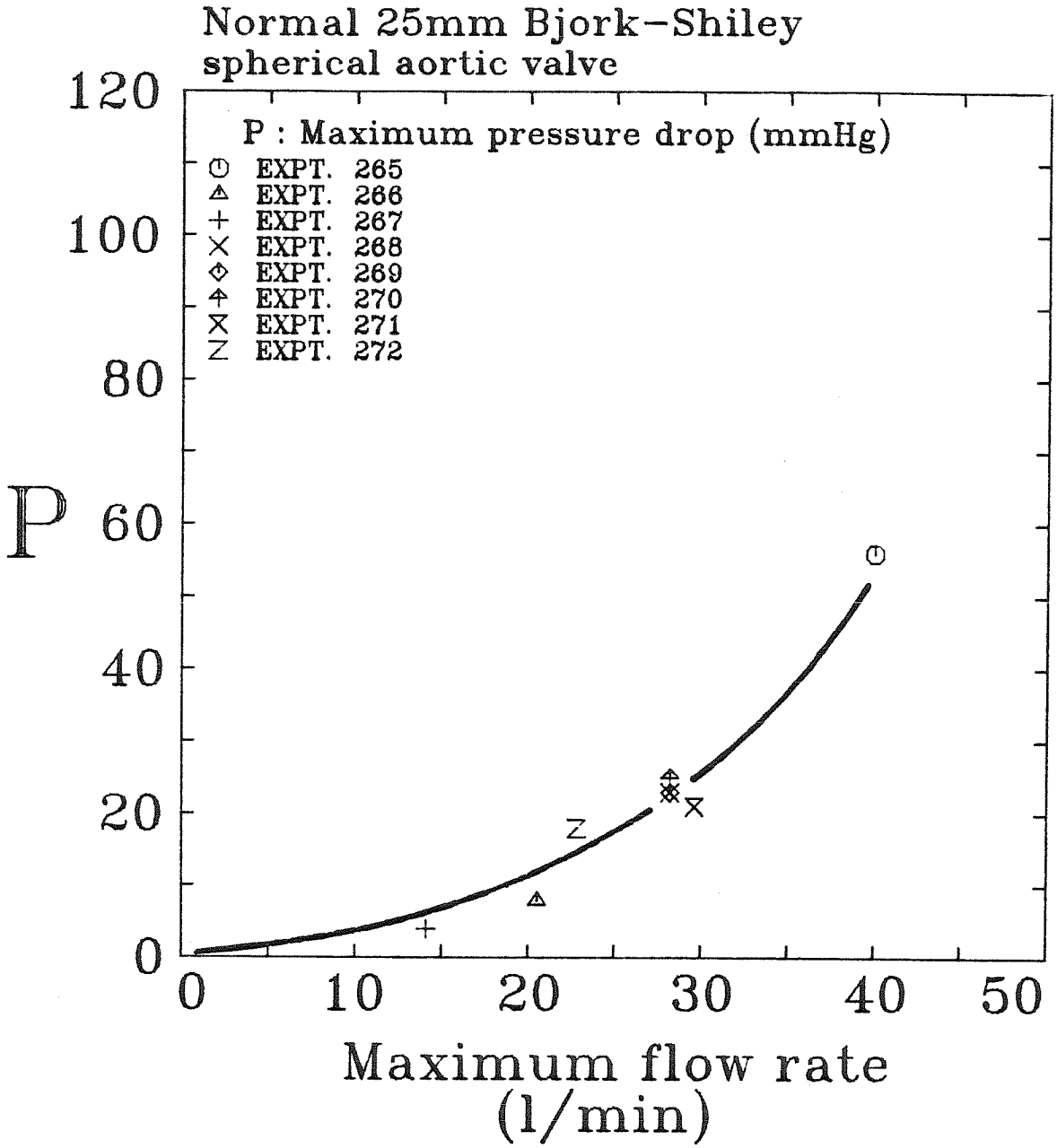

Figure 6-1 Maximum pressure gradient vs. maximum flow rate for the experiments with the normal 25mm Bjork-Shiley spherical aortic prosthesis.

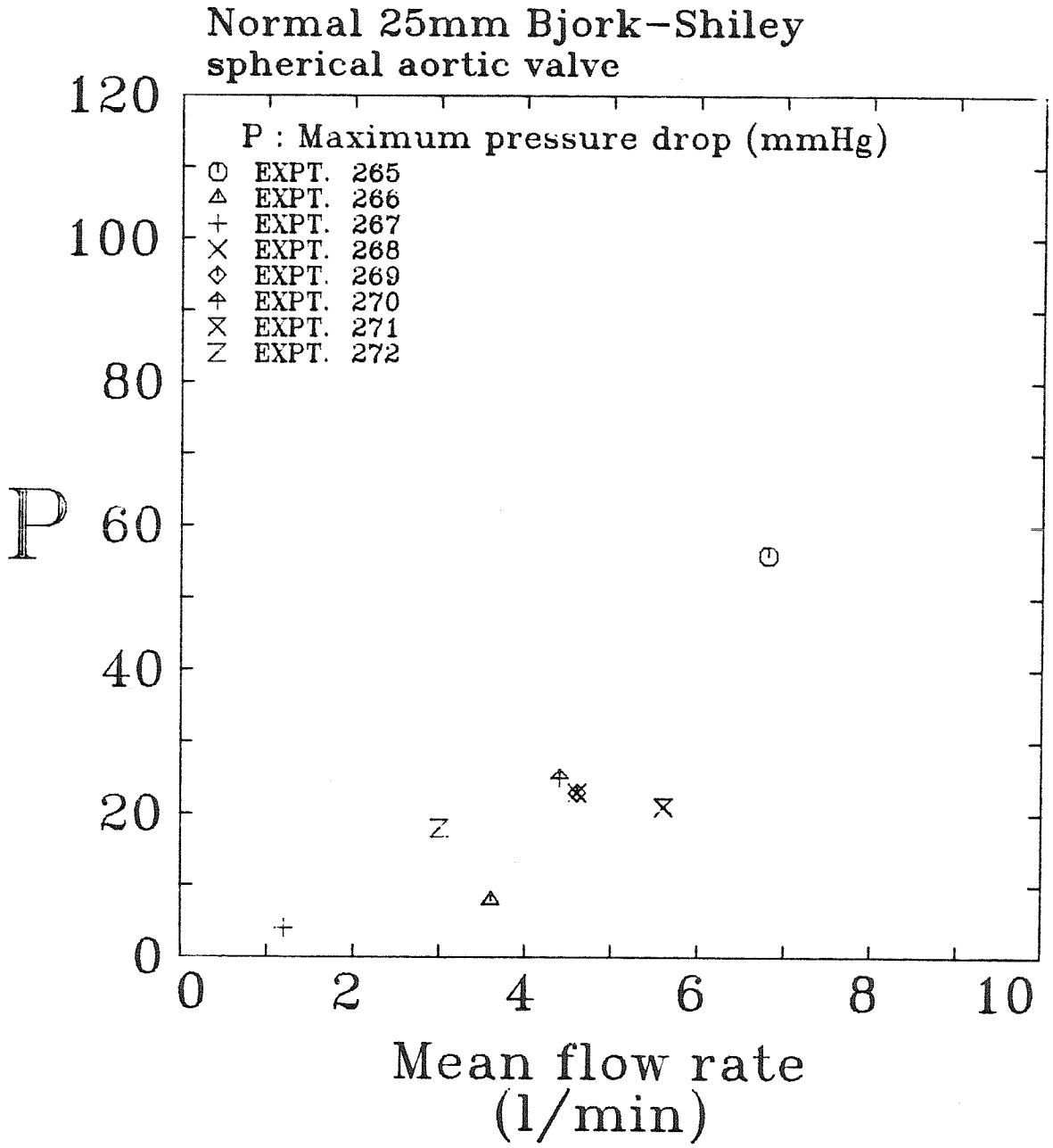

Figure 6-2 Maximum pressure gradient vs. mean flow rate for the experiments with the normal 25mm Bjork-Shiley shperical aortic prosthesis.

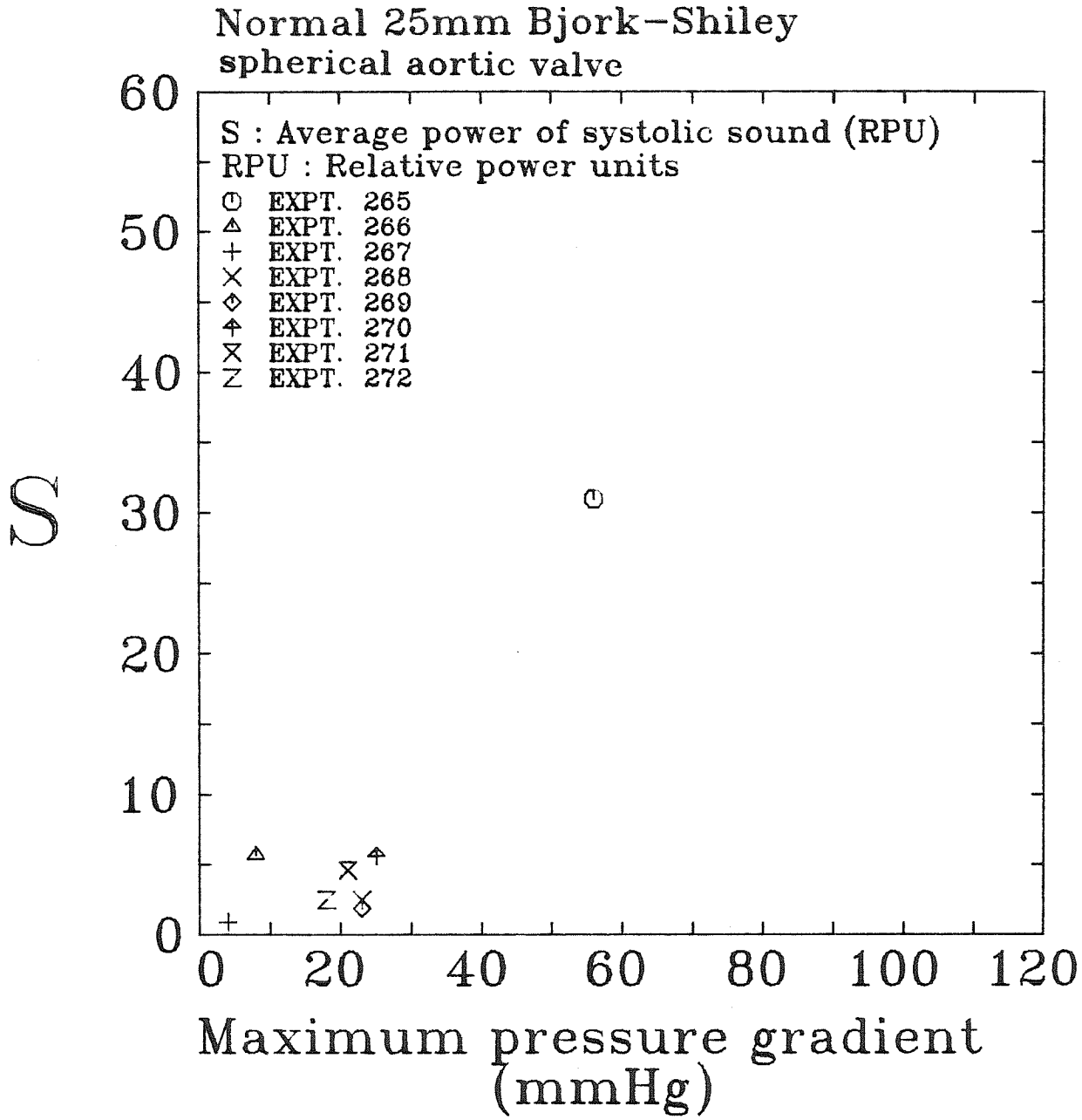

Figure 6-3 Average total-power of systolic sound vs. maximum pressure gradient for the experiments with the normal 25mm Bjork-Shiley spherical aortic prosthesis.

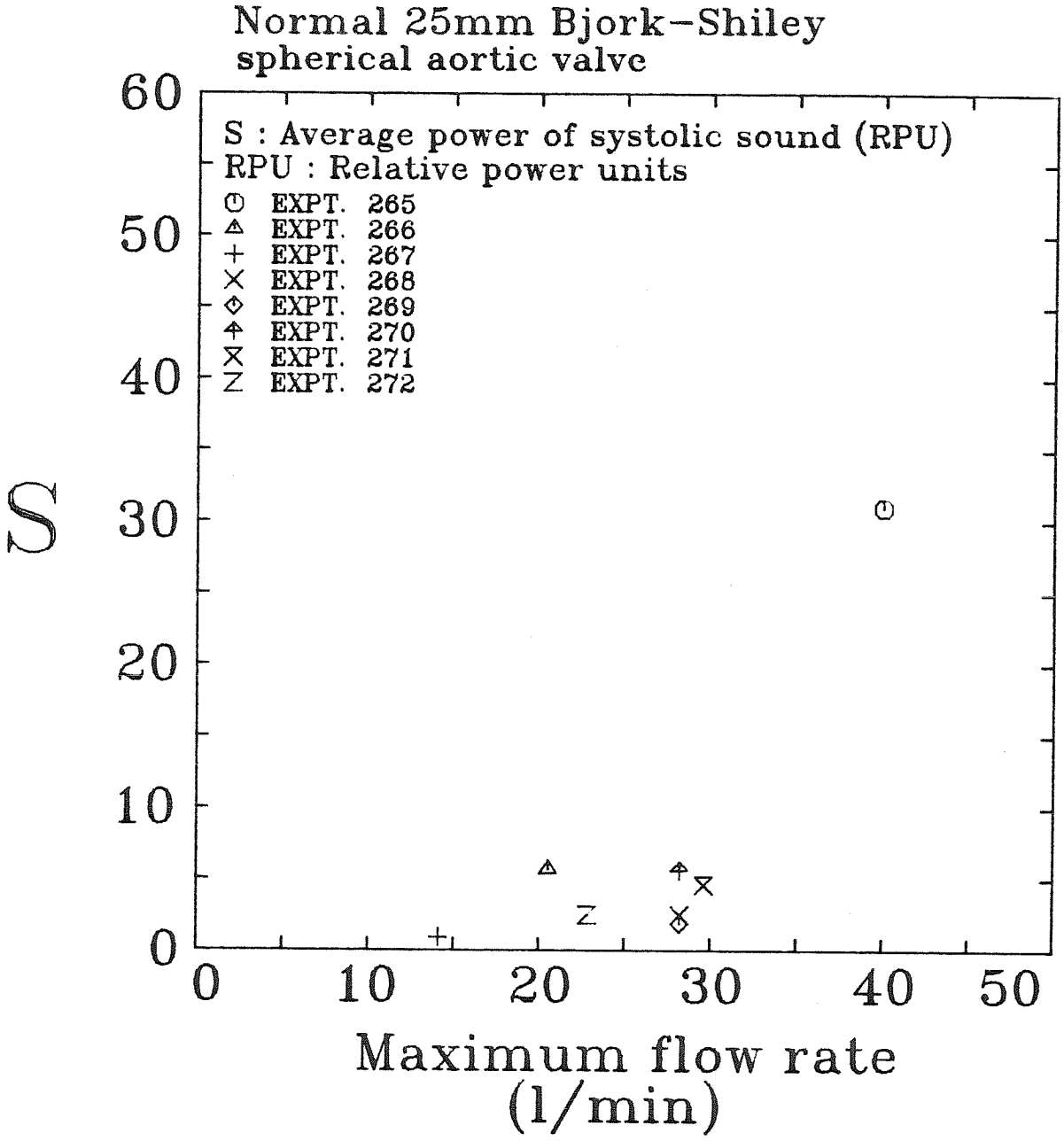

Figure 6-4 Average total-power of systolic sound vs. maximum flow rate for the experiments with the normal 25mm Bjork-Shiely spherical aortic prosthesis.

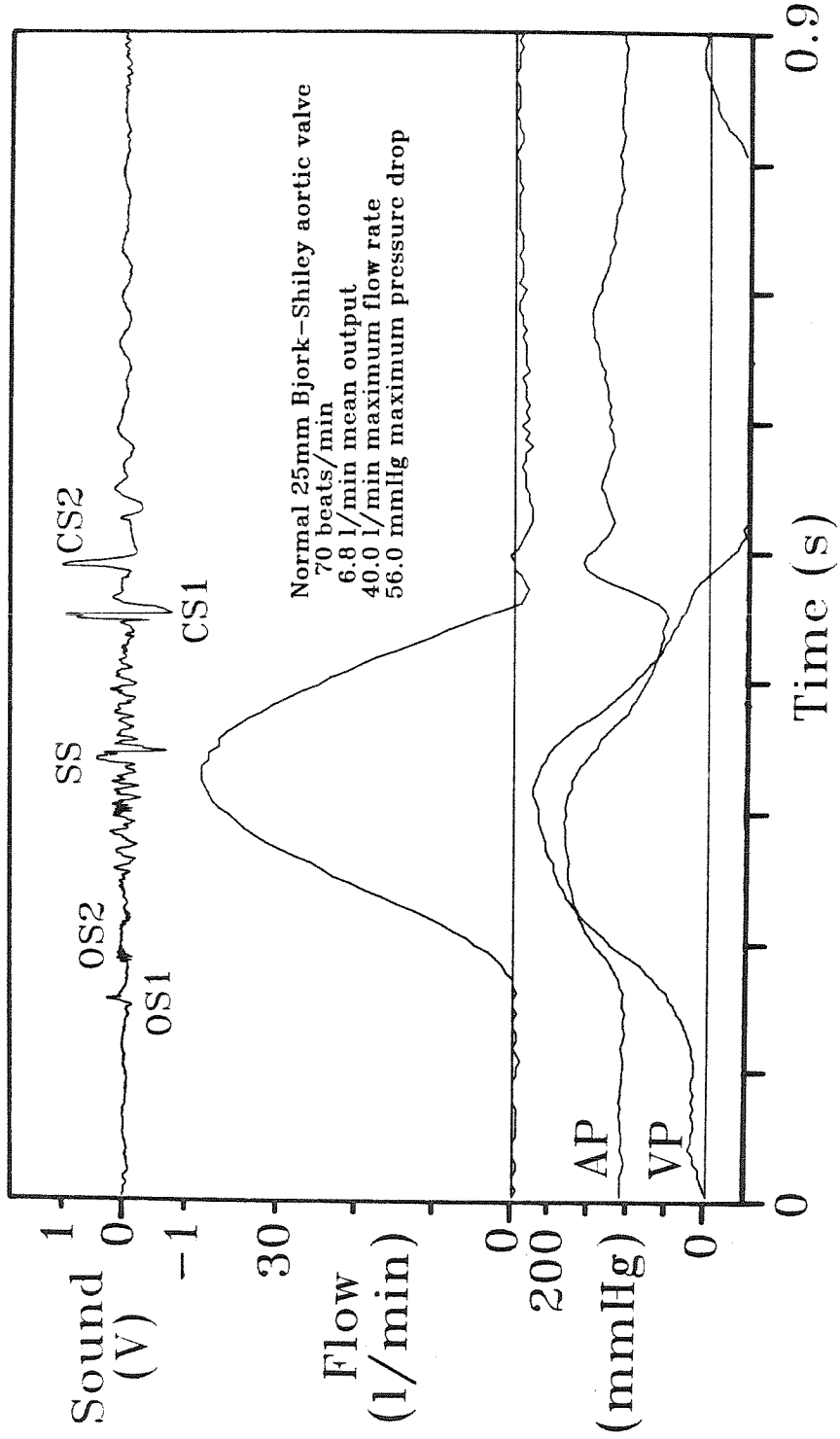

Figure 6-5a Amplitude vs. time tracings of sound, flow rate, aortic pressure and ventricular pressure associated with a typical cycle of experiment 265.

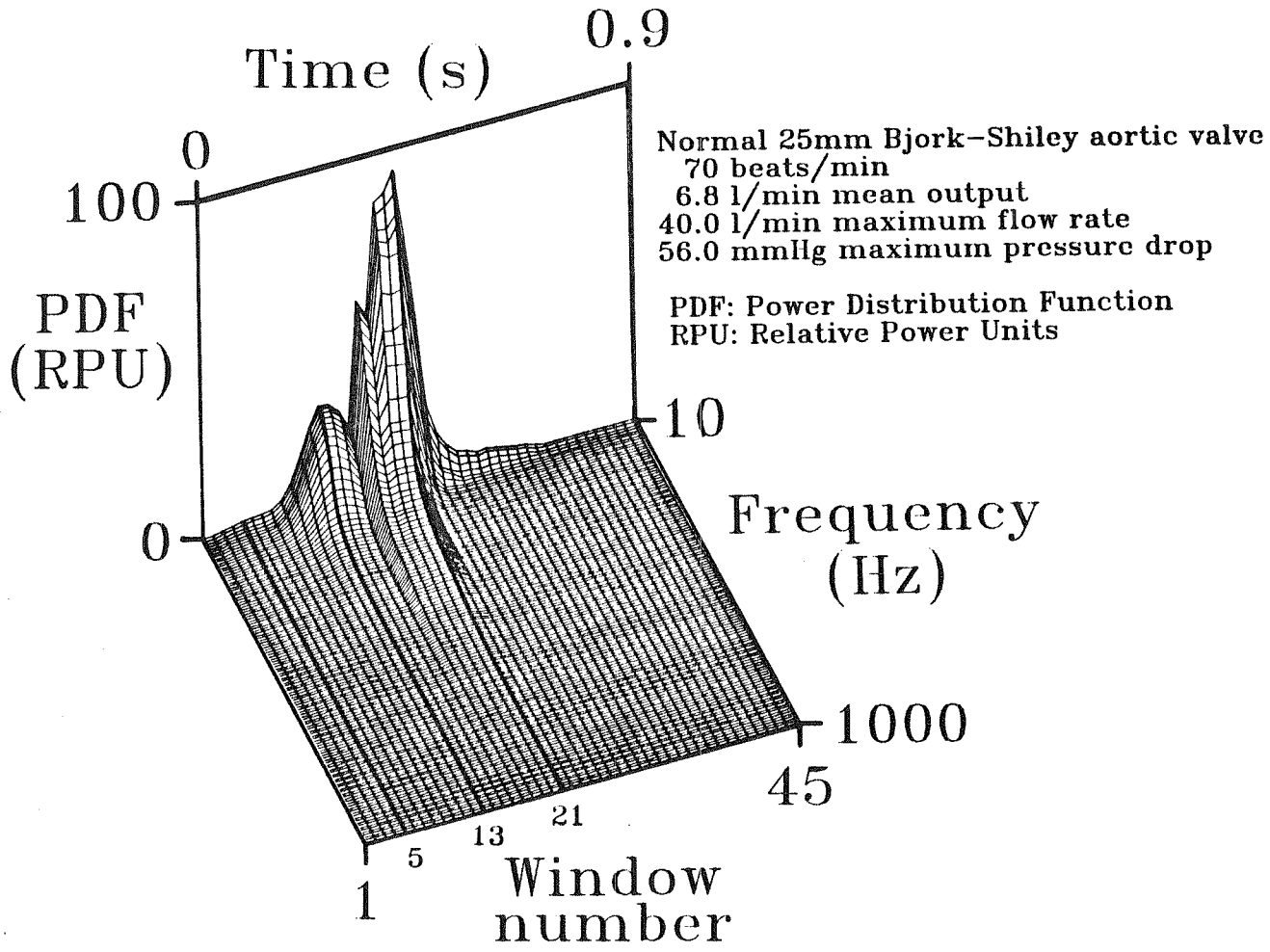

Figure 6-5b Three-dimensional power-frequency-time surface averaged over ten cycles of experiment 265.

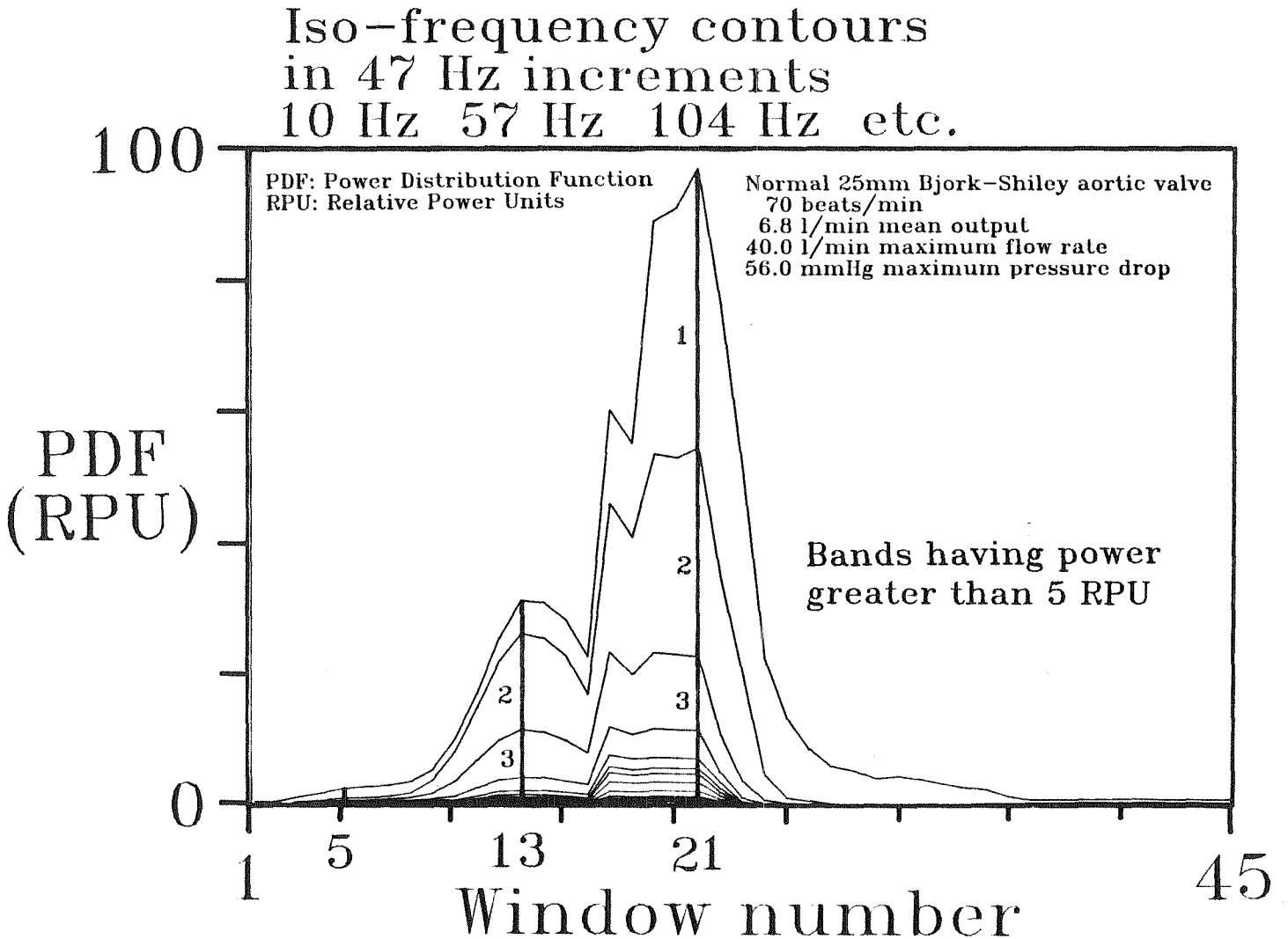

Figure 6-5c Auxiliary view perpendicular to the time axis of the 3-D power-frequency-time surface of experiment 265 showing iso-frequency contours.

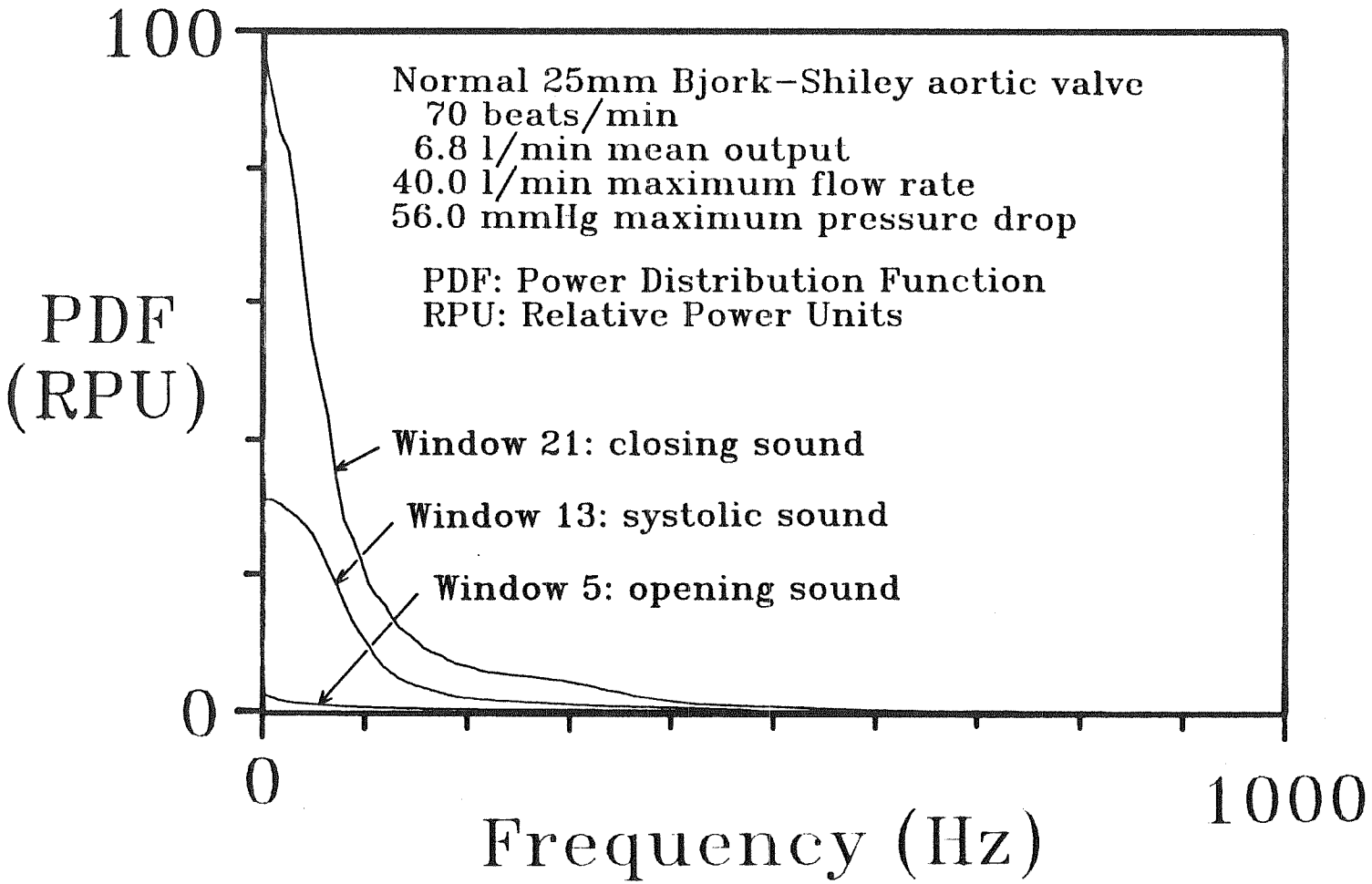

Figure 6-5d Auxiliary view perpendicular to the frequency axis of the 3-D power-frequency-time surface of experiment 265 showing power power distributions associated with windows encompassing the opening, systolic, and closing sounds.

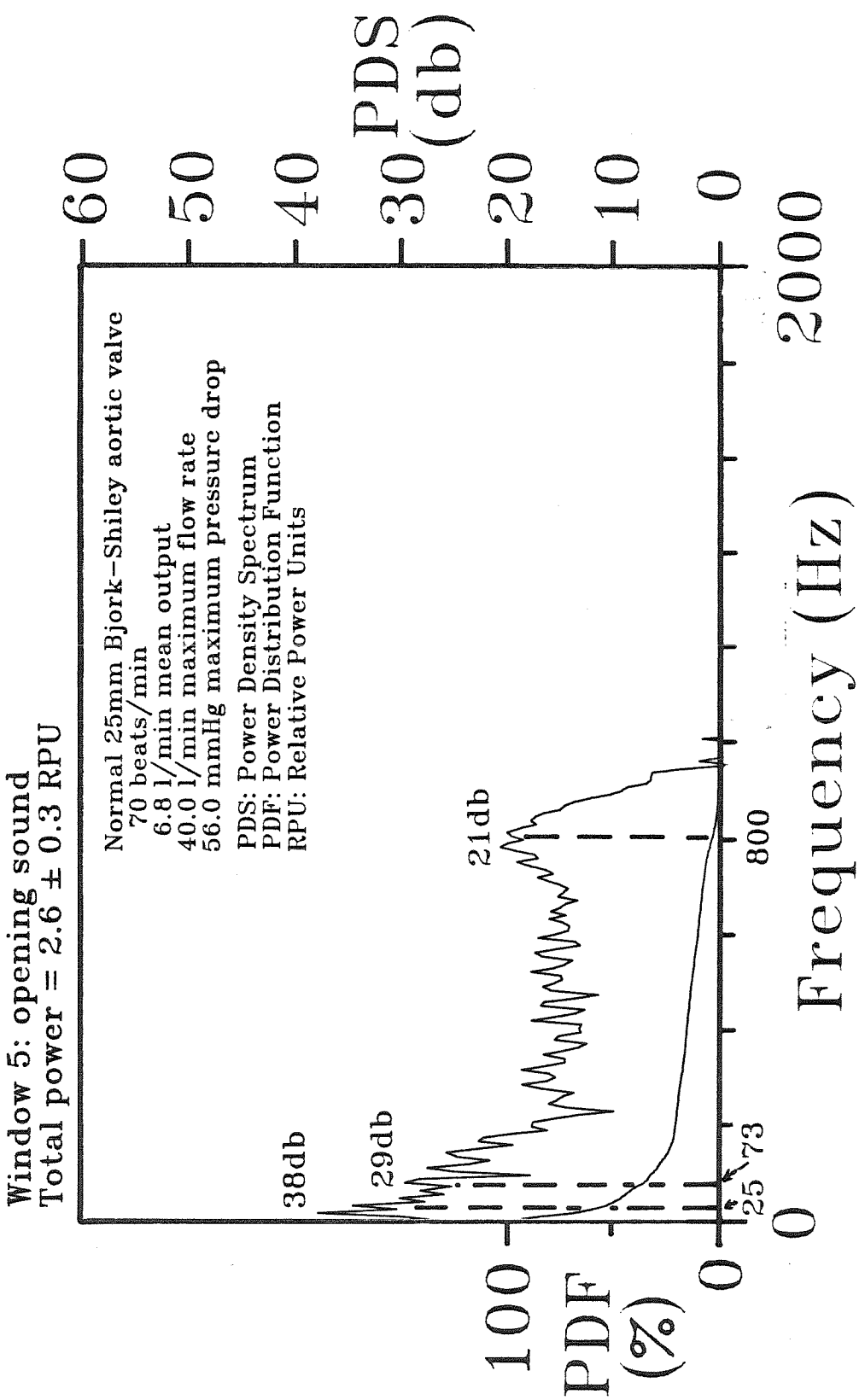

Figure 6-5e Power-density spectra and power distribution of the opening sound of experiment 265.

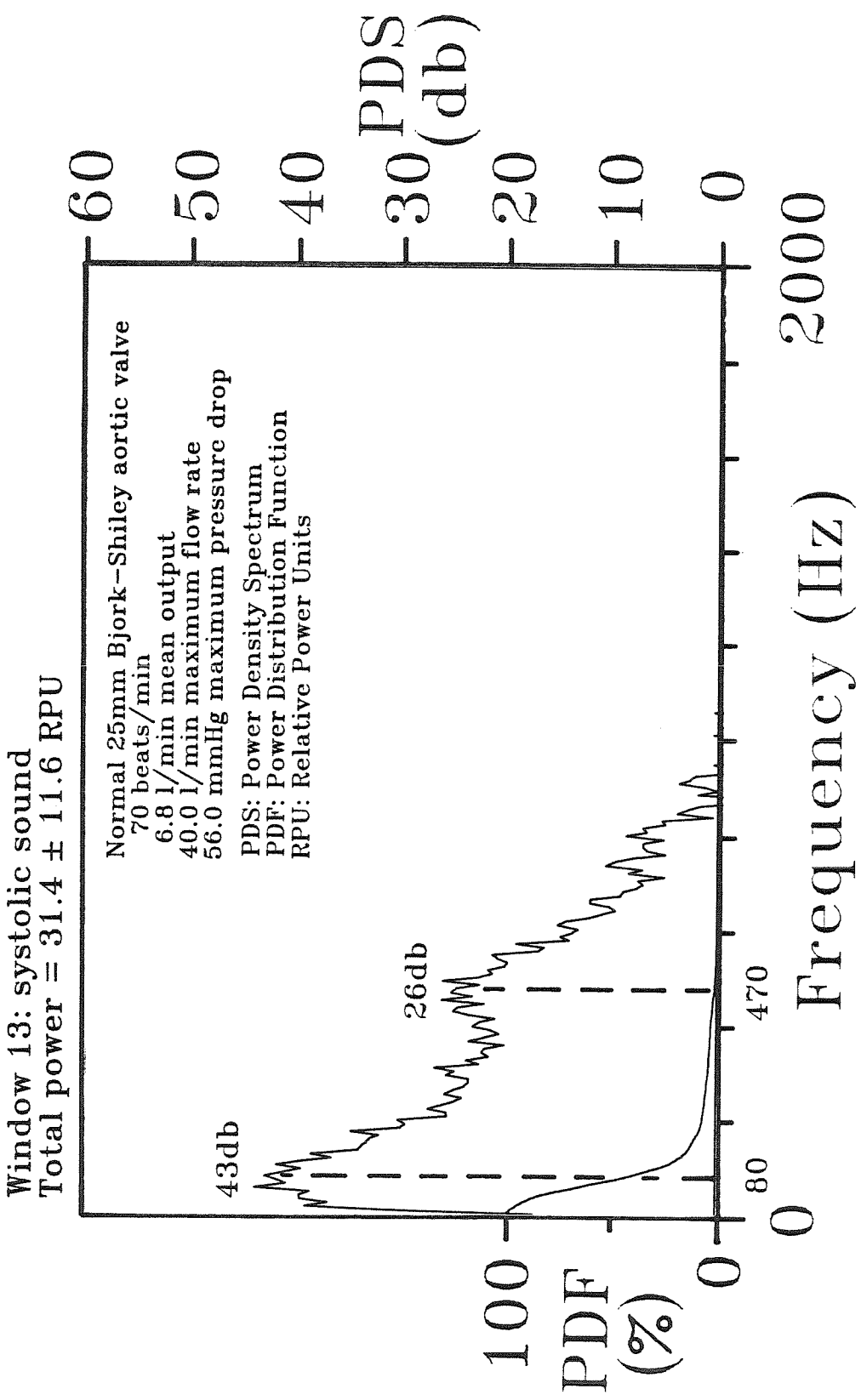

Figure 6-5f Power-density spectra and power distribution of the systolic sound of experiment 265.

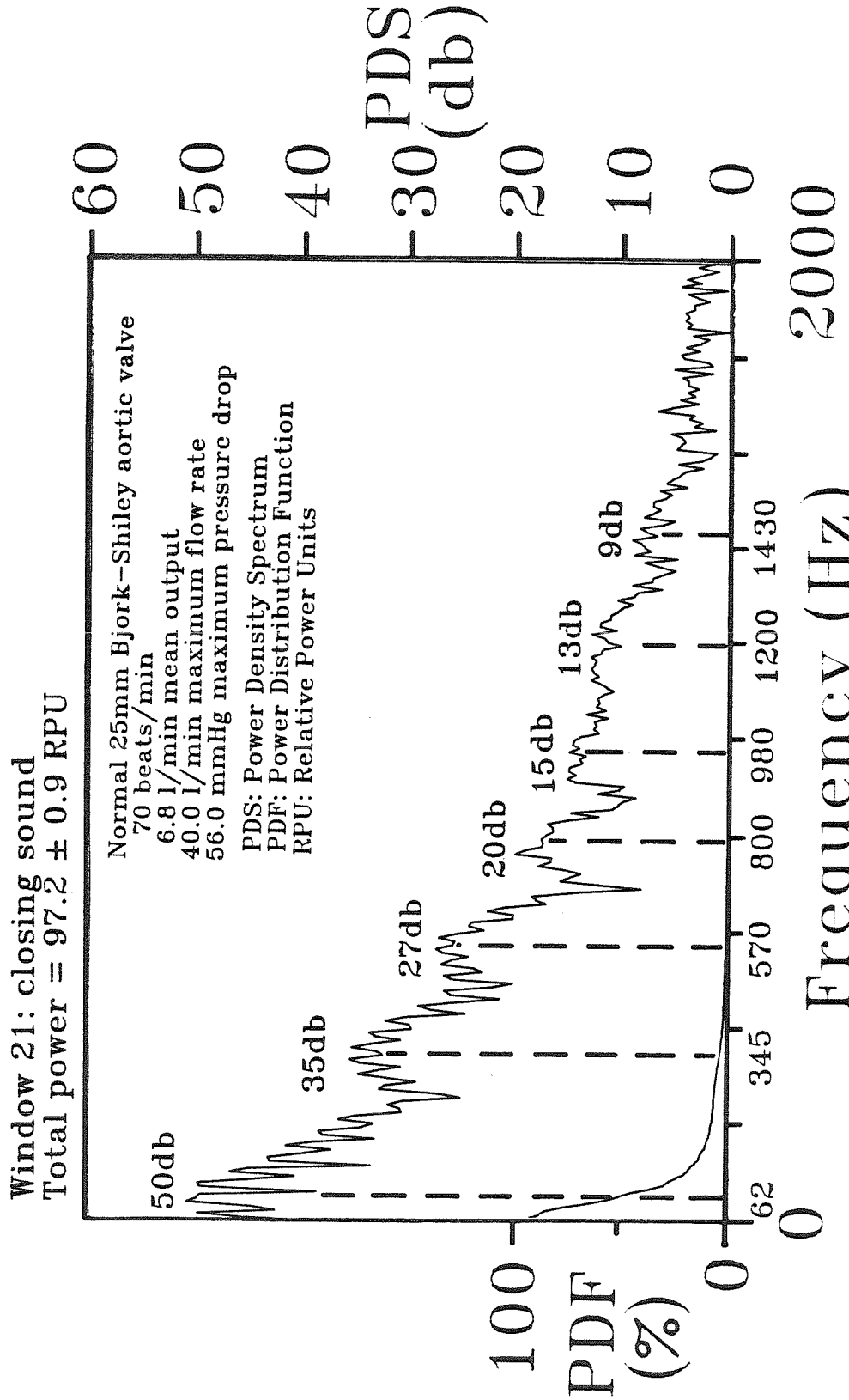

Figure 6-5g Power-density spectra and power distribution of the closing sound of experiment 265.

Parameters Estimated for

Significant Harmonic Peaks

Experiment 265

Event	Frequency, $f_{f,i}$; Decay, k_i; Power-Density, G_i (Hz,Hz,db)
Opening Sound	25, 5,38
Window 5	73,15,29
	800,65,21
Systolic Sound	80,45,43
Window 13	470,45,26
Closing Sound	62,40,50
Window 21	345, 65,35
	570, 65,27
	800, 55,15
	980, 55,15
	1200,110,13
	1430, 80, 9

Table 6-2 Parameters estimated from significant harmonic peaks of experiment 265.

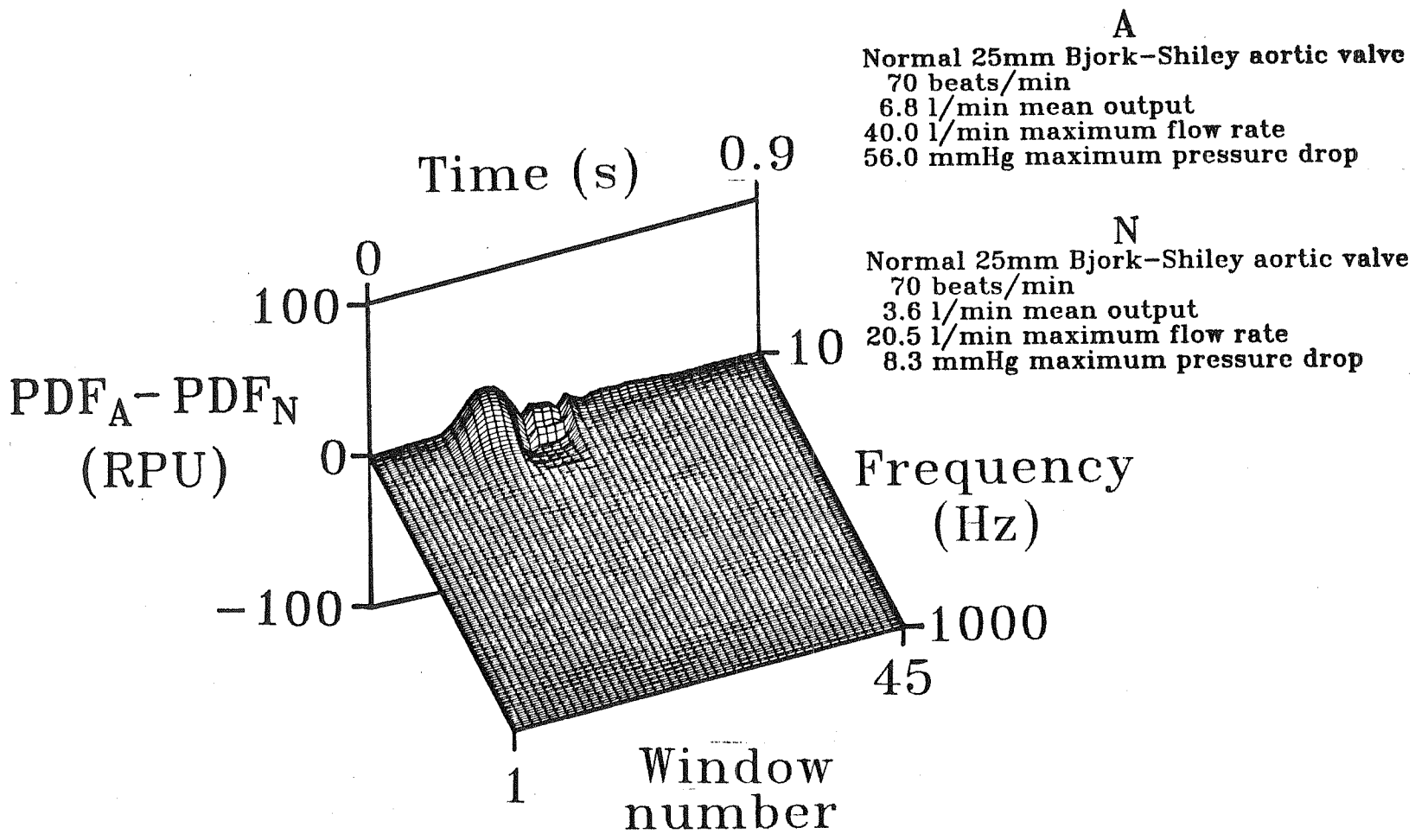

Figure 6-5h Three-dimensional surface depicting the difference between the power-frequency-time surfaces associated with experiments 265 and 266.

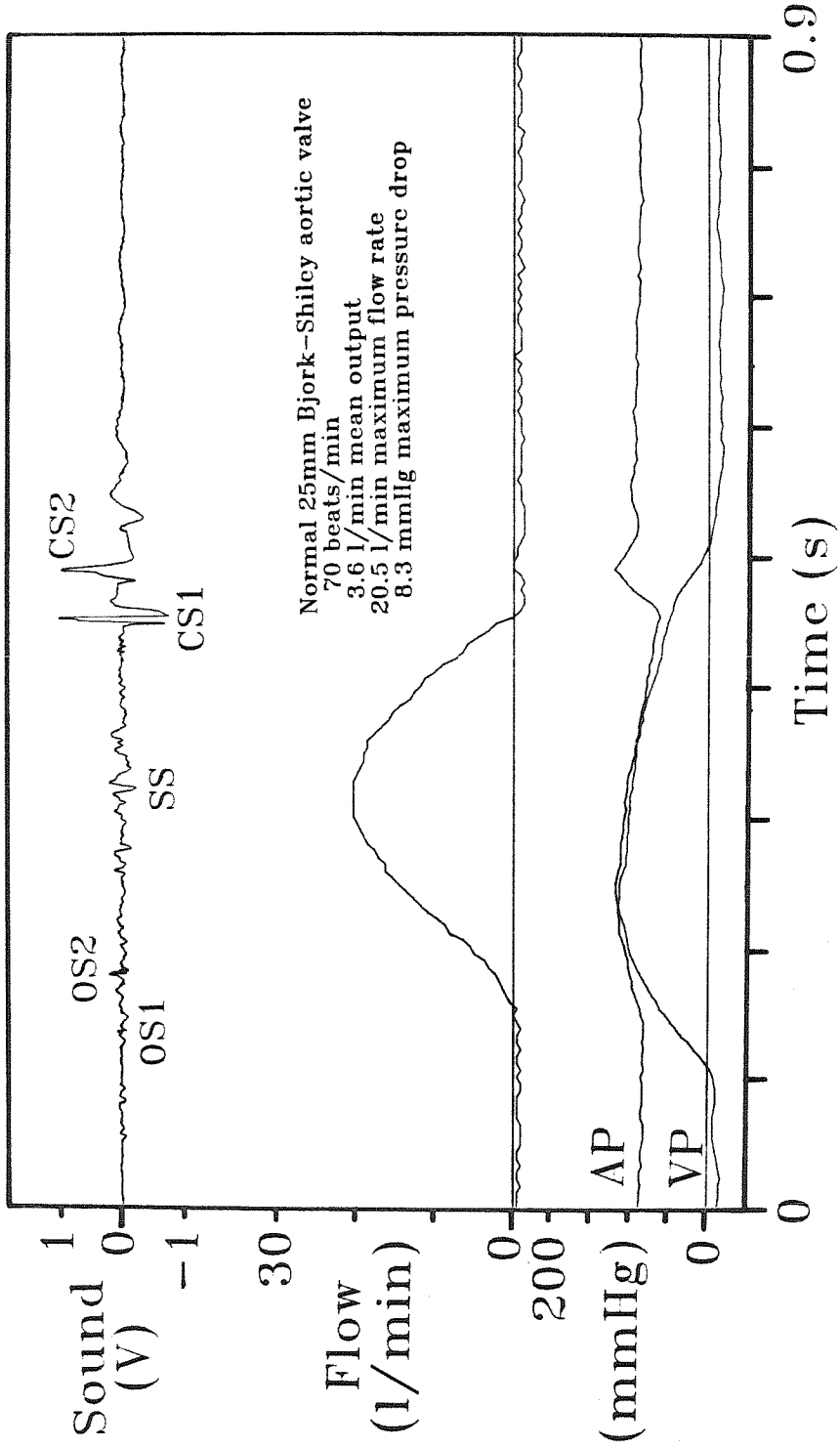

Figure 6-6a Amplitude vs. time tracings of sound, flow rate, aortic pressure and ventricular pressure associated with a typical cycle of experiment 266.

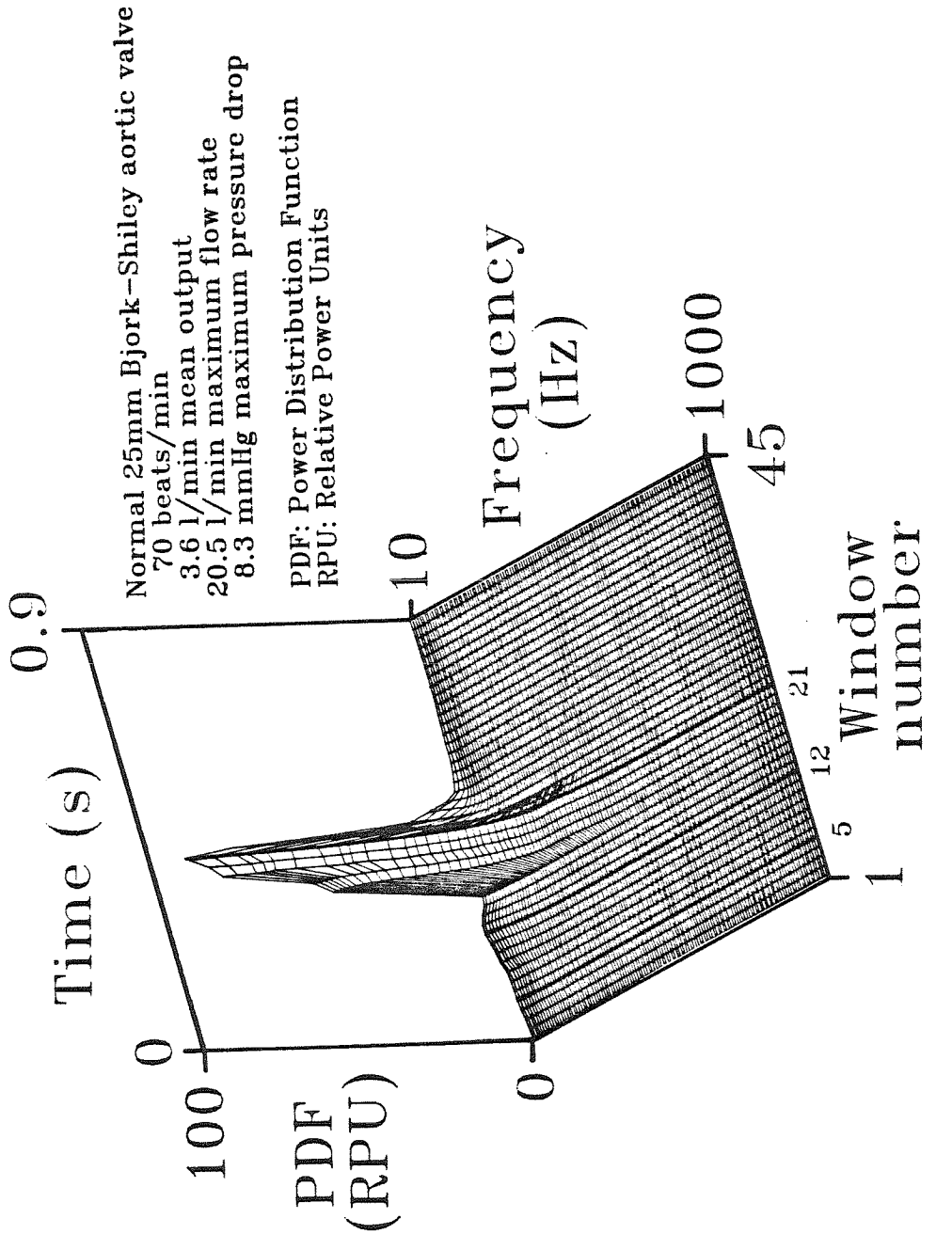

Figure 6-6b Three-dimensional power-frequency-time surface averaged over ten cycles of experiment 266.

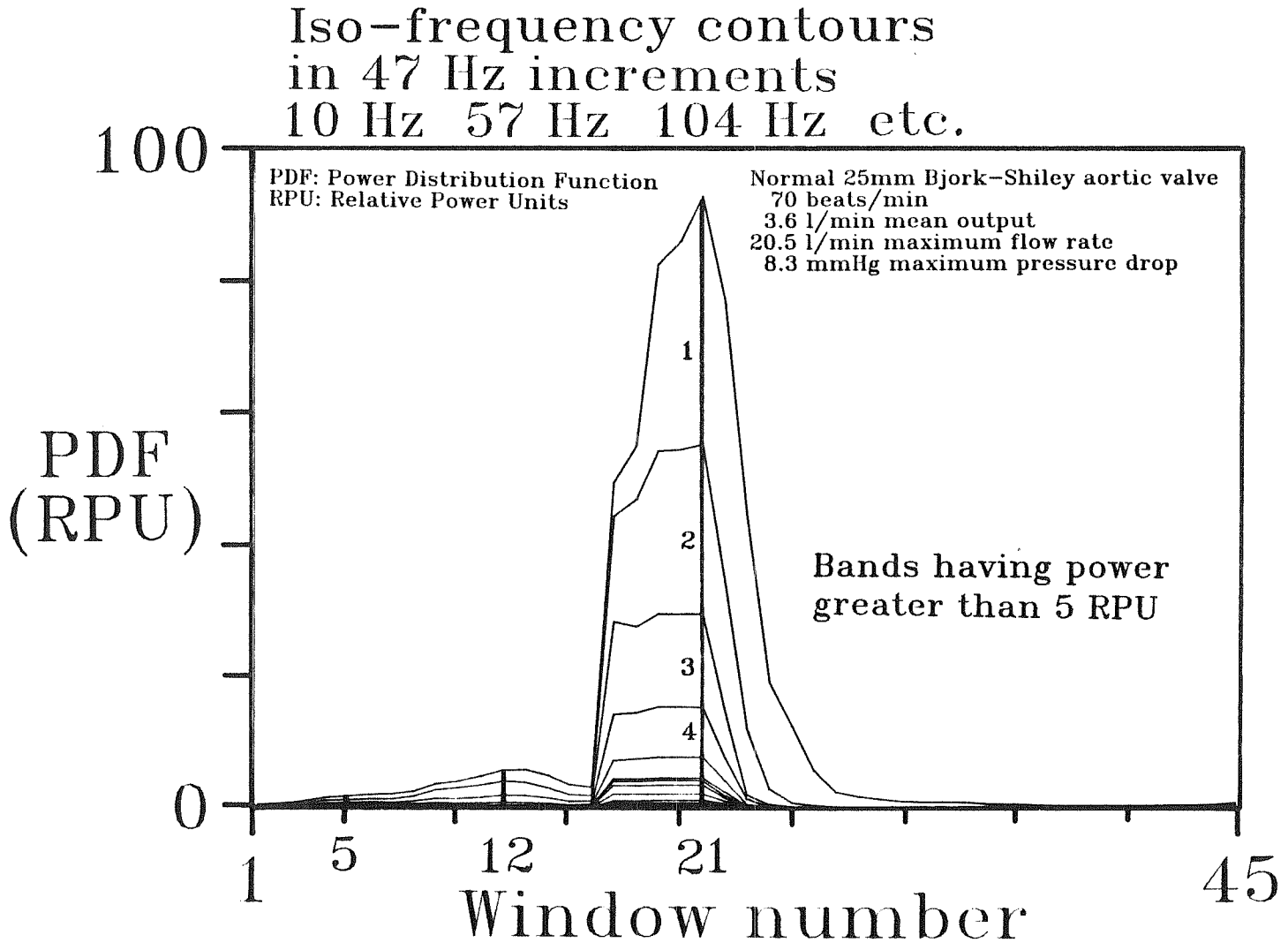

Figure 6-6c Auxiliary view perpendicular to the time axis of the 3-D power-frequency-time surface of experiment 266 showing iso-frequency contours.

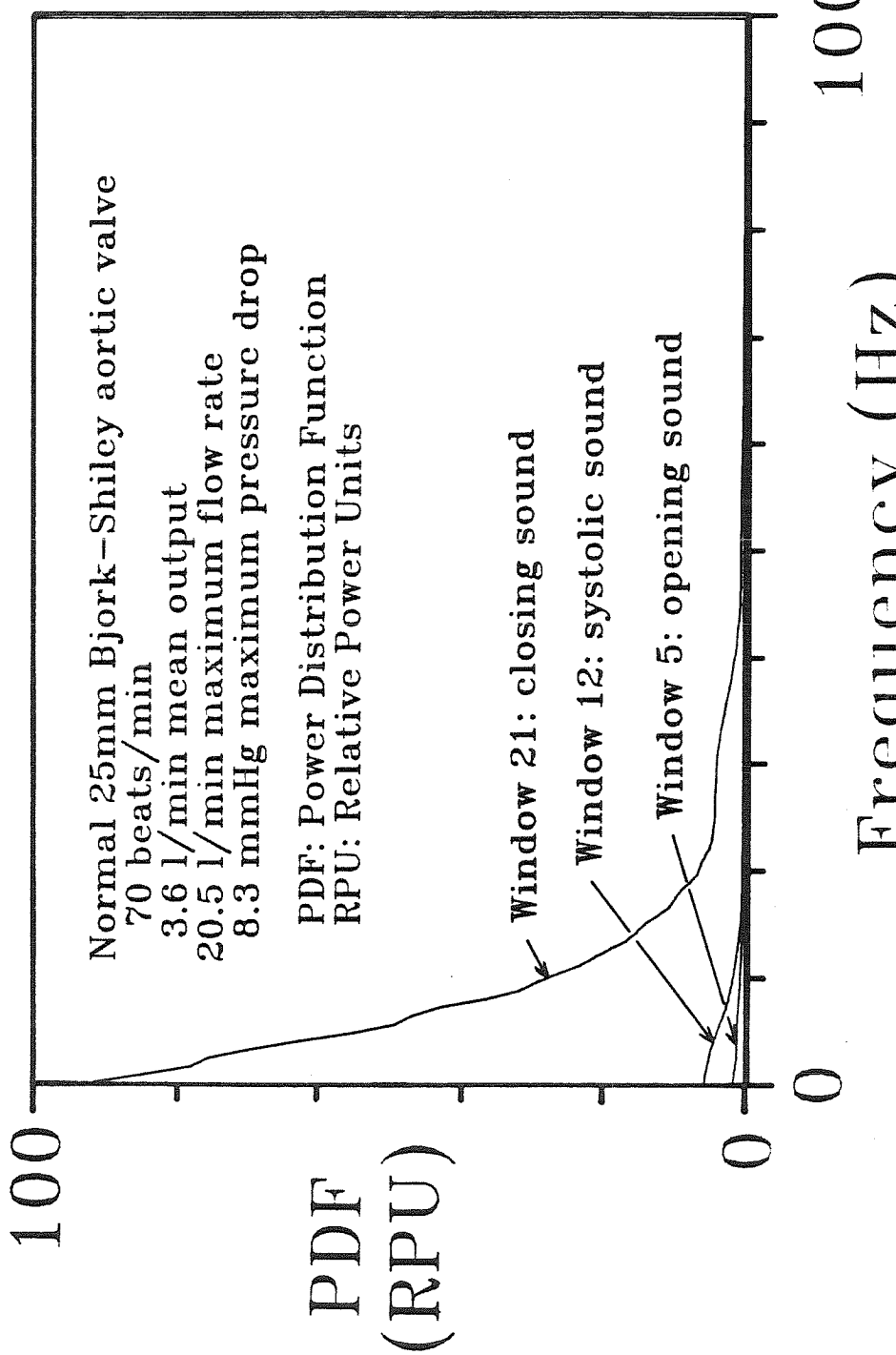

Figure 6-6d Auxiliary view perpendicular to the frequency axis of the 3-D power-frequency-time surface of experiment 266 showing power power distributions associated with windows encompassing the opening, systolic, and closing sounds.

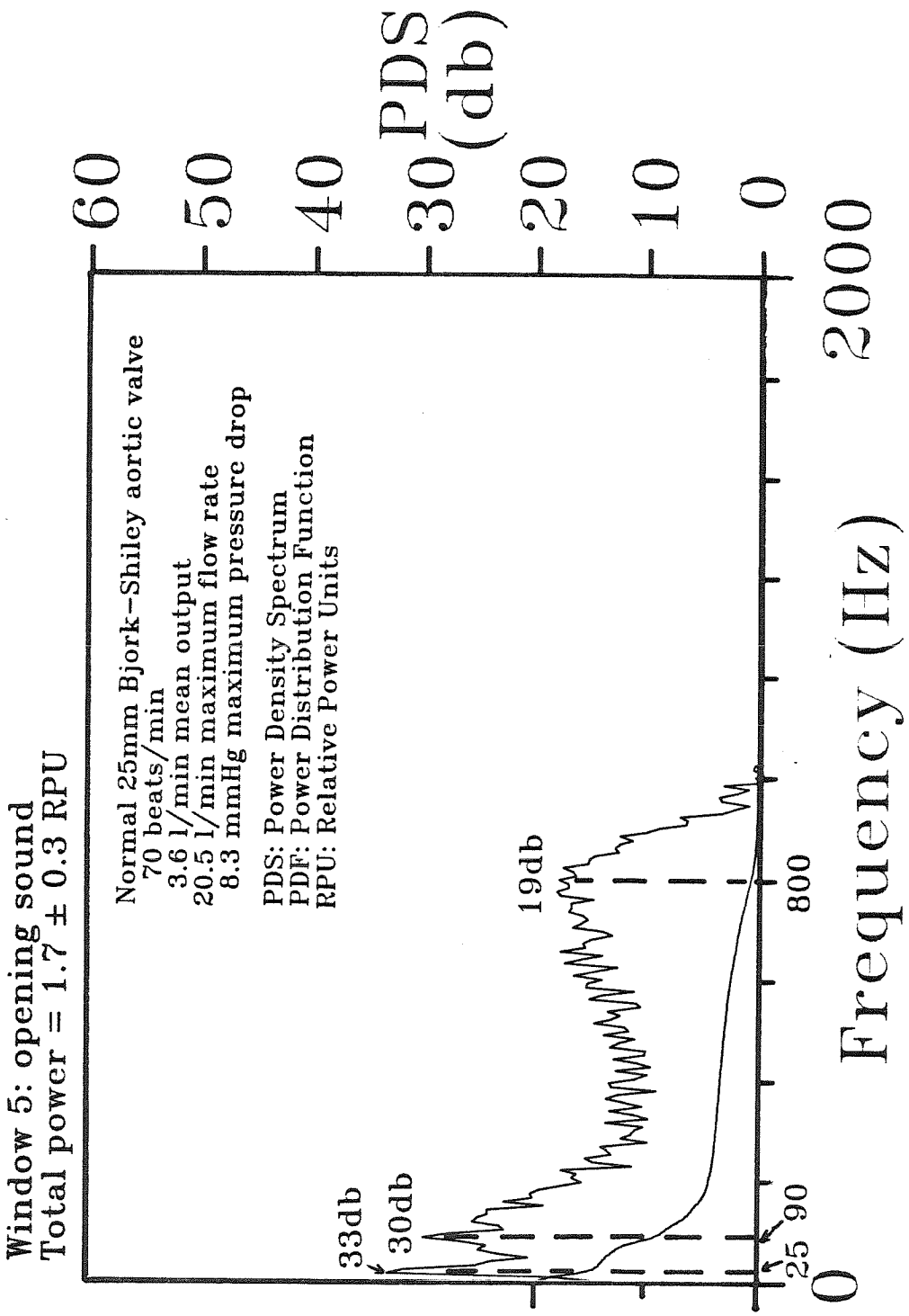

Figure 6-6e Power-density spectra and power distribution of the opening sound of experiment 366.

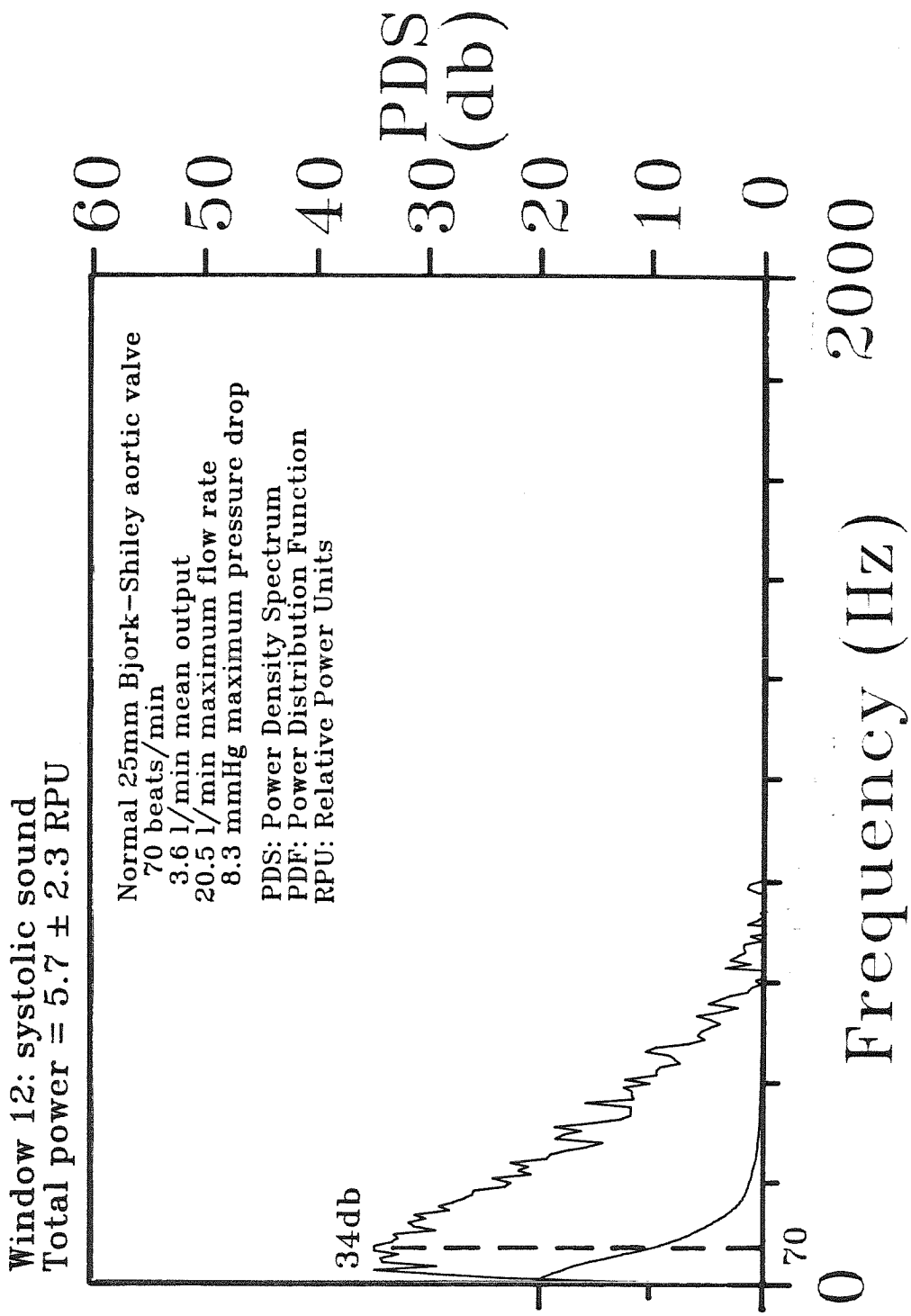

Figure 6-6f Power-density spectra and power distribution of the systolic sound of experiment 266.

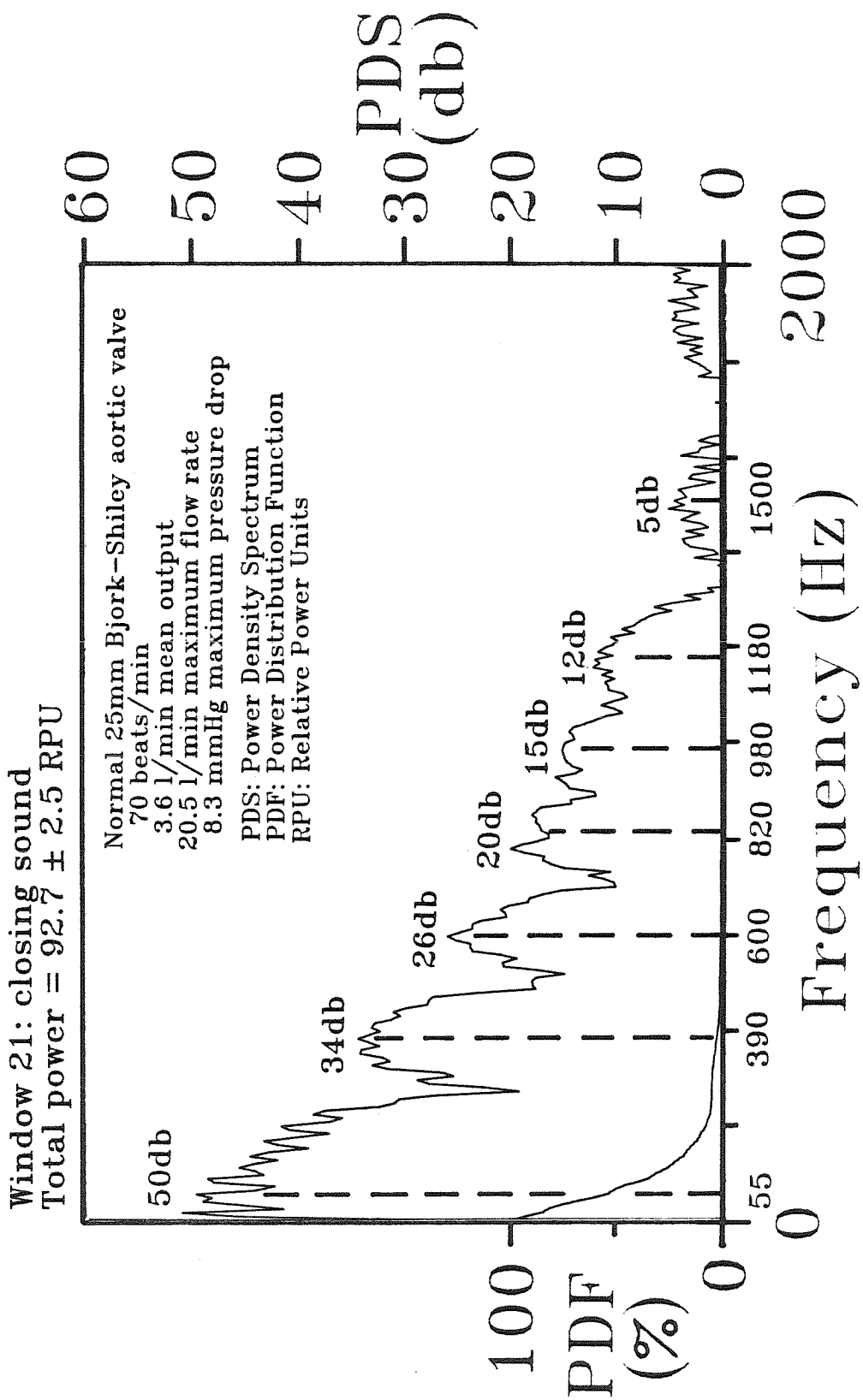

Figure 6-6g Power-density spectra and power distribution of the closing sound of experiment 266.

Parameters Estimated for

Significant Harmonic Peaks

Experiment 266

Event	Frequency, $f_{f,i}$; Decay, k_i; Power-Density, G_i (Hz,Hz,db)
Opening Sound	25, 5,33
Window 5	90,10,30
	800,80,19
Systolic Sound	
Window 12	70,45,34
Closing Sound	55,40,50
Window 21	390, 65,34
	600, 45,26
	820, 65,20
	980, 70,15
	1180, 80,12
	1500,120, 5

Table 6-3 Parameters estimated from significant harmonic peaks of experiment 266.

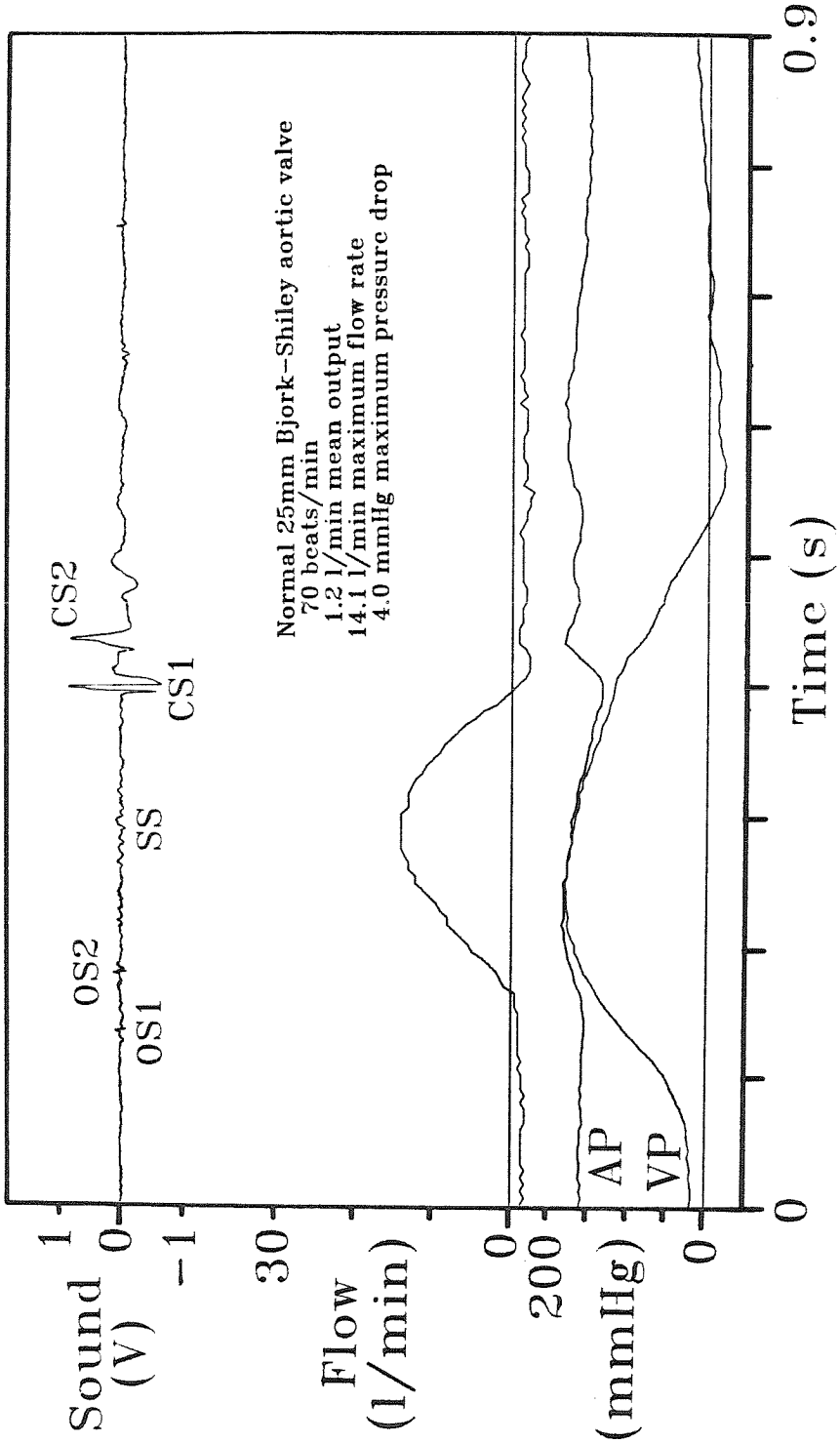

Figure 6-7a Amplitude vs. time tracings of sound, flow rate, aortic pressure and ventricular pressure associated with a typical cycle of experiment 267.

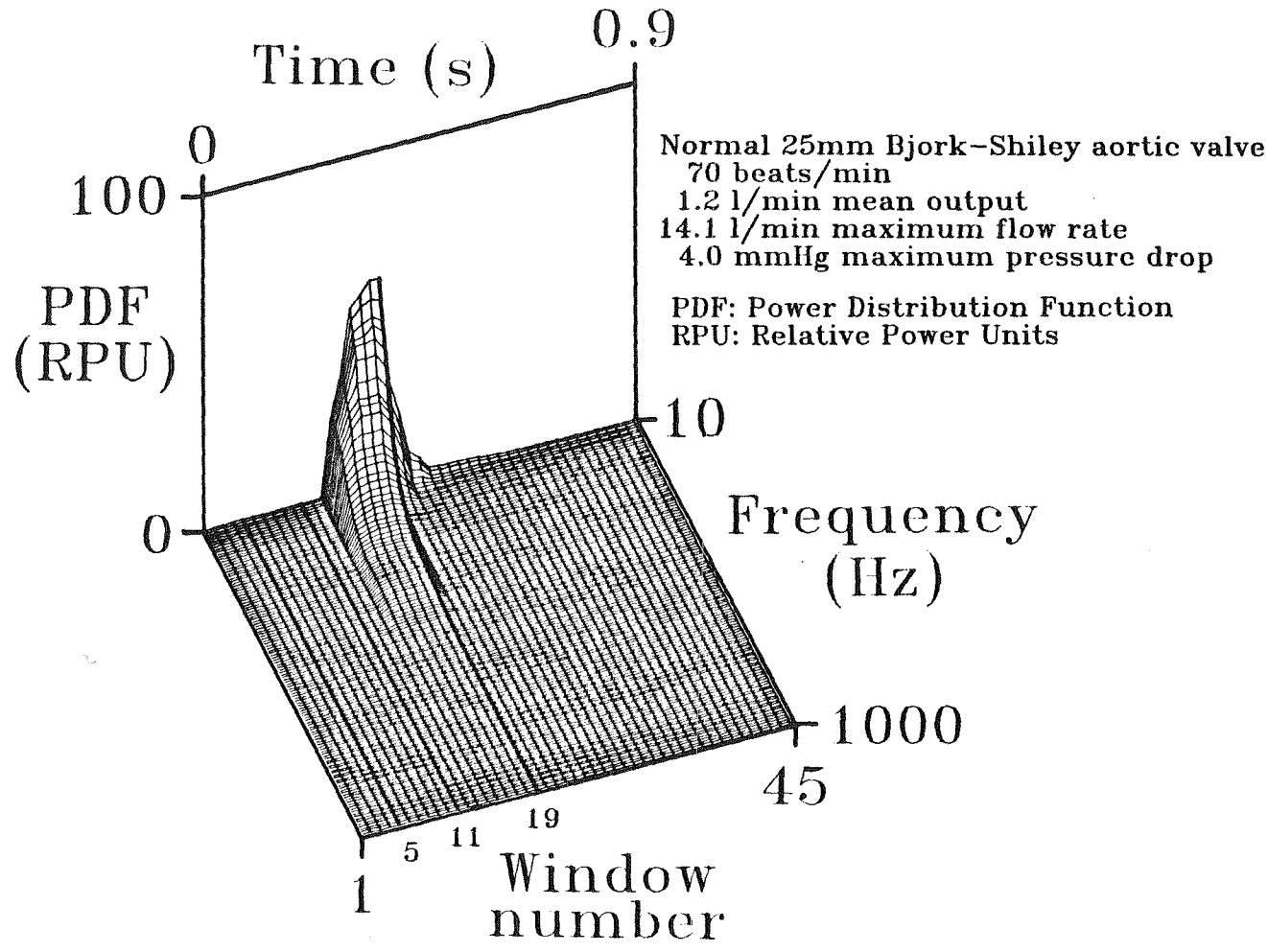

Figure 6-7b Three-dimensional power-frequency-time surface averaged over ten cycles of experiment 267.

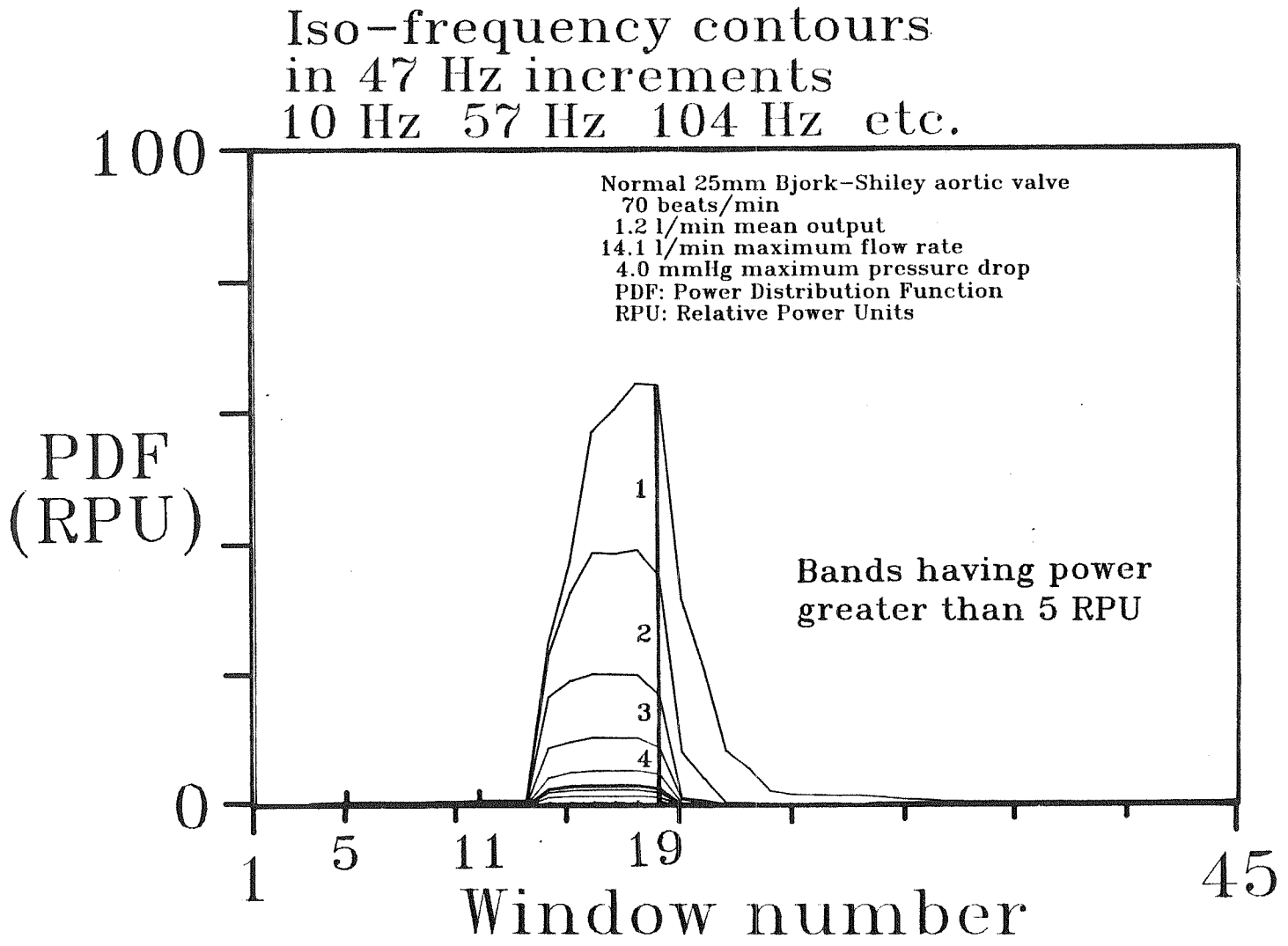

Figure 6-7c Auxiliary view perpendicular to the time axis of the 3-D power-frequency-time surface of experiment 267 showing iso-frequency contours.

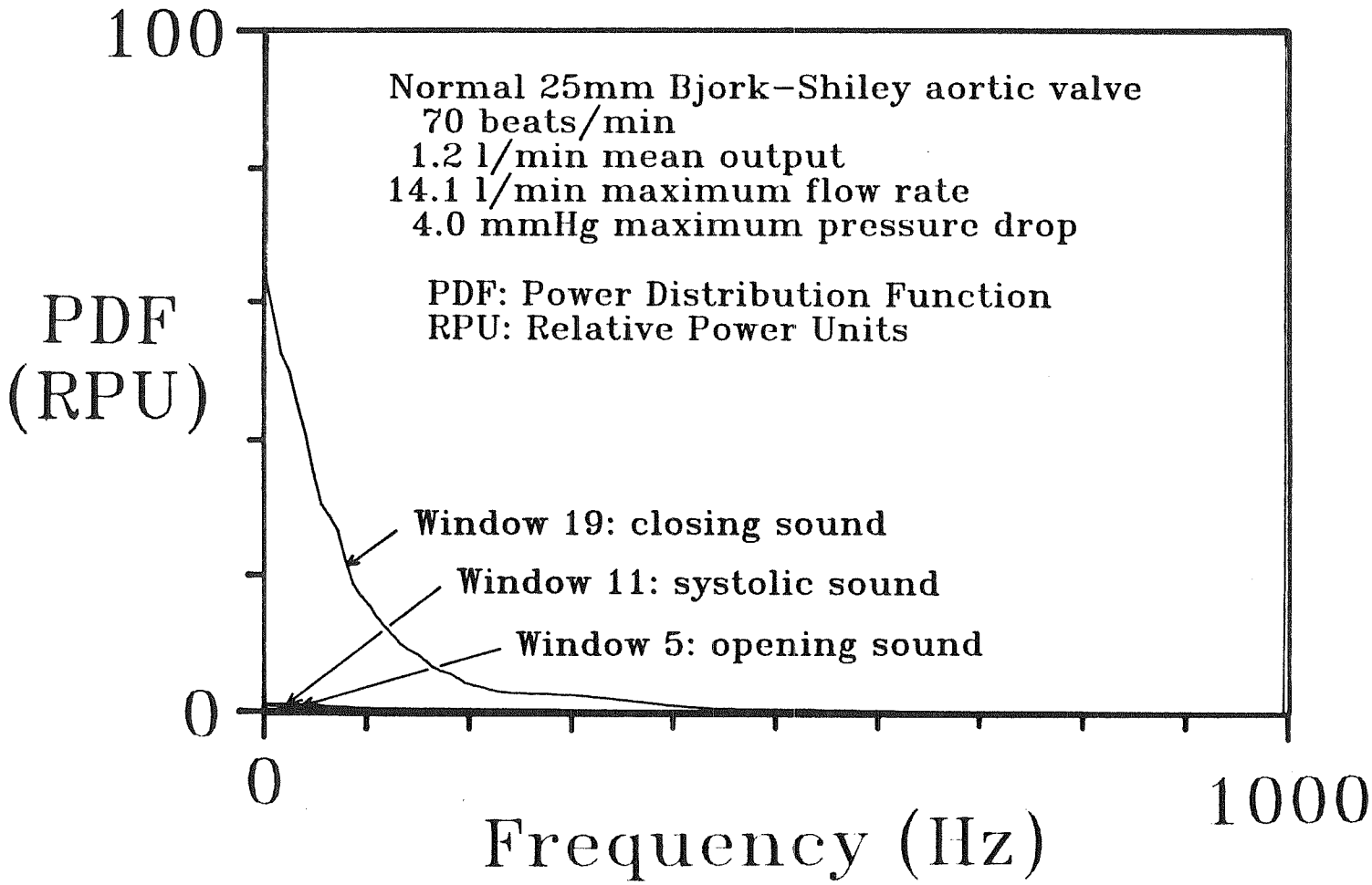

Figure 6-7d Auxiliary view perpendicular to the frequency axis of the 3-D power-frequency-time surface of experiment 267 showing power power distributions associated with windows encompassing the opening, systolic, and closing sounds.

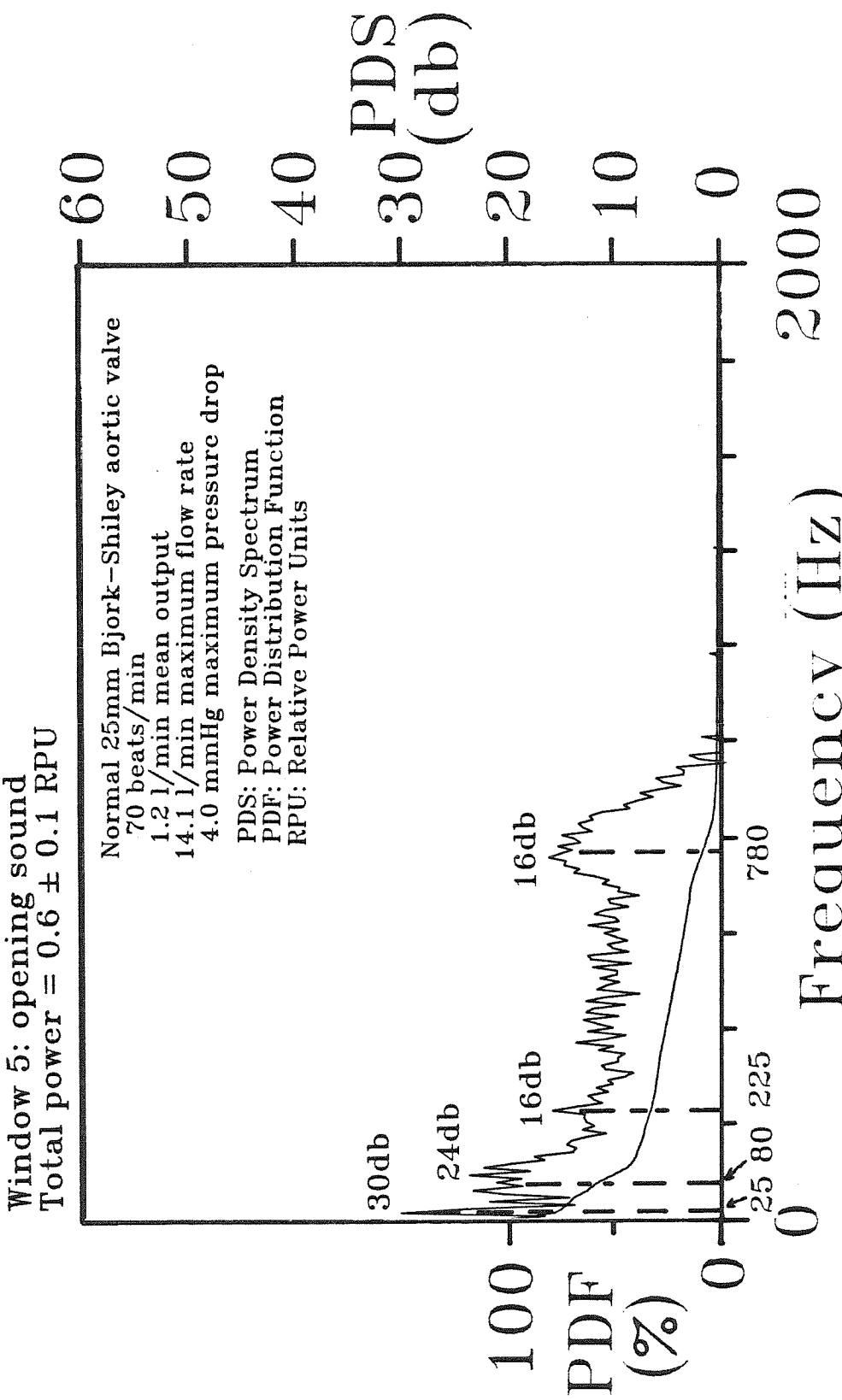

Figure 6-7e Power-density spectra and power distribution of the opening sound of experiment 267.

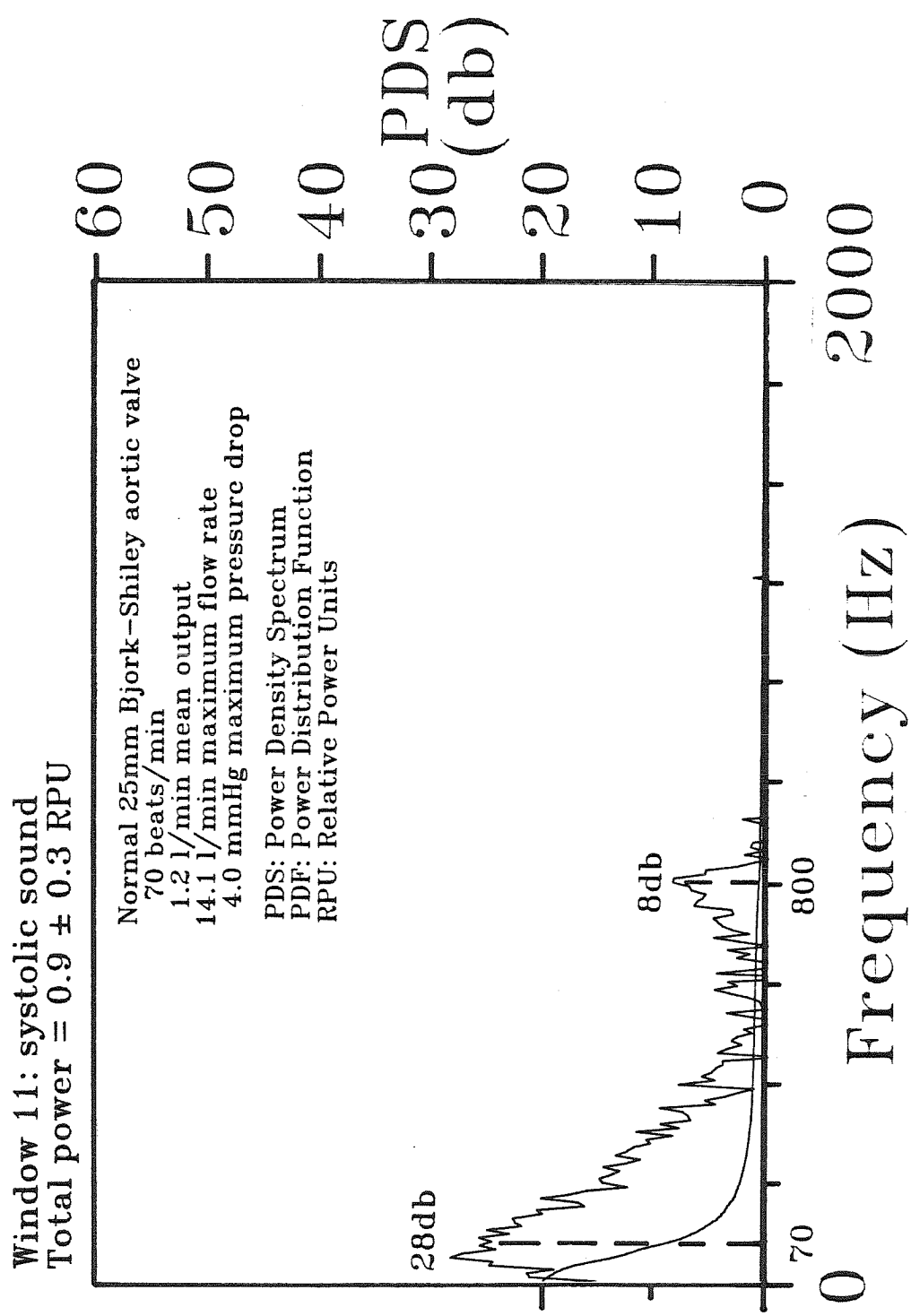

Figure 6-7f Power-density spectra and power distribution of the systolic sound of experiment 267.

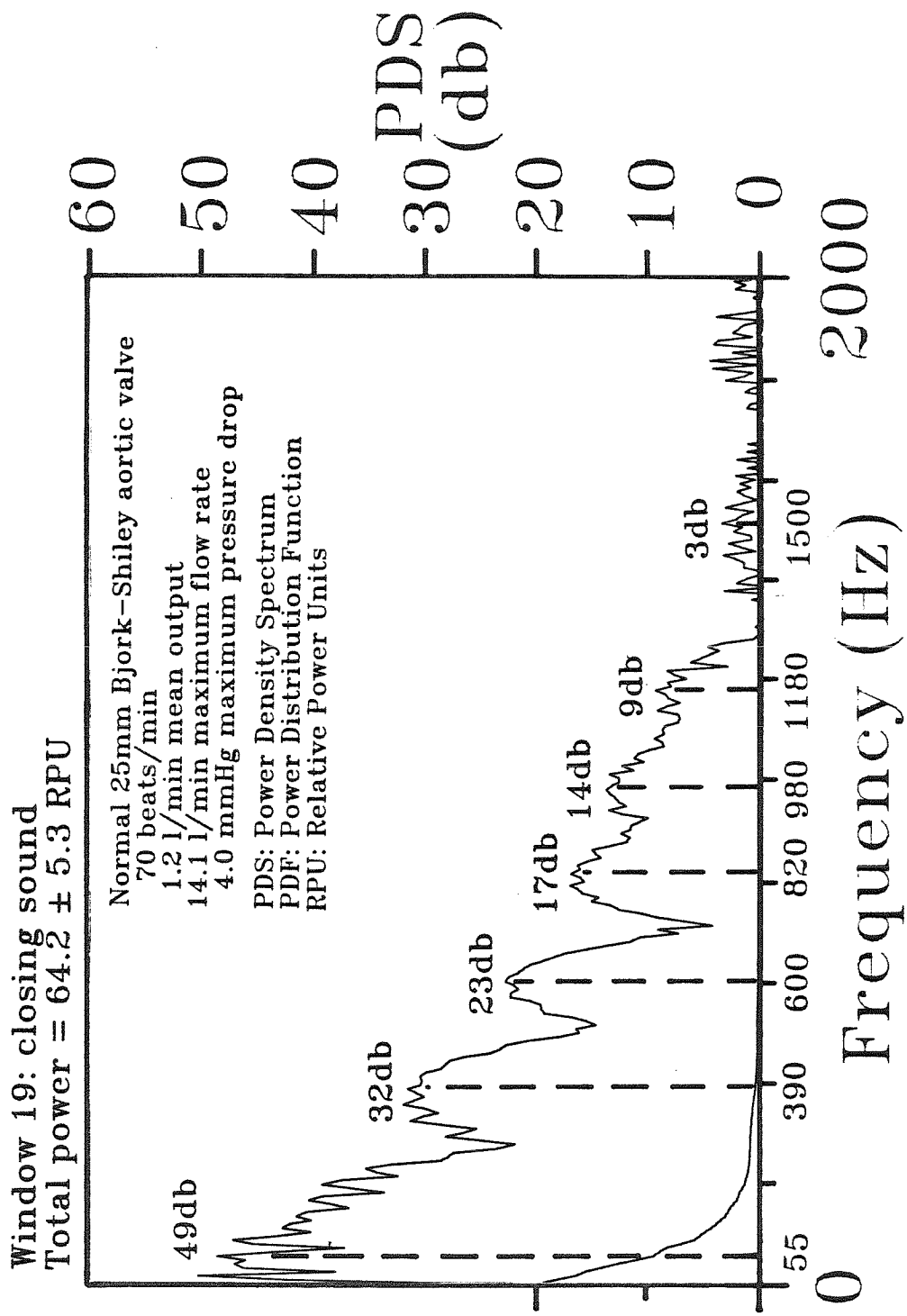

Figure 6-7g Power-density spectra and power distribution of the closing sound of experiment 267.

Parameters Estimated for

Significant Harmonic Peaks

Experiment 267

Event	Frequency, $f_{f,i}$; Decay, k_i; Power-Density, G_i (Hz,Hz,db)
Opening Sound	25, 5,30
	80,35,24
Window 5	225,25,16
	780,60,16
Systolic Sound	70,40,28
Window 11	800,35, 8
Closing Sound	55, 35,49
	390, 65,32
	600, 55,23
	820, 60,17
Window 19	980, 70,14
	1180, 70, 9
	1500,140, 3

Table 6-4 Parameters estimated from significant harmonic peaks of experiment 267.

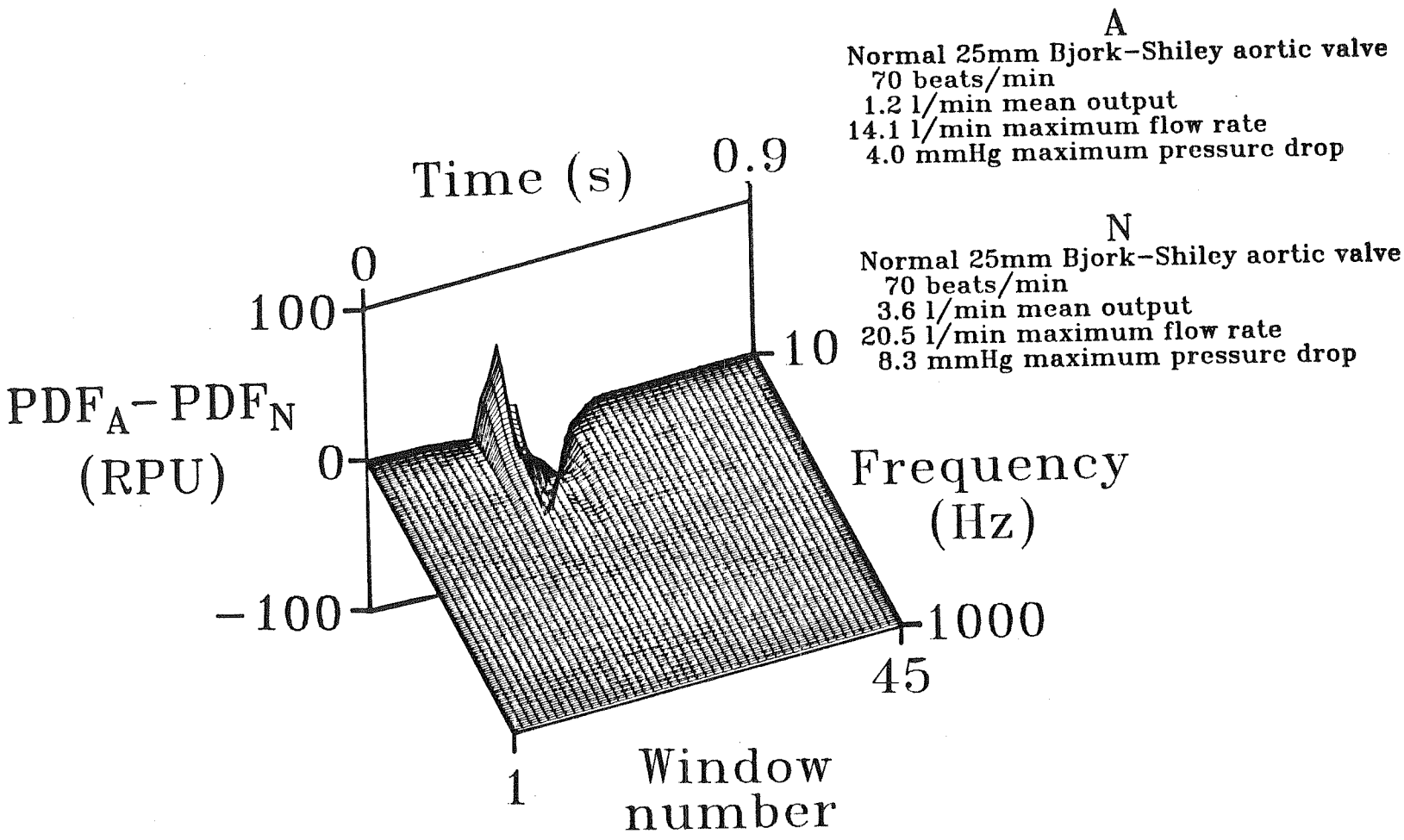

Figure 6-7h Three-dimensional surface depicting the difference between the power-frequency-time surfaces associated with experiments 267 and 266.

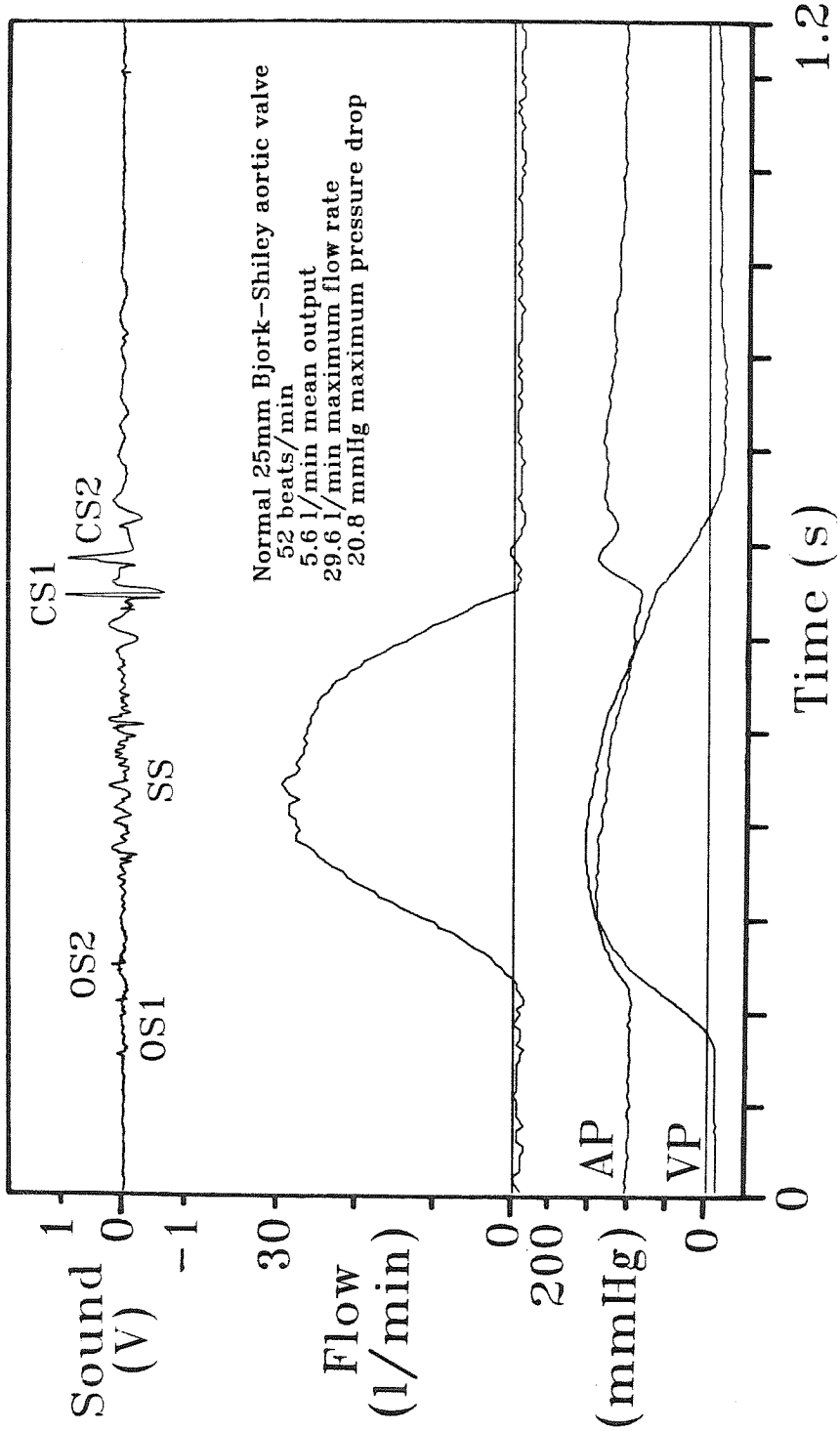

Figure 6-8a Amplitude vs. time tracings of sound, flow rate, aortic pressure and ventricular pressure associated with a typical cycle of experiment 271.

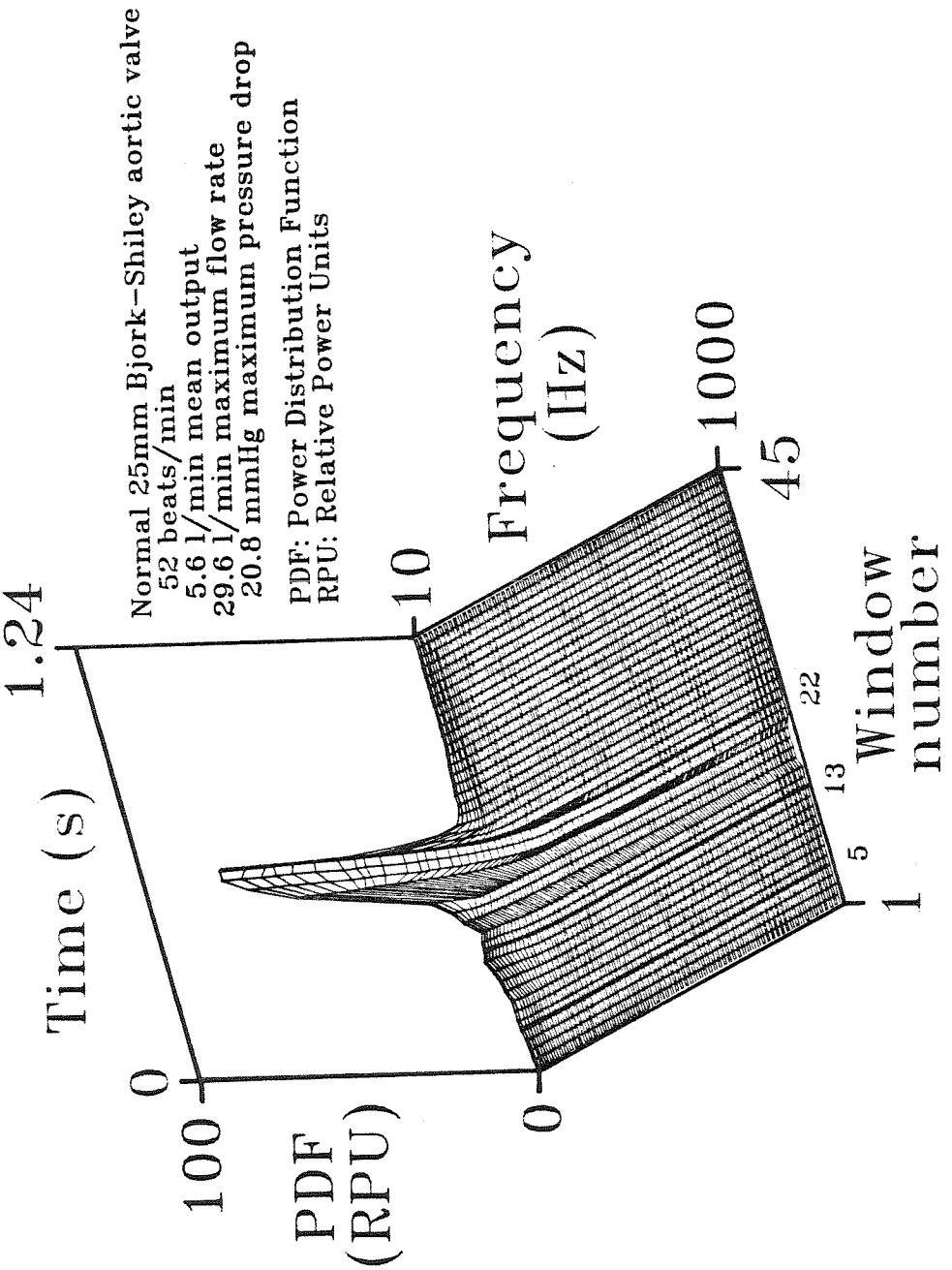

Figure 6-8b Three-dimensional power-frequency-time surface averaged over ten cycles of experiment 271.

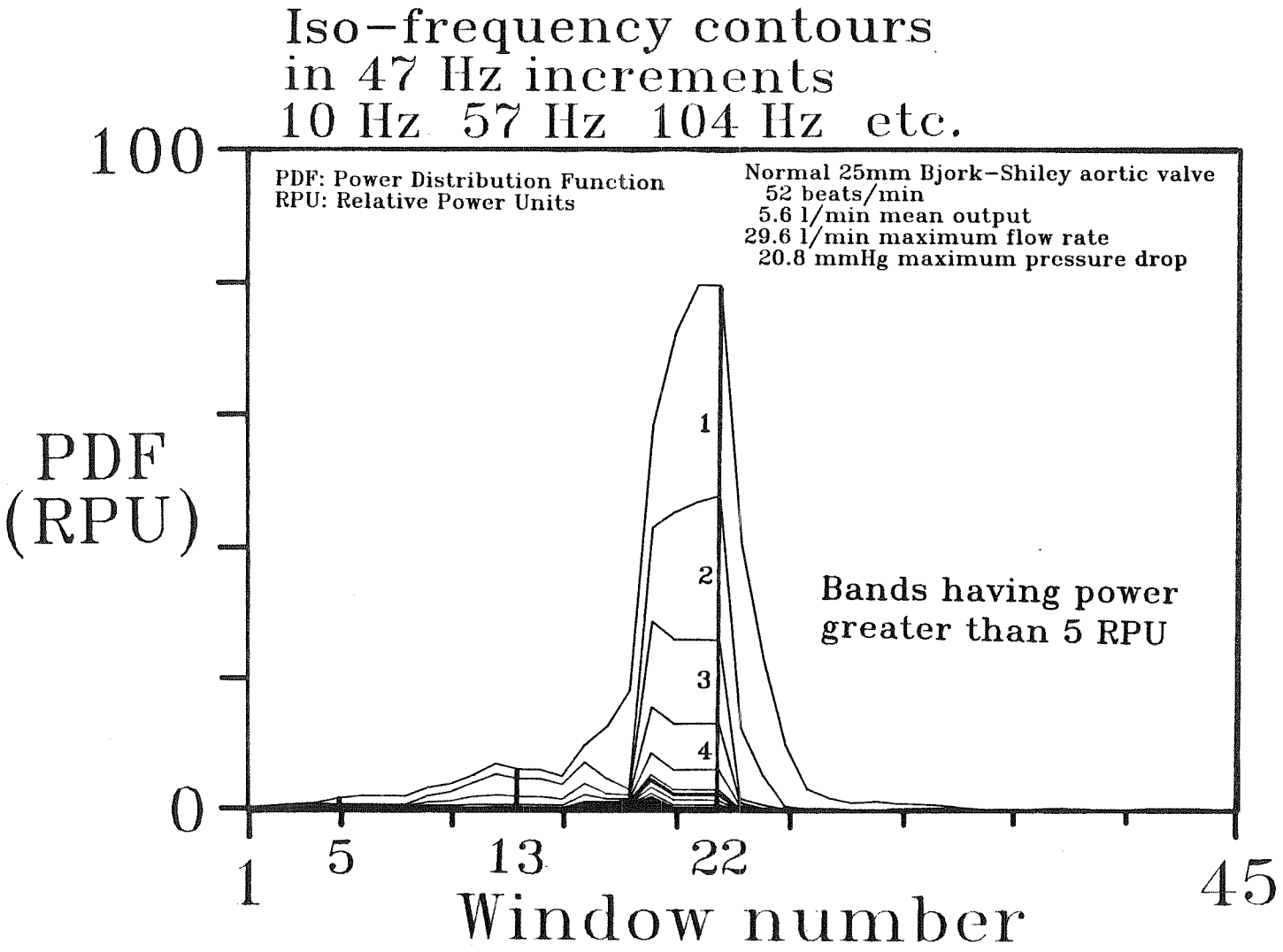

Figure 6-8c Auxiliary view perpendicular to the time axis of the 3-D power-frequency-time surface of experiment 271 showing iso-frequency contours.

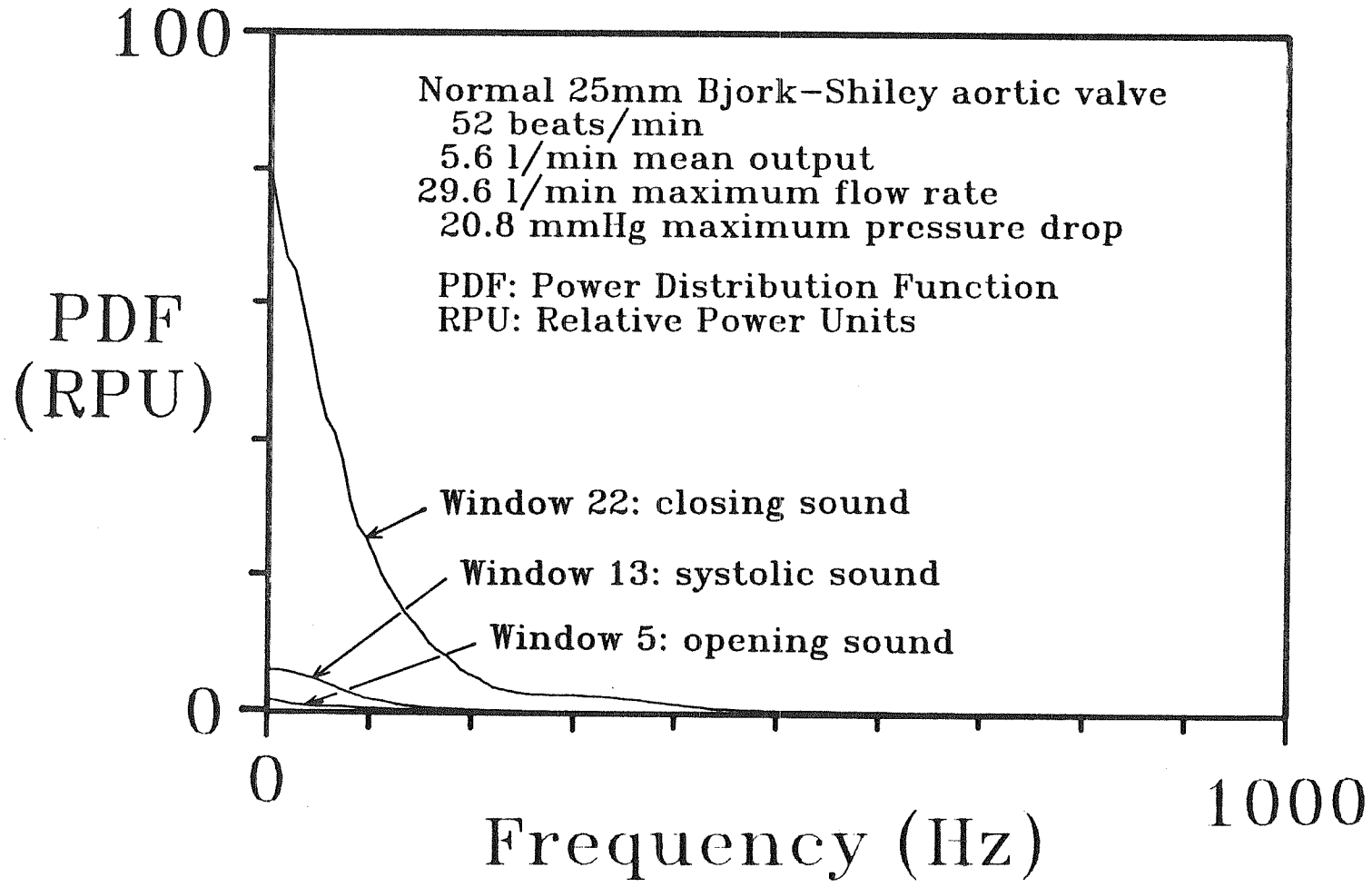

Figure 6-8d Auxiliary view perpendicular to the frequency axis of the 3-D power-frequency-time surface of experiment 271 showing power power distributions associated with windows encompassing the opening, systolic, and closing sounds.

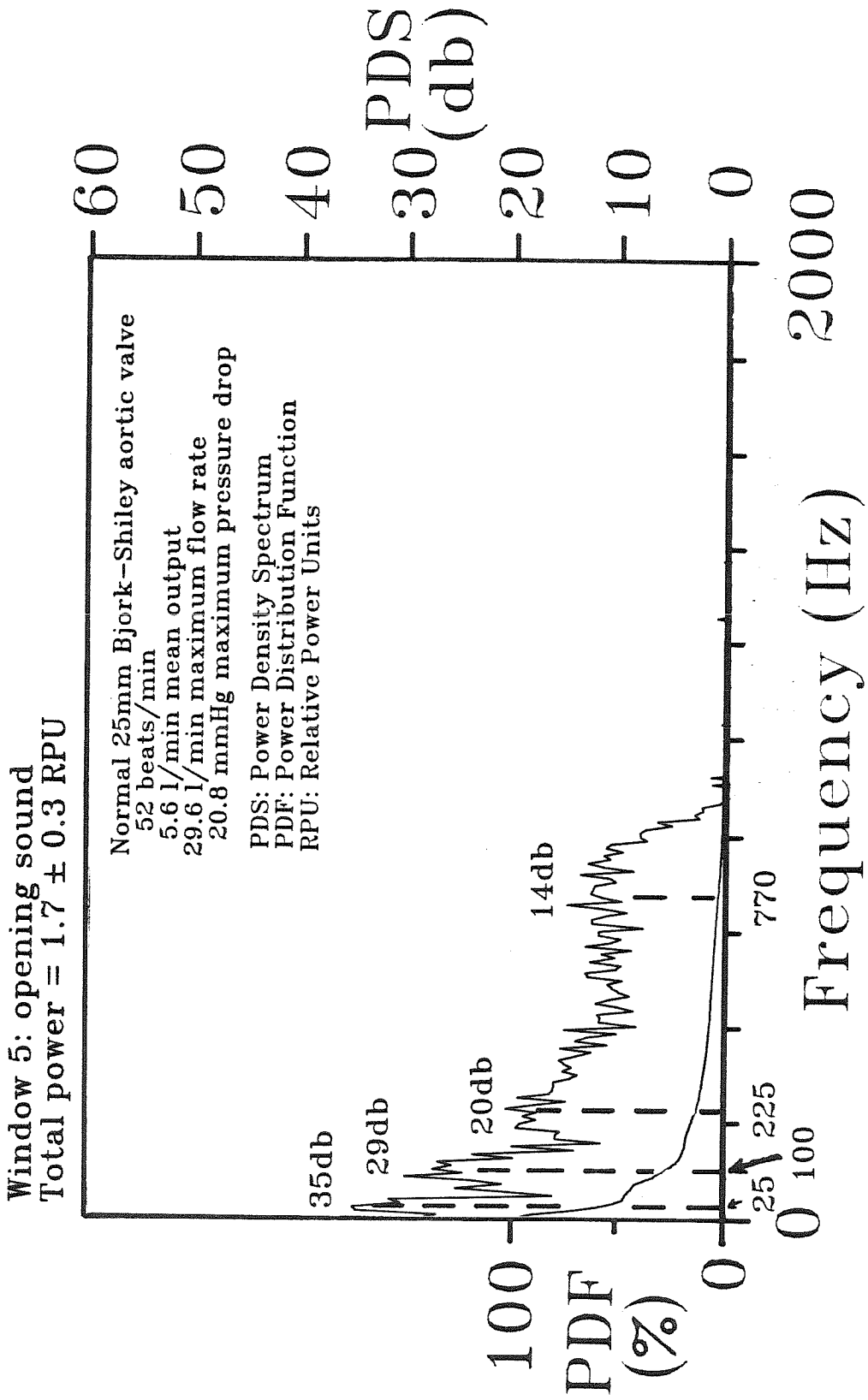

Figure 6-8e Power-density spectra and power distribution of the opening sound of experiment 271.

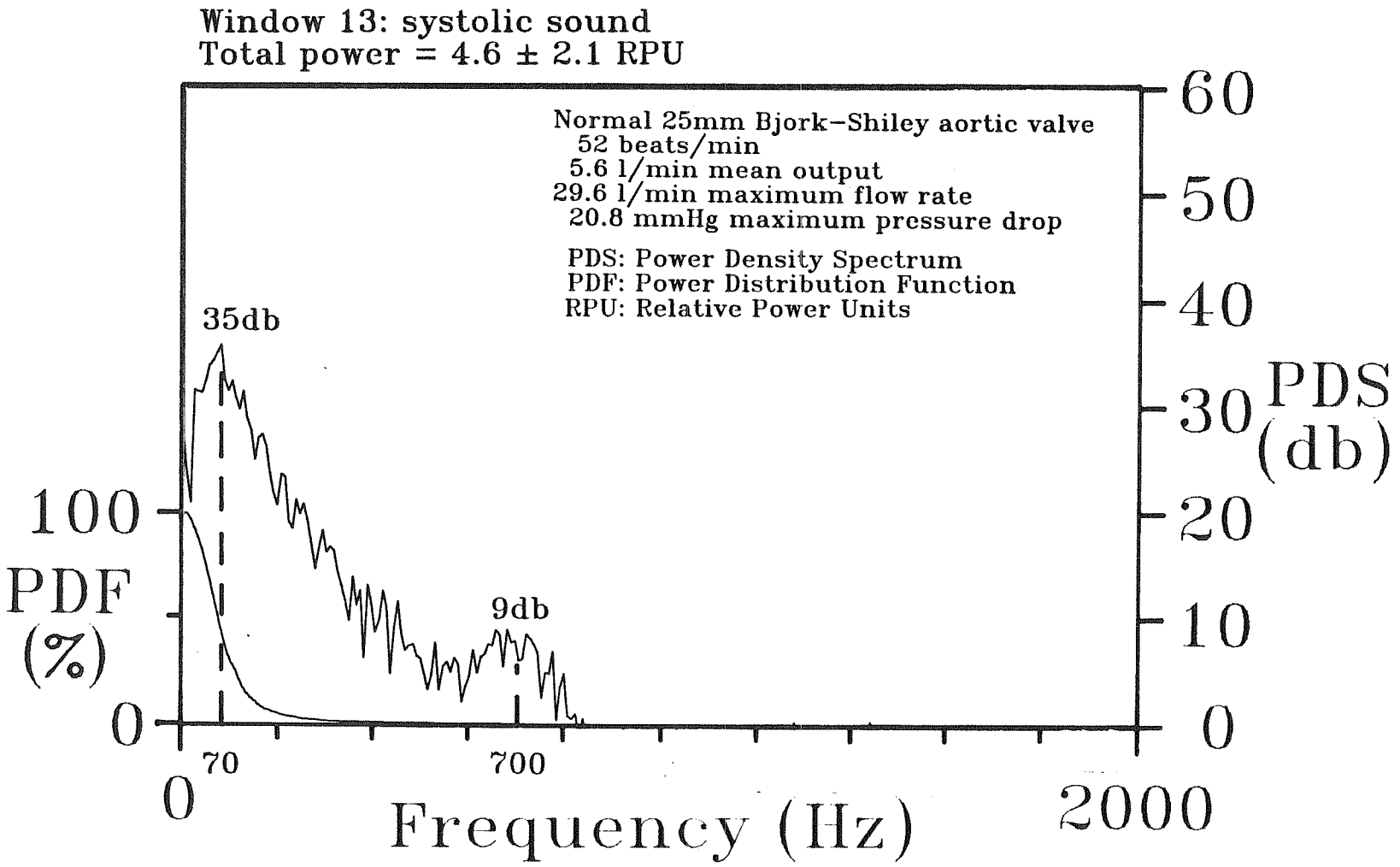

Figure 6-8f Power-density spectra and power distribution of the systolic sound of experiment 271.

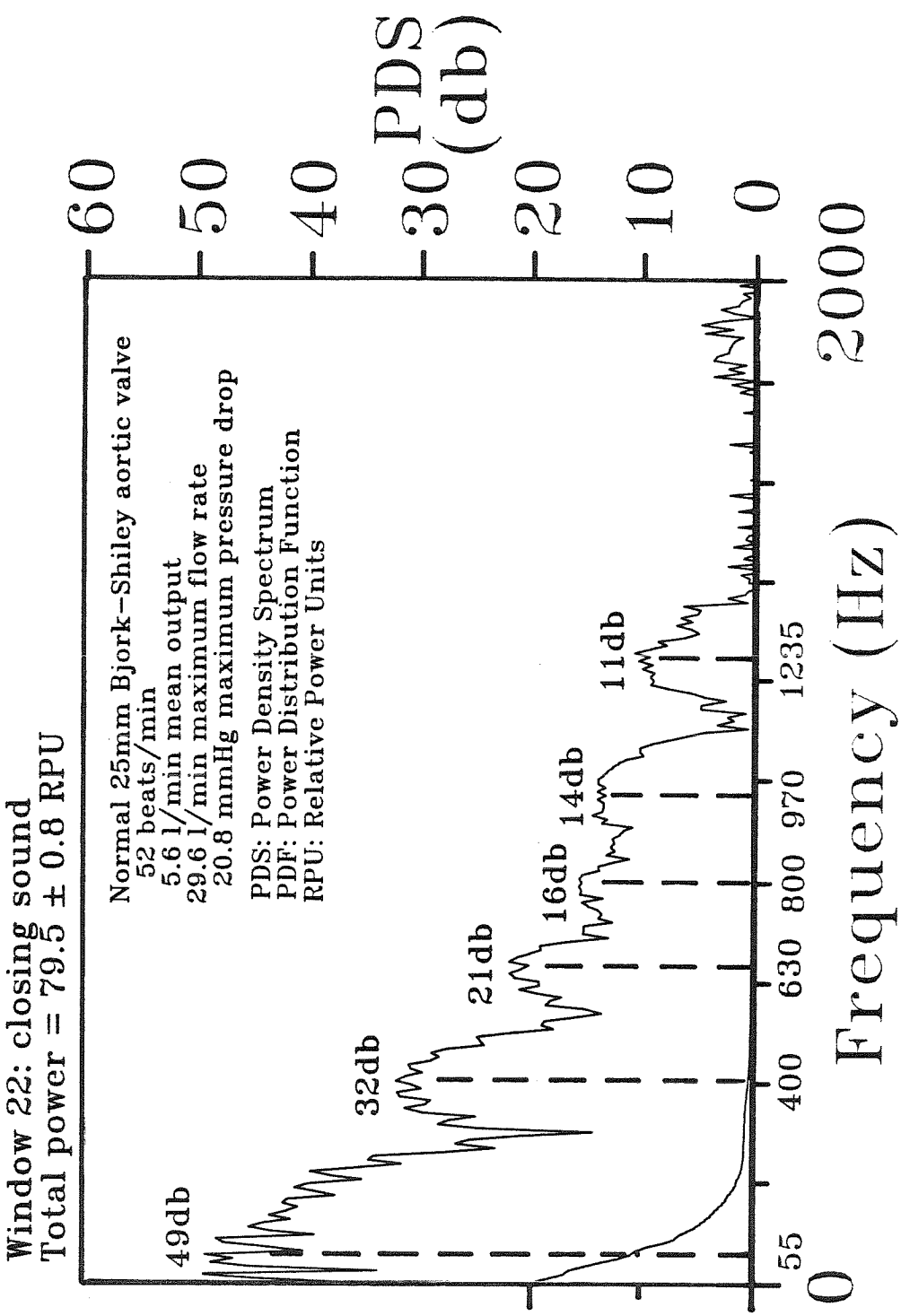

Figure 6-8g Power-density spectra and power distribution of the closing sound of experiment 271.

Parameters Estimated for

Significant Harmonic Peaks

Experiment 271

Event	Frequency, $f_{I,i}$; Decay, k_i; Power-Density, G_i (Hz,Hz,db)
Opening Sound	25, 15,35
	100, 30,29
Window 5	225, 40,20
	770,110,14
Systolic Sound	70,45,35
Window 13	700,80, 9
Closing Sound	55,40,49
	400,55,32
	630,55,21
Window 22	800,65,16
	970,65,14
	1235,65,11

Table 6-5 Parameters estimated from significant harmonic peaks of experiment 271.

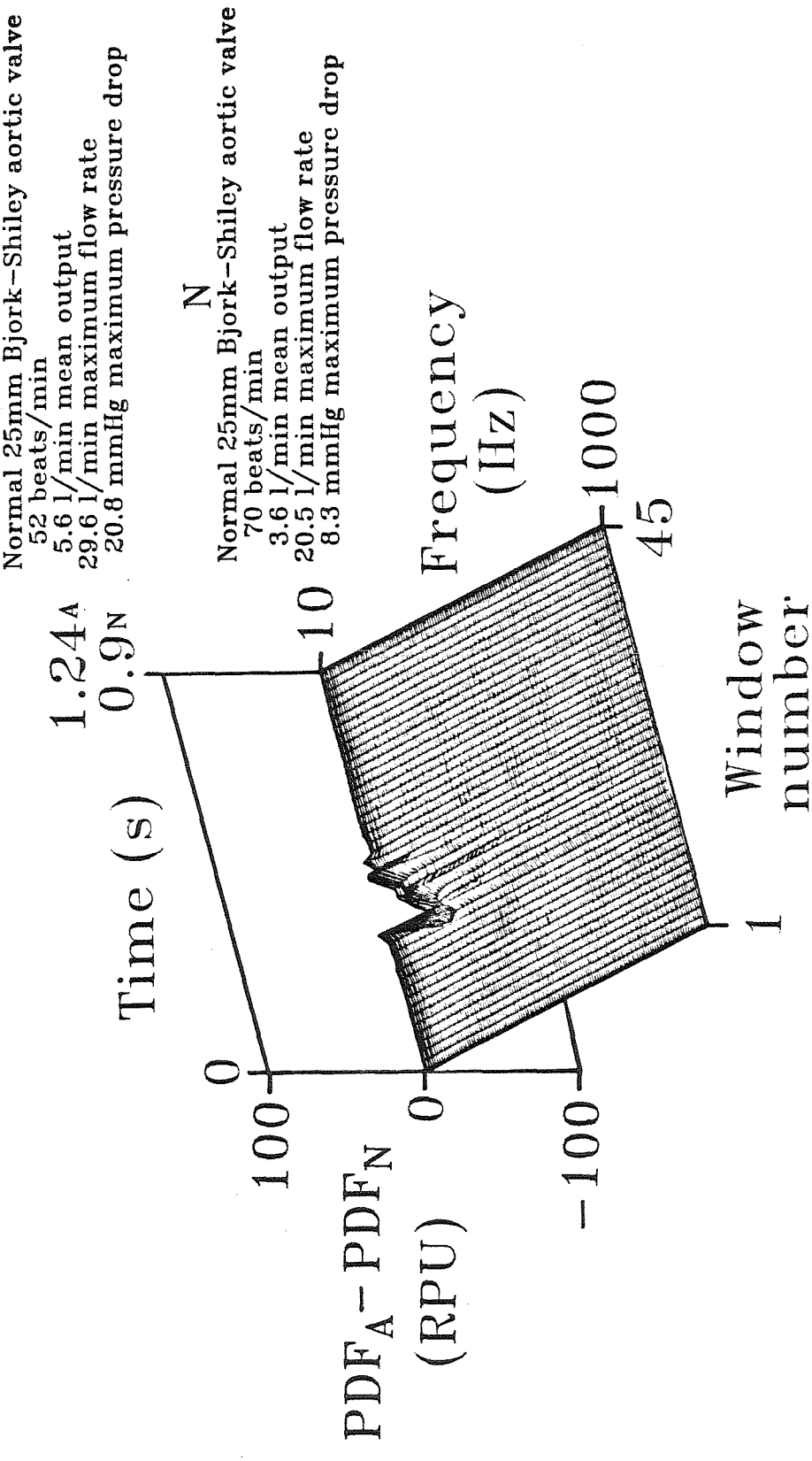

Figure 6-8h Three-dimensional surface depicting the difference between the power-frequency-time surfaces associated with experiments 271 and 266.

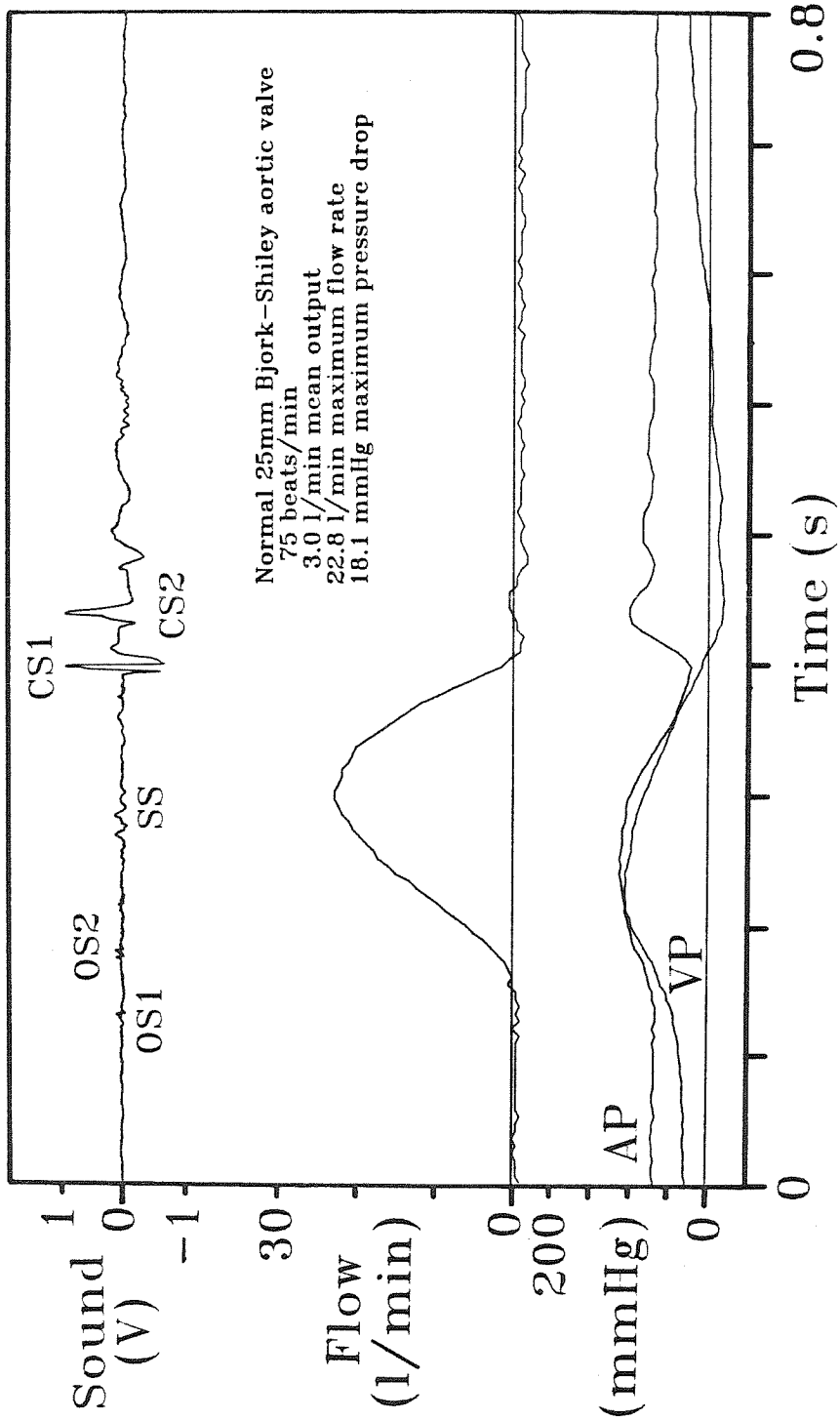

Figure 6-9a Amplitude vs. time tracings of sound, flow rate, aortic pressure and ventricular pressure associated with a typical cycle of experiment 272.

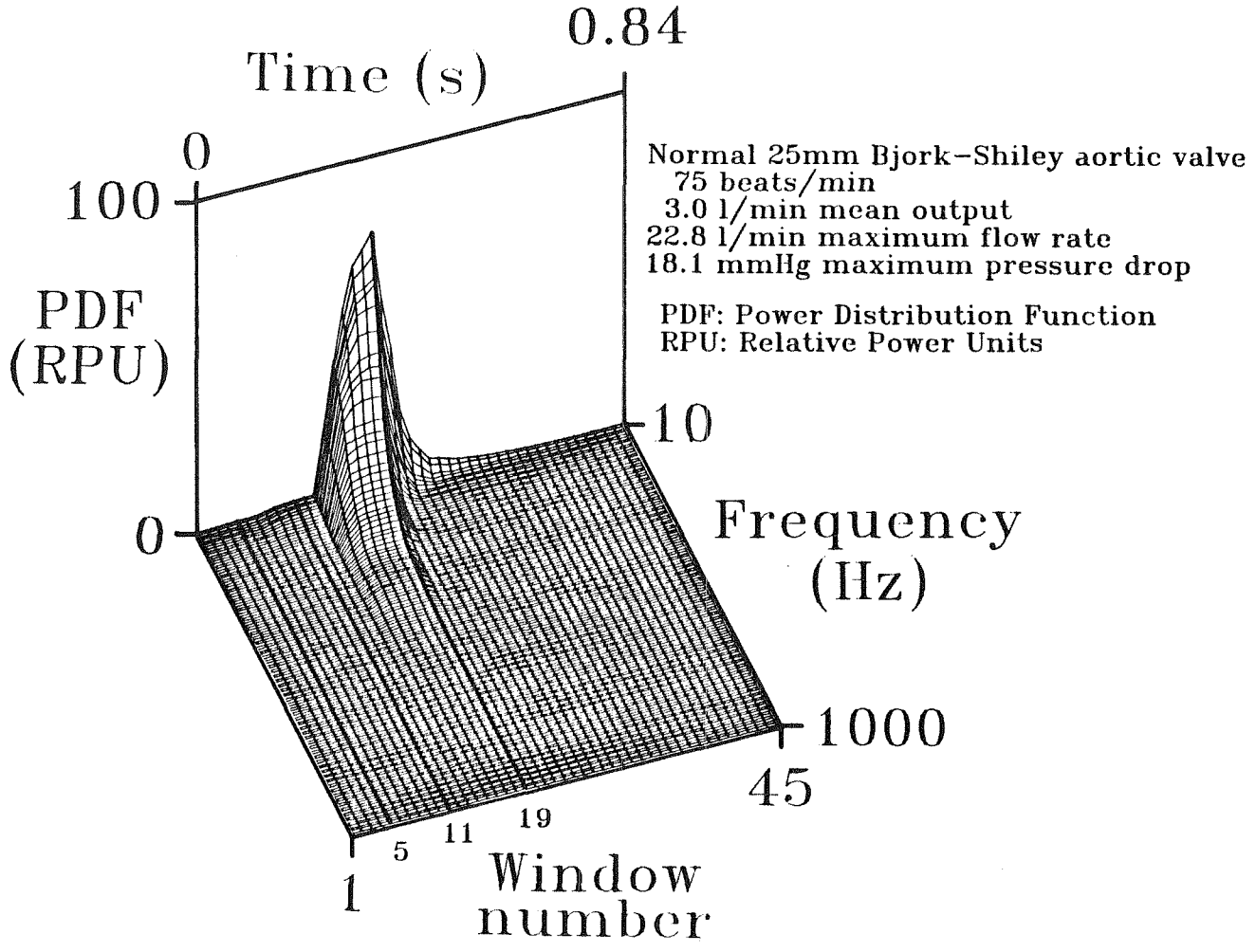

Figure 6-9b Three-dimensional power-frequency-time surface averaged over ten cycles of experiment 272.

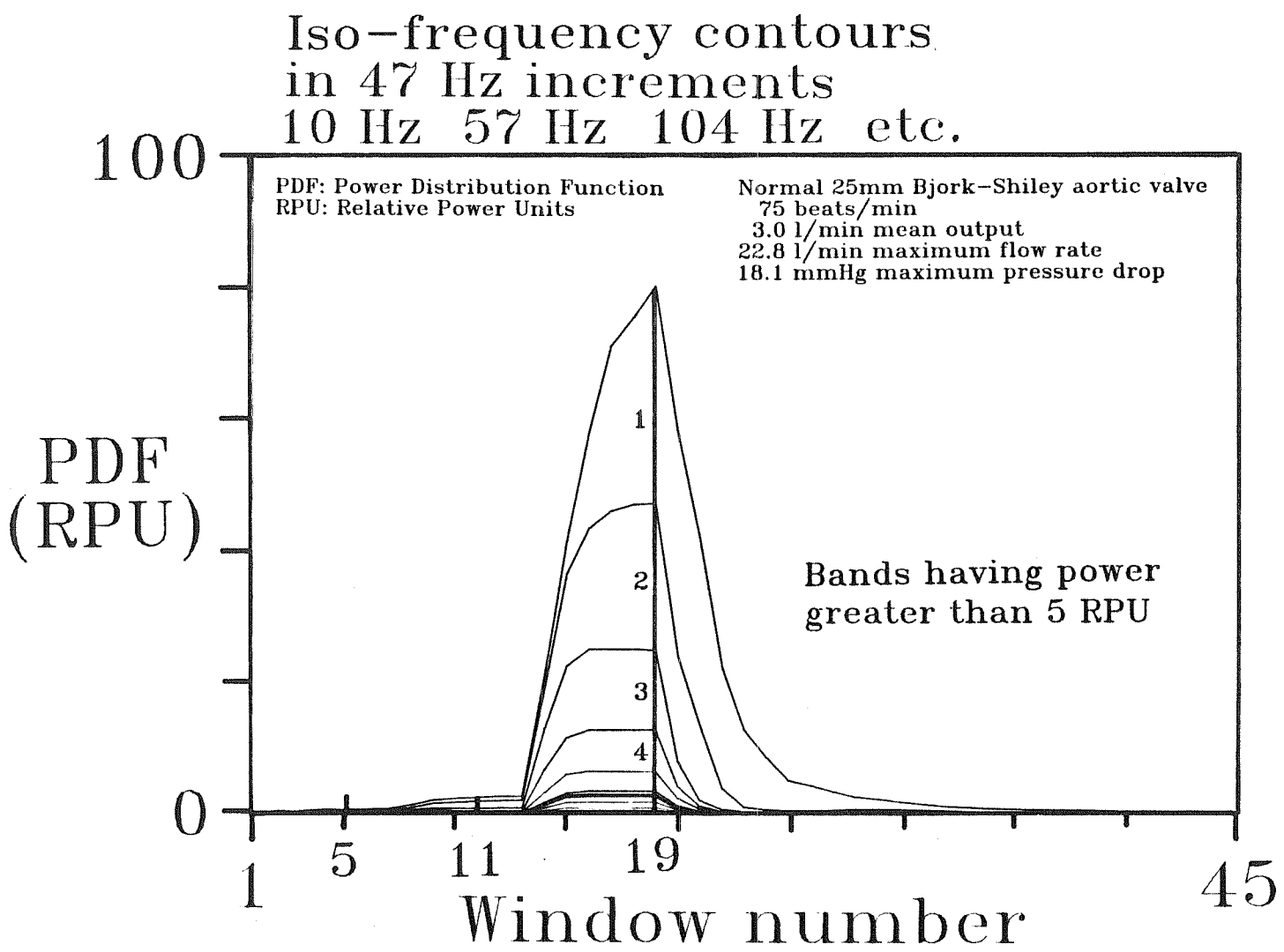

Figure 6-9c Auxiliary view perpendicular to the time axis of the 3-D power-frequency-time surface of experiment 272 showing iso-frequency contours.

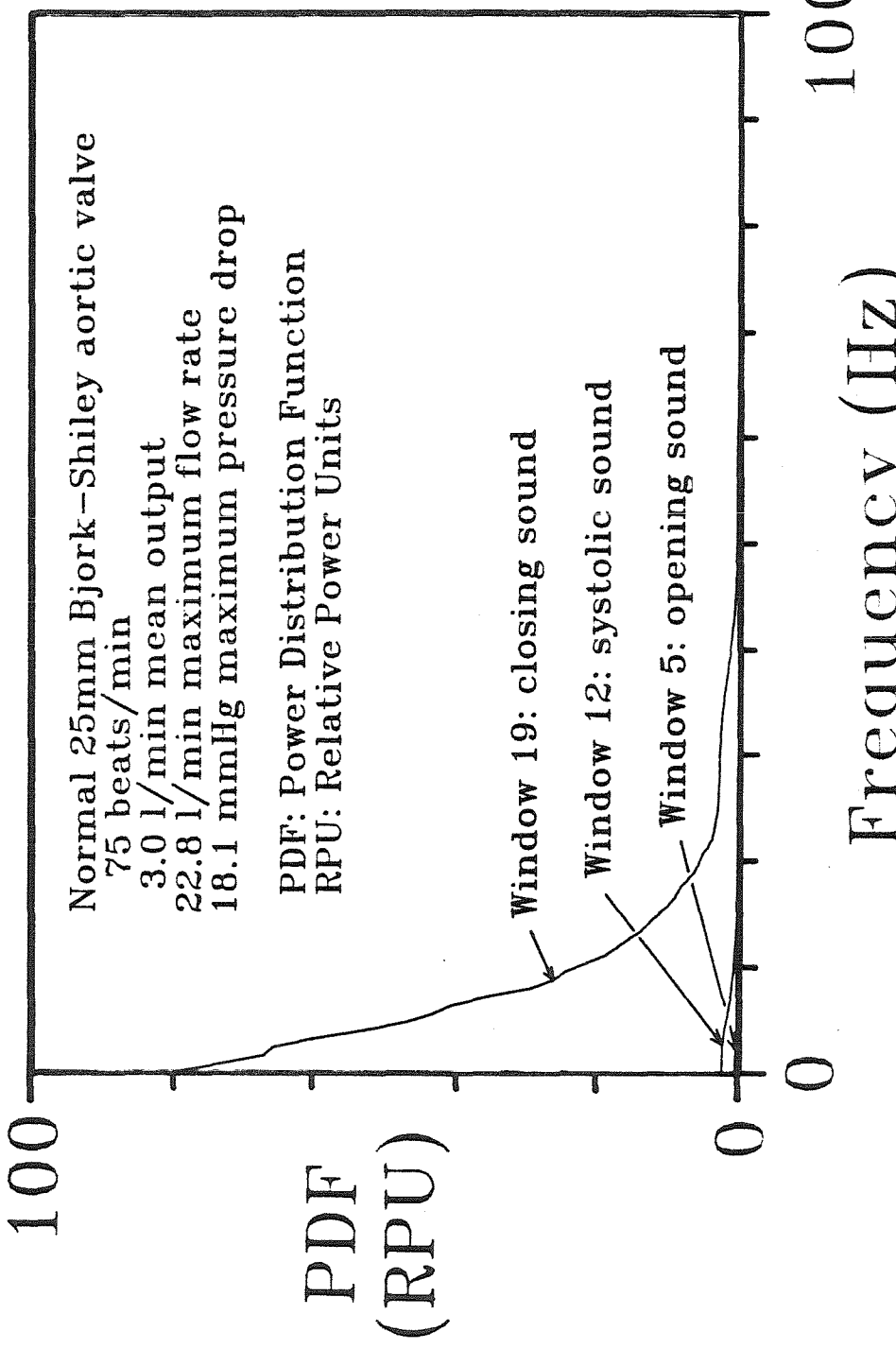

Figure 6-9d Auxiliary view perpendicular to the frequency axis of the 3-D power-frequency-time surface of experiment 272 showing power power distributions associated with windows encompassing the opening, systolic, and closing sounds.

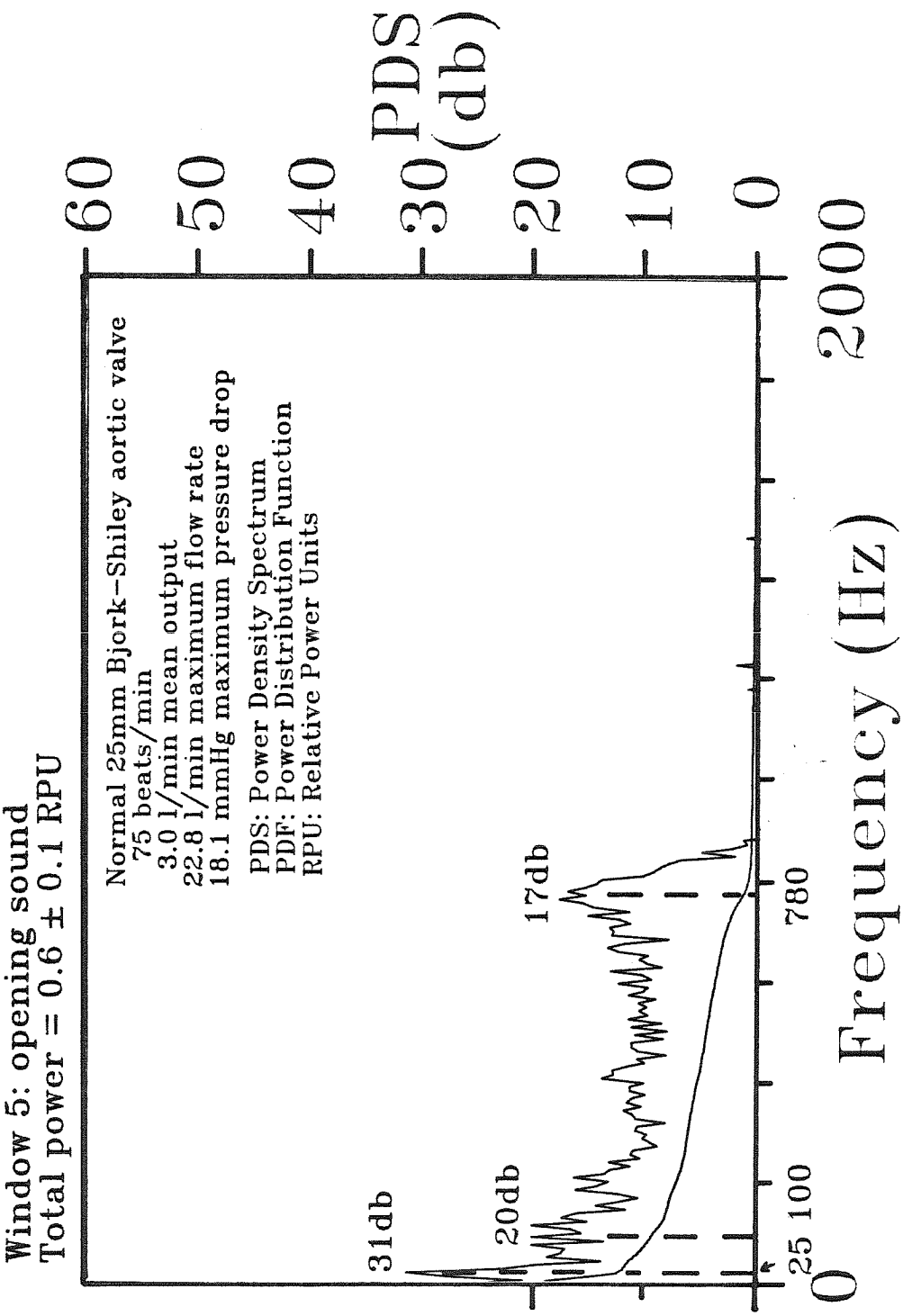

Figure 6-9e Power-density spectra and power distribution of the opening sound of experiment 272.

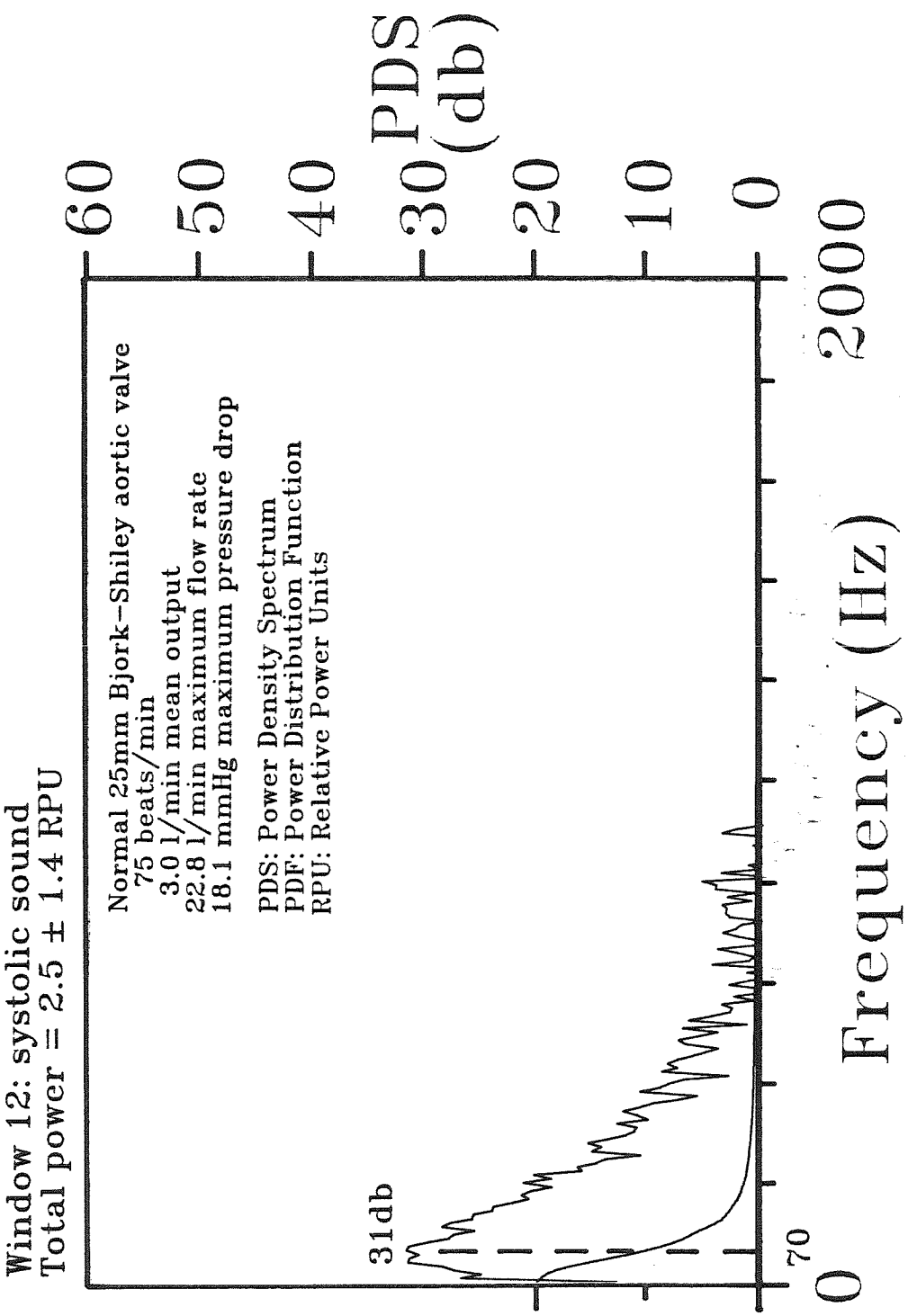

Figure 6-9f Power-density spectra and power distribution of the systolic sound of experiment 272.

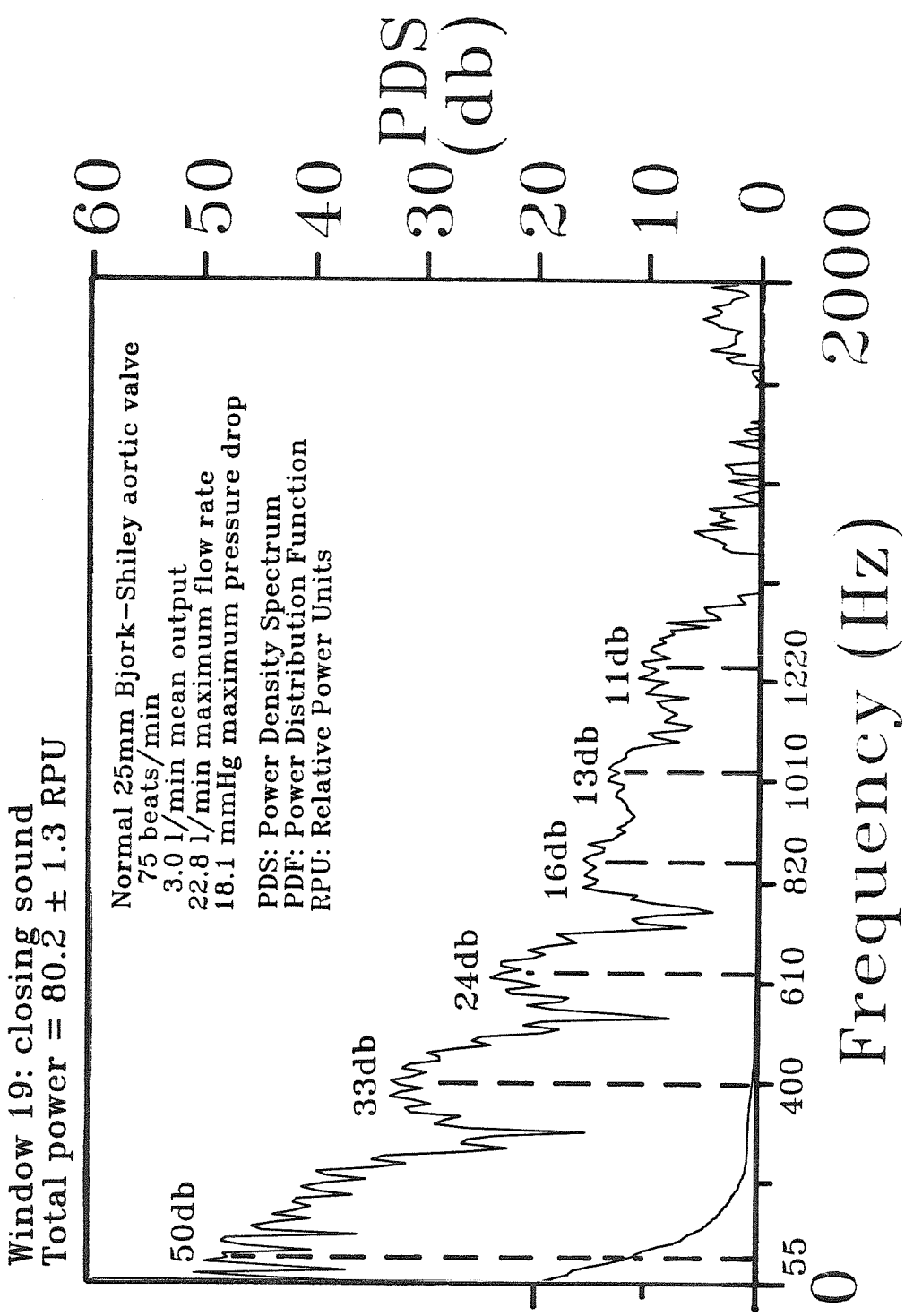

Figure 6-9g Power-density spectra and power distribution of the closing sound of experiment 272.

Parameters Estimated for

Significant Harmonic Peaks

Experiment 272

Event	Frequency, $f_{f,i}$; Decay, k_i; Power-Density, G_i (Hz,Hz,db)
Opening Sound	25, 5,31
Window 5	100,45,20
	780,40,17
Systolic Sound	
Window 12	70,45,31
Closing Sound	55,45,50
	400,60,33
	610,55,24
Window 19	820,55,16
	1010,65,13
	1220,80,11

Table 6-6 Parameters estimated from significant harmonic peaks of experiment 272.

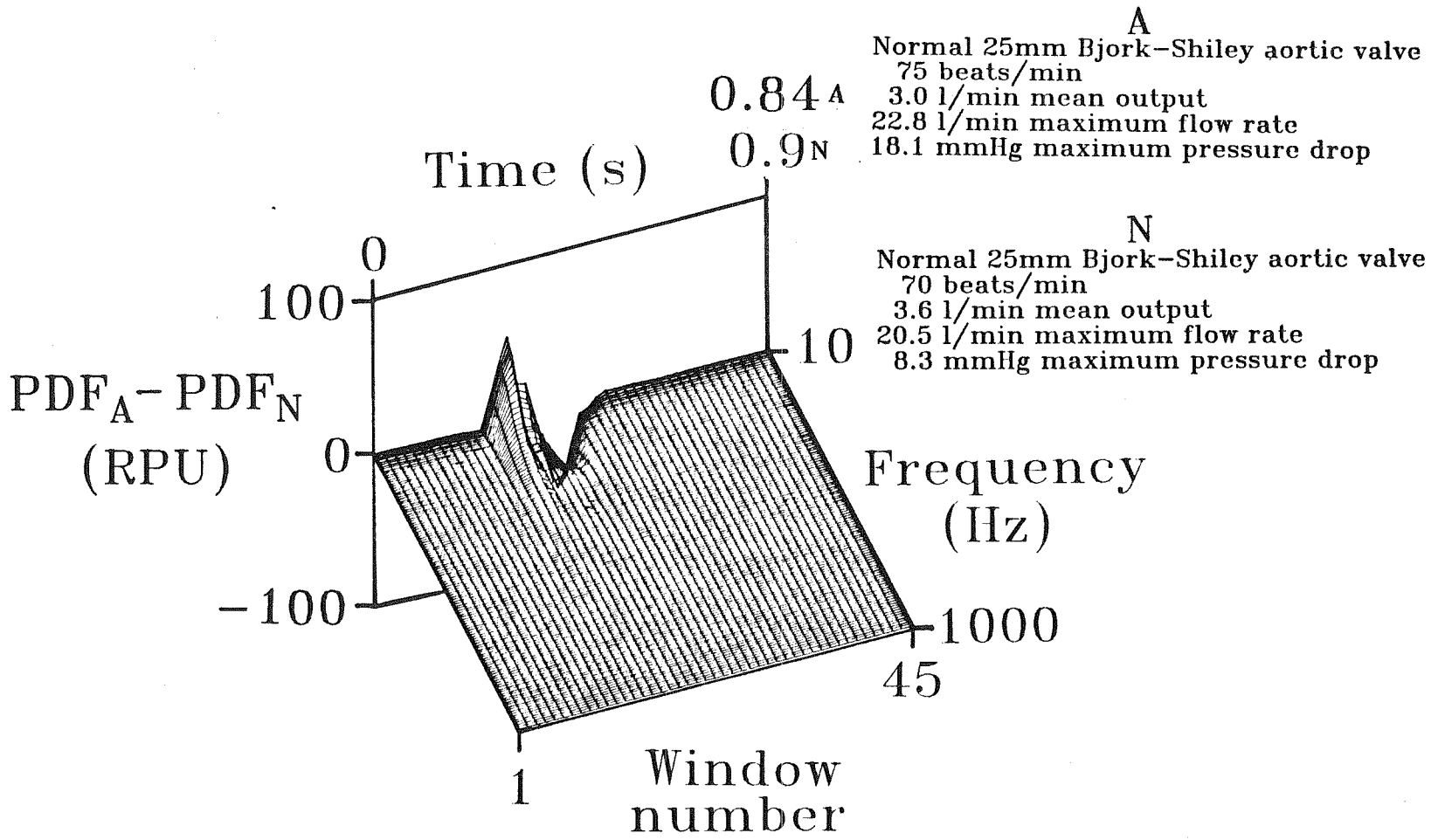

Figure 6-9h Three-dimensional surface depicting the difference between the power-frequency-time surfaces associated with experiments 272 and 266.

6.4 DISCUSSION OF RESULTS

6.4.1 Effects of Pulse Rate on the Sounds

The Bjork-Shiley prosthesis was pulsed at three different pulse rates. These pulse rates were 70, 52, and 75 beats/min which corresponded to experiments 266, 271 and 272, respectively. The important values defining the pulse mode for these three experiments are listed in the second and final columns of Table 6-1a. The ventricular ejection time was corrected by normal factors for these three pulse rates in order to simulate the natural, rate-dependent systolic and whole-cycle times. As a result the ratio of the systolic time interval to the whole-cycle time was not a constant but rather increased with the pulse rate. When the pulse rate varied between experiments, adjacent windows were shifted an amount proportional to the time of one complete cycle. As a result, windows 1 and 45 corresponded to the same relative moment within two consecutive cycles. During these three experiments, the stroke volume, maximum flow rate, and maximum pressure gradient decreased as the pulse rate increased. These changes resulted from maintainance of the mean output near values of 3.6, 5.6 and 3.0 L/min for experiments 266, 271 and 272, respectively.

6.4.1.1 The Opening Sounds

The opening sounds, OS, produced by the Bjork-Shiley valve for these three experiments occurred as two distinct events which we have labeled OS1 and OS2 nearest their occurrence along the upper tracings of Figures 6-6a, 6-8a and 6-9a. Flow visualization experiments confirmed that OS1 was produced when the occluder was still in its closed position while OS2 was produced when the occluder was at its totally open position. The four tracings in Figures 6-6a, 6-8a and 6-9a show that OS1 occurred at the time forward flow began. It was also clear that OS2 occurs approximately 50 ms after OS1 for each of the three

experiments. The occluder rotated from the orifice to its full opening angle at a rate that was not significantly affected by the pulse rates and stroke volumes that occurred during these three experiments. Based on these facts, we would expect to see similarities in the opening sounds for these experiments.

The opening sounds were chosen to correspond to window 5 of our analysis. No significant changes were observed in the values of the rate of change of the ventricular pressure prior to the opening sound OS2. We did not observe much change between the power-density spectra of the opening sounds for these three experiments. This can be seen by examining the spectra shown in Figures 6-6e, 6-8e and 6-9e and the correspond parameters listed in Tables 6-2, 6-5 and 6-6. The Figures show that the each significant peak of the spectra had similar center-frequencies. Like the spectra of the opening sounds of the Starr-Edwards 2400 valve, which we discussed in Part IV, each of the present spectra exhibited two low-frequency peaks and one high-frequency peak centered near 25 Hz, 100 Hz and 800 Hz, respectively. The amplitudes and widths of these peaks varied with the pulse rate. As the pulse rate decreased and the stroke volume increased from 58 to 116 cm^3, the distribution of power between the low- and high-frequency peaks shifted toward the low-frequency end of the bandwidth as shown by the distributions plotted in Figures 6-6e and 6-8e. The two, low-frequency peaks are probably associated with the first component of the opening sound which occurred when the valve was closed. Estimates of the flow rates through the annular gap which would be required to produce vortex-shedding of these frequencies gave values of 0.062 and 0.220 L/min for the 25-Hz and 90 Hz peaks, respectively. These values of the flow rate are quite possibly present at the time the valve begins to open. The flow rate of 0.062 L/min associated with the 25-Hz peak is also very similar to that corresponding with the 510-Hz peak associated with the opening sound of the Smeloff valve which had a value of

0.065 L/min. Also, the amplitude of the 25-Hz peak for the present case increased with decreasing pulse rate. This inverse relationship would be possible if the occluder remained in the orifice for a longer period, which could happen at slower pulse rates. The peak near 770 Hz broadened significantly and decreased in amplitude by 5 db as the pulse rate decreased. We have attributed this peak to the collision of the disc with the struts as the occluder rotates into its fully open position. Damping and less power of this mode indicates a possible reduction of the forces involved with the opening process.

Power distributions of these opening sounds can be observed by comparing contours of window 5 in all of the other subfigures corresponding to these three experiments. These figures include Figure 6-6 , Figure 6-8 and Figure 6-9, subfigures b,c,d, and h. Here we can compare their powers to those of the systolic and closing sounds as well as the latter's relative times in the cycle. The opening sound was the least powerful of the three major sounds of the Bjork-Shiley valve. The total-power of the opening sound never exceeded 3 RPU during any experiment. Both difference-surfaces shown in Figures 6-8h and 6-9h show flat contours for windows 3 through 8 which corresponded to the opening sound. The power axis was again scaled to permit the plotting of the more powerful closing sounds, therefore, these difference-surfaces did not clearly show differences between these less powerful opening sounds.

6.4.1.2 The Systolic Sounds

The systolic sound, SS, of experiments 265, 271 and 272 is labeled nearest its occurrence along the upper tracings of Figures 6-6a, 6-8a and 6-9a, respectively. Unlike the opening sounds, the systolic sounds were not similar for experiments 266, 271 and 272. These differences were primarily a result of differences in the

value of the maximum systolic flow rates which were 20.5, 29.6 and 22.8 L/min for experiments 266, 271 and 272, respectively. The maximum intensity of the systolic sound occurred at the same time as the maximum flow-rate and the maximum pressure-gradient. It is clear from these figures that the systolic sound-intensity increased with the maximum flow-rate and the maximum pressure-gradient. A correlation was observed between the total-power of the systolic sound and the value of the maximum flow rate. This correlation is shown in Figure 6-4 for these three experiments. An additional correlation was observed between the power of the sound produced during systole and the value of the maximum systolic pressure gradient across the valve. This correlation is shown in Figure 6-3 for these three experiments.

The time-amplitude tracings in subfigures **a** also show that the systolic sound occurred earlier, within window 11, during experiment 272, and later, within window 12, during experiment 266. The **normal** systolic window was window 12 during experiment 271. These differences resulted from a smaller stroke volume of 47 cm^3 during experiment 272 and a larger stroke volume of 116 cm^3 during experiment 271 compared with the **normal** stroke volume of 58 cm^3. As with the other two valvar designs, the Bjork-Shiley valve exhibits similar trends relative to the acoustical changes associated with changes of the stroke volume. The systolic sound is early or later than **normal** depending whether the stroke volume has decreased or increased, respectively. A very good correlation was observed between the total power of the systolic sound and the value of the maximum flow rate. This correlation is shown in Figure 6-4 for these three experiments. In addition, a correlation existed between the power of the sound produced during systole and the value of the maximum systolic pressure gradient. This correlation is shown in Figure 6-3 for these three experiments. We see comparable changes when we inspect the information in the frequency

domain.

The power-density spectra depicted in Figures 6-6f, 6-8f and 6-9f show these differences in the frequency domain. The spectrum of the systolic sound of experiment 271 is noticeably different from the other two experiments. This difference is the peak in the spectrum at 700 Hz in Figure 6-8f. Since this peak is near the same center frequency as that attributed to the opening sound OS2, we conclude that the occluder is bouncing abnormally in the open position at this reduced pulse rate. A larger systolic flow rate was probably responsible for this extra bouncing. The spectra of the **normal** systolic sound of experiment 266 as shown in Figure 6-6f, depicts no such peak. Flow visualization experiments confirm this lack of bouncing during **normal** systole for the Bjork-Shiley valve relative to the Smeloff or Starr-Edwards 2400 valves. The low-frequency peaks have comparable center-frequencies but differ in amplitude. Experiment 271 had less power near 25 Hz. This reduction accounted for the 1.1 RPU loss of total power relative to **normal**. Experiment 272 had 2 to 4 db less-power over all frequencies accounting for the 3.2 RPU, or 55%, loss of total power relative to **normal**.

Subfigures 6-6, 6-8 and 6-9, subfigures b,c,d, and h show these differences in terms of the distribution functions. The power of the systolic sounds were large enough relative to the closing sounds to enable one to see differences between them as shown in these figures. They particularly show the differences in the magnitude of the total power of the systolic sound. The systolic sound generally had more power than the opening sound but less power than the closing sound. The difference-surfaces at first appear to have flat contours near the systolic sound, windows 10 to 13. This is true for Figure 6-8h, but Figure 6-9h has a small valley at those contours encompassing the systolic sound. This valley is only about 3 RPU deep and must be inspected closely to be seen.

6.4.1.3 The Closing Sounds

The closing sounds, CS, of experiments 266, 271 and 272 were very similar to each other. These sounds were comprised of two events which we have labeled CS1 and CS2 near their occurrence along the upper tracings of Figures 6-6a, 6-8a and 6-9a. One can see from the other tracings included in these figures that the closing sound, CS1, occurred at the same time as the maximum backflow, the dichrotic notch of the aortic pressure curve, and the beginning of the rapid decrease of the ventricular pressure curve. The second closing sound CS2 occurred at the same time as the maximum value of the diastolic aortic pressure. We observed a 40-ms early closing sound during the experiment having increased pulse rate and 20% less stroke volume. We also observed a 20-ms late closing sound during the experiment having decreased pulse rate and 100% more stroke volume. These changes were estimated in the normalized time-domain.

From the appearance of these sounds in the time-domain we would expect them to have similar power-density spectra. These spectra are shown in Figures 6-6g, 6-8g and 6-9g. Like the experiments involving the Smeloff and Starr-Edwards 2400 valves, the spectra of the closing sounds were similar to each other but much unlike either of the spectra associated with the opening or systolic sounds. The "intra-sonic" similarity was in the number, location, shape and amplitude of corresponding peaks. Each spectrum shown in Figures 6-6g, 6-8g and 6-9g has essentially six peaks. These peaks have similar center-frequencies as listed in Table A-5. The amplitudes of the peaks of the spectrum of the closing sound of the APS have from 1 to 2 db less power-density relative to normal. This decrease of power for distinct peaks was reflected in the decreased, average total-power of the sounds, from a normal value of 92.7 RPU to approximately 80

RPU for both of the two **APS** . The normalized, distribution functions plotted below the spectra were identical for each experiment. Similarities of the closing sounds between valvar designs suggest either the aortic flow section is involved with these additional peaks because the general effect is not valvar dependent, or the nature of the forces involved in closure are responsible for stimulating similar vibrational modes of the valves. There are clear differences between the groupings of the peaks for each valvar design which would suggest that the design does have some additional influence on the location and shape of the peaks. At this time we can not relate these peaks with more certainty to specific physical vibrations of the system. Estimates of the flow rates required to produce vortex-shedding at the time of closure gave values ranging from 0.12 to 3.75 L/min corresponding to the peaks from 55 to 1500 Hz, respectively. Table 7-2 lists the results of these estimates for closing sounds of the three valvar designs. Of the flow rates estimated, those corresponding to values less than 2.0 L/min were physically realistic. Therefore, peaks centered at 55 Hz were most probably related to vortex-shedding.

The power distributions of the closing sounds that are indicated by windows 21, 22 and 19 in Figures 6-6, 6-8 and 6-9, subfigures b,c,d and h, respectively, were similar in form but differed significantly in their relative magnitudes and timing within the pulse-cycle. These differences are directly depicted by the valley between 10 and 600 Hz along the contours of windows 20 and 21 in Figure 6-8h. This asymmetrical valley/peak combination indicates that the closing sound during this **APS** had significantly less power between 10 and 600 Hz and it occurred late relative to the **normal** closing sound. Similarly, the peak/valley combination along the 10 Hz contour between windows 13 and 25 in Figure 6-9h, indicates that the closing sound was early during this experiment. The symmetry of this peak indicates that the power distributions were similar for the

two experiments.

6.4.1.4 Summary of Comparisons of Pulse-Rate Experiments

The effect of pulse rates of 52, 70 and 75 beats/min upon the opening sounds of the Bjork-Shiley valve was minor. A significant reduction of the total power of this sound was observed for the case having a reduced stroke volume.

The effect of pulse rate upon the systolic sound was primarily to shift this sound earlier in systole as the stroke volume decreased, and to increase the power of the non-transient component, centered near 100 Hz, as the stroke volume increased. A peak centered near 800 Hz for the case having a greater maximum systolic flow rate indicated that the occluder bounced more during flow for this experiment.

The effect upon the closing sound was to decrease the power of harmonic peaks by 1 to 3 db as the pulse rate decreased. There was an early or delayed closing sound during the APS depending whether the stroke-volume was greater or less than **normal**, respectively. Time was estimated using a time scale normalized with respect to the cycle-time.

6.4.2 Effects of Stroke Volume on the Sounds

The Bjork-Shiley valve was pulsed at three different stroke volumes while maintaining a pulse rate of 70 beats/min. The experiments which will be compared are 265, 266, and 267. The important values which define the pulsatile state for these experiments are listed in the the first three columns of Table 6-1a. The stroke volumes corresponding to these experiments were 105, 58, and 32 cm^3 and corresponded to mean flow rates of 6.8, 3.6, and 1.2 L/min, respectively. As the stroke volume corresponding to these three experiments increased, we

observed an increase of the maximum flow-rate and maximum pressure-gradient

6.4.2.1 The Opening Sounds

In a manner similar to the previous comparisons involving changes of pulse rate, the opening sounds, OS, produced by the Bjork-Shiley valve for these three experiments occurred as two events which we have labeled OS1 and OS2 nearest their occurrence along the upper tracings of Figures 6-5a, 6-6a and 6-7a. The sound, OS1, occurred at about the time that the flow curve began to rise. Flow visualization experiments confirmed that the occluder began its motion at the time OS1 occurred and arrived at its fully open position at the time OS2 occurred. The time interval between OS1 and OS2 was approximately 40 ms for all three experiments. The opening sounds corresponded to window 5 of our analysis. Significant changes were observed in the value of the rate of change of the ventricular pressure immediately prior to the opening sound for the case involving increased stroke-volume. The normal rate-of-change was 1.6 mmHg/ms while the rate-of-change during the APS was 2.6 mmHg/ms. These changes may be responsible for the differences between the power-density spectra of the opening sounds for these three experiments.

Subfigures 6-5e, 6-6e and 6-7e depict these spectra and the corresponding parameters are listed in Tables 6-2, 6-3 and 6-4. The spectra had essentially two peaks below 100 Hz and one peak near 800 Hz. These peaks had approximately the same location within the spectra, but had amplitudes which varied significantly with the stroke-volume. The peak at 25 Hz increased by 8 db and the peak at 80 Hz increased by 5 db above their normal values during the experiment having increased stroke-volume. As a result of these changes, the

corresponding total-power of the opening sounds increased from 0.6 RPU to 2.6 RPU. The peaks near 800 Hz had peak-powers of 16 db when the stroke-volume was 32 cm^3, and 21 db when the stroke-volume was 105 cm^3. These facts together with the increase of the rate of change of the ventricular pressure and reduced OS1-OS2 interval suggest that the forces on the occluder increased with increasing stroke-volume.

These opening sounds can be compared further by inspecting contours of window-5 in Figure 6-5 , Figure 6-6 and Figure 6-7, subfigures b,c,d, and h. Unfortunately, the power-scales of these figures again do not allow clear comparisons between these sounds. They do show, however, that the opening sound was comparable in power to the systolic sound for the two experiments having lowest stroke-volumes, and that the opening sound had much less power than the closing sound during all three experiments. The difference-surfaces shown in Figures 6-5h and 6-7h, show a very shallow valley and peak, respectively, along the window-5 contour, indicating the 10-RPU differences between the total power of these power distributions.

6.4.2.2 The Systolic Sounds

The systolic sounds were quite different for experiments 292, 295 and 296. Again, differences are immediately apparent in the time tracings of the systolic sound, SS, depicted at the top of Figures 6-5a, 6-6a and 6-7a. This primary difference was the amplitude and time of the sounds. These changed with the value of the maximum systolic flow rate which was 40.0, 20.5 and 14.1 L/min for experiments 265, 266 and 267, respectively. Again, by examining all four tracings in these figures, one can see that the maximum intensity of the systolic sound occurred at the same time as the maximum flow-rate and the maximum

pressure-gradient. And it is also clear that the systolic sound-intensity again increased with the maximum flow-rate and the maximum pressure-gradient. This correlation between systolic sound and maximum flow-rate and pressure-gradient is shown in Figures 6-4 and 6-3, respectively.

The time-amplitude tracings in subfigures a show that the maximum amplitude of the systolic sound occurred later, within window 13, during experiment 265, and earlier, within window 11, during experiment 267 when compared with the **normal** window 12. As we have noted with the Smeloff and Starr-Edwards 2400 valves, the time of maximum systolic sound correlated quite well with the stroke volume, maximum flow rate, or alternatively the mean flow rate.

The power-density spectra depicted in Figures 6-5f, 6-6f and 6-7f clearly show these differences between systolic sounds. Each spectrum has a low-frequency peak centered near 70 Hz. The amplitude of this peak was 28, 34 and 43 db for stroke volumes of 32, 58 and 105 cm^3, respectively. The spectrum corresponding to the experiment having low stroke volume, shown in Figure 6-7f, has a small 8-db peak centered at 800 Hz. The **normal** spectrum had no corresponding peak. This high-frequency peak was probably produced by sounds made by the occluder as it vibrated in the open position. We observed a similar high-frequency peak in the spectrum of the systolic sound of experiment 271 which also had a stroke volume greater than **normal**. The occluder bounced more at the greater of the three stroke-volumes. This is assuming that the peak at 470 Hz in Figure 6-5f is not related to such bouncing. This peak at 470 Hz in the spectrum of the high-stroke-volume experiment is unique for the systolic sounds of this valvar design. It physical significance is not known. Possible explanations of its origin include abnormal vibrational modes of the valve, the catheter, and the aortic flow section. Estimated values of the Strouhal number at the strut and catheter based on the frequency of this peak were 0.22 and

0.29, respectively. These values are listed in Table 7-2. Any general remarks made earlier with regard to the relationships between stroke-volume and systolic sounds for the experiments involving different pulse rates also applies to the experiments involving changes of stroke-volume alone.

Subfigures 6-5, 6-6 and 6-7, subfigures b,c,d, and h, show these differences very clearly in terms of the power-distributions. The total systolic power of experiment 265 is clearly greater than that of experiments 266 or 267. The total power of the systolic sounds of each experiment are greater than that of the corresponding opening sound and less than that of the corresponding closing sound. The large peak along the window-13 contour between 10 and 300 Hz in Figure 6-5b, for example, is clearly different from corresponding contours of Figures 6-6b and 6-7b. Figure 6-7h shows a shallow valley along the window-12 contour at frequencies between 10 and 200 Hz. Figure 6-5h shows a large peak along the window-12 contour at frequencies between 10 and 200 Hz.

6.4.2.3 The Closing Sounds

The closing sounds, CS, of experiments 265, 266 and 267 are very similar to each other when seen in the time domain. Figures 6-5a, 6-6a and 6-7a show these sounds along the top tracing. These sounds were comprised of two events which we have labeled CS1 and CS2 nearest their occurrence along these tracings. The rate of change of pressure at closing is significantly different for these three experiments. These values are given in Table 6-1a. The closing sound CS1 occurred at the same time as the maximum backflow, the dichrotic notch of the aortic pressure curve, and the beginning of the rapid decrease of the ventricular pressure curve. The second closing sound, CS2, occurred at the same time as the highest value of the diastolic aortic pressure.

Each of the spectra of the closing sounds that are shown in Figures 6-5g, 6-6g and 6-7g has seven peaks. The spectra of the closing sounds for each experiment were again more similar to each other than to either of the spectra associated with the opening or systolic sounds. There were, however, significant differences between these spectra. The amplitudes of corresponding peaks between experiments 267 and 266 were 1 to 3 db less for the **APS** . These values accounted for the reduction of the total power of the closing sound associated with experiment 267 from a **normal** value of 93 RPU to 64 RPU. It is not clear why such a change occurred. The rate of change of ventricular pressure had decreased, but not significantly. This experiment involved a degree of hypertension. The mean aortic pressure was 164 mmHg. This fact combined with the low stroke-volume should have increased the drag forces on the occluder. We cannot explain this result. The major difference between the spectrum of experiment 265 and the **normal** spectrum was that the peaks normally centered at 390, 600, 820, and 1500 Hz were shifted between 30 to 50 Hz lower in frequency. The total power, however, is only 5 db greater than **normal**.

The power distributions of the closing sounds are depicted by windows 21, 21 and 19 in Figures 6-5, 6-6 and 6-7, subfigures b,c,d and h, respectively. These figures also show the power distributions of these closing sounds as they relate to the opening and closing sounds. Particularly clear is the reduced power of the closing sound of experiment 267. The 3-D power-frequency-time surfaces, subfigures **b**, also show closing sounds that are similar in form but different in amplitude. These differences appear in the difference surfaces shown in Figures 6-5h and 6-7h. The window-20 contour in Figure 6-5h indicated that the closing sound of the experiment having a large stroke-volume had a distribution of power toward lower frequencies between 10 and 200 Hz while maintaining a comparable total-power. The peak/valley combination between windows 13 and 25

shown in Figure 6-7h indicated that the closing sound of experiment 267, having a small stroke-volume and mean-aortic pressure of 165 mmHg, had a closing sound which occurred 60 ms early.

6.4.2.4 Summary of Comparisons of Stroke-Volume Experiments

The effect of stroke volumes of 32, 58, and 102 cm^3 upon the opening sounds of the Bjork-Shiley valve was significant for the case having the largest stroke volume. At this alternate pulsatile condition a reduced rate-of-change of ventricular pressure occurred prior to opening of the valve. The vibrational modes corresponding to the center-frequencies observed in the spectra of these sounds were essentially the same. Only the powers of these modes changed with Stroke-Volume. These changes were probably caused by changes of the rate of change of ventricular pressure at the time of OS2. In general, a reduction of stroke-volume produced a less powerful opening sound at frequencies between 10 and 1000 Hz.

The effect of the stroke-volume upon the systolic sound was primarily to shift this sound later in systole as the stroke volume increased and increase the power of the non-transient component, centered near 70 Hz, as the stroke volume increased. The transient peak appeared at 800 Hz during low stroke-volumes and disappeared at both **normal** and high stroke-volumes. A peak appeared at 470 Hz during the experiment having a large stroke-volume. This 470-Hz peak was probably produced by vortex shedding at the phonocatheter and struts during the high flow rates associated with this experiment. These overall changes of the systolic sound reflect the changing dynamics of the occluder and turbulence as a result of the corresponding changes of maximum flow rate during these experiments.

The effect of stroke volume upon the closing sound was not as easily explainable compared with corresponding explanations of changes of the opening and systolic sounds. A significant reduction of 28 RPU was observed in the total power of the closing sound of the case having a stroke-volume less than **normal**. It was suggested that this could have resulted from the combined effects of stroke-volume and hypertension during this experiment. The closing sound of the experiment having a large stroke volume was **normal**.

6.4.3 Effects of Hypertension on the Sounds

The Bjork-Shiley valve was pulsed at two different states of mean-aortic pressure at a pulse rate of 70 beats/min. These two experiments, 266 and 267, have been compared as part of the experiments involving changes of the stroke-volume in the previous section. A separate comparison of these experiments is not necessary. The comments made in that section of text for these two experiments are valid for a comparison of the effects of hypertension. These effects include a reduction of stroke-volume and maximum systolic flow-rate, early closing sound relative to the opening sound, a reduction of the total power of the opening sound, and a small shift of the center-frequencies of the closing sound toward lower values. The reduction of the total-power of the closing sound was noted above. This change could not be related to hypertension alone and were considered to be primarily caused by the change of stroke volume.

6.5 CONCLUSIONS AND RECOMMENDATIONS

It is apparant from the results presented in this paper that the effects of pulse rate, stroke volume and hypertension upon the three major sounds of the Bjork-Shiley valve were significant.

The opening sounds under all of the pulsatile conditions did not change significantly relative to corresponding changes of the systolic and closing sounds. We did observe an increase of the total power of the opening sound with an increase of the stroke volume and rate of change of ventricular pressure.

Of the three major sounds, the most significant changes occurred with respect to the systolic sounds. This sound occurred early or late depending whether the stroke volume was greater or less than **normal**. We observed that the total-power of the systolic sound changed dramatically and correlated very well with the stroke volume, maximum systolic flow rate, mean flow rate, and maximum systolic pressure gradient. A low-frequency peak, associated with the flow, was always present in the spectrum, whereas a high-frequency peak associated with the bouncing occluder appeared during the experiments having small-stroke volume and low pulse rate. A unique peak at 470 Hz appeared in the spectrum of the systolic sound for the experiment having a maximum systolic flow rate of 40 L/min. This peak was associated with sounds produced by vortex-shedding at the phonocatheter and struts.

The closing sounds of the valve were very powerful relative to both the opening and systolic sounds. The time of closure was later with increasing stroke volume. The total power of the closing sound increased with stroke volume and rate of change of ventricular pressure. The spectra of these sounds were very similar for each experiment except for the case having a large mean aortic pressure. The peaks of this spectrum had **normal** center-frequencies but the amplitudes of the peaks were each 2 to 4 db below **normal**. For this case, the total power of the closing sound was 28 RPU less than the **normal** value of 93 RPU. This particular experiment also involved a small stroke-volume. These combined effects produced this reduction of acoustical power at the time of closing.

We observed some general similarities between valvar designs. We speak here in general terms when we say "similarities". For example, the distribution of peaks in the spectrum of the opening sound of one valve, say A, may be more similar to valve B than to valve C. The spectra of the opening sounds of the Bjork-Shiley valve were more similar to those of the Starr-Edwards 2400 valve than to those of the Smeloff valve. The Shiley and Edwards designs produced opening sounds with peaks located in the bands 10 to 1000 Hz with a rapid decline of little power at frequencies above 1000 Hz. The Smeloff valve had no such rapid decline of power at the frequencies we studied. The corresponding systolic sounds were also similar for the Bjork-Shiley and Starr-Edwards 2400 prostheses as compared with the Smeloff valve. No two valve designs had closing sounds which were different to a lesser or greater degree from the third valvar design.

The differences between spectra produced by two different valve designs could clearly be distinguished for any two spectra chosen at random from those we have presented. No change of the pulsatile mode could produce a spectrum which could be mistakenly associated with another valvar design. Therefore, we conclude the method, as we have applied it to these data, produced very unique and specific results relative to valvar design.

The systolic sounds were sensitive to flow conditions for all three designs. The opening and closing sounds were insensitive to all pulsatile conditions we have studied relative to the sensitivity of the corresponding systolic sounds. The Bjork-Shiley and Starr-Edwards 2400 valves did, however, show some sensitivity of the opening sounds to changes of stroke volume and time-rate-of-change of ventricular pressure at the time of opening. The Smeloff valve showed no comparable sensitivity. Peaks in the spectra of the closing sounds of all three valves had center-frequencies which were insensitive to changes of the pulsatile

conditions. The amplitudes of these peaks, however, did increase with increasing stroke volume and time-rate-of-change of ventricular pressure at the time of closure.

6.6 ACKNOWLEDGEMENTS

Funding for this project was provided by the Donald E. Baxter Foundation, the Children's Heart Foundation of Southern California, and the American Heart Association, Greater Los Angeles Affiliate.

PAPER 7

A Quantitative Method for the *In Vitro* Study of Sounds Produced by Prosthetic Aortic Heart Valves Part VII: Consideration of Vortex-Shedding as a Mode of Sound Production

A Quantitative Method for the *In Vitro* Study of Sounds Produced by Prosthetic Aortic Heart Valves Part VII: Consideration of Vortex-Shedding as a Mode of Sound Production

ABSTRACT

One possible mode of sound production during opening, systole and closing phases of the valvar-cycle is related to vortex-shedding at the the orifice, struts, occluder and phonocatheter.

Assuming each peak in the density-spectra of the opening and closing sounds was related to such shedding, we estimated the effective mean velocity and associated flow rate which would produce shedding having the center-frequency of each peak. These estimates were based on the dimensions of the annular gaps that existed between the occluder and the orifice of the Smeloff and Bjork-Shiley valves. A gap width comparable to that of the Smeloff valve was assumed for the Starr-Edwards 2400 prosthesis. The resulting effective flow rates associated with these peaks were small relative to the systolic flows through the valves. Based on the results of these calculations and flow visualization studies, we concluded that vortex shedding was a possible mode of production of the first components of both the opening and closing sounds for all three valvar designs.

Assuming each peak in the density-spectra of the systolic sounds was related to vortex shedding, we estimated the effective mean velocity and associated flow rate which would produce shedding having the center-frequency of each peak. These values were estimated separately for flows at the struts and phonocatheter and were based on the dimensions of each of these strutures. We also estimated the Strouhal number for flows at the struts of each valvar design and at the phonocatheter. The results of these estimates indicated that the low-

frequency peak at 170 Hz in the systolic sound of the Smeloff valve was related to shedding at the catheter. A peak at 470 Hz in the systolic sound of the Bjork-Shiley valve was related to shedding at the struts and/or catheter. And the low-frequency peak at 80 Hz in the systolic sound of the Starr-Edwards 2400 valve was associated with shedding at the catheter.

Key Words-Strouhal number, vortex-shedding, sound, fast Fourier-transform, prosthetic heart-valve, *in vitro* comparison

7.1 INTRODUCTION

In this paper we discuss the relationships between the frequencies of sounds, generated by vortex-shedding of flows around valvar structures, gaps and phonocatheters, and the corresponding flow rates associated with these frequencies. Natural heart valves and many designs of prosthetic heart valves seal totally when they are closed. There are many designs of prosthetic heart valves, however, that have occluders with diameters smaller than the diameter of the orifice. These valves can normally never close totally. For these types of valves, either forward flow or backward flow can occur during early systole and diastole, respectively. Flows through these small gaps or around small objects like struts can produce sounds having frequencies that depend on the geometry of the flow - primarily the gap-width or strut-diameter - the flow rate, and the Strouhal Number. The Strouhal number observed for a wide variety of geometries and flow rates has values between 0.1 and 0.2. The Strouhal number of flows past rigid cylinders is between 0.19 and 0.21 for Reynolds numbers, based on the cylinder-diameter, between 200 and 10000. For flows through thin annular gaps, the gap-width is commonly used as the characteristic length for these flows. Blevins (1977) and Berger and Wille (1972) provide plots of the Strouhal number for a variety of geometries and Reynolds numbers.

We have observed resonance peaks within the power-density spectra of sounds produced by forward flows through prosthetic heart valves when these valves are in their closed position. We have observed such sounds being produced by the Smeloff and Bjork-Shiley prostheses which do not totally occlude upon closure. We have not, however, observed these sounds during the pulsing of the Starr-Edwards 2400 valve. This difference may result from the fact that

the occluder of this valve does totally occlude the orifice upon closure. These facts suggest the physical cause of these sounds was related to the difference in the flow-dynamics at opening and closing that result from these design differences. It was possible to have forward flow prior to opening. For those valves which did not totally occlude, forward flow may not be large enough to produce sufficient drag on the occluder and the pressure-gradient may not contribute sufficient force upon the occluder to force its downstream-motion until a critical amount of forward flow has developed. If these facts are true, then, a small flow-rate through the valve prior to both opening and closure could produce vortex shedding downstream of the annular gap. These vortices could shed at frequencies which correlate with those of the significant peaks of the acoustical power-density spectra. The relationship between the characteristic mean velocity and this predominate frequency of the sounds produced by such flows would be provided by the Strouhal number.

Another type of flow which could be responsible for sounds produced by flow in and around prosthetic heart valves is that related to vortices shed as the fluid flows around struts. Analogous phenomena would occur during flow past a phonocatheter inserted into the flow. Struts of prosthetic heart-valves are generally circular in cross-section but can have very complex, spanwise geometries depending on the valvar design. Most phonocatheters, on the other hand, have a simple, cylindrical shape.

The geometries of the struts for each valvar design used in our studies were quite different. Figure 7-1 shows photographs of typical Starr-Edwards 2400, Smeloff and Bjork-Shiley valves. The Starr-Edwards 2400 valve had three upstream struts. These struts projected downstream perpendicularly to the orifice and then curved inward at their extremities, meeting at the "apex." Since the flow must go around the central occluder, it must flow around these struts.

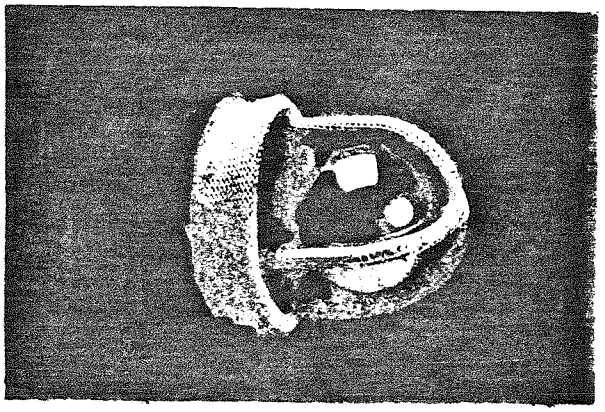

Starr-Edwards 2400-10A ball valve

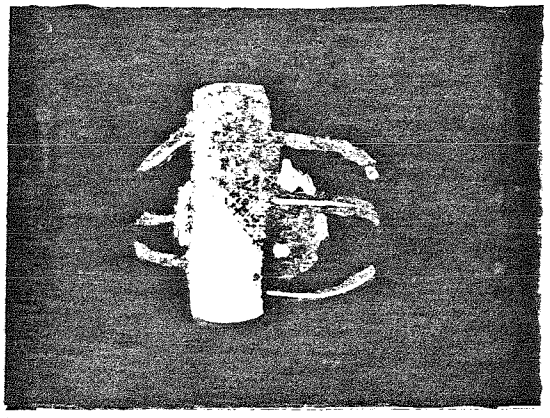

Smeloff-Cutter A-5 ball valve

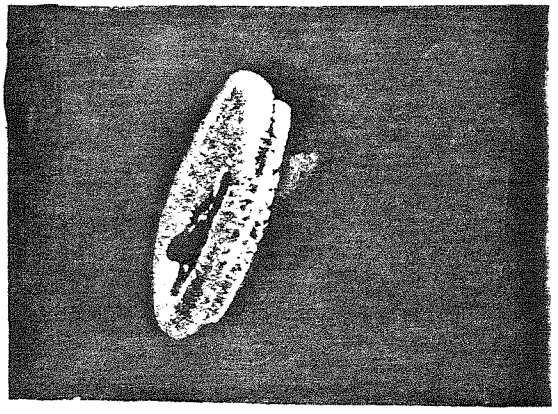

Björk-Shiley tilting disc valve

Figure 7-1 Photographs of the Starr-Edwards 2400, Smeloff and Bjork-Shiley Prostheses used for these studies.

Flow visualization experiments have shown that the streamlines during systole were inclined at angles between 20 and 40 degrees relative to the axis of the struts. This angle depended on the axial position. The Smeloff valve had three upstream and three downstream struts each of which projected perpendicular to the orifice and then curved inward at their extremities as shown in Figure 7-1. Unlike the Starr-Edwards 2400 valve, the struts of the Smeloff valve did not connect to form an "apex." Again the flow must go around the struts. Flow visualization again showed that the streamlines during systole were inclined at angles between 20 and 40 degrees relative to the struts. Figure A-3 of Appendix A shows photographs of frames of a video tape showing the position of the occuluder, the sound tracing, particle trajectories and the flow-rate tracing for three specific times of a typical cycle of the Smeloff valve. The three sounds depicted are from the top to the bottom: the sound produced prior to opening of the valve, the sound at peak systolic flow, and the sound produced at closure. Flows are to the right in the top two pairs of figures and to the left in the bottom pair of figures. The maximum systolic flow rate was approximately 25 L/min during the experiment depicted in Figure A-3. A third valvar design, the Bjork-Shiley valve, had a single, complexly shaped upstream strut and a similar downstream strut. A photograph of this valve is shown in Figure 7-1. Unlike the struts of the Smeloff valve, these struts are perpendicular to the flow. When this valvar design was fully open, large portions of the struts were adjacent to the occluder and did not extend into the bulk flow. Approximately 50% of the strut surface-area extended from the occluder to the orifice. At these latter surfaces, the fluid flowed entirely around the strut. These exposed regions were in the lower, "minor" flow-region associated with this valve. For comparable flow-rates, the struts of the Bjork-Shiley valve would, therefore, be exposed to relatively small velocities as compared to the struts of either the Smeloff or Starr-Edwards 2400

prostheses. Figure A-4 shows frames of a video tape depicting the occluder, sound and flow tracings and particle trajectories through the Bjork-Shiley valve. Corresponding frames are similar to those described for Figure A-3. The maximum systolic flow rate during this experiment was approximately 25 L/min.

The most powerful sounds produced by vortex-shedding near any strut would probably occur during systole at the time of the largest forward-flows. Such vortex-shedding may be responsible for peaks that have been observed in the power-density spectra of the systolic sounds of flows in and around each valvar design. Vortices could also be shed as a result of the systolic flows past a phonocatheter. The frequency of vortex-shedding that results from flow past such a phonocatheter inserted perpendicular to the flow would be the same for each systolic sound provided the free-stream velocities were similar.

It is important to remember that we are also discussing "confined" flows. The walls of the aortic flow-section, complex geometry of the sinuses of Valsalva and each, individual valvar design produced a very unique, complex flow in the region of the valve. In this paper, we will give estimates of the flow rates that would be necessary for sound production for frequencies we have observed during experiments involving the three valvar prostheses. These estimates have been based upon Strouhal numbers for flows past rigid cylinders and the corresponding relation between the Strouhal number and Reynolds number. We were not able to estimate the Strouhal number for many of the examples we will discuss because the flow rates were too small to be estimated from the output of the flowmeter. We will use examples from experiments discussed in Parts IV, V and VI of this series to illustrate vortex-shedding for flows through gaps, past struts and past the phonocatheter. These examples indicate typical extents of these effects for each valvar design.

7.2 METHOD OF ANALYSIS

7.2.1 The Strouhal Number

The Strouhal number, S, is the proportionality constant between the predominate frequency of vortex shedding, f, and the free stream velocity, V, divided by the characteristic width, D, of the object generating the vortices free-stream velocity, D:

$$S = \frac{f\,D}{V} \quad . \tag{7-1}$$

If the cylinder is inclined with respect to the flow, the velocity component normal to the axis of the cylinder is used in the above equation. Using the velocity component perpendicular to the cylinder-axis, Chui and Lienhard (1967) demonstrated that for flows past yawed cylinders, vortices were shed at a single, predominate frequency. Sound could therefore be produced having a single, predominate frequency and a relatively narrow bandwidth for flow past these inclined struts. The Strouhal number is a function of geometry and Reynolds number for low Mach number flows. The Mach number for the flows through normal prosthetic heart valves is always less than 0.002. The relationship can be used for pulsatile flows and dynamic boundaries provided the characteristic time of maintainance of the flow-rate and geometry is greater than that of the vortex shedding. The characteristic time of the pulse for our experiments was approximately 1 second. The maximum systolic flow rate was maintained within 10% of maximum for a duration of approximately 50 to 100 ms during the experiments we will be discussing. The duration of the flow and geometries at the time of opening were much less than that of the systolic flows. This fact explains the transient quality of these flow-related non-transient sounds. They

normally decay within 20 to 40 ms. The corresponding durations of the flow and geometries at the time of closing were larger than those durations corresponding to opening because the occluder was held in position by the struts. We assumed, therefore, that the annular shape is maintained at the time of opening for a sufficient duration to allow flow to develop and produce vortex-shedding downstream of the annular gap. No such assumption was necessary for the systolic and closing sounds.

7.3 RESULTS OF ANALYSIS

7.3.1 Sounds Related to Flow through Annular Gaps

7.3.1.1 First Components of Opening Sounds

This section focuses attention upon sounds produced by vortex shedding as a result of forward flow through the annular gap of each closed valve immediately prior to opening. The calculations in this section were based upon Equation 7-1. We could not estimate the flow rate at the time of valvar opening, consequently we could not estimate the mean velocity in order to solve for the Strouhal number. We did, however, assume a value for S and solved for V. The mean velocity in the gap between the orifice and the occluder, V_{gap}, was estimated by the following relation:

$$V_{gap} = \frac{f\, D_{gap}}{S} \quad , \tag{7-2}$$

where, D_{gap} was the measured width of the thin, annular gap. The Strouhal number used in Equation 7-2 was assumed to be 0.20. An effective flow rate through the gap, $\dot{Q}_{gap}$, was then estimated based on the mean velocity in the gap and the area of the gap, A_{gap}, using the following relation:

$$\dot{Q}_{gap} = V_{gap} A_{gap} \quad . \tag{7-3}$$

We now discuss the estimated values of the effective flow rates for each valve design based on the frequencies of the significant peaks in the spectra of the opening sounds.

7.3.1.1.1 The Smeloff Prosthesis

We used experiment 292 of Part V of this series of papers to illustrate a typical example of the non-transient sound related to normal flow through the annular gap of the Smeloff prosthesis. This flow could only produce the first component of the opening sound. This component was labeled OS1 in Figure 5-5a. The power-density spectrum of the total opening sound, including OS1 and OS2, is depicted in Figure 5-5e. It has three significant peaks centered at 25, 200 and 510 Hz. Using the gap-width of the valve of 0.010 cm, and a Strouhal number of 0.2, the corresponding mean-velocities estimated using Equation 7-1 were 1.2, 10 and 25.5 cm/s, respectively. Based on an annular area of 0.045 cm^2 for this valve, these mean velocities correspond to effective flow-rates of 0.003, 0.027 and 0.065 L/min, respectively. Another experiment involving the Smeloff valve, experiment 295, had a lower, rate-of-change of the ventricular pressure at the time of opening. A similar estimate of the mean velocities and effective flow rates for the sound produced during this experiment yielded, for peaks centered at 25, 180 and 580 Hz, 1.25, 9.0 and 25.5 cm/s and .003, .022 and .068 L/min, respectively. These mean velocities and effective flow rates are listed in Table 7-1 for these sounds and other sounds that will be discussed later in this section. It appears that the opening sounds of these two pulse states were similar with respect to the mean velocities and effective flow rates which we have estimated and listed in Table 7-1. The values of the flow-rate given above were too small to

Mean Velocities and Effective Flow Rates
Associated with Vortex-Shedding of Flows through Annular Gaps
Estimated From Center-Frequencies of Significant Acoustical Peaks
in the Spectra of Opening and Closing Sounds

Valvar Design	Experiment Number	Opening Sound f (Hz)	Opening Sound V_{gap} (cm/s)	Opening Sound Q_{gap} (L/min)	Closing Sound f (Hz)	Closing Sound V_{gap} (cm/s)	Closing Sound Q_{gap} (L/min)
Smeloff	292	25	1.2	0.003	130	6.5	0.018
		200	10.0	0.027	440	22.0	0.059
		510	25.5	0.065	710	35.5	0.096
					1100	55.0	0.149
					1590	79.5	0.214
					1820	91.0	0.246
	295	25	1.2	0.003	130	6.5	0.018
		180	9.0	0.022	420	21.0	0.057
		570	28.5	0.068	690	34.5	0.093
					1050	52.5	0.142
					1280	64.0	0.173
					1520	76.5	0.205
					1750	87.5	0.236
Bjork-Shiley	266	25	0.62	0.062	55	1.2	0.12
		90	2.25	0.220	390	10.0	1.00
		800	20.0	2.000	600	15.0	1.50
					980	24.0	2.40
					1180	29.0	2.90
					1500	37.5	3.75
	265	25	0.62	0.062	62	1.5	0.15
		75	1.87	0.187	345	8.6	0.86
		800	20.0	2.000	570	14.2	1.42
					800	20.0	2.00
					980	24.5	2.45
					1200	30.0	3.00
					1430	35.7	3.57
Starr-Edwards 2400	306	90	4.5	0.013	70	3.5	0.010
		360	18.0	0.049	165	8.7	0.025
		780	39.0	0.110	380	19.0	0.055
					490	24.5	0.071
					665	33.2	0.096
					825	41.2	0.120
					1035	50.2	0.145
					1355	67.7	0.196
					1700	85.0	0.246
	309	110	5.5	0.016	60	3.0	0.009
		360	18.0	0.049	410	20.5	0.060
		610	30.5	0.088	635	31.7	0.092
		760	38.0	0.110	820	41.0	0.118
					1045	52.2	0.151
					1310	65.5	0.189

be measured with our flow-meter or observed in the films we have made of the flow tracing and valvar motion, but they are each certainly within the range of possible values of the instantaneous flow-rate through the closed valve at the time of opening.

7.3.1.1.2 The Bjork-Shiley Prosthesis

Experiment 266 of Part VI was used to illustrate a typical example of the non-transient sound related to flow through the annular gap of the Bjork-Shiley prosthesis. Figure 6-6a depicts the sound, OS1, in the time-domain for a typical cycle of this valve. Figure 6-6e depicts the power-density spectrum corresponding to a window that encompassed the opening sounds OS1 and OS2. This spectrum has significant peaks centered at 25, 90 and 800 Hz. Using these frequencies, the gap-width of the valve of 0.005 cm, and a Strouhal number of 0.2, the mean-velocities were estimated to be 0.625, 2.25 and 20 cm/s, respectively. Based on the annular area for this valve of 0.16 cm^2, these free velocities correspond to effective flow-rates of 0.0625, 0.22 and 2.0 L/min, respectively. Flow visualization experiments have shown that the Bjork-Shiley prosthesis opens earlier than the Smeloff valve at corresponding pulsatile states. Other factors being equal, then, the mean flow-rate through the annulus of the Bjork-Shiley valve could not develop to as great a value as for flow through the corresponding gap of Smeloff valve. One possibility is that the peak related to vortex shedding was that centered at 510 Hz for the Smeloff valve and that at centered 25 Hz for the Bjork-Shiley valve. The effective flow rates estimated from Equation 7-3 were 0.65 and 0.625 L/min, respectively. The opening sound of experiment 265, having a larger stroke-volume, was analyzed in the same manner. The rate of change of ventricular pressure was greater during this experiment relative to experiment 266. The resulting values from these

calculations are shown in Table 7-1. They did not differ significantly from those of the previous experiment. Again, the change of the dynamic state had little effect on the values of the effective flow rates required to produce vortices having the required frequencies.

7.3.1.1.3 The Starr-Edwards 2400 Prosthesis

Experiment 306 of Part IV illustrates a typical example of the non-transient sound related to flow through the annular gap of the Starr-Edwards 2400 prosthesis. Figure 4-5a depicts the sound OS1 curing a typical cycle for this valve and Figure 4-5e depicts the power-density spectrum corresponding to a window that encompassed the opening sounds OS1 and OS2. It is important to note that OS1 was a very low amplitude sound of relatively low frequency. This spectrum had significant peaks centered at 90, 360 and 780 Hz. Since this valve closed totally, the calculations we have made correspond to flows that would be present when the valve was partially open with a gap width of 0.010 mm. Using the observed frequencies, the gap-width of the valve of 0.010 cm, and a Strouhal number of 0.2, the mean-velocities were estimated to be 4.5, 18.0 and 39.0 cm/s, respectively. Based on an annular area of 0.45 cm^2 for the Starr-Edwards 2400 valve, the effective mean flow-rates corresponding to the mean-velocities cited above were 0.013, 0.049 and 0.11 L/min, respectively. Flow visualization experiments have shown that the Starr-Edwards 2400 prosthesis opened later than the Bjork-Shiley valve and at a time comparable to that of the Smeloff valve, all relative to similar times in the flow tracing. Other factors being equal, then, these facts about the pre-systolic dynamics of the occluder indicate that the mean flow-rate through the early-systolic annular gap of the Starr-Edwards 2400 valve could have developed to as great a value as for flow through the corresponding gap of Smeloff valve. It is interesting to note, then, that the peak centered at

360 Hz in the spectrum of the opening sound of the Starr-Edwards 2400 valve corresponded to an effective flow rate of 0.049 L/min. This value is comparable to the two peaks that were thought to be related to OS1 of the Smeloff and Bjork-Shiley valves. Perhaps all three designs open at or near the same critical flow rate. A similar estimate was made for a second experiment, number 309, involving the Starr-Edwards 2400 valve. Again, this experiment had a stroke volume much greater than the previous normal case. The results of these calculations, given in Table 7-1, indicate no significant change of the frequencies, mean velocities or effective flow rates associated with the corresponding sounds.

It is equally possible that the peak at 360 Hz in the spectrum of the opening sound of the Starr-Edwards 2400 valve was contributed by the sound OS2. More precise information is necessary about the relationship between the position of the occluder and the value of the flow rate at these times in the cycle as well as the precise frequency content of OS1 to accurately determine if the OS1-events are related to vortex shedding. The data we have examined indicate that vortex induced sounds can occur during the opening sounds of the Smeloff and Bjork-Shiley valves, but are not as probable in the case of the Starr-Edwards 2400 valve.

7.3.1.2 First Components of Closing Sounds

Similar calculations have been made relative to the sounds produced at the time of closure of these three valves. Equations 7-2 and 7-3 were again used for estimating the mean velocity and effective flow through the annular gap.

Unlike the opening sound, the motion of the occluder at the time of valvar closure was checked by the upstream struts. Any backflow relative to the occluder velocity at the time of this deceleration was "pinched off". This tran-

sient flow phenomenon should produce sounds having frequencies related to the magnitude of the reverse-flow-rate at the time this deceleration occurred. The windows of the spectra we have used to obtain the center frequencies of the resonance peaks encompassed the entire closing sound including CS1 and CS2. This complicated the problem of separating those peaks which belonged to CS1. An additional complication was provided by the number of peaks in the spectra of the closing sounds of all three valvar designs. As with OS1, it would be advisable to select other window positions which would only contain spectral information about CS1. These windows encompassing CS1 would need to be short so as not to include the late systolic sounds. The results of our estimates for experiments 292 and 295 involving the Smeloff valve, experiments 265 and 266 involving the Bjork-Shiley valve and experiments 306 and 309 involving the Starr-Edwards 2400 valve are summarized in Table 7-1.

7.3.1.2.1 The Smeloff Prosthesis

The normal closing sound of the Smeloff valve exhibited two components, CS1 and CS2, in the time-domain as shown in Figure 5-5a. The corresponding spectrum, is depicted in Figure 5-5g. This spectra exhibited seven peaks centered at 130, 440, 710, 1100, 1590, and 1820 Hz. We estimated corresponding mean-velocities of 6.5, 22, 35.5, 55, 79.5, and 91 cm/s and corresponding effective flow rates of 0.018, 0.59, 0.96, 0.149, 0.214 and 0.25 L/min. Similar estimates for experiment 295 are given in Table 7-1. The results were similar for both closing sounds.

7.3.1.2.2 The Bjork-Shiley Prosthesis

The normal closing sound of the Bjork-Shiley valve exhibited two components in

the time-domain as shown in Figure 6-6a. The corresponding spectrum is depicted in Figure 6-6g. The corresponding spectrum exhibited seven peaks centered at 55, 390, 600, 980, 1180, and 1500 Hz. We estimated corresponding mean-velocities of 1.25, 10, 15, 24, 29, and 37.5 cm/s and effective flow rates of 0.125, 1.0, 1.5, 2.4, 2.9 and 3.75 L/min. Similar results were obtained for the closing sound of experiment 265.

7.3.1.2.3 The Starr-Edwards 2400 Prosthesis

The closing sound of the normal Starr-Edwards 2400 valve exhibited two components in the time-domain as shown in Figure 4-5a. The corresponding spectrum is depicted in Figure 4-5g. This spectrum exhibited nine peaks centered at 70, 165, 380, 490, 665, 825, 1035, 1355, and 1700 Hz. We estimated corresponding mean-velocities of 3.5, 8.75, 19, 24.5 33.2, 41.2, 50.2, 67.7, and 85 cm/s and effective flow rates of 0.010, 0.025, 0.055, 0.071, 0.096, 0.12, 0.14, 0.20 and 0.25 L/min. Again, the results of experiment 309 having increased stroke-volume were similar.

7.3.1.2.4 Summary of Results of the Closing Sounds

A comparison of the effective flow rates corresponding to the peaks of the spectra of the closing sounds for the three valvar designs clearly shows the dramatically greater values of the Bjork-Shiley valve for comparable frequencies as compared with the other two. valvar designs. This increase contradicts the expected decrease that would result from the earlier closing of this valvar design. The only other conclusion we can reach at this time about these calculations relative to the closing sound is that they are all physically realistic based on observed backflows through these valves at the time of closing. More detailed

studies may yield information relative to the precise assignments of the peaks of the spectra of these closing sounds.

7.3.2 Sounds Related to Flow around Struts and Phonocatheter

In this section, the estimation of mean velocities required to produce sounds of frequencies that were observed in the systolic sounds of prosthetic heart valves were made assuming these sounds result from flow past the struts and/or the phonocatheter. The strut diameters were 1.6 mm for the Smeloff valve, 1.0 mm for the Bjork-Shiley valve and 2.0 mm for the Starr-Edwards 2400 valve. The diameter of the phonocatheter was 1.6 mm. The following relations, derived for each specific case from Equation 7-1, was used to estimate the mean velocity corresponding to the four dimensions listed above:

$$\bar{V}_{strut} = \frac{f\, D_{strut}}{S} , \tag{7-4}$$

$$\bar{V}_{catheter} = \frac{f\, D_{catheter}}{S} . \tag{7-5}$$

The Strouhal number must be known or assumed in order to use these expressions to estimate mean velocities. We used a Strouhal number of 0.2 for all of the calculations based upon Equations 7-4 and 7-5. As stated previously, mean velocities estimated using these equations would correspond to the velocity component perpendicular to the axis of the cylinder.

An alternative approach to estimating the presence of vortex shedding was to calculate the Strouhal number directly using the flow rate during systole. This was possible for the systolic sounds because the flow rate was sufficiently large to be estimated from the experimental apparatus. A characteristic, mean velocity associated with flow at the struts would be that calculated by dividing the

maximum systolic flow rate, Q_{max}, by the area of the orifice, $A_{orifice}$. A characteristic, mean velocity associated with flow at the phonocatheter would be that calculated by dividing the maximum systolic flow rate, Q_{max}, by the area of the aorta,A_{aorta}. We estimated the Strouhal number for these two cases using the follow relations:

$$S_{strut} = \frac{f\, D_{strut}\, A_{orifice}}{Q_{max}} , \qquad (7\text{-}6)$$

and,

$$S_{catheter} = \frac{f\, D_{catheter}\, A_{aorta}}{Q_{max}} . \qquad (7\text{-}7)$$

7.3.2.1 The Smeloff Prosthesis

The power-density spectrum associated with the normal systolic sound of the Smeloff valve is depicted in Figure 5-5f. The spectrum had two significant peaks with center-frequencies of 170 and 560 Hz. Using Equations 7-4, 7-5, 7-6 and 7-7 we estimated mean velocities and Strouhal numbers for flows around the struts and catheter. The resulting values are listed in Table 7-2. The Strouhal number estimated for the peak at 560 Hz based on flow past the phonocatheter is 0.89, a value too high to correspond to vortex shedding. A similar conclusion can be reached from the corresponding Strouhal number, 0.55, of the systolic sound of experiment 295 which had a 55% larger maximum systolic flow rate. The corresponding Strouhal numbers for the peak centered near 560 Hz based on flow past the struts were 0.36 and 0.44 for experiments 292 and 295, respectively. It was possible that these consistent values are associated with vortex shedding near the struts. The factor of two separating these values and other observed values of the Strouhal could be explained by the fact that we probably underestimated the free stream velocity associated with flow through the orifice.

Table 7-2
Mean Velocities and Strouhal numbers
of Flows Associated with Vortex-Shedding
Estimated From Center-Frequencies of Significant Acoustical Peaks
of the Systolic Sounds

Valvar Design	Experiment (Maximum Flow-Rate)	Center Frequency f (Hz)	Flow at Struts V_{strut} (cm/s)	S_{strut}	Flow at Catheter $V_{catheter}$ (cm/s)	$S_{catheter}$
Smeloff	292 (512 cc/s)	170	136	0.103	136	0.27
		560	448	0.36	448	0.89
	295 (791 cc/s)	180	144	0.08	144	0.19
		540	432	0.44	432	0.55
Bjork-Shiley	266 (341 cc/s)	70	35	0.065	56	0.17
	265 (637 cc/s)	80	40	0.038	64	0.061
		470	235	0.22	376	0.290
Starr-Edwards 2400	306 (443 cc/s)	80	80	0.066	64	0.18
		690	690	0.37	562	1.59
	309 (785 cc/s)	110	80	0.051	64	0.14
		790	790	0.37	632	1.02

Visualization experiments have shown that the velocity profile at the orifice was less turbulent than that at the phonocatheter and consequently more "pointed" in shape. Nevertheless, mean velocities estimated for these peaks had physically reasonable values, near 140 cm/s, for the peaks near 170 Hz. The corresponding values of the peaks near 560 Hz are 448 and 432 cm/s, respectively. These large values of velocity suggest that these peaks were not related to vortex shedding at the strut or at the phonocatheter. We conclude then that the peaks most probably related to vortex shedding were those near 170 Hz and that the corresponding shedding probably occurred at the phonocatheter.

7.3.2.2 The Bjork-Shiley Prosthesis

If we examine the spectrum of the systolic sound produced by the normal Bjork-Shiley valve which is shown in Figure 6-6f we find one significant peak having a center-frequency of 70 Hz. Using Equation 7-3, we estimated a corresponding mean velocity of 35 cm/s for this peak. The systolic sound of experiment 265, having a 100% larger maximum systolic flow-rate, had two significant peaks in its spectrum. One peak was centered at 80 Hz the other peak at 470 Hz. The Strouhal numbers based on flow past the struts and catheter are listed in Table 7-2. The Strouhal numbers 0.65 and 0.38 for the peaks centered near 70 Hz indicated that these peaks were probably not associated with vortex shedding at the struts. The peak at 470 Hz in the systolic sound of experiment 265 was probably produced by flow past the struts as suggested by the Strouhal number of 0.22 and the comparable values of the characteristic mean-velocities of 235 and 212 cm/s calculated from both Equation 7-4 and by dividing the flow rate by the area of the orifice, respectively. We conclude that any peaks associated with vortex shedding for these systolic sounds were the peaks near 70 Hz, associated with shedding near the phonocatheter, and the peak near 470 Hz associated

with shedding near the struts.

7.3.2.3 The Starr-Edwards 2400 Prosthesis

Examining the spectrum of the systolic sound produced by the normal Starr-Edwards 2400 valve, experiment 306, which is shown in Figure 4-5f, we found two significant peaks having center-frequencies of 80 and 690 Hz. Similar peaks were observed in the spectrum of experiment 309. The Strouhal numbers associated with the high-frequency peaks were large as indicated in Table 7-1. The corresponding mean velocities were also very large. It is unlikely that these peaks were related to vortex shedding. If they were, however, then shedding would probably have occurred at the struts because the velocities estimated using Equation 7-4 were comparable to those estimated by dividing the flow rate by the area of the orifice. Similar results from these two different estimations support each other. The low-frequency peaks could be related to shedding near the catheter. The Strouhal numbers of these peak were 0.18 and 0.14. For experiment 306 we estimated a mean velocity at the catheter of 87 cm/s based on the area of the aorta and a mean velocity of 64 cm/s based on a Strouhal number of 2.0. These results suggest that the low-frequency peaks could have been caused by vortex shedding at the phonocatheter. The corresponding values of the Strouhal number and mean velocities associated with shedding near the struts, 0.066 and 80 cm/s respectively, were significantly different from values which would support shedding at the struts for these low-frequency peaks.

7.4 CONCLUSIONS

7.4.1 Summary of Results for Opening Sounds Related to Vortex Shedding at the Annular Gap

Each of the effective flow rates estimated from the center-frequencies of each significant peak in the spectra of the opening sounds for each valvar design could be associated with vortex shedding based on our calculations. The mean velocities that were estimated were all within the range of physically real values.

Of the three peaks in its opening spectra, the peaks near 510 Hz for the case of the Smeloff valve were most probably related to flows through the annular gap. The effective flow rate corresponding to this peak was 0.065 L/min.

The peaks near 25 Hz for the case involving the Bjork-Shiley valve were most probably related to flows through the annular gap. The effective flow rates associated with these peaks were 0.063 L/min.

The peaks near 360 Hz for the case involving the Starr-Edwards 2400 valve were most probably related to flows through the early, systolic gap. The effective flow rates associated with these peaks were 0.049 and 0.051 L/min for experiments 306 and 309, respectively.

These three effective flow rates were within the realm of possible flow states at the times when these sounds occurred. Therefore, we conclude that vortex-shedding could be responsible for the first components of the opening sounds of these prostheses having these frequencies. It is more likely that this shedding occurred during the opening of Smeloff and Bjork-Shiley valves than during the opening of the Starr-Edwards 2400 design. Comparisons of the opening sounds for two different pulse states of each valvar design indicate no significant changes in the estimated values of the mean velocities or effective flow rates.

7.4.2 Summary of Results for Closing Sounds Related to Vortex Shedding at the Annular Gap

Since we could not relate particular peaks to the shedding frequency, these results were not very informative, however, we know that the Bjork-Shiley valve begins to close during the deceleration phase of the flow curve. That is to say, the Bjork-Shiley valve is virtually closed before any backflow can develop. In addition, Figure 6-6a indicates 1-2 L/min backflow at the time of closure of the Bjork-Shiley valve. The Smeloff valve required more backflow to close. Visualization experiments show that the Smeloff valve was totally open when backflow began at the end of systole. Figure 5-5a indicates 5 L/min backflow at the time of closure of the Smeloff valve. The Starr-Edwards 2400 valve began to close during the deceleration phase of the systolic cycle at a time later than that of the Bjork-Shiley valve and earlier than that of the Smeloff valve. Figure 4-5a indicates approximately 0-1 L/min backflow at the time of closure of the Starr-Edwards 2400 valve. If we compare the facts just stated, about the valvar motion and time of sounds, with the estimates of the mean velocities made previously from center-frequencies of the closing sounds for each valve design, we find that the data suggest that a correlation exists between these mean velocities and the relative velocity of the occluder at the time of CS1. If we also assume that the frequencies associated with CS1 are those of the upper half of the bandwidth, then the spectra indicate significant loss of power at these frequencies for the sounds produced by the Bjork-Shiley valve as compared with the other two valvar designs and a significant reduction of the mean velocity associated with backflow at the time of closing of the Bjork-Shiley valve.

7.4.3 Summary of Results for Systolic Sounds Related to Vortex Shedding near Struts and Phonocatheter

The results of this section are the most informative of this paper. Spectra associated with the systolic sounds possessed only one or two peaks. Assigning each peak to a particular type of flow was therefore easier than that of the opening and closing sounds. For the case of the Smeloff valve, the low-frequency peak near 170 Hz was assigned to vortex shedding at the phonocatheter and the high-frequency peak near 560 Hz was assigned to vortex shedding at the struts. Strouhal numbers estimated for experiments 292 and 295 for these flows were 0.27 and 0.19 for the shedding at the phonocatheter and 0.36 and 0.44 for the shedding at the struts, respectively.

The low-frequency peak of the systolic sound of the Bjork-Shiley valve centered at 70 Hz was assigned to shedding at the phonocatheter and the high-frequency peak was assigned to shedding at the struts. The Strouhal numbers estimated for experiments 266 and 265 were 0.167 and 0.061 associated with shedding at the phonocatheter, respectively, and for experiment 265, 0.22 associated with shedding at the struts.

The low-frequency peak of the systolic sound of the Starr-Edwards 2400 valve centered at 80 Hz was assigned to shedding at the phonocatheter and the high-frequency peaks centered near 700 Hz were assigned to collisions of the occluder with the struts and not related to vortex shedding. The Strouhal numbers estimated for experiments 306 and 309 were 0.184 and 0.142, respectively, for shedding at the phonocatheter.

7.5 RECOMMENDATIONS

We recommend that a closer, more specific examination be made of the spectra corresponding to windows which encompass only OS1 and CS1 rather than both components of the opening and closing sounds. This examination would isolate and reduce the number of peaks associated with the spectra of these specific components. A further examination of the flow-rates at the time of valvar opening and closing would enable the direct calculation of the Strouhal number associated with each peak in the spectra of these sounds. The results from these two studies would help us understand the physical nature of the peaks in these sounds, especially the closing sounds.

7.6 ACKNOWLEDGEMENTS

Funding for this project was provided by the Donald E. Baxter Foundation, the Children's Heart Foundation of Southern California, and the American Heart Association, Greater Los Angeles Affiliate.

7.7 REFERENCES

[1] Blevins, R.D., 'Flow-induced Vibration," Van Nostrand Reinhold Co., New York, pp. 15-19(1977).

[2] Berger, E. and R. Wille, 'Periodic Flow Phenomena," *Annual Review of the Journal of Fluid Mechanics*, p. 332 (1972).

[3] Chui, W.S., and J.H.Lienhard, "On Real Fluid Flow over Yawed Circular Cylinders," *J. Basic Eng.* , **89**,851-870(1967).

7.8 NOMENCLATURE

A_{aorta}	Area associated with the aortic flow section at the axial position of the phonocatheter, m^2
A_{gap}	Area associated with the annular gap between the occluder and the orifice of the valve, cm^2
$A_{orifice}$	Area associated with the orifice of the valve, m^2.
D	Characteristic dimension of a bluff body, m
$D_{catheter}$	Diameter of phonocatheter, m
D_{gap}	Width of annular gap, m
D_{strut}	Diameter of strut, m
f	Frequency, Hz
$\dot{Q}_{max}$	Maximum systolic flow rate, m^3/s
$\dot{Q}_{gap}$	Effective flow rate in the annular gap, m^3/s
S	Strouhal number, dimensionless
S_{strut}	Strouhal number estimated using characteristic velocities estimated at the strut, dimensionless
$S_{catheter}$	Strouhal number estimated using characteristic velocities estimated at the catheter, dimensionless
V	Effective mean velocity, m/s
V_{gap}	Effective mean velocity in the annular gap, m/s

PART VIII

OVERALL CONCLUSIONS AND RECOMMENDATIONS

OVERALL CONCLUSIONS AND RECOMMENDATIONS

Overall conclusions will be discussed in terms of contributions provided by the *in vitro*-analytical method and by results of its application in this study.

Merits of the present *in vitro* study of sound produced by prosthetic heart-valves included: knowledge of the valvar design, size, orientation and condition; isolation of aortic-valvar sounds; control and measurement of the pulsatile state; simultaneous recording of sounds and visualization of the valve; control of the path of acoustical propagation; and control of all other non-valvar aspects of the investigation.

Application of the linearized equations of change provided information about the modes of sound propagation in the aorta. Planar modes were found to propagate while non-planar modes decayed exponentially with axial distance from the valve.

Linear vibrational theory provided an adequate model for understanding the modes of vibration of the valve which were found to be responsible for the significant resonance peaks in the spectra of the opening and closing sounds of the valves studied. The changing values of parameters estimated from the spectra of the sounds produced by normal and abnormal valves indicated changes of the effective mass of specific vibrational modes. These modes were characterized by their respective resonance peaks.

The digital method described in Part I and applied in Parts II through VI provided a general means for analysis of sounds produced by heart valves. The Fast Fourier Transform was satisfactory in providing the needed transformation into the frequency domain. The method described provided satisfactory resolution in both the time and frequency domain. A rapid, overall presentation and

comparison of two sounds was accomplished by depicting the power-frequency-time data in terms of a three-dimensional surface. After becoming familiar with these surfaces, the investigator was able to detect and interpret the significant information in them which had only previously been described in terms of the individual power-density spectra associated with fragments of the cardiac cycle. The analytical method can be applied *in vivo* by using a phonocatheter or by replacing the phonocatheter with a surface microphone. It can be applied to a wide variety of situations of clinical importance. We have estimated that a dedicated device could generate the plots and list desired values in approximately 30-60 minutes.

Application of the method *in vitro* yielded many important results. For the Starr-Edwards 2400, Smeloff and Bjork-Shiley spherical valves a number of similarities were observed as well as an even greater number of differences.

Under all pulsatile and valvar states, each valve design produced an opening, systolic and closing sound. The opening and closing sounds were generally comprised of events, or components, which were indicative of the dynamics of the occluder at the times of these events. Visualization showed that these events in the opening sound were related to both flow around the occluder before the valve had begun to open (OS1) and collisions of the occluder with the structures of the valve as it reached its fully-open position (OS2). The systolic sound was comprised of a broadband noise associated with flow through the valve and around the phonocatheter (SSNT) as well as transient sounds produced by the bouncing of the occluder (SST) for those cases involving the caged-ball designs. The disk of the Bjork-Shiley valve did not bounce during systole. The closing sound of the three valves was also comprised of two components. One was the sound produced as the occluder collided with the struts as it reached the closed position (CS1). The other component was produced shortly

after the preceeding one and was associated with either flow back through the valve or a second seating of the occluder due to bouncing of the occluder after the first collision during closure (CS2). Other general similarities between these three normal valve designs were their relatively powerful closing sounds compared with opening and systolic sounds at normal pulsatile states.

In the study of the effects of pulsatile states on the sounds produced by these three normal valves, each of the three valves exhibited little change in the spectra of their opening and closing sounds under changing pulse rate, stroke volume and mean aortic pressure. For each valve design, however, an increase in stroke volume, or cardiac output, increased the power at corresponding frequencies in the spectrum of the systolic sound. These changes were indicated by increases of the total power of the systolic sounds with increasing cardiac output.

Differences between the sounds of these valvar designs were extensive. Under all pulsatile and valvar states, the frequency characteristics of the opening sounds of each of the three designs were distinctly different from each other. This included the location, amplitude and widths of the resonance peaks. The spectra of the opening sounds of the Starr-Edwards 2400 and Bjork-Shiley valves extended with significant power levels to much higher frequencies than those of the Smeloff valve. The effect of simulated tissue overgrowth on the inner apical surface of the Starr-Edwards 2400 design, significantly altered the spectrum of the opening sound by reducing the amplitude of the resonance peak associated with the collision of the stellite occluder with the stellite "track" of this design. This change was not such that it could then be confused with another valvar design, or alternate pulsatile mode of the Starr-Edwards 2400 valve.

Differences between the systolic sounds of the valves depended primarily on the materials and dynamics of the occluder. If the occluder was relatively rigid and bounced during systole, as was the case for the Starr-Edwards 2400 valve, then a significant resonance peak occurred in the systolic spectrum in the high-frequency region. This peak was generally distinct from the broader, low-frequency peak commonly associated with sound caused by the flow. For the case having simulated apical overgrowth, the high-frequency peak of the systolic spectrum was not significantly changed indicating near-normal bouncing of the ball when this overgrowth was present. A high-frequency peak was observed in the systolic spectrum of the Bjork-Shiley valve only under extremely high cardiac outputs. Visualization of the Bjork-Shiley valve showed that the disk did not move at these pulsatile states. This specific peak was later associated with periodic vortex shedding at the struts. The systolic spectra of the Smeloff valve had one resonance peak of low frequency and comprised of sound produced by both occluder-bouncing and sounds related to flow. For the abnormal valvar case involving simulated overgrowth on the upstream struts, the systolic sound was abnormally early causing an abnormally powerful opening sound and an abnormally weak systolic sound in terms of the total power associated with these events.

Closing sounds for each of the three designs possessed many more resonance peaks than their corresponding opening and systolic sounds. The center-frequencies, amplitudes and widths of these peaks were also different between valvar designs. The spectra of these sounds exhibited harmonic qualities. Many of the peaks were nearly equally spaced in the frequency domain. Of the three major sounds produced by these three valves, the closing sounds were the most similar when compared between designs.

A measure of the velocities of the occluder prior to opening and closing would provide information about forces present on the occluder at those times. A relationship between the rate of change of ventricular pressure, the drag on the occluder, and its velocity during opening and closing would be useful in better understanding the importance of these effects on the power of the opening and closing sounds.

A faster A/D rate would allow one to decrease the record length of each window while maintaining the same frequency resolution or alternatively, it would allow one to increase the frequency resolution while maintaining the record length. This increased rate would allow one to investigate the components of the opening sounds and closing sounds individually or more accurately, respectively.

Information provided by pulsed ultrasound and laser doppler anemometry about the fluid velocity field in the region near the valve would be useful to correlate with the information provided by the audible sound. Steady flow studies done in our laboratory with the Smeloff valve indicate that the pressure fluctuations of the sound and velocity fluctuations of the turbulence at the phonocatheter correlate well with the mean flow rate over the frequency domain from 0 to 2000 Hz. This correlation also applied to sound measured internally using the phonocatheter and externally using a surface microphone strapped to the lucite, aortic flow-section. Such studies would be useful for future applications of totally non-invasive clinical estimates of the effective flow area of heart valves. Sound would provide information about the pressure gradient and pulsed ultrasound would provide information about the flow rate. The effective flow area could be estimated using the orifice equation and the estimated pressure gradients and flow rates.

APPENDIX A

This appendix contains a figure of the analog filter characteristics, Figure A-1, and a figure showing the orientation of the valves for each experiment, Figure A-2. Figure A-3 and A-4 show photographs of the occluder position, particle trajectories, oscilloscope tracings of sound and flow during three important acoustical events of the Smeloff and Bjork-Shiley valves, respectively. Six tables provide rapid comparisons of the center-frequencies and amplitudes of the significant peaks of the opening, systolic and closing sounds of the three valvar designs we studied.

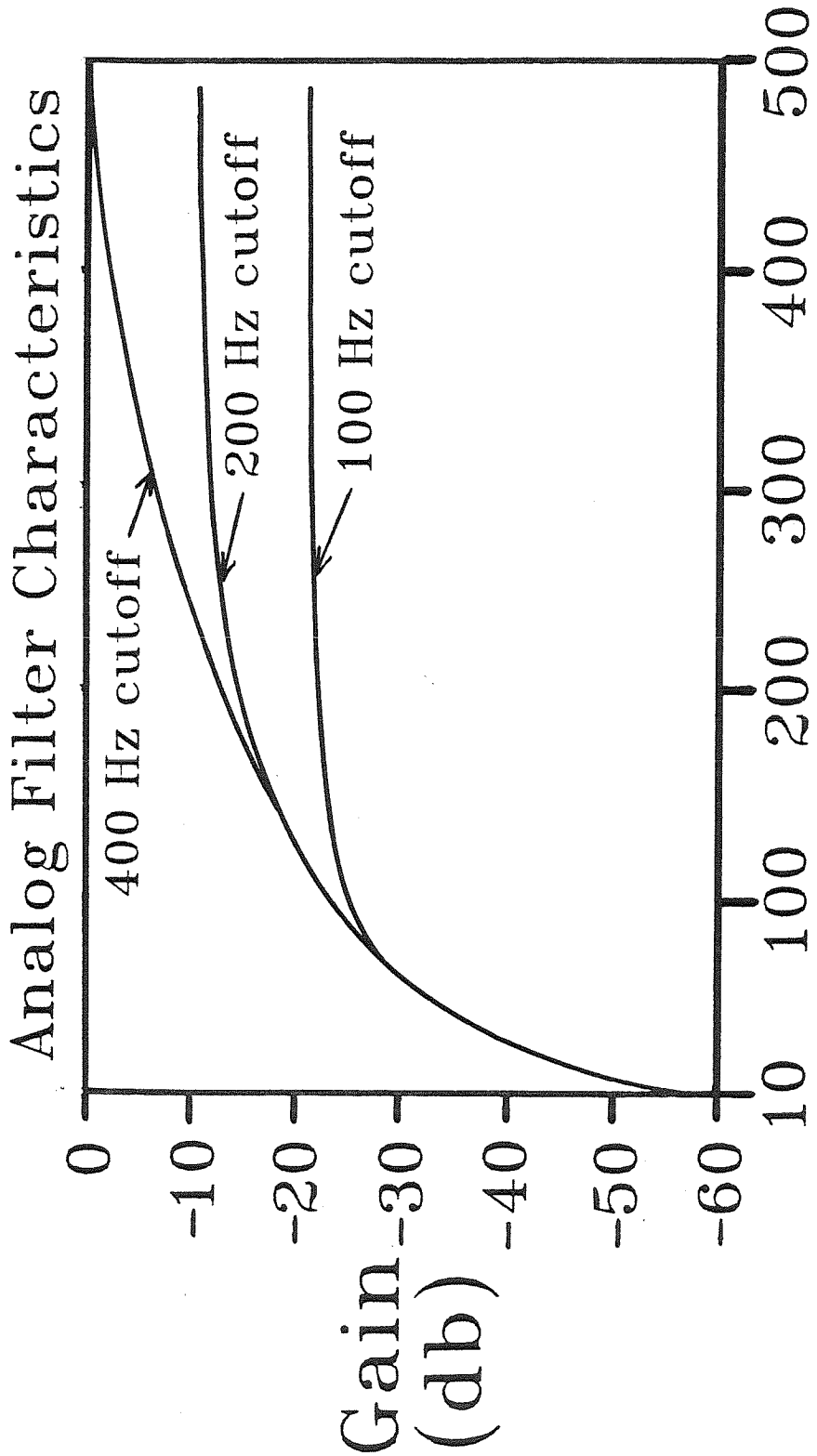
Analog Filter Characteristics
400 Hz cutoff
200 Hz cutoff
100 Hz cutoff
0
-10
-20
-30
-40
-50
-60
Gain (db)
10
100
200
300
400
500
Frequency (Hz)

Figure A-1

Figure A-2

Orientation of Valves

Starr-Edwards 2400

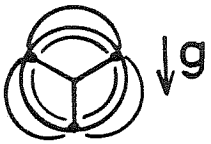

Experiment Numbers 306-311

Smeloff

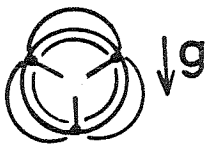

292-298 300

Bjork-Shiley

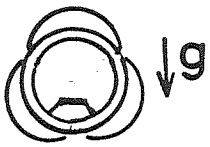

265-267, 271,272

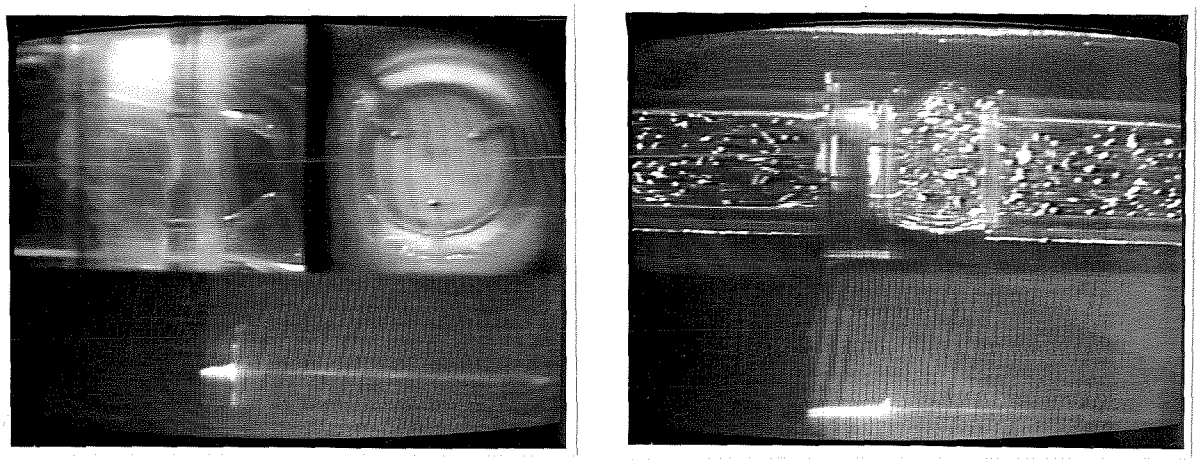

Time of Opening Sound: OS1

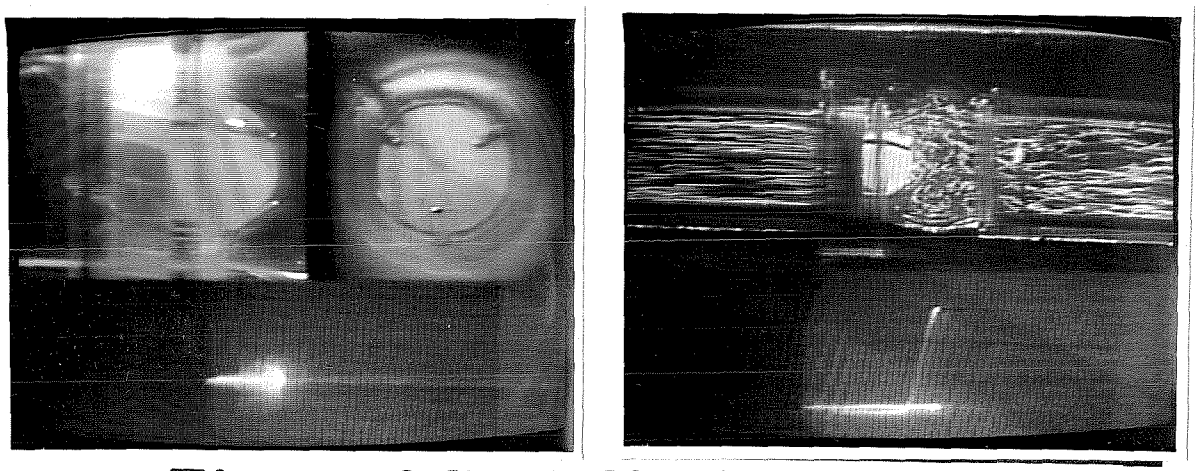

Time of Systolic Sound: SS

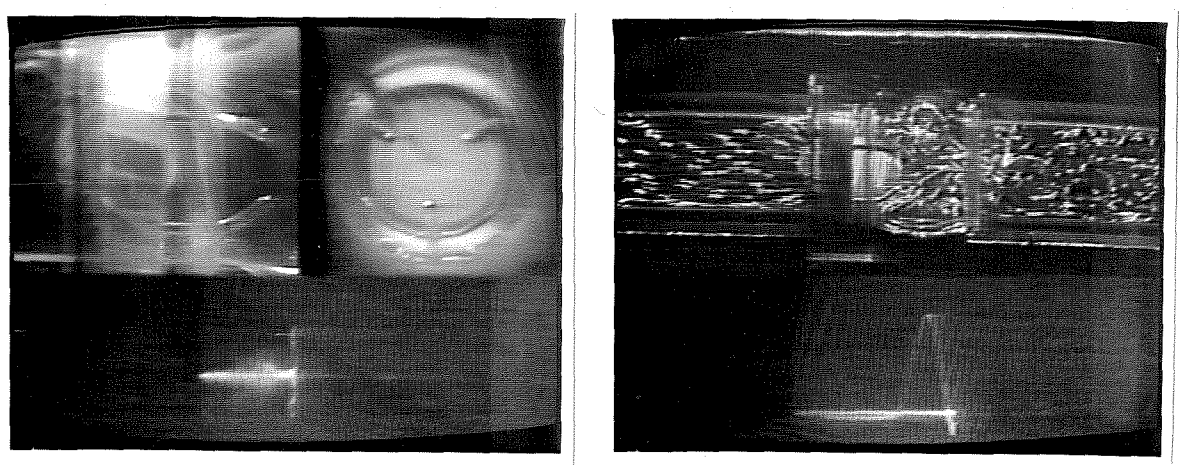

Time of Closing Sound: CS2

Figure A-3 Photographs of occluder positions, particle trajectories, and sound/flow rate tracings for the Smeloff valve at three specific times of the cardiac cycle.

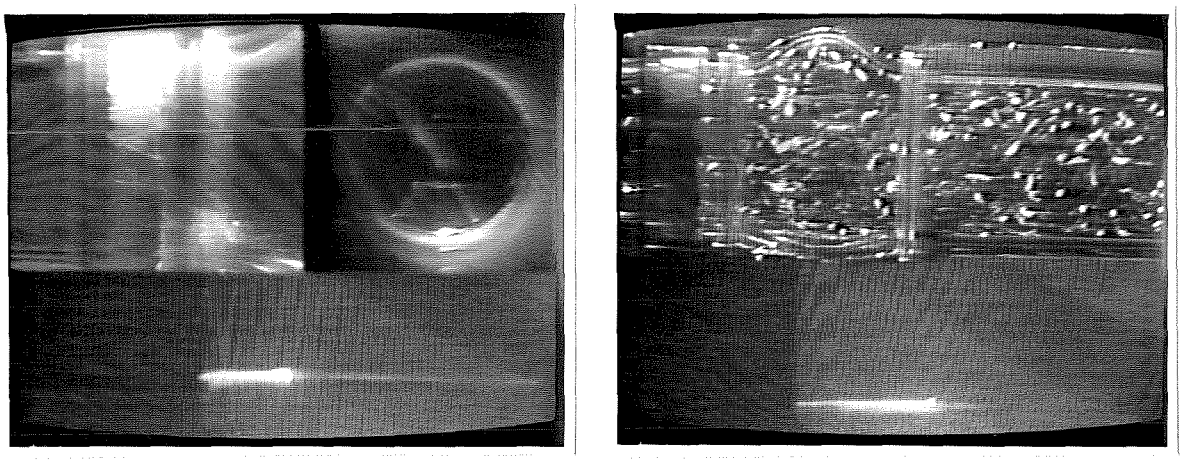

Time of Opening Sound: OS1

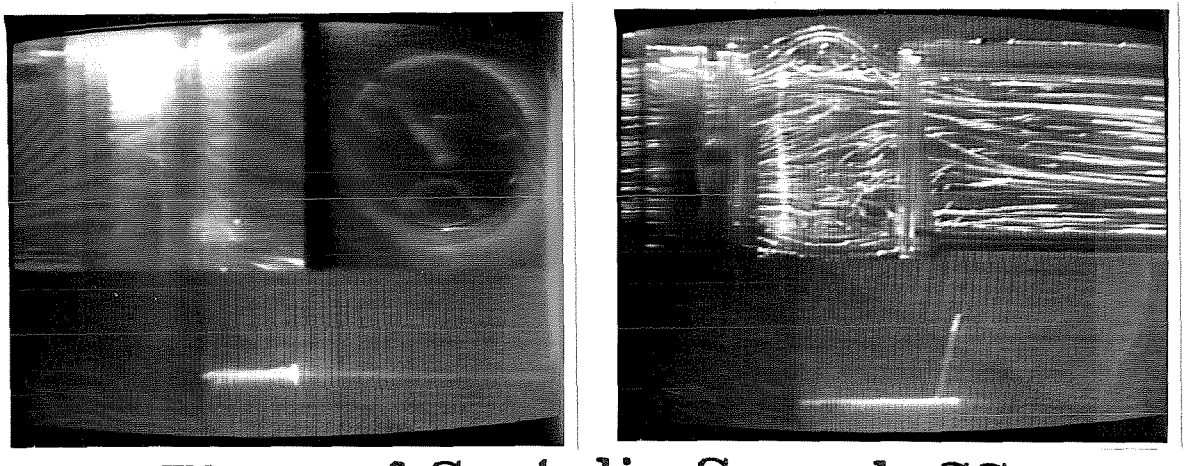

Time of Systolic Sound: SS

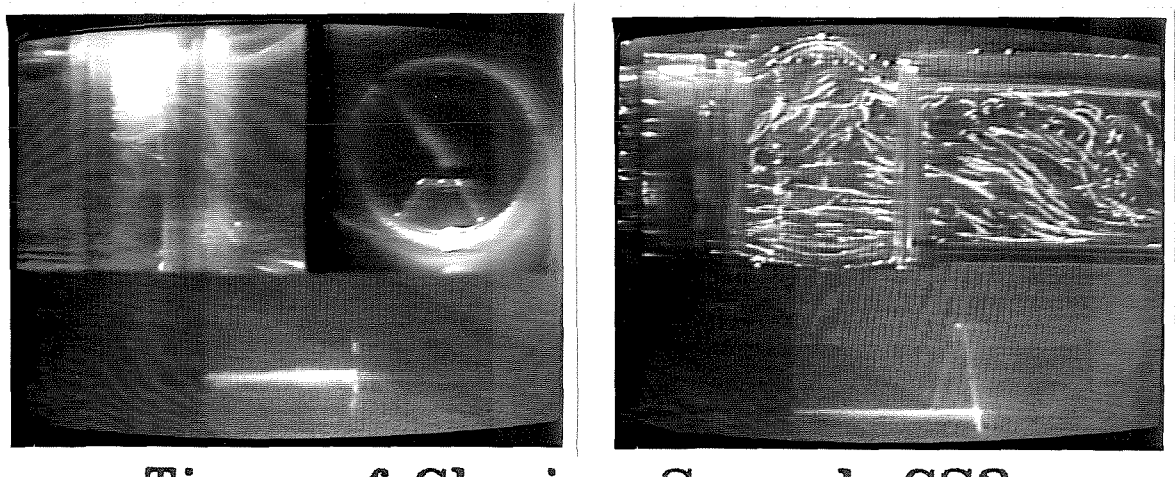

Time of Closing Sound: CS2

Figure A-4 Photographs of occluder positions, particle trajectories, with sound and flow rate tracings for the Bjork-Shiley valve and three specific times in the cardiac cycle.

Table A-1

Center Frequencies of Significant Peaks of the Opening Sounds of the Bjork-Shiley, Smeloff and Starr-Edwards 2400 Prostheses

Valvar Design	Experiment Number	Center-Frequencies (Hz)					
Bjork-Shiley	265	25	73				800
	266	25	90				800
	267	25	80	225			780
	271	25	100	225			770
	272	25	100				780
Smeloff	292	25		200		510	
	293	25		210		530	
	294	25		200		520	
	295	25		180		570	
	296	25		210		525	
	297	25		190		515	
	298	25		200		510	
	300	25		190		530	
Starr-Edwards 2400	306		90		360		780
	307		90		360	580	820
	308	20			360	580	
	309		110		360	610	760
	310	45		250	345	470	760
	311	65		250	345	633	780

Table A-2

Amplitudes of Significant Peaks of the Opening Sounds of the Bjork-Shiley, Smeloff and Starr-Edwards 2400 Prostheses

Valvar Design	Experiment Number	Amplitude (db)					
Bjork-Shiley	265	38	29				21
	266	33	30				19
	267	30	24	16			16
	271	35	29	20			14
	272	31	20				17
Smeloff	292	41		43		28	
	293	39		42		28	
	294	38		41		27	
	295	31		38		18	
	296	35		42		27	
	297	35		41		25	
	298	35		42		25	
	300	37		43		27	
Starr-Edwards 2400	306		29		24		24
	307		29		32	25	24
	308	37			26	17	
	309		32		26	25	25
	310	31		28	29	25	23
	311	29		27	31	23	24

Table A-3

Center Frequencies of Significant Peaks of the Systolic Sounds of the Bjork-Shiley, Smeloff and Starr-Edwards 2400 Prostheses

Valvar Design	Experiment Number	Center-Frequencies (Hz)		
Bjork-Shiley	265	80	470	
	266	70		
	267	70		800
	271	70		700
	272	70		
Smeloff	292	170	560	
	293	200	510	
	294	180	580	
	295	180	540	
	296	190	510	
	297	190	510	
	298	190	510	
	300	200	590	
Starr-Edwards 2400	306	80		690
	307	35		690
	308	45		690
	309	110		790
	310	35		690
	311	25		690

Table A-4
Amplitudes of Significant Peaks of the Systolic Sounds of the Bjork-Shiley, Smeloff and Starr-Edwards 2400 Prostheses

Valvar Design	Experiment Number	Amplitudes (db)		
Bjork-Shiley	265	43	26	
	266	34		
	267	28		8
	271	35		9
	272	31		
Smeloff	292	45	36	
	293	44	28	
	294	45	36	
	295	49	42	
	296	44	28	
	297	43	25	
	298	45	26	
	300	43	32	
Starr-Edwards 2400	306	26		15
	307	27		15
	308	31		15
	309	39		23
	310	31		13
	311	28		13

Table A-5

Center Frequencies of Significant Peaks of the Closing Sounds of the Bjork-Shiley, Smeloff and Starr-Edwards 2400 Prostheses

Valvar Design	Experiment Number	Center-Frequencies (Hz)									
Bjork-Shiley	265	62		345		570	800	980	1200	1430	
	266	55		390		600	820	980	1180	1500	
	267	55		390		600	820	980	1180	1500	
	271	55		400		630	800	970	1235		
	272	55		400		610	820	1010	1220		
Smeloff	292		130	440			710	1100	1350	1590	1820
	293		130	440			730	1100	1350	1620	
	294		110	420			690	1010	1260	1510	
	295		130	420			690	1050	1280	1520	1750
	296		100	420			720	1090	1330	1590	1840
	297		110	420			710	1090	1330	1590	1820
	298		110	430			710	1100	1360	1590	1820
	300		130	410			710	1070	1320	1600	1880
Starr-Edwards 2400	306	70	165	380	490	665	825	1035	1355		1700
	307	70	165	380	490	665	825	1070	1310		
	308	70	190	390	550	710	810	1035			
	309	60		410		633	820	1045	1310		
	310	80	170	380	570		820	1010	1310		1710
	311	70	170	390	590	725					1710

Table A-6

Amplitudes of Significant Peaks of the Closing Sounds of the Bjork-Shiley, Smeloff and Starr-Edwards 2400 Prostheses

Valvar Design	Experiment Number	Amplitudes (db)									
Bjork-Shiley	265	50		35		27	15	15	13	9	
	266	50		34		26	20	15	12	5	
	267	49		32		23	17	14	9	3	
	271	49		32		21	16	14	11		
	272	50		33		24	16	13	11		
Smeloff	292		48	35			27	22	19	14	11
	293		47	35			25	23	19	15	
	294		45	34			26	20	18	15	
	295		46	35			27	20	16	15	12
	296		46	36			27	22	19	16	13
	297		46	35			26	22	19	15	12
	298		47	36			27	21	18	16	13
	300		47	36			27	22	19	15	13
Starr-Edwards 2400	306	48	40	34	28	25	23	18	11		9
	307	48	41	33	27	24	22	18	13		
	308	48	41	34	28	26	23	16			
	309	49		31		27	22	18	15		
	310	47	40	33	27		23	23	12		10
	311	47	41	32	28	25					8

APPENDIX B

This appendix is a copy of a typical example of Fortran software used to generate the data presented and discussed in this thesis. The copy presented here was used to generate the plots and information in Part V. The program was used to generate all plots of acoustical data and it calculated the pressure and flow data listed in Table 5-1. The program was run on an IBM370 computer at Booth computing center of the California Institute of Technology. The user must provide a digital tape containing sound, pressure, and flow information to be analyzed. Subroutine READTP was written to read a very specific tape format. This format includes the channel numbers of the sound, pressure and flow information. The user must also provide the window length, test voltage of the heart-sound amplifier's gain, initiation time for ten pulsatile cycles and the windows numbers corresponding to the opening, systolic and closing sounds for which detailed plots and information are generated. Typical examples of these user-supplied data are provided at the end of the program.

```
//SMELOF  JOB (36654,DSS,CHE),'4 CHAN. SCAN',TIME=(9,59)
/*JOBPARM TAPES=(,1),PLT=4000,IOC=220,REGION=712K,L=20
/*REQUEST SMELOF,9L,R:
//  EXEC FORTG
//FORT DD *
C    ANALYSIS OF FOUR-CHANNEL DATA SET-UP ON A PDP-11/50 COMPUTERSYSTEM.
C    THE DATA ON THE RESPECTIVE CHANNELS MUST BE AS FOLLOWS:
C                    1) FILTERED SOUND;CHANNEL 3.
C                    2) UPSTREAM PRESSURE;CHANNEL 5
C                    3) DOWNSTREAM PRESSURE;CHANNEL 7
C                    4) VOLUMETRIC FLOW RATE;CHANNEL 9.
C
C    ARRAY SETUP.....
     INTEGER*4 C
     LOGICAL*1 A(512),B
     INTEGER*2 A2(256),B2(2)
     EQUIVALENCE (A(1),A2(1)),(C,B2(1))
     DIMENSION U(14000),V(605),W(605),X(605)
     DIMENSION T(4800),U1(4800),V1(250),W1(250),X1(250)
     DIMENSION TSTART(45),NUMSEG(45),BPOWER(45),WPOWER(45)
     DIMENSION FREQ(256),AMP(256),THETA(256),AS(256),BS(256)
     DIMENSION DPF(256),AMATRX(256),BMATRX(256),CMATRX(256)
     DIMENSION AMB(45,256),CNPDF(45,256),CPDFN(45,256),CPDFAB(45,256)
     DIMENSION AF(45,256),BF(45,256),THET(45,256),BPDIFF(45,256)
     DIMENSION TSTAR(10),IMAX(5),IWP(3),AK(45),ENTIM(45)
     DIMENSION INV(512),S(512),DD(6),ZERO(2),N(45),UU(530)
C
C    DEFINE THREE-DIMENSIONAL PLOTTING FIELD LENGTHS AND POSITIONING.
     COMMON/XYZLEN/XLONG,YLONG,ZLONG,XOFF,YOFF,SIDEZ
     XLONG=5.0
     YLONG=5.0
     ZLONG=5.0
     XOFF=10.0
     YOFF=4.825
     SIDEZ=5.0
C
C    DEFINING VARIABLE LABEL PARAMETERS FOR PLOTTING ROUTINES: VLABEL.
     COMMON/LBLCOM/ITEST,SLBL,STTL,SSCL,STICK
     ITEST=1
     SLBL=0.00
     STTL=0.0
     SSCL=0.0
     STICK=0.15
C
C    SETTING TWO POINTS FOR BASE-LINE PLOTTING PURPOSES.
     ZERO(1)=0.0
     ZERO(2)=0.0
```

```
C    THE FOLLOWING PARAMETERS WILL OR WILL NOT PRINT AND PLOT VARIOUS DATA DE-
C    PENDING ON WHETHER THE VALUE IS '1' OR '0' RESPECTIVELY.
     IODA=   1
     IOPRFL= 1
     IODAPL= 1
     IOPDF=  1
     IOCOMP= 1
     IOPT=   1
     IOPF=   1
     IOFRVU= 1
C
C    NEXP IS THE ANALOG EXPERIMENT NUMBER.
C    TVMV IS THE TEST VOLTAGE IE. SOUND AMP GAIN, IN MILLIVOLTS.
C    WINLGT IS THE WINDOW LENGTH IN SECONDS.
C    NSKIP IS THE NUMBER OF FILES SKIPPED FORWARD ON COMPUTER TAPE.
C    TSTAR1 IS THE STARTING TIME OF THE FIRST WINDOW.
C    NP AND NP2 ARE THE DIGITIZATION RATES OF THE SOUND AND REMAINING
C    THREE CHANNELS RESPECTIVELY.
C    TIMINC IS THE TIME INCREMENT BETWEEN SUCCESSIVE WINDOWS.
C    SEGLGT IS THE THE AMOUNT OF FILE PLACED INTO THE LARGE ARRAYS EACH TIME
C    SUBROUTINE 'READTP' IS CALLED (NOTE WINDOWS CAN NOT CROSS SEGMENTS).
C    NW IS THE TOTAL NUMBER OF WINDOWS ANALYSED FOR EACH CYCLE.
C    MM IS THE BINARY POWER WHICH SETS THE SIZE OF THE ARRAY TO BE TRANSFORMED.
C    CYCTIM IS THE CYCLE TIME IN SECONDS (LESS THAN 1.2)
C    NSPW IS THE NUMBER OF SPECIAL WINDOWS FOR DETAILED PLOTS AND DATA
C
     NSKIPP=0
     NWPCYC=45
     NSPW=3
     NP=4000
     NP2=200
     SEGLGT=3.005
     MM=8
     ND=2**MM
     NWIN1=1
     CALL ERRSET(213,256,0,1)
     CALL ERRSET(218,256,0,1)
     DD(1)=0.0
     DD(3)=1.0
C
C
C    THIS IS THE BEGINNING OF THE MAIN MAIN DO LOOP THAT HANDLES EACH FILE.
     DO 1 NFILE=1,7
     READ(5,2)NEXP,NW,NSKIP,TVMV,WINLGT,CYCTIM
2    FORMAT(3I10,3F10.3)
     WRITE(6,3)NEXP,NW,NSKIP,TVMV,WINLGT,CYCTIM
3    FORMAT(1H ,'NEXP=',I5,3X,I3,2X,'CYCLES AVERAGED',10X,'NSKIP=',I3,
    Z3X,'TVMV=',F10.3,5X,'WINLGT=',F10.3,5X,'CYCLE TIME =',F10.3)
```

```
      TIMINC=0.020*(CYCTIM/0.860)
      NWINF=NP*CYCTIM+0.5
      NNW=NW
      AW=1.0*NW
      NWIN=WINLGT*NP+1.5
      NWIN2=NP2*CYCTIM+0.5
      DO 51 I=1,NW
   51  READ(5,50)TSTAR(I)
   50  FORMAT(F10.3)
      DO 35 I=1,3
      READ(5,36)IWP(I)
   36  FORMAT(1I10)
   35  CONTINUE
C
C     SELECTION OF SEGMENT WHERE ALL NW WINDOWS ARE FOUND.
      CALL DATBLK(NUMSEG,SEGLGT,NW,WINLGT,TSTAR)
      INW=1
      DO 52 I=1,NWPCYC
      WPOWER(I)=0.0
      DO 53 J=1,ND
      AMB(I,J)=0.0
      IF(NFILE.GT.1)GO TO 54
      CPDFN(I,J)=0.0
   54  CPDFAB(I,J)=0.0
  111  CNPDF(I,J)= 0.0
      BPDIFF(I,J)= 0.0
      THET(I,J)= 0.0
      AF(I,J)=   0.0
      BF(I,J)=   0.0
   53  CONTINUE
   52  CONTINUE
C
C
C
C     THE BEGINNING OF THE MAIN SUB-LOOP FOR ITERATION ON WINDOW NUMBER.
      IW=1
      IF(NSKIPP.EQ.1)GO TO 18
      JCOUNT=0
   59  IF(INW.NE.1)GO TO 18
C
C     CALLING OF READRC TO GET PAST FIRST RECORD OF IDENTIFICATION.
      CALL READRC(A,NB)
    5  JCOUNT=JCOUNT+1
      WRITE(6,55)JCOUNT
   55  FORMAT(1H ,'JCOUNT=',I3)
      CALL READTP(U,V,W,X,ICHECK)
   18  NS=NUMSEG(INW)
      IF(NS.EQ.0)GO TO 6
      IF(NS.NE.JCOUNT)GO TO 5
```

```
C    SHIFTING OF STARTING TIMES FOR EACH SEGMENT VALUE.
56    TSTART(IW)=TSTAR(INW)+(IW-1)*TIMINC
     TS=TSTART(IW)-(NS-1)*SEGLGT
     NTS=TS*NP
     NTS2=TS*NP2
C
C    SHIFTING OF FLOW AND PRESSURE DATA FOR PLOTTING AND ANALYSIS.
     IF(INW.GT.1)GO TO 33
     IF(IW.GT.1)GO TO 33
     DO 9 JJ=1,NWIN2
     V(JJ)=V(JJ+NTS2)
     W(JJ)=W(JJ+NTS2)
9    X(JJ)=X(JJ+NTS2)
C
C    THE ANALYSIS OF THE PRESSURE AND FLOW DATA.
     IF(IOPRFL.EQ.0)GO TO 33
     CALL PRTPRE(V,V1,W,W1,X,X1,NWIN2,NP2)
C
C    SHIFTING OF SOUND DATA FOR PLOTTING.
33    IF(IW.GT.1)GO TO 37
     IF(INW.GT.1)GO TO 37
     DO 28 J=NWIN1,NWINF
     U1(J)=U(J+NTS)
28    T(J)=1.0*J
C
C    SHIFTING AND NORMALIZATION OF SOUND DATA FOR ANALYSIS.
37    DO 8 J=1,NWIN
8     UU(J)=U(J+NTS)/TVMV
C
C    THE FREQUENCY ANALYSIS!
     CALL FORIA(UU,MM,INV,S,IERR,NP,TL,DF,FREQ,AMP,NWIN,THETA,AS,BS,DPF
    Z,TOTP)
C
     WRITE(6,57)INW,IW,TOTP,NTS,NS
57    FORMAT(1H ,'CYCLE:',I3,5X,'WINDOW:',I3,5X,'TOTAL POWER:',F12.8,5X,
    Z'FIRST DATA POINT:',I5,5X,'IN SEGMENT:',I3)
C    SETTING UP ARRAY FOR THE TOTAL POWER ASSOCIATED WITH EACH WINDOW.
     WPOWER(IW)=TOTP/AW+WPOWER(IW)
C
C    CREATION OF TWO-DIMENSIONAL ARRAYS FOR 3-D PLOTTING.
     DO 13 J=1,ND
     AMB(IW,J)=10.0*(ALOG10(AMP(J))+11.0)/AW+AMB(IW,J)
     AF(IW,J)=AS(J)/AW+AF(IW,J)
     BF(IW,J)=BS(J)/AW+BF(IW,J)
     THET(IW,J)=THETA(J)/AW+THET(IW,J)
     CNPDF(IW,J)=(1.0-DPF(J))/AW+CNPDF(IW,J)
     INZ=46-IW
```

```
      IF(NFILE.GT.1)GO TO 38
      CPDFN(INZ,J)=TOTP*(1.0-DPF(J))/AW+CPDFN(INZ,J)
      GO TO 13
38    CPDFAB(INZ,J)=TOTP*(1.0-DPF(J))/AW+CPDFAB(INZ,J)
13    CONTINUE
30    GO TO 16
6     WRITE(6,32)IW
32    FORMAT(1H ,'WINDOW IGNORED IS: ',I4)
C
C     TERMINATION OF MAIN SUB-LOOP.
16    IW=IW+1
      IF(IW.GT.NWPCYC)GO TO 58
      GO TO 56
58    INW=INW+1
      IW=1
      IF(INW.GT.NNW)GO TO 60
      GO TO 59
C
C     DO LOOP FOR PRINTING OF DATA FOR AVERAGED SURFACE.
60    IF(IODA.EQ.0)GO TO 17
      DO 61 I=1,NSPW
      IW=IWP(I)
      WRITE(6,62)IW
62    FORMAT(1H ,'WINDOW:',I3)
      INZ=46-IW
      WRITE(6,120)
120   FORMAT(1H ,2X,'FREQUENCY',9X,'I',13X,'R',12X,'AMB',10X,'PHASE',9X,
     Z'CNPDF',6X,'DISTRIBUTION'/)
      DO 29 J=1,127
      IF(NFILE.GT.1)GO TO 63
      WRITE(6,121)FREQ(J),AF(IW,J),BF(IW,J),AMB(IW,J),THET(IW,J),CNPDF(I
     ZW,J),CPDFN(INZ,J)
121   FORMAT(1H ,F12.3,2X,5(E12.5,2X),F12.8)
      GO TO 29
63    WRITE(6,121)FREQ(J),AF(IW,J),BF(IW,J),AMB(IW,J),THET(IW,J),CNPDF(I
     ZW,J),CPDFAB(INZ,J)
29    CONTINUE
      DO 123 J=130,255,5
      IF(NFILE.GT.1)GO TO 124
      WRITE(6,121)FREQ(J),AF(IW,J),BF(IW,J),AMB(IW,J),THET(IW,J),CNPDF(I
     ZW,J),CPDFN(INZ,J)
      GO TO 123
124   WRITE(6,121)FREQ(J),AF(IW,J),BF(IW,J),AMB(IW,J),THET(IW,J),CNPDF(I
     ZW,J),CPDFAB(INZ,J)
123   CONTINUE
61    CONTINUE
C
C     SIMULTANEOUS PLOTS WITH RESPECT TO TIME OF THE FOUR CHANNELS OF DATA.
17    IF(IODAPL.EQ.0)GO TO 20
      CALL TIMPLT(U1,V1,W1,X1,NWIN2,NWINF,DD,ZERO)
```

```
C    PLOTTING OF POWER BANDS IN 47 HZ INCREMENTS VS. TIME.
20   IF(IOPT.EQ.0)GO TO 39
     DO 201 K=1,NWPCYC
201  AK(K)=K*1.0
     CALL BOX
     DO 202  J=1,127,6
     DO 203  K=1,NWPCYC
203  ENTIM(K)=CNPDF(K,J)*WPOWER(K)
     LAB=0
     IF(J.EQ.127)LAB=-1
     CALL XYPLOT(NWPCYC,AK,ENTIM,-14.,60.,-.0167,.0667,DD,LAB)
     LAB=0
202  CONTINUE
C
C    PLOTTING OF 3D SURFACES FOR THE NORMAL, ABNORMAL CASES.
39   IF(IOPDF.EQ.0)GO TO 41
     IF(NFILE.GT.1)GO TO 40
     CALL T3DAX
     CALL CPLT3D(CPDFN,0.05,0.0,45,256,1,1,45,1,1,127,1,45.0,70.0,.TRUE
    Z.)
     GO TO 41
40   CALL T3DAX
     CALL CPLT3D(CPDFAB,0.05,0.0,45,256,1,1,45,1,1,127,1,45.0,70.0,.TRU
    ZE.)
C
C    PLOTTING OF COMPARISON SURFACE BY ELEMENT DIFFERENCE METHOD.
41   IF(NFILE.EQ.1)GO TO 44
     IF(IOCOMP.EQ.0)GO TO 44
     DO 42 J=1,ND
     DO 43 IW=1,NWPCYC
     BPDIFF(IW,J)=CPDFAB(IW,J)-CPDFN(IW,J)+0.05
43   CONTINUE
42   CONTINUE
     DO 65 I=1,NSPW
     IW=IWP(I)
     INZ=46-IW
     DO 66 J=1,256,5
     WRITE(6,67)IW,J,BPDIFF(INZ,J),BPDIFF(INZ,J+1),BPDIFF(INZ,J+2),BPDI
    ZFF(INZ,J+3),BPDIFF(INZ,J+4)
67   FORMAT(1H ,2(I5,5X),5(F12.8,3X))
66   CONTINUE
65   CONTINUE
     CALL C3DAX
     YOFF=3.929
     CALL CPLT3D(BPDIFF,0.1,0.0,45,256,1,1,45,1,1,127,1,45.0,70.0,.TRUE
    Z.)
C    CALL SLOPFT(BPDIFF,FREQ)
     YOFF=4.825
```

```
C    PLOTTING OF POWER DENSITY AND NORMALISED DISTRIBUTION FOR IWP(I).
44    IF(IOPF.EQ.0)GO TO 45
      DO 46 I=1,NSPW
      IW=IWP(I)
      WRITE(6,47)IW
47    FORMAT(1H ,'DENSITY AND NORMALISED DISTRIBUTION PLOTTED FOR WINDOW
     Z',I5)
      DO 48 J=1,ND
      AMATRX(J)=AMB(IW,J)
48    BMATRX(J)=CNPDF(IW,J)
      CALL BOX
      CALL XYPLOT(ND,FREQ,AMATRX,-660.,2640.,10.0,110.0,DD,0)
      CALL XYPLOT(ND,FREQ,BMATRX,-660.,2640.,-1.0,4.0,DD,-1)
46    CONTINUE
C       PLOTTING OF 3D VIEW PERPENDICULAR TO FREQ/POWER PLANE.
45    IF(IOFRVU.EQ.0)GO TO 71
      LAB=0
      CALL BOX
      LAB=0
      DO 68 I=1,NSPW
      IW=IWP(I)
      IF(I.EQ.NSPW)LAB=-1
      DO 69 J=1,ND
69    CMATRX(J)=CNPDF(IW,J)*WPOWER(IW)
      CALL XYPLOT(ND,FREQ,CMATRX,-330.,1320.,-0.0167,0.0667,DD,LAB)
      LAB=0
68    CONTINUE
C
C    READING OF TAPE TO GET TO THE END OF THE FILE.
71    IF(NSKIP.LT.0)NSKIPP=1
      IF(NSKIP.GE.0)NSKIPP=0
      IF(NSKIP.LT.0)GO TO 72
      DO 24 JCOUNT=1,30
      CALL READTP(U,V,W,X,ICHECK)
      IF(ICHECK.EQ.1)GO TO 25
24    CONTINUE
C
C    SKIPPING OF MAGNETIC TAPE TO NEXT SPECIFIED FILE.
25    K=0
26    IF(K.EQ.NSKIP)GO TO 72
      K=K+1
27    CALL READRC(A,NB)
      IF(NB.EQ.0)GO TO 26
      GO TO 27
C
C    END OF MAIN DO-LOOP, AND END OF MAIN PROGRAM.
72    WRITE(6,73)NSKIP,NSKIPP
73    FORMAT(1H ,'NSKIP=',I5,10X,'NSKIPP=',I5)
1     CONTINUE
      STOP
      END
```

```
      SUBROUTINE DATBLK(N,S,NW,WL,T)
      DIMENSION T(1),N(45)
      DO 1 I=1,NW
      DO 2 J=1,25
      C=J*S
      IF(T(I).LT.C)GO TO 3
    2  CONTINUE
    3  TK=T(I)+WL
      N(I)=J
      IF(TK.GT.C)N(I)=0
    1  CONTINUE
      RETURN
      END
      SUBROUTINE READTP(U,V,W,X,ICHECK)
      INTEGER*4 C
      LOGICAL*1 A(512),B
      INTEGER*2 A2(256),B2(2)
      EQUIVALENCE (A(1),A2(1)),(C,B2(1))
      DIMENSION U(1),V(1),W(1),X(1)
      DATA MASK/Z000007FF/,MASK2/Z0000F800/,MASK3/Z00007800/
      ICHECK=0
      B2(1)=0
      I1=1
      I2=1
      I3=1
      I4=1
      DO 1 IR=1,54
      CALL READRC(A,NB)
      IF(NB.EQ.0)GO TO 2
      NC=NB/2
      DO 3 I=1,NC
      J=2*I
      K=J-1
      B=A(K)
      A(K)=A(J)
    3  A(J)=B
      DO 4 I=1,NC
      B2(2)=A2(I)
      K=IAND(C,MASK3)
      C=IAND(C,MASK)
      J=IAND(C,1024)
      IF(J.NE.0)C=IOR(C,MASK2)
      IF(K.EQ.6144)GO TO 5
      IF(K.EQ.10240)GO TO 6
      IF(K.EQ.14336)GO TO 7
      IF(K.EQ.18432)GO TO 8
      GO TO 4
    5  U(I1)=B2(2)
      I1=I1+1
      GO TO 4
```

```
6    V(I2)=B2(2)
     I2=I2+1
     GO TO 4
7    W(I3)=B2(2)
     I3=I3+1
     GO TO 4
8    X(I4)=B2(2)
     I4=I4+1
     GO TO 4
4    CONTINUE
1    CONTINUE
     GO TO 9
2    ICHECK=1
9    RETURN
     END
     SUBROUTINE PRTPRE(V,V1,W,W1,X,X1,NWIN2,NP2)
     DIMENSION V(1),W(1),X(1),DELTAP(250),V1(1),W1(1)
     DIMENSION X1(1),DPDT(250),DQDT(250)
     CONVP=84.75/102.4
     CONVF=23.3/102.4
     DO 1 J=1,NWIN2
     V1(J)=V(J)*CONVP
     W1(J)=W(J)*CONVP
     X1(J)=X(J)*CONVF
1    DELTAP(J)=V1(J)-W1(J)
     JM=NWIN2-1
     WRITE(6,2)
2    FORMAT(1H ,'TIME',5X,'VP',7X,'AOP',7X,'DELTA-P',4X,'DP/DT',7X,'FLO
    ZW',5X,'DQ/DT')
     WRITE(6,4)
4    FORMAT(1H ,' MS',5X,'MMHG',6X,'MMHG',7X,'MMHG',6X,'MMHG/S',5X,'L/M
    ZIN',5X,'L/MIN/S'/)
     DO 6 J=1,JM
     ITIME=J*5
     DPDT(J)=(V1(J+1)-V1(J))*NP2
     DQDT(J)=(X1(J+1)-X1(J))*NP2
     WRITE(6,5)ITIME,V1(J),W1(J),DELTAP(J),DPDT(J),X1(J),DQDT(J)
5    FORMAT(1H ,I3,4X,F7.2,2X,F7.2,5X,F7.2,3X,F8.2,3X,F7.2,3X,F9.2)
6    CONTINUE
     G=0.0
     D=0.0
     E=0.0
     EE=0.0
     DN=0.0
     DP=0.0
     K=0
     K1=0
     CONVF2=0.005/60.
     DO 3 J=1,JM
```

```
      IF(DELTAP(J).GT.G)G=DELTAP(J)
      IF(DELTAP(J).GT.0.0)E=E+DELTAP(J)
      IF(DELTAP(J).GT.0.0)K=K+1
      EE=EE+W1(J)
      D=D+X1(J)
      IF(X1(J))10,10,11
10     DN=X1(J)*CONVF2+DN
      GO TO 3
11     DP=X1(J)*CONVF2+DP
3     K1=K1+1
      E=E/K
      EE=EE/JM
      D=D/K1
      WRITE(6,7)G
      WRITE(6,8)E
      WRITE(6,15)EE
      WRITE(6,9)D
      WRITE(6,14)DP
      WRITE(6,13)DN
7     FORMAT(1H ,' MAX SYSTOLIC PRESSURE DROP (MMHG)=',F12.4)
8     FORMAT(1H ,'MEAN SYSTOLIC PRESSURE DROP (MMHG)=',F12.4)
15     FORMAT(1H ,'MEAN AORTIC PRESSURE (MMHG)=',F12.4)
9     FORMAT(1H ,'CARDIAC OUTPUT (L/MIN)=',F12.4)
13     FORMAT(1H ,'NEGATIVE FLOW PER STROKE (L)=',F12.4)
14     FORMAT(1H ,'POSITIVE FLOW PER STROKE (L)=',F12.4)
      RETURN
      END
      SUBROUTINE FORIA(U,MM,INV,S,IERR,NP,TL,DF,FREQ,AMP,NWIN,THETA,AS,B
     ZS,DPF,TOTP)
      DIMENSION U(1),INV(1),S(1),AMP(1),FREQ(1),WEFAC(100),THETA(1)
      DIMENSION AS(1),BS(1),E1(256),DPF(1)
C     IF ICOS=1 THEN COSINE WEIGHING FACTORS ARE USED.
C     IF ICOS=0 THEN ALL WEIGHING FACTORS = 1 . NORMALLY ICOS=1
      ICOS=1
      IF(ICOS.EQ.0) GO TO 11
      ICOWIN=NWIN/10
      DO 50 I=1,ICOWIN
50     WEFAC(I)=(1.0+SIN(3.1416*(I-1)/(ICOWIN-1)+1.5*3.1416))/2.0
      DO 60 I=1,ICOWIN
60     U(I)=U(I)*WEFAC(I)
      DO 70  I=1,ICOWIN
70     U(NWIN-ICOWIN+I)=U(NWIN-ICOWIN+I)*WEFAC(ICOWIN+1-I)
11     N=2**MM
      NI=2*N
      IF(NWIN.GT.NI)GO TO 25
      NWI=NWIN+1
      DO 10 J=NWI,NI
 10   U(J)=0.0
 25   ANP=NP
      DT=1./ANP
      TLG=(NI-1)*DT
      THF=TLG/2.
```

```
      CALL RHARM(U,MM,INV,S,IERR)
      DO 30 J=1,N
      J1=2*J
      J2=2*J-1
      AMB=U(J1)*U(J1)+U(J2)*U(J2)
      AMP(J)=AMB*THF
      FREQ(J)=(J-1)/TLG
      AS(J)=U(J2)
      BS(J)=U(J1)
      IF(U(J2).EQ.0.0)GO TO 29
      THETA(J)=ATAN(U(J1)/U(J2))
      GO TO 30
29    THETA(J)=90.
30    CONTINUE
      K=N-1
      G=0.0
      DO 2 J=2,K
      G=(AMP(J)+AMP(J+1))/2.0+G
      E1(J)=G
2     CONTINUE
      DO 3 J=2,K
      DPF(J)=E1(J)/E1(N-1)
3     CONTINUE
      DPF(1)=0.0
      DPF(N)=1.0
      TOTP=E1(N-1)
5     TL=TLG
      DF=FREQ(2)
      RETURN
      END
      SUBROUTINE TIMPLT(U1,V1,W1,X1,NWIN2,NWINF,DD,ZERO)
      DIMENSION U1(1),V1(1),W1(1),X1(1),DD(1),ZERO(1)
      YMAX=70.0
      YMIN=-30.
      CALL CPLOT(X1,NWIN2,NWIN2,DD,YMAX,YMIN,0)
      CALL CPLOT(ZERO,2,2,DD,YMAX,YMIN,0)
      YMAX=950.
      YMIN=-50.
      CALL CPLOT(V1,NWIN2,NWIN2,DD,YMAX,YMIN,0)
      CALL CPLOT(W1,NWIN2,NWIN2,DD,YMAX,YMIN,0)
      CALL CPLOT(ZERO,2,2,DD,YMAX,YMIN,0)
      YMAX=256.
      YMIN=-1024.
      CALL CPLOT(U1,NWINF,NWINF,DD,YMAX,YMIN,-1)
      RETURN
      END
      SUBROUTINE BOX
      CALL SYSPLT(3.,2.,3)
      CALL SYSPLT(3.,8.,2)
      CALL SYSPLT(12.,8.,2)
      CALL SYSPLT(12.,2.,2)
      CALL SYSPLT(3.,2.,2)
      RETURN
      END
```

```
      SUBROUTINE T3DAX
      CALL SYSPLT(5.053,3.625,3)
      CALL SYSPLT(5.303,3.625,2)
      CALL SYSPLT(5.303,7.286,2)
      CALL SYSPLT(10.,8.487,2)
      CALL SYSPLT(10.,4.825,2)
      CALL SYSPLT(5.053,7.286,3)
      CALL SYSPLT(5.303,7.286,2)
      CALL SYSPLT(5.303,7.536,2)
      CALL SYSPLT(10.,8.737,3)
      CALL SYSPLT(10.,4.825,2)
      CALL SYSPLT(10.25,4.825,2)
      CALL SYSPLT(11.967,1.500,3)
      CALL SYSPLT(11.717,1.500,2)
      CALL SYSPLT(11.717,1.278,2)
      CALL SYSPLT(7.02,0.300,3)
      CALL SYSPLT(7.02,0.068,2)
      RETURN
      END
      SUBROUTINE C3DAX
      CALL SYSPLT(6.162,2.847,3)
      CALL SYSPLT(5.3030,2.669,2)
      CALL SYSPLT(5.0530,2.669,2)
      CALL SYSPLT(5.303,2.669,3)
      CALL SYSPLT(5.3030,6.581,2)
      CALL SYSPLT(5.0530,6.331,3)
      CALL SYSPLT(5.3030,6.331,2)
      CALL SYSPLT(10.,7.531,2)
      CALL SYSPLT(10.,7.781,3)
      CALL SYSPLT(10.,5.7,2)
      CALL SYSPLT(10.25,5.7,2)
      CALL SYSPLT(11.967,2.3730,3)
      CALL SYSPLT(11.717,2.3730,2)
      CALL SYSPLT(11.717,2.143,2)
      CALL SYSPLT(7.0200,1.153,3)
      CALL SYSPLT(7.0200,0.943,2)
      CALL SYSPLT(5.3030,4.5,3)
      CALL SYSPLT(5.0530,4.5,2)
      RETURN
      END
      SUBROUTINE CPLT3D(A,AMAX,AMIN,IDIM,JDIM,ISTART,IDELTA,ISTOP,JSTART
     1,JDELTA,JSTOP,MODE,THEDEG,PHIDEG,NOAXIS)
      DIMENSION A(IDIM,JDIM),BCDW(22)
      COMMON/XYZLEN/XLONG,YLONG,ZLONG,XOFF,YOFF,SIDEZ
      INTEGER RTIME
      LOGICAL OPAQUE,BLOCK,ARRAY,NOAXIS,NOLABL
      BMAX=AMAX
      ARRAY=IDIM.NE.1
      BLOCK=MODE.EQ.2.OR.MODE.EQ.4
      OPAQUE=MODE.EQ.3.OR.MODE.EQ.4
      THETA=(3.1416/180.)*THEDEG
      PHI=(3.1416/180.)*PHIDEG
```

```
      SIDEX=ISTOP-ISTART
      SIDEY=JSTOP-JSTART
6     XH=XLONG*SIN(PHI)
      YH=YLONG*COS(PHI)
      XV=XLONG*COS(PHI)*COS(THETA)
      YV=YLONG*SIN(PHI)*COS(THETA)
      TX=(XH-YH)/2.+3.
      TY=(XV+YV)/2.+4.5
      JMAX=JSTOP
      JMIN=JSTART
      TM=ZLONG*SIN(THETA)
      CALL SYSPLT(XOFF,YOFF,3)
      IF(NOAXIS) GO TO 35
      CALL SYSPLT(XOFF,TM+YOFF,2)
      CALL SYSPLT(YH+XOFF,-YV+YOFF,3)
      CALL SYSPLT(XOFF,YOFF,2)
      CALL SYSPLT(-XH+XOFF,-XV+YOFF,2)
   35 CONTINUE
      NOW=RTIME(KKK)
      CALL CPTT3D (A,BMAX,AMIN,IDIM,JDIM,ISTART,IDELTA,ISTOP,JSTART,
     *JDELTA,JSTOP,THETA,PHI,OPAQUE,BLOCK,ARRAY,XLONG,YLONG,ZLONG)
      CALL SYSEND(-1,1)
      RETURN
      END
      SUBROUTINE SLOPFT(E,F)
      DIMENSION E(1,1),F(1),SLOP(45,256)
      DO 1 I=2,45
      DO 2 J=1,256
      IF(I.EQ.2)SLOP(1,J)=1.0
      SLOP(I,J)=1.0+(E(I,J)-E(I-1,J))/0.02
2     CONTINUE
1     CONTINUE
      CALL C3DAX
      CALL CPLT3D(SLOP,2.000,0.,45,256,2,1,45,1,1,127,1,45.,70.,.TRUE.)
      DO 3 I=1,45
      DO 4 J=2,256
      IF(J.EQ.2)SLOP(I,1)=0.001
      SLOP(I,J)=0.001+(E(I,J)-E(I,J-1))/F(2)
4     CONTINUE
3     CONTINUE
      CALL C3DAX
      CALL CPLT3D(SLOP,0.002,0.,45,256,1,1,45,1,1,127,1,45.,70.,.TRUE.)
      RETURN
      END
//LOAD DD *
//READRC01 DD LABEL=(08,NL,,IN),UNIT=TPDD,DISP=OLD,
//  DCB=(RECFM=U,BLKSIZE=512),VOL=SER=SMELOF
//SYSPLTDN DD SYSOUT=(N,,GSW4)
//DATA DD *
```

```
  292      10       0  100.000    0.125    0.855
 0.680
 1.535
 3.245
 4.100
 4.955
 6.665
 7.520
 9.230
10.085
10.940
     5
    13
    23
  293      10       1  100.000    0.125    0.651
 0.483
 1.785
 3.738
 5.040
 6.342
 7.644
 9.597
10.899
12.201
13.503
     5
    10
    24
  295      10       0  100.000    0.125    0.858
 0.734
 1.595
 3.330
 4.180
 6.762
 7.660
 9.356
10.214
12.808
13.666
     5
    14
    23
  296      10       0  100.000    0.125    0.863
 0.891
 1.754
 3.480
 4.343
 6.069
 6.932
 7.795
 9.521
10.384
12.110
     5
     8
    23
```

```
  297      10       0  100.000    0.125    0.867
 0.655
 1.522
 3.236
 4.103
 4.970
 7.571
 9.285
10.152
12.753
13.620
     5
     8
    20
  298      10       1  100.000    0.125    0.860
 0.070
 0.930
 1.790
 3.510
 4.370
 6.110
 6.970
 7.830
 9.550
10.430
     5
     7
    22
  300      10       0  100.000    0.125    0.855
 0.085
 0.940
 1.815
 3.525
 4.380
 6.090
 6.965
 7.820
 9.530
10.385
     5
    12
    23
//
```

APPENDIX C

This appendix contains a copy of the United States Patent 4,378,022 granted to the inventors Suobank, Harrison and Corcoran, entitled: "Energy-Frequency-Time Heart Sound Analysis." The patent describes a preferred non-invasive method of application of the acoustical analysis *in vivo*.

Cir 1638

United States Patent [19]

Suobank et al.

[11] **4,378,022**

[45] **Mar. 29, 1983**

[54] **ENERGY-FREQUENCY-TIME HEART SOUND ANALYSIS**

[75] Inventors: **David W. Suobank**, Pasadena; **Earl C. Harrison**, South Pasadena; **William H. Corcoran**, San Gabriel, all of Calif.

[73] Assignee: **California Institute of Technology**, Pasadena, Calif.

[21] Appl. No.: **225,251**

[22] Filed: **Jan. 15, 1981**

[51] **Int. Cl.**[3] **A61B 5/02**; A61B 7/00

[52] **U.S. Cl.** **128/715**

[58] **Field of Search** 128/696, 701, 715, 773

[56] **References Cited**

U.S. PATENT DOCUMENTS

3,799,147	3/1974	Adolph et al.	128/715 X
3,878,832	4/1975	Tickner et al.	128/696
4,181,134	1/1980	Mason et al.	128/690 X
4,220,160	9/1980	Kimball et al.	128/773 X
4,226,248	10/1980	Manoli	128/773

OTHER PUBLICATIONS

Iwata, A. et al, "Algorithm for Detecting the First and the Second Heart Sounds by Spectral Tracking," Med. & Biol. Energy & Computing, Jan. 80, pp. 19–26.

Iwata, A. et al, "Pattern Classification of the Phonocardiogram Using Linear Prediction Analysis," Med. & Biol. Eng. & Comp., Jul. 77, pp. 407–412.

Hearn, T. C. et al, "Temporal & Heart Size Effects on First Heart Sound Spectra," Med. & Biol. Eng. & Comput., Sep. 1979, pp. 563–568.

Primary Examiner—Kyle L. Howell
Assistant Examiner—Francis J. Jaworski
Attorney, Agent, or Firm—Marvin E. Jacobs

[57] **ABSTRACT**

A method for determining the operability status of heart valves IN VIVO. Accoustical data emanating from a heart valve to be analyzed is gathered. The data are divided into time slices, and the power, energy, and frequency relations for each time slice are calculated. The energy ratio of known peak frequencies is compared between the analysis data as gathered and known energy levels for a properly operating valve. The energy ratio of known frequency bands is also compared between the analysis data as gathered and known energy levels for a properly operating valve. Valve malfunctioning is indicated by the presence of a high change in the power and/or energy ratio at the selected key frequencies and bands.

36 Claims, 12 Drawing Figures

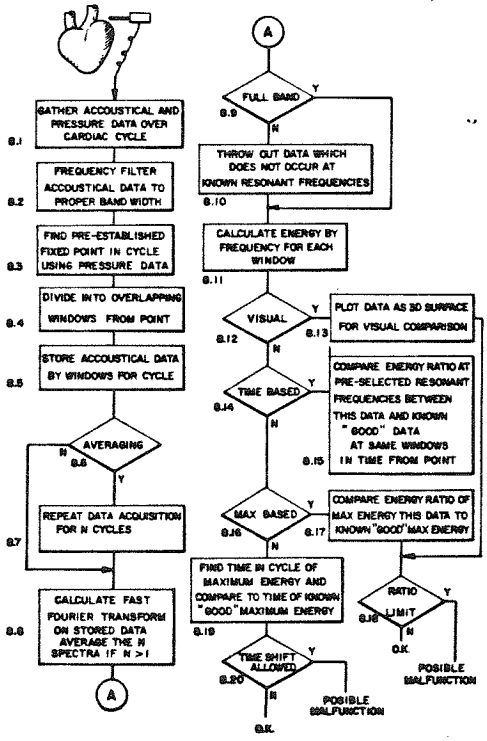

U.S. Patent Mar. 29, 1983 Sheet 1 of 7 4,378,022

Fig. 1.

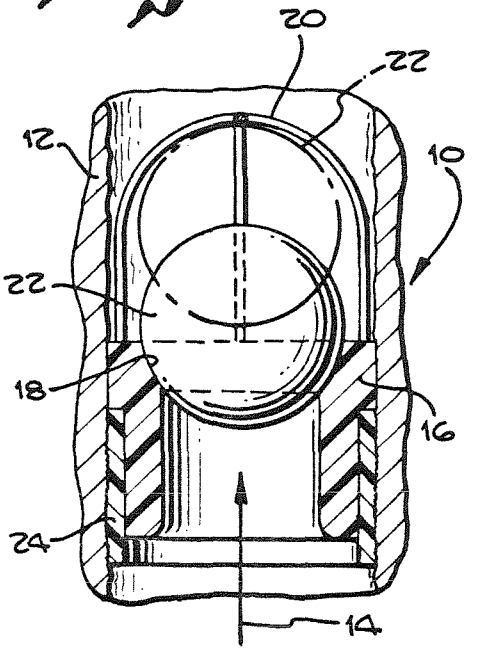

Fig. 3.

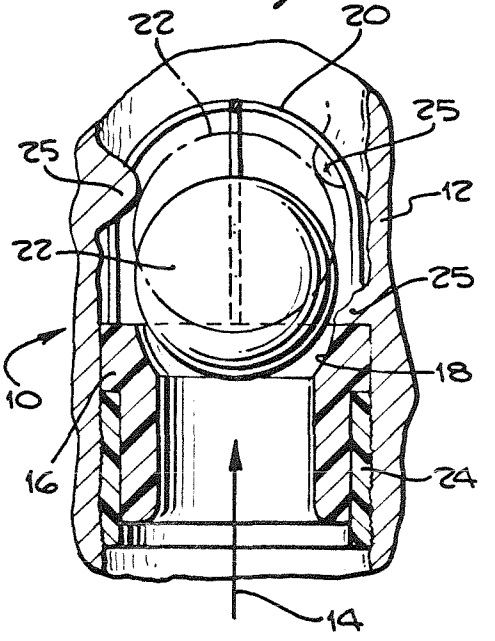

Fig. 2.

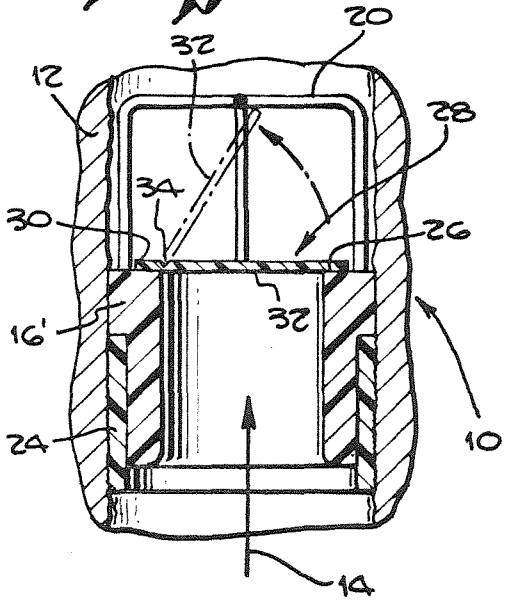

Fig. 4.

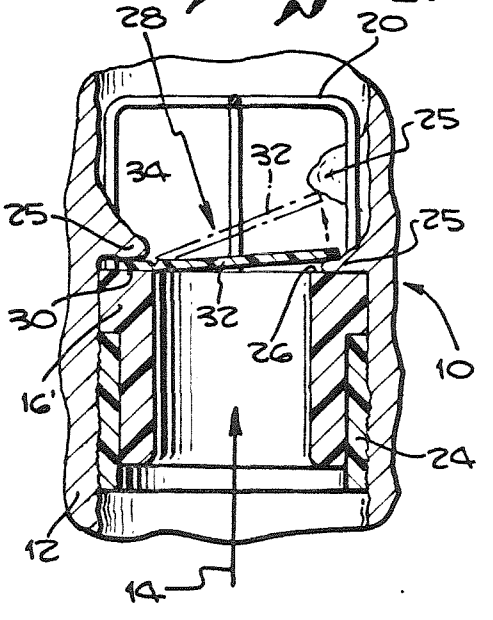

Fig. 5.

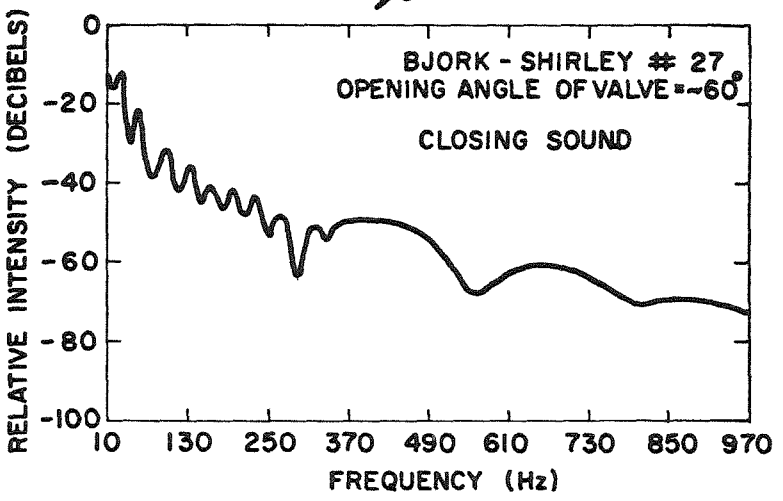

Fig. 6.

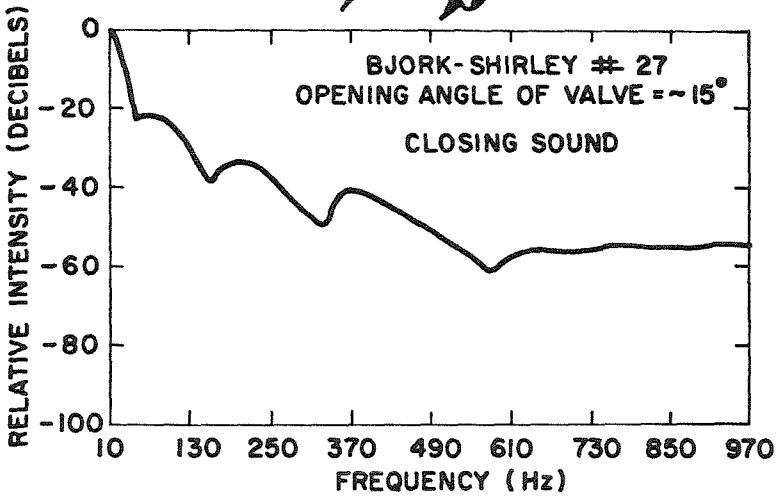

Fig. 7.

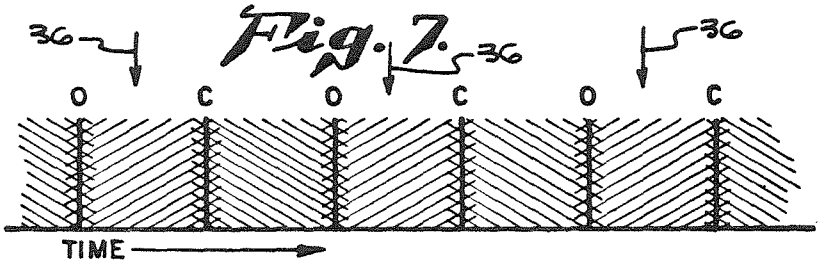

Fig. 8.

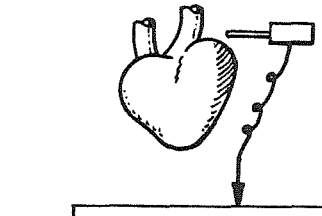

8.1 GATHER ACCOUSTICAL AND PRESSURE DATA OVER CARDIAC CYCLE

8.2 FREQUENCY FILTER ACCOUSTICAL DATA TO PROPER BAND WIDTH

8.3 FIND PRE-ESTABLISHED FIXED POINT IN CYCLE USING PRESSURE DATA

8.4 DIVIDE INTO OVERLAPPING WINDOWS FROM POINT

8.5 STORE ACCOUSTICAL DATA BY WINDOWS FOR CYCLE

8.6 AVERAGING — N / Y

8.7 REPEAT DATA ACQUISITION FOR N CYCLES

8.8 CALCULATE FAST FOURIER TRANSFORM ON STORED DATA AVERAGE THE N SPECTRA IF N > 1

A

A

8.9 FULL BAND — Y / N

8.10 THROW OUT DATA WHICH DOES NOT OCCUR AT KNOWN RESONANT FREQUENCIES

8.11 CALCULATE ENERGY BY FREQUENCY FOR EACH WINDOW

8.12 VISUAL — Y / N

8.13 PLOT DATA AS 3D SURFACE FOR VISUAL COMPARISON

8.14 TIME BASED — Y / N

8.15 COMPARE ENERGY RATIO AT PRE-SELECTED RESONANT FREQUENCIES BETWEEN THIS DATA AND KNOWN "GOOD" DATA AT SAME WINDOWS IN TIME FROM POINT

8.16 MAX BASED — Y / N

8.17 COMPARE ENERGY RATIO OF MAX ENERGY THIS DATA TO KNOWN "GOOD" MAX ENERGY

8.18 RATIO LIMIT — Y / N

O.K.

POSIBLE MALFUNCTION

8.19 FIND TIME IN CYCLE OF MAXIMUM ENERGY AND COMPARE TO TIME OF KNOWN "GOOD" MAXIMUM ENERGY

8.20 TIME SHIFT ALLOWED — Y / N

POSIBLE MALFUNCTION

O.K.

Fig. 9.

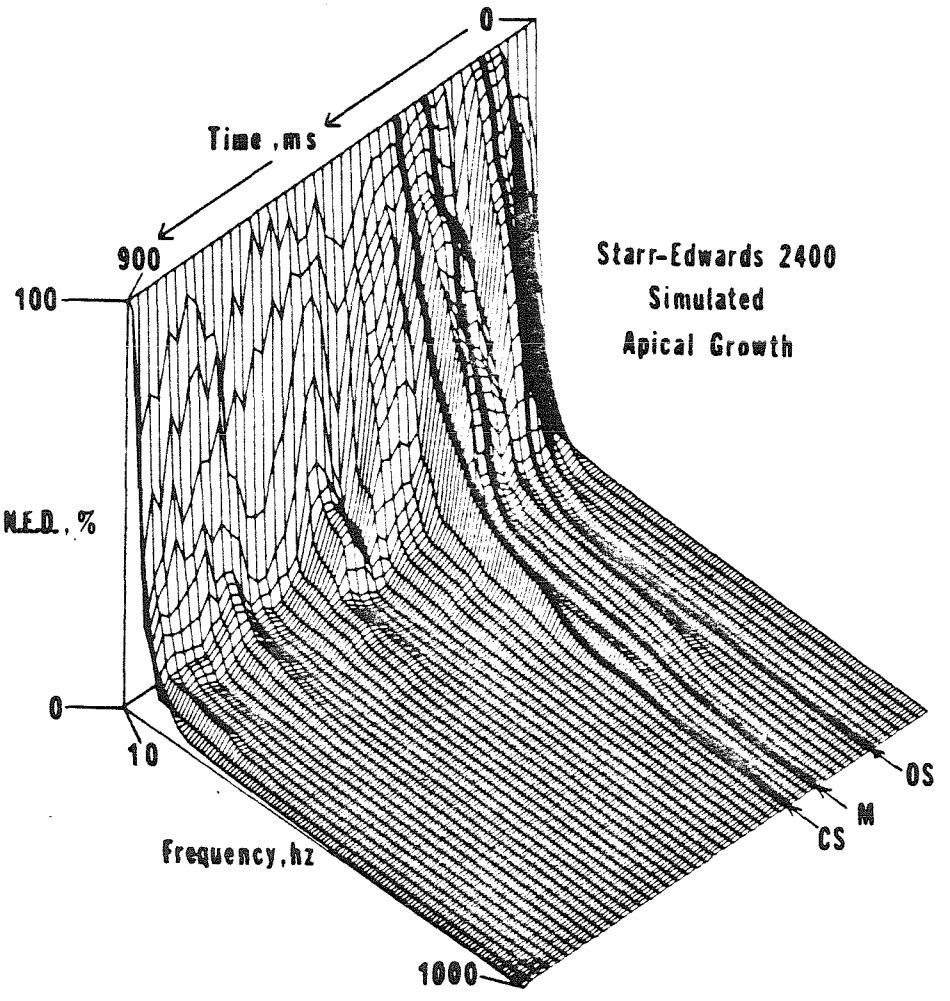
0
Time, ms
900
100
N.E.D., %
0
10
Frequency, hz
1000
Starr-Edwards 2400
Simulated
Apical Growth
OS
M
CS

Fig. 10.

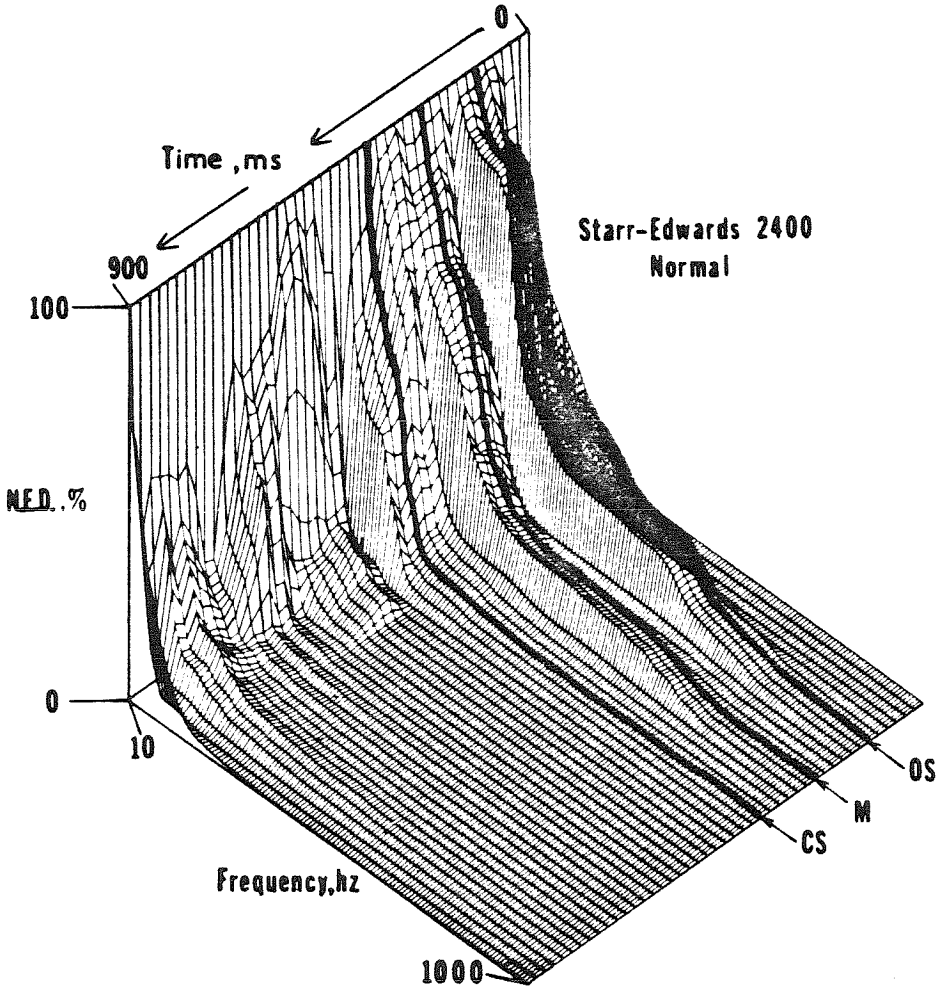
0
Time ,ms
900
Starr-Edwards 2400
Normal
100
N.E.D. .%
0
10
OS
M
CS
Frequency,hz
1000

Fig. 11.

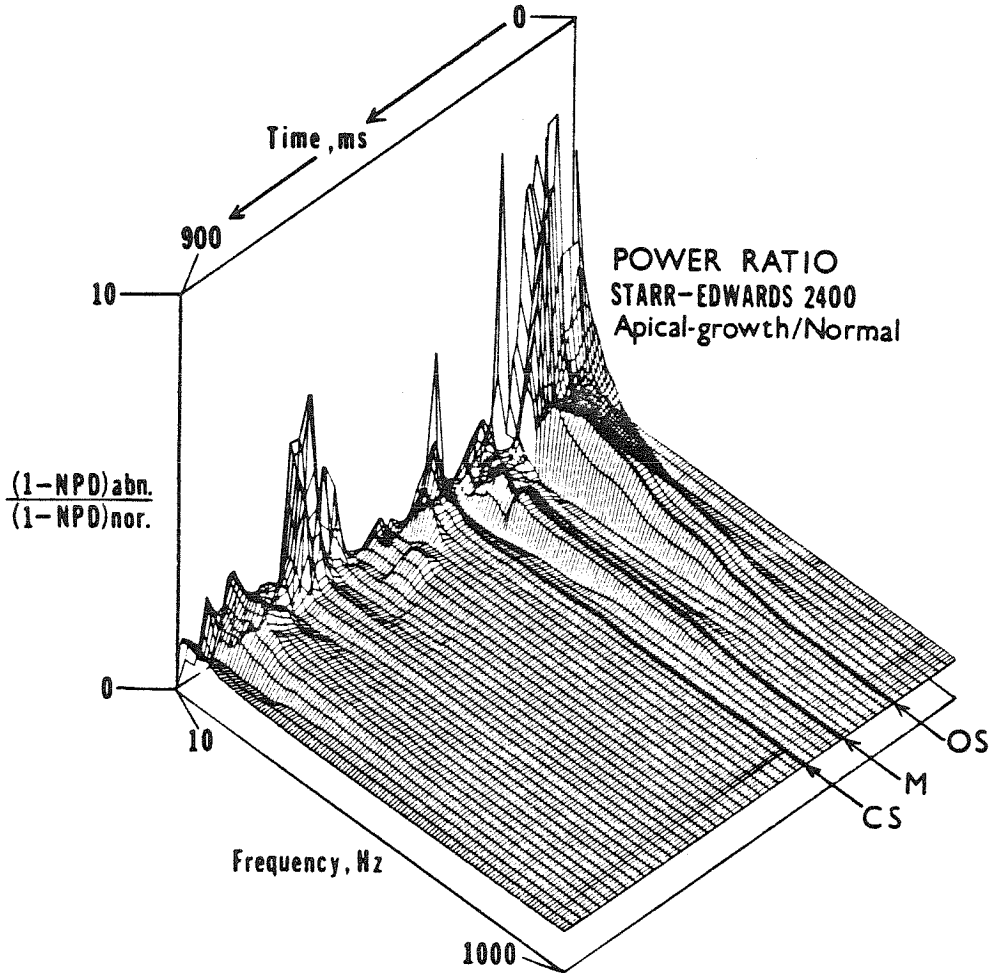
0
Time, ms
900
10
POWER RATIO
STARR-EDWARDS 2400
Apical-growth/Normal
(1-NPD)abn.
(1-NPD)nor.
0
10
OS
M
CS
Frequency, Hz
1000

Fig. 12.

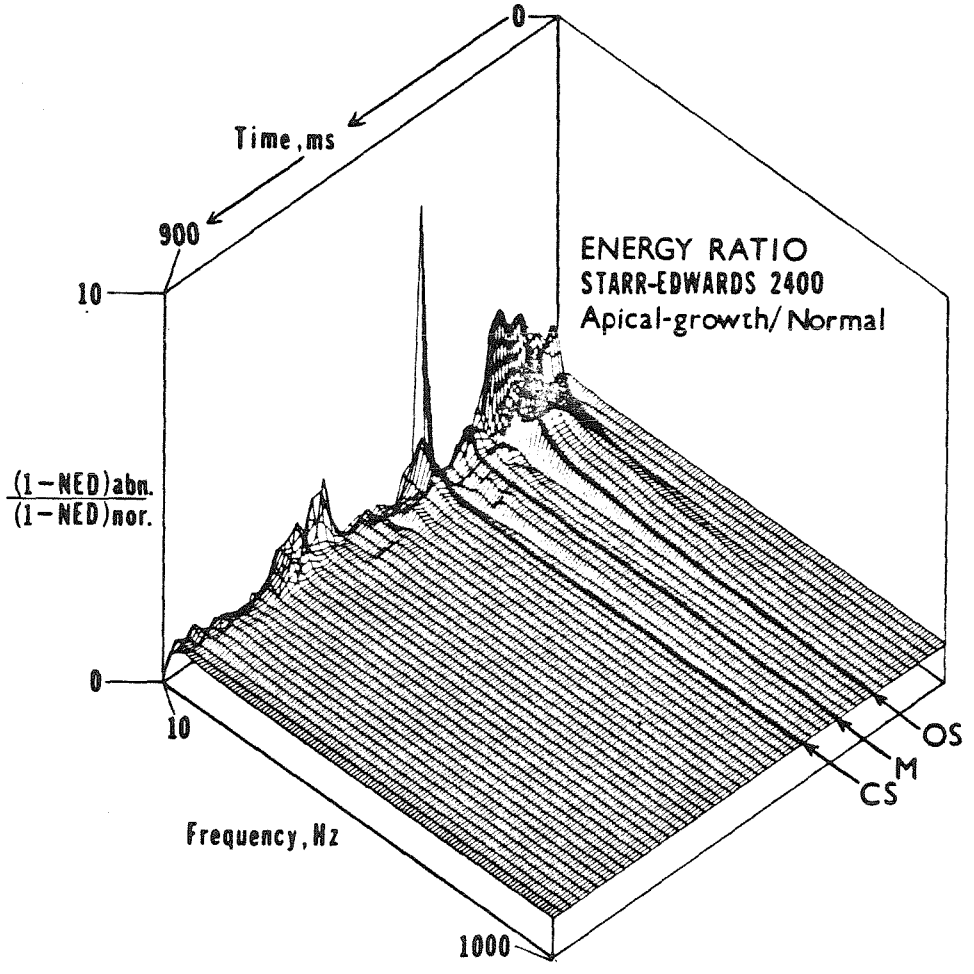
0
Time, ms
900
10
ENERGY RATIO
STARR-EDWARDS 2400
Apical-growth/ Normal
(1-NED)abn.
(1-NED)nor.
0
10
Frequency, Hz
1000
OS
M
CS

ENERGY-FREQUENCY-TIME HEART SOUND ANALYSIS

BACKGROUND OF THE INVENTION

The present invention relates to methods of in vivo analysis and, in particular, to methods for determining the operability status of heart valves and the like. Heart valve prostheses have been used successfully since 1960. As stated by one author, the decade of 1960 will probably be remembered most in the annals of cardiology as the decade in which cardiac valve replacement became a reality. Of the nearly fifty different heart valves introduced over the last sixteen years, many have been discarded due to their lack of success. Of those remaining, several modifications have been made or are presently being made.

The most commonly used basic types of valves at present are the caged ball, the tilting disc, the caged disc, and tissue or porcine valves. A caged-ball-type valve is shown IN SITU within the blood stream in simplified form in operation in FIG. **1**. A tilting-disc type is shown in similar manner in FIG. **2**. At present, over ninety thousand prosthetic valves of different designs are used annually throughout the world.

Even after sixteen years of experience, the problems associated with heart-valve prostheses have not been totally eliminated. The most serious problems and complications associated with them are red-cell destruction, thrombosis formation, damage to the endothelial lining of the aortic walls, valve failure due to material fatigue or chemical change, leaks caused by failure of the valve to close properly, infection, and tearing of sewing sutures.

Because of the above mentioned problems, implanted prosthetic valves eventually show some degree of malfunction. If the malfunction of a prosthetic valve is not detected, it could be fatal to the patient. Except for a few valves of recent design, the moving parts of most prosthetic valves contain only plastic materials (specifically non-metallic) such that easily accomplished non-invasive testing cannot be done. Low intensity X-ray analysis through the injection of radiopaque dyes into the heart via catheterization is neither pleasant nor without certain dangers.

Wherefore, it is the object of the present invention to provide a simple non-invasive method of analysis of the operability of heart valves IN VIVO.

SUMMARY

The foregoing objectives have been met by the method of the present invention comprising the steps of disposing of phono-cardiographic transducer in a position to gather time-amplitude acoustical information emanating from the heart valve and adjacent area; gathering the output signal from the transducer over a cardiac cycle; determining the point of a pre-established point in the cardiac cycle within the data; dividing the data of the cardiac cycle into time slices beginning with the pre-established point; calculating the power versus frequency curve for each time slice; comparing the power or energy level associated with the valve being contested at pre-established frequencies within each time slice to corresponding power or energy levels for the same frequency at the same time slice for a known good valve; and, indicating valve malfunction if the power and/or energy ratio of measured data to a known good data is greater than a pre-established amount for over a pre-established threshold number of compared values.

In the ideal state and preferred method of the present invention, the known good data are obtained from the same valve by the same steps performed at a time when it is known that the valve is properly operating. In the case of prosthetic valves, this can be accomplished by gathering such data closely after the implantation thereof.

In the preferred embodiment, the data are digitized at a rate of 2000 samples per second, and only information associated with frequencies between 10 Hz and 1000 Hz is retained. An analog high-pass filter is used to reduce the energy of sound for frequencies less than 100 Hz. Moreover, each cardiac cycle to be analyzed is divided into overlapping windows of 100-ms duration, and the beginning of each successive window occurs at increments of 20 ms.

DESCRIPTION OF THE DRAWINGS

FIG. **1** is a side cut-away elevation through a caged-ball-type prosthetic heart valve in its proper operating condition.

FIG. **2** is a cut-away side elevation through a tilting-disc-type prosthetic heart valve in proper operating condition.

FIG. **3** is a cut-away side elevation of the valve of FIG. **1** in a malfunctioning condition.

FIG. **4** is a cut-away side elevation of the valve of FIG. **2** in a malfunctioning condition.

FIG. **5** is a frequency-versus-intensity curve of a normally operating Bjork-Shiley valve in a single-time slice in a closing mode. (unfiltered sound)

FIG. **6** is a frequency-versus-intensity plot for the same time slice for the valve of FIG. **5** in a malfunctioning mode. (unfiltered sound)

FIG. **7** is a drawing depicting the occurrence of data during normal heart operation showing the opening and closing cycles.

FIG. **8** is a flowchart showing the method of the present invention with several testing options.

FIG. **9** is a 3D plot of a malfunctioning Starr-Edwards valve.

FIG. **10** is a 3D plot of a normally operating Starr-Edwards valve.

FIG. **11** is a 3D plot of the Power Ratio of the data of FIGS. **9** and **10**.

FIG. **12** is a 3D plot of the Energy Ratio of the data of FIGS. **9** and **10**.

DESCRIPTION OF THE PREFERRED EMBODIMENT

Referring once again to FIG. **1**, a caged-ball-type valve is shown and generally indicated as **10**. Valve **10** is implanted within a blood vessel such as, the aorta **12** wherein blood flow is in the direction of arrow **14**. Valve **10** comprises a cylindrical body portion **16** having a valve seat **18** at the top inner surface thereof. A metallic wire cage **20** is disposed above valve seat **18** and connected to body portion **16**. A ball **22** is placed within cage **20**. As blood attempts to pass through valve **10** in the proper direction, ball **22** is forced out of valve seat **18** against the top of wire cage **20**, whereby the blood can pass up through valve seat **18** and around ball **22** and, therefore, through aorta **12**. Any attempt for blood to flow in the opposite direction (i.e. opposite arrow **14**) causes ball **22** to be forced into valve seat **18**

thereby blocking the flow of blood in the wrong direction through valve **10**. Typically, the body portion **16** is provided with a Dacron surface **24**.

Turning to FIG. **3**, typically after a period of time the endothelial tissue in the area around valve **10** may grow because of the stimulation of valve **10** as a foreign body. Excess tissue growth can result in the formation of projections **25** which can interfere with both the opening and/or the closing of the valve **10**.

Turning now to FIGS. **2** and **4**, the same general situation is shown with respect to a tilting disc type valve such as that sold under the name of Bjork-Shiley. In such a valve, the top **26** of the cylindrical body portions **16'** forms the valve seat and a tilting disc **28** replaces the ball. Tilting disc **28** has a portion **30** fastened to the top **26** of body portion **16'**. The remaining portion **32** of tilting disc **28** is connected to portion **30** by a so-called living hinge **34**. Thus, portion **32** is free to rotate about living hinge **34** between the closed position and open (ghosted) positions as shown. Within FIG. **4**, these same phenomena of projections **25** as may be caused by the growth of the endothelial tissue of aorta **12** can cause impairment to the operation of the portion **32** by preventing full opening and/or full closure.

In arriving at the present invention, the closing sounds produced by six different aortic prostheses were analyzed for their frequency content by the Fast Fourier Transform (FFT). In addition, the frequency spectrum of the closing sounds of a normal and abnormal aortic prosthesis were compared in order to see if the FFT technique could be used to detect malfunctioning prosthetic valves. All experiments were conducted at California Institute of Technology using its pulse duplicator system. For repeatability and, therefore, more valid comparative results, the experiments were conducted IN VITRO in a simulated environment. The sounds were measured by a Millar phonocatheter (PC-480) which was placed in the aortic flow channel via a wall pressure tap. Therefore, all sounds in the near vicinity of the aortic prosthesis were readily obtained. When the valve is operational, sounds are produced by the operation and vibration of the valve itself as well as by the flow of blood passing through and around the parts of the valve as well as emanating from vibrations in the surrounding tissue itself. Experiments were conducted at a heart rate of 70 beats per minute, an average cardiac output of 5 liters per minute, and a pressure range of 128 mm Hg. The test fluid used in the pulse duplicator was a Polyol V-10 solution (Wyandotte Chemicals) with a viscosity of 3.5 cp at 22° C.

The IN VITRO sounds obtained from the phonocatheter were passed through a heart-sound amplifier (Hewlet Packard model 8813A) and were high-pass filtered at 12 db octave with a cutoff frequency of 100 Hz. The sounds were then recorded, together with the aortic pressure, ventricular pressure, and flow, and the time base on a Hewlett Packard model 3960 FM tape recorder. In actual human testing, this pressure information is most easily obtained by taking the carotid or Korotkoff pressure of the cardiovascular system. The recorded signals were then played back from the tape recorder through, an analog to digital converter at the California Institute of Technology computer center and 30 to 45 second epochs of data were digitized for each experiment. A digitization rate of 2,000 points-per-second was used. The digitized data were stored on a magnetic tape. This tape was then used to generate time plots of the valve sounds on a Calcomp plotter.

Ten to fifteen 100 ms time segments, or windows, containing the closing sounds of the aortic valve were selected. A frequency spectrum of each of these 100-ms time segments was obtained using the Fast Fourier Transform algorithm. Finally, a mean-frequency spectrum for each valve was obtained by averaging the spectra of ten to fifteen closing sounds. This average spectrum was corrected for the 12 db octave filtering, and the resulting spectrum was plotted in graphical form. By analyzing ten to fifteen closing sounds of each valve, any variability introduced by the pulse duplicator was averaged out.

The frequency spectrum obtained showed that in the frequency range of about 10 to 200 Hz there exist some sharp resonant peaks, and beyond that range there are some smooth, wide peaks. The phenomena were observed in the frequency spectrum of a number of different types of valves studied. No resonant peaks were observed above 750 Hz. The reproducibility of the results were verified by performing sound recordings on each valve about two weeks after the first set of experiments and obtaining sound spectra which possessed resonance peaks that were centered within plus or minus 10 Hz of the peaks in the original sound spectrum.

The results of the frequency analysis indicated that with the exception of the Bjork-Shiley valve, the other tested valves have sharp resonant peaks which are quite similar. These six aortic prostheses, however, have characteristic smooth, wide resonant peaks which distinguish each one of them. A mathematical analysis indicated that each of the six frequency spectra obtained were different and distinguishable. That is, early tests indicated that a normal operating prosthetic heart valve had sound characteristics which were reproducible, unique, and identifiable with respect to each type of valve. The next question which presented itself in the evolution of a solution for the stated objectives of the present invention was whether a malfunctioning valve would have sound characteristics which could possibly distinguish it from the normally operating valve.

In order to use the frequency analysis technique as a method to monitor the functional integrity of a prosthetic aortic valve, it was proposed to use the frequency spectrum of the opening and/or closing sound of each normally functioning prosthesis as its own baseline and investigate to see how it changed when pathologically realistic modifications were made to the prosthesis. It was known that the Bjork-Shiley tilting disc aortic prosthesis has been observed to have pathological problems associated with it that impede the opening of the disc as previously discussed with reference to FIGS. **2** and **4**. Some of the Bjork-Shiley valves that have been recovered only open to an angle of about 15°, whereas the normal Bjork-Shiley valve opens to an angle of 60°. A previously tested Bjork-Shiley valve was constrained in a pathologically realistic way to open up only to an angle of about 15°, and the sound measurements as previously described were made. It was observed that the intensities of the closing sounds for both experiments were only slightly different and could not be differentiated by the human ear. It was possible to listen to the sounds of the prosthesis via the audiophone output on the heart sound amplifier which was set at a constant gain for both experiments. The frequency spectrum of the closing sounds, however, were very different as shown in FIGS. **5** and **6**. The frequency spectrum of the normally functioning Bjork-Shiley

valve (FIG. 5) had nine sharp resonant peaks in the frequency range of 25 to 325 Hz, and two smooth, wide peaks at 394 and 665 Hz, respectively. The frequency spectrum of the closing sounds of the malfunctioning valve (FIG. 6) however, had no sharp resonant peaks and had three smooth, wide peaks at 58, 234 and 378 Hz respectively. These results indicated quite clearly that the frequency content of the closing sounds of the normally operating and malfunctioning Bjork-Shiley valve are different and distinguishable.

At present, physicians listen to the intensity of the closing click of the Bjork-Shiley aortic valve in order to judge if the valve is opening completely. The above described in vitro experiment conducted in the pulse duplicator suggested not only that a non-invasive technique for analysis of prosthetic valves to determine malfunctioning was not only probably viable, but, additionally, that the change in sound intensity of a normally functioning valve in a valve that opens to about 15° cannot be detected by the human ear. Thus, if a physician were to use the intensity of the closing click of the Bjork-Shiley aortic valve as a method for detecting any malfunctioning of the valve, he could endanger the life of his patient. Consequently, the evolution of a truly dependable non-invasive method of testing such prosthetic valves appeared not only desirable, but mandatory from a life endangering point of view.

To arrive at a truly viable method for prosthetic-heart-valve testing using acoustical techniques, the operation of the actual cardiovascular system was considered. As shown in symbolic graphic manner in FIG. 7, over a period of time the valves of the heart go through repeated opening and closing cycles separated by periods of stability. The valves of the heart neither open nor close instantaneously, whether it is the actual living heart valve or a prosthetic implant. Thus, while the vertical lines labeled "O" and "C" indicating the opening and closing cycle limits are drawn as lines, as shown by the overlapping cross-hatching, the change in cycle takes a period of time. In the single cross-hatched portion of the time domain of each cycle, the valve and surrounding cardio-vascular tissue as well as the blood flow obtains a stable nature. It is convenient to detect the blood pressure in order to establish a repeating fixed point within each cardiac cycle. For example, the dichrotic notch is a very easily identifiable point within each cardiac cycle. Thus, if data are gathered over a complete cardiac cycle, both as to the acoustical nature and the simultaneous blood pressure associated therewith, a pre-established point within the cardiac cycle can be determined, as symbolized by the arrows 36 in FIG. 7, and from that pre-established point, selected stable portions of the cardiac cycle can be employed as the data base for comparison.

According to the preferred embodiment of the present invention, as finally established, acoustical information in the form of a time-amplitude, analog signal is obtained using standard phono-cardiographic transducers placed either externally or internally near the source of the sound. The unfiltered analog signal is amplified and recorded on FM analogue tape. Analog filtering of the raw data is also done during the recording process. Once the experimental data are stored on tape in files, they are digitized by a standard analog to digital converter at 2,000 points per second and stored on magnetic computer tape. By establishing the location within the data of the pre-established point within the cardiac cycle, the data file of interest is plotted so that a typical cardiac cycle can be chosen along with it starting and ending times. A typical cardiac cycle is of approximately 0.860-second duration. From the total data a series of time slices of data are established. In the preferred embodiment, these time slices are in the form of windows of data in overlapping relationship. Preferably, a window length is chosen of approximately 100 milliseconds, and the time of the beginning of each successive window is incremented 20 milliseconds. Thus, for a 100-millisecond window length and a 20-millisecond increment, it will take 43 windows to cover the entire 860 millisecond cardiac cycle.

While hand calculation of the data would, of course, be possible, modern computer technology makes the calculations and comparisons necessary to implement the technique of the present invention much more practical. For each window, the spectra corresponding to the data line within the time range associated with the window must be calculated. This analysis is most conveniently accomplished by implementing a calculation employing a Fast Fourier algorithm to obtain real and imaginary parts of the complex Fourier coefficients associated with the data within the windows. It is preferred that a modified Hanning window be used to minimize undesirable effects caused by sampling in the time domain. According to one technique as employed and tested, the calculations are performed for each window, and, having obtained the spectra for each of the forty-three windows, a three-dimensional surface plot is generated having time as the third axis associated with the increment of the starting time of successive windows. The 3D surface thus plotted is characteristic of the energy distribution associated with a cardiac system's acoustical state for a specific time range and frequency band width. The foregoing information can be visually checked by a physician or technician for malfunctions. Specifically, the plot of a presently functioning valve is compared against a similar plot for a known properly functioning valve of the same type. Examples of such 3D plots for a normal and a malfunctioning valve are shown in FIGS. 10 and 9, respectively. While specifically developed for detecting malfunctioning prosthetic valves, the present invention appears to also have value in the analysis of living heart valves and, in fact, various other bodily functions. For such latter analysis, a file history of acoustical spectra on individual patients would have to be maintained for later comparison to determine changes therein. While it is possible to have pre-established acoustical spectra on individual prosthetic valves, it is likewise preferred that such data be secured in vivo from the individual patient. That is, following a prosthetic implant is it preferred that an acoustical spectra of "normal" operation be obtained and retained for later comparison during malfunction testing. In addition to the visual comparison possible employing the three-dimensional plot technique, the data can also be compared numerically either manually or by computer.

The information obtained according to the foregoing techniques is valuable for specifically predicting the physical changes occuring in a sound producing system, such as prosthetic heart valves operating within the heart. The energy content of specific valve-related sounds in specific frequency bands has been shown to be a function of the operational state of the valve, specifically the nature of the materials that are in juxtaposition at the time of collision (e.g. the valve poppet and flow orifice). An example of the results of the invention for a

specific valve show that the energy ratio between a normal valve and a valve having thrombosis is 3:1, with the specific frequency band 150–300 Hz at the time corresponding to a 100 ms window containing the maximum acoustical energy of the closing sound. That is, the data when employing the present invention can be compared on two bases. According to one technique, specific windows occurring at the same position within a cardiac cycle from the pre-established point within that cycle are compared for known good operational data and the data under test. The total energy ratio across the frequency spectrum can be compared, or, preferably, the energy ratios of those frequencies known to produce resonant peaks in normal operation are compared. An energy ratio higher than a pre-established amount is indicative of a malfunction.

A particularly useful tool in the analysis of the data is a normalized three-dimensional surface plot of the power or energy ratio. Such plots are shown in FIGS. **11** and **12**, respectively, corresponding to the data of FIGS. **9** and **10**. If the data were identical, the ratio would produce no points plotted off of the time-frequency plane. Therefore, the three-dimensional nature of the plot quickly shows a variation of the power/energy associated with the abnormal performance as compared to that associated with the normal performance. Thus, the normalized plots such as those of FIGS. **11** and **12** add significantly to understanding the comparison between a normal valve and an abnormal valve.

The normalized energy and power distributions employed and preferred are defined as follows:

Normalized Energy Distribution (N.E.D.) is defined by the relationship:

$$1 - NED(n\Delta f) = \frac{\frac{1}{2}\sum_{k=0}^{n}\left[\frac{[a(k\Delta f)]^2 + [b(k\Delta f)]^2}{kf} + \frac{[a((k+1)\Delta f)]^2 + [b((k+1)\Delta f)]^2}{(k+1)f}\right]}{\frac{1}{2}\sum_{k=0}^{N}\left[\frac{[a(k\Delta f)]^2 + [b(k\Delta f)]^2}{k\Delta f} + \frac{[a((k+1)\Delta f)]^2 + [b((k+1)\Delta f)]^2}{(k+1)\Delta f}\right]}$$

Normalized Power Distribution (N.P.D.) is defined by the analogous relationship:

$$1 - NPD(n\Delta f) = \frac{\frac{1}{2}\sum_{k=0}^{n}[a(k\Delta f)]^2 + [b(k\Delta f)]^2 + [a((k+1)\Delta f)]^2 + [b((k+1)\Delta f)]^2}{\frac{1}{2}\sum_{k=0}^{N}[a(k\Delta f)]^2 + [b(k\Delta f)]^2 + [a((k+1)\Delta f)]^2 + [b((k+1)\Delta f)]^2}$$

for n=0, 1, 2, . . . , N

and where, Δf is the frequency resolution (9.8 Hz) and $a(\omega)$ and $b(\omega)$ are the real and imaginary part of the complex Fourier coefficient for frequency ω.

Rather than establishing specific window-to-window comparisons on a fixed-time position, one can also search the total data for windows having maximum energy data either across the frequency spectrum or at selected frequencies and compare these maximum data for their energy ratio regardless of the time occurrence within the cardiac cycle. In this latter approach, both the energy ratio and the time-phase shift between the occurrence of this maximum energy data could be indicative of malfunction. That is, a change in the energy of the sound produced would tend to indicate a change in the operation of the valve characteristics as would a delay in the occurence of the maximum energy from its expected time of occurence within the cardiac cycle. Such a delay in time could, for example, indicate that a valve was opening completely but was being impeded in its time of operation by tissue growth which would shortly completely stop full operation.

Turning now to FIG. **8**, the logic accomplished by the various options within the preferred embodiment as set forth above is shown schematically in low-chart form. The procedure begins at block **8.1** wherein the acoustical and blood-pressure data are gathered over at least one cardiac cycle. In block **8.2**, the acoustical data are frequency filtered to the proper band width. As seen previously, in the typical prosthetic heart valve as tested to date, this filtering would be to reduce the energies of frequencies below 100 Hz and above 1000 Hz. The specific filtering would, of course, be dependent upon the system being checked, particularly the valve design.

Next, the bood-pressure data are checked in box **8.3** to find a pre-established fixed point in the cardiac cycle. The easiest point to establish is, of course, the dichrotic notch which occurs between the systolic and diastolic portions of the heart action as mentioned previously.

In box **8.4**, the data are divided into overlapping windows using the pre-established point as a starting point. That is, one cardiac cycle is, by definition, the duration of data existing from the pre-established point to the same pre-established point in the next cycle. Because the cardiac cycle in its pressure response generally behaves according to known, pre-established characteristics, having once found a known point, the entire cycle can be mapped out from beginning to end and the data taken in any sequence desired. In forming the overlapping windows of data, it is preferred, as previously mentioned, to use 100 ms windows at 20 ms intervals with a digitization rate of 2000 Hz.

In box **8.5**, the acoustical data by windows is stored for the entire cycle. While not shown, it is inherent that the data be stored in a sequential manner such that its time within the cycle is retained.

In question block **8.6**, the logic checks to see if averaging is occurring. By "averaging", it is meant that more than one cardiac cycle is being employed in order to eliminate extraneous or inconsistent data. If averaging is not occurring, box **8.7** is bypassed as shown. If averaging is occurring, in the logic represented by box **8.7** the data-acquisition steps of blocks **8.1** through **8.5** are repeated and the data stored as a replacement for the single-cycle data stored in box **8.5**.

In box **8.8**, the Fast Fourier Transform is used to calculate the parameters of interest for each cycle of the stored data and averaging of the spectra is performed in the frequency domain. Other methods could be used, of course. The Fast Fourier Transform is preferred in that it provides the necessary information at a much faster rate than possible by other methods. The Fast Fourier

Transform and its use, of course, are well known in the art and, per se, form no point of novelty in the present invention.

At question block 8.9, the logic next checks to see if the full band of frequencies are being employed. That is, are all the frequencies within the filtered data are being employed. Typically, only the data associated with the known resonant frequencies for the valve under test are employed. The remaining data are discarded by the logic of box 8.10. The box 8.11, the energy by frequency for each window is calculated. The basic data are, of course, provided by the Fast Fourier Transform calculated in box 8.8 and the logic associated with box 8.11 contemplates merely placing the data in a usable form for the balance of the logic.

In decision blocks 8.12, the logic next checks to see if only a visual presentation of the data is desired. If "yes", the logic of box 8.13 plots the data as a three dimensional surface for visual comparison. While the entire process can be accomplished mechanically, with computer logic, it has been found that an analysis of the data in a three dimensional time-frequency-power plot by one skilled in the cardiac art provides insight and decision making capabilities not possible with the single repetitive logic of a computer. In particular, in the preferred manner of implementation, the known good valve IN SITU is tested according to the preceeding logic and, at this point, its data are plotted for visual analysis. The cardiologist then analyzes the data for the particular patient and stores the responses, known as "good" data, for later comparison when possible malfunction is being checked for the same patient. In this manner, the "good" data for each patient is highly individualized to the patient.

When non-visual presentation is being made, the logic next begins a series of checks to determine which of the various data testing options are to be employed. As the balance of the logic illustrated shows, only one type of testing is implemented. As will be readily recognizable to the those skilled in the art, additional logic of a non-inventive nature could be incorporated to cause the foregoing logic to produce more than one, and even all, of the tests described without the necessity for the entire test being repeated. This logic provides no inventive level to the present invention, and is therefore, omitted for simplicity.

In decision box 8.14, the logic checks to see if the test is to be time based. By time based, the test data are compared to the known "good" data at the same window in time within the cardiac cycle. As stated in box 8.15, if a time based check is selected, the energy ratio at pre-selected resonant frequencies is compared between these data and the known data at the same windows in time from the pre-selected point.

If time-based testing is not selected, the logic next checks to see if maximum based testing is desired in decision box 8.16. If "yes", the logic within box 8.17 searches the data for this valve to find the maximum energy in any window. This value is compared to the maximum energy associated with known "good" data. Whether box 8.15 or box 8.17 logic is employed, the results of the comparison are subjected to decision box 8.18 wherein the ratio of the compared data is compared to an appropriate pre-established limit for the test being conducted. If the ratio between the tested data and the known good data is greater than the pre-established allowable amount, a possible malfunction is indicated while if the ratio is not greater than the limit, the valve is indicated as being performing acceptably. While not specifically indicated, it is preferred that the logic within decision box 8.18 include the further limitation that the ratio be greater than the limit for a pre-established number of points which may be one or greater. Typically, a greater number of points is employed in order to throw out a single piece of spurious data. It has been found that, in practice, it is preferred that the data being compared be taken from windows wherein the valve is not in a transitory state. That is, occuring within the single cross-hatched or "stable" area of FIG. 7.

If max-based testing is not indicated in decision box 8.16, the default-testing procedure of "time in cycle" is accomplished beginning with the logic of box 8.19. This method is the previously discussed case where the logic determines the maximum energy occuring within the cycle and then determines the time within the cycle wherein this maximum energy has occurred. This time is compared to the time within the cycle wherein maximum energy occurs for a known "good" valve. In decision logic 8.20 which follows, possible malfunction is indicated if the time shift between the occurrence of the two maximum energies is greater than the allowed amount, and probable valve proper functioning is indicated if the time shift is less than the maximum amount allowed.

With particular reference to the question of data filtering in the present invention, the preferred method of digitizing the data limits the analysis to the broad frequency band of 10–100 Hz. If analog filtering is desired, this can be done. In that case, the preferred method is to employ a filter having a 12 db/octave slope and a 100 Hz lower cutoff frequency. This causes the reduction (but not elimination) of the acoustical energy between 10–100 Hz while leaving the energy in the band 100–1000 Hz unchanged. Although the energy in the 10–100 Hz band is filtered, the residual energies are still of interest since it cannot be totally eliminated. Thus, the results are plotted for the total band of 10–1000 Hz.

It should be understood that power or energy can be measured and compared in accomplishing the objectives of the present invention. Thus, either or both can be employed. In the foregoing description and the claims which follow, the term "power" is usually employed for convenience and simplicity. Whenever "power" or "energy" alone is encountered, the broader "power and/or energy" is implied and considered to be within the scope of the description and claims of the present invention.

Wherefore, having thus described our invention, we claim:

1. The method of determining the operability status of a heart valve in vivo comprising the steps of:

(a) disposing a phonocardiographic transducer in a positon to gather time-amplitude-acoustical information emanating from the heart valve and adjacent areas;

(b) gathering the output signal from the transducer from a cardiac cycle;

(c) determining the location of a pre-established point in the cardiac cycle within the data;

(d) dividing the data of the cardiac cycle into time slices beginning with the pre-established point;

(e) calculating the power v. frequency curve for each time slice;

(f) comparing the power level associated with the valve being tested at pre-established frequencies within each time slice to corresponding power levels for the same frequencies at the same time slice for a known good valve; and,

(g) indicating valve malfunction if the power ratio of measured data to known good data is greater than a pre-established amount over a pre-established threshold number of compared values.

2. The method of claim 1 wherein:

the power ratio is a Normalized Power Distribution (NPD) defined by the relationship:

$$1 - NPD(n\Delta f) = \frac{\frac{1}{2}\sum_{k=0}^{n}[a(k\Delta f)]^2 + [b(k\Delta f)]^2 + [a((k+1)\Delta f)]^2 + [b((k+1)\Delta f)]^2}{\frac{1}{2}\sum_{k=0}^{N}[a(k\Delta f)]^2 + [b(k\Delta f)]^2 + [a((k+1)\Delta f)]^2 + [b((k+1)\Delta f)]^2}$$

for n=0, 1, 2, . . . , N

and where, Δf is the frequency resolution (9.8 Hz) and a(ω) and b(ω) are the real and imaginary part of the complex Fourier coefficient for frequency ω.

3. The method of claim 1 wherein:

the known good data are obtained from the same valve from steps (a) through (e) of claim 1 performed at a time when the valve is known to be properly operating.

4. The method of claim 1 or claim 3 wherein:

step (b) of gathering the output signal includes filtering the signal to remove data associated with frequencies below 100 Hz and above 1000 Hz.

5. The method of claim 1 or claim 4 wherein said step (d) of dividing the data into time slices comprises:

dividing the data into overlapping time windows having a length of duration longer than the increment between windows.

6. The method of claim 5 wherein:

each window is about 100 ms in duration, and the windows are taken at 20 ms increments.

7. The method of claim 1 or claim 3 wherein said step (c) of determining the location of a pre-established point in the cardiac cycle within the data includes the steps of:

(c1) gathering simultaneous blood-pressure data with said acoustical data;

(c2) storing said pressure data in association with said acoustical data as an identifier thereof;

(c3) searching said pressure data for a pre-established point in the cardiac cycle identifiable by its pressure characteristics; and

(c4) using the acoustical data associated with said pressure identifiable point in the cardiac cycle as a starting point for step (d).

8. The method of determining the operability status of a heart valve in vivo comprising the steps of:

(a) gathering simultaneously and retaining time-amplitude acoustical information emanating from the heart valve and adjacent area as well as the carotid or Korotkoff pressure within the cardiovascular system as produced by the heart for a cardiac cycle;

(b) searching the retained pressure data for a pre-established point within the cardiac cycle;

(c) using the pre-established point within the data found in step (b) as a starting point and dividing the acoustical data into a series of overlapped data windows for one cardial cycle wherein the duration of each window is longer than the increment between windows;

(d) calculating the power v. frequency curve for each window;

(e) comparing the power level associated with the valve being tested at pre-established known resonant frequencies to the power level at the same frequencies for the same windows in the cardiac cycle for a known good valve; and,

(f) indicating valve malfunction if the ratio of the compared power levels is greater than a pre-established amount for greater than a pre-established number of values.

9. The method of claim 8 wherein:

the power ratio is a Normalized Power Distribution (NPD) defined by the relationship:

$$1 - NPD(n\Delta f) = \frac{\frac{1}{2}\sum_{k=0}^{n}[[a(k\Delta f)]^2 + [b(k\Delta f)]^2 + [a((k+1)\Delta f)]^2 + [b((k+1)\Delta f)]^2]}{\frac{1}{2}\sum_{k=0}^{N}[[a(k\Delta f)]^2 + [b(k\Delta f)]^2 + [a((k+1)\Delta f)]^2 + [b((k+1)\Delta f)]^2]}$$

for n=0, 1, 2, . . . , N

and where, Δf is the frequency resolution (9.8 Hz) and a(ω) and b(ω) are the real and imaginary part, respectively, of the complex Fourier coefficient for frequency ω.

10. The method of claim 8 wherein;

the known good data are obtained from the same valve by steps (a) through (e) of claim 8 performed at a time when the valve is known to be properly operating.

11. The method of claim 8 or claim 10 wherein:

step (b) of gathering the output signal includes filtering the signal to remove data associated with frequencies below 100 Hz. and above 1000 Hz.

12. The method of claim 8 wherein:

each window is about 100 ms in duration and the windows are taken at 20 ms increments.

13. The method of claim 8 wherein:

only data associated with windows wherein the valve is in a non-transition state between open and closed is employed for step (e) of comparing.

14. The method of determining the operability status of a heart valve in vivo comprising the steps of:

(a) gathering simultaneously and retaining time-amplitude acoustical information emanating from the heart valve and adjacent area as well as the carotid or Korotkoff pressure within the cardiovascular system as produced by the heart for one cardiac cycle;

(b) searching the retained pressure data for a pre-established point within the cardiac cycle;

(c) using the pre-established point within the data found in step (b) as a starting point and dividing the

acoustical data into a series of overlapped data windows for one cardiac cycle wherein the duration of each window is longer than the increment between windows;

(d) calculating the power v. frequency curve for each window;

(e) finding the maximum power level associated with the valve being tested at pre-established frequencies during the cardiac cycle;

(f) comparing the maximum power level for the valve being tested to the maximum power for a known good valve; and,

(g) indicating valve malfunction if the ratio of the compared maximum power levels is greater than a pre-established amount.

15. The method of claim 14 wherein:

the power ratio is a Normalized Power Distribution (NPD) defined by the relationship:

$$1 - NPD(n\Delta f) = \frac{\frac{1}{2}\sum_{k=0}^{n}[[a(k\Delta f)]^2 + [b(k\Delta f)]^2 + [a((k+1)\Delta f)]^2 + [b((k+1)\Delta f)]^2]}{\frac{1}{2}\sum_{k=0}^{N}[[a(k\Delta f)]^2 + [b(k\Delta f)]^2 + [a((k+1)\Delta f)]^2 + [b((k+1)\Delta f)]^2]}$$

for n=0, 1, 2, . . . , N

and where, Δf is the frequency resolution (9.8 Hz) and a(ω) and b(ω) are the real and imaginary part of the complex Fourier coefficient for frequency ω.

16. The method of claim 14 wherein:

the known good data are obtained from the same valve from steps (a) through (e) of claim 14 performed at a time when the valve is known to be operating properly.

17. The method of claim 14 or claim 16 wherein:

step (b) of gathering the output signal includes filtering the signal to remove data associated with frequencies below 100 Hz and above 1000 Hz.

18. The method of claim 14 wherein:

each window is about 100 ms in duration and the windows are taken at 20 ms increments.

19. The method of determining the operability status of a heart valve IN VIVO comprising the steps of:

(a) disposing a phonocardiographic transducer in a positon to gather time-amplitude-acoustical information emanating from the heart valve and adjacent areas;

(b) gathering the output signal from the transducer from a cardiac cycle;

(c) determining the location of a pre-established point in the cardiac cycle within the data;

(d) dividing the data of the cardiac cycle into time slices beginning with the pre-established point;

(e) calculating the energy v. frequency curve for each time slice;

(f) comparing the energy level associated with the valve being tested at pre-established frequencies within each time slice to corresponding energy levels for the same frequencies at the same time slice for a known good valve; and,

(g) indicating valve malfunction if the energy ratio of measured data to known good data is greater than a pre-established amount over a pre-established threshold number of compared values.

20. The method of claim 19 wherein:

the energy ratio is a Normalized Energy Distribution (NED) defined by the relationship:

$$1 - NED(n\Delta f) = \frac{\frac{1}{2}\sum_{k=0}^{n}\left[\frac{[a(k\Delta f)]^2 + [b(k\Delta f)]^2}{k\Delta f} + \frac{[a((k+1)\Delta f)]^2 + [b((k+1)\Delta f)]^2}{(k+1)\Delta f}\right]}{\frac{1}{2}\sum_{k=0}^{N}\left[\frac{[a(k\Delta f)]^2 + [b(k\Delta f)]^2}{k\Delta f} + \frac{[a((k+1)\Delta f)]^2 + [b((k+1)\Delta f)]^2}{(k+1)\Delta f}\right]}$$

for n=0, 1, 2, . . . , N

and where, Δf is the frequency resolution (9.8 Hz) and a(ω) and b(ω) are the real and imaginary part of the complex Fourier coefficient for frequency ω.

21. The method of claim 19 wherein:

the known good data are obtained from the same valve from steps (a) through (e) of claim 19 performed at a time when the valve is known to be properly operating.

22. The method of claim 19 or claim 21 wherein:

step (b) of gathering the output signal includes filtering the signal to remove data associated with frequencies below 100 Hz and above 1000 Hz.

23. The method of claim 19 or claim 22 wherein said step (d) of dividing the data into time slices comprises:

dividing the data into overlapping time windows having a length of duration longer than the increment between windows.

24. The method of claim 23 wherein:

each window is about 100 ms in duration, and the windows are taken at 20 ms increments.

25. The method of claim 19 or claim 21 wherein said step (c) of determining the location of a pre-established point in the cardiac cycle within the data includes the steps of:

(c1) gathering simultaneous blood-pressure data with said acoustical data;

(c2) storing said pressure data in accordance with said acoustical data as an identifier thereof;

(c3) searching said pressure data for a pre-established point in the cardiac cycle identifiable by its pressure characteristics; and

(c4) using the acoustical data associated with said pressure identifiable point in the cardiac cycle as a starting point for step (d).

26. The method of determining the operability status of a heart valve in vivo comprising the steps of:

(a) gathering simultaneously and retaining time-amplitude acoustical information emanating from the heart valve and adjacent area as well as the carotid or Korotkoff pressure within the cardiovascular system as produced by the heart for a cardiac cycle;

(b) searching the retained pressure data for a pre-established point within the cardiac cycle;

(c) using the pre-established point within the data found in step (b) as a starting point and dividing the acoustical data into a series of overlapped data

windows for one cardial cycle wherein the duration of each window is longer than the increment between windows;

(d) calculating the energy v. frequency curve for each window;

(e) comparing the energy level associated with the valve being tested at pre-established known resonant frequencies to the energy level at the same frequencies for the same windows in the cardiac cycle for a known good valve; and,

(f) indicating valve malfunction if the ratio of the compared energy levels is greater than a pre-established amount for greater than a pre-established number of values.

27. The method of claim 26 wherein:

the energy ratio is a Normalized Energy Distribution (NED) defined by the relationship:

$$1 - NED(n\Delta f) \approx \frac{\frac{1}{2}\sum_{k=0}^{n}\left[\frac{[a(k\Delta f)]^2 + [b(k\Delta f)]^2}{k\Delta f} + \frac{[a((k+1)\Delta f)]^2 + [b((k+1)\Delta f)]^2}{(k+1)\Delta f}\right]}{\frac{1}{2}\sum_{k=0}^{N}\left[\frac{[a(k\Delta f)]^2 + [b(k\Delta f)]^2}{k\Delta f} + \frac{[a((k+1)\Delta f)]^2 + [b((k+1)\Delta f)]^2}{(k+1)\Delta f}\right]}$$

for n=0, 1, 2, . . . , N

and where, Δf is the frequency resolution (9.8 Hz) and a(ω) and b(ω) are the real and imaginary part of the complex Fourier coefficient for frequency ω.

28. The method of claim 26 wherein:

the known good data are obtained from the same valve by steps (a) through (e) of claim 26 performed at a time when the valve is known to be properly operating.

29. The method of claim 26 or claim 28 wherein:

step (b) of gathering the output signal includes filtering the signal to remove data associated with frequencies below 100 Hz. and above 1000 Hz.

30. The method of claim 26 wherein:

each window is about 100 ms in duration and the windows are taken at 20 ms increments.

31. The method of claim 26 wherein:

only data associated with windows wherein the valve is in a non-transition state between open and closed is employed for step (e) of comparing.

32. The method of determining the operability status of a heart valve IN VIVO comprising the steps of:

(a) gathering simultaneously and retaining time-amplitude acoustical information emanating from the heart valve and adjacent area as well as the carotid or Korotkoff pressure within the cardiovascular system as produced by the heart for one cardiac cycle;

(b) searching the retained pressure data for a pre-established point within the cardiac cycle;

(c) using the pre-established point within the data found in step (b) as a starting point and dividing the acoustical data into a series of overlapped data windows for one cardiac cycle wherein the duration of each window is longer than the increment between windows;

(d) calculating the energy v. frequency curve for each window;

(e) finding the maximum energy level associated with the valve being tested at pre-established frequencies during the cardiac cycle;

(f) comparing the maximum energy level for the valve being tested to the maximum energy for a known good valve; and,

(g) indicating valve malfunction if the ratio of the compared maximum power levels is greater than a pre-established amount.

33. The method of claim 32 wherein:

the energy ratio is a Normalized Energy Distribution (NED) defined by the relationship:

$$1 - NED(n\Delta f) \approx \frac{\frac{1}{2}\sum_{k=0}^{n}\left[\frac{[a(k\Delta f)]^2 + [b(k\Delta f)]^2}{k\Delta f} + \frac{[a((k+1)\Delta f)]^2 + [b((k+1)\Delta f)]^2}{(k+1)\Delta f}\right]}{\frac{1}{2}\sum_{k=0}^{N}\left[\frac{[a(k\Delta f)]^2 + [b(k\Delta f)]^2}{k\Delta f} + \frac{[a((k+1)\Delta f)]^2 + [b((k+1)\Delta f)]^2}{(k+1)\Delta f}\right]}$$

for n=0, 1, 2, . . . , N

and where, Δf is the frequency resolution (9.8 Hz) and a(ω) and b(ω) are the real and imaginary part of the complex Fourier coefficient for frequency ω.

34. The method of claim 32 wherein:

the known good data are obtained from the same valve from steps (a) through (e) of claim 32 performed at a time when the valve is known to be operating properly.

35. The method of claim 32 or claim 34 wherein:

step (b) of gathering the output signal includes filtering the signal to remove data associated with frequencies below 100 Hz and above 1000 Hz.

36. The method of claim 32 wherein:

each window is about 100 ms in duration and the windows are taken at 20 ms increments.

* * * * *